Investigating the Pathogenesis of Mitochondrial Dysfunction in Mitochondrial and Other Myopathies

Amy Elizabeth Vincent

MSci (Hons)

This thesis is submitted for the degree of Doctor of Philosophy at Newcastle University

Institute of Neuroscience

Wellcome Trust Centre for Mitochondrial Research

May 2017

Author Declaration

This thesis is submitted for the degree of Doctor of Philospy at Newcastle University. The research was conducted in the Wellcome Trust Centre for Mitochondrial Research, Institute of Neuroscience, Newcastle University under the supervision of Prof Sir D M Turnbull, Prof R W Taylor and Dr R Barresi. In addition some of the research was completed in Prof. M Picard's lab, Department of Psychiatry, Division of Behavioural Medicine, Columbia University, New York USA. All work is my own unless otherwise stated.

I certify that none of the material presented here in this thesis has previously been submitted by me for a degree or qualification at this or any other university.

For Mum and Dad,

With love

Abstract

Skeletal muscle contains a large number of mitochondria, known for their production of ATP via oxidative phosphorylation, which is of vital importance for energy-demanding muscle contraction. However, the mitochondria also have a plethora of other functions such as; calcium ion homeostasis, iron-sulphur cluster formation, redox signalling and apoptotic signalling, which are of similarly high importance to skeletal muscle function. As such, it is of little surprise that mitochondrial dysfunction has been linked to a large number of neuromuscular conditions as well as healthy skeletal muscle ageing and sarcopenia. However, the mechanisms by which the dysfunction occurs and its pathological and clinical relevance remains to be understood. This thesis therefore aims to advance the understanding of mechanisms and pathological significance of mitochondrial dysfunction in mitochondrial disease, myofibrillar myopathy, dysferlin myopathy and skeletal muscle ageing.

The project was approached from three very different angles. Firstly, by exploring mitochondrial dysfunction in myofibrillar myopathy, dysferlinopathy and looking for potential links to disease pathology. Secondly, by attempting to understand mechanisms and factors effecting clonal expansion of mitochondrial DNA (mtDNA) mutations, which accumulate with age in post mitotic tissues in both healthy individuals and those affected by neuromuscular and neurodegenerative disorders. Both of these approaches were investigated using histochemical, immunocytochemical and single cell genetic methodologies. Finally, possible links between mitochondrial morphology, ultrastructure and function were investigated using electron microscopy techniques.

This work provides novel insights into mitochondrial involvement in neuromuscular disease pathology. Key findings include; the reduction of mitochondrial mass in myofibrillar myopathy, increased respiratory chain deficiency in some patients with dysferlinopathy, the spectrum of mitochondrial ultrastructural defects in mitochondrial myopathy, the anisotropic nature of the skeletal muscle mitochondria, the perinuclear origins of mtDNA deletions and their clonal expansion due to retrograde signalling and mitochondrial biogenesis.

Acknowledgments

Firstly, and foremost, I would like to thank my supervisors Professor Sir Doug Turnbull, Professor Robert Taylor and Dr Rita Barresi for the opportunity to undertake my PhD, but also for their unwavering support and advice along the way. In particular Doug's belief in my ability, and the new challenges he has presented to me have been a welcome motivator.

Secondly, I thank my collaborator Professor Martin Picard who has been; a fantastic guide into the nanoscale world of EM, a source of additional support and a great mentor through the later part of my PhD. Prof. Picard also allowed me the opportunity to work for 3 months with him at Columbia University, and being there to see the birth of the Picard lab was a pleasure.

I then must thank a few key contributors to my work. Firstly, Dr. Georgia Campbell who designed the primers used for long range PCR. Then to, Richard, Julie and Matt at the MIU and Gavin and Tom in the diagnostic lab who facilitated my access to tissue. A big thanks also to Drs Kathryn White and Tracey Davey from Electron Microscopy Research services who prepared all samples run on EM, helped with SBFSEM imaging set-up and have always been keen to try new experimental approaches to investigate mitochondrial structure. Dr. Trevor Booth from Bioimaging has always been helpful with imaging advice. In addition, Dr. Yi Ng and Dr. Charlotte Alston have been a fantastic source of clinical information and genetic knowhow respectively. Last but not least, Dr. John Grady's statistical magic has been absolutely essential!

Next to some key members in the MRG family; Drs Amy Reeve, Oliver Russell, Karolina Rygiel, Anne Grunewald, Helen Tuppen, Mariana Rocha. Jono Philips, Alexia Chrysostomou and also to Nicole Mai and Pavendeep Rai. Each of whom have always been happy to share their knowledge and experience with me and many of whom I have been lucky enough to share laughs and friendship with also. An extra special thanks to my colleague and living compadre Joel and partner in crime Hannah for being right there with me through all of this. You've made the worst parts bearable and been fantastic friends in the process! To Chen, you've very literally held my hand through the writing process, providing moral support, lunch and much needed breaks, thank you! Hannah, Amy, Joel and Jono have also provided excellent moral support, caffeine breaks and biscuits throughout the writing process. I also can't forget the help of my canine friends Bella and Darwin, who provided much needed dog therapy and solid scientific opinions.

To my Newcastle family (the inhabitants of 73 Osborne road). In particular, the breakfast club (Gwenno and Gemma), who have always been so supportive and understanding of my hectic schedule. I also cannot thank them enough for coming to visit me in NY and for all the good times over the last three years. I also extend my thanks to NMHC and in particular the lovely Ladies 1s. Hockey is a welcome distraction and it is made all the better when you have fantastic team mates. These friendships along with those at the MRG have kept me sane(ish) and made living in Newcastle the best years of my life.

I can't then forget to thank my family including Mum, Dad, Charlotte, my grandparents and Pippa, all of whose support throughout my PhD and before has

been fundamental to my achievements. In particular, my mum and dad have been a rock throughout and I do not know what I would do without out them. Thanks also to Dot and Becca who are now pretty much family and have always been there to listen and offer advice when I've had a bad day.

I would like to extend my gratitude to the MRC for funding my studentship and thus allowing me to undertake my PhD. Further thanks to the MRC supplementary award committee at Newcastle University for granting me additional funding to undertake a period of work at Columbia University with Prof. Martin Picard.

Finally, the work included here would not be possible without the consent of the patients. Thank you, I sincerely hope that advances over the coming years improve the livelihoods of you, your families and future generations living with mitochondrial disease. The close partnership between the patients, clinicians and researchers found at the WTCMR is quite rare and this is essential to making the research as translational as possible.

Publications list:

Amy E. Vincent, Hannah S. Rosa, Charlotte L. Alston, John P. Grady, Karolina A. Rygiel, Mariana C. Rocha Rita Barresi, Robert W. Taylor, Doug M. Turnbull: *Dysferlin mutations and mitochondrial dysfunction*. Neuromuscular Disorders 08/2016; DOI:10.1016/j.nmd.2016.08.008

Amy E. Vincent, John P. Grady, Mariana C. Rocha, Charlotte L. Alston, Karolina A. Rygiel, Rita Barresi, Robert W. Taylor, Doug M. Turnbull: *Mitochondrial dysfunction in myofibrillar myopathy*. Neuromuscular Disorders 08/2016; DOI:10.1016/j.nmd.2016.08.004

Amy E Vincent, Yi Shiau Ng, Kathryn White, Tracey Davey, Carmen Mannella, Gavin Falkous, Catherine Feeney, Andrew M Schaefer, Robert Mcfarland, Grainne S Gorman, Robert W Taylor, Doug M Turnbull, Martin Picard: *The Spectrum of Mitochondrial Ultrastructural Defects in Mitochondrial Myopathy*. Scientific Reports 09/2016; 6. DOI:10.1038/srep30610

Martin Picard, **Amy E Vincent**, Doug M. Turnbull: *Expanding Our Understanding of mtDNA Deletions*. Cell Metabolism 07/2016; 24(1). DOI:10.1016/j.cmet.2016.06.024

Virgilio J. J. Cadete, Sonia Deschênes, Alexanne Cuillerier, François Brisebois, Ayumu Sugiura, **Amy Vincent**, Doug Turnbull, Martin Picard, Heidi M. McBride, Yan Burelle: *Formation of Mitchondrial-derived vesicles is an active and physiologically relevant mitochondrial quality control process in the cardiac system*. The Journal of Physiology 06/2016; DOI:10.1113/JP272703

Karolina A. Rygiel, Helen A. Tuppen, John P. Grady, **Amy Vincent**, Emma L. Blakely, Amy K. Reeve, Robert W. Taylor, Martin Picard, James Miller, Doug M. Turnbull: *Complex mitochondrial DNA rearrangements in individual cells from patients with sporadic inclusion body myositis*. Nucleic Acids Research 04/2016; 44(11). DOI:10.1093/nar/gkw382

Mariana C Rocha, John P Grady, Anne Grünewald, **Amy Vincent**, Philip F Dobson, Robert W Taylor, Doug M Turnbull, Karolina A Rygiel: *A novel immunofluorescent assay to investigate oxidative phosphorylation deficiency in mitochondrial myopathy: Understanding mechanisms and improving diagnosis*. Scientific Reports 10/2015; 5. DOI:10.1038/srep15037

Courses and conferences attended

Expansion microscopy and lattice light sheet microscopy – Training course at Janelia farm research campus, USA (2016)

Mitochondrial Medicine, United Mitochondrial Disease Foundation Symposium – Poster presentation. Seattle, USA (2016)

Mitochondrial Medicine – Poster presentation. Cambridge, UK (2016)

20th International congress of the World Muscle Society – Poster presentation. Brighton, UK (2015)

Introduction to teaching and learning in higher education – Training course. Newcastle, UK (2015)

9th Annual UK Neuromuscular Translational research conference – Flash presentation and poster presentation. Oxford, UK (2015)

8th Annual UK Neuromuscular Translational research conference – Poster presentation. Newcastle, UK (2015)

7th Annual UK Neuromuscular Translational research conference – Poster presentation. London, UK (2014)

Update in Neuromuscular disorders – Poster presentation. London, UK (2014)

Abbreviations

A	Adenine
ADP	Adenosine diphosphate
ANT	Adenine nucleotide Translocator
ATP	Adenosine Triphosphate
ATPase	Adenosine Triphosphate synthase
BAG3	BCL2-Associated Athanogene 3
BpB	Bromo phenol Blue
C	Cytosine
Ca^{2+}	Calcium ion
COX	Cytochrome c Oxidase
CPEO	Chronic Progressive External Opthalmoplegia
CRYAB	Crystallin Alpha B
Ct	Threshold cycle
DAB	Diaminobenzadine
DEPC	Diethylpyrocarbonate
DES	Desmin
dH_2O	Distilled water
D-Loop	Displacement loop
DMAT	Distal Myopathy with Anterior Tibialis onset
DNA	Deoxyribonucleic Acid
dNTP	Deoxynucleotide
DYSF	Dysferlin
EDTA	Ethylenediaminetetraacetic acid
ETC	Electron transport chain
Fe-S	Iron-sulphur
G	Guanine
H^+	Proton
H_2O	Water
HCl	Hydrochloric acid
H strand	Heavy strand

HVR	Hypervariable region
IMM	Inner mitochondrial membrane
IMS	Intermembrane space
Kb	Kilobase
KSS	Kearn-Sayre Syndrome
LDB3	LIM Domain Binding Protein
LGMD2B	Limb Girdle Muscular Dystrophy Type 2B
L strand	Light strand
Leu	Leucine
Lys	Lysine
M	Molar
MELAS	Mitochondrial Enchephalomyopathy, Lactic Acidosis and Stroke-like episodes
MERRF	Myoclonic Epilepsy with Ragged Red Fibres
MFM	Myofibrillar myopathy
$MgCl_2$	Magnesium Chloride
MICOS	Mitochondrial Internal Cristae Organising System
ml	millilitre
mM	millimolar
MM	Myoshi Myopathy
mRNA	messenger Ribonucleic Acid
mtDNA	Mitochondrial DNA
mtSSB	Mitochondrial Single Strand Binding protein
mt-tRNA	mitochondrial transfer Ribonucleic Acid
MYOT	Myotilin
Na^+	Sodium ion
nDNA	nuclear DNA
nm	nanometer
O_H	Origin of heavy strand replication
O_L	Origin of light strand replication
OMM	Outer mitochondrial membrane
OPA1	Optic Atrophy 1

OXPHOS	Oxidative phosphorylation
PBS	Phosphate buffered saline
PCR	Polymerase chain reaction
PEO	Progressive external opthalmoplegia
PMS	Phenazine methosulphate
POLG	Polymerase Gamma
rCRS	Revised Cambridge reference sequence
ROS	Reactive oxygen species
RNA	Ribonucleic Acid
RRF	Ragged red fibre
RRM2B	Ribonucleotide Reductase subunit M2 B
SDH	Succinate Dehydriogenase
SBF-SEM	Serial Block Face Scanning Electron Microscopy
SKM	Skeletal Muscle
smPCR	Single molecule PCR
SR	Sarcoplasmic reticulum
T	Thymidine
TAE	Tris-Acetate EDTA
TCA	Tricarboxylic Acid
TEM	Transmission Elctron Microscopy
tRNA	transfer ribonucleic acid
T_m	Melting temperature
TWNK	Twinkle helicase
UPR^{mt}	Mitochondrial unfolded protein response
VDAC	Voltage Dependant Anion Channel
ZASP	Z-band Alternatively Spliced Protein
µm	micromolar
µl	microlitre

Table of Contents

List of Figures

List of Tables

Chapter 1. Introduction

1.1 Mitochondrial origins

Mitochondria reside in almost every eukaryotic cell and produce adenosine triphosphate (ATP) to power normal cellular function. Mitochondrial origins within eukaryotic cells are thought to have arisen due to an endosymbiotic relationship (Sagan, 1967).

There are two potential theories proposed to explain eukaryotic origins. One hypothesis suggests that nucleated Archeazoa diverged from prokaryotes, with Archeazoa including the host for the mitochondrial endosymbiont (Cavalier-Smith, 1987; Moreira and Lopez-Garcia, 1998). This hypothesis is based on the small subunit ribosomal RNA (rRNA) phylogenetic tree. The alternative suggests that the endosymbiotic event occurred before the diversion of eukaryotes from prokaryotes, with the subsequent diversion and development of a nucleus forming the eukaryotic cell (Martin and Muller, 1998). This second theory is now thought to be more plausible, since many genes in eukaryotic nuclei are more closely related to eubacteria homologues than archaebacterial homologues.

Although there is debate over the host cell, the endosymbiont has been easier to trace phylogenetically. The endosymbiont is thought to be an α-proteobacteria, due to the similarities between present day mitochondrial DNA (mtDNA) and some of the genes encoded by the α-proteobacteria genome (Esser *et al.*, 2004). Phylogenetic analysis of cytochrome b oxidase and cytochrome *c* oxidase genes of *Rickettsia prowazekii* confirmed the ancestor of mitochondria to be α-proteobacteria of the *Rickettsiaceae* family (Sicheritz-Ponten *et al.*, 1998).

1.2 Mitochondrial structure

Mitochondria are double membrane organelles, with the inner mitochondrial membrane (IMM) enclosing the matrix and the outer mitochondrial membrane (OMM) enclosing the intermembrane space (IMS). Early work on mitochondrial structure produced the baffle model of cristae structure (Palade, 1953), suggesting that the

IMM forms wide invaginations. This has been found to be inaccurate with the cristae actually being connected to the IMS by tubular cristae junctions (Daems and Wisse, 1966). In addition to this, regular cristae structure are known to take two formations; tubular and lamella-like, which are both connected to the IMS by 30 nm tubular connections (Mannella *et al.*, 1997; Perkins *et al.*, 1997; Frey and Mannella, 2000; Nicastro *et al.*, 2000). **Figure 1.1** shows a schematic representation of mitochondrial structure along-side an electron micrograph.

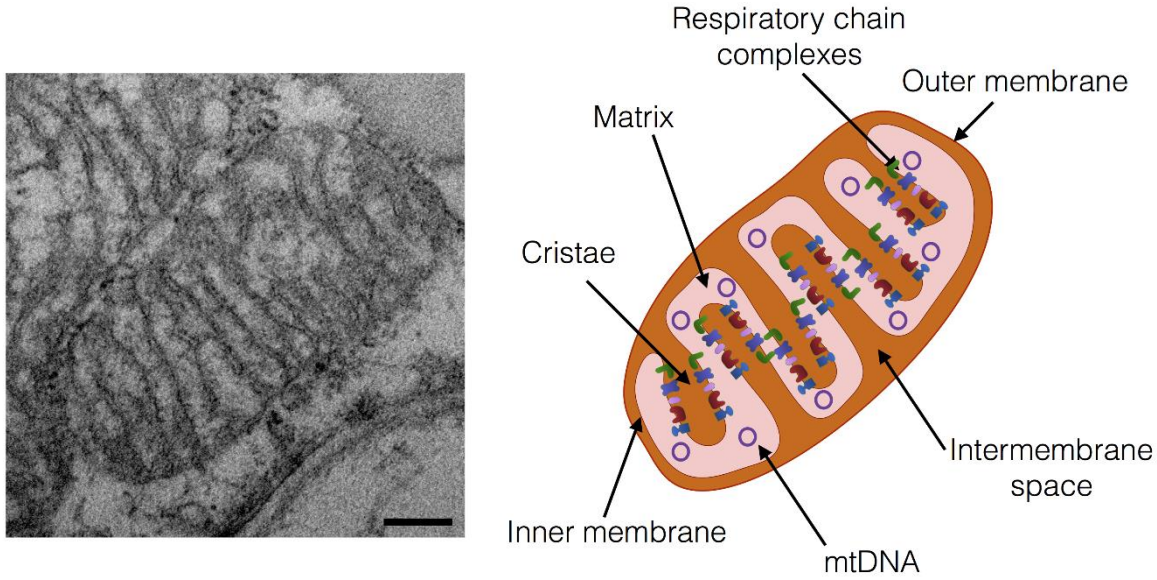

Figure 1.1 *Normal mitochondrial ultrastructure. Electron micrograph (left) and schematic (right) showing normal mitochondrial ultrastructure. Scale bar; 200 nm*.

The double membrane provides strict transport regulation for metabolites and ions both into and out of the mitochondria. The OMM is similar in composition to that of the cell membrane, thus allowing lipid soluble molecules to diffuse into the IMS. In comparison, proteins and hydrophilic molecules are transported across the OMM through protein channels such as the voltage-dependent anion channel (VDAC) (Ponnalagu and Singh, 2016).

The IMM is less permeable than the OMM, providing the stringency of mitochondrial transport into and out of the mitochondria, which is necessary for oxidative phosphorylation. In comparison to the OMM, the IMM has a greater ratio of protein to phospholipid, 70% protein to 30% lipid (Fleischer *et al.*, 1961), due to the large number of proteins required for metabolic pathways and high levels of cardiolipin. The IMM forms a series of invaginations, and consists of three topologically different regions. The inner boundary membrane is situated closest to the OMM, a large percentage of respiratory chain complex II are localised to the inner boundary membrane (Wilkens *et al.*, 2013; Cogliati *et al.*, 2016). The inner boundary membrane bends inwards at regular intervals forming cristae junctions; tubular structures, which are tightly regulated by the mitochondrial cristae organising system (MICOS) proteins. The final region is the cristae membrane, which delves into the mitochondrial matrix space. Respiratory chain complexes I, III and IV as well as ATP synthase localise to the cristae membrane (Wilkens *et al.*, 2013; Cogliati *et al.*, 2016). ATP synthase is known to form dimers at the apex of the cristae (Paumard *et al.*, 2002; Dudkina *et al.*, 2005; Strauss *et al.*, 2008). ATP synthase dimerisation and cristae morphology is described in detail in **6.1.2**.

The matrix is a continuous regulated environment where many mitochondrial biochemical processes, such as iron-sulphur (Fe-S) cluster formation and the tricarboxylic acid (TCA) cycle, occur. Multiple copies of the nucleoid packaged mtDNA are found in the matrix along with the machinery required for transcription and translation.

Nuclear encoded proteins, possessing a mitochondrial targeting sequence, can enter the mitochondria via the outer (TOM) and inner (TIM) mitochondrial translocases (Herrmann and Neupert, 2000; Rehling *et al.*, 2004). Depending on the protein function and its targeting sequence, these can be targeted to the matrix, IMS or be inserted into the OMM or IMM (Rehling *et al.*, 2004). Further detail on the

organisation and regulation of normal mitochondrial structure can be found in **Chapter 6**, along with analysis and discussion of abnormal mitochondrial ultrastructure.

1.3 Mitochondrial dynamics and morphology

Mitochondria were originally considered to be discrete, bean shaped organelles and are still commonly depicted in this way in scientific textbooks. However, it has now be known for some time that the mitochondria are in fact highly dynamic organelles, constantly undergoing fission and fusion (Bereiter-Hahn, 1978; Bereiter-Hahn and Voth, 1994). The balance of these determines their morphology and subsequently function. The frequency of these events alters mitochondrial morphology and in turn mitochondrial morphology can be used to predict the likelihood of fission or fusion events (Westrate *et al.*, 2014). Maintaining the balance is crucial and may shift dependent on cellular requirements. With increased mitochondrial fusion increasing mtDNA stability (Chen *et al.*, 2010) but allowing functional complementation to mitigate cellular stress and fission allowing selective removal of damaged mitochondria (Youle and van der Bliek, 2012). Defects in fission and fusion have been associated with numerous human diseases e.g. Parkinson's disease (Van Laar and Berman, 2009), Alzheimer's disease (Santos *et al.*, 2010) and Charcot-Marie-Tooth (CMT) disease (Palau *et al.*, 2009).

Mitochondrial dynamics have been found to vary substantially between different cell types (Kuznetsov *et al.*, 2009), with some cell types such as neurons having highly dynamic mitochondria while skeletal and cardiac mitochondria are less so. To date, the understanding of how frequently fission and fusion events occur in intact myofibres is limited and cultured myoblasts and myotubes do not have the regular lattice-like structure of mitochondrial arrangement found in fully developed muscle so are unlikely to be representative of *in vivo* mitochondrial dynamics. So far, the best models of mitochondria dynamics in skeletal muscle are live cell imaging of intact mouse muscle (Pham *et al.*, 2012), demonstrating that mitochondria are dynamic and fusion competent despite their static appearance.

1.1.1 Fission

Fission is the process by which one mitochondrion divides to form two mitochondria (***Figure 1.2***). Early work to identify the fission machinery was completed in yeast where Dnm1 and Fis1 were identified (Bleazard *et al.*, 1999; Mozdy *et al.*, 2000). Mammalian homologues of these proteins, dynamin related protein 1 (Drp1) and mitochondrial fission 1 protein (Fis1), were subsequently identified (Smirnova *et al.*, 2001; James *et al.*, 2003). Functional studies have demonstrated that knockdown of either protein causes mitochondria to elongate and become hyperfused whilst over expression fragments the mitochondrial network (Lee *et al.*, 2004).

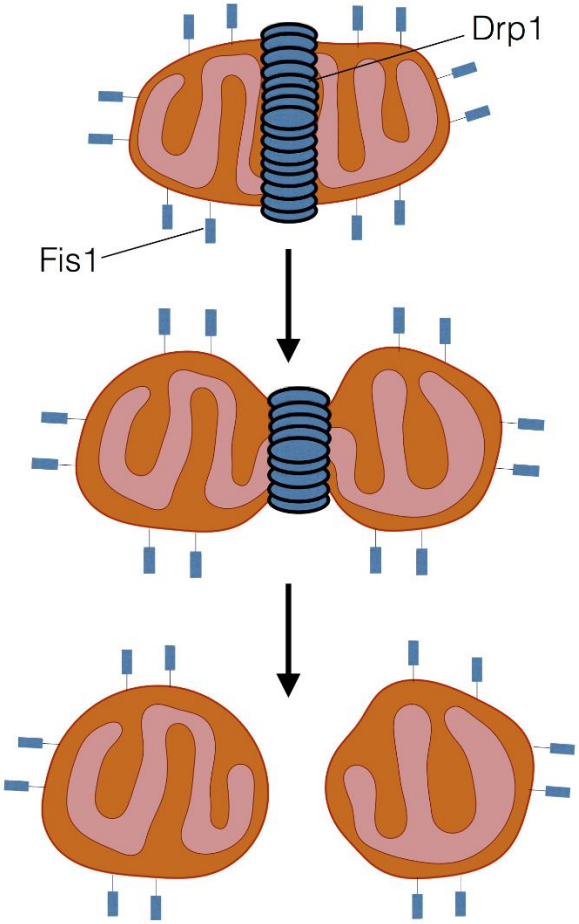

Figure 1.2 *Mitochondrial fission. Schematic representing mitochondrial fission and demonstrating the localisation of Dynamin related protein 1(Drp1) and mitochondrial fission 1 protein (Fis1). Fis1 is found to be evenly distributed across the full OMM and may play a role in Drp1 recruitment. Drp1 forms a helix around the mitochondrion. Contraction of this helix septates the membranes forming two mitochondria.*

In mammals, Drp1 is recruited from the cytosol and oligomerises forming a helix which, through the process of GTP hydrolysis constricts the mitochondrion ultimately resulting in membrane scission (Legesse-Miller *et al.*, 2003; Mears *et al.*, 2011). Drp1 recruitment and function are highly regulated by a number of post translational modifications (Chang and Blackstone, 2010). Furthermore, numerous proteins have been found to interact with Drp1 and are thus thought to play a role in its recruitment. These include Mff, Fis1, MID49 and MID51 (Mozdy *et al.*, 2000; Loson *et al.*, 2013). Recently, Septin 2 was found to localise to fission sites and interact with Drp1, depletion of Septin 2 significantly decreases the recruitment of Drp1 thus confirming its importance (Pagliuso *et al.*, 2016). The exact mechanism and roles that all of the proteins mentioned above play is not yet completely resolved.

Mitochondrial fission is important for the isolation and selective degradation of damaged mitochondria by mitophagy. A reduction in membrane potential results in fission, if the membrane potential remains low the mitochondrion cannot fuse back into the mitochondrial network and is targeted for mitophagy (Twig *et al.*, 2008), as described in **1.4.2**.

Due to the double membrane of the mitochondria, the fission process is a two-step process, requiring independent fission of the inner and outer membranes. Although the mechanism of mitochondrial fission is not yet completely understood, the proteins involved are well characterised.

1.1.2 Fusion

Fusion is the process by which two mitochondria combine to form a single mitochondrion with continuous inner and outer membranes (***Figure 1.3***). OMM fusion is regulated by GTPases MFN1 and MFN2, which form homo- or heterodimers (Chen *et al.*, 2003), that are all competent for fusion (Chen *et al.*, 2005). Both MFN1 and MFN2 perform similar roles but are both required for successful fusion, though they have differential importance in different tissues (Chen *et al.*, 2003; Chen *et al.*, 2005). MFN2 has also been demonstrated to perform a number of additional roles for which MFN1 cannot compensate e.g. tethering of mitochondria to the endoplasmic reticulum (de Brito and Scorrano, 2008) and normal glucose homeostasis (Sebastian *et al.*, 2012). The process of OMM fusion requires hydrolysis of GTP by the GTPase

domain, which induces a conformational change allowing the membranes to fuse (Chan, 2006).

IMM fusion is thought to be mediated by OPA1 (Cipolat *et al.*, 2004), which localises to the IMM. OPA1 undergoes alternative splicing and thus can exist in a number of functionally different isoforms (Delettre *et al.*, 2001). Upon low membrane potential or low ATP levels, Oma1 is activated leading to the proteolytic cleavage of Opa1 and preventing fusion (Head *et al.*, 2009).

Loss of the fusion machinery has been associated with disease in a number of tissues including heart (Papanicolaou *et al.*, 2011), brain (Chen *et al.*, 2007) and muscle (Chen *et al.*, 2010). However, the importance of the fusion machinery varies in a tissue specific manner, as such some defects, such as knockout of MFN2 in kidney, only result in a phenotype when the mitochondria are stressed (Gall *et al.*, 2012).

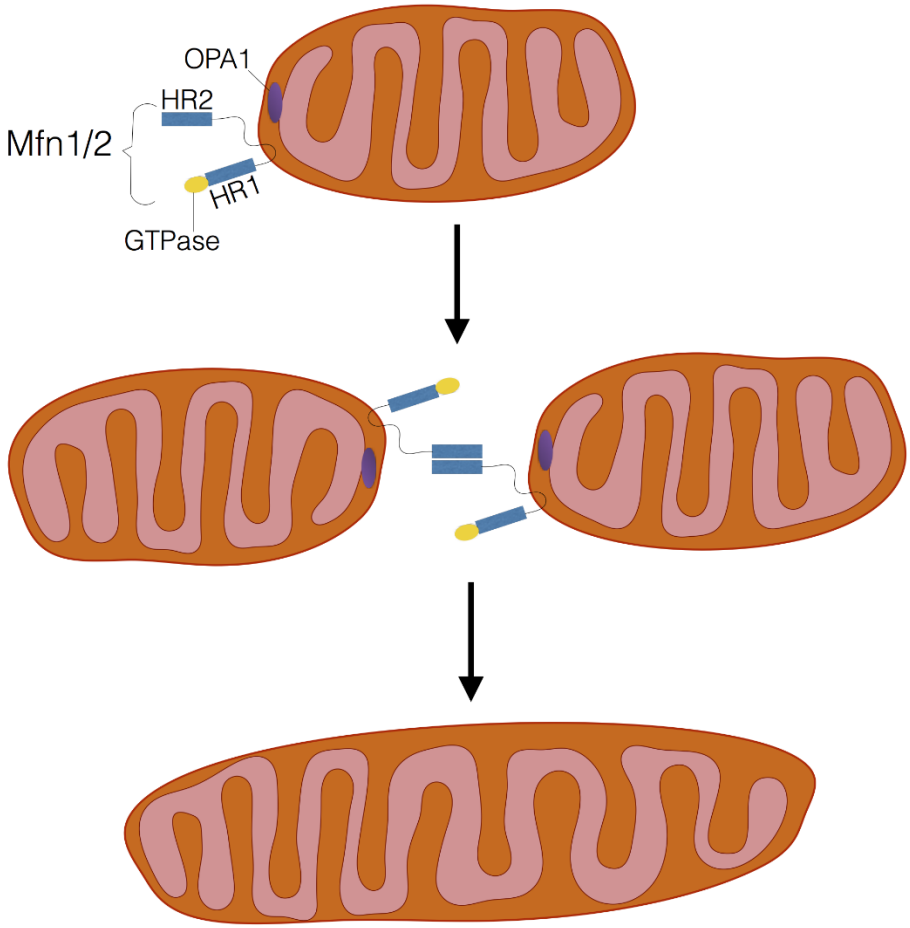

Figure 1.3 *Mitchondrial fusion. Schematic representing mitochondrial fusion and demonstrating the localisation of Opa1 and Mfn1/2. Binding of Mfn1/2 to the membrane and dimerisation is necessary for tethering of the two mitochondria prior to GTP hydrolysis and fusion of the outer mitochondrial membrane. Opa1 mediates fusion of the inner mitochondrial membrane.HR1 and HR2; heptad repeat region 1 and 2.*

1.1.3 Mitochondrial transport

Along with fission and fusion, mitochondrial dynamics also include small Brownian-like movements and transport over longer distances within the cell. However, the degree of motility varies on a tissue-specific basis, in some cells such as neurons and pancreatic cells, mitochondria can move quickly and continuously (Boldogh and Pon, 2007). Mitochondrial transport is particularly important in neurons, where it is used to balance changing energy needs of the subcellular locations (Hollenbeck and Saxton, 2005).

In neurons anterograde mitochondrial transport takes mitochondria from the cell body into the axon towards the synapse and is generated by Kinesin-1 (Hurd and Saxton, 1996; Glater *et al.*, 2006), which interacts with Miro through adapter protein Milton (Stowers *et al.*, 2002; Glater *et al.*, 2006), in a calcium dependent manner (Wang and Schwarz, 2009). Retrograde transport of mitochondria back to the cell body is achieved by a dynein motor (Martin *et al.*, 1999).

However, in mature, cardiac and skeletal muscle, mitochondrial transport is not observed. In mice with photoactivatable mitochondria the mitochondrial appear immotile (Eisner *et al.*, 2014) and in rat cardiomyocytes it has been demonstrated that mitochondria do not make large scale movements, only Brownian-like vibrations (Beraud *et al.*, 2009). This may largely be due to the dependence of mitochondria on interactions with the cytoskeleton which gives the skeletal muscle mitochondria a crystal-like organisation (Vendelin *et al.*, 2005). Specifically, mitochondria are known to be localised to the z-band in skeletal muscle and are tethered here by a protein complex containing desmin and plectin (described in more detail in **1.8.1**), other members of this complex have yet to be identified.

Work in cultured myoblasts has demonstrated that many of the proteins required for transport of mitochondria in other cell types are also expressed in myoblasts, although some kinesin heavy chain isoforms are not expressed (Iqbal and Hood, 2014). To date, this is the only work that has looked at mitochondrial transport in muscle and due to the change in cell architecture and mitochondrial positioning during myoblast differentiation and skeletal muscle development, the extent of mitochondrial transport in skeletal muscle *in vivo* is largely unknown.

1.4 Oxidative phosphorylation and ATP production

1.2.1 TCA cycle

The generation of ATP for cellular energy is a multi-step process starting with the anaerobic glycolysis, which feeds into the tricarboxylic acid cycle (TCA) or Kreb's cycle in the mitochondrial matrix, before reaching the respiratory chain and oxidative phosphorylation. Anaerobic glycolysis **Equation 1.1**, which occurs in the cytosol, produces two molecules of pyruvate (Berg *et al.*, 2012b). Pyruvate is either imported

into mitochondria, to the Kreb's cycle, or used to restore cytoplasmic NAD^+ pools for further glycolysis. The process of creating NAD^+ is either via fermentation in yeast or reduction of pyruvate to lactate by lactate dehydrogenase.

$$Glucose + 2[NAD^+] + 2[ADP] + 2[P_i] \rightarrow 2\ [pyruvate]\ 2[NADH] + 2[H^+] + 2[ATP] + 2[H_2O]$$

Equation 1.1 *Glycolysis reaction (Berg et al., 2012a).*

NADH molecules created by glycolysis cannot cross the IMM as such electrons are transferred via the glycerol 3-phosphate shuttle (Berg *et al.*, 2012a). NADH donates $2e^-$ to dihydroxyacetone in the cytosol, producing NAD and glycerol 3-phophate. Glycerol 3-phosphate dehydrogenase oxidises glycerol 3-phophate back to dihydroxyacetone and the $2e^-$ are transferred to flavin adenine dinucleotide (FAD) to produce $FADH_2$. $FADH_2$ is oxidised and ubiquinone (Q) reduced to ubiqinol (QH_2) in the matrix (Berg *et al.*, 2012a).

The Kreb's cycle or tricarboylic acid (TCA) cycle occurs in the mitochondrial matrix. The initial reaction is a conversion of pyruvate to acetyl CoA, catalysed by pyruvate dehydrogenase (**Equation 1.2**) (Berg *et al.*, 2012c). Acetyl CoA for the Kreb's cycle can also be produced via β-oxidation of fatty acids.

$$Pyruvate + CoA + NAD^+ \rightarrow Acetyl\text{-}CoA + NADH + H^+ + CO_2$$

Equation 1.2 *Pyruvate decarboxylation reaction catalysed by pyruvate dehydrogenase (Berg et al., 2012c).*

The Kreb's cycle (Krebs and Johnson, 1937) is a series of reactions that produces one molecule of ATP and CO_2 plus three NADH and two $FADH_2$ electron carriers that are subsequently involved in oxidative phosphorylation (**Equation 1.3**) (Berg *et al.*, 2012c). Oxaloacetate and Acetyl-CoA are converted to citrate catalysed by citrate

synthesis. A series of reactions then produces NADH, $FADH_2$ and ATP and returns citrate to oxaloacetate (Berg *et al.*, 2012c).

$$\text{Acetyl-CoA} + 3[NAD^+ + FAD + ADP + Pi + 2[H_2O] \rightarrow CoA + 3[NADH] + 2[H^+] + FADH_2 + ATP + 2[CO_2]$$

Equation 1.3 *The Kreb's cycle overall reaction*

1.2.2 Oxidative phosphorylation

The final stage of respiration is oxidative phosphorylation which couples the transport of electrons along the respiratory chain complexes I to IV with the translocation of protons across the IMM (***Figure 1.4***). Thus producing a chemiosmotic gradient, which results in the flow of electron back through ATP synthase, generating the energy required to produce ATP. This coupling of electron transport and ATP production was first described by Mitchell in 1961 and is termed the chemisomotic theory (Mitchell, 1961).

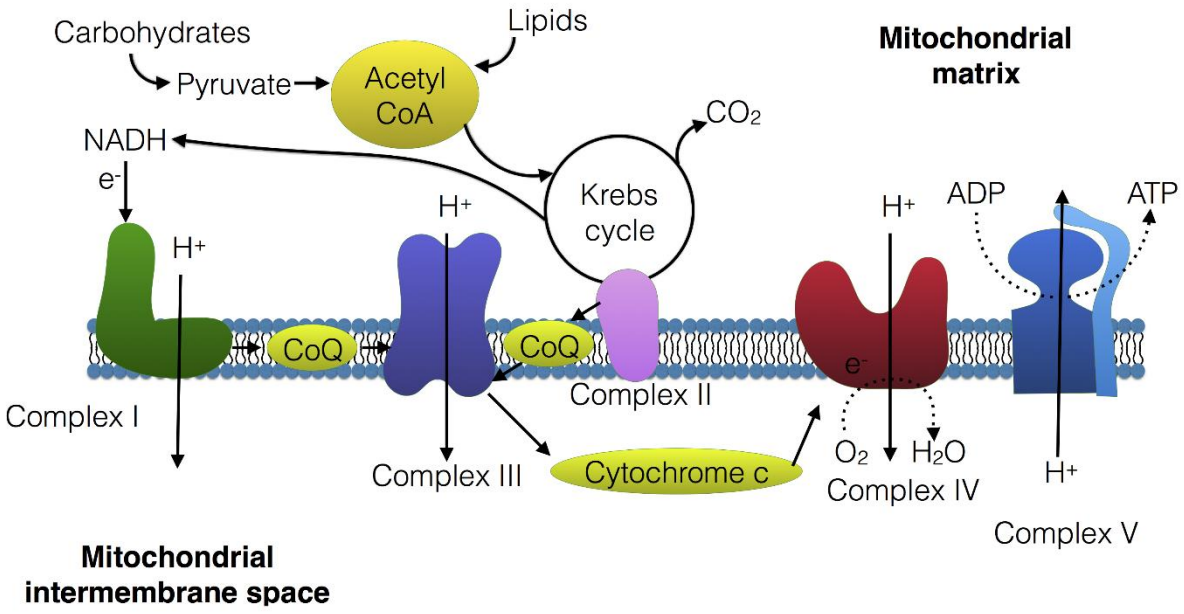

Figure 1.4 *Oxidative phosphorylation. Respiratory chain complexes I-IV are embedded into the inner mitochondrial membrane (IMM). Oxidative phosphorylation couples electron transport and proton translocation to ATP generation. Electrons can enter the electron transport chain at complex I or complex II and are shuttled to complex IV via cytochrome c. The transfer of electrons provides the energy to translocate protons from the matrix to the intermembrane space. Complex V or ATP synthase uses the proton gradient to produce ATP.*

1.2.3 Complex I or NADH: Ubiquinone Oxidoreductase

Complex I was first isolated in 1961 (Hatefi *et al.*, 1961). Composed of 45 subunits (of which seven are mitochondrial-encoded), complex I is the largest respiratory chain complex (almost 1000 kDa) (Zhu *et al.*, 2016). Fully assembled, complex I is L shaped, with a hydrophobic arm embedded in the IMM and one arm protruding into the matrix.

Complex I, schematically represented in ***Figure 1.5***, can be subdivided into three functional modules (Brandt, 2006); the N-module, Q-module and P-module. The N-module is located in the matrix arm and binds NADH oxidising it, transferring two electrons to a flavin mononucleotide (FMN) to form $FMNH_2$. The electrons are then transferred to Q via a chain of Fe-S clusters in the Q modules, also located in the matrix arm (Sazanov, 2007). Within the Fe-S clusters, electrons transiently reduce Fe^{3+} to Fe^{2+} prior to oxidation back to Fe^{3+}. Transfer of electrons to QH_2 also requires $2H^+$ from the matrix (Sazanov, 2007), the product QH_2 is released into the IMS. The

reduction of Q is coupled to proton translocation and can be inhibited for experimental purposes by rotenone, piericidin A, barbiturates (e.g. Amytal), Demerol and mercuricals. The overall reaction catalysed by complex I, is presented below (**Equation 1.4**). The final module is the P-module, which is IMM embedded and contains the seven mtDNA encoded subunits (Anderson *et al.*, 1981), acts as a proton pump. The transfer of electrons in the matrix arm, causes a conformational change in both arms, opening the channel and permitting the translocation of protons out of the matrix and across the IMM (Efremov *et al.*, 2010; Efremov and Sazanov, 2011).

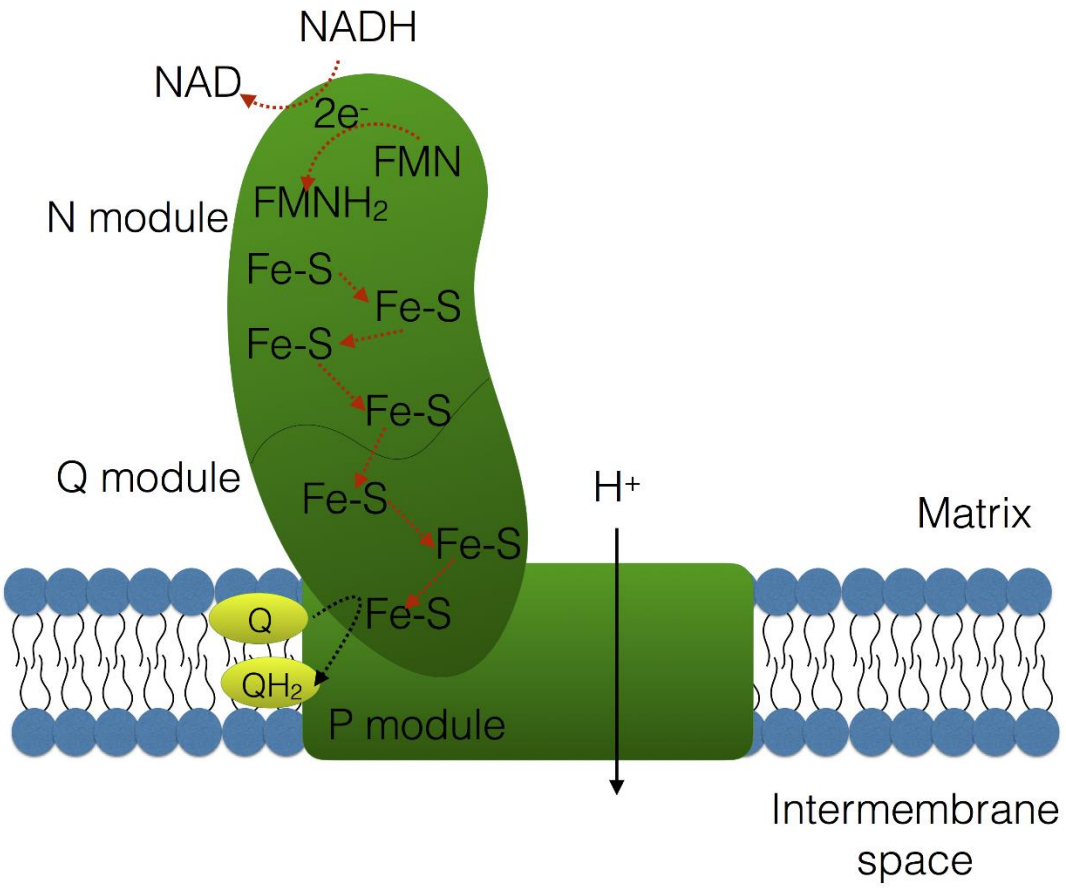

Figure 1.5 *Complex I. The schematic shows a simplified structure of respiratory chain complex I. Electrons are accepted from NADH and transferred to FMN. They are shuttled along a chain of iron sulphur clusters (Fe-S) and transferred to ubiquinone (Q). This shuttling of electrons is coupled to the transfer of a proton from the matrix to the intermembrane space across the inner mitochondrial membrane.*

$$NADH + Q + 5[H^+]_{matrix} \rightarrow NAD^+ + QH_2 + 4[H^+]_{cytoplasm}$$

Equation 1.4 *Complex I reaction (Berg et al., 2012b).*

Recently, complexasome profiling was implemented to study the assembly of complex I (Guerrero-Castillo *et al.*, 2016) and demonstrated a stepwise assembly. P_P-b is the central building block to which Q/P_P-a and P_D-a are added. However, data so far is inconclusive as to the order these join the complex. Subsequently, P_D-b is attached completing the Q and P modules. The final addition is the N-module, along with a few remaining accessory subunits. Of note, NDUFB8 belonging to PD-b is a commonly targeted subunit when assaying complex I levels via immunofluorescent protocols(Grünewald *et al.*, 2014; Rocha *et al.*, 2015) or western blotting (Lopez-Fabuel *et al.*, 2016).

1.2.4 Complex II or succinate:ubiquinone oxidoreductase dehydrogenase

Complex II (124kDa), was initially discovered by Thunberg in 1909, solubilised by Morton in 1950 and purified in 1971 (Davis and Hatefi, 1971; Hatefi, 1985). The enzymatic component is called succinate dehydrogenase or (SDH). Complex II consists of only four subunits (***Figure 1.6***), which are completely encoded by the nuclear genome. SDHC and SDHD are embedded in the IMM and SDHA and SDHB which are in the matrix and form the catalytic core (Hagerhall, 1997; Sun *et al.*, 2005). Complex II is not involved in the transfer of H^+ across the IMM, but catalyses the oxidation of succinate to fumarate and transfer of the electrons to ubiquinone via FAD and Fe-S clusters in SDHB (Hagerhall, 1997), thus acting as the second and last point of entry for electrons into the respiratory chain. The generation of fumarate is important for the TCA cycle.

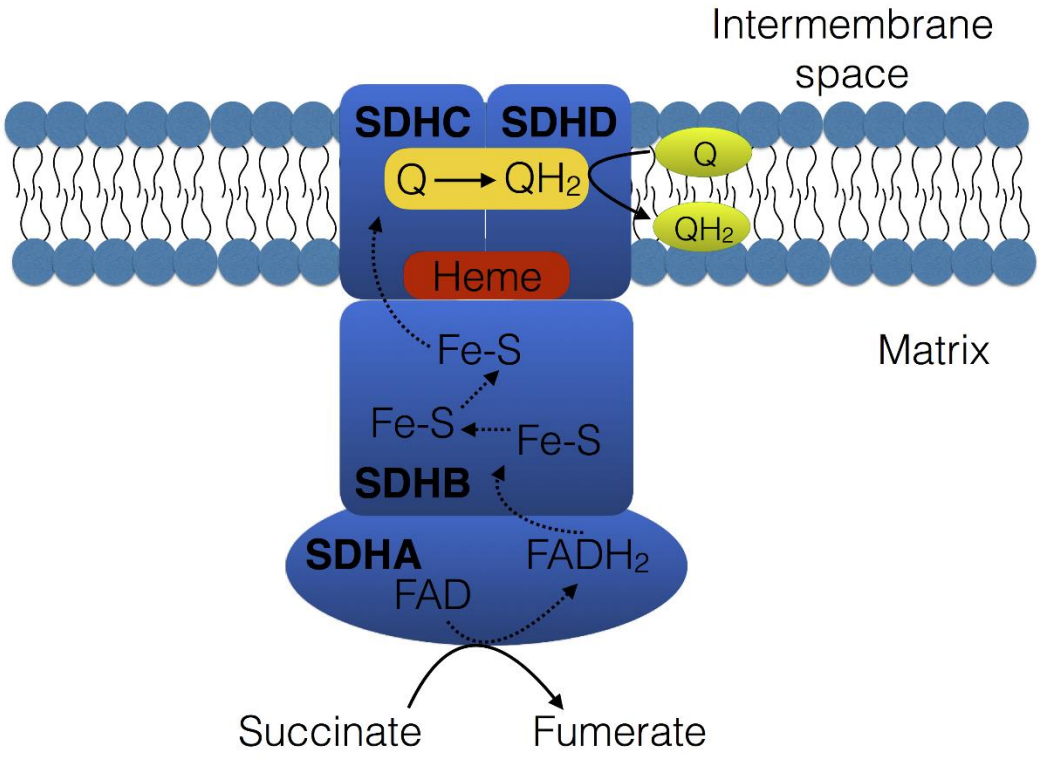

Figure 1.6 *Complex II. Schematic shows a simplified structure of complex II including pathway of electron transport. Complex II is the second point of entry for electrons into the oxidative phosphorylation system. Electrons are transferred from succinate to FAD, reducing it to $FADH_2$. Electrons are then shuttled along Fe-S clusters to ubiquinone*.

Succinate +FAD +2[H^+] +Q → Fumerate +$FADH_2$ + Q → fumerate +FAD +QH_2

Equation 1.5 *Complex II reaction (Berg et al., 2012b).*

1.2.5 Complex III or Ubiquinol cytochrome c oxidoreductase

Complex III, was first purified from bovine heart mitochondria in 1961 (Hatefi, 1976) and subsequent crystallisation showed that it consists of 11 subunits (Xia *et al.*, 1997; Iwata *et al.*, 1998), a simplified schematic is presented in **Figure 1.7**. Of the 11 subunits only cytochrome b is mitochondrially encoded.

Complex III catalyses the transfer of electrons from ubihydroquinone (QH_2) to cytochrome *c* as part of the Q cycle (Mitchell, 1976), which processes two QH_2 molecules in succession (**Equation 1.4**). For each QH_2, $2H^+$ are released into the IMS, and the electrons diverge down different routes. One electron is passed to cyctochrome *c* via the Riske Fe-S cluster and cytochrome c_1 and the second to cytochrome b where it binds to first low affinity haem (b_L), then high affinity haem (b_H) before reducing ubiquinone to a semiquinone intermediate. The process is repeated again and semiubiquione is reduced to QH_2.

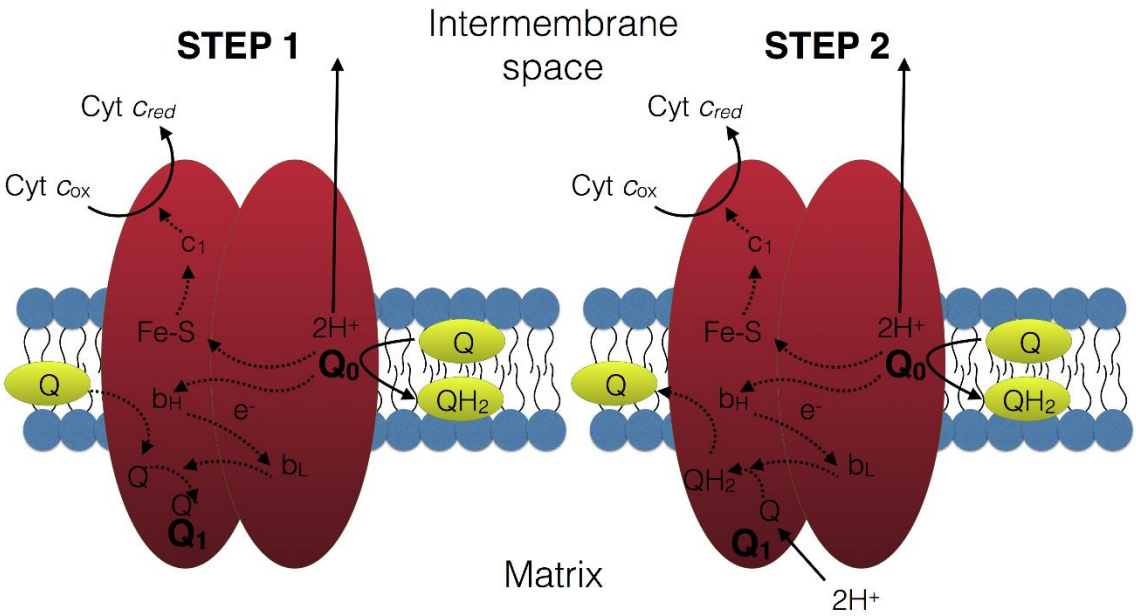

Figure 1.7 *Complex III. Schematic demonstrates a simplified structure of complex II, electron pathway and translocation of protons. Electrons are shuttled from ubihydroquinone via sulphur clusters and haem to ubiquinone and cytochrome c. This shuttling of electrons is coupled with the translocation of protons from the matrix to the intermembrane space.*

$$2[QH_2] + Q + 2[\text{Cyt c}]_{ox} + 2[H^+]_{matrix} \rightarrow 2\,[Q] + QH_2 + 2[\text{Cyt c}]_{red} + 4[H^+]_{cytoplasm}$$

Equation 1.6 *Complex III reaction (Berg et al., 2012b).*

1.2.6 Complex IV or cytochrome c oxidase (COX)

Complex IV or cytochrome c oxidase (COX) is the final complex of the electron transport chain and is responsible for the reduction of oxygen to water. COX is comprised of 13 subunits (**Figure 1.8**), of which three (MTCOI, MTCOII and MTCOIII) are mitochondrially encoded (Tsukihara *et al.*, 1996).

Electrons from cytochrome *c* are transferred via two haem groups and two copper centres (CuA and CuB) to O_2. Overall, four cytochrome *c* molecules are oxidised, donating four electrons. One passes via Cu_A and haem a to haem a_3 before reducing Cu_B. The next passes via Cu_A to haem a, allowing O_2 to bind to Cu_B and haem a

generating a peroxide bridge (Faxen *et al.*, 2005). The same process happens with the next two electrons, but this time $2H^+$ binding cleaves the peroxide bridge and a further two $2H^+$ to complete the reduction of O_2 to H_2O (Faxen *et al.*, 2005).

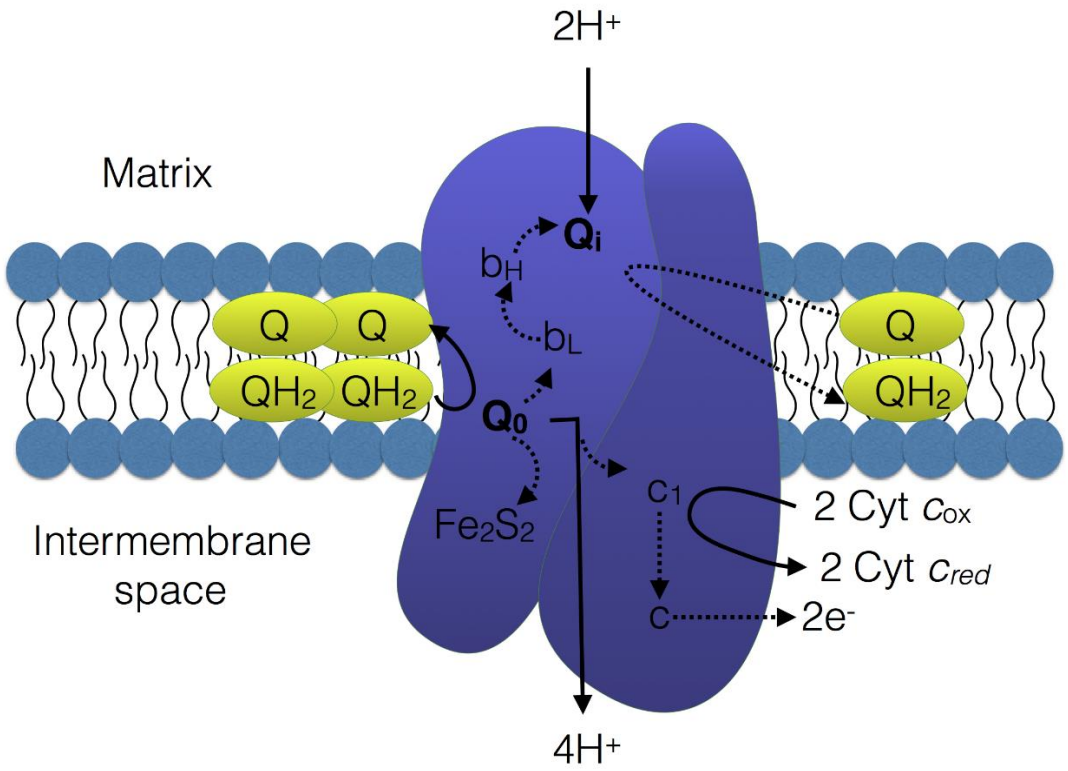

Figure 1.8 *Complex IV. Schematic demonstrates simplified structure transport of electrons and translocation of protons. Electrons from cytochrome c are transferred via two heam groups and two copper centres, allowing the binding of molecular oxygen and hydrogen atoms to form water. The shuttling of electrons is also couples to the translocation of protons from the matrix to the intermembrane space.*

$$4[\text{Cyt c}]_{red} + 8[H^+]_{matrix} + O_2 \rightarrow 4[\text{Cyt c}]_{ox} + 2H_2O + 4[H^+]_{cytoplasm}$$

Equation 1.7 *Complex IV reaction (Berg et al., 2012b).*

1.2.7 Complex V or ATP synthase

ATP synthase catalyses the final step in the synthesis of ATP. ATP synthase uses the electrochemical gradient generated by complexes I, III and IV to drive rotation of the F_0 rotary ring phosphorylating ADP to form ATP. ATP synthase consists of the F_0 portion which is situated in the IMM and the F_1 portion which protrudes into the matrix space (***Figure 1.9***). F_0 is made up of a c-ring and subunits a, b, d, F_6 and oligomycin sensitivity-conferring protein (OSCP), in addition subunits e, f, g and A6L are all associated with F_0 (Jonckheere *et al.*, 2012). Subunits a and A6L are the only two ATP synthase subunits to be encoded for by the mtDNA genes, *ATP6* and *ATP8* respectively (Anderson *et al.*, 1981). F_1 consists of three alternating α and β subunits plus one γ, one δ and one ε subunit.

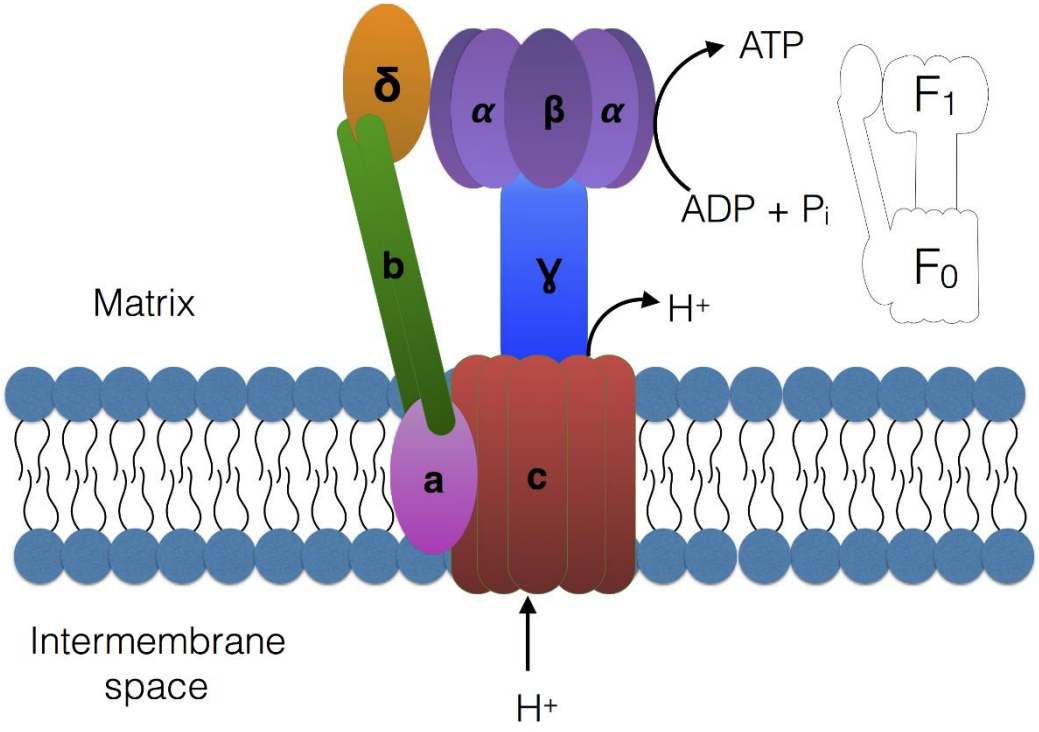

Figure 1.9 *Complex V or ATP Synthase. Schematic shows subunit arrangement, translocation of protons and generation of ATP. ATP synthase catalyses the synthesis of ATP from ADP and inorganic phosphate. This reaction is powered by the transport of protons through ATP synthase from the intermembrane space to the matrix. This flow occurs due to an electrochemical gradient generated by complexes I to IV. The silhouette to the left demonstrates the F_1 and F_0 portions.*

The proton gradient establishes a proton motive forces, and movement of protons through the c-ring is coupled with the rotation of two rotary motors; the c-ring (F_0) and γ, δ and ε subunit. As F_1 rotates, the β subunits to which ADP and P_i are bound undergoes a conformational change (Noji *et al.*, 1997). Thus, the turning generates the energy required to phosphorylate ADP and release ATP. A full 360° rotation is coupled to the transfer of eight protons and produces three ATP molecules (Watt *et al.*, 2010). ATP synthase can also reverse this process hydrolysing ATP, when mitochondrial membrane potential falls and pumping protons across the IMM to restore membrane potential.

ATP synthase has been demonstrated by electron cryo-tomography to dimerise at the apex of the cristae (Strauss *et al.*, 2008), such a dimersation induces a bend in the IMM. The cristae acts as a proton trap and ATP synthase dimerisation increases the electron-gradient, creating a proton sink at the apex of the cristae. Thus, leading to efficient ATP synthesis under proton limiting conditions.

1.2.8 Supercomplexes

Respiratory chain complexes I, II and IV, assemble into supercomplexes which improves complex stability and it has been hypothesised may reduce ROS production and lead to more efficient substrate channelling. Initially, a solid state model was proposed, suggesting that the complexes were organised in a large particle called the oxasome (Chance *et al.*, 1963). However, later findings of isolated complexes and the diffusion couples process of electron transport weaken this hypothesis. Subsequently, a fluid-state model was proposed (Hackenbrock *et al.*, 1986), before the proposition of supercomplexes, for which there is now substantial experimental support (Schagger and Pfeiffer, 2000). Thus, it is now believed that majority of complex I, is found bound as a complex II dimer and complex IV (known as the respirasome), with a smaller proportion just bound to a complex III dimer. There is also another supercomplex with dimerised complex III bound to complex IV (Schagger and Pfeiffer, 2000; Schägger and Pfeiffer, 2001). In addition, use of cryoEM has demonstrated that the respirasome is found in two structural conformations ‘tight’ and ‘loose’, for which it is unclear whether there is a transition

between the two states or if these are structurally different conformations (Gu *et al.*, 2016; Letts *et al.*, 2016).

1.5 Mitochondrial functions

Mitochondria are commonly referred to as 'the powerhouse of the cell' however mitochondria have long been known to perform functions, aside from ATP, production that are just as important to cell survival. These functions include calcium homeostasis, iron sulphur (Fe-S) cluster formation and a role in apoptotic signalling each of which is described in more detail below.

1.3.1 Calcium ion buffering

Calcium (Ca^{2+}) is an important cellular signal and as such cytosolic Ca^{2+} concentration is fundamental to numerous cellular processes. Ca^{2+} buffering in the cell is regulated by modulating translocation of Ca^{2+} into and out of the mitochondria. Ca^{2+} uptake by the mitochondria is achieved via the Ca^{2+} uniporter in the IMM in an electrochemical gradient dependent manner (Baughman *et al.*, 2011; De Stefani *et al.*, 2011) and release is via an ion exchange with Na^{+} (Palty *et al.*, 2010). Findings suggest this occurs in a $3Na^{+}/1Ca^{2+}$ ratio (Boyman *et al.*, 2013), with the mitochondrial membrane potential and Na^{+} concentration gradient driving calcium release.

Control of intracellular Ca^{2+} concentration in muscle is critically important for controlling muscle contraction. Motor neurons innervate muscle forming neuromuscular junctions at which an action potential opens Ca^{2+} channels causing an influx of extracellular Ca^{2+} into the neuron triggering release of acetylcholine into the synaptic cleft. Acetylcholine binds to receptors on the post-synaptic cleft and induces Na^{+} and K^{+} channel opening and depolarisation of the sarcolemmal membrane and opening of L-type Ca^{2+} channels in the sarcoplasmic reticulum (SR) triggering the release of Ca^{2+} into the cytosol. This cytosolic Ca^{2+} is increased which initiates actin/myosin cross bridging and movement of the myosin head to cause muscle contraction (Gehlert *et al.*, 2015). As the depolarisation spreads across the sarcolemma, it reduces the voltage dependent activation of L-type Ca^{2+} channels and

conformational change closes the channel. Muscle relaxation requires reuptake of calcium by the SR via ATP-dependent Ca^{2+} pumps, sarcoplasmic/endoplasmic reticulum calcium ATPase (SERCA) 1 and 2 (Brini and Carafoli, 2009).

1.3.2 Iron Sulphur cluster formation

Iron Sulphur clusters are an essential cofactor for OXPHOS and are present in oxidative phosphorylation complexes I-IV. Within the complexes iron sulphur clusters facilitate the transfer of electrons by repeated redox reactions. Reduced iron is transported into the matrix by mitoferrins (Zhu *et al.*, 2016). Following this, iron is donated to Isu1 and Nfu scaffold proteins via frataxin and an iron sulphur cluster is formed (Tong *et al.*, 2003; Yoon and Cowan, 2003). The sulphur for the cluster is provided in the form of sulphide ions generated from the release of sulphur from cysteine by cysteine dysulphurase (Tong and Rouault, 2000).

1.3.3 Apoptosis

Apoptosis is the process of controlled cell death which was initially expected to be a fully nuclear driven event (Kerr *et al.*, 1972). Contrary to this, it is now known that the mitochondria have a significant role in the control of this process (Estaquier *et al.*, 2012). A reduction in mitochondrial membrane potential and mitochondrial fission is temporally coupled to apoptosis with mitochondrial network fragmentation occurring prior to apoptosis, and Dnmp1 (yeast DRP1 homologue) has been found to mediate fragmentation and apoptosis like cell death in yeast (Fannjiang *et al.*, 2004). Furthermore, Drp-deficient cells with hyperfused mitochondria have been found to be resistant to apoptosis (Frank *et al.*, 2001).

Apoptosis is regulated in part by the Bcl-2 family of proteins, specifically pro-apoptotic (e.g. Bax and Bak) and anti-apoptotic (e.g. Bcl-2) which interact at the mitochondrial IMM (Cory and Adams, 2002). Activation of Bax and Bak or inhibition of Bcl-2 by the Bh3 family of proteins regulates the release of pro-apoptotic factors including cytochrome *c* from the IMS into the cytosol (Zong *et al.*, 2001).

Factors including cytochrome *c* interact with apoptosis proteinase-1 activating factor (Aparf-1) and caspase-9 in an 'apoptosome', which induces the caspase cascade (Wang and Youle, 2009). Apoptosis can be inhibited at the apoptosome level but inhibition can be relieved by proteins such as Smac and DIABLO which are also mitochondrially derived (Srinivasula *et al.*, 2001). Furthermore, apoptosis inducing factor which is responsible for chromatin condensation and degradation of nuclear DNA is also released by the mitochondria (Candé *et al.*, 2002).

The exact route by which apoptotic factors are released from the IMS is a topic of some debate. Loss of Opa1 oligomers during apoptosis releases the cristae junctions to facilitate release of IMS proteins (Scorrano *et al.*, 2002; Frezza *et al.*, 2006). This process is regulated by Oma1 which inhibits AAA protease YME1L cleavage of Opa1 (Head *et al.*, 2009). Prior to this, suggestions include a change in membrane permeabilisation (Kroemer *et al.*, 1995), due to opening of the mitochondrial permeability transition pore (PTP) which conists of; VDAC (Shimizu *et al.*, 1999) and ANT (Marzo *et al.*, 1998) or via Bax generated openings (Kuwana *et al.*, 2002).

1.3.4 Reactive oxygen species (ROS)

Reactive nitrogen and oxygen species cause damage to both protein and DNA (Cui *et al.*, 2012). The close proximity of the mitochondrial proteins and mtDNA to the respiratory chain, which produces ROS, makes them highly susceptible to ROS induced damage (Turrens, 2003).

The most common ROS produced is superoxide (O_2^-). Superoxide is produced by an electron leak from the respiratory chain which results in electrons being accepted directly by molecular oxygen (Turrens, 2003). Superoxide dismutase in the cell is able buffer superoxide by converting it to hydrogen peroxide (H_2O_2), which is more stable but still highly toxic. Hydrogen peroxide can be broken down to water and oxygen by catalase.

Although ROS are highly damaging, they play important functional roles in cell signalling (Droge, 2002). ROS signalling has been demonstrated to be important for cell adaptations to hypoxia (Chandel *et al.*, 1998), regulation of autophagy (Scherz-Shouval *et al.*, 2007), immunity (West *et al.*, 2011) and apoptosis (Pierce *et al.*,

1991). Interestingly, it has also been linked to upregulation of mitochondrial biogenesis and mitophagy promoting mitochondrial turnover in the heart (Bartz *et al.*, 2015).

1.6 Mitochondrial turnover

Mitochondrial turnover occurs at a tissue specific rate. For instance, mitochondrial half-life in the mouse heart has been found to be around 17 days compared to around four days for the mouse liver (Kim *et al.*, 2012). Mitochondrial turnover can be considered to be the result of a fine balance between mitochondrial biogenesis and mitophagy. The turnover of mitochondria occurs independently of the cell cycle and thus still occurs in post-mitotic tissues.

1.4.1 Mitochondrial biogenesis

Mitochondrial biogenesis is the process by which cells increase their mitochondrial mass and mtDNA copy number. This is particularly important in skeletal muscle where periods of contractile activity, in the form of exercise, induce mitochondrial biogenesis and lead to an increase in mitochondrial mass and oxidative capacity (Holt *et al.*, 1989). Central to mitochondrial biogenesis is peroxisome proliferator-activated receptor gamma coactivator 1-alpha (PGC-1α), a transcriptional co-activator which upregulates expression of nuclear respiratory factor-1 (NRF-1), estrogen related receptor alpha (ERRα) and peroxisome proliferator-activated receptor alpha (PPARα) (**Figure 1.10**). Muscle specific knockout of PGC-1α in mice has been found to cause a reduction in mitochondrial mass and a fibre type shift from slow type I to fast IIx/IIb (Handschin *et al.*, 2007). PGC-1α is activated by AMPK mediated phosphorylation and SIRT1 mediated deacetylation in response to energy deprivation signalled by increasing AMP/ATP ratio and NAD+/NADH ratios, respectively (Canto et al., 2009).

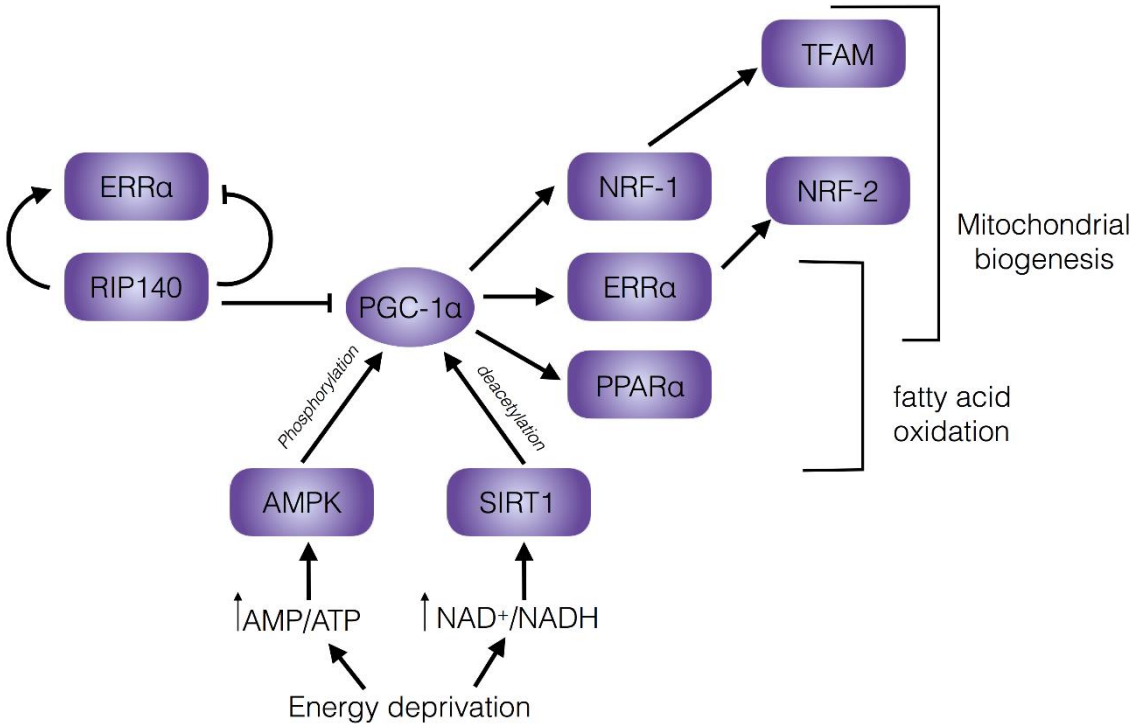

Figure 1.10 *Signalling pathway for mitochondrial biogenesis. Peroxisome proliferator-activated receptor gamma coactivator 1-alpha (PGC-1α) governs mitochondrial biogenesis. PGC-1α is regulated in response to AMP/ATP and NAD⁺/NADH levels which are indicators of energetic status. PGC-1α functions through its transcriptional regulation of nuclear respiratory factor 1 (NRF1), estrogen related receptor alpha (ERRα) and peroxisome proliferator-activated receptor alpha (PPARα). NRF1 transcriptionally activates TFAM, which regulates mtDNA transcription and replication. Adapted from Scarpulla (2011).*

ERRα activates transcription of NRF-2, which along with NRF-1 and ERRα drives transcription of mitochondrial mtDNA (Schreiber et al., 2004). ERRα also stimulates RIPI40 expression (Nichol et al., 2006), suggesting a possible negative feedback mechanism inhibiting PGC-1α activity and thus tightly regulating mitochondrial biogenesis. NRF-1 is responsible for the activation of transcription factor A, mitochondrial (TFAM) which is a transcriptional activator for the mtDNA (Virbasius and Scarpulla, 1994).

1.4.2 Mitophagy

Mitophagy is the selective degradation of damaged mitochondria (Kanki and Klionsky, 2008) and is proceeded by fission of the damaged mitochondrion (Twig *et al.*, 2008) (**Figure 1.11**). The dysfunctional mitochondrion has a loss of membrane potential, which activates Oma1 cleaving Opa1 and preventing re-fusion into the mitochondrial network (Duvezin-Caubet *et al.*, 2006).

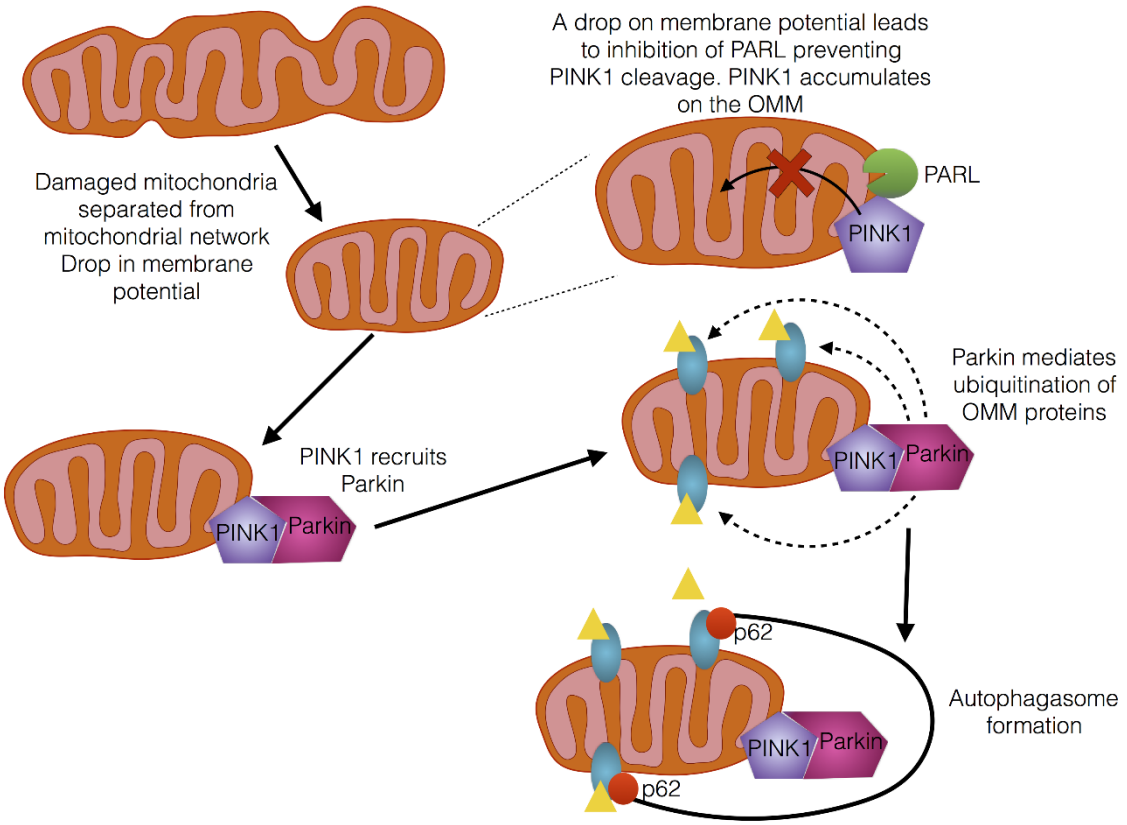

Figure 1.11 *Signalling pathway for mitophagy and autophagasome formation. Damaged mitochondria are separated from the mitochondrial network due to low membrane potential. The low membrane potential prevents presenilins-associated rhomboid-like protein (PARL) cleavage of PTEN-induced putative kinase 1 (PINK1), which accumulates on the outer mitochondrial membrane and recruits parkin. Parkin mediates the ubiquitination of the outer membrane proteins which leads to recruitment of p62 and autophagasome formation.*

Mitophagy involves two key proteins; PINK1 and Parkin which when mutated cause familial Parkinson's disease (Kitada *et al.*, 1998; Valente *et al.*, 2004). Under normal cellular conditions PINK1 is imported into the IMS by the TOM transporter and is

cleaved by PARL (Meissner *et al.*, 2011). However, when a mitochondrion becomes dysfunctional and the membrane potential is reduced PINK1 import and cleavage by PARL is blocked and instead it locates to the OMM and recruits Parkin (Narendra *et al.*, 2008). Parkin mediates the ubiquitination of OMM proteins and p62 is recruited to the OMM (Narendra *et al.*, 2010). Interaction of p62 with the ubiquitinated proteins and also with LC3 recruits lysosomes containing hydrolytic enzymes and forms an autophagasome for mitochondrial degradation.

1.7 Mitochondrial stress response

Mitochondria are involved in apoptotic cell death and as such their response to cellular stress is essential in deciding whether a cell survives and recovers or undergoes apoptosis. Mitochondria respond to cellular stresses in a number of ways including changes in morphology, release of damage associated mitochondrial proteins (DAMPs) and possibly activation of the mitochondrial unfolded protein response (UPR^{mt}). Each of these responses will be specific to dealing with the stress to which the cell has been exposed and each is described in more detail below.

1.5.1 Morphology and dynamics

It has been demonstrated that under low levels of cellular stress, mitochondria fuse to become a connected network (Tondera *et al.*, 2009; Shutt and McBride, 2013; Picard *et al.*, 2014; Leduc-Gaudet *et al.*, 2015), likely allowing functional complementation and increasing the ability of mitochondria to cope with the stress. However, at higher levels of mitochondrial stress the mitochondrial network fragments and mitochondria swell. Mitochondrial swelling appears to occur due to an influx of water caused by higher ion concentrations in the matrix over the cytosol as a result of mitochondrial permeability transition pore (PTP) opening (Di Lisa *et al.*, 2001) due to calcium overload (Halestrap *et al.*, 1986) and depolarisation of the mitochondria (Minamikawa *et al.*, 1999).

An alternative to mitochondrial swelling, is the formation of donut or toroid shaped mitochondria (Long *et al.*, 2015). Toroid mitochondria have an increase in mitochondrial volume but also have an advantage over swollen mitochondria since

return to normal mitochondria is easier upon removal of mitochondrial stress (Liu and Hajnoczky, 2011).

1.5.2 Mitochondrial derived vesicles

Mitochondrial derived vesicles have been found to be an early response to oxidative stress occurring prior to mitochondrial depolarisation (Soubannier *et al.*, 2012a; Soubannier *et al.*, 2012b) and are thus form an essential housekeeping and quality control mechanism. Targeting of HeLa cells with a subtoxic dose of ROS, produced MDVs detectable by electron microscopy and confocal microscopy, prior to mitochondrial fragmentation which are targeted to lysosomes (Soubannier *et al.*, 2012a). There are two species of MDVs which differ based on their subcellular destination and protein composition, with peroxisome targeted MDVs containing MAPL and lysosomal targeted MDVs containing TOM20 (Neuspiel *et al.*, 2008; Soubannier *et al.*, 2012a). Electron microscopy has demonstrated MDVs to be of a regular spherical shape around 80 to 120 nm in size (Neuspiel *et al.*, 2008).

Mechanistic studies suggest GTP hydrolysis is not essential for MDV formation suggesting the process to be independent of DRP1 (Soubannier *et al.*, 2012b). More recently, treatment of HeLa cells transfected with GFP-parkin with antimycin A lead to parkin recruitment to the OMM (McLelland *et al.*, 2014). Furthermore, parkin mutants did not generate MDVs and MDV formation was found to require PINK1 similar to mitophagy (McLelland *et al.*, 2014). The involvement of PINK1 and parkin, in both quality control processes, has led to the suggestion that when mitochondrial damage exceeds a threshold level, the membrane potential dissipates and PINK1 detects this change and orchestrates the switch from MDV formation to mitophagy (McLelland *et al.*, 2014).

1.5.3 The mitochondrial unfolded protein response

The mitochondrial unfolded protein response is a mechanism for dealing with proteotoxic stress specifically in the mitochondria. Although originally identified in cultured rat hepatoma cells (Martinus *et al.*, 1996), the molecular mechanisms involved in the UPR^{mt} have mainly been investigated in *Caenorhabditis elegans* (*C.*

elegans) (Pellegrino *et al.*, 2013), as such the mammalian UPR^{mt} has not yet been fully elucidated.

The mitochondrion, as a double membrane organelle, presents a proteostasis risk for the cell since they require import of numerous proteins to specific locations within the mitochondrion. Thus, the mitochondria are equipped with numerous chaperone proteins that aid in the correct folding and localisation of the imported mitochondrial proteins (Bukau *et al.*, 2006). In addition to this, a number of proteases (e.g. Lon protease, ClpXP, YME1L and paraplegin) are also found within the mitochondria and degrade those proteins that are misfolded (Tatsuta and Langer, 2009).

To date, the established signalling pathway (**Figure 1.12**), for the induction of the UPR^{mt} in *C. elegans*, is initiated by ClpP which degrades misfolded proteins to peptides, which are pumped across the IMM and detected by ATFS-1 (Pellegrino *et al.*, 2013). ATFS-1 is a transcription factor and upon activation localises to the nucleus activating UPR^{mt} genes including chaperone proteins mtHsp70 and Hsp60. In comparison, the mammalian UPR^{mt} (**Figure 1.13**) is not completely characterised but appears to have two signalling pathways one for the matrix and one for the IMS. The matrix UPR^{mt} functions by activating the JNK2 signalling pathway which activates the transcription factor CHOP, which upregulates UPR^{mt} genes including Hsp60, mtDnaJ, ClpP and CHOP (Zhao *et al.*, 2002). The IMS UPR^{mt} functions via the AKT signalling pathway which activates ERα increasing expression of Htra2, NRF1 and activating proteasome activity (Papa and Germain, 2011). No mammalian homologue of ATFS-1 has been identified.

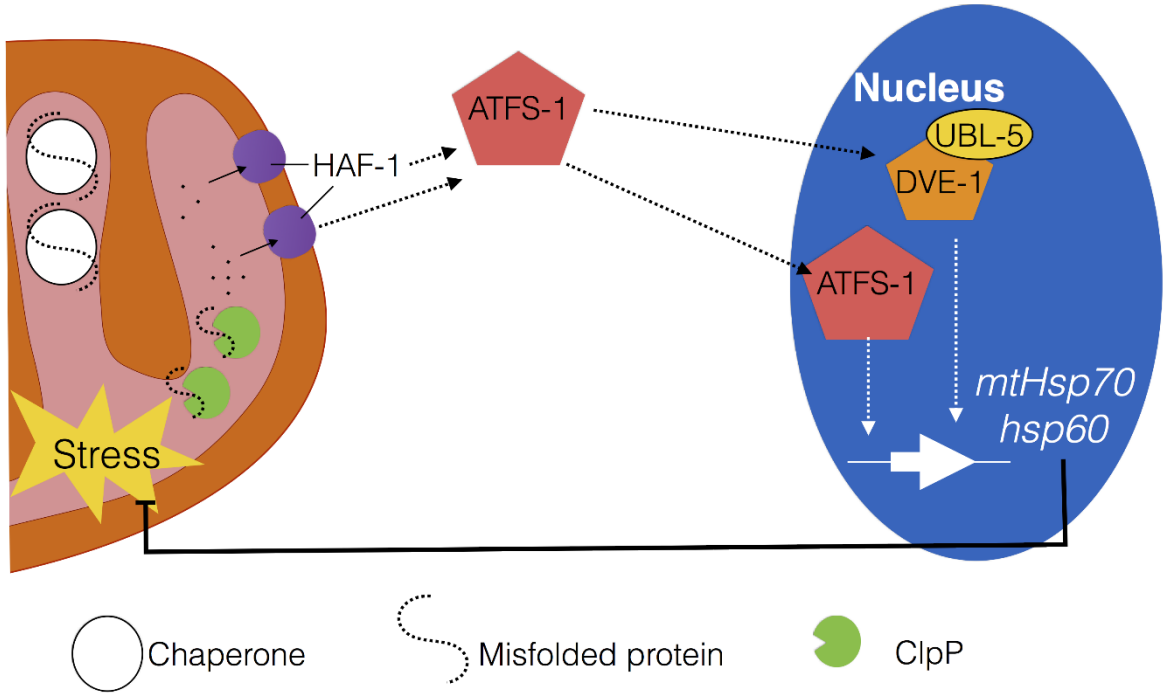

Figure 1.12 *The mitochondrial unfolded protein response (UPR^{mt}) signalling pathway in C. elegans. Unfolded proteins are degraded by ClpP protease and undergo HAF-1 mediated export from the mitochondria. HAF-1 mediated peptide release leads to the nuclear accumulation of ATFS-1, UBL-5 and DVE-1 in the nucleus. This leads to the transcriptional activation of Hsp60 and mtHsp70 to restore correct protein folding. Figure adapted from. Figure adapted from Pellegrino et al. (2013).*

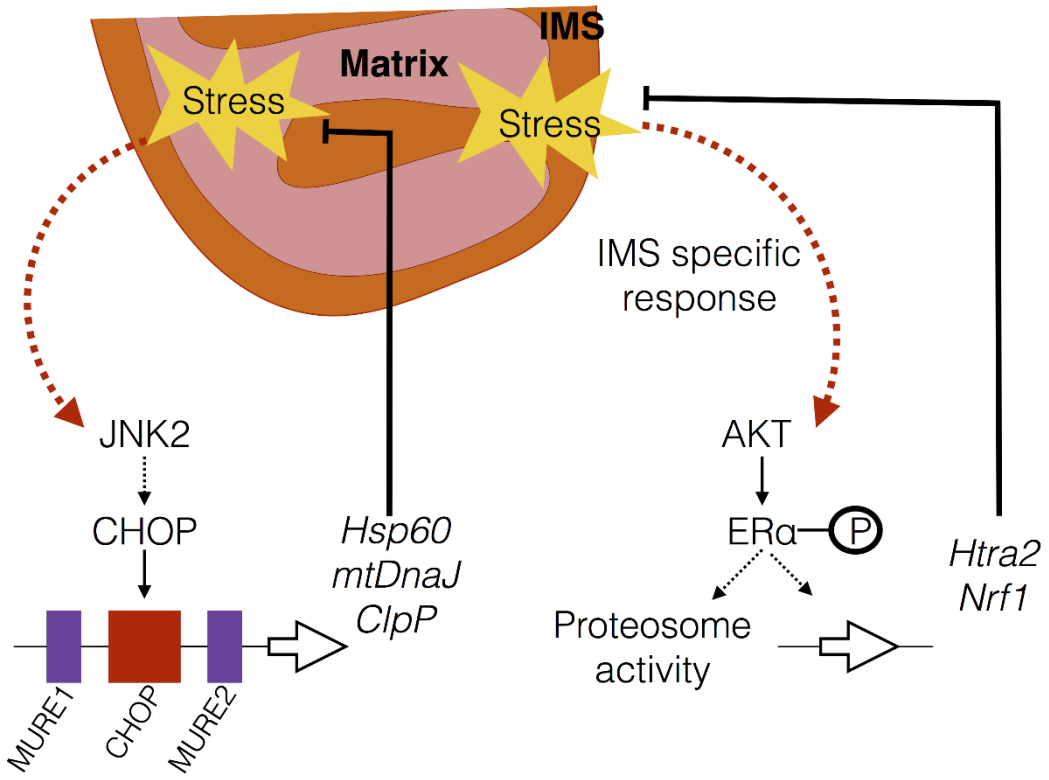

Figure 1.13 *The mitochondrial unfolded protein response (UPRmt) signalling pathway in mammals. The pathway has not been fully elucidated, however it is thought that there are two branches a matrix stress specific and an intermyofibrillar space (IMF) specific. Accumulation of unfolded proteins in the matrix signals the upregulation of CHOP via JNK and c-Jun. CHOP transcriptionally activates the expression of ClpP protease, Hsp60 chaperone protein and mtDnaJ. Accumulation of unfolded protein in the IMS leads to AKT dependent phosphorylation of ERα. Which transcriptionally activates Htra2 protease and Nrf1 transcription factor expression. Figure adapted from Pellegrino et al. (2013).*

1.8 Mitochondrial genetics

1.5.4 Mitochondrial genome

The mitochondrial genome is a double stranded, negatively-coiled, 16569bp circular genome encoding 22 tRNAs, two rRNAs and 13 subunits of the oxidative phosphorylation complexes (***Figure 1.14***). The mtDNA was originally sequenced by Anderson *et al.* (1981) and later revised by Andrews *et al.* (1999). Compared to the organisation of the nuclear genome, the amount of non-coding DNA is extremely low, with tRNAs typically punctuating the coding regions of the respiratory chain subunits and rRNA (Ojala *et al.*, 1981). The majority of these genes (both rRNAs, 14 tRNAs and 12 proteins) are transcribed from the heavy strand, named as such due to it being guanine rich, the remaining genes are transcribed from the light strand. In addition, to the mentioned genes the mtDNA also has a non-coding region (NCR), which has two hypervariable regions (HSV1 and HSV2) and three conserved sequence blocks (CSB1-3) (Walberg and Clayton, 1981). It is here in the NCR, where the displacement loop (D-Loop) is found. The D-loop is a displaced region of heavy strand DNA with 7S DNA bound to the light strand (***Figure 1.14***).

The mitochondrial genome exists in numerous copies per cell, with the number of copies varying on a cell-type specific basis e.g. approximately 100000 in the mature oocyte (Shoubridge and Wai, 2007), 7000 in cardiomyocytes and 3600 skeletal muscle fibres (Miller *et al.*, 2003).The mtDNA has been demonstrated to be packaged in a nucleoprotein complex called a nucleoid which is found to interact with the IMM (Wang and Bogenhagen, 2006). Super resolution microscopy has been used to elucidate that some of the protein machinery necessary for replication and transcription of the mtDNA including mitochondrial transcription factor A (TFAM) single stranded binding protein and the twinkle helicase (Garrido *et al.*, 2003; Brown *et al.*, 2011).

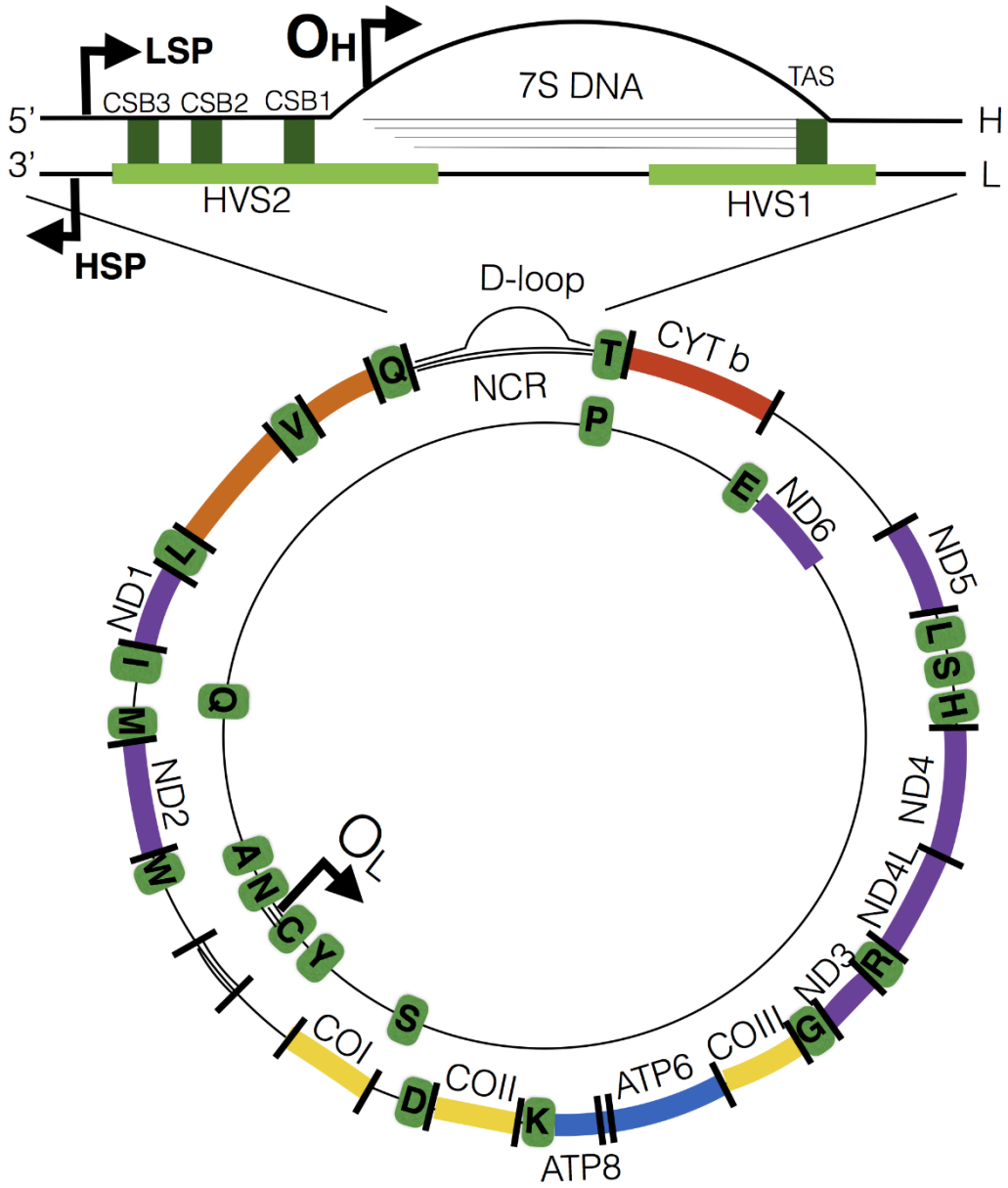

Figure 1.14 *Mitochondrial genome organisation. The protein encoded genes are colour coded for: complex I, purple; complex III, red; complex IV, yellow and complex IV, blue. Ribosomal RNA genes are in orange and the tRNAs in green. The origins of replication; O_H (heavy strand) and O_L (light strand) are also shown. The non-coding region (NCR) also contains the displacement loop (D-loop), which is shown in greater detail. The NCR includes three conserved sequence blocks (CSB) and two hypervariable sequences (HVS), as well as the heavy strand promotor (HSP), light strand promotor (LSP) and origin of heavy strand replication (O_H). Binding of 7S DNA sometimes displaces a region of the heavy strand leading to a region of the D-loop being triple stranded. Adapted from Nicholls and Minczuk (2014).*

1.5.5 Mitochondrial DNA Replication

Replication of the mtDNA requires a small repertoire of proteins. These proteins include; Polymerase gamma (POLG) which replicates the mtDNA, Twinkle (TWNK) the mtDNA helicase which is involved in the unwinding of the mtDNA, mitochondrial DNA ligase III mitochondrial single strand binding protein (mtSSB) which stabilises the single stranded mtDNA, POLRMT which synthesises the RNA primer, RNaseH1 which removes the RNA primer and topoisomerase which unwinds the DNA as the replication fork progresses (**Figure 1.15**) (Wanrooij and Falkenberg, 2010; Young and Copeland, 2016).

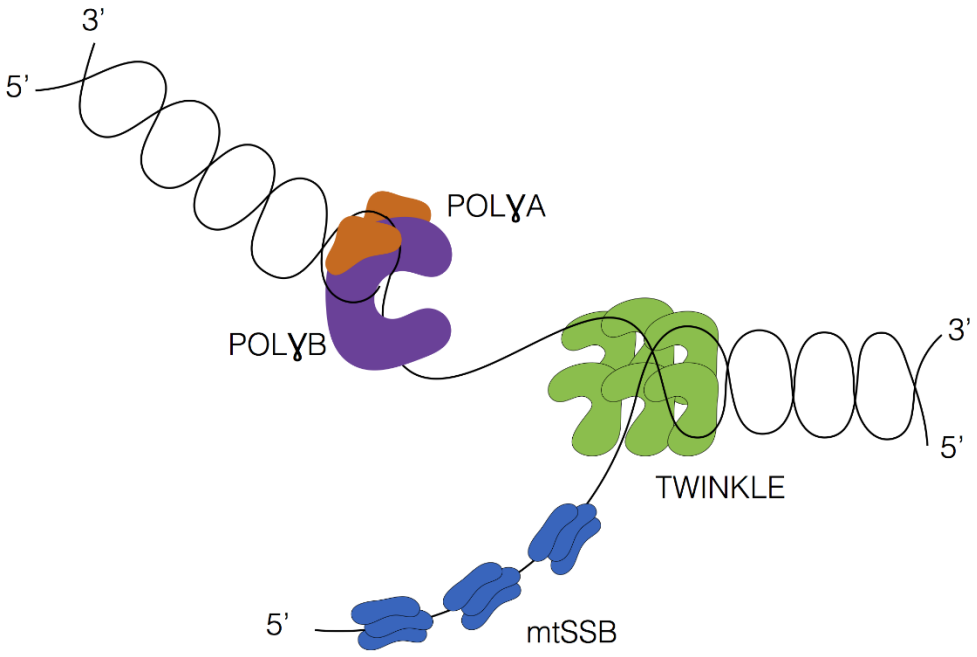

Figure 1.15 *Mitochondrial DNA replication fork. The mtDNA is replicated by polymerase gamma (POLG). POLG is assisted by a number of proteins including the twinkle helicase which unwinds the DNA at the replication fork and single strand binding protein (mtSSB) which binds the single stranded mtDNA protecting it.*

Replication is initiated at the H-strand origin of replication (O_H) located within in the D-Loop and requires RNA primers produced during transcription originating at the LSP (Chang and Clayton, 1984). As such, initiation of replication is dependent on the premature termination of transcription from the LSP thus transcription and replication the mtDNA is linked (Bonawitz *et al.*, 2006).

Replication of the mitochondrial DNA occurs via relaxed replication, that is it occurs independently from the cell cycle (Bogenhagen and Clayton, 1977) and is proposed to occur by one of two models; asynchronous or synchronous.

Strand asynchronous replication (***Figure 1.16***) was first proposed by (Clayton, 1982) and suggests that replication initiates at O_H, then after two thirds of the heavy strand is replicated the O_L is exposed and light strand replication is initiated. Heavy strand replication then continues in a clockwise direction and light strand replication in a counter-clockwise direction. The replication of the light strand lags behind that of the heavy strand thus the strands can also be termed lagging and leading strands. Once replication is complete, the mtDNA is circularised and becomes supercoiled. Finally, the D-loop is replicated and it is hypothesised that this serves as a template for its replication (Clayton, 1982).

The synchronous model of replication (***Figure 1.16***) was originally proposed by (Robberson *et al.*, 1972) and further developed and supported by data from (Holt *et al.*, 2000). This theory suggests that replication of the heavy strand is initiated at O_H and light strand replication occurs simultaneously through priming of replication by short oligonucleotide Okazaki fragments (Holt *et al.*, 2000). However, the presence of the okazaki fragments has yet to be demonstrated (Wanrooij and Falkenberg, 2010). ChIP-seq used to map the binding of mtSSB to the D-loop and the retention of primers at the origins of replication in RNaseH1 deficient cell lines is suggestive that mtDNA replication is more likely to occur via a strand-displacement mechanism (Miralles Fusté *et al.*, 2014; Young and Copeland, 2016).

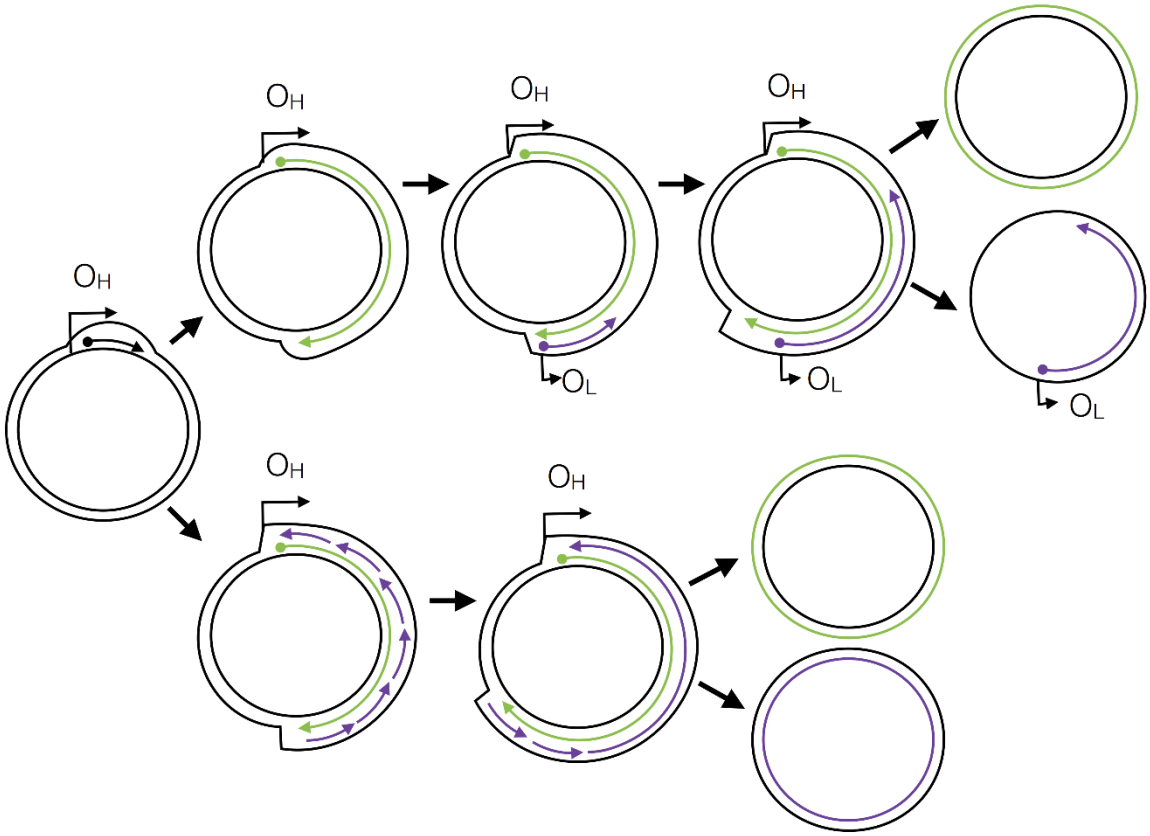

Figure 1.16 *Models of mtDNA replication. Strand asynchronous replication (top), starts at the heavy strand origin of replication O_H and replicates the heavy strand until the origin of light strand of replication is reached and light strand replication is imitated from O_L. Strand synchronous replication (bottom), also starts at O_H however priming and replication of the light strand starts prior to the O_L being reached by generation of a series of short okazaki fragments.*

1.5.6 Transcription

Transcription of the light strand is imitated at the light strand promotor (LSP) and transcription of the heavy strand at the heavy strand promotor (HSP) from two sites (H1 and H2) (Montoya *et al.*, 1983). Initiation at H1 generates a short transcript for the two rRNAs. Whereas initiation at H2 generates a transcript for the majority of the mtDNA (Chang and Clayton, 1984; Zollo *et al.*, 2012). Due to the lack of non-coding DNA the mtDNA is transcribed as polycistronic mRNAs, which is subsequently cleaved into different transcripts aided by folding of the transcripts at the tRNA coding regions, creating a site for RNA processing enzymes (Ojala *et al.*, 1981).

Mitochondrial transcription is performed by mitochondrial RNA polymerase (POLMRT) which also requires a number of transcription factors; TFAM, transcription

factors B2 (TFB2M) (Falkenberg *et al.*, 2002; Litonin *et al.*, 2010). Initially, POLRMT and TFAM bind to the promotor forming a transcription-incompetent pre-initiation complex in which the elements of POLRMT that bind and melt the promoter are not in a position to interact with the DNA (Morozov *et al.*, 2014). Following this, TFB2M binds causing the promoter to melt and the pre-initiation complex to convert into a transcription competent initiation complex (Morozov *et al.*, 2015).

Transcription initiated at HSP1 is terminated downstream of the 16sRNA gene, which is regulated by mitochondrial termination factor (mTERF). In addition, mTERF has been found by Martin *et al.* (2005) to have a role in transcription initiation from HSP1 and HSP2 by allowing recycling of the initiation machinery, and to play a role in termination of transcripts initiated at the LSP. However, termination of heavy strand transcripts at the distal site within the D-loop is not understood (Guja and Garcia-Diaz, 2012).

1.5.7 Translation

Mitochondrial translation differs from the cytosolic translation first since the ribosome is much smaller, with a sedimentation coefficient of 55S and secondly since it only requires 22 tRNAs. The smaller requirement of tRNAs is explained by the “Wobble hypothesis” which proposes that the first base of the tRNA can form non Watson-Crick pairing and thus recognise multiple codons (Crick, 1966; Barrell *et al.*, 1980).

Prior to translation, all mitochondrially encoded mRNA transcripts with the exception of MTND6 are processed, mainly at the tRNA sites (Ojala *et al.*, 1981), and matured by the addition of a poly-A tail by the mitochondrial poly (A) polymerase (mtPAP) (Tomecki *et al.*, 2004; Slomovic *et al.*, 2005).

Translation can be broken down into initiation, elongation termination and recycling (***Figure 1.17***). The first step in initiation is the recruitment of mt-mRNA to the mitochondrial small subunit (mt-SSU) and binding to initiation factor mtIF3 thus preventing premature association with large subunit (mt-LSU). Following this, mtIF2 facilitates the binding of $tRNA^{fmet}$ and GTP at the ribosome P-site (Ma and Spremulli, 1996), $tRNA^{fmet}$ is only used during initiation, during elongation non-formylated $tRNA^{met}$ is used (Takeuchi *et al.*, 1998). Following the binding of $tRNA^{fmet}$, the mt-LSU

can bind to complete the ribosome, triggering hydrolysis of the GTP and the release of initiation factors IF2/3 (Mai *et al.*, 2016).

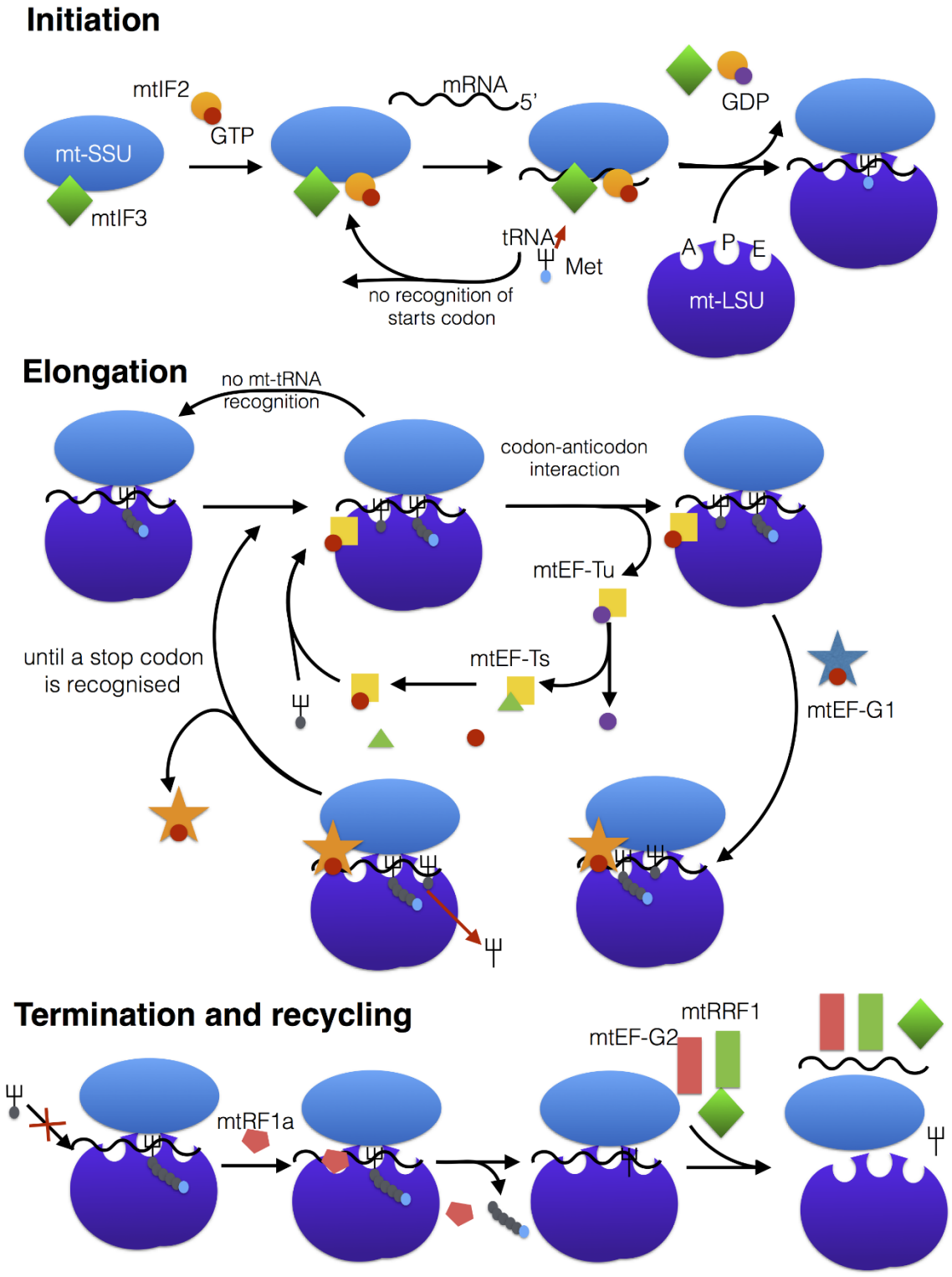

Figure 1.17 *Mitochondrial translation. Mitochondrial translation can be broken down into initiation, elongation and termination and recycling. Details of each step are described in section 1.5.7, along with abbreviations. Figure was adapted from Mai et al. (2016).*

The next step is elongation which requires the elongation factor mtEFTu, GTP and a charged mt-tRNA forming a ternary complex which can enter the ribosomal A-site. The presence of the correct codon:anticodon pairing results in GTP hydrolysis, the release and recycling of mtEF-Tu (Jeppesen *et al.*, 2005) and the subsequent formation of a peptide bond at the peptidyl transferase centre in the mt-LSU. The P-site of the mitoribosome now contains a deacetylated mt-tRNA and the di-peptidyl-tRNA is present at the A-site. Interaction of elongation factor mtEF-G1 causes a conformational change that results in movement of the tRNA in the A-site to the E-site and the di-peptidyl-tRNA to the A-site (Katunin *et al.*, 2002). This process cycles and the newly synthesised polypeptide moves through the ribosome to the matrix where it is folded (Smits *et al.*, 2010).

When the mitoribosome receives a stop codon at the A-site termination occurs and mitochondrial translation release factor mtRF1a (Soleimanpour-Lichaei *et al.*, 2007), enters the ribosome hydrolysing the ester bond holding the peptide in the P-site causing its release (Martin Schmeing *et al.*, 2005). Following peptide release, two ribosome recycling factors mtRRF-1 and mtEF-G2 promote the disassociation of the mito-ribosome and release of the mRNA and tRNA (Rorbach et al., 2008; Tsuboi et al., 2009). The human mitoribosome has been found to invoke a -1 frameshift at rare arginine codons AGA or AGG triplets, which are termed “hungry codons” (Temperley *et al.*, 2010).

1.5.8 Mitochondrial DNA repair

Mitochondria were originally thought to have no mechanism of DNA repair, based on evidence that no mechanism for pyrimidine dimer repair existed in mammalian mitochondria (Clayton *et al.*, 1974). However, since then a number of repair mechanisms have been identified.

Base excision repair (BER) has been found to occur in mitochondria in a similar manner to BER in the nucleus and repair alkylation and oxidative DNA lesions. Most importantly in the mitochondria, BER can be used to repair damage caused by ROS which includes thymine glycol (TG) and 8-oxoguanine (8-oxoG) lesions. BER can proceed via two pathways. Both require recognition and cleavage of the damaged site by a glycosylase specific for the damage leaving an abasic site. The abasic site

is cleaved at the 5' end by an AP endonuclease generating a nick with a 5'deoxyribose phosphate (5'dRP) flap. For single nucleotide BER the POLG can then fill the gap and cleave the 5'dRP flap before ligation (Longley *et al.*, 1998). However, some oxidative damage cannot be repaired in this way since it inhibits replication and thus interferes with POLG performing short-patch BER. Alternatively, long patch BER requires the endonucleases FEN1 and DNA2 (Liu *et al.*, 2008; Zheng *et al.*, 2008) to displace the 5' flap structure prior to ligation by ligase III.

Single strand breaks (SSB) can form in mtDNA due to ROS damage, collision of topoisomerase with RNA polymerase during transcription or failed BER. The repair of SSB follows a similar process to BER and it is generally suspected that the same machinery is used (Kazak *et al.*, 2012). In comparison, double strand breaks have also been found to occur in the mtDNA and there has been a lot of debate as to whether the mitochondria are able to repair these by recombination as in the nucleus. However, the presence of repeat sequences at many break points reported in MitoBreak (Damas *et al.*, 2014a), provides potential evidence for homologous recombination. Furthermore, use of a mitochondrially targeted *Sca*I restriction endonuclease in mice demonstrated evidence for recombination (Bacman *et al.*, 2009) and a mouse model expressing an inducible restriction endonuclease provided evidence for both homologous and non-homologous recombination by as yet undefined mechanisms (Fukui and Moraes, 2009).

1.5.9 Mitochondrial DNA copy number regulation

Studies in cultured mouse and human cells have estimated the mitochondrial copy number to be highly variable and by approximately 1000 to 5000 copies per cell (Shmookler Reis and Goldstein, 1983; Alexander *et al.*, 2000). Furthermore, evidence suggests that mitochondrial DNA copy number is tightly regulated and varies in a tissue specific manner, dependent on the energy demands of the tissue. In most instances, the mtDNA copy number appears to be linked to mitochondrial mass. However, the mechanism by which mitochondrial DNA copy number is regulated has not been conclusively shown and a number of hypotheses have been proposed.

Tang *et al.* (2000), proposed that mtDNA copy number is regulated indirectly by controlling the size of dNTP pools, meaning that the number of mtDNA copies will increase if the genome size is smaller. Another hypothesis suggests that TFAM regulates copy number by switching the mode of replication, evidence for this includes the depletion of mtDNA in TFAM knockout mice (Pohjoismaki *et al.*, 2006). However, changes in mtDNA packaging due to lack of TFAM could also be argued to cause this. Clay Montier *et al.* (2009), proposed that copy number is regulated dependent on the current ATP requirement for the cell. However, so far no evidence supporting this has been found. This model however, does fit with tissue specific variances in energy demands and mtDNA copy number.

More recently, investigation of CpG island methylation around the *POLG* gene has indicated a role for epigenetic regulation of the mtDNA maintenance machinery in the regulation of mtDNA copy number (Kelly *et al.*, 2012). This work finds a correlation between mtDNA copy number and *POLG* CpG island methylation. However, previous data indicates that the mtDNA replication factors increase significantly when mtDNA copy number decreases (Schultz *et al.*, 1998). Thus, epigenetic regulation of POLG would appear to be a long term mechanism for tissue specific copy number regulation rather than a homeostatic mechanism for short term fluctuations in mtDNA copy number.

1.5.10 Heteroplasmy and the threshold effect

The mitochondrial DNA exists as multiple copies within an individual cell, as such it is possible that some but not all of these will contain polymorphic or even pathogenic variants. If all copies of the mtDNA are identical the cell is said to be homoplasmic, however if more than one mtDNA species is present within a single cell the cell is said to be heteroplasmy (**Figure 1.18**). Heteroplasmy is measured as a percentage of the total copy number and percentage heteroplasmy can vary between 0 - 100%. Since the mtDNA is regularly replicated a mutated molecule may replicate increasing in heteroplasmy until it out numbers the wild type copy number, this process is known as clonal expansion.

The effect that a mutation will have on the function of the mitochondria is based on a principle known as the threshold effect (**Figure 1.18**) (Rossignol *et al.*, 2003). Low

level heteroplasmy typically does not cause a biochemical deficiency and thus does not affect the cell phenotype due to the compensatory effect of the wild type mtDNA. However, if the mutational heteroplasmy exceeds the phenotypic threshold, the mutation can no longer be compensated for and thus a biochemical deficiency and cell phenotype becomes apparent (Rossignol *et al.*, 2003).

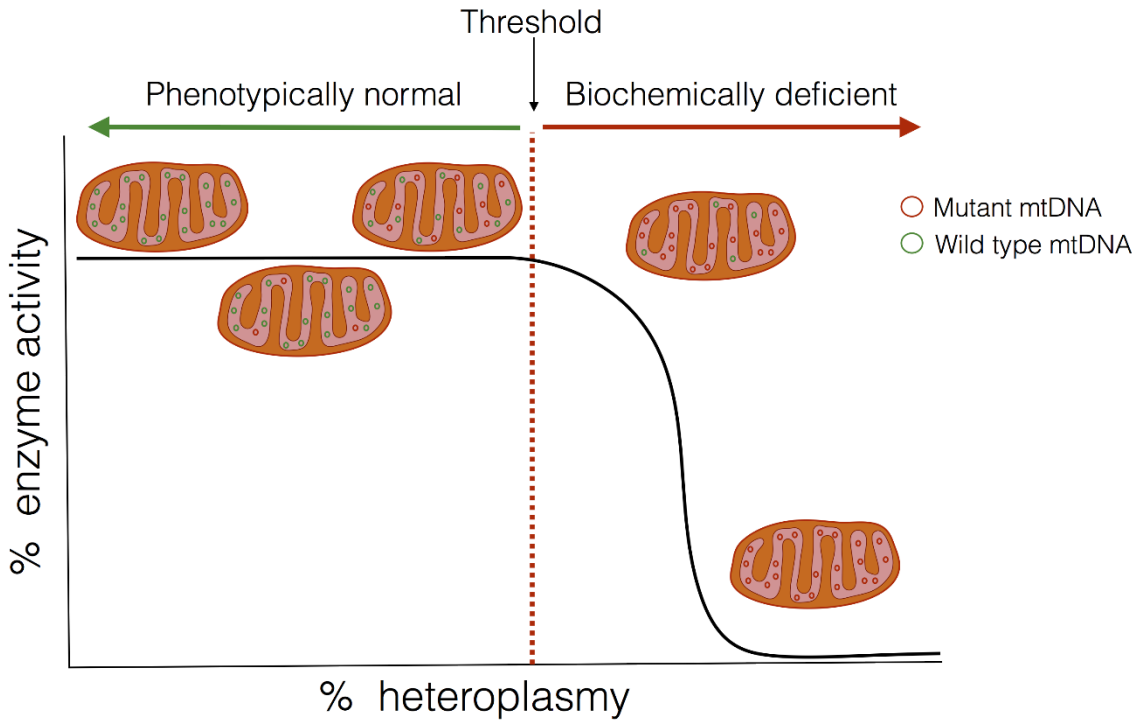

Figure 1.18 *Heteroplasmy and the threshold effect. Mitochondrial DNA exists in numerous copies per mitochondrion as such an mtDNA mutation can exist at anywhere between 0 and 100% heteroplasmy. At low levels of heteroplasmy a mitochondrion may be biochemically normal, due to the presence of wild type mtDNA. However, above a functional threshold (red dotted line) the oxidative phosphorylation chain enzyme activity is diminished.*

The threshold effect has been found to vary both between mutation types and also between tissues. Mitochondrial DNA deletions in skeletal muscle are reported to have a threshold anywhere between 50% (Porteous *et al.*, 1998) and 90% (Sciacco *et al.*, 1994). This large variability in threshold is likely to be due to the substantial variation in deletion size and location, therefore affecting the impact the deletion is likely to have on the respiratory chain. Point mutations show an even greater variation in threshold with the m.8344A>G $tRNA^{Lys}$ mutation reported to have a threshold of 97% (Moslemi *et al.*, 1997) and the m.3243A>G $tRNA^{Leu(UUR)}$ mutation a

threshold of 50% (Jeppesen *et al.*, 2006) in skeletal muscle. The higher threshold for some mt-tRNA mutations may be due to the fact that these are generally accepted to be functionally recessive (Al-Dosary et al., 2009; Tuppen et al., 2010), however findings of dominant mt-tRNA mutations challenges this assumption (Sacconi et al., 2008). Interestingly, in skeletal muscle the mutational heteroplasmy can vary along the length of a myofibre as well as between fibres.

One of the complications when investigating mitochondrial disease pathogenesis is the lack of correlation between mutational heteroplasmy and disease severity (Morgan-Hughes *et al.*, 1995). Furthermore, identical mutations can have different phenotypic presentations, for example patients with the m.3243A>G $tRNA^{Lys}$ mutation may present with mitochondrial encephalomyopathy, lactic acidosis, and stroke-like episodes (MELAS), maternally inherited diabetes and deafness (MIDD) and CPEO as well as additional symptoms (Nesbitt and McFarland, 2011).

1.5.11 Maternal inheritance and the mitochondrial bottle neck

Unlike the nuclear genome, the mtDNA is inherited solely down the maternal lineage (Giles *et al.*, 1980), with the mitochondria from the sperm being selectively degraded. Pathogenic variants in the mtDNA are therefore passed from the mother to her offspring, however there can a large amount of variability in the number of mutated mtDNA molecules passed on and siblings can end up with very different heteroplasmy levels (Taylor and Turnbull, 2005). This variation is attributed to a phenomena termed the mitochondrial bottle neck (Howell *et al.*, 2000). The mitochondrial bottleneck is the result of rapid replication after fertilisation (Cree *et al.*, 2008), with variation in heteroplasmy of an mtDNA variant in an embryo resulting from random genetic drift during replication (Brown *et al.*, 2001).

1.9 Mitochondrial DNA mutations

The mtDNA is prone to high levels of mutagenesis, with a mutation rate approximately 10 times higher than that of the nuclear genome (Brown *et al.*, 1979).

The high mutation rate may be due to a number of factors and more than likely to a combination of these factors. The first to consider is the close proximity of the mtDNA to the respiratory chain complex and thus the exposure to damaging ROS produced by the respiratory chain. A second issue is that the mtDNA polymerase POLG has a much lower fidelity than that of the nuclear polymerase (Kunkel and Loeb, 1981). Further to this, the mitochondrial DNA is replicated much more frequently than the nuclear genome (Bogenhagen and Clayton, 1977) and therefore the probability of an error during replication that is incorrectly repaired is much more likely. In addition to the high mutation rate, since the mitochondrial genome consists almost entirely of coding regions mutations are much more likely to occur in a coding region and as such be pathogenic.

1.6.1 Point mutations

Point mutations are a single base substitution and occurrence in the mitochondrial genome is highest in the tRNA genes, with 50% of all point mutations occurring here (Schaefer *et al.*, 2008). Pathogenic point mutations are known to cause a number of mitochondrial diseases and can be maternally inherited or sporadic. The most common and thus most well characterised point mutations are the m.3243A>G $tRNA^{Leu(UUR)}$ and the m.8344A>G $tRNA^{Lys}$ (Gorman *et al.*, 2015).

The m.3243A>G mutation is the most common cause of MELAS causing approximately 80% of all cases (Urata *et al.*, 2004). However, the phenotypic spectrum of m.3243A>G mutations is very variable. MIDD is most common but patients also present with Leigh's syndrome and CPEO, and isolated symptoms are also reported (Nesbitt and McFarland, 2011; Mancuso et al., 2014). The m.8344A>G point mutations has been reported to cause 80-90% of all myoclonic epilepsy with ragged red fibres (MERRF) cases (Wu *et al.*, 2010). However, m.8344A>G, similar to m.3243A>G, also causes a wider variety of symptoms including migraine, psychiatric disorders, hearing impairment, respiratory and gastrointestinal symptoms (Mancuso *et al.*, 2013; Altmann *et al.*, 2016).

1.6.2 Single large-scale mtDNA deletions

Large-scale single mtDNA deletions arise sporadically during embryogenesis due to errors in either mtDNA replication or repair (Shoffner *et al.*, 1989; Krishnan *et al.*, 2008; Dong *et al.*, 2014) and the same deletion species is found at variable heteroplasmy in each cell. Clinically these account for 12% of adult mitochondrial disease cases (Gorman *et al.*, 2015). Patients can present with chronic progressive external ophthalmoplegia (CPEO), Kearns-Sayre Syndrome and Pearson Syndrome as well as non-syndromic disease symptoms, with the most common symptoms being ptosis, ophthalmoparesis and muscle weakness (Mancuso *et al.*, 2015). The most common single, large-scale mtDNA deletion is the 4977bp common deletion between nucleotides 8482 and 13460 of the mtDNA, and typically has a 13bp repeat either side of the breakpoint as reported in MitoBreak (Damas *et al.*, 2014a). The common deletion has been reported to account for approximately one third of all single mtDNA deletions (Pitceathly *et al.*, 2012a), but also commonly accumulates with age (Williams *et al.*, 2013).

Early investigations into single, large-scale mtDNA deletions found there to be a lack of relationship between mtDNA genetics, biochemical function and clinical phenotype (Zeviani *et al.*, 1988; Holt *et al.*, 1989; Moraes *et al.*, 1989). However, more recently reports have found relationships between mtDNA deletion heteroplasmy, age of onset and disease phenotype i.e. larger deletions lead to a more severe phenotype (Yamashita *et al.*, 2008; Lopez-Gallardo *et al.*, 2009). However, mtDNA deletion size is found to both have a correlation with disease phenotype (Yamashita *et al.*, 2008) and not to have a relationship (Lopez-Gallardo *et al.*, 2009). Furthermore, both of the above studies found that deletion location can impact disease severity. (Yamashita *et al.*, 2008), find that a deletion affecting *MT-COI, MT-COII, MT-COIII*, *MT-ATP6* or *MT-ATP8* have significantly earlier onset, while (Lopez-Gallardo *et al.*, 2009) found that deletions affecting *MT-CYB* are associated with a severe KSS phenotype.

1.6.3 Disorders of mtDNA maintenance

Mitochondrial DNA deletions have been associated secondary mitochondrial diseases due to nuclear mutations and also with a number of neuromuscular (Oldfors *et al.*, 2006; Rygiel *et al.*, 2016) and neurodegenerative disorders (Bender *et al.*,

2006), as well as accumulating with age in healthy post-mitotic tissues (Muller-Hocker *et al.*, 1993; Brierley *et al.*, 1998; Kraytsberg *et al.*, 2006; Meissner *et al.*, 2006).

They most commonly occur in the major arc of the mtDNA, however the frequency at which deletions are detected in the minor arc has increased in recent years. They are typically found to accumulate throughout life, with the highest levels identified in the post-mitotic tissues e.g. neurons and myofibres (Bender *et al.*, 2006). Mitochondrial DNA deletions which typically arise secondary to a nuclear mutations in a gene involved in the maintenance or replication of the mtDNA, but are also associated with neuromuscular and neurodegenerative diseases and healthy ageing. Genes associated with mtDNA deletions encode proteins involved in replication (e.g. *POLG* (Van Goethem *et al.*, 2001), *TWNK* (Spelbrink *et al.*, 2001)), synthesis of dNTPs (e.g. *RRM2B* (Tyynismaa *et al.*, 2009)) and mitochondrial fission and fusion (e.g. *OPA1* and *MFN2* (Amati-Bonneau *et al.*, 2008; Rouzier *et al.*, 2012)). Additional genes that cause multiple mtDNA deletions are continually being identified. Phenotypically mtDNA deletions range from isolated progressive external opthalmoplegia (PEO) to fatal multi-systemic PEO-plus syndromes. The other symptoms encompassed in the PEO-plus category can be very diverse, and disease onset ranges from infantile to late adulthood. Accumulation of deletions with age is termed clonal expansion, theories of how this occurs and the process by which deletions are expected to form is explored in more detail in **Chapter 4**.

1.10 Mitochondrial disease

1.7.1 Disease prevalence

Mitochondrial diseases are multi-systemic disorders that typically present with symptoms affecting some of the most energetically demanding organs such as the central and peripheral nervous systems and the skeletal muscle. The prevalence of mitochondrial disease is difficult to accurately assess, due to the clinical and genetic heterogeneity. The most recent assessment in the North East of England finds the prevalence of mitochondrial disease caused by mutations of both the mitochondrial and nuclear genomes to be approximately 1 in 4300 (Gorman *et al.*, 2015). In comparison, the minimum prevalence of mtDNA mutations is reported to be 1 in

5000. The study finds the m.3243A>G mutation to be the most prevalent pathogenic point mutation with a prevalence of 7.8 per 1000000. Although, single deletions are still the most common cause of mitochondrial disease (minimum prevalence = 1.5×10^{-5}).

1.11 Skeletal muscle structure

Skeletal muscle is a highly structured tissue, consisting of a hierarchical structure. Each myofibre consists of repeats of contractile units called sarcomeres and is composed of a bundle of myofibrils surrounded by the sarcolemma and endomysium (Leiber, 2010). Myofibres are then bundled together into 'fascicles', which are held together by perimysium, which also provides entry for the capillary bed and motor neurons to innervate the myofibres. Finally, the entire muscle is surrounded by the epimysium.

1.8.1 The sarcomere

Within each myofibre, 85-90% of the volume is occupied by myofibrils arranged in parallel. The myofibrils are composed of series of repeating units called sarcomeres of approximately 2.5-3 µm in length (**Figure 1.19**). Each sarcomere is made up of thick and thin filaments. The thick filament is anchored to the z-band by elastic protein titin, which regulates the spatial relationship between the thick and thin filaments (Dubowitz, 2007).

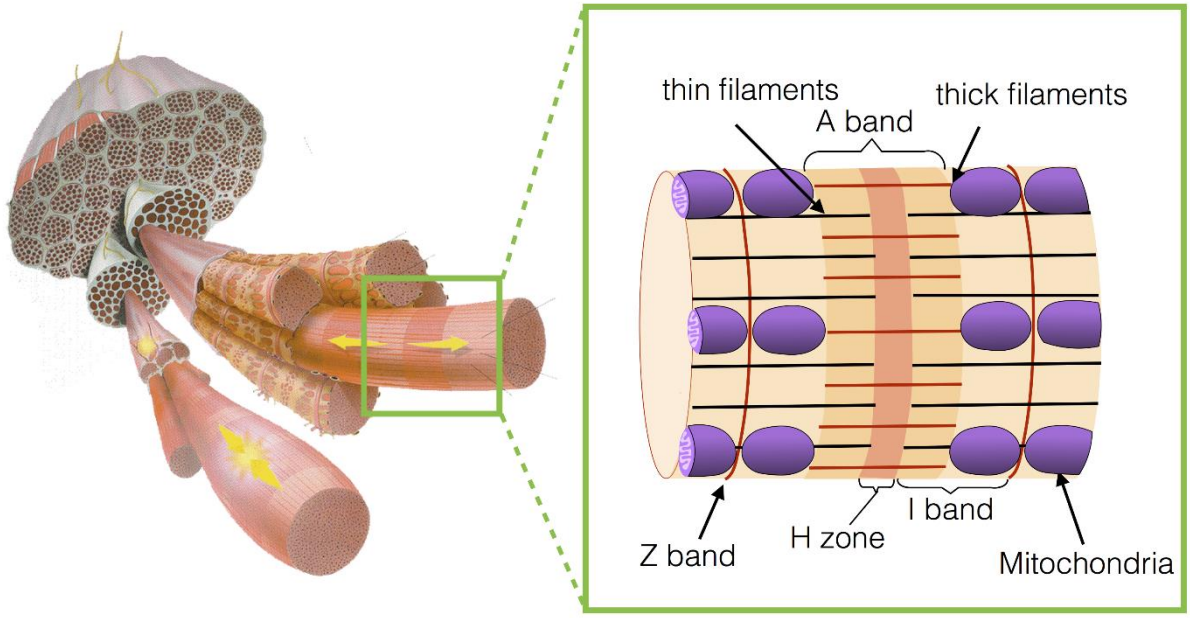

Figure 1.19 *Skeletal muscle structure and structure of the sarcomere. Mitochondria are located at the z-band.*

A number of the proteins localised to the z-band are associated with Myofibrillar myopathy, which has been reported to have changes to mitochondrial function and positioning. These proteins are discussed below in the context of sarcomeric structure.

Desmin is found at the z-band and inserts into the costamere, linking adjacent myofibrils (Dubowitz, 2007), and synchronizes contraction of the myofibres. Desmin also interacts with the heat shock protein αB-crystallin, which is involved in desmin polymerization and plectin which, together with desmin, anchors the mitochondria in pairs at the z-band (Reipert *et al.*, 1999). Both αB-crystallin and plectin gene mutations are associated with aggregation of desmin protein as seen in MFM (Vicart *et al.*, 1998; Schroder *et al.*, 2002). Due to the role of desmin in mitochondrial localisation, mutations in desmin have been suggested and reported to have an impact on mitochondrial positioning and function. Myotilin also localises to the z-band as part of a complex of actin cross-linking proteins, which control myofibril assembly and help to stabilise the Z-band (Salmikangas *et al.*, 2003). Mutations in the *MYOT* gene lead to protein aggregates which typically label for the presence of both myotilin

and desmin. Z-band alternatively spiced protein (Zasp) or LIM domain binding 3 (LDB3), is also located at the Z-band. Proteins with LIM domains and PDZ motifs typically interact with other proteins often guiding them to multiprotein complexes (Faulkner *et al.*, 1999). Zasp is thought to play a role in protein kinase C-mediated signalling. Mutations in the *ZASP* gene lead to protein aggregates positive for the presence of myotilin, desmin or both.

1.8.2 Myogenesis

Skeletal myofibres formed during embryogenesis at regions along the embryo from small clusters or somites of mesoderm progenitor cells called myoblasts (Yusuf and Brand-Saberi, 2012). Initially, clusters of myoblasts fuse to form multinucleated myotubes. Subsequently, a secondary myotube will arise beneath the basal lamina of the primary myotube, using the primary myotube as a scaffold for support. Continued fusion of myotubes both radially and longitudinally forms the myofibre beneath the basal lamina and myonuclei from the fused cells will migrate to below the sarcolemma membrane (Leiber, 2010). A small portion of myoblasts will remain unfused and become satellite cells, which are the stem cells of the muscle and remain for purpose of myofibre regeneration. As the myofibres mature, primary and secondary myotubes will separate, each contained in a basal lamina with myonuclei and satellite cells (Leiber, 2010). Myoblast differentiation and formation of myofibres is transcriptionally regulated by four myogenic regulatory factors (MRFs). Early differentiation is regulated by *MYOD* and *MYF5* and terminal differentiation is regulated by myogenin (Braun and Gautel, 2011). The final MRF, MRF4 appears to have a dual role in both terminal differentiation but also in determination of embryonic cells to mesoderm progenitor cells (Kassar-Duchossoy *et al.*, 2004).

Once a muscle fibre is fully differentiated, although post-mitotic, it can undergo regeneration through a process of satellite cell fusion. Satellite cells are the progenitor cells of the skeletal muscle, which retain proliferative capacity. Upon muscle fibre damage and necrosis a satellite cell can fuse with a muscle fibre and allow regeneration of the muscle fibre (Charge and Rudnicki, 2004). Evidence demonstrates that satellite cells harbour similar levels of mtDNA mutations as muscle fibres in mitochondrial myopathy patients (Spendiff *et al.*, 2013).

A fully differentiated muscle fibre will have multiple peripherally located nuclei. Each nucleus will have a nuclear domain, which is defined as a region of the muscle fibre cytoplasm for which the nucleus is transcriptionally responsible. The size of the nuclear domain has been found to vary between muscle fibre types (Mishra *et al.*, 2015).

1.8.3 Muscle fibre types

Skeletal muscles typically consist of a mixture of muscle fibre types, with the proportions of each fibre type influencing the oxidative capacity of that muscle. The growth and differentiation of these muscle fibres is transcriptionally regulated based on electrical impulses from the nervous system. Discharge rates of 10 and 100Hz influence the pattern of gene expression and thus the development of fast and slow fibre types (Schiaffino *et al.*, 1999).

Grouping of muscle fibre types is based on morphological, contractile and metabolic characteristics (Burke *et al.*, 1971; Peter *et al.*, 1972; Reiser *et al.*, 1985). Type I muscle fibres are the most oxidative, have a higher mitochondrial content but low ATP consumption due to their slow contraction rate. Type IIA fibres are defined as fast oxidative glycolytic have a high mitochondrial content, high ATP consumption and a fast contraction rate. Finally, type IIB fibres are fast glycolytic with a low mitochondrial content, high ATP consumption and fast contraction rate (Leiber, 2010).

1.8.4 Skeletal muscle mitochondria

In skeletal muscle mitochondria can be found in two subcellular populations, the intermyofibrillar (IMF) mitochondria and the subsarcolemmal (SS) mitochondria. The two populations are topologically, morphologically and functionally different. The intermyofibrillar mitochondria are located in pairs either side of the z-band and are held here by a z-band protein complex known to contain desmin and plectin proteins among others (Milner *et al.*, 2000). As such, the intermyofibrillar mitochondria form a rigid lattice structure and are relatively immotile compared to mitochondria described in other cells such as the neurons (Huang *et al.*, 2013). The subsarcolemmal

mitochondria can usually be found in a small, perinuclear cluster just below the sarcolemma of the myofibre.

Proteomic and biochemical comparison in rats finds the IMF mitochondria to have higher level of respiratory chain activity, consistent with their location between the myofibrils to power muscle contraction (Ferreira *et al.*, 2010). This is consistent with structural findings in rat cardiomyocytes, that SS mitochondrial cristae are more lamella and IMF more tubular, which may provide an increased proton gradient due to smaller intracristae space (Riva *et al.*, 2005). In comparison to IMF mitochondria, SS mitochondria are thought to produce ATP mainly for the function of the membrane and nuclei (Hood, 2001). The different proteomic composition also leads to IMF mitochondria being more susceptible to apoptotic stimuli, likely due to their large numbers and importance in sensing and triggering apoptosis (Adhihetty *et al.*, 2005).

1.8.5 COX-deficiency in skeletal muscle

When examined in transverse orientation, skeletal muscle can be seen to present with a mosaic pattern of COX-deficiency (Johnson *et al.*, 1983; Sciacco *et al.*, 1994). In addition, when the muscle is examined longitudinally the COX-deficiency is found to be segmental. Bua *et al.* (2006), reported that at 49 years ~6% of myofibres will have a COX-deficient segment somewhere along the length. Furthermore, this was found to increase to ~22% at 67 years and reach ~31% by 92 years.

A number of studies in humans and animal models have found the segmental deficiency to be concomitant with high levels of mtDNA deletion (Lee *et al.*, 1998; Wanagat *et al.*, 2001; Bua *et al.*, 2006; Herbst *et al.*, 2007; Campbell *et al.*, 2014). Many studies have also found increased skeletal muscle fibre atrophy and breakage in regions with segmental deficiency, suggesting a possible link (Wanagat *et al.*, 2001; Herbst *et al.*, 2007).

Although it is now widely accepted that mtDNA deletions are causative of respiratory chain deficiency in skeletal muscle. The mechanisms by which these arise and lead to a biochemical defect are not fully understood. Another puzzling question is what

restricts the longitudinal spread along the myofibre and whether this is a defensive mechanism to protect the myofibre from the spread of damage?

1.12 Overall aims and objectives

The overall aim of this project was to improve the understanding of mitochondrial pathogenesis in skeletal muscle and more specifically to explore the mechanisms by which mtDNA mutations accumulate in skeletal muscle fibres and segmental respiratory chain deficiency arises. This included three aims:

1) To investigate two neuromuscular conditions, myofibrillar myopathy and dysferlinopathy, for which mitochondrial dysfunction was suspected. The hypothesis was that protein aggregates in myofibrillar myopathy would cause aberrations in mitochondrial positioning and dynamics and that Dysferlin myopathy due, to its inflammatory nature, may present with similar mitochondrial pathology to inclusion body myositis.
2) To assessed a range of muscle biopsies for the presence of small regions of respiratory chain deficiency that may represent the earliest stages of respiratory chain deficiency in a muscle fibre and thus the initial events of mtDNA deletion clonal expansion. The purpose of this was to find and investigate the early stages of mutation accumulation and thus the spread of respiratory chain deficiency through the muscle fibre.
3) To develop mechanisms to assess the variability of the mitochondrial network in human skeletal muscle of the control population, to contrast this with cases of mitochondrial myopathy and potentially gain an insight into the importance of mitochondrial morphology in skeletal muscle pathogenesis.

Chapter 2. Materials and methods

2.1 Reagents, equipment, solutions and consumables:

2.1.1 Equipment and software

Equipment or Software	Supplier
ABI Step one software v2.0	Applied Biosystems
ABI Step-one Plus Real Time PCR system	Applied Biosystems
ABI verti-96 well Thermo Cycler	Applied Biosystems
Autoclave	Prior Clave
Axiovison	Zeiss
Biorad Chemidoc	Biorad
Corning LSE Vortex mixer	Sigma Alderich
Cryostat	Bright OTF 5000
Digital Micrograph v2.31.734.0	Gatan
Eppendorf Thermomixer	Eppendorf
GeneAmp PCR system 9700	Applied Biosystems
Image lab v4	Biorad
Imaris v7.7.2	Bitplane
IMOD v4.7.15	Boulder Lab
Laminar flow hood	Jencons-PLS
Leica Laser microdissection system	Leica
Microflow biological safety hood	J. Marston engineers
Minitab 17	Minitab
Nanodrop ND-1000 Spectrophotometer	Labtech International
NANOpurell Water Purification System	Barnstead
ND-1000 software	Labtech International
Palm Robo v4.6	Zeiss
Pipette boy	Integra
Prism v7.0	Graph pad
Serial block face scanning electron microscope	Gatan 3-view

R v3.3.0	R
R Studio v0.99.896	R Studio
Stereo Investigator	MBF Bioscience
Stereology microscope	Olympus BX51
Sterilizing oven	Laboratory Thermal Equipment Ltd.
Transmission Electron Microscope	Philips CM100
UV hood (PCR clean room)	Astec
UV hood (UV room)	Bioair
Vortex genie 2	Scientific Industries
Zeiss axioimager	Zeiss
ZEN blue	Zeiss

Table 2.1 *Equipment and software*

2.2 Reagents

2.2.1 Molecular genetics

Reagent	**Supplier**
Agilent Bioanalyzer DNA High Sensitivity kit	Agilent
DEPC treated water	Ambion
DNA Away	Thermo Fisher
dNTPS	TaKaRa
QIAmp DNA Blood Mini Kit	Qiagen
Ethylenediaminetetraacetic acid (EDTA)	GIBCO
Expand Long template PCR kit	Roche
LA Taq	TaKaRa
Nuclease free water	Ambion
Prime STAR GXL	TaKaRa
Primers	Eurofinns
Proteinase K solution	Fisher Scientific
Real Time PCR primers	Applied biosystems
Tamra labelled probes (ND1, ND4, Dloop)	Applied biosystems
Taqman mastermix	Applied biosystems
Tris-EDTA	Fluka analytic

Table 2.2 *Molecular genetics reagents*

2.2.2 Chemicals

Chemical	**Supplier**
Liquid Nitrogen	BOC
3,3' Diaminobenzidine Tetrahydrochloride	Sigma
Catalase	Sigma
Cytochrome C	Sigma
DAPI	Sigma
DPX	BDH
Eosin	CellPath
Ethanol Analar	Merck
Haemotoxylin	TCS Biosciences Ltd.
Histoclear	National diagnostics
Methanol	Merck
Nitro Blue Tetrazolium	Sigma
Normal Goat Serum	Sigma
Paraformaldehyde (4%) (PFA)	Santa Cruz Biotech
Paraformaldehyde (16%) (EM grade)	Agar Scientific
Phosphate Buffered Saline tablets	Sigma
Prolong Gold	Life Technolodies
Sodium Azide	Sigma
Sodium Cacodylate	Sigma
Sodium Dodecycl Sulphate (SDS)	BDH
Sodium succinate	Sigma
TAE buffer (10x)	Sigma
Trizma base	Sigma
Tween-20	Sigma

Table 2.3 *Chemicals and supplier*

2.3 Solutions

Solution	Recipe
5x TBST pH 7.4 (2L)	121 g Trizma Base 90 g NaCl 5 ml Tween Concentrated HCl
COX-EM fixative	2% Glutaraldehyde 0.1 M Sorrenson's buffer (pH7.4)
DNA Loading buffer	0.25% (w/v) Bromophenol blue 0.25% (w/v) Xylene Cyanol 30% (v/v) Glycerol
DNA electrophoresis gel buffer (1L)	100 ml 10x TAE (0.4 M Tris-acetate, 10 mM EDTA, pH 8.3) 900ml Nanopure water
DNA electrophoresis running buffer (1L)	100 ml 10x TAE (0.4 M Tris-acetate, 10 mM EDTA, pH 8.3) 900ml Nanopure water
smPCR lysis buffer (1ml)	5 ml SDS 945 ml 10mM EDTA 50 µl proteinase K
Single cell lysis buffer (500µl)	250 µl 1% Tween 20 50 µl 0.5M TrisHCl pH 98.5 195 µl dH_2O 5 µl proteinase K
Phosphate Buffered Saline (PBS)	1 tablet in 100ml dH_2O
TEM fixative (pH 7)	2% Glutaraldehyde 0.1 M Sodium Cacodylate

Table 2.4 *Buffers and recipes*

2.4 Consumables

Consumables	Supplier
0.2ml Thin-walled PCR tubes	Star Lab
0.5ml Thin-walled PCR tubes	Star Lab
1.5ml Eppendorf	Eppendorf
2ml Eppendorf	Eppendorf
5ml Eppendorf	Eppendorf
96 Well Fast Optical Reaction Plates	Applied Biosystems
96 Well semi-skirted Plate, with raiser rim	Starlab
Electronic pipettes	Ranin
Gilson pipette (P2, P10, P20, P100, P200, P1000)	Anachem
Glass slides	Thermo Scientific
Gloves	Starlab
PEN slides	Leica
QIAmp DNA micro kit	Qiagen
Scalples	Swann Morton
Serological pipettes	Cellstar
SlideRita 5 Mailer	CellPath
Starseal advanced Polyelfin film	Thermo scientific
Weigh boats	VWR
Filter pipette tips	Tip One
QIAamp DNA midi kit	Qiagen

Table 2.5 *Consumables*

2.5 Patient cohort

2.5.1 Controls

Controls fell in to either “healthy disease controls” (those referred to the NGS mitochondrial disease diagnostic service but were found not to have mitochondrial disease) or “healthy control” groups (muscle donated during routine ligament surgery.) All controls are selected to be age matched for the required study and relevant information for these can be found in Table 2.6. In addition a single disease control with pathogenic, recessively inherited *RRM2B* variants, previously reported by Pitceathly *et al.* (2012b), was also used in **Chapter 3** and **Chapter 4**. Patient details are provided in **Table 2.6**. Control blood (previously tested for mtDNA deletions) was also provided by NGS mitochondrial disease diagnostic service for DNA extraction.

Control	Classification	Age/years	Gender	Chapters
C1	Healthy disease	18	F	3
C2	Healthy disease	34	F	3
C3	Healthy disease	52	F	4,3
C4	Healthy disease	63	F	4
C5	Healthy	23	M	7
C6	Healthy	33	M	7
C7	Healthy	28	M	7
C8	Healthy	27	M	7
C9	Healthy	25	F	7
C10	Healthy	25	M	7
C11	Healthy	35	F	7
C12	Healthy	45	F	7

Table 2.6 *Control case information**.** Healthy disease controls were referred to the NGS mitochondrial disease diagnostic service but found not to have mitochondrial disease. Healthy controls agreed to donate muscle during routine anterior cruciate ligament surgery. M; male, F; female.*

2.5.2 Dysferlinopathy patients

Dysferlinopathy (n = 8) patients were identified through the Rare Diseases Advisory Group Service for Neuromuscular Diseases. Selection was based on immunohistochemistry using anti-Ham1/3 antibody against the C-terminus of Dysferlin as well as a genetic diagnosis. Patient details including clinical and pathological findings are summarised in **Table 2.7**, these patients are investigated in **Chapter 3**.

Patient	Gender	Age at onset (if known)	Age at biopsy	Mutation	CK	Phenotype
P1	F	10 (distal myopathy)	15.7	c.855+1delG; c.3031G>C, p.(Gly1011Arg)	3012	MM
P2	F	26	20.5	c.2434dup p.(His812Profs*53); c.1745G>T p.(Arg582Leu)	7586	LGMD2B
P3	F	26	21.9	Hom. c.2163-1G>T	13000	LGMD2B
P4	M	Birth	24.7	Hom. c.1480+18T>C; c.4999G>A, p.(Glu1667Lys)	400-700	LGMD2B
P5	M	9	28.9	exon 5-10 deletion; c.757C>T, p.(Arg253Trp)	5000	LGMD2B
P6	M	Late teens (distal myopathy)	30.4	Hom. c.3059dupC, p.(Glu1021Glyfs*10)	20000	MM
P7	F	N/K	47.1	c. 5509G>A, p.(Asp1837Asn); c.6124C>T, p.(Arg2042Cys)	5110	LGMD2B
P8	M	13	52.5	c.3512_3513delCT, p.(Ser1171Phefs*3); c.5908C>T, p.(Pro19070Ser)	6000	LGMD2B

Table 2.7 *Dysferlinopathy patient information. Patients are organised in age order and all mutation nomenclature uses the primary transcript (NM_003494.3). All biopsies were taken from the Quadriceps via needle biopsy. N/K; not known, M; male, F; female, Hom.; homozygous, LGMD2B; Limb girdle muscular dystrophy type 2B, MM; Myoshi myopathy. Adapted from Vincent et al. (2016c).*

2.5.3 Myofibrillar myopathy patients

Myofibrillar myopathy patients (n = 9) were identified through the Rare Diseases Advisory Group Service for Neuromuscular Diseases. Selection was based on the presence of protein aggregates in skeletal muscle cryosections labelled for myotilin and desmin immunohistochemistry as well as a genetic diagnosis. Patient details including clinical and pathological findings are summarised in **Table 2.8**, these patients are investigated in **Chapter 4**.

Patient	Gender	Mutated gene	Mutation	CK	Biopsy Site	Age at biopsy	Age at onset (if known)
P9	M	*DES*	Het. c.1069G>C, p.(Ala357Pro)	480	Quadriceps	31.2	29
P10	M	*DES*	Het. c.1069G>C, p.(Ala357Pro)	NK	NK	32.1	NK
P11	M	*DES*	Hom. c.46C>T, p.(Arg16Cys)	450	Quadriceps	33.8	20's
P12	F	*DES*	Het. c.735+20C>T (MAF=0.01); c.638C>T, p.(Ala213Val)	NK	Quadriceps	51.3	Early childhood
P13	F	*DES*	Het. c.638 C>T, p.(Ala213Val)	74	Quadriceps	53	40's
P14	F	*DES*	Het. c.1346A>C , p.(Lys449Thr)	287	NK	64.3	46
P15	M	*MYOT*	Het. c.179C>G, p.(Ser60Cys)	446	Quadriceps	60.5	55
P16	M	*MYOT*	c.179C>G, p.(Ser60Cys)	400-500	Tibialis Anterior	65.7	NK
P17	F	*LDB3* or *ZASP*	Het. c.494C>T, p.(Ala165Val); Het. c.728C>T, p.(Pro243Leu)	300	Quadriceps	69.6	60’s

Table 2.8 *Clinical and diagnostic information for Myofibrillar myopathy patients examine in Chapter 4 (n = 9). Patients are organised by gene then age order and all mutation nomenclature uses the primary transcripts for DES (NM_001927) and MYOT (NM_006790) and for LDB3 or ZASP transcript variant 2 (NM_001080114.1). DES; desmin, MYOT; myotilin, Hom.; homozygous, Het.; heterozygous, MA; minor allele frequency, CK; creatine kinase, NK; not known. Adapted from Vincent et al. (2016a)*.

2.5.4 Patients for clonal expansion experiments (Chapter 5)

A cohort of mitochondrial disease patients has been selected for investigation throughout this thesis. In **Chapter 5**, a range of patients including; multiple mtDNA deletions (n = 7), single, large-scale mtDNA deletions (n = 4), inclusion body myositis (IBM) (n = 5), are used to investigate mechanisms of clonal expansion. Relevant clinical information for these patients is presented in **Table 2.9**. Patient 28 is also investigated in **Chapter 6**. All patients mentioned above were identified through the NGS mitochondrial disease diagnostic service.

Patient	Gender	Age at onset	Age at biopsy	Gene	Mutations (c.DNA; amino acid)	% COX deficiency	% RRF	Clinical phenotype	Reported previously?
P18	F	N/A	31	*TWNK*	c.1121G>A, p.(Arg374Gln)	10%	1%	adPEO	nr
P19	M	14	37	*RRM2B*	c.431 C>T; p.(Thr141Ile) and c.817G>A; p.(Gly273Ser)	>40%	20%	arPEO, muscle weakness	Pitceathly et al. Brain (2012), Patient 19
P20	F	11	43	*RRM2B*	c.556A>G; p.(Arg186Gly) and c.653C>T; p.(Thr218Ile)	30%	5%	arPEO plus	Pitceathly et al. Brain (2012), Patient 20
P21	F	38	64	*RRM2B*	c.208G4A; p.(Asp70Asn)	8%	3%	adPEO, ptosis, ataxia	Pitceathly et al. Brain (2012), Patient 5
P22	F	N/A	66	*POLG*	c.1399G>A, p.(Ala467Thr); c.2799T>G p.(Ser933Arg)	24%	6%	arPEO, ataxia	nr
P23	F	N/A	69	*TWNK*	c.907c>T, p.(Arg303Trp)	30%	8%	adPEO, ptosis	nr
P24	M	N/A	80	*POLG*	c.752C>T, p.(Thr251Ile); c.1760C>T, p.(Pro587 Leu); c.1399G>A p.(Ala467Thr)	20%	4%	arPEO	nr
P25	M	N/A	27	mtDNA	single deletion	25%	5%	CPEO, ptosis	nr
P26	F	N/A	32	mtDNA	single deletion	40%	1%	CPEO	nr
P27	F	N/A	35	mtDNA	single deletion	25%	1%	CPEO, proximal	nr

P28	F	N/A	47	mtDNA	single deletion	20%	10%	muscle weakness CPEO	nr
P29	F	20	66	mtDNA	single deletion	20%	1%	CPEO, ptosis	nr
P30	M	44	48	N/A	N/A	79%	0%	IBM	Rygiel et al. Nucl Acid Res (2016) Patient 7
P31	F	44	47	N/A	N/A	10%	0%	IBM	Rygiel et al. Nucl Acid Res (2016) Patient 9
P32	F	61	64	N/A	N/A	23%	0%	IBM	Rygiel et al. Nucl Acid Res (2016) Patient 5
P33	F	69	79	N/A	N/A	24%	0%	IBM	Rygiel et al. Nucl Acid Res (2016) Patient 4
P34	M	78	81	N/A	N/A	5%	0%	IBM	Rygiel et al. Nucl Acid Res (2016) Patient 8

Table 2.9 *Case information for patients examined in Chapter 5 for clonal expansion experiments, including patients with; Multiple mtDNA deletions (n = 7), Single, large-scale mtDNA deletions (n = 4), Inclusion body myositis (IBM) (n = 5). adPEO, autosomal dominant progressive external ophthalmoplegia; arPEO, autosomal recessive progressive external ophthamoplegia; CPEO, chronic progressive external ophthalmoplegia; nr, not reported.*

2.5.5 Patients for electron microscopy studies (Chapter 6 and Chapter 7)

In **Chapter 6** a group of seven patients are examined; m.8344A>G (n = 3), m.3243A>G (n = 1), single, large-scale mtDNA deletions (n = 3). Of the patients examined in **Chapter 6** all but one single deletion patient (P28) is also examined in **Chapter 7**. The relevant clinical information for these patients is presented in **Table 2.10**. Patient 28 was also investigated in **Chapter 5**. All patients mentioned above were identified through the NGS mitochondrial disease diagnostic service.

Patient #	Sex	Age at biopsy	Genetic diagnosis	Heteroplasmy (if applicable)	% COX deficiency	% RRF	CK (IU/L)	Lactate (mmol/L)	Clinical phenotype	Diagnostic notes
P28	F	47	Large-scale single mtDNA deletion	N/A	20	10	226	2.4	CPEO, proximal myopathy	-
P35	F	62	Large-scale single mtDNA deletion	34	20	15	122-197	2.1-3.1	CPEO, proximal myopathy	-
P36	F	70	Large-scale single mtDNA deletion	22	18	9	318-1238	1.4-2	CPEO, proximal myopathy	Asymmetric myopathy
P37	F	22	m.8344A>G	97	97	10	145-291	7.4	Axial, proximal myopathy, lactic acidosis	-
P38	F	50	m.8344A>G	63	22	7	43	1.6	Mild myopathy	Mother of Patient 7.4
P39	F	20	m.8344A>G	40	COX intermediate	0	267	1.2	Asymptomatic	Sister of Patient 7.4
P40	F	69	m.3243A>G	21	3	2	180-375	1.3	Diabetes mellitus, deafness, gut dysmotility	-

Table 2.10 *Patient information for the biopsies examined in electron microscopy investigations in Chapter 6 (P28, 35-40) and Chapter 7 (P34-40). N/A: non-available; % COX: proportion of muscle fibres with cytochrome c oxidase deficiency; RRF: ragged red fibres; CK: creatine kinase; CPEO: chronic progressive external opthalmoplegia; HCM: hypertrophic cardiomyopathy; OA: optic atrophy; MERRF: myoclonic epilepsy with ragged red fibres. Deletions position and sizes for P28: N/A; P35: m.8482-13460, 4978bp; P36: m.8576-12968, 4392bp. Normal clinical range for CK: 25-200 IU/L; lactate: <2.2 mmol/L. All biopsies from the tibialis anterior muscle, none of these patients were previously reported.*

2.6 Ethical guidelines

All work presented here was previously approved by the Newcastle and North Tyneside Local Research Ethics Committees (reference 2002/205) and is now approved under Newcastle and North Tyneside Local Research Ethics Committees (reference 16NE/0267). Control biopsies from routine ACL surgery were approved by Newcastle and North Tyneside Local Research Ethics Committees (reference 12/NE/0395, project number 42). Prior informed consent was obtained from all participants and all experiments were carried out in accordance with the approved guidelines.

2.7 Newcastle Mitochondrial Disease Adult Scale (NMDAS)

Due to the multi-systemic nature of mitochondrial disease and the large degree of clinical severity observed in mitochondrial disease, standardisation of clinical assessment is invaluable. Clinicians at the Wellcome Trust Centre for Mitochondrial research developed the Newcastle Mitochondrial Disease Adult Scale (NMDAS) in order to provide a standardised assessment (Schaefer *et al.*, 2006). The NMDAS consists of a number of sections with the first portion being a questionnaire filled in by the patients and the second portion consisting of more clinical measurements. Thus for each clinical assessment a patient will receive a score for each symptom specific sub-section (e.g. myopathy or diabetes) and an overall NMDAS score. The NMDAS is a valuable tool to both standardise assessment within the centre and externally and has proven to be a good means of assessing patient disease progression. An example of the NMDAS questionnaire is included in **Appendix 1**.

2.8 Histochemistry

2.8.1 Haematoxylin and eosin

Tissue sections were removed from -80 °C storage and air dried on the bench for one hour. Slides were immersed in Haemotoxylin for 10 minutes and subsequently washed in tap water until the water turns clear. A drop of ammonia was added for

blueing and the slides were rinsed again. Slides were immersed in eosin for one minute and washed with tap water until the water turns clear. Sections were rapidly dehydrated in an ascending ethanol gradient (70%, 90%, 100%, 100%) and cleared in two washes of histoclear before mounting in DPX medium.

2.8.2 COX histochemistry

Tissue sections were removed from -80 °C storage and air dried on the bench for one hour, during which time they were encircled with a hydrophobic pen. Sections were rinsed briefly in 1 M PBS whilst the COX incubation medium was prepared. COX reagents were defrosted at 55 °C and combined in the following quantities; 200 µl cytochrome C, 800 µl DAB and a pinch of catalase. Sufficient reaction medium was applied to each section (roughly 200 µl). Sections were incubated for 45 minutes at 37 °C, after which they were washed for three five minute intervals in 1 M PBS. Slides were dehydrated in an ascending ethanol gradient by placing for 10 minutes in each ethanol (70%, 90%, 100% and 100%) and cleared in two pots of histoclear for 10 minutes each before mounting in DPX.

2.8.3 SDH histochemistry

Tissue sections were removed from -80 °C storage and air dried on the bench for one hour, during which time they were encircled with a hydrophobic pen. Sections were rinsed briefly in 1 M PBS. Reagents for SDH reaction medium were defrosted at 55 °C and combined in the following quantities; 100 µl sodium succinate, 100 µl PMS, 10 µl sodium azide and 800 µl NBT. Sufficient reaction medium was applied to each section (roughly 200 µl). Sections were incubated for 40 minutes at 37 °C. Sections were incubated for 45 minutes at 37 °C, after which they were washed for three five minute intervals in 1 M PBS. Slides were dehydrated in an ethanol gradient by placing for 10 minutes in each ethanol (70%, 90%, 100% and 100%) and cleared in two pots of histoclear for 10 minutes each before mounting in DPX.

2.8.4 Sequential COX/SDH histochemistry

Tissue sections were removed from -80 °C storage and air dried on the bench for one hour, during which time they were encircled with a hydrophobic pen. Sections were rinsed briefly in 1 M PBS whilst the COX incubation medium was prepared. COX reagents were defrosted at 55 °C and combined in the following quantities; 200 µl cytochrome C, 800 µl DAB and a pinch of catalase. Sufficient reaction medium was applied to each section (roughly 200 µl). Sections were incubated for 45 minutes at 37 °C, after which they were washed for three five minute intervals in 1 M PBS. Reagents for SDH reaction medium were defrosted at 55 °C and combined in the following quantities; 100 µl sodium succinate, 100 µl PMS, 10 µl sodium azide and 800 µl NBT. Sufficient reaction medium was applied to each section (roughly 200 µl). Sections were incubated for 40 minutes at 37 °C, after which they were washed for three five minute intervals in 1 M PBS. Slides were dehydrated in an ethanol gradient, with 10 minutes in each ethanol (70%, 95%, 100% and 100%) and cleared in two pots of histoclear for 10 minutes each before mounting in DPX.

2.9 Immunofluorescence

2.9.1 Quadruple immunofluorescence

Tissue sections were removed from -80 °C storage and air dried for one hour during which the slides were labelled as either primary antibody or no primary control (NPC) and each section encircled using a hydrophobic pen. Sections were fixed in 4% cold PFA over a period of three minutes. Slides were rinsed quickly twice with TBST, followed by 10 minutes in 1X TBST. Sections were dehydrated and rehydrated in a methanol series; 70% (10 minutes), 95% (10 minutes), 100% (20 minutes), 95% (10 minutes), 70% (10 minutes), followed by three five minute washes in 1X TBST. Sections were then blocked for one hour at room temperature with 10% NGS in TBST. Approximately 200 µl primary antibody cocktail was applied to one section from each patient and a no primary control (NPC) cocktail applied to a corresponding NPC section. Both cocktails were made in 10% NGS and all primary antibody concentrations can be found in **Table 2.11**. Sections were placed at 4 °C overnight.

Sections were washed for three five minute washes in 1X TBST. Approximately 200µl secondary antibody cocktail was added to all sections and sections incubated at 4 °C for two hours. Secondary antibody concentrations can be found in **Table 2.12**.

Sections were washed for three five minute periods in 1X TBST. If a streptavidin conjugated secondary antibody was being used this was added next. Approximately 200 µl was applied to each section and sections incubated for 2 hours at 4 °C. Slides were washed for three periods of five minutes in 1X TBST, mount in Prolong Gold mounting medium for fluorescence (Life Tech) and encircled with nail varnish.

Antibody	**Supplier**	**Product number**	**Dilution**
Mouse anti-desmin (IgG1)	Dako	M076029-2	1:400
Rabbit anti-laminin (polyclonal)	Sigma	L9393	1:50
Mouse anti-MTCOI (IgG2a)	Abcam	ab14705	1:100
Mouse anti-myotilin (IgG2a)	Santa Cruz Biotechnologies	sc-393958	1:100
Mouse anti-NDUFB8 (IgG1)	Abcam	ab110242	1:100
Mouse anti-SDHA (IgG1)	Abcam	Ab14715	1:100
Mouse anti-VDAC1 IgG2b	Abcam	ab14734	1:100

Table 2.11 *Primary antibodies used in immunofluorescence and dilutions used.*

Antibody	**Supplier**	**Serial number**	**Dilution**
Anti-IgG1-biotinylated	Life Technologies	S32357	1:200
Anti-IgG2a-Alexa Fluor 488	Life Technologies	S21131	1:200
Anti-IgG2b-Alex Fluor 546	Life Technologies	A21143	1:200
Anti-Rabbit-Alexa Fluor 405	Life Technologies	A31556	1:200
Streptavidin-Alex Fluor 647	Life Technologies	S21374	1:100

Table 2.12 *Secondary antibodies used for immunofluorescence and dilutions used.*

2.9.2 Counterstaining of COX/SDH histochemistry or immunofluorescence with DAPI.

Counterstaining with DAPI was completed following incubation with SDH reaction medium and PBS washes for COX/SDH histochemistry and following TBST washes after the final secondary antibody incubation for immunofluorescence. Sections were washed thoroughly in either PBS (histochemistry) or TBST (immunofluorescence) before counterstaining with DAPI at a concentration of 2 µg/ml in PBS for 5 minutes. Sections were washed again and mounted in ProLong Gold.

2.9.3 Fluorescence microscopy

Fluorescent images were captured at either 10x, 20x or 40x magnification using a Zeiss axioimager M1 and either axiovision or ZEN blue software with a monochrome digital camera (AxioCam MRm) and filter cubes for dyes at 405 nm, 488 nm, 546 nm and 647 nm. A motorised stage and software tiling function allowed automated scanning of full muscle biopsy sections. Exposure times for each channel were chosen to avoid over exposure and minimise background detected on primary controls. Exposure times were used for all cases and controls within an experiment. Following imaging .zvi files were stitched to generate a .czi file for image analysis.

2.9.4 Imaris image analysis

Imaris version v7.7.2 was used to quantify mean fluorescent intensity per fibre for each channel. Individual fibres were isolated using the membrane marker laminin to create surface one. Surface one was masked and a second surface created over each fibre. Unwanted areas were removed either by thresholding of the analysis or manually removed at the end. The mean optical density for the 488, 546 and 647 channels was automatically measured.

2.9.5 R statistical analysis of quantitative immunofluorescence

Data generated by analysis of quadruple immunofluorescence in Imaris was statistically analyzed using an R-script written by Dr John Grady. The R script first corrected for background in each channel by subtracting the average optical density (OD) for each channel in the no primary control from the values generated from the section labelled with all primary antibodies. Background corrected values were log transformed to normalise data and the VDAC distribution was checked to confirm that it was normally distributed. Mean and standard deviation of the control population were obtained and z-scores determined for VDAC, complex I and IV based on the expected level of each calculated using the VDAC level as a mitochondrial mass marker. A z-score for each control and patient fibre is generated for each channel. This z-score allows each fibre to be classified as positive, intermediate positive, intermediate negative or negative for complex I and IV and very low, low, normal, high or very high for VDAC. The boundaries of categories were tested and validated by Rocha *et al.* (2015), and further details of statistical analysis are also described.

2.10 DNA extraction and cell lysis

2.10.1 Laser microdissection

Individual cells were captured by laser microdissection using a Zeiss Laser Capture Microdissection microscope with Palm Robo v4.6. Single muscle fibres were traced using the RoboLPC function and with cut settings; energy = 33 and focus =71 and LPC settings; energy = 15 and delta = 1. Two 0.2 ml eppendorfs were inserted into the tube collection holder and 15 µl of lysis buffer appropriate for the downstream application (**2.10.2** or **2.10.3**) added to each cap. Cell traces were selected and assigned to Tube 1 or Tube 2 and upon initiation the laser cut around the cell and fired it into the target cap. After cutting tubes containing cells were kept on ice and then were centrifuged briefly using the “short spin” function to bring lysis buffer and cell to the bottom prior to incubating for the appropriate lysis protocol (**2.10.2** or **2.10.3**).

2.10.2 Tris-Tween single cell lysis

Tris-Tween-Protinase K lysis buffer (0.5 M Tris-HCl, 0.5% Tween 20, 1% Proteinase K, pH 8.5) is made up in a UV hood. Cells were captured into 15µl lysis buffer, centrifuged briefly and incubated at 55°C for three hours, followed by 10 minutes at 95 °C.

2.10.3 SDS-EDTA single cell lysis

SDS-EDTA-Protinase K lysis buffer (0.5% SDS, 10 mM EDTA, 5% proteinase K) is made up in a clean room with a laminar flow hood. Cells were captured into 15 µl lysis buffer, vortexed for 30 seconds, centrifuged briefly and incubated at 37 °C for two hours.

2.10.4 DNA extraction from blood homogenate

10 ml of anonymised frozen control blood was provided by NGS mitochondrial disease diagnostic service for DNA extraction. DNA extraction was completed using a QIAGEN Mini extraction kit following the manufacturer's instructions. The blood was split and processed in 10 x 1 ml samples. Columns were left to stand for 5 minutes in AE buffer to increase DNA yield and samples were eluted into 50 µl of nuclease free water rather than TE buffer in case of incompatibility with any downstream applications. DNA was quantified using the Nanodrop with the lowest concentration being 63 ng/µl.

2.11 PCRs and sequencing

2.11.1 D-loop/MT-ND1/MT-ND4 triplex real rime PCR deletion assay

A triplex real time PCR assay was used to quantify mtDNA deletion level as described previously (Rygiel *et al.*, 2015a). This method quantifies relative levels of

MT-ND4 (commonly deleted) and *MT-ND1* (rarely deleted) and D-Loop (rarely deleted), using TaqMan chemistry. Primers and TaqMan MGB probes to detect *MT-ND1*, *MT-ND4* and D-Loop used have been previously reported (Rygiel *et al.*, 2015a). *MT-ND1*, *MT-ND4* and D-Loop probes were coupled with VIC, FAM and NED fluorophores, respectively. PCR amplification was carried out as described previously (Rygiel *et al.*, 2015a), in a 25 µl reaction in triplicate for each sample, with each plate containing a serial dilution of p7D1 plasmid for standard curve generation. Real time primer details can be found in **Table 2.13** and probe details in **Table 2.14**.

Primer pair	Primer name	Primer position	Sequence
D-Loop	D-Loop forward	chrM:16536-16557	5′-CCCACACGTTCCCCTTAAATAA-3′
	D-Loop reverse	chrM:34-9	5′-CGTGAGTGGTTAATAGGGTGATAGAC-3′
MT-ND1	MT-ND1 forward	chrM:3485-3504	5’-CCCTAAAACCCGCCACATCT-3’
	MT-ND1 reverse	chrM:3532-3553	5’-GAGCGATGGTGAGAGCTAAGGT-3’
MT-ND4	MT-ND4 forward	chrM:12087-12109	5’-CCATTCTCCTCCTATCCCTCAAC-3
	MT-ND4 reverse	chrM:12170-12140	5’–CACAATCTGATGTTTTGGTTAAACTATATTT-3’

Table 2.13 *Real time PCR primer positions and sequences. All primer sequences are based on the revised Cambridge reference sequence (NC_012920.1).*

Probe	Primer position	Sequence
D-Loop	chrM:16559–6	NED-5′-ACATCACGATGGATCAC-3′-MGB
ND1	chrM:3506-3529	VIC-5’-CCATCACCCTCTACATCACCGCCC-3’-MGB
ND4	chrM:12111-12138	FAM-5’-CCGACATCATTACCGGGTTTTCCTCTTG-3’-MGB

Table 2.14 *Real time probe positions and sequences. All probe sequences are based on the revised Cambridge reference sequence (NC_012920.1).*

2.11.2 Long range PCR primer design and selection (work by Dr. Georgia Cambell)

A large number of primer pairs were designed to amplify roughly 16 Kb amplicons from the mitochondrial genome. Primers were designed using the PrimerBLAST (NCBI) web programme and based on the Revised Cambridge reference sequence (rCRS), GenBank accession number NC_012920.1 for human mtDNA. These

primer sets were then grouped dependent by size, melting temperature (T_m) and location in the mtDNA. Following this the primers were narrowed down. Primers were required to have a one or two base pair (bp) GC-clamp (primers with a 3' Guanine or Cysteine bind more efficiently and greater than 2 bp GC-clamp have an increased risk of non-specific binding) and not have a greater than 4 bp repeat of a single nucleotide (poly X repeat).

Finally, one primer pair for each set of reaction conditions and mtDNA location was selected to order and test. The final 16 Kb primer pairs selected can be found in **Table 2.15**. In addition, when working with single cell lysates it sometimes become necessary to implement a second round of amplification, which is commonly more successful using nested primers, as such 30 second round (three per first round pair, **Table 2.16**) were designed and ordered also.

Primer pair	Primer	Primer position	Primer Length (bp)	Amplicon size (bp)	T_m (°C)	Gene located in
1	1F	chrM:3-27	25	16358	60	D-Loop
	1R	chrM:16360-16336	25			
2	2F	chrM:2700-2724	25	15876	63	16S
	2R	chrM:1956-1932	25			
3	3F	chrM:2699-2724	26	15822	67	16S
	3R	chrM:2006-1982	25			
4	4F	chrM:3086-3115	30	15882	60	16S
	4R	chrM:2339-2310	30			
5	5F	chrM:2862-2891	30	16070	63	16s
	5R	chrM:2362-2333	30			
6	6F	chrM:122-150	29	16188	63	D-Loop
	6R	chrM:16309-6281	29			
7	7F	chrM:2180-2209	30	16178	67	12S
	7R	chrM:1789-1760	30			
8	8F	chrM:458-490	34	15848	63	D-Loop
	8R	chrM:16305-16273	33			
9	9F	chrM:1371-1405	35	16306	67	12S
	9R	chrM:1108-1074	35			
10	10F	chrM:442-476	35	16090	67	D-loop
	10R	chrM:16531-16497	35			

Table 2.15 *16 Kb long range PCR first round primer pairs selected for optimisation. Primer pairs were selected to have a range of melting temperatures (T_m) and primer lengths as well as for the gene in which they bind. Primers are designed using the revised Cambridge reference sequence (rCRS), GenBank accession number NC_012920.1, for human mtDNA.*

First round primer pair	Second round primer pair	Primer	Primer position	Primer Length (bp)	Amplicon size (bp)	T_m (°C)
1	1A	1AF	chrM:116-140	25	16131	60
		1AR	chrM:16246-16222	25		
	1B	1BF	chrM:261-285	25	16031	60
		1BR	chrM:16291-16267	25		
	1C	1CF	chrM:126-150	25	16179	60
		1CR	chrM:16304-16281	24		
2	2A	2AF	chrM:2768-2793	26	15534	63
		2AR	chrM:1733-1758	26		
	2B	2BF	chrM:2860-2884	25	15480	63
		2BR	chrM:1771-1749	24		
	2C	2CF	chrM:2939-2967	29	15488	63
		2CR	chrM:1858-1830	29		
3	3A	3AF	chrM:2974-3001	28	15512	67
		3AR	chrM:1917-1893	25		
	3B	3BF	chrM:3015-3040	26	15505	67
		3BR	chrM:1951-1926	26		
	3C	3CF	chrM:2769-2794	26	15752	67
		3CR	chrM:1952-1926	27		
4	4A	4AF	chrM:3269-3297	29	15534	60
		4AR	chrM:2260-2234	27		
	4B	4BF	chrM:3273-3302	30	15561	60
		4BR	chrM:2265-2239	27		
	4C	4CF	chrM:3210-3236	27	15445	60
		4CR	chrM:2086-2060	27		
5	5A	5AF	chrM:3039-3068	30	15793	63
		5AR	chrM:2263-2235	29		
	5B	5BF	chrM:3087-3116	30	15744	63
		5BR	chrM:2262-2234	29		
	5C	5CF	chrM:2939-2967	29	15846	63
		5CR	chrM:2216-2188	29		
6	6A	6AF	chrM:333-362	30	15900	63
		6AR	chrM:16233-16204	30		
	6B	6BF	chrM:358-386	29	15874	63
		6BR	chrM:16232-16204	29		
	6C	6CF	chrM:448-476	29	15802	63
		6CR	chrM:16250-16222	29		
7	7A	7AF	chrM:2330-2359	30	15951	67
		7AR	chrM:1712-1683	30		
	7B	7BF	chrM:2328-2412	30	15967	67
		7BR	chrM:1726-1697	30		
	7C	7CF	chrM:2331-2359	29	15883	67

		7CR	chrM:1645-1616	30		
8	8A	8AF	chrM:648-677	30	15522	63
		8AR	chrM:16170-16141	30		
	8B	8BF	chrM:580-309	30	15532	63
		8BR	chrM:16112-16084	29		
	8C	8CF	chrM:720-748	29	15512	63
		8CR	chrM:16232-16204	29		
9	9A	9AF	chrM:1413-1442	30	16186	65
		9AR	chrM:1030-1001	30		
	9B	9BF	chrM:1530-1559	30	16071	65
		9BR	chrM:1032-1003	30		
	9C	9CF	chrM:1560-1588	29	15980	65
		9CR	chrM:971-944	28		
10	10A	10AF	chrM:719-748	30	15703	65
		10AR	chrM:16422-16394	29		
	10B	10BF	chrM:608-635	28	15703	65
		10BR	chrM:16311-16281	31		
	10C	10CF	chrM:582-609	28	15711	65
		10CR	chrM:16293-16267	27		

Table 2.16 *16 Kb long range PCR second round primer. For each first round primer three second round primer pairs were designed and these have been labelled using the number of the first round primer pair they correspond to and the letters A to C. For each primer pair the T_m (meting temperature) and length is generally similar to the first round primer pair. Primers are designed using the revised Cambridge reference sequenc (rCRS) GenBank accession number NC_012920.1 for human mtDNA.*

2.11.3 Optimisation of long range PCR

All twenty primer pairs were trialed with LA Taq and PrimeSTAR taq polymerase using two sets of cycling conditions for each taq polymerase. Initial testing was completed using 50 µl reaction volumes for both polymerases and 1x mastermix (**Table 2.17**) volumes were decided based on the manufacturer's guidance. Cycling conditions are summarised in **Table 2.18**.

PrimeSTAR GXL 1x mastermix		**LA Taq 1x mastermix**	
Nuclease free water	32 µl	Nuclease free water	33.5 µl
5x PrimeSTAR GXL buffer	10 µl	10x LA Taq buffer	5 µl
dNTPs (2.5 µm)	4 µl	dNTPs (2.5 µm)	8 µl
Forward primer (10 µm)	1 µl	Forward primer (10 µm)	1 µl
Reverse primer (10 µm)	1 µl	Reverse primer (10 µm)	1 µl
PrimeSTAR GXL polymerase	1 µl	LA Taq polymerase	0.5 µl

Table 2.17 *1x reaction master mix for PrimeSTAR GXL and LA Taq.*

Polymerase	**Cycling protocol 1**	**Cycling protocol 2**
PrimeSTAR GXL	40 cycles of 98 °C for 10 seconds followed by 68 °C for 16 minutes. Hold at 4°C	35 cycles of 98 °C for 10 seconds followed by 68 °C for 11 minutes. Hold at 4 °C
LA Taq	Initial denaturation at 94 °C for 30 seconds followed by 35 cycles of 94 °C for 30 second, 58 °C for 30 seconds and 68 °C for 11 minutes. Then a final extension of 72 °C for 10 minutes and hold at 4 °C.	Initial denaturation at 94 °C for 30 seconds followed by 35 cycles of 94 °C for 30 second and 68 °C for 15 minutes. Then a final extension of 72 °C for 10 minutes and hold at 4 °C.

Table 2.18 *Cycling conditions trialled for PrimeSTAR GXL and LA Taq*

Results of initial trials for 16 Kb primer pairs can be found in **Figure 2.1**. Primer pairs that successfully amplified a product from the 1 in 10 (10^{-1}) dilution of wild type blood homogenate were carried forward and tested on serial dilutions from 10^{-1} to 10^{-5} to test which primers work best at lower concentrations of blood homogenate (**Figure 2.2**), which would be similar to that achieved from a single cell lysate.

Following this the best conditions were selected for each polymerase, this was the 3-temperature cycling protocol (protocol 1) for LA taq and the 11 minutes extension time and 35 cycles (protocol 2) for PrimeSTAR GXL to be carried forward for trial on single cell lysates.

Interestingly, for the primers for 16 Kb long range PCR ranking of primer pair for each of LA taq and PrimeSTAR GXL demonstrates that the best primers are 30 bp in length and melting temperature varies substantially. Whereas for LA Taq the best primer pairs have a high T_m of 66 or 67 °C but vary in length. Therefore, it appeared that primer length was most important for successful amplification with PrimeSTAR GXL whereas T_m is important for LA taq.

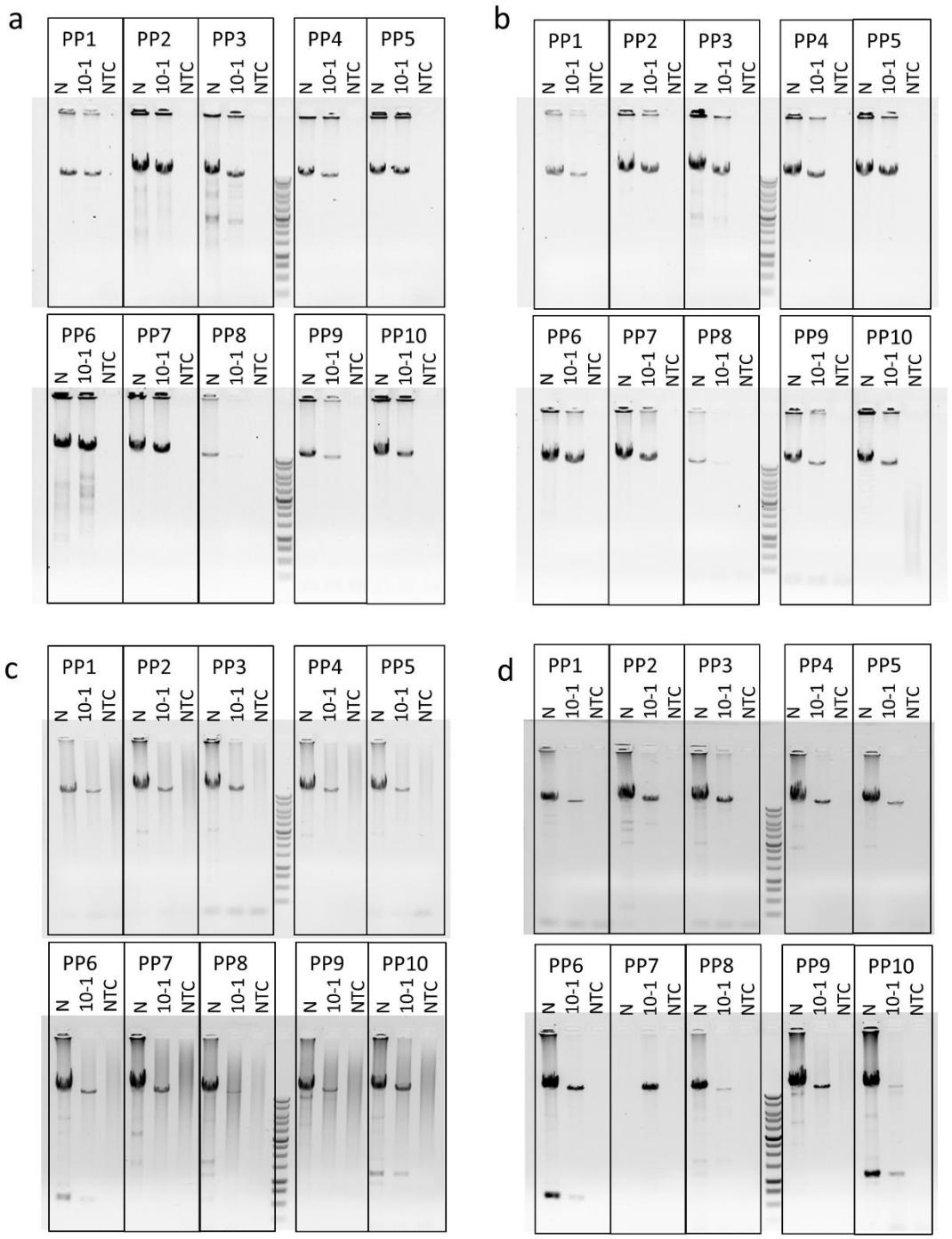

Figure 2.1 *16 Kb Long range PCR testing primer pairs (PP) 1 to 10 on wild type blood homogenate DNA. (a) PrimerSTAR GXL taq polymerase with 16 minute extension time and 40 cycles. (b) PrimerSTAR GXL taq polymerase with 11 minute extension time and 35 cycles. (c) LA taq polymerase using the two temperature step protocol. (d) LA taq polymerase using a three temperature step protocol. L; 1Kb ladder (Promega), N; neat, 10^{-1}; 1 in 10 dilution of N and NTC; no template control.*

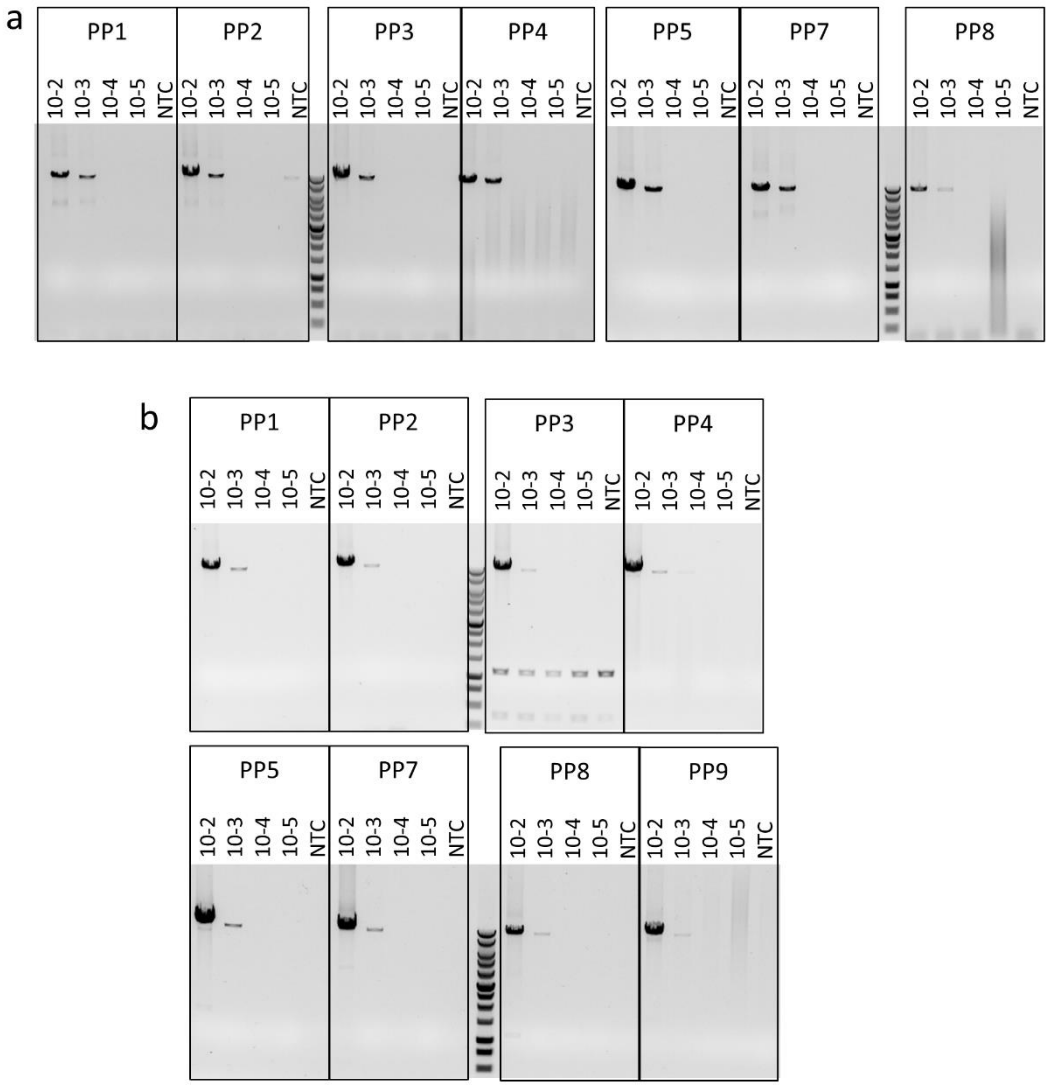

Figure 2.2 *16Kb Long range PCR testing for primer pairs down to 10^{-5}. (a) PrimerSTAR GXL taq polymerase with primer pairs 1 to 5, 7 and 8 (b) LA taq polymerase with primer pairs 1-5 and 7 to 9. Ladder; 1 Kb ladder (Promega), 10^{-2}; 1 in 100, 10^{-3}; 1 in 10 dilution of 10^{-2}, 10^{-4}; 1 in 10 dilution of 10^{-3}, 10^{-5}; 1 in 10 dilution of 10^{-4}, and NTC; no template control.*

Based on serial dilution success the two most successful primers for each polymerase were selected for trial on multiple deletion single cell lysates. Single cells were laser microdissected from a SDH stained muscle section of a patient 20, with *RRM2B* variants. Previous work using single cell lysates for long range PCR and real time PCR demonstrated a difference in success of different lysis methods e.g. SDS-EDTA-proteinase K lysis is not successful with real time PCR. As such two lysis methods were trialed; 10 fibres were captured into a tris-tween proteinase K lysis buffer and 10 fibres captured into a SDS-EDTA-proteinase K lysis buffer and incubated as stated in 2.10.2 and 2.10.3. A 10^{-3} wild type blood homogenate was run as a positive control on every PCR plate alongside the no template control.

This demonstrated better amplification with SDS-EDTA-proteinase K lysis buffer than tris-tween-proteinase K lysis buffer with both LA taq and PrimeSTAR for the selected primer pairs. For 16 Kb long range on single cell lysates it was often the case that a product would not be detectable following the first round therefore a set of three second round nested primers were designed for each of the 16 Kb first round primer pairs. After an unsuccessful or partially successful first round of PCR second round primers were then trialed to see if this boosted amplification, which it often did.

Successful primer pairs were trialed for reduced reaction volumes including 25 µl and 10 µl as this is necessary in order to be cost effective when preforming both long range and most importantly single molecule PCR. **Figure 2.3** demonstrates amplification of wild type and deletion molecules from COX negative fibres from patient 20 with RRM2B variants and multiple mtDNA deletions. This was completed in 10 µl reaction volumes in quadruplicate and the gel presented is a second round reaction.

The most successful 16 Kb primer, taq and cycling condition combination for amplification of single cell lysates was PrimeSTAR GXL, using 11 minutes extension and 35 cycles with primer pair number six (122F/16309R) and second round primer pair 6A (333F/16233R). These were trialed unsuccessfully for single molecule PCR, This would require further optimisation to use in future. Subsequently primer pair 6 was no longer viable, therefore primer pair 7 (2180F/1789R) with PrimeSTAR GXL was subsequently used for long range PCR in 2.11.4 and Chapters 3 and 4.

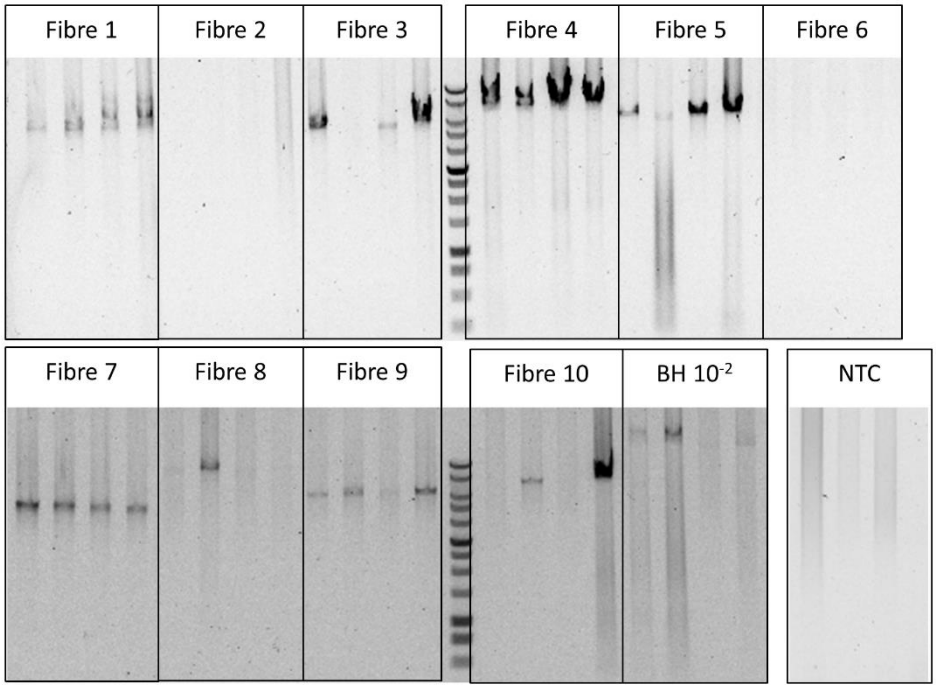

Figure 2.3 *16 Kb Long range PCR using primer pair 6 (122F/16309R) and second round primer pair 6B (333F/16233R) on single fibre lysates. COX negative fibres 1 to 10 from patient 20 with RRM2B variants and multiple mtDNA deletions and blood homogenate and no template.*

2.11.4 Final Long range PCR protocol

Two rounds of PCR were employed to screen single muscle fibre lysates for large-scale mtDNA rearrangements using PrimeSTAR GXL (TaKaRa, Clonetech). The reaction was prepared as follows: 1 µl cell lysate, 1x PrimeSTAR GXL reaction buffer, 0.2 µM dNTPs, 0.2 µM forward and reverse primers and 0.625 unit polymerase, in a total volume of 50 µl. The first round of PCR amplified a 16179 bp region using primer pair 7 (2180F/1789R) (**Table 2.15**) and the second round reaction amplified a 16029bp region using the reverse primer from primer pair 7 and the forward primer from primer pair 7A (2330F/1789R) (**Table 2.16**). Cycling conditions were: 35 cycles of 10 seconds at 98 °C and 11 minutes at 68 °C. PCR products were separated through a 0.7% agarose gel with a 1 Kb ladder used to size amplicons.

2.11.5 Agarose gel electrophoresis

Agarose was dissolved in 1 x TAE by heating in a microwave until boiling. For long range and smPCR products which were in excess of 10 Kb in length 0.7% agarose gel was used. 4 µl of gel red was added per 100 ml for DNA visualisation. This was emptied into a gel cassette and a well comb inserted. The gel was allowed to set before transfer to an electrophoresis tank filled with 1 x TAE running buffer. 1 µl of loading dye was added to each well of the plate and 5 µl of each sample was loaded on to the gel. 5 µl of an appropriately sized DNA ladder was also loaded for sizing of products. The gel was run out at 140 volts until the PCR products were sufficiently separated. PCR products were visualised and imaged using the BioRad ChemiDoc.

2.12 Electron microscopy techniques

2.12.1 Transmission electron microscopy

Muscle fibre bundles were teased from a fresh biopsy and lightly fixed overnight in 2% glutaradehyde (in Sorenson's buffer (0.1M, pH7.4)) at 4 °C. All subsequent processing of samples was completed by Drs Kathryn White and Tracey Davey in Electron Microscopy Research Services (EMRS). Fibres were post fixed in 1% osmium tetroxide for one hour. Samples are dehydrated in a graded series of acetone (25%, 50%, 75%, 100%) before being embedded in epoxy resin (TAAB medium grade) and polymerised at 60 °C. Sections are cut on an ultramicrotome, firstly semi-thin sections (0.5 µm) are stained with toluidine blue for LM to identify the area of interest/confirm orientation of tissue. Ultrathin sections (70 nm) are then cut and picked up onto copper grids. Sections were stained with uranyl acetate and lead citrate before being viewed on the TEM (Philips CM100). Images were captured using an AMT CCD camera (Deben). Scanning for regions of interest 5800x and initial images were captured at 7900x, more detailed images were captured at 13500x. Fibres selected for analysis had to have no more than two z-lines separated by a minimum of 10–15 µm in order to be deemed optimally transverse in orientation.

2.12.2 Serial block face scanning electron microscopy

Processing of samples was completed by Drs Kathryn White and Tracey Davey in EMRS. Tissue was fixed in 2% glutaraldehyde in 0.1 M cacodylate buffer. It is then treated with a series of heavy metals as described previously (Deerinck T *et al.*, 2010). Briefly, tissue was immersed in 3% potassium ferrocyanide + 2% osmium tetroxide, followed by 0.1% thiocarbohydrazide, then 2% osmium tetroxide and finally left overnight in 1% uranyl acetate (with water washes between each step). The next day the samples were immersed in 0.6% lead aspartate solution and then dehydrated in graded acetone and embedded in epoxy tab 812 hard resin. After polymerisation the block was trimmed and sectioned for TEM to identify the area of interest before performing serial block face SEM. Fibres with a high mitochondrial content were selected, from cases with specific mitochondrial pathology detected via TEM and a z- stack was captured using the Gatan 3view system and digital micrograph software to allow further analysis of mitochondrial pathology.

2.13 Statistical analyses

Graphs were produced in Prism v7.0 and statistical analysis was performed in a combination of R v3.3.0, Prism v7.0 and Mini tab 17. Normality tests and histograms were performed to assess normality where appropriate and then data normalised (if possible) prior to selecting the appropriate parametric or non-parametric statistical test. Specific tests area specified in the methods and results sections of individual chapters.

Chapter 3. Dysferlinopathy and mitochondrial dysfunction

3.1 Introduction:

3.1.1 Dysferlin and ferlin proteins

The ferlin protein group to which dysferlin belongs all have Ca^{2+} sensitive C2 domains (Lek *et al.*, 2010), dysferlin itself has seven C2 domains with variable affinities for Ca^{2+} (Abdullah *et al.*, 2014). As a group ferlin proteins play roles in vesicle and membrane fusion events.

Dysferlin is encoded by the *DYSF* gene, the loci for which is 2p13 (MIM*603009). Dysferlin localises to the sarcolemmal membrane (**Figure 3.1**) and is a membrane resealing protein which repairs damage to the sarcolemmal membrane caused by the mechanical stress due to muscle contraction. It has previously been demonstrated that an influx of Ca^{2+} through the site of membrane injury binds to the C2 domains of dysferlin and triggers dysferlin-mediated membrane repair (Bansal *et al.*, 2003). Membrane rupture results in an influx of Ca^{2+} which binds to dysferlin, this triggers fusion of cytosolic vesicles and localisation to the site of membrane resealing where the vesicles fuse with the membrane repairing the damage. **Figure 3.2** is a schematic showing how membrane resealing occurs. Patients with dysferlin mutations often have impaired membrane resealing, this is of particular importance in skeletal muscle where Ca^{2+} concentration is highly important.

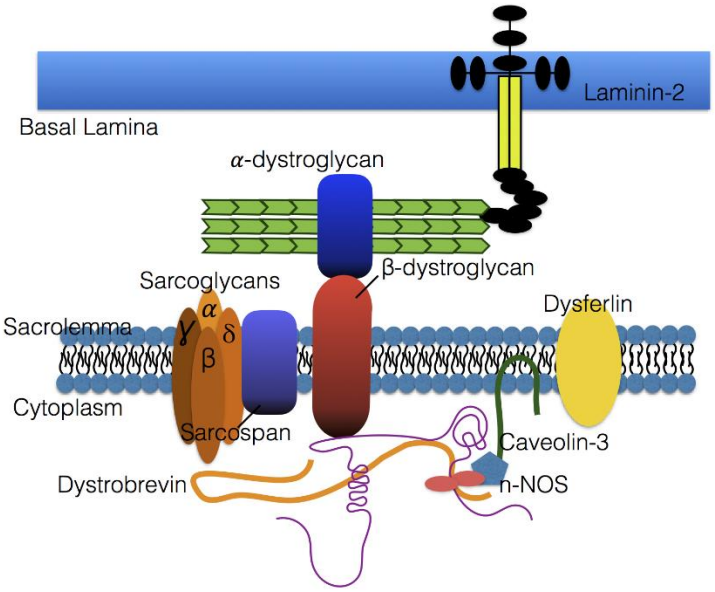

Figure 3.1 *Dystroglycan complex and localisation of dysferlin in the sarcolemma.*

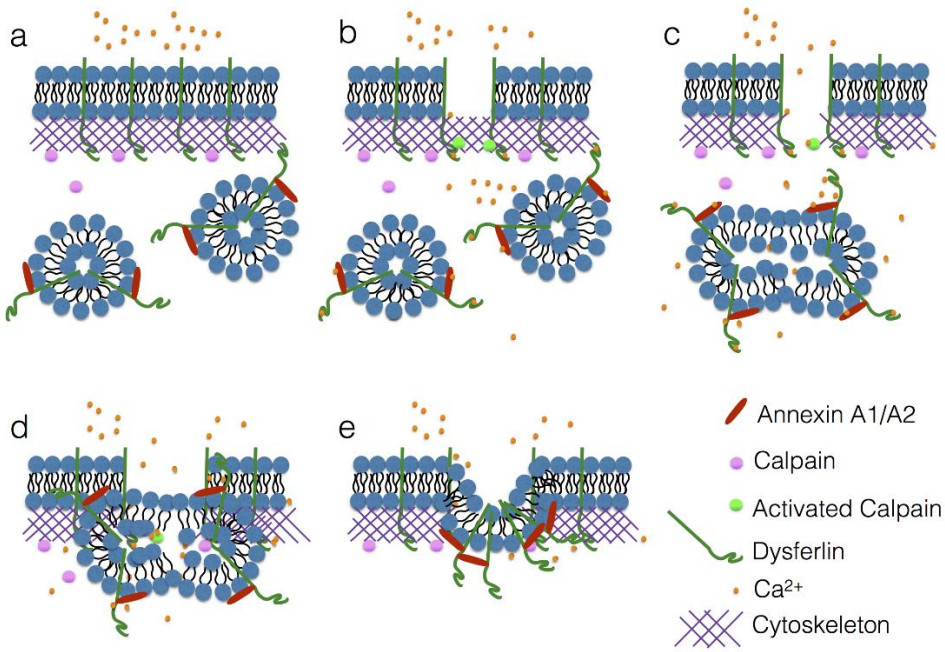

Figure 3.2 *Schematic demonstrating the mechanism of dysferlin mediated membrane repair. (a) Before membrane damage, (b) membrane damage and influx of calcium which binds to annexin A1/A2 and dysferlin. (c) Cytoplasmic vesicles fuse and (d) move to the site of membrane damage. (e) Vesicles fuse with the membrane sealing the hole.*

3.1.2 Dysferlinopathy

Mutations of the *DYSF* gene generate a heterogeneous clinical phenotype presenting as; limb girdle muscular dystrophy type 2B (LGMD2B), Miyoshi Myopathy (MM) (Bashir *et al.*, 1998; Liu *et al.*, 1998), distal myopathy with anterior tibialis onset (DMAT) (Bansal and Campbell, 2004) or muscular dystrophy with congenital onset (Paradas *et al.*, 2009). MM (MIM*254130) is typically autosomal recessive in inheritance, with onset during young adult hood. Although MM is caused by mutations in *DYSF,* it is genetically heterogeneous and mutations in *ANO5* are also known to cause MM. LGMD2B (MIM*253601), also fits an autosomal recessive pattern of inheritance, with typical onset between 15 and 25 years (Bashir *et al.*, 1994). DMAT (MIM*606768) has an autosomal recessive pattern of inheritance and has reported onset between 14 and 28 years.

3.1.3 Inflammatory myopathies and mitochondria

Inflammatory myopathies are a group of conditions characterised by inflammation and inflammatory infiltrates. These include; polymyositis, dermatomyosistis and inclusion body myositis (IBM) (Dubowitz, 2007). A proportion of these have been found to be associated with skeletal muscle mitochondrial abnormalities (Oldfors *et al.*, 1993; Levine and Pestronk, 1998), these are most prominent in sporadic IBM. In sporadic IBM, percentage COX-deficiency of up to 5% (Oldfors *et al.*, 1995) has been reported and around 50% of these COX-deficient fibres have been shown to have one or more large-scale mtDNA rearrangements (Rygiel *et al.*, 2016). Interestingly, inflammatory infiltrates also correlate with the level of respiratory chain deficiency and myofibre atrophy (Rygiel *et al.*, 2015b). Mutations in the *DYSF* gene have been associated with inflammatory myopathy (Fanin and Angelini, 2002; Yin *et al.*, 2015) and it is due to this commonality between sporadic IBM and dysferlinopathy researchers have become interested in how mitochondria function in patients with *DYSF* mutations.

3.1.4 Dysferlin and mitochondria

In addition to the inflammatory nature of both IBM and dysferlinopathies, mitochondria have been demonstrated to accumulate at the site of membrane damage and inhibition of mitochondrial function inhibits healing of injured myofibres in intact myofibres (Sharma *et al.*, 2012). This further suggest that mitochondria may be pathologically involved in disease pathology of patients with *DYSF* mutations.

Two reports have so far demonstrated mitochondrial abnormalities in patients with dysferlin variants. The first report found an accumulation of subsarcolemmal mitochondria in some patients' myofibres including one patient with COX or complex IV deficient ragged red fibres (RRF) and paracrystalline inclusions (Gayathri *et al.*, 2011). The second investigation reported up to 10% of myofibres to be COX-deficient, and some of these fibres have increased mitochondrial mass (Liu *et al.*, 2016). The same study also observed a decreased complex IV and complex III levels of activity in some patients, whilst others showed a significant reduction of complex I and complex IV and a mild decrease in complex III activities.

Recent work looking at membrane repair in mdx mice which have a C>T transition in exon 23 of the dystrophin gene and are a disease model for Duchenne muscular dystrophy has found mitochondria to be important in dysferlin mediated membrane repair (Vila et al., 2016). They report that in mdx mice mitochondrial accumulation at the site of injury and mitochondrial mass is significantly reduced compared to wild type mice and dysferlin protein levels are increased. This increase in dysferlin relieves the cellular stress induced by membrane rupture but is not sufficient to repair the fibre. Furthermore, in dysferlin and dystrophin double knock out mice they find that this increases severity of disease when DYSF knockout alone causes no phenotype at the same age. The underlying mechanism was not demonstrated, however they hypothesise this may be due to reduced muscle fibre bioenergetics and calcium handling.

The findings presented here have been published (Vincent *et al.*, 2016c), this paper can be found in **Appendix 2**.

3.2 Aims of this investigation:

This study aimed to characterise the degree of mitochondrial dysfunction in a cohort of dysferlinopathy patients and determine the mechanisms of mitochondrial involvement in DYSF mutation pathogenesis.

3.3 Methodology:

3.3.1 Patient cohort:

Muscle biopsies were taken for diagnostic purposes from patients (n = 8), with a suspected neuromuscular condition; all patients consented to the use of the sample for research. Diagnostic immunohistochemistry and western blotting showed an absence of dysferlin protein and sequencing of the *DYSF* gene identified pathogenic mutations confirming a diagnosis of dysferlinopathy. Relevant clinical and diagnostic details for all eight patients included in this study can be found in **Table 2.7**. Six were diagnosed with LGMD2B and the remaining two with MM. A previously reported patient with recessive Ribonucleoside-diphosphate reductase subunit M2 B (*RRM2B*) variants (Patient 20,

Table 2.9) (Pitceathly *et al.*, 2012b), mtDNA maintenance disorder and multiple mtDNA deletions was used as a positive control. This patient has multiple mtDNA deletions due to an imbalance in the dNTP pools caused by the mutation in RRM2B, the product for which is involved in dNTP synthesis. In addition three healthy control biopsies were also used; Controls 1, 2 and 3 which were 18, 35 and 52 years respectively. The healthy disease control information can be found in **Table 2.6**. Ethical approval was granted by the Newcastle and North Tyneside Local Research Ethics Committees (reference 2002/205).

3.3.2 Histochemistry:

Three serial cryosections (10 µm) were reacted for COX, SDH and sequential COX/SDH histochemistry as described in **2.8.2**, **2.8.3** and **2.8.4**. A serial section was stained with haematoxylin and eosin (H&E) (as described in **2.8.1**) to examine muscle morphology.

3.3.3 Stereology

Numbers of COX-deficient fibres were counted in a defined area for each section using the meander scan function in Stereo Investigator and a Stereology microscope. Sections were assessed independently by two investigators (myself and Hannah Rosa), due to the subjectivity of assessment by eye. Myofibres were classified as COX-negative (blue), intermediate-negative (blue-grey), Intermediate-positive (brown-grey) and positive (brown) (**Figure 3.3**), in order to be more comparable with quantitative immunofluorescent assessment.

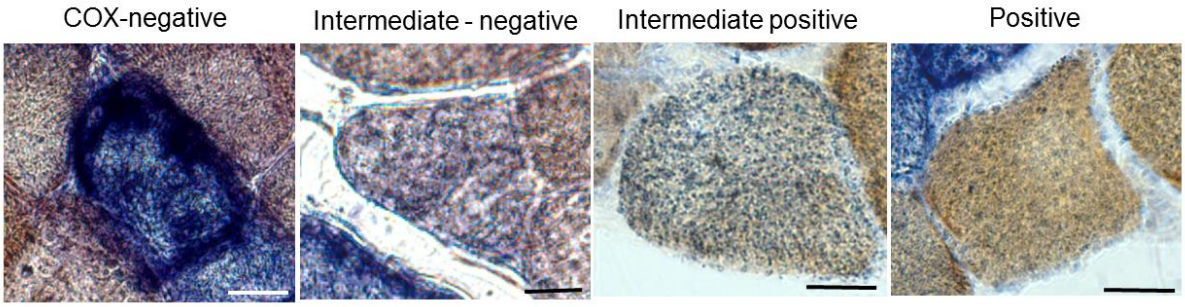

Figure 3.3 *Guide to classification of fibres as COX-negative, intermediate negative, intermediate positive and positive, for comparison to the quadruple immunofluorescence assay.*

3.3.4 Laser microdissection and cell lysis

Three serial cryosections (15 µm) were cut and the first and last muscle sections underwent sequential COX/SDH histochemistry (as described in **2.8.4**) and were used to assess COX deficiency of myofibres. The second tissue section underwent SDH histochemistry (as described in **2.8.3**) only and was used for mtDNA analysis. Single myofibres were laser microdissected as described in **2.10.1** and captured into 15 µl SDS-EDTA-Proteinase K lysis buffer as described in **2.10.3**.

3.3.5 Long Range PCR

Long range PCR was performed on single cell lysates of 20 fibres per patient as described in **2.10.4**. Primer information is detailed in **Table 2.15** and **Table 2.16**. PCR products were separated through a 0.7 % agarose gel with a 1 Kb ladder used to size amplicons.

3.3.6 Immunofluorescent analysis of respiratory chain protein expression profiles

A quantitative immunofluorescent assay was used to assess levels of complex I and complex IV relative to mitochondrial mass (Rocha *et al.*, 2015). Immunofluorescence was completed as described in **2.9.1** with primary antibodies being anti-MTCOI, anti-NDUFB8, anti-VDAC and laminin and secondary antibodies, anti-IgG2a Alexa Fluor 488, anti-IgG2b Alexa Fluor 546, Biotinylated IgG1 and Streptavidin conjugated Alexa Fluor 647. All antibody dilutions can be found in **Table 2.11** and **Table 2.12**. Images were captured on a Zeiss Axioimager and AxioCam MRm with Axiovision and then stitched using ZEN (blue edition). Image analysis using Imaris (v.7.7.2) and statistical analysis as described in **2.9.4** and **2.9.5**.

3.4 Results:

3.4.1 Histochemistry

H&E staining demonstrated fibre size variability (**Figure 3.4a**), muscle fibre necrosis (**Figure 3.4b**), internal nuclei (**Figure 3.4c**), inflammatory fibres (**Figure 3.4d**) and in some muscle biopsies inflammatory infiltrates. Inflammatory infiltrates were mostly associated with (but not limited to) necrotic fibres (**Figure 3.5**, left column). Sequential COX/SDH histochemistry showed a small number (typically less than 1%) of COX-deficient fibres (**Figure 3.5**, right column). However, many biopsies had a large number of fibres that appeared to have intermediate levels of COX deficiency, which was difficult to assess by eye (**Figure 3.5**, Patient 3). Stereo Investigator and a stereology microscope were used to count the number of COX positive, intermediate-positive, intermediate-negative and negative fibres in a defined region (**Table 3.1**). Due to very small numbers of completely COX-deficient fibres and larger numbers of

COX-intermediate myofibres, percentage deficiency was likely to be under- or overestimated. Furthermore, counts were completed by two investigators and inter-investigator variability substantial, due to a large number of fibres intermediate for COX activity. This demonstrated the necessity of using quantitative immunofluorescence (Rocha *et al.*, 2015) for objective classification of complex I and IV deficiency.

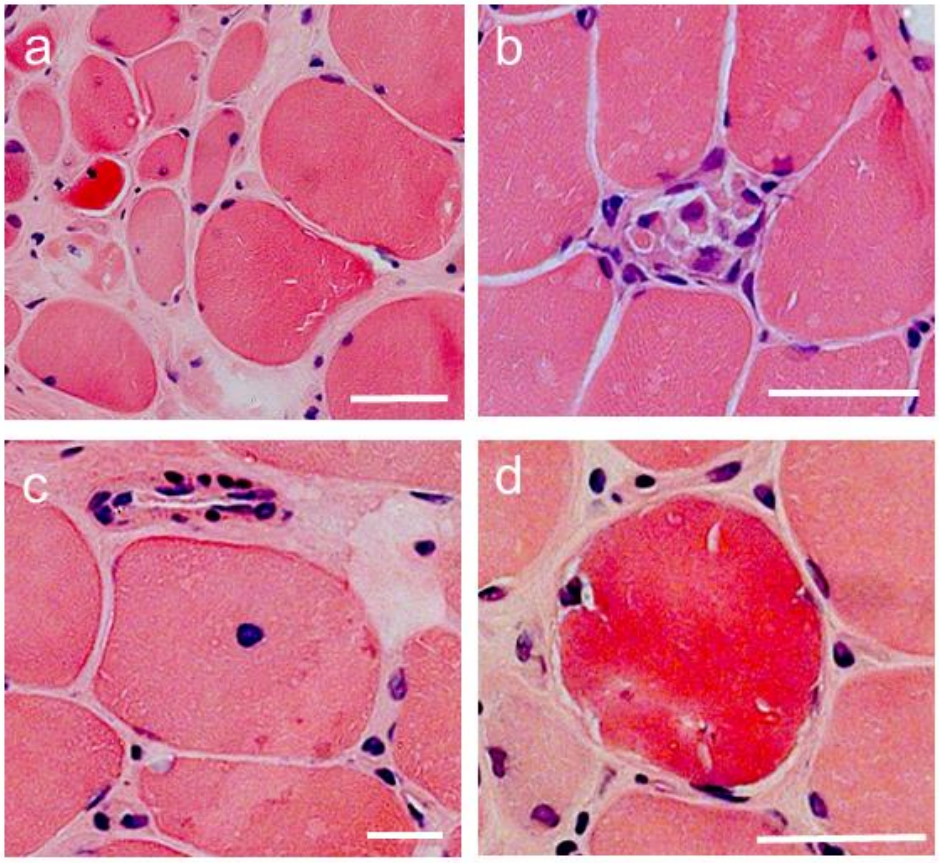

Figure 3.4 *H and E for dysferlin patients. H and E showed (a) muscle fibre size variation, (b) necrotic fibres (occasionally with inflammatory infiltrates), (c) internal nuclei and (d) inflammatory fibres with vacuoles.*

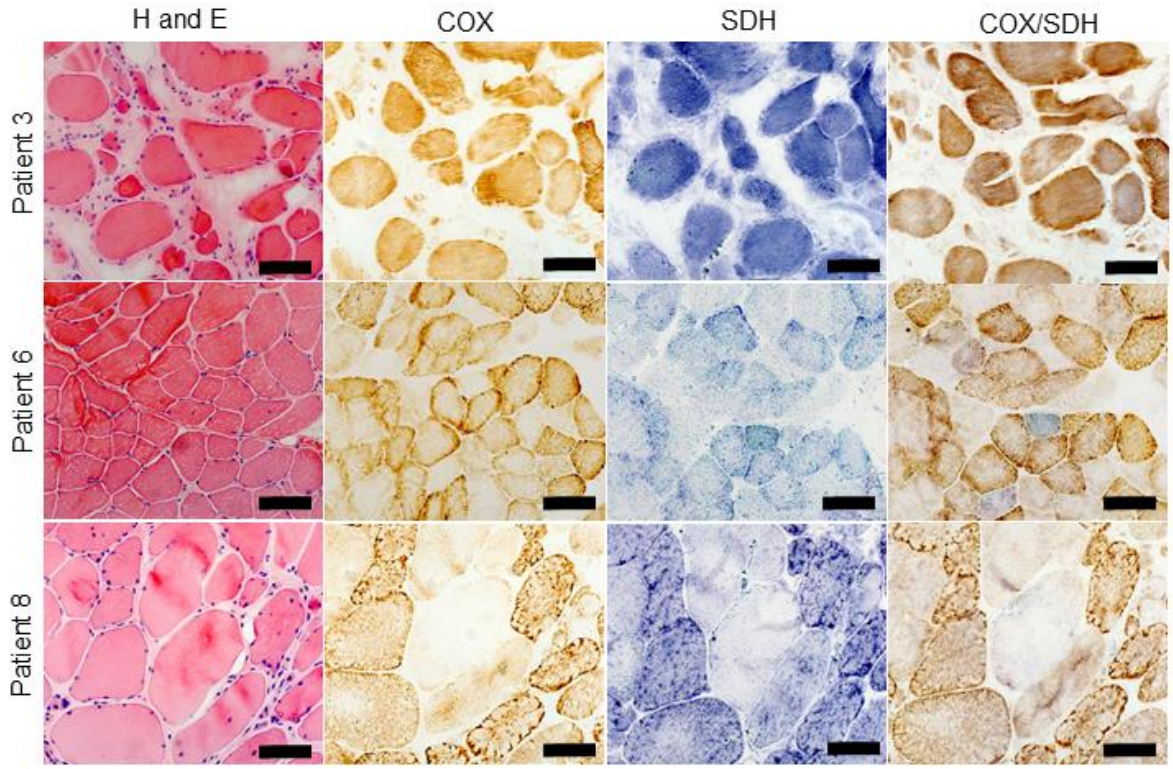

Figure 3.5 *Histochemical analysis of Dysferlin patient muscle. Serial muscle sections from P3, P6 and P8, for H&E, COX, SDH and sequential COX/SDH histochemistry. H&E demonstrates large variation in fibre size, with occasional internal nuclei and inflammation. Only P6 shows a clear cut COX negative fibre but all three biopsies show evidence of intermediate fibres. Adapted from Vincent et al. (2016c).*

Investigator	Patient	Total fibers	% COX positive	% Intermediate positive	% Intermediate negative	% COX negative
1	P1	1491	98.2%	1.8%	0.0%	0.0%
	P2	577	75.4%	18.4%	6.1%	0.1%
	P3	963	65.5%	21.9%	11.9%	0.6%
	P4	1774	97.7%	5.0%	0.1%	0.0%
	P5	397	86.9%	12.8%	0.3%	0.0%
	P6	563	80.8%	17.9%	0.9%	0.4%
	P7	132	69.7%	30.3%	0.0%	0.0%
	P8	453	92.5%	4.9%	2.0%	0.7%
2	P1	1357	83.6%	16.3%	0.07%	0.0%
	P2	382	71.7%	26.9%	1.5%	0.0%
	P3	328	65.9%	30.4%	3.7%	0.0%
	P4	1131	97.1%	2.6%	0.2%	0.1%
	P5	395	77.7%	22.0%	0.3%	0.0%
	P6	726	70.4%	27.1%	1.9%	0.6%
	P7	135	58.5%	31.1%	10.4%	0.0%
	P8	463	78.2%	20.3%	1.2%	0.4%

Table 3.1 *COX deficiency for dysferlin patients (n = 8) as assessed by sequential COX/SDH histochemistry. Fibres were classified as COX-positive, COX-intermediate positive, COX-intermediate negative or COX-negative for comparison with immunofluorescent assessment. Adapted from Vincent et al. (2016c).*

3.4.2 Immunofluorescent analysis

Quadruple immunofluorescence allowed objective quantification of complex I and complex IV protein abundance. A summary of results can be found in **Table 3.2**. Representative immunofluorescent images for all patients are presented in **Figure 3.6**, these show complex I and complex IV deficient fibres in a small number of patients (patients 2, 4, 5, 6 and 8). Controls 1 (18 years) and 2 (34 years) had no complex I deficiency, but the control 3 (52 years) had approximately 0.5% complex I deficiency. In comparison, percentage complex I deficiency ranged from 0% in two patients up to 29.4% in patient 3. Complex I deficiency detected was higher than expected in age matched healthy individuals but lower than levels detected in the patient with recessive *RRM2B* variants (36.2%).

Patient	Age/years	Complex I negative/%	Complex I deficient/%	Complex IV negative/%	Complex IV deficient/%
P1	15.7	2.03	12.26	0.58	6.62
C1	18.0	0.00	0.00	0.00	0.00
P2	20.5	0.00	0.00	0.00	0.05
P3	21.9	26.10	29.4	0.00	11.10
P4	24.7	0.09	0.85	1.13	4.70
P5	28.9	0.15	0.48	0.12	0.33
P6	30.4	1.78	7.43	1.24	3.05
C2	34.0	0.18	0.60	0.18	0.30
P7	47.1	0.00	0.00	0.00	5.05
C3	52.0	0.00	0.00	0.00	0.00
P8	52.5	1.96	10.79	0.44	1.31

Table 3.2 *Immunofluorescent analysis of respiratory chain protein expression in Dysferlin patients. For each fibre a z_score for complex I and complex IV described variation from the control population. The z-scores allowed fibres to be classified into positive, intermediate positive, intermediate negative and negative groupings for complex I and IV. These groups were validated by Rocha et al. (2015). Summary of percentage of fibres classified as complex I and complex IV negative or deficient (negative and intermediate positive and intermediate negative categories combined). Controls and patients are organised in age order for easy comparison and controls are shaded grey. Adapted from Vincent et al. (2016c).*

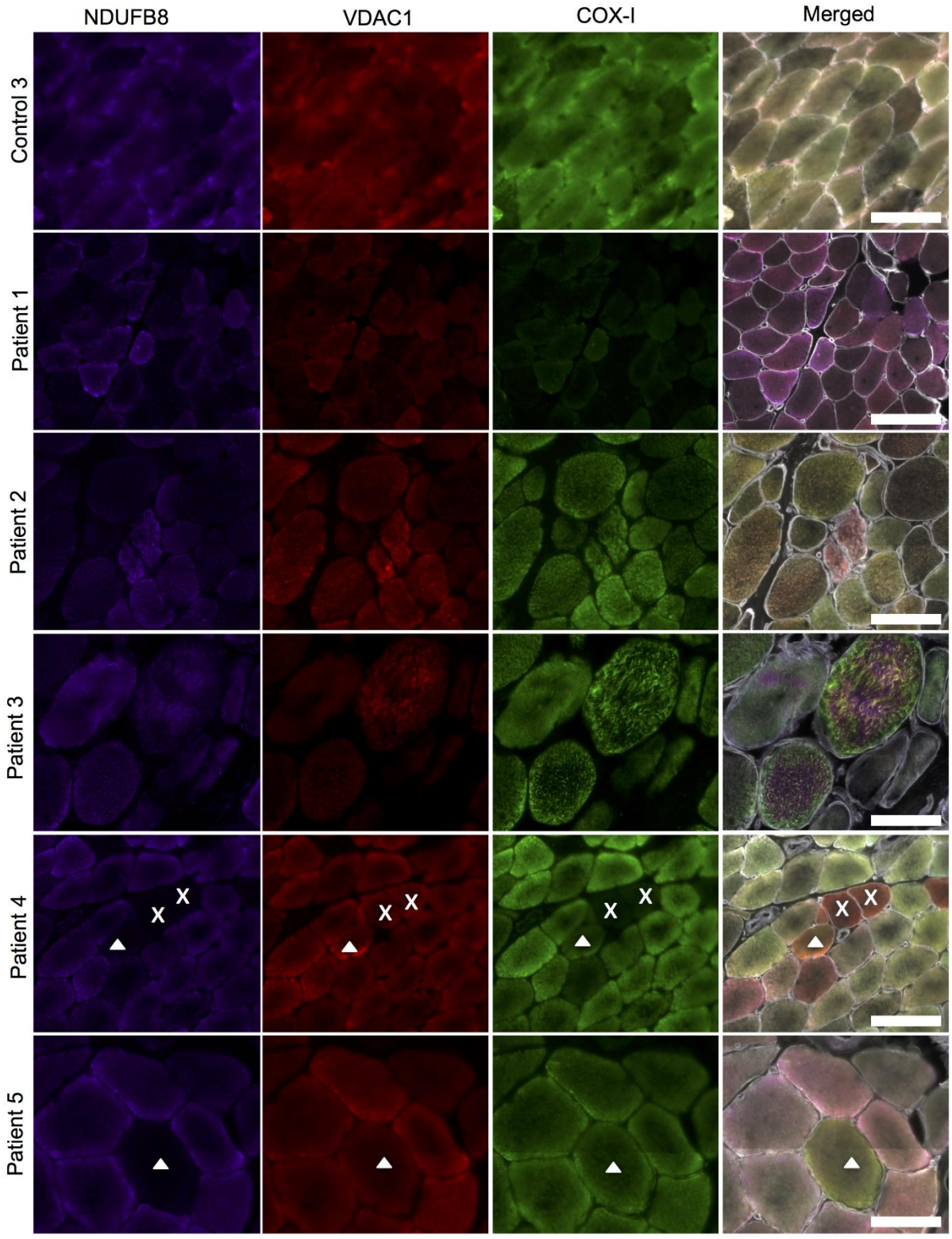
NDUFB8
VDAC1
COX-I
Merged
Control 3
Patient 1
Patient 2
Patient 3
Patient 4
Patient 5

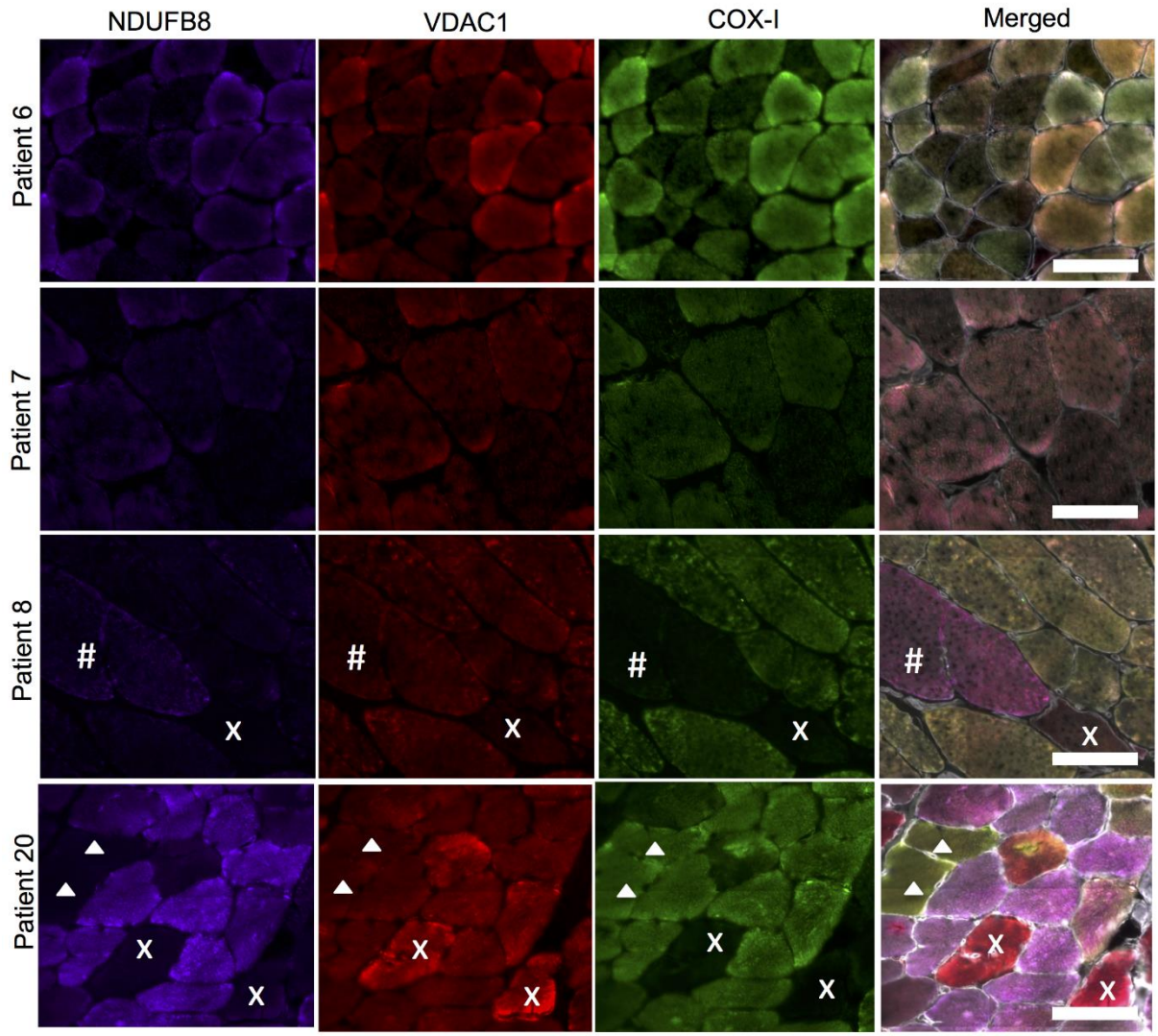

Figure 3.6 *Quadruple immunofluorescent analysis of mitochondrial respiratory chain deficiency in Dysferlin patients, control 3 and patient 20 with RRM2B variants. Representative images of NDUFB8 (complex I) (purple), VDAC1 (red) and COX-I (complex IV) (red). Immunofluorescent staining in a Control 3 (52 years) negative control and patients 1-8. Fibres deficient for; both complex I and complex IV (x in P4 and P8), complex IV only (# in P8) and complex I only (arrow head in P5 and P8) can be seen. Scale bar 100 µm. Adapted from Vincent et al. (2016c).*

Muscle biopsies from control 1 (18 years) and control 2 (35 years) had no complex IV deficient fibres and the muscle biopsy of control 3 (52 years) had approximately 0.5% complex IV deficiency. In comparison to this, 0.1-11.1% of DYSF patients' muscle fibres had evidence of complex IV deficiency. A higher percentage of myofibres were complex IV deficient than in the age-matched controls tested here and previous reports of age-related complex IV deficiency (Bua *et al.*, 2006). However, in

comparison to the patient 20, with *RRM2B* variants, whose biopsy harboured 23.2% complex IV deficient fibres, the degree of deficiency in the dysferlin patient is low.

The respiratory expression profiles in ***Figure 3.7*** show three patterns of mitochondrial respiratory chain protein levels. Dysferlin patients 1, 3 and 6 (***Figure 3.7*** **a, c** and **f** respectively) present with a large number of complex I deficient myofibres. Dysferlin patient 4 (***Figure 3.7*****d**) showed a greater number of complex IV deficient fibres than complex I deficient fibres. DYSF patients, 2, 5, 7 and 8 (***Figure 3.7*** **b, e, g and h** respectively) demonstrated very little deficiency affecting either respiratory chain complex. All DYSF patients had lower levels of complex I and complex IV deficiency than the patient 20, with *RRM2B* variants (***Figure 3.7*****i**). At 43 years of age, this disease control is older than the majority of dysferlin patients (many of whom are below the age of 35 years), however the *RRM2B* variants rather than age is likely to explain the difference in deficiency.

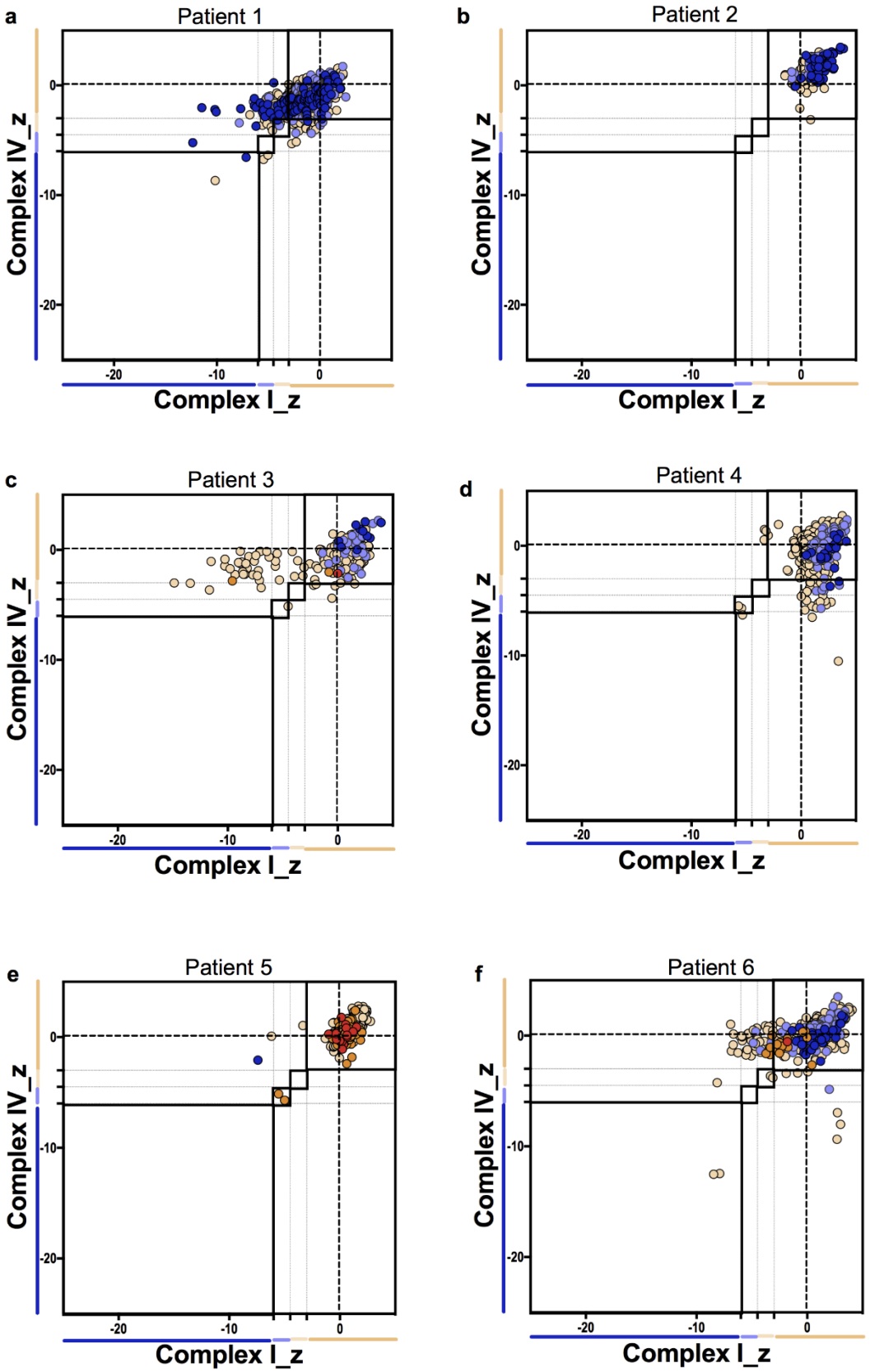
a
Patient 1
Complex IV_z
Complex I_z
b
Patient 2
Complex IV_z
Complex I_z
c
Patient 3
Complex IV_z
Complex I_z
d
Patient 4
Complex IV_z
Complex I_z
e
Patient 5
Complex IV_z
Complex I_z
f
Patient 6
Complex IV_z
Complex I_z

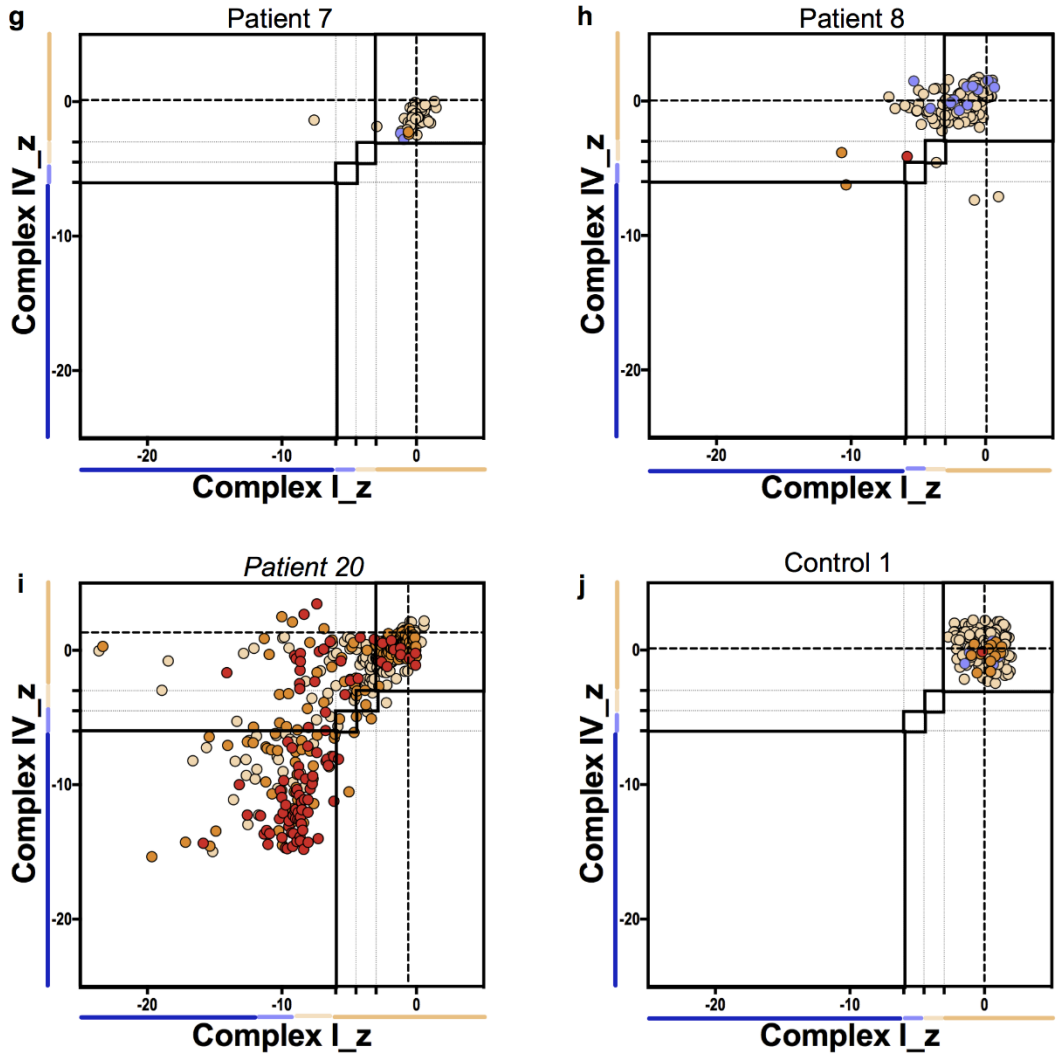

Figure 3.7 *Mitochondrial respiratory chain expression profiles displaying complex I, complex IV and VDAC1 levels in patients with DYSF mutations and an RRM2B mutation as a mitochondrial disease control. (a) patient 1, (b) patient 2, (c) patient 3, (d) patient 4, (e) patient 5, (f) patient 6, (g) patient 7, (h) patient 8 and (i) patient 20 (RRM2B patient) positive control. Each point gives the complex I and complex IV z-scores for a single fibre and is colour coded to indicate the VDAC1 category of the fibre (very low, dark blue; low, light blue; normal, beige; high, orange; or very high, red). Bars next to the X and Y-axes indicate category of complex I or complex IV levels (dark blue, negative; light blue, intermediate negative; light beige, intermediate positive and beige, normal). Adapted from Vincent et al. (2016c).*

3.4.3 Mitochondrial DNA deletions

Patients 4, 6 and 8 were selected for genetic analysis, based on the presence of COX-deficient fibres in sections reacted for sequential COX/SDH histochemistry. Long-range PCR indicated a lack of deletions in all fibres for which a product was successfully amplified for each patient (**Figure 3.8a**) whilst the positive control, patient 20, with compound *RRM2B* variants showed multiple clonally-expanded mtDNA deletions (**Figure 3.8b**). For each case examined a small number of fibres failed to amplify, which is common in single cell long range PCR. This was less frequently seen for patient 20 and can likely be attributed to the fact that fibres selected from the RRM2B patient were more commonly ragged red and therefore the mtDNA concentration was higher.

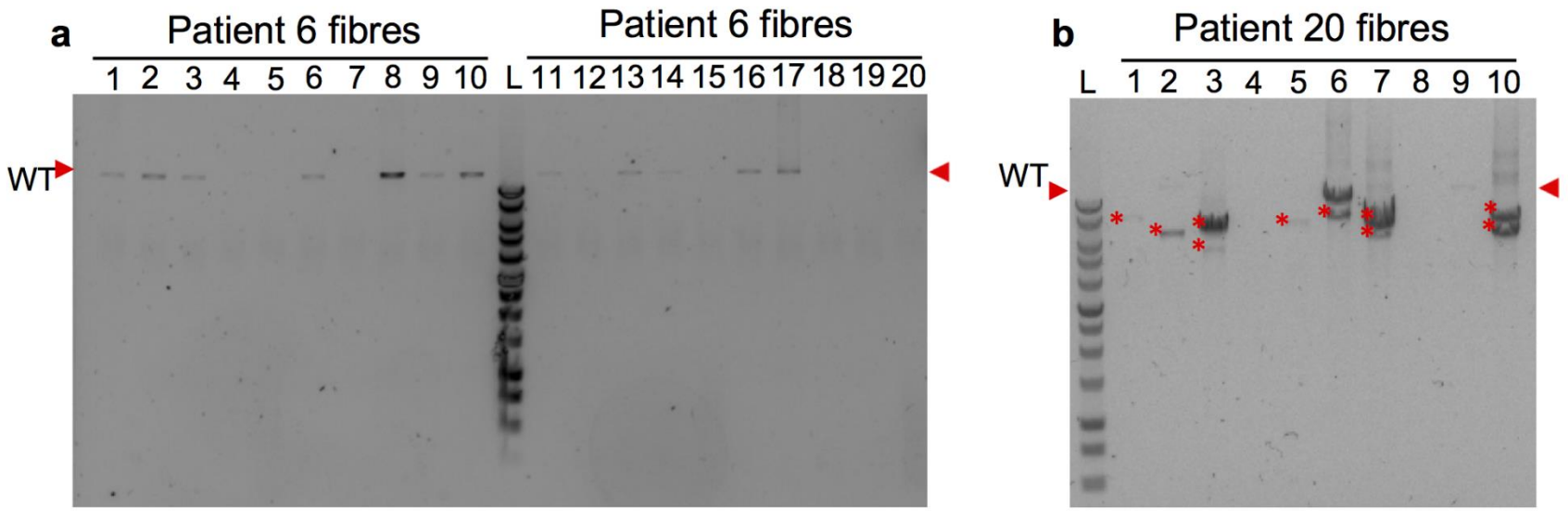

Figure 3.8 *Long range PCR analysis of mtDNA. Long range analysis of dysferlin patient 6 (representative). Red arrows on all gels indicates wild type mitochondrial DNA size. 1 Kb ladder (Promega) run on every agarose gel to size bands and a non-deleted, wild type DNA sample and a no template were included as controls. (a) Long range PCR results for 20 single fibre lysates from patient 6 showed no deletions to be present whilst (b) patient 20, the RRM2B positive controls, long-range PCR results showed multiple large-scale mtDNA deletions detected(*). Adapted from Vincent et al. (2016c).*

3.5 Discussion

This study has demonstrated that the levels of complex IV (COX) and complex I deficiency are higher in some DYSF patients examined than in age-matched controls. The majority of fibres that were deficient were classified as intermediate-positive or intermediate-negative rather than completely negative. Additionally, the percentage of complex I-deficient fibres were commonly higher than the percentage of complex IV deficient fibres.

Long range PCR analysis of mtDNA from three patients, with a high percentage of complex I and complex IV deficient fibres, produced full length mtDNA amplicons. Despite an absence of large-scale mtDNA deletions detected, it is still possible that the respiratory chain dysfunction may be due to either deletions smaller than the resolution of the technique or duplications which are unlikely to be detected here (due to the larger amplicon size). It is also possible that the respiratory chain deficiency is due to point mutations, however I believe deletions or dupications to be more-likely given the inflammatory nature of dysferlin myopathy.

As there is a larger percentage of complex I and complex IV deficiency in patients than observed in controls and since mutations in the *DYSF* gene cause a defect in membrane resealing causing an increase in intracellular Ca^{2+} this could also have an impact on the mitochondria. If so mitochondrial respiratory chain dysfunction may be secondary to a change in mitochondrial morphology in response to increased cytosolic Ca^{2+}. Dysferlin, which has ferlin Ca^{2+} binding domains with variable affinities for Ca^{2+}, functions to regulate cytosolic Ca^{2+} by repairing membrane damage (Gayathri *et al.*, 2011). In the absence of normal levels of functional dysferlin, myofibre cytosolic Ca^{2+} levels increase to abnormal levels. Since Ca^{2+} homeostasis is also a role of the mitochondria, a shift in Ca^{2+} concentration will alter mitochondrial function. Increased cytosolic Ca^{2+} results in increased mitochondrial fission, fragmenting the mitochondrial network (Han *et al.*, 2010). Mitochondrial fusion is important for stability of the mtDNA and tolerance of mtDNA mutations, since it allows dilution of mutated mtDNA reducing the impact on mitochondrial function and equilibration of mtDNA maintenance machinery (Chen *et al.*, 2010). Therefore, mutations in the *DYSF* gene impairing Ca^{2+} homeostatic ability of the muscle, result in an increase in cytosolic Ca^{2+}, fragmentation of the mitochondrial

network and thus allows mitochondrial dysfunction to accrue and have a negative impact on muscle function.

In addition, mitochondria are also known to accumulate at the site of membrane injury in wild-type mice and therefore this suggests they play a role in membrane resealing (Sharma *et al.*, 2012; Vila *et al.*, 2016). Increased dysfunction of mitochondria may therefore cause a negative feedback further perturbing membrane resealing. Given that perturbed membrane resealing following injury related muscle damage is likely to lead to an immune response and increased inflammation, this could also be causative of mitochondrial damage.

3.5.1 Limitations

Here no mtDNA deletions were detected however fibres for genetic analysis were selected based on COX/SDH histochemistry. Given that the majority of fibres with complex IV deficiency fell into the intermediate complex IV categories when assessed by immunofluorescence and the fact that complex I deficiency was more prominent it would have been better to use the immunofluorescent sections for selection of fibres.

Tissue culture and assessment of patient myoblasts for calcium handling defects and mitochondrial morphology, would have been valuable. Unfotunately no myoblasts were available for any patients reported here.

3.5.2 Future work

Since patients 1, 3 and 6 showed a trend towards more complex I deficiency than COX deficiency and patient 4 more complex IV deficiency than complex I, it would be interesting to investigate deficient pools of fibres from these patients for both mtDNA deletions and point mutations. Previous findings using this immunofluorescent assay has demonstrated a correlation between the pattern of deficiency observed and the genetic cause which would be interesting to investigate here. Furthermore given that a correlation between inflammatory infiltrates and mitochondrial dysfunction is noted in IBM it may be interesting to look for a similar correlation in dysferlin patients.

Due to the relevance of calcium in these patients, investigating calcium homeostasis by fluorescence imaging of *DYSF* patient myoblasts to detect fluorescence intensity of Rhod2/AM (mitochondrial Ca^{2+} concentration) and Fluo3 (Cytoplasmic Ca^{2+} concentration), as previously described (Csordás and Hajnóczky, 2003), may be very interesting. However, this would need to be approached in a new cohort of patients since myoblasts are not available for the patients included here. Although this is unlikely to be an ideal model given the difference in cytoarchitecture and mitochondrial arrangement in myoblasts and myotubes from full differentiated muscle this may shed some light on the pathogenic mechanisms.

3.5.3 Conclusion

The results presented here demonstrate that percentage of complex I and complex IV deficient myofibres is higher in patients with *DYSF* mutations than in age-matched controls. This can be explained if calcium homeostasis is disrupted due to the mutation in Dysferlin and defect in membrane resealing. Further testing is required to test this hypothesis and to understand what role the mitochondria play in membrane resealing since they are found to relocate to the site of injury, however it could provide a potential therapeutic target.

Chapter 4. Myofibrillar myopathy and mitochondrial dysfunction

4.1 Introduction:

4.1.1 Myofibrillar myopathy

Myofibrillar myopathies (MFMs) are a group of myopathies characterised by focal myofibrillar destruction and aggregation of z-disk proteins. MFMs are clinically and genetically heterogeneous and age of onset is most commonly between 10 and 61 years. However, incidents of infantile presentation have been recorded (Piñol-Ripoll *et al.*, 2009).

Muscle weakness can present as proximal or distal but is usually progressive (Ferrer and Olive, 2008; Olivé *et al.*, 2011), cardiomyopathy and isolated cardiomyopathy are also common. Mutations causing MFM have been identified in genes encoding a range of cytoskeletal proteins including; desmin (*DES*) (Goldfarb *et al.*, 1998), αB-crystallin (*CryAB*) (Vicart *et al.*, 1998), myotilin (*MYOT*) (Selcen and Engel, 2004), filamin C (*FLNC*) (Vorgerd *et al.*, 2005), *LDB3* or ZASP (Selcen and Engel, 2005) and *BAG3* (Selcen *et al.*, 2009). The function of each of these proteins, cellular location and disease association are presented in **Table 4.1**.

Protein	Loci	Cellular location	Function	Disease
DES	2q35	Cytoplasm, z-disk	Desmin forms filaments tethering myofibrils to each other and to the plasma membrane. Anchors mitochondria at the Z-disk.	MFM1, dilated cardiomyopathy 1, Limb-girdle muscular dystrophy type 2R, neurogenic scapuloperoneal syndrome
CRYAB	11q23.1	Cytoplasm, Nucleus	Protein chaperone	MFM2, fatal infantile hypertonic myofibrillar myopathy
MYOT	5q31.2	z-line	Actin cross-linking proteins.	MFM3, Limb-girdle muscular dystrophy 1A, Spheroid body myopathy
LDB3* or *ZASP	10q23.2	Localized to the cytoplasm around nuclei. Colocalises with ACTN2 at the z-lines.	Protein kinase C-mediated signalling	Dilated cardiomyopathy 1C, Left ventricular non-compaction 3, MFM4
TTN	2q31.2	Cytoplasm, Nucleus	Contributes to the fine balance of forces between the two halves of the sarcomere.	Hereditary myopathy with early onset respiratory failure (HMERF), MFM, dilated cardiomyopathy 1G, Familial hypertrophic cardiomyopathy 9, LGMD2J, early onset myopathy with fatal cardiomyopathy, tibial muscular dystrophy, proximal myopathy with early respiratory muscle involvement

Table 4.1 *Genes mutated in myofibrillar myopathy, their protein functions, cellular location and clinical disease associated with mutations in the gene presentation.*

Reports of desmin protein aggregates and fibres with reduced COX and SDH on sequential histochemistry, indicative of reduced mitochondrial mass and abnormal mitochondrial morphology and positioning in a patient with a plectin related Epidermolysis Bullosa Simplex and muscular dystrophy (Schroder *et al.*, 2002), may indicate that plectin is involved also. To date, only 50% of MFM causing mutations have been identified and large-scale proteomic studies are being pursued to identify novel candidate genes (Kley, 2014).

4.1.2 Myofibrillar myopathy and mitochondrial dysfunction

Interest in understanding mitochondrial dysfunction in myofibrillar myopathies stems from the role of desmin in localisation of the mitochondria at the z-band, where they are required to meet the energy demands of muscle contraction. As such, it was of great interest when a number of studies discovered that mitochondria are often relocated in patients with MFM and that respiratory chain deficiency also appears to be more common. However, this presents an intriguing question: why do mutations in other MFM genes cause mitochondrial dysfunction? It could be hypothesised that this is likely due to secondary effects of Desmin aggregation in many MFM cases.

Investigations into mitochondrial dysfunction, positioning and dynamics in myofibrillar myopathies are limited to desminopathy, αB-crystallinopathy, zaspopathy, and myotilinopathy. Henderson *et al.* (2013), examined a 12 year old male and his 11 year old sister. Both proband and sister were heterozygous for two *DES* variants; c.266delA (p.Thr76fs*21) and c.322G>T (p.Glu108*). The proband showed 5% COX deficiency but lacked signs of any mtDNA copy number variation, rearrangements or deletions. There were no mitochondrial structural abnormalities reported however the size and distribution of mitochondria varied.

Dold *et al.* (2012), examined three patients with mutations in *DES*. The first two patients showed COX-negative fibres, as well as fibres with diminished or irregular COX activities, mtDNA deletions and histochemical and biochemical mitochondrial dysfunction. One of these also presented with mitochondrial proliferation and a reduction in respiratory chain activity, while the other and the

third patient had changes in mitochondrial morphology. The third patient showed no mtDNA deletions or biochemical or histochemical abnormalities. No mitochondrial positional rearrangements were reported.

Claeys *et al.* (2008), examined mitochondrial positioning in muscle biopsy sections from genetically confirmed MFM patients with; *DES* (n = 9), *CRYAB* (n = 5), *LDB3* (n = 3) and *MYOT* (n = 2) mutations. Seven of the desminopathy patients showed mitochondria in a sandwich-like formation around protein deposits, which were located parallel to the z-line. The majority of desminopathy patients had a normal mitochondrial structure and size. One patient presented with paracrystalline inclusions. However there was nothing else remarkable noted about this patient. For αB-crystallinopathy they found that, although mitochondria were structurally normal they were accumulated in the subsarcolemmal region of the fibres and were depleted in areas of intraplasmic granulofilamentous masses. One *CRYAB* patient also had a few mitochondria with paracrystalline inclusions. For patients with *LDB3* mutations, they found that the mitochondria had a normal structure but were completely absent from filamentous bundles and areas of filamentous accumulation and aggregated around filamentous bundles. Finally, for patients with *MYOT* mutations they found no mitochondria present within tubulofilamentous or filamentous bundles but an accumulation of mitochondria on the periphery of myofibres.

A study of five patients with a histopathalogical diagnosis of MFM but without genetic confirmation was also completed (Reimann *et al.*, 2003). Ages ranged from 50 to 78 years. Of these four patients presented with 0.7%, 0.6%, 3.8% and 1.8%, COX-deficient fibres respectively and the majority of COX deficiency was due to myofibrillar pathology. All five had higher subsarcolemmal COX and SDH activity relative to the intermyofibrillar region. Two patients had low complex I activity and one had low complex IV activity. No decrease in complex II or III activities were demonstrated. Uneven COX, NADH and SDH histochemical activity across the fibres indicated changes in mitochondrial positioning. No mtDNA deletions were found and screening for m.8344A>G $tRNA^{Lys}$ and m.3243A>G $tRNA^{Leu(UUR)}$ point mutations was negative. However the authors do not provide details of nuclear DNA screening, so a confirmed MFM diagnosis is not given; contacting the author confirmed that a genetic

diagnosis was never completed and is no longer possible (J. Reimann – personal communication).

Schroder *et al.* (2003), examined one 40 year old, male patient with slowly progressive muscle weakness since the age of 18. Sequencing of the full *DES* gene showed a c.5141_5143insA (p.Lys239fs*4). This caused a frame shift and premature stop codon, 4 codons downstream of the insertion and resulted in a truncated protein. Muscle analysis showed an increase in fibre diameter and basophilic inclusions. Mitochondria were depleted in some regions but a focal increase found in others. COX-deficient fibres were present at less than 2%, and there were no ragged red fibres. Mitochondrial foci co-localised with protein aggregates and depletion of mitochondria was found to co-localise with granulofilamentous inclusions. Respiratory chain analysis showed normal levels of complex I, complex IV and citrate synthase activity and normal COX/citrate synthase and complex I/citrate synthase ratios. However isolated saponin-permeabilized cells, which are more representative of the *in vivo* state, demonstrated reduced maximal respiratory rates and higher amytal sensitivity, Since amytal is an inhibitor of respiration, that blocks electron transport between complex I and coenzyme Q, this indicates complex I inhibition.

In addition, Winter *et al.* (2016) examined muscle biopsies from three desmin patients in conjunction with studies of the heterozygous and homozygous *DES* knock-in mice carrying c.1045_1047delAGG>insCCC (p.Arg349Pro) mutation. They report few COX-deficient fibres but a large number of ‘rubbed-out’, which are fibres with little COX or SDH staining on sequential histochemistry, indicative of reduced mitochondrial mass. Electron microscopy on patient muscle showed subsarcolemmal accumulation of mitochondria, in association with protein aggregates. Long range PCR demonstrated large-scale mtDNA deletions in two of three patients and heterozygous mice. Interestingly, where patients and heterozygous mice both had wild type products, with additional mtDNA deletion products, homozygous mice displayed prominent mtDNA deletion products with only a few wild type products. They also examined mtDNA copy number and found a reduction of mtDNA copy number in their oldest patient, homozygous knock-in and homozygous knock-out mice.

This chapter investigates a cohort of eight MFM patients and has previously been reported (Vincent *et al.*, 2016a). This paper can also be found in **Appendix 3**.

4.2 Aims of this investigation:

This work aimed to characterise the degree of mitochondrial dysfunction in a cohort of myofibrillar myopathy patients and determine what role if any mitochondrial dysfunction has in the pathogenesis of mitochondrial myopathy.

4.3 Methodology:

4.3.1 Patient cohort

Myofibrillar myopathy patients (n = 9) were identified through the Rare Diseases Advisory Group Service for Neuromuscular Diseases. Selection was based on the presence of protein aggregates in myotilin and desmin immunohistochemistry as well as a genetic diagnosis. A previously reported patient with recessive Ribonucleoside-diphosphate reductase subunit M2 B (*RRM2B*) variants (Patient 20,

Table 2.9) (Pitceathly *et al.*, 2012b), mtDNA maintenance disorder and multiple mtDNA deletions was used as a positive control. This patient has multiple mtDNA deletions due to an imbalance in the dNTP pools caused by the mutation in RRM2B, the product for which is involved in dNTP synthesis. Control 3 (52 years) and control 4 (63 years) were used as age matched controls. Patient details including clinical and pathological findings (where appropriate) are summarised in **Table 2.8**. Ethical approval was previously approved by the Newcastle and North Tyneside Local Research Ethics Committees (reference 2002/205).

4.3.2 Histology

Serial muscle cryosections (10 µm) were stained for Haematoxyin and Eosin or treated for COX, SDH and sequential COX/SDH histochemistry as described in sections **2.8.1**, **2.8.2**, **2.8.3** and **2.8.4**.

4.3.3 Stereology

COX/SDH histochemistry sections were analysed by outlining the full biopsy section and using the meander scan function in Stereo Investigator and a stereology microscope. The minimum number of fibres counted was 127 in patient 11. Fibres were classified by eye with brown fibres categorised as COX positive, grey-brown as COX intermediate positive, blue-grey as COX intermediate negative and blue as COX negative. These categories were used to make the stereology results comparable with the immunofluorescent quantification.

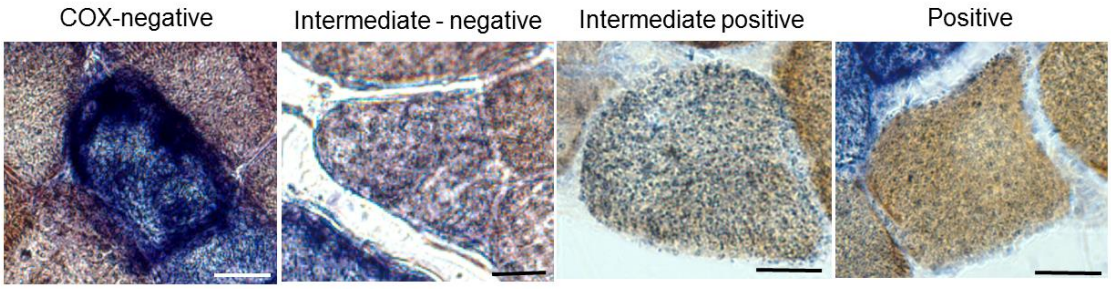

Figure 4.1 *Guide to classification of fibres in COX/SDH histochemistry. Fibres can be classified as; COX-negative, intermediate negative, intermediate positive and positive, for comparison to the quadruple immunofluorescence assay.*

4.3.4 Cryosectioning and histochemistry for single cell genetic analysis

Four serial muscle sections were cryosectioned the first and last were 10 µm sections and were treated for sequential COX/SDH histochemistry before being dehydrated and mounted as a reference for COX efficiency of the fibres. The second and third were 15 µm sections, cut on to membrane slides for laser microdissection and were treated for SDH histochemistry only. These sections were dehydrated prior to laser microdissection.

4.3.5 Laser microdissection

Individual cells were captured by laser microdissection into 15 µl of lysis buffer as in **2.10.1**. The same fibre from serial sections was captured into different lysis buffers for two downstream applications. Tris-Tween-Proteinase K lysis (as in **2.10.2**) was used for real time PCR and SDS-EDTA-proteinase K (as in **2.10.3**) for long range PCR. Tubes were centrifuged briefly to bring lysis buffer and cell to the bottom prior to incubating for the appropriate lysis protocols (**2.10.2** and **2.10.3**).

4.3.6 Long Range PCR and agarose gel

Two round of long range PCR were performed using PrimesStar GXL as described in **2.11.4**. The first round used primer pair 7 (2180F/1789R) and the second round the reverse primer from primer pair 7 and the forward primer of primer pair 7A (2330F/1789R). Primer details can be found in **Table 2.15** and **Table 2.16**. PCR products were separated through a 0.7 % agarose gel with a 1 Kb ladder used to size amplicons, as in 2.11.5.

4.3.7 D-loop/MT-ND1/MT-ND4 triplex real time PCR

A triplex real time PCR assay, targeting D-Loop, *MT-ND1* and *MT-ND4*, to quantify deletion level was used as described in **2.11.1**. All primer details are provided in **Table 2.13** and probe details in **Table 2.14** of Chapter 2.

4.3.8 Immunofluorescent analysis of respiratory chain protein expression profiles

An immunofluorescent assay was used to assess levels of complex I and complex IV relative to mitochondrial mass (Rocha *et al.*, 2015). Immunofluorescence was completed as described in **2.9.1** with primary antibodies being anti-MTCOI, anti-NDUFB8, anti-VDAC and laminin and secondary antibodies, anti-IgG2a Alexa Fluor 488, anti-IgG2b Alexa Fluor 546, Biotinylated IgG1, streptavidin conjugated Alexa Fluor 647. All antibody dilutions can be found in **Table 2.11** and **Table 2.12**. Images were captured on a Zeiss axioimager (microscope details) using Axiovision and then stitched using ZEN (blue edition). Analysis was completed in Imaris (v7.7.2) software and statistical analysis was completed as described in **2.9.4** and **2.9.5** and also by (Rocha *et al.*, 2015).

4.3.9 Measurement of mitochondrial mass across myofibres

A total pool of normal (n = 10), low (n = 10) and very low VDAC (n = 10) fibres were selected to assess VDAC level across the myofibre. The profile tab in ZEN (blue edition) was used to draw a segmenting line across the full myofibre and generate a graph of fluorescent intensity in each channel across the fibre

4.3.10 Assessment of mitochondrial mass

To assess mitochondrial mass, expression of a second marker, succinate dehydrogenase subunit A (SDHA) was compared to VDAC1. Cryosectioned muscle (10 µm) was stained following a similar protocol, as in **4.3.8** but without anti-MTCOI and replacing anti-NDUFB8 with anti-SDHA (1:100). Imaging and image analysis was completed as in **4.3.8**.

4.3.11 Analysis of MFM protein aggregates and mitochondrial mass

Muscle sections were co-stained with antibodies for laminin, desmin (Dako), myotilin (Leica Biosystems) and VDAC1. Image were capture, processed and analysed as in **4.3.8**. Myofibres that contained very low (n = 436), low (n = 338) and normal VDAC1 (n = 150) content (across all patients) were analysed in turn and grouped as either being positive or negative for the presence of desmin and/or myotilin aggregates. Following this, fibres with or without aggregates were plotted against z-score for VDAC1 protein level as an indicator of mitochondrial mass. Imaging and image analysis were completed as described in 4.3.8.

4.3.12 Analysis and statistics

For quantitative immunofluorescence, an R script written by Dr. John Grady was used to generate z-scores for each patient fibre to describe deviation from the control population and classify the fibre as normal, intermediate positive, intermediate negative or negative for each protein (complex I, complex IV and VDAC1). The average OD for each channel from the negative (no primary antibody) control for each case was subtracted from that of the sections stained with primary antibodies to correct for non-specific background. NDUFB8 and COX-1 intensity was normalised to VDAC1 intensity as a mitochondrial mass marker. Control values then created a “normal population” for which the patient fibres were assigned a z-score describing their deviation from the normal population. Statistical analysis is described in **2.9.5** and by Rocha *et al.* (2015). Total fibres analysed was dependent on section size and ranged from n = 111 to n = 1883 in patients and controls.

Percentage classification of fibres for complex I, complex IV and VDAC1 were compared between the patient group and control group, using a Wilcoxen Signed-Rank test. Spearman’s rank correlation (src) was used to assess the relationship between fibre area and complex I, complex IV and VDAC1 protein levels.

4.4 Results:

4.4.1 Histochemistry

Haematoxylin and eosin (H&E) staining revealed a variety of pathological features, consistent with a diagnosis of myofibrillar myopathy including; fibre size variation, rimmed vacuoles, internal nuclei, nuclear bags, basophilic and eosinophilic inclusions, fibre splitting and necrotic and regenerating fibres. Sequential COX/SDH histochemistry showed a small number of COX-deficient fibres (typically not more than 5%) (**Table 4.2**). Often fibres that had decreased COX activity also had decreased SDH activity, indicating low mitochondrial content rather than COX deficiency (**Figure 4.2**). Core-like lesions, which is defined as reduction of COX and SDH activity in the centre of the fibre, was also observed (e.g. patient 10, **Figure 4.2**). Fibre type distribution was not assessed, as it is generally not affected in MFM patients, except where signs of peripheral neuropathy are present. However in these cases grouping of atrophic fibres of both types is present (Dubowitz, 2007).

Patient	Total fibres	COX positive	Intermediate positive	Intermediate negtative	COX negative
P9	494	94.3	4.45	1.01	0.202
P10	611	87.7	10.3	1.80	0.164
P11	127	81.9	18.1	0.0	0.0
P12	863	95.6	4.06	0.348	0.0
P13	1086	93.6	5.06	0.829	0.552
P14	248	45.16	39.1	12.9	2.82
P15	848	96.6	2.48	0.943	0.0
P16	697	91.1	5.67	3.73	0.0
P17	835	99.4	0.479	0.120	0.0

Table 4.2 *COX deficiency counts for myofibrillar myopathy patients based on sequential COX/SDH histochemistry. Adapted from Vincent et al. (2016a).*

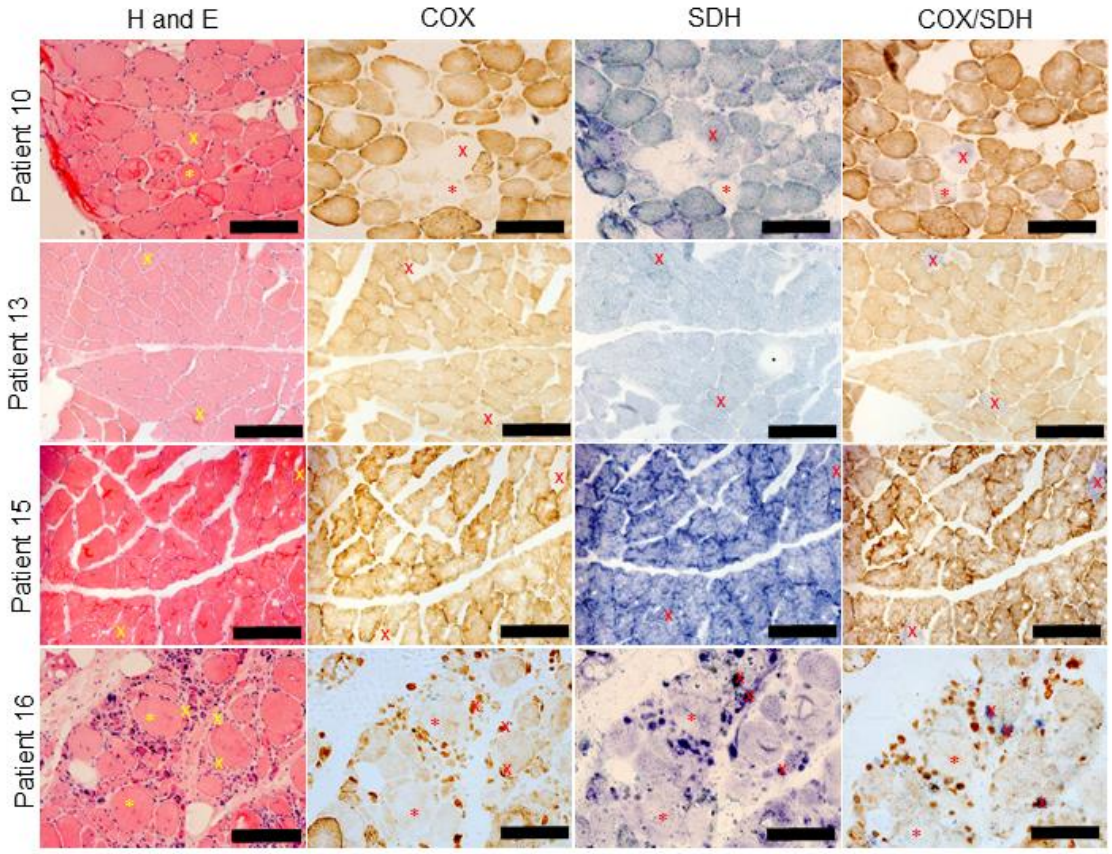

Figure 4.2 *Histochemistry for serial muscle sections from myofibrillar myopathy patients. Images of sections from P10, P13, P15 and P17 treated for H&E staining, COX histochemistry, SDH histochemistry and sequential COX/SDH histochemistry. H&E staining demonstrates morphological changes compatible with diagnosis. Many fibres appear COX-deficient but also demonstrate low SDH reactivity, indicative of a reduction in mitochondrial mass. X indicates COX-deficient fibres and asterisks fibres that are core-like or have low mitochondrial mass. Scale bar 200 µm. Adapted from Vincent et al. (2016a).*

4.4.1 Mitochondrial DNA deletions

Six patients with *DES* (n = 3), *MYOT* (n = 1) and *LDB3* (n = 1) were selected for further mtDNA genetic analysis. Selection was based on the percentage of COX-deficient fibres as assessed by sequential COX/SDH histochemistry. For every single fibre analysed, both long range PCR and real time PCR were implemented to search for clonally-expanded mtDNA deletions. For each MFM patient, 20 single fibre lysates were analysed, 20 fibres were also analysed from patient 20 (recessive *RRM2B* variants,

Table 2.9), as a positive control.

Long range PCR analysis of 20 fibres from patient 20 demonstrated full length wild type amplicons and products of varying size indicative of different sized mtDNA deletions (**Figure 4.3 a**). In comparison to the patient 20, only five fibres (P12: n = 1, P13: n = 1 and P17: n = 3) from the six MFM patients (total fibres n=120) had an mtDNA deletion detected (**Figure 4.3 b-d**).

Failure to amplify a product is common in long range PCR from single cell lysates, since the concentration of DNA is low and this also occurred in two fibres from patient 20. The percentage of fibres that did not amplify is lower in the patient 20. I hypothesise that this is due to a difference in mtDNA content of MFM patient myofibres and those patient 20, which is based on the observation of ragged-red fibres indicative of high mitochondrial mass in the patient 20 and core-like fibres suggesting low mitochondrial mass in the MFM patients.

Real time PCR analysis is presented in **Figure 4.4**, as *MT-ND4* to *MT-ND1* ratio and *MT-ND1* to D-Loop ratio. Due to the potential for the D-Loop region to be triple stranded, when assessing *MT-ND1* to D-Loop, a percentage deletion was required to be above 33% in order to confirm an *MT-ND1* deletion (red box), as highlighted by Rygiel *et al.* (2015a). However, it is interesting to note that some of the potential *MT-ND1* deletions highlighted by the blue box appear to be confirmed as true low level deletions by the *MT-ND4/MT-ND1* results. Similar to the long range PCR results, the real time PCR shows the greatest number of deletions in patient 17, with the level of *MT*-ND4 deletions and the number of fibres affected, close to that of the patient 20.

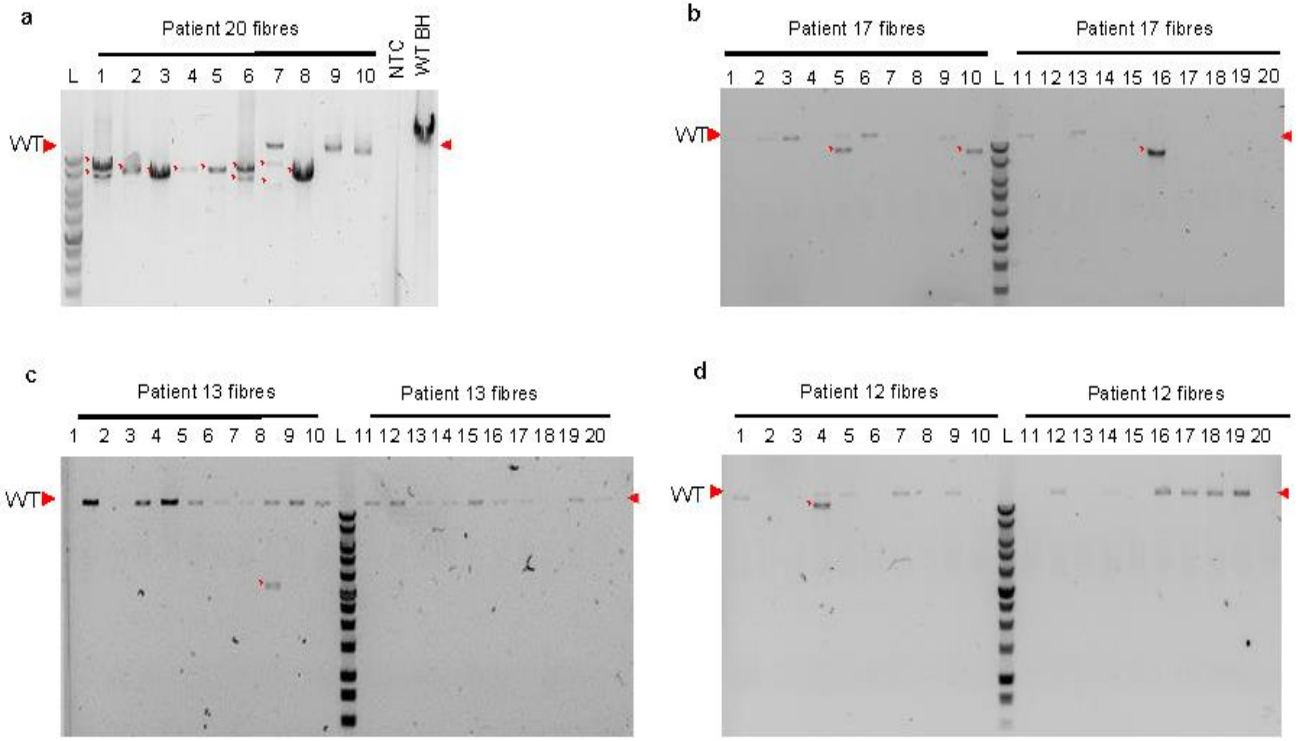

Figure 4.3 *Long range PCR results for single fibre lysates of MFM patients. In long range PCR gels (a-d) red arrows indicate size of wild type mtDNA product, red asterisk (*) indicates deletion products. (a) Long range PCR results for 10 single fibre lysates relative to a wild type blood homogenate (WT BH), no template control (NTC) and 1 Kb ladder (Promega), multiple and single deletions present due to variants in P20. (b) Long range PCR results for 20 single fibre lysates from P17 demonstrating three fibres with a single deletion. (c) Long range PCR results for 20 single fibre lysates from P13 demonstrating one fibre with an mtDNA deletion. (d) Long range PCR results for 20 single fibre lysates from demonstrating one fibre with an mtDNA deletion. Adapted from Vincent et al. (2016a).*

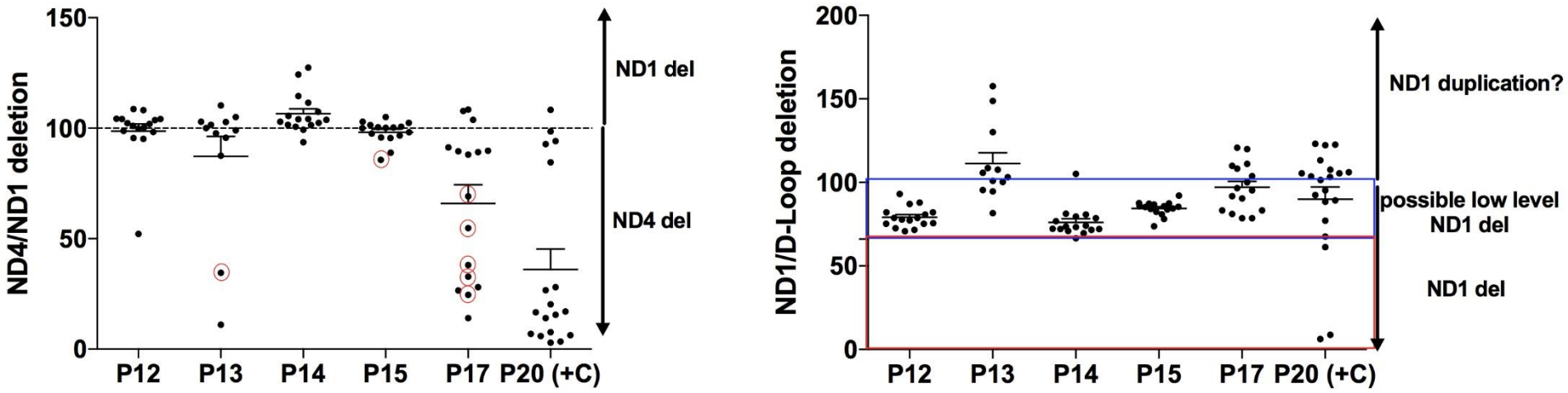

Figure 4.4 *Real time PCR results for MFM patients P12, P13, P14, P15 and P17. Graphs show ratios of MT-ND4 to MT-ND1 (left) and ND1 to D-Loop (right). Since the D-Loop region is likely to be partially triple stranded quantification of MT-ND1 deletion cannot be exact as such the red box indicates a definite deletion and blue box a potential deletion. In addition, there are a small number of fibres for which MT-ND1 is present in a greater proportion than D-Loop, which could be explained by an MT-ND1 duplication which would not have been detected by long range PCR. The dashed line at 100 (left) represents 0% deletion of MTND4. In both graphs, mean and standard error of the mean (SEM) are plotted for each case. Fibres circled in red (graph left) are those for which a deletion was detected on real time but not long range. Adapted from Vincent et al. (2016a).*

Out of the 120 fibres, on which both long range PCR and real time PCR were completed, a deletion was found by both methods in five fibres. A further seven fibres were shown to have a deletion by real time PCR alone. In these seven fibres, unfortunately no long range product was amplified. Inclusion of the D-loop allowed confirmation that MFM patient fibres did not contain any deletions affecting *MT-ND1* (**Figure 4.4**). This was in agreement with long range PCR.

4.4.2 Immunofluorescent analysis of respiratory chain protein expression

Based on lack of genetic defect and histochemistry results, a quantitative immunofluorescence approach was used to explore the nature of the respiratory chain protein expression further. Quantitative analysis allowed comparison of the protein expression levels of VDAC1, NDUFB8 (complex I) and COX-I (complex IV) in patients and controls.

Immunofluorescent analysis allowed comparison of the myofibrillar myopathy patients to age matched controls and a patient with compound heterozygous *RRM2B* variants. Immunofluorescent images showed a number of complex I, complex IV deficient fibres and combined complex I and IV deficiency as well as fibres with reduced mitochondrial mass (**Figure 4.5**). A summary of results can be found in **Table 4.3** and protein expression profiles for all MFM patients and patient 20 are presented in **Figure 4.6**.

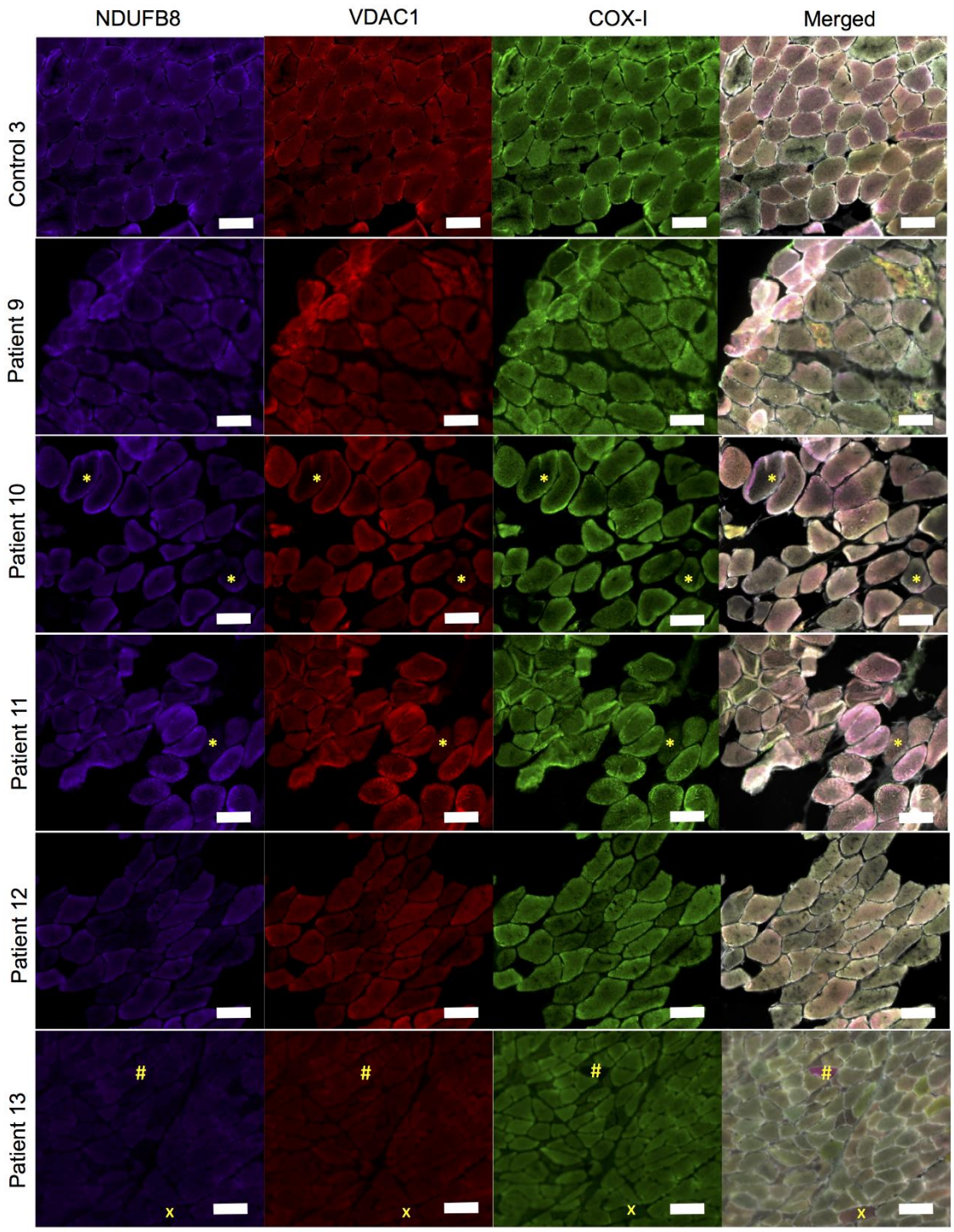
NDUFB8
VDAC1
COX-I
Merged
Control 3
Patient 9
Patient 10
Patient 11
Patient 12
Patient 13

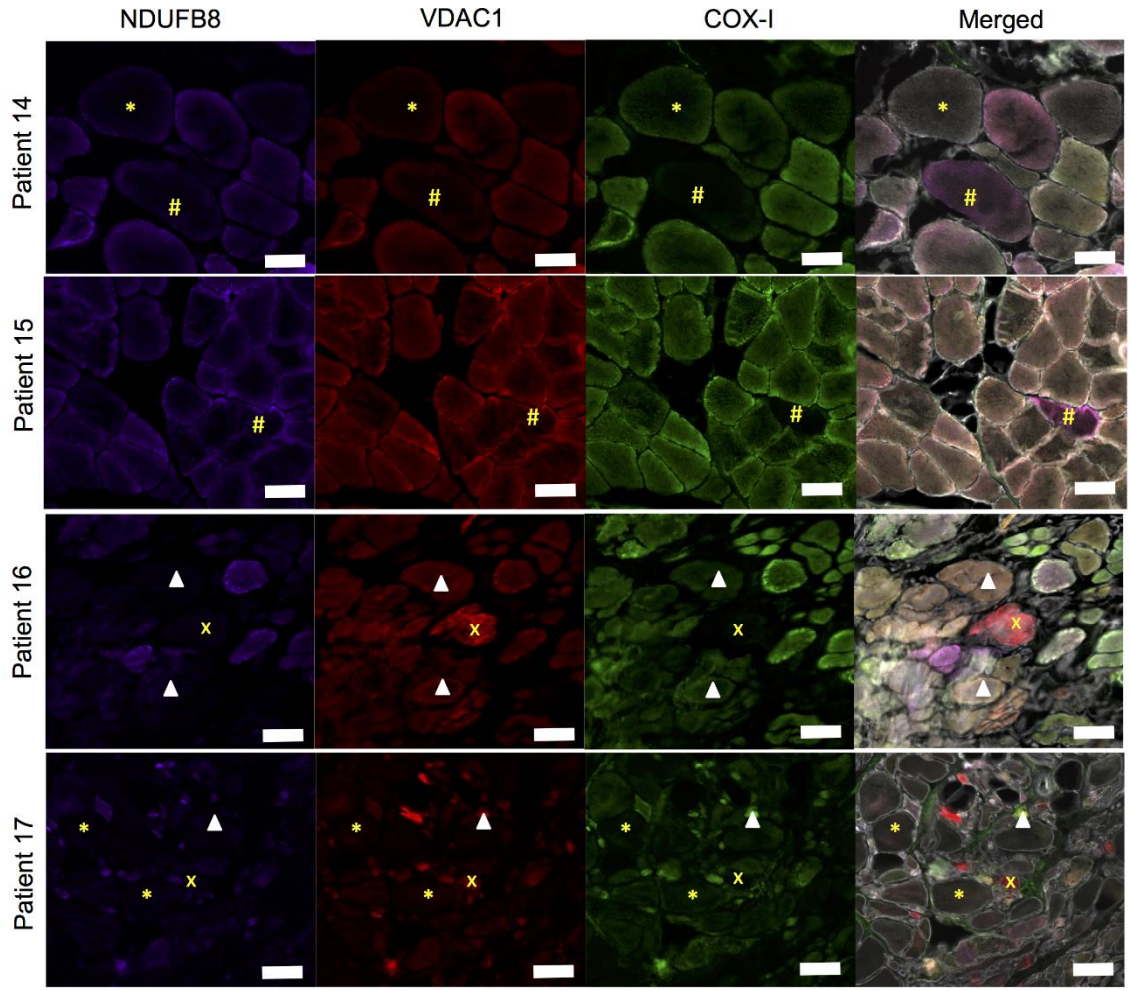

Figure 4.5 *Representative immunofluorescence images for NDUFB8 (complex I), VDAC1 and COX-I (complex IV) in C3 and P9 to P17. Complex I and complex IV deficient fibres, complex IV deficient fibres and complex I deficient fibres can be seen. Most strikingly fibres with low VDAC1, complex I and complex IV can be seen in a number of patients, most pronounced in P17(*). Arrow head; complex I negative, hash; complex IV deficient, cross; complex I and IV deficient, asterisk; low complex I, IV and VDAC1. Scale bar 100 µm. Adapted from Vincent et al. (2016a).*

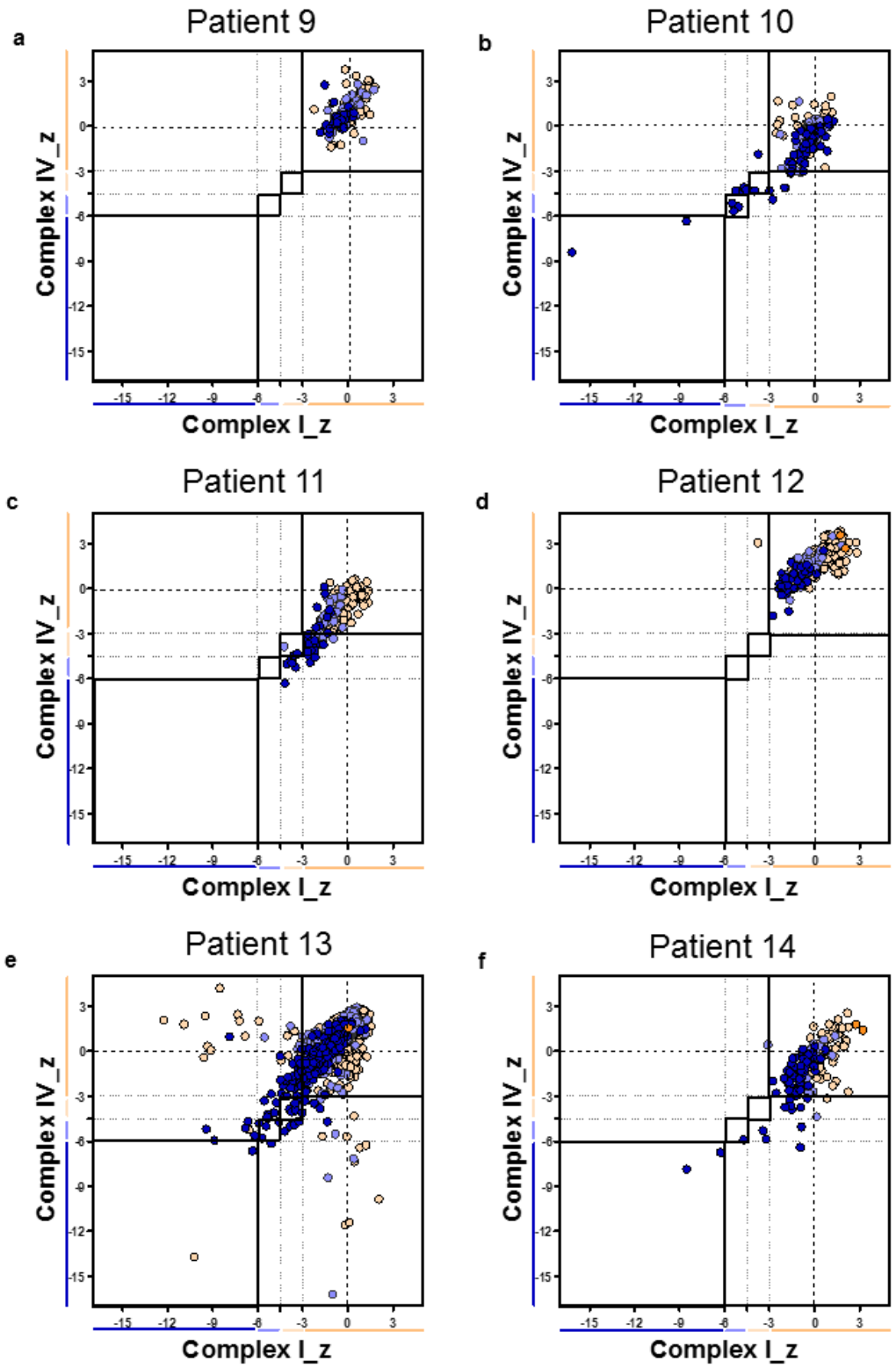
a
Patient 9
Complex IV_z
Complex I_z
b
Patient 10
Complex IV_z
Complex I_z
c
Patient 11
Complex IV_z
Complex I_z
d
Patient 12
Complex IV_z
Complex I_z
e
Patient 13
Complex IV_z
Complex I_z
f
Patient 14
Complex IV_z
Complex I_z

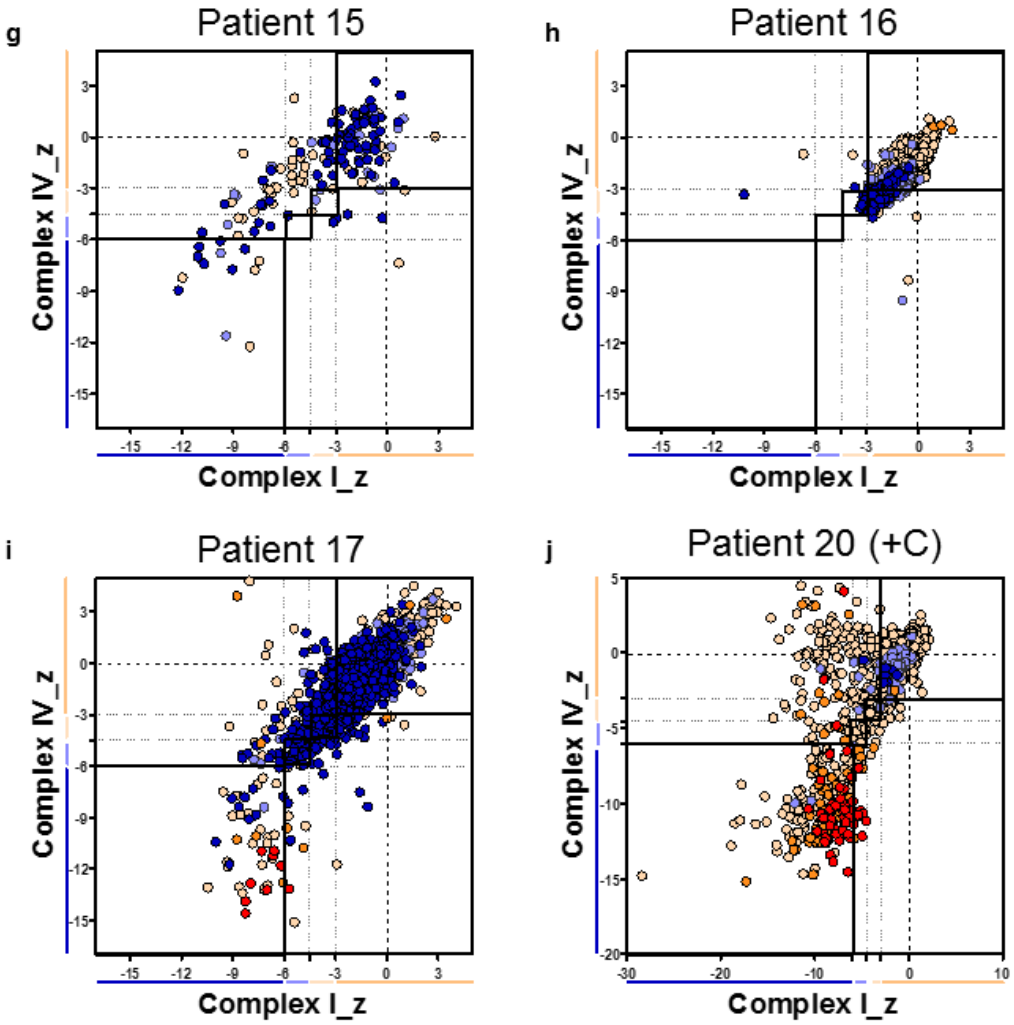

Figure 4.6 *Immunofluorescence results for MFM patients and RRM2B patient positive control. Graphs demonstrate distribution of z-scores for complex I and complex IV with each point colour coded for VDAC1 category. (a) P9, (b) P10, (c) P11, (d) P12 , (e) P13, (f) P14, (g) P15, (h)P16, (i) P17, (j) P20. Each point gives the COX and complex I z-scores for a single fibre and is colour coded to indicate the VDAC1 category of the fibre (very low; dark blue, low; light blue, normal; beige, high; orange or very high; red). Bars next to the X and Y-axes indicate category of COX or complex I levels (dark blue; negative, light blue; intermediate negative, light beige; Intermediate positive and beige; normal.) Additionally solid and dashed lines running vertically and horizontally also mark the boundaries between each category of complex I and complex IV. Adapted from Vincent et al. (2016a).*

Controls 3 and 4 showed no complex I or complex IV deficiency (**Figure *4.6* k and l**). In comparison, desmin patients showed higher levels of complex I and complex IV deficiency (**Figure *4.6* a-f**), reaching 6.5% and 4.2% deficient fibres for complex I and complex IV respectively. The myotilin patients exhibited even higher levels of deficiency, with one patient reaching deficiency of 45.5% for complex I and 24.7% for complex IV. Finally, the *LDB3* patient (P17) had 11.5% complex I deficient fibres and 9% complex IV deficient fibres.

When these patients are compared with the *RRM2B* patient with 32.6% complex I and 23% complex IV deficiency, it is apparent that the patient 15 and 17 in particular exhibit levels of deficiency similar to that of a mitochondrial disease patient.

Patient	Age/years	Complex I negative /%	Complex I deficient /%	Complex IV negative /%	Complex IV deficient/ %	Total fibres analysed
P9	31.2	0.00	0.00	0.00	0.00	111
P10	32.1	0.12	6.48	0.12	3.62	174
P11	33.8	0.00	0.00	0.58	4.18	162
P12	51.3	0.00	0.00	0.00	0.00	224
C3	52.0	0.00	0.00	0.00	0.00	581
P13	53.0	0.79	1.41	0.8	1.63	1883
C4	60.0	0.00	0.73	0.07	0.07	395
P14	60.5	0.18	0.18	0.12	0.44	669
P15	64.3	1.91	2.50	3.52	4.99	149
P16	65.7	38.5	45.51	13.57	24.73	177
P17	69.6	6.43	11.47	5.34	8.96	1348

Table 4.3 *Immunofluorescent analysis of respiratory chain protein expression in MFM patinets. Summary of percentage of fibres classified as complex I and complex IV negative or deficient (negative and intermediate categories). Controls and patients are organised in age order for easy comparison. Adapted from Vincent et al. (2016a).*

4.4.3 Immunofluorescent analysis of mitochondrial mass

MFM patients have between 11% and 51.4% very low VDAC1 fibres. Low and very low VDAC1 fibres are presented by light blue and dark blue circles in the respiratory chain expression profiles in (**Figure 4.6**). There is a significant difference in percentage of normal ($p = 0.03$), low ($p = 0.03$) and very low ($p = 0.04$) VDAC1 fibres between patients and controls.

During the image analysis process, the surface created in Imaris does not cover the full area within the laminin membrane staining. Previous reports and findings presented here suggest core-like depletion of mitochondria in the intermyofibrillar regions and aggregation in the subsarcolemmal regions. If this is the case, it is possible the image analysis process may miss some of the mitochondria, explaining the low VDAC1 fibres. This was tested by analysis across the full diameter of the fibre, using the plot profile function in Zen, described in section **4.4.4**.

4.4.4 Investigating reduction in mitochondrial mass

In order to test whether this is the case the fluorescent signal intensity was analysed across a pool of normal, low and very low VDAC1 fibres. This showed that low and very low VDAC1 fibres have a lower fluorescent intensity across the full width of the fibre (**Figure 4.7**).

To validate mitochondrial mass reduction, sections were labelled for VDAC1 and SDHA, a subunit of complex II, which is nuclearly encoded and therefore a good marker of mitochondrial mass. When SDHA is linearly regressed against VDAC1, the r^2 values suggest a strong positive relationship in the cases with the largest range of VDAC1 and SDHA levels. For those cases with a smaller range the relationship was still apparent but the r^2 value was smaller due to the spread of the data points. This indicates that mitochondrial mass is reduced in a higher percentage of myofibrillar myopathy patient fibres compared to controls (2.6% and 6.4%).

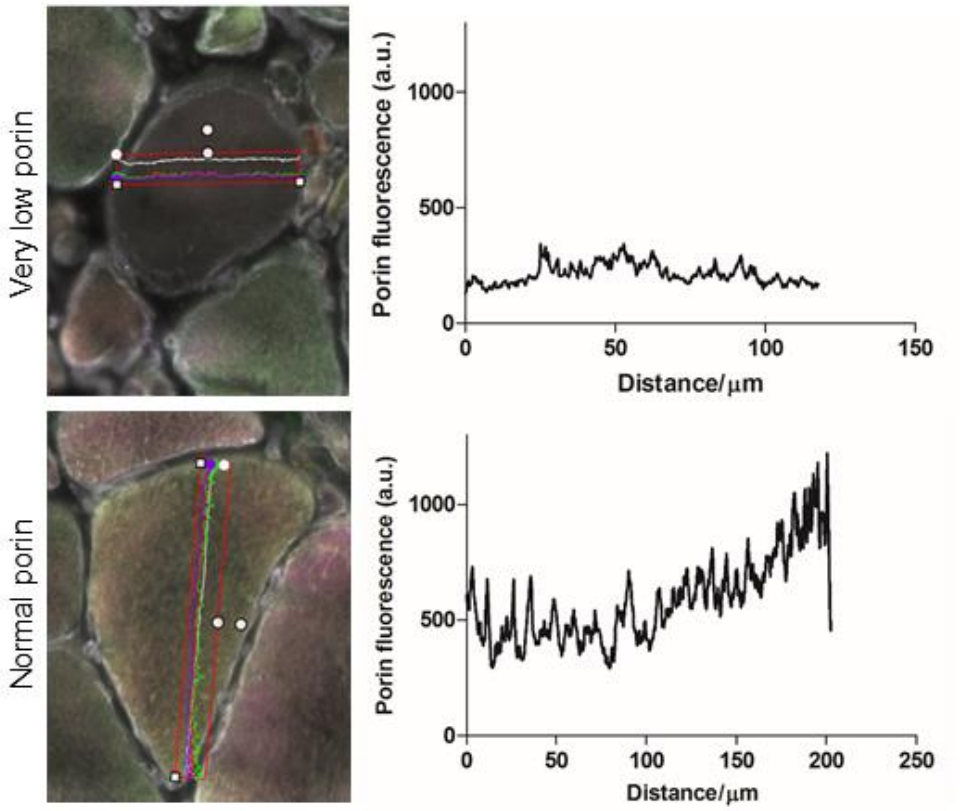

Figure 4.7 *Representative examples of analysis of VDAC1 fluorescent intensity across the myofibres of MFM patients. Indicated that in very low VDAC1 fibres VDAC1 fluorescent intensity is lower across the full fibre. Adapted from Vincent et al. (2016a).*

4.4.5 Relation of respiratory chain deficiencies, mitochondrial mass and fibre size

To determine whether levels of VDAC1, complex I and complex IV could be related to fibre atrophy we compared fluorescent intensity for each channel with fibre area. Correlation was examined using Spearman's rank correlation (src) coefficient (summarised in **Table 4.4**). Regression of myofibre area against complex I level (**Figure 4.8**) demonstrated a positive correlations for patients P13 (src = 0.2600, $p < 0.0001$) and P11 (src = 0.4389, $p = < 0.0001$) but a negative correlation for P14 (src = −0.4817, $p < 0.0001$). For myofibre area and complex IV levels (**Figure 4.9**), only very weak to no correlation was demonstrated. In addition, a negative correlation between myofibre area and VDAC1 level (**Figure 4.10**) for P17 (src = −0.4487, $p < 0.0001$) and P14 (src =

−0.4583, $p < 0.0001$) was noted. Spearman's rank correlations were also significant for P10, P13, P14, P15 and P16; it should be noted however, the correlation between VDAC1 and myofibre area was weak in these patients (**Table 4.4**). VDAC1 level plotted against myofibre area, for patient P17, in particular, shows that large myofibres all have a low VDAC1 level whilst smaller myofibres have a range of high to low VDAC1. Low Spearman's rank correlations in some patients appear to be due to the smaller range of fibre area.

Patient	VDAC1		Complex I		Complex IV	
	src	p value	src	p value	src	p value
P9	-0.0564	0.5546	0.1389	0.144	0.09819	0.303
P10	-0.2492	0.0009	0.1161	0.1261	-0.1738	0.0214
P11	0.3776	< 0.0001	0.4389	< 0.0001	0.2808	0.0003
P12	0.06009	0.3707	0.1249	0.0619	0.05067	0.4504
P13	-0.1733	< 0.0001	0.2600	< 0.0001	0.2933	< 0.0001
P14	-0.4583	< 0.0001	-0.4817	< 0.0001	-0.3073	0.0001
P15	-0.2093	< 0.0001	-0.09169	0.0187	-0.2006	< 0.0001
P16	0.1302	0.1064	0.2428	0.0023	0.0483	0.5506
P17	-0.4487	< 0.0001	-0.1716	< 0.0001	-0.1634	< 0.0001

Table 4.4 *Analysis of myofibre area and respiratory chain expression profiles in MFM patients. Summary of Spearman's rank correlation (src) analysis of myofibre area against levels of VDAC1, complex I and complex IV. Adapted from Vincent et al. (2016a).*

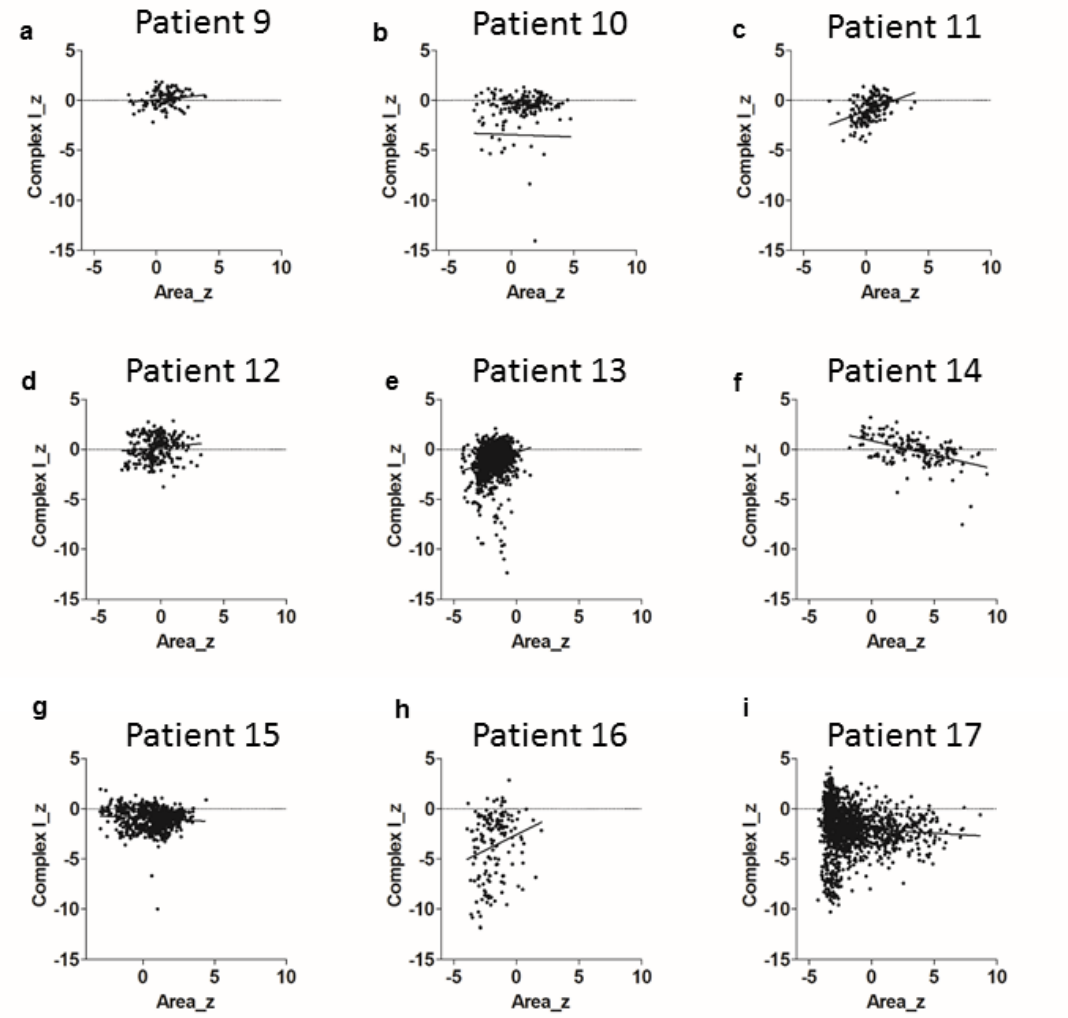

Figure 4.8 *Complex I z score (Complex I_z) against fibre area z score (Area_z) for: (a) P9, (b) P10, (c) P11, (d) P12, (e) P13, (f) P14, (g) P15, (h) P16 and (i) P17. Spearman rank correlation and p values in Table 4. Adapted from Vincent et al. (2016a).*

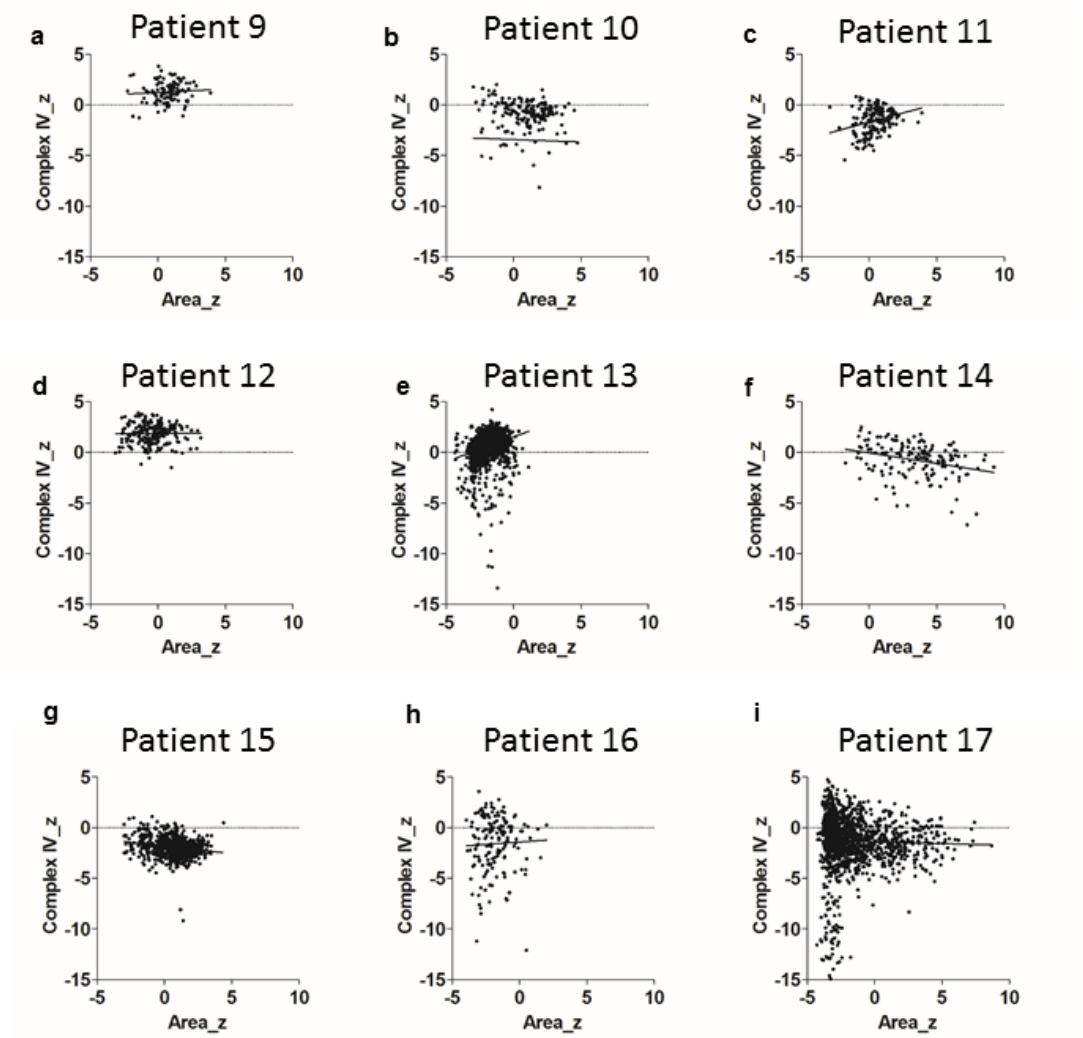

Figure 4.9. *Plots of Complex IV z score (Complex IV_z) against fibre area z score (Area_z) for: (a) P9, (b) P10, (c) P11, (d) P12, (e) P13, (f) P14, (g) P15, (h) P16 and (i) P17. Spearman rank correlation and p values in Table 4. Adapted from Vincent et al. (2016a).*

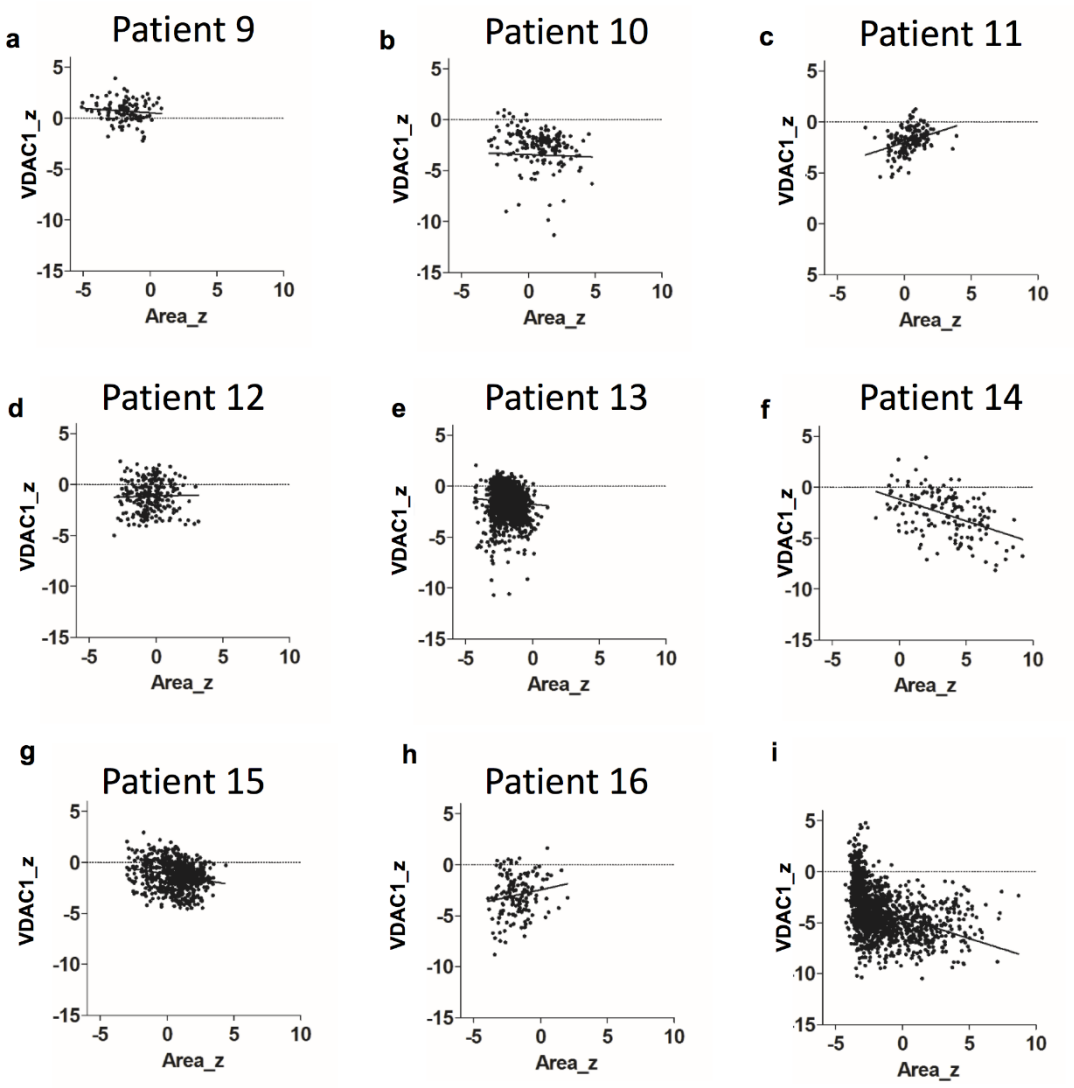

Figure 4.10 *VDAC1 z score (VDAC1_z) against fibre area z score (Area_z) for: (a) P9, (b) P10, (c) P11, (d) P12, (e) P13, (f) P14, (g) P15, (h) P16 and (i) P17. Spearman rank correlation and p values in Table 4. Adapted from Vincent et al. (2016a).*

4.4.6 Analysis of low mitochondrial mass and protein aggregates:

As the hallmark of myofibrillar myopathy, aggregates may be mechanistically linked to the low VDAC1 fibres. Analysis of sections co-stained with antibodies for myotilin, desmin, VDAC1 and laminin demonstrated a similar percentage of low and very low VDAC1 fibres relative to controls as previously shown. Very low and low VDAC1 fibres were analysed for the presence of myotilin and

desmin aggregates. This analysis demonstrates no significant relationship between presence of protein aggregates and mitochondrial mass (**Figure 4.11**)**.** Furthermore, in fibres with aggregates in patient 7 (the patient with the highest percentage of low VDAC1 fibres), only 22.9 % had very low mitochondrial mass. Throughout the analysis however, it became apparent that in cases where large aggregates are present, there is a lack of VDAC1 and therefore reduction of mitochondrial mass. Mitochondria are accumulated in the subsarcolemmal regions or other myofibrillar regions of the fibres, which agrees with previous studies using electron microscopy.

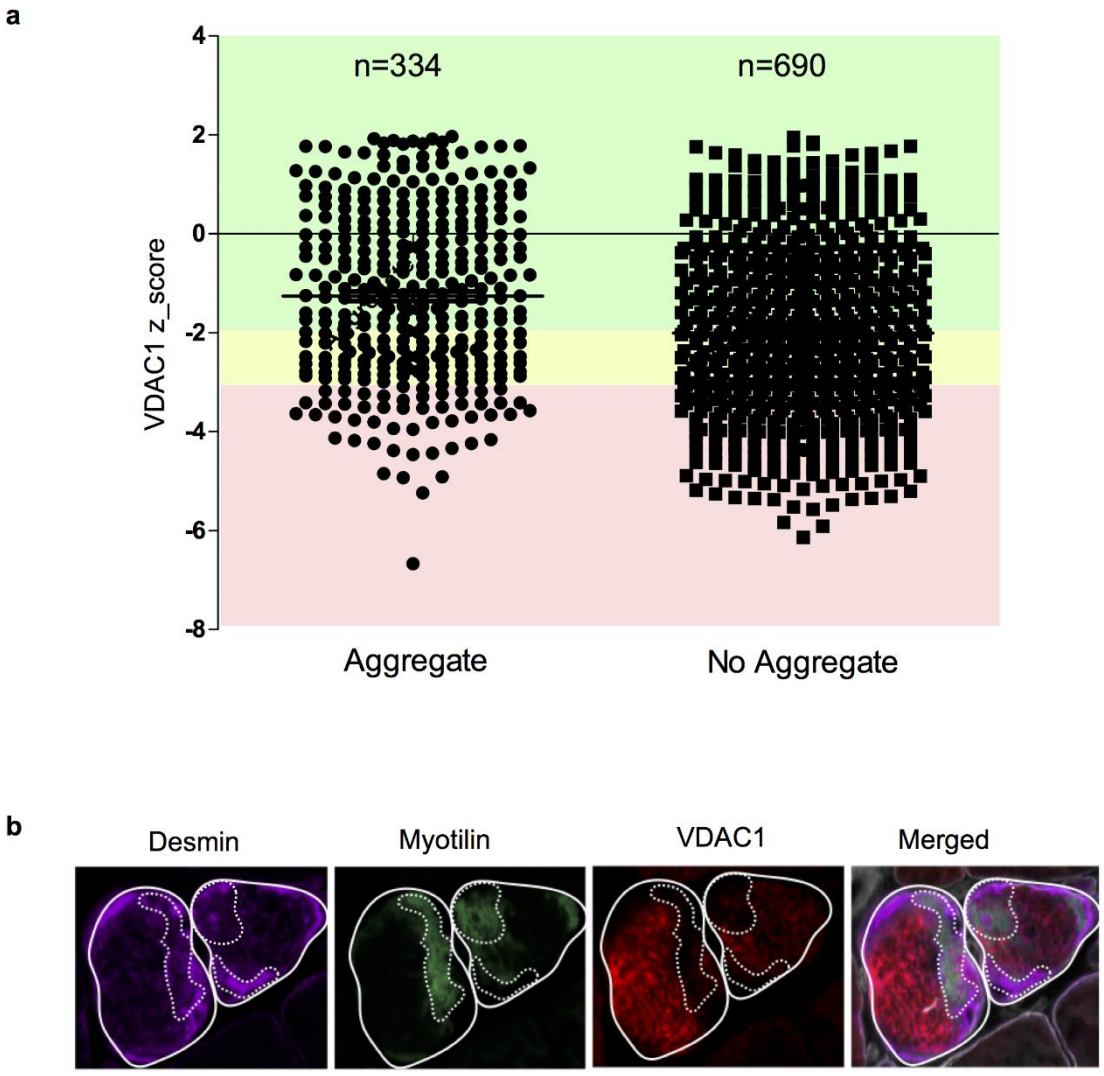

Figure 4.11 *Immunofluorescent analysis of mitochondrial mass and MFM aggregates. P17 as a representative example of analysis of desmin and myotilin protein aggregation and mitochondrial mass. (a) P17 fibres classified as very low (pink), low (yellow) or normal (green) VDAC1 fibres analysed for presence of aggregates. No clear relationship detected. Very low VDAC1 fibres accounted for 22.9% of all fibres with aggregates. (b) Immunofluorescent images from P17 showing individual channel images (desmin, myotilin, VDAC1) and merged. The staining demonstrates a lack of VDAC1 in regions with large aggregates (regions within dashed lines). Adapted from Vincent et al. (2016a).*

4.5 Discussion

Skeletal muscle from patients with myofibrillar myopathy has previously been shown to accumulate mitochondrial respiratory chain deficiency (Schroder *et al.*, 2003; Dold *et al.*, 2012; Henderson *et al.*, 2013) and clonally-expanded mtDNA deletions (Dold *et al.*, 2012; Joshi *et al.*, 2014) and show changes in mitochondrial positioning (Claeys *et al.*, 2008). It could be hypothesised that, the mutation of *DES* or other MFM causative genes, which cause protein aggregates containing desmin protein, may result in the mislocalisation of mitochondria within skeletal muscle. As such, the aim of this investigation was to examine a cohort of myofibrillar myopathy patients for the presence of mitochondrial dysfunction and attempt to understand what correlation, if any, this has with disease pathology.

Here, clonally expanded mtDNA deletions are identified in a small number of fibres from MFM patients by both long range PCR and real time PCR. A further seven fibres were found to have deletion real time PCR but failed to amplify a product with long range PCR, a common problem with single cell long range PCR especially if mtDNA content is low as in MFM myofibres. Based on the age of the patients and the propensity for sporadic mtDNA deletions to accumulate with age (McKenzie *et al.*, 2002) it is concluded that these deletions arise, at least in part due to age in addition to disease pathogenesis. In particular patient 17 where the most deletions were detected, is the oldest patient. However, due to the fact that only one *ZASP* patient was investigated, it is difficult to conclude to what extent this is due to genotype or ageing.

In COX-deficient fibres, where no clonally-expanded mtDNA deletion was detected, it is possible that deficiency has arisen due to an mtDNA point mutation or mtDNA depletion, both of which can cause respiratory chain deficiency. Evidence from immunofluorescence would suggest it is more likely to be mtDNA depletion since mitochondrial mass is reduced. Copy number comparison between COX positive and COX negative fibres would be required to test this. It should be noted, that based on COX/SDH and immunofluorescent analysis COX-deficient fibres are less frequent than those with reduced mitochondrial mass. Both quantification of mtDNA copy number and deep

sequencing would be a valuable addition to this work to assess these possibilities.

Immunofluorescent analysis demonstrated a higher percentage of complex I and complex IV deficiency than would be expected in age matched controls for four out of six desmin patients one of two MYOT patients (P15) and a ZASP patient (P17). More interestingly, VDAC1 is often reduced in a significantly high percentage of fibres relative to controls in all patients, indicating a reduction in mitochondrial mass. This reduction in mitochondrial mass may simply be due to the depletion of mitochondria in the intermyofibrillar space and aggregation in the subsarcolemmal space, as previously described in myofibrillar myopathy patients (Schroder *et al.*, 2003; Claeys *et al.*, 2008; Henderson *et al.*, 2013). Careful analysis of low VDAC1 fibres, for labelling intensity across the fibre to assess if this is in fact an artefact of the method, revealed that this is not the case. Furthermore, there is no correlation between the presence of desmin and myotilin protein aggregates and the reduction in VDAC1. This is in agreement with recent work by Winter *et al.* (2016), who reported that presence of 'rubbed out' or core-like areas are independent of protein aggregates. Throughout the analysis however, it was noted that in some fibres where large protein aggregates are present mitochondria are depleted in this area (**Figure 4.11b**), which may explain the core-like findings on COX/SDH histochemistry. These fibres also show an accumulation of subsarcolemmal mitochondria, which agrees with previous studies using electron microscopy.

It has been demonstrated that aggregate prone desmin mutations alter Ca^{2+} homeostatic ability, due to a change in mitochondrial positioning further from the sarcoplasmic reticulum (Smolina *et al.*, 2014). Therefore, it may be that aggregate prone mutations in MFM related genes, including *MYOT* and *ZASP* have the same outcome, also leading to increased cytoplasmic Ca^{2+}. An increase in cytoplasmic Ca^{2+} concentration in the neurons, causes an increase in mitochondrial fission and therefore fragmentation of the mitochondrial network (Han *et al.*, 2008). Since, mitochondrial fusion and interaction of the mitochondrial network is necessary for mitochondrial DNA stability and ability to cope with mtDNA mutation (Chen *et al.*, 2010) this might give rise to clonally-expanded mtDNA deletions.

Comparison of complex I and complex IV levels with myofibre cross sectional area yielded mixed relationships, this makes it hard to determine whether complex I and complex IV levels may be linked to myofibre atrophy or hypertrophy. In contrast to this, comparison of myofibre area with mitochondrial mass showed a negative relationship in the majority of patients. This relationship suggests that hypertrophic myofibres with a greater area typically have a lower level of VDAC1 than atrophic fibres with a smaller area which have more variable levels of VDAC1. This seems to indicate that mitochondrial mass is not involved in the process of muscle atrophy but may indicate either a lack of mitochondrial biogenesis or increased mitophagy during myofibre hypertrophy. It seems the most likely explanation is that a lack of mitochondrial biogenesis is responsible for the low levels of VDAC1, leading to a dilution of mitochondrial mass during myofibre hypertrophy. However, further testing would be needed to confirm this.

The low occurrence of clonally-expanded mtDNA deletions, lack of relationship between complex I and IV deficiency and myofibre cross sectional area and between pathological protein aggregates and mitochondrial dysfunction, found here, are very different to previous findings in sporadic inclusion body myositis (IBM). In sporadic IBM, ~50% of COX-deficient fibres were found to have one or more large-scale mtDNA rearrangements (Rygiel *et al.*, 2016). Additionally, inflammatory infiltrates were directly correlated with mitochondrial respiratory chain deficiency and myofibre atrophy (Rygiel *et al.*, 2015b). Therefore, in comparison to sporadic IBM, where it can be concluded that mitochondrial dysfunction is pathologically important, and to mitochondrial myopathies where clear mechanistic links exist between mutations in mtDNA maintenance genes, mtDNA deletions and mitochondrial respiratory chain deficiency, additional work needs to be undertaken to determine the pathological relevance of mitochondrial dysfunction in MFM. Nevertheless, the decrease in mitochondrial mass and weak relationship between mitochondrial mass and myofibre cross sectional area, infers that mitochondrial dysfunction may be both mechanistically and pathologically relevant.

4.5.1 Limitations

In this study fibres were selected for genetic analysis based on sequential COX/SDH histochemistry. This is both subjective and in many MFM patients misleading, as to the level of respiratory chain deficiency. It may have been more informative to subsequently revisit the genetic analysis using quadruple immunofluorescence to assess respiratory chain deficiency and select muscle fibres.

Since the cohort consist of six *DES* patients, two *MYOT* and one *LDB3,* with the MYOT and LDB3 patients being the oldest, it is difficult to differentiate between ageing and genotype as factors affecting levels of mitochondrial respiratory chain deficiency and mtDNA deletions. Furthermore, for the *DES* patients the variability in age and mutations within the gene, with mutations in different domains known to have different effects of protein and disease phenotype, it means it is difficult to make conclusions linking disease pathogenesis to mitochondrial dysfunction.

Due to the fact that all experiments are completed in skeletal muscle cryosections, this work also only examines a static time point. Tissue culture and live cell imaging for patient myoblasts may have been more informative for gaining mechanistic insight into disease pathogenesis and potential relevance of mitochondrial dysfunctions.

4.5.2 Future work

Since it is hypothesised that the reason for reduced mitochondrial mass is a reduction in mitochondrial biogenesis it would be interesting to assess the levels of the proteins involved in the mitochondrial biogenesis pathway (e.g. PGC1α, TFAM, NRF-1 and NRF-2) (Scarpulla, 2011).

Furthermore since mitochondria are likely to be repositioned within the myofibres, Calcium homeostasis and mitochondrial dynamics may be altered. As such, it would be interesting to both examine mitochondrial location, ultrastructure and morphology but also Calcium homeostasis in cultured patient myotubes. Furthermore, culturing myotubes would have allowed a more

dynamic visualisation of mitochondrial morphology and turnover using live cell imaging. Although this was intended for the future of the project, only two *DES* mutant cell lines were obtained, of these cell lines one failed to differentiate, as such these experiments were not completed.

An alternative and better model to assess the effects of Desmin mutants *in vivo* could be crossing a DES mutant mouse such as that used by Winter *et al.* (2016) with the mito-Dendra2 mice (Pham *et al.*, 2012) with photoactivatable mitochondria and live-tissue imaging as performed by Pham *et al.* (2012). This would have been a better model for the in vivo situation since the cytoarchitecture and thus mitochondrial positioning is not full formed until muscle is completely differentiated, as such even differentiated myotubes are far from the *in vivo* organisation.

4.6 Conclusions

In conclusion, this work demonstrates clonally-expanded mtDNA deletions in a small number of single myofibre lysates, similar to previous findings in muscle homogenate DNA from MFM patients. It is further noted that the frequency of these deletions is highest in the oldest patient (P17) with a *LDB3* mutation. Given this and previous work it is concluded that mtDNA deletions likely arise due to the combined effect of sarcopenia and disease pathogenesis. The reason for this conclusion is that the two most severely affected patients are the oldest, however they also have the most severe mitochondrial dysfunction and MFM muscle pathology both of which are reported to be causative of mtDNA deletions. Evidence that myofibrillar myopathies can manifest depletion of mitochondria and respiratory chain deficiency of varying degrees among patients, is also presented. Previous reports show a core-like reduction of mitochondria, which is confirmed here. Such a depletion of mitochondria may be a contributing factor to overall disease pathogenesis and could be linked to hypertrophy of the myofibres.

When taken with previous findings, the involvement of mitochondria in MFM disease pathology still appears to be very heterogeneous and mechanistically unclear. Furthermore, it seems likely that the extent of mitochondrial

involvement is altered depending on the mutation and which gene is affected, whether the mutation is heterozygous or homozygous and the age of the patient. As such, the small scale studies and studies with a large mixture of genotypes, including the work presented here are not sufficient to identify patterns and determine the pathological importance of each of these factors.

Chapter 5. Clonal expansion of mitochondrial DNA deletions

5.1 Introduction:

Clonal expansion is the term used to describe the accumulation of a single mutant species mtDNA to higher levels of heteroplasmy. Eventually, the number of mutant mtDNA molecules will outnumber the number of wild type mtDNA molecules and subsequently exceed the mutational threshold required to cause a biochemical defect (described in more detail in **1.7**). This process is highly relevant to the pathogenesis of both inherited and sporadic mtDNA mutations and equally applicable to both mtDNA deletions and mtDNA point mutations. Furthermore, due to the prevalence of mtDNA mutations in neuromuscular and neurodegenerative diseases, as well as in normal tissue ageing, this is mechanistically-relevant to a variety of disease and non-disease pathologies.

5.1.1 mtDNA deletion formation

Mitochondrial DNA deletions have been proposed to form either during replication or mtDNA repair. The first model proposed that deletions form during replication due to a slip-replication mechanism (Shoffner *et al.*, 1989) (**Figure 5.1**), this model assumes that mtDNA is replicated by the strand-asynchronous mechanism (See **1.5.5**). If a slipped strand were to occur, the light strand would misalign so that the 3’ repeat of the light strand anneals to the 5’ end of the heavy strand, generating a single strand loop which would be susceptible to a single strand break and degradation. Continued replication would generate a wild type molecule from the heavy strand and a deleted molecules from the light strand (Shoffner *et al.*, 1989).

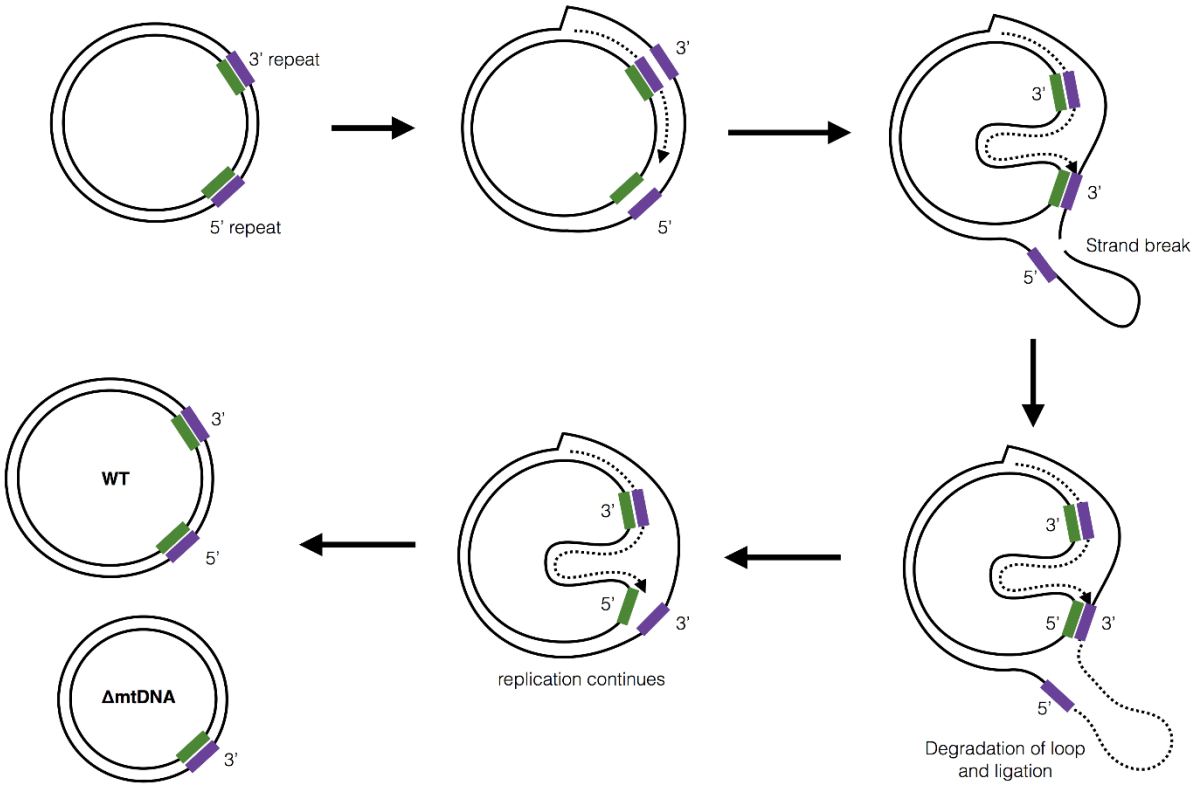

Figure 5.1 *Deletion formation by a slippage replication mechanism. Replication of the 3' repeat occurs after which the displaced 3' repeat misaligns with the 5' repeat. This forms a displaced look and subsequently a strand break. The loop is degraded by endonucleases and the ends ligated before replication continues. This generates a wild type and a deleted mtDNA molecule (ΔmtDNA). Figure based on (Shoffner et al., 1989; Krishnan et al. (2008)).*

However, this necessitates the 3' and 5' repeats coming together to form a single stranded loop that is subsequently degraded when the mtDNA break occurs (Krishnan *et al.*, 2008). Based on this an alternative hypothesis was proposed, that suggests mtDNA deletions are formed during mtDNA repair of double strand breaks, by the annealing of homologous regions created by exonuclease activity at double strand breaks (Krishnan *et al.*, 2008). The problem with this hypothesis is that it only accounts for homology dependent recombination, whereas there are deletions reported, for example in in the substantia nigra (Reeve *et al.*, 2008), which have no repeats.

Findings in a mouse model with an inducible mitochondrially-targeted restriction endonuclease (Fukui and Moraes, 2009) lead to the suggestion that mtDNA deletions

are formed during mtDNA repair of double-strand breaks by both homology-dependent and homology-independent mechanisms. In these mice double-strand breaks were induced in adult neurons and resulted in deleted mtDNA molecules resembling those naturally occurring with age and in neurodegenerative diseases such as Parkinson's disease. The spectrum of mtDNA deletions observed was consistent with a mixture of both homologous recombination and non-homologous end-joining.

5.1.2 Theories of clonal expansion

Mitochondrial DNA deletions and point mutations have been found to accumulate to high levels in ageing and disease. Many theories have been proposed to explain clonal expansion of mtDNA mutations, but to date no one theory explains all of the biological data reported. Wallace (1989), proposed the 'survival of the smallest' hypothesis which suggests that there is a replicative advantage for mtDNA with a larger deletion, since the time taken to replicate the mtDNA is reduced. Thus smaller genomes can replicate faster and out compete the wild type mtDNA to exceed a threshold level (**1.5.10**), within a cell.

However, since this hypothesis was proposed numerous papers have questioned its validity. In particular, this theory only explains clonal expansion of mtDNA deletions and would not fit for point mutations which do not significantly alter the size of the mtDNA molecule and yet are found to clonally expand through-out life. For instance the m.12320A<G mutation was reported to increase from 70 to 90% over a 12 year period in four consecutive muscle biopsies of a patient with isolated mitochondrial myopathy (Weber *et al.*, 1997). Similarly mtDNA point mutations were found to be present in early adulthood at low levels and higher clonally expanded levels and to increase with age (Greaves *et al.*, 2014).

Furthermore, Campbell *et al.* (2014) investigated the possibility of a replicative advantage by analysing mtDNA deletion size and size of respiratory chain deficient segments, as a measure of rate of clonal expansion. By sequencing the breakpoints of 62 small COX-deficient segments and 60 large COX-deficient segments they concluded that no replicative advantage was apparent. Also, recent data looking at

two mtDNA deletions in *Caenorhabditis elegans* finds that both smaller and larger genomes accumulate to similar levels (Gitschlag *et al.*, 2016).

In contrast to these findings, an *in vitro* study of mtDNA repopulation following mtDNA deletion by Diaz *et al.* (2002), found that mitochondria were predominantly repopulated with smaller mtDNA molecules under relaxed copy number control conditions. Furthermore, they demonstrate the hybrid cells containing two mtDNA deletion species tend to retain the smallest genomes. In keeping with these observations, cell lines containing homoplasmic mtDNA deletions also repopulate their mtDNA copy number faster than wild type cell lines (Moraes *et al.*, 1999). However, under tight copy number control which constitutes normal non-selective conditions, a decrease of deleted mtDNA genomes is demonstrated over time, likely due to the faster growth of cells with higher levels of wild type mtDNA. Other studies have also demonstrated that cell doubling time is highest in cells with higher levels of mtDNA deletion (Hayashi *et al.*, 1991). Thus the evidence for or against replicative advantage of deleted mtDNA molecules to date is inconclusive and results are dependent on cellular conditions.

A second hypothesis, often referred to as the “survival of the slowest” hypothesis was proposed by de Grey (1997). This suggested that the mtDNA mutation lowers the respiratory capacity of the mitochondria, resulting in a reduction in damage caused by free radicals. As such these mitochondria are not targeted for mitophagy but instead undergo preferential replication. In comparison, otherwise normal mitochondria produce high levels of ROS leading to damage to the mitochondrial membrane proteins, depolarisation of the IMM and selective degradation (Kim *et al.*, 2007). The main problem with this theory is that it requires mitochondrial respiratory deficiency and therefore only explains the clonal expansion of an already established deletion species.

Both of the above hypotheses suggest a selective advantage of mitochondria containing mutant mtDNA. In contrast to this a third hypothesis, termed ‘random genetic drift’, was proposed by Elson *et al.* (2001) which suggests that no selective advantage is required. This hypothesis is based on the theory of relaxed replication, which describes the regular turnover of mtDNA independently of the nuclear DNA which is replicated with each new cell cycle (Bogenhagen and Clayton, 1977). Elson *et al.* (2001), modelled replication based on replicative dynamics previously

demonstrated (Shadel and Clayton, 1997) and found that relaxed replication is sufficient to explain the clonal expansion of mtDNA deletions. The model demonstrated that clonal expansion to high levels of heteroplasmy, required the vast majority of mtDNA mutation events to occur before 30 years of age with 30% occurring before 15 years of age. Mutation events that happened after this, according to the model, would not have sufficient time to accumulate.

Another study modelled the accumulation of mtDNA mutations in cancerous epithelial stem cell to mutational homoplasmy (Coller *et al.*, 2001). The model assumed that the mtDNA was mutated, replicated and segregated during cell divisions randomly and found that after only 70 generations a mutation can reach homoplasmy.

This is further supported by data from the colon of the mtDNA mutator mouse (Baines *et al.*, 2014), however does not predict the same levels of mitochondrial respiratory chain deficiency and levels of heteroplasmy as observed in human biological ageing data. The model by Elson *et al.* (2001), predicts 4% of post-mitotic cells would be COX-deficient over an 80 year period, however 40% of substantia nigra neurons are found to be COX-deficient at 80 years with up to 90% deletional heteroplasmy (Itoh *et al.*, 1996; Kraytsberg *et al.*, 2006).

Kowald and Kirkwood (2014), proposed another alternative hypothesis which suggested that the driving mechanism is the link between transcription and replication of mtDNA. This was supported by *in silico* data, with these authors proposing that *MT-ND4*, *MT-ND5* and *MT-ND6* are potential candidates for this feedback mechanism. While it is true that these proposed genes are more commonly absent in clonally expanded deletion species, they are not always deleted. Furthermore their increased frequency could simply be due to their location relative to mtDNA mutation hotspots (Damas *et al.*, 2014b), rather than them driving a feedback mechanism. Certainly there are clonally expanded deletions reported via MitoBreak (Damas *et al.*, 2014a), that only affect the minor arc whilst many more reported that only affect the major arc. As such, a single candidate gene that could theoretically provide this feedback mechanism seems unlikely.

Finally, two recent publications have used *C. elegans* as a model organism to investigate the importance of the mitochondrial unfolded protein response (UPR^{mt}) (Gitschlag *et al.*, 2016; Lin *et al.*, 2016) in clonal expansion of mtDNA deletions. Both

papers show that wild type mtDNA copy number is tightly regulated in *C. elegans*, furthermore according to data in both papers, the expansion of mtDNA deletions involves retrograde mito-nuclear signalling to upregulate the UPR^{mt} and increase total mtDNA copy number. Lin *et al.* (2016), demonstrate that activating transcription factor associated with stress-1 (ATFS-1) fails to be imported into depolarised mitochondria and its cytosolic location activates the UPR^{mt}. Although, similar in approach these studies reach different conclusions. Gitschlag *et al.* (2016) present data that shows the UPR^{mt} reduces mitophagy and it is this that allows the mtDNA deletions to accumulate. In contrast, Lin *et al.* (2016) demonstrate that the UPR^{mt} induces mitochondrial biogenesis and promotes mitochondrial fission and fusion. Although the UPR^{mt} has not been characterised in humans and to date no equivalent to ATFS-1 has been identified, these studies raise questions of whether there is a similar mito-nuclear signalling mechanism in humans.

5.1.3 The proliferative perinuclear niche hypothesis

Based on these data and the previous theories presented above a novel hypothesis to explain the clonal expansion of mtDNA deletion in skeletal muscle was proposed and termed the ‘proliferative perinuclear niche’ hypothesis. The mtDNA would need to be actively replicating in order for the mtDNA deletions to clonally expand a process which requires nuclear encoded replication machinery. As such the perinuclear niche hypothesis proposes that the initial events of clonal expansion would be perinuclear. This further makes sense if we consider previous data which suggests that mitochondria closest to the nuclei are replicating faster (Davis and Clayton, 1996), that signaling is limited by diffusion distance and that mechanisms previously reported in *C. elegans* involve retrograde signaling to changes in mitochondrial biogenesis, mitophagy and mitochondrial dynamics (Gitschlag *et al.*, 2016; Lin *et al.*, 2016). Furthermore, it was hypothesised that in a tissue with the highly organised cytoskeletal such as the skeletal muscle, limited mitochondrial movement should make the initial events of clonal expansion easily traceable.

5.2 Aims of this investigation:

This investigation aimed to; identify the smallest region of COX deficiency and thus the earliest visible signs of clonal expansion in skeletal muscle. Subsequently, the investigation was intended to characterise the frequency at which they occur, the level of mtDNA deletion in regions of focal COX-deficiency relative to the remainder of the fibre and the effect of mitochondrial morphology on the spread of mtDNA deletions through the myofibre.

5.3 Methodology:

5.3.1 Patient cohort

Muscle biopsies from patients with single, large-scale mtDNA deletions and inclusion body myositis (IBM) were selected from large cohorts of recently diagnosed patients, by screening for good muscle morphology and a reasonable degree of COX deficiency (>5%). Patients with multiple mtDNA deletions were similarly selected from a larger cohort of cases with confirmed genetic diagnoses. Cases included those with inherited variants in *TWNK*, *RRM2B* and *POLG* genes. Normal human ageing samples were obtained from the Hertfordshire cohort, these samples were used to screen for the presence of COX negative foci in a non-quantiative manner, to assess if these were observed in aged samples also. Relevant patient information is detailed in **Table 2.9**.

Ethical approval was previously granted by the Newcastle and North Tyneside Local Research Ethics Committees (reference 2002/205) and is now approved under Newcastle and North Tyneside Local Research Ethics Committees (reference 16NE/0267). Prior informed consent was obtained from each participant. All experiments were carried out in accordance with the approved guidelines.

5.3.2 Sequential COX/SDH histochemistry

Cryosections (10 µm) were treated for sequential COX/SDH histochemistry as described in **2.8.4** for initial screening of foci and stereological assessment. For

analysis of foci proximity to nuclei, 8 µm serial cryosections were cut to allow reconstruction of myofibres for three dimensional assessment of nuclear proximity. These were treated for COX/SDH histochemistry as described in **2.8.4** and then counter stained with DAPI as described below in **5.3.3**.

5.3.3 Counterstaining of COX/SDH histochemistry or immunofluorescence with DAPI

Counterstaining with DAPI was completed following incubation with SDH reaction medium and 1x PBS washes for COX/SDH histochemistry and following 1x TBST washes after the final secondary antibody incubation for immunofluorescence. Sections were washed thoroughly in either 1x PBS (histochemistry) or 1x TBST (immunofluorescence) before counterstaining with DAPI at a concentration of 2 µg/ml in PBS for 5 minutes. Sections were washed again and mounted in ProLong Gold.

5.3.4 Immunofluorescence for quantitative analysis of foci

This experiment was completed in collaboration with Hannah Rosa with both parties contributing equally (Hannah Rosa completed the immunofluorescent staining, we both imaged the sections and stitched the images and I performed the image analysis).

Serial cryosections (8 µm) were obtained from patient 24 with *POLG* variants. The first and last section were treated as no primary controls with 16 serial section in the middle treated for full immunofluorescence. Sections were treated for immunofluorescence as described in **2.9.1** using anti-MTCOI (1:100), anti-SDHA (1:100) and anti-laminin (1:50) primary antibodies and anti-mouse IgG_{2a} Alexa Fluor 488 (1:200), biotinylated anti-mouse IgG1 (1:200), anti-rabbit Alexa Fluor 405 (1:200) and Streptavidin conjugated Alexa Fluor 647 (1:100). No primary controls were labelled with anti-laminin as the only primary antibody and all secondary antibodies. Imaging was completed as described in **2.9.3**. Images were stitched before analysis using the profile function in Zen (Blue edition) to plot fluorescent intensity across the myofibre.

5.3.5 Stereology

Cryosectioned skeletal muscle from patients with large scale single mtDNA deletions (n = 5), IBM (n = 4) and multiple mtDNA deletions (n = 7) were reacted for COX/SDH histochemistry (performed by Gavin Falkous, Dr Karolina Rygiel and Dr Georgia Cambell, respectively). Prior to assessment both investigators assessed one section together and agreed on assessment criteria. It was decided that all fibres that were not fully COX-negative (blue) (**Figure 5.2**) or containing foci, would be classified as "other" (**Figure 5.2**). In order for a fibre to be classified as containing a foci it had to have a small clearly defined foci of COX deficiency with the remainder of the fibre being COX-positive (**Figure 5.2**). Finally, the remainder of the fibres which were classified as COX-positive were counted to give a total number of fibres assessed. The methodology was designed to capture only the earliest events of COX deficiency and subsequently allow us to compare frequency of these to fully deficient fibres to infer how quickly COX deficiency spreads from the foci across the full myofibre. Counts were made in Stereo investigator using the meander scan function and using an Olympus BX51 Stereology microscope. It was agreed that I would assess each section first, defining a region using the meander scan function in Stereo investigator and capturing an image of the annotated region. The annotated image was then used by Hannah Rosa to assess the same region independently.

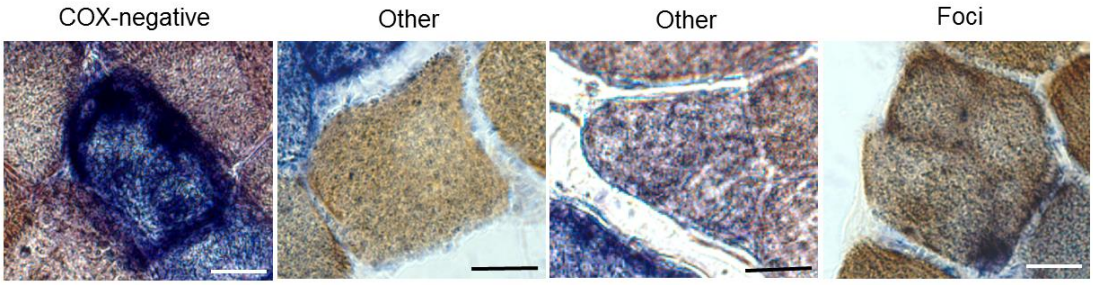

Figure 5.2 *Guide to classification of fibres by stereology for the purpose of assessing the frequency of full COX-negative muscle fibres and muscle fibres with early stage focal COX deficiency.*

5.3.6 Laser microdissection and cell lysis for triplex real time PCR

Three patients with mtDNA maintenance disorders and multiple mitochondrial deletions were selected for genetic assessment, these patients had variants in *RRM2B* (n = 2, patient 20) and *POLG* (n = 2, patients 22 and 24). Eight serial cryosections (15 µm) were cut and treated for COX/SDH histochemistry as described in section.

Foci from myofibres were laser capture microdissected (**2.10.1**), along with identically sized COX-positive regions from the same myofibre. Full COX-positive and COX-negative fibres were captured for comparison and all samples were captured into Tris-tween-proteinase K lysis buffer (**2.10.2**). Triplex real time PCR with amplicons in the D-Loop (rarely deleted), *MT-ND1* (occasionally deleted) and *MT-ND4* (commonly deleted), was run as described in **2.11.1**. For each plate a standard curve of plasmid p7D1 and at least two fully COX-negative and fully COX-positive fibres were included on each plate. All samples were analyzed in triplicate and each foci were compared to two identically sized regions of the same fibre.

5.3.7 Statistical analysis

For clonal expansion experiments statistical significance was tested using a combination of two-tailed unpaired (whole myofibre) and paired (matched sub-cellular regions) T-tests. Statistical significance was set at 0.05. All analyses were performed

in Prism v7.0 (Graph Pad).

5.4 Results:

5.4.1 Initial screen

An initial screen of previously prepared cryosections that had been treated for COX/SDH histochemistry were surveyed to assess if focal regions of deficiency were present, which may represent the origin of clonally expanded mtDNA deletions and thus COX deficiency. Once identified examination of a variety of biopsies from patients with multiple mtDNA deletions, single large scale mtDNA deletions, IBM, myofibrillar myopathy and aging confirmed that it is a wide spread observation (**Figure 5.3**). In addition, to the frequently reported fully COX-negative (**Figure 5.3b**) and COX-intermediate myofibres observed in both transverse and longitudinally orientated myofibres subsarcolemmal foci of COX-deficiency and fibres with larger segments of COX deficiency in cross section were also observed (**Figure 5.3**).

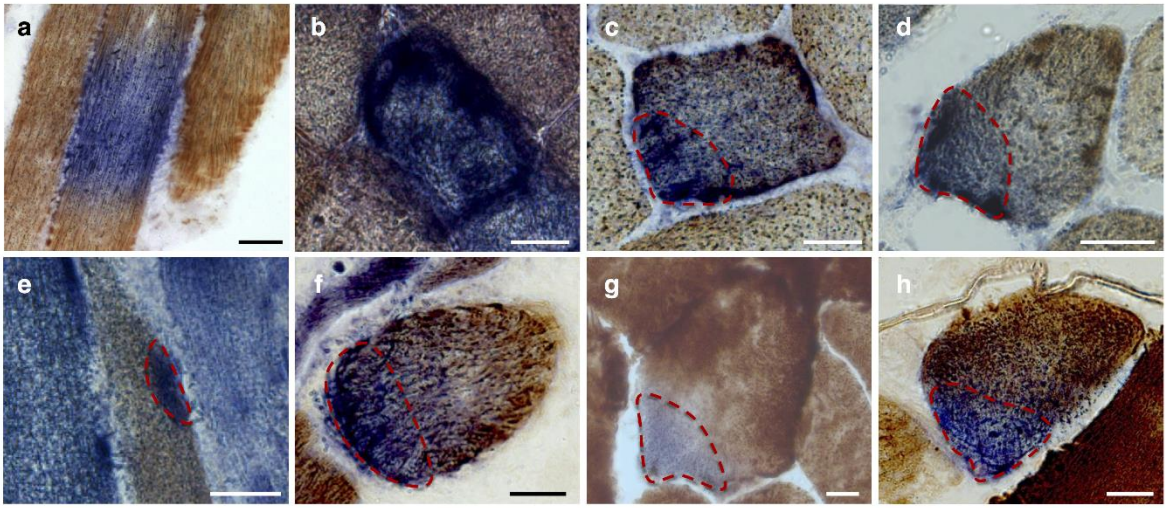

Figure 5.3 *Sequential COX/SDH for the localisation of COX deficiency in human skeletal muscle. (a) Three myofibres in longitudinal orientation from a case of inclusion body myositis (IBM), note segmental COX deficiency in the central fibre. (b) Fully COX-deficient myofibre in transverse orientation. (c) Focal COX deficiency in a case of single, large-scale mtDNA deletion, and (d) multiple mtDNA deletions in transverse orientation. (e) Focal COX deficiency in a case of multiple mtDNA deletions in longitudinal orientation. Note the restricted nature of deficiency. (f) Focal COX deficiency in cross-section from cases of IBM; (g) mechanically-ventilated diaphragm; and (h) normal aging. Examples shown in A and B are commonly observed in both disease and aging, whereas examples shown in C-H (encircled in red dashed line) are rarer. Exact prevalence of myofibres with complete and focal COX deficiency is listed in* ***Table 5.1****. Scale bars, 25 μm.*

5.4.2 Quantifying frequency of focal COX deficiency

Stereological assessment of skeletal muscle biopsies, was performed in order to assess; the frequency of COX-deficient foci, whether the frequency is higher in a specific patient group or with increased percentage COX deficiency of the overall biopsy. Counts were performed by myself and Hannah Rosa and averages are presented in **Table 5.1**. Intra-investigator variability was noted, however, this was mainly due to how we classified fibres with low levels of intermediate deficiency. Of the total fibres analysed (n = 20595, averaging n = 1373 fibres per patient), 47 fibres contained foci and 1644 were COX-deficient. Therefore, on average muscle biopsies contained on average 9.7% (range 0.8 – 30.5%) fully COX-deficient fibres, compared to 0.16% (range 0 – 0.57%) COX-negative foci. This demonstrated the frequency of COX-negative foci to be 1:807 of all myofibres analysed, or 1:64 fully COX-deficient myofibres.

Patient #	Diagnosis	Total counted	% COX negative	% Foci	% Foci / COX negative
P18	multiple mtDNA deletions	469	8.53	0.00	0.00
P19	multiple mtDNA deletions	719	30.48	0.14	0.23
P20	multiple mtDNA deletions	2421	16.20	0.33	2.04
P21	multiple mtDNA deletions	1658	0.78	0.12	15.38
P23	multiple mtDNA deletions	1251	9.52	0.16	1.26
P24	multiple mtDNA deletions	2615	5.66	0.15	2.71
P25	single mtDNA deletion	788	19.16	0.38	1.66
P26	single mtDNA deletion	1364	5.79	0.15	2.55
P27	single mtDNA deletion	1221	8.52	0.08	0.48
P28	single mtDNA deletion	349	12.34	0.57	3.53
P29	single mtDNA deletion	2430	3.29	0.08	1.88
P30	IBM	626	15.02	0.16	1.06
P31	IBM	1319	4.78	0.00	0.00
P32	IBM	1745	4.70	0.06	0.61
P34	IBM	1620	1.05	0.00	0.00
	Average	1373	9.72	0.16	1.43

Table 5.1 *Quantification of cytochrome c oxidase (COX) deficient myofibres and foci in muscle biopsies from; multiple mtDNA deletions (n = 6), single, large-scale mtDNA deletions (n = 5) and inclusion body myositis (IBM) (n = 4). Counts presented here are averages of two investigators (Hannah Rosa and myself).*

5.4.3 Subcellular localization of focal deficiency

Analysis of approximately 94,000 myofibres from 16 skeletal muscle biopsies of patients described in **Chapter 2 Table 2.9**, demonstrated that partial respiratory chain deficiency is always restricted to the subsarcolemmal region of the myofibre and never the centre or intermyofibrillar region (dotted line, **Figure 5.3b-f**). Similar subsarcolemmal deficiency was also identified by Martin Picard in mechanically-ventilated diaphragm where COX deficiency is associated with mtDNA deletions (**Figure 5.3d**) (Picard *et al.*, 2012). In addition to diseased muscle biopsies, muscle of healthy adults 68 - 77 years of age (n = 79, **Figure 5.3h**), were also analysed and confirmed the previously observed pattern of subsarcolemmal focal deficiency. As such it would appear this pattern is conserved across numerous neuromuscular disorders and healthy ageing.

Immunofluorescent labelling of nuclear encoded SDHA and mtDNA encoded MTCOI further confirmed this pattern (**Figure 5.4a**). More interestingly, when serial sections reacted for COX/SDH histochemistry and immunofluorescence were counter-stained with DAPI the foci are always associated to a nucleus (**Figure 5.4b and c**). Quantitative assessment of fluorescently stained sections demonstrated that 97% of all identified foci contained a nucleus within the foci either on the same section or on a serial section. **Figure 5.4d** shows a COX deficiency surface map which allowed visualisation of level of focal deficiency in **Figure 5.4a**. Using electron microscopy we found close proximity of mitochondria to the nuclear pores facilitating mito-nuclear signaling (**Figure 5.4e**), furthermore close proximity to capillaries providing nutrients and oxygen for mitochondrial biogenesis was also observed (**Figure 5.4f**).

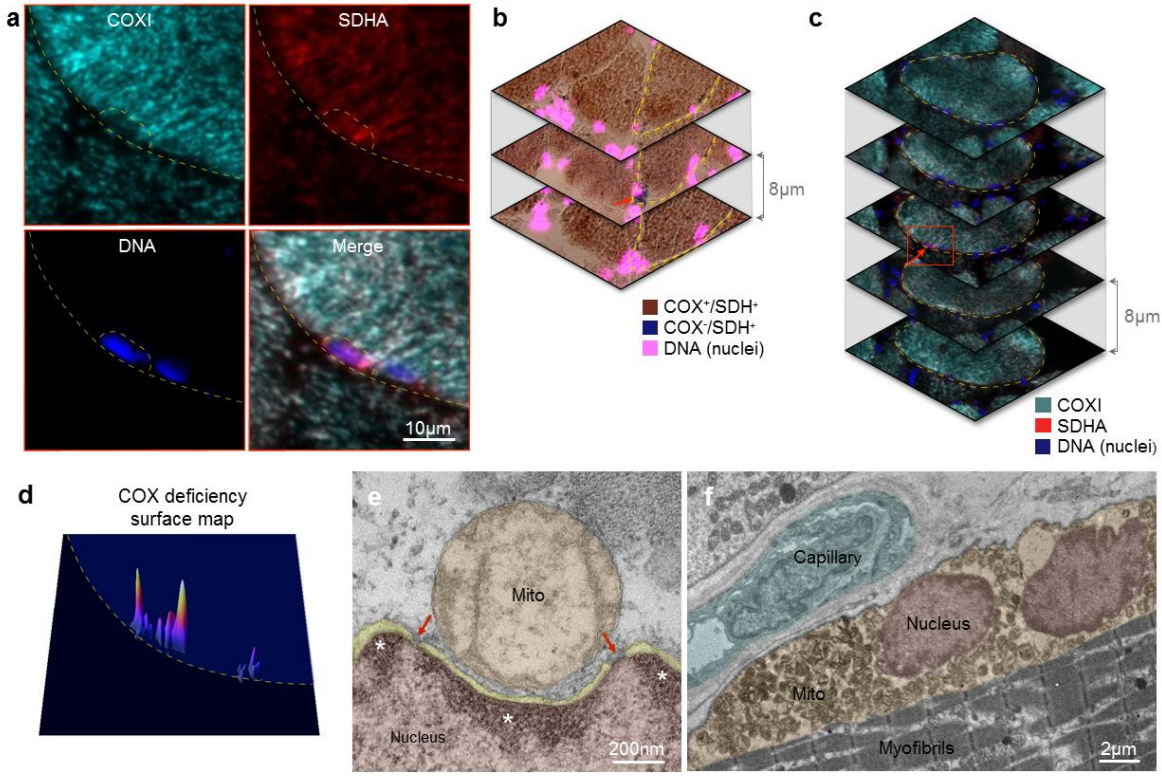

Figure 5.4 *Foci of respiratory chain deficient mitochondria are located in the subsarcolemmal region and colocalise with nuclei. (a) Magnified area showing selective absence of MTCOI staining in the perinuclear niche area outlined. (b) Serial cryosections reacted for sequential COX/SDH histochemistry and DAPI. Note the foci of COX deficiency in the outlined cell restricted to the middle section (red arrow), indicating that the foci is less than 8µm in length. (c) Serial cryosections labelled by triple immunofluorescence for MTCOI, SDHA, and DAPI for nuclei, showing focal COX deficiency restricted to the middle section (red arrow). (d) Intensity profile for [1/(MTCOI/SDHA)] ratio for the myofibre region shown in (a) (created by Martin Picard). Regions of high COX deficiency are marked by high peaks of red, orange and yellow and no deficiency shows no peak. (e) Pseudocoloured transmission electron micrograph (TEM) showing a mitochondrion in close proximity to nuclear pores within the nuclear envelope (arrows), representing a window onto the euchromatin and heterochromatin (*) where transcriptional regulation occurs.(f) Pseudocoloured TEM electron micrograph showing subsarcolemmal mitochondria in proximity to a capillary and two nuclei, which provide resources for increased mitochondrial biogenesis. Example from skeletal muscle of m.8344A>G tRNA^{Lys} skeletal muscle.*

5.4.4 Quantitative analysis of COX deficiency across the myofibre

From the immunofluorescently labelled serial sections MTCOI/SDHA intensity profiles were generated to precisely map and quantitatively assess the distribution of complex IV deficiency with sub-cellular resolution. A range of MTCOI deficiency was noted from no deficiency (**Figure 5.5a**), to small foci confined to the perinuclear region (**Figure 5.5b**), to partially deficient (**Figure 5.5c**) to completely deficient (**Figure 5.5d**).

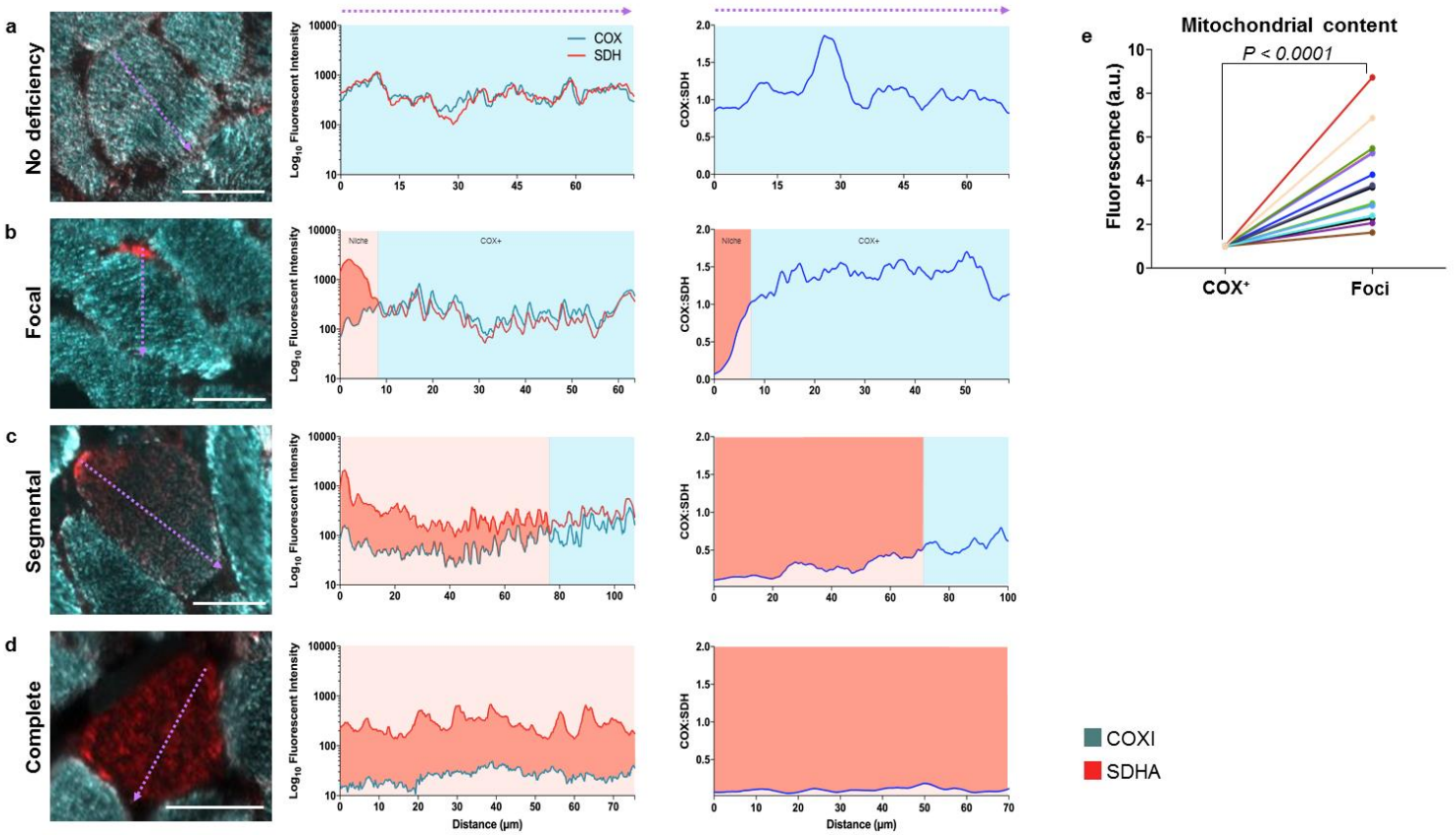

Figure 5.5 *Foci distribution of COX deficiency and mitochondrial content by immunofluorescence in human myofibres. (a) MTCOI and SDHA immunofluorescent labelling and quan*tification of a normal COX-*positive* myo*fibre (left), with fluorescence intensity plotted along the profile denoted by the arrow (middle), and CO*X:SDH ratio (right). (b) Myo*fibre with a niche of focal COX deficiency denoted in red in fluoresce*nce intensity plots. (c) Myo*fibre with segmental COX deficiency spread through approximately 70% of the cell*'s longest diameter. (d) Myo*fibre with complete COX deficiency.(e) Quantification of mitochondrial content based on SDHA fluorescence intensity in COX- foci and in matched COX+ subsarcolemmal r*egions within individual myo*fibres (n = 15, two-tailed paired T test). Data is plotted relative to COX+ regions. Scale bars, 50 µm.*

This pattern would be consistent with spread of mtDNA deletions and respiratory chain deficiency from an initial subsarcolemmal foci across the transvers myofibre. Comparison of SDHA fluorescent intensity in the COX-deficient foci and the COX-positive remainder of the same fibre showed higher SDHA fluorescent intensity in the COX-deficient foci (**Figure 5.5e**). This is consistent with an increase in mitochondrial mass in areas of respiratory chain deficiency and is also comparable to COX-positive and COX-negative fibres.

5.4.5 Quantification of deletion level in COX-deficient foci

Genetic analysis was performed in patients with mtDNA maintenance disorders due to mutations in either *RRM2B* (n = 1) or *POLG* (n = 2) (patients 6.3, 6.5 and 6.7). Laser microdissection of COX-deficient foci and equivalently sized regions of the remainder of the fibre (**Figure 5.6a**) were compared to assess whether the focal deficiency observed, was due to a higher mtDNA deletion level in the focal region of deficiency than observed in the COX-positive portion of the fibre.

As expected triplex real time PCR showed that the majority of COX-deficient foci contained *MT-ND4* deletions with a smaller proportion also containing *MT-ND1* deletions. In comparison the COX-positive regions of the same fibre contained either no mtDNA deletion or lower levels of deletion (**Figure 5.6b**). On average deletion level (as assessed by *MT-ND4/MT-ND1* relative abundance) was significantly higher in COX-deficient foci than in the corresponding COX-positive regions (**Figure 5.6c**). When this is compared to COX positive and negative fibres analysed here and previously the deletion pattern is comparable (**Figure 5.6d**).

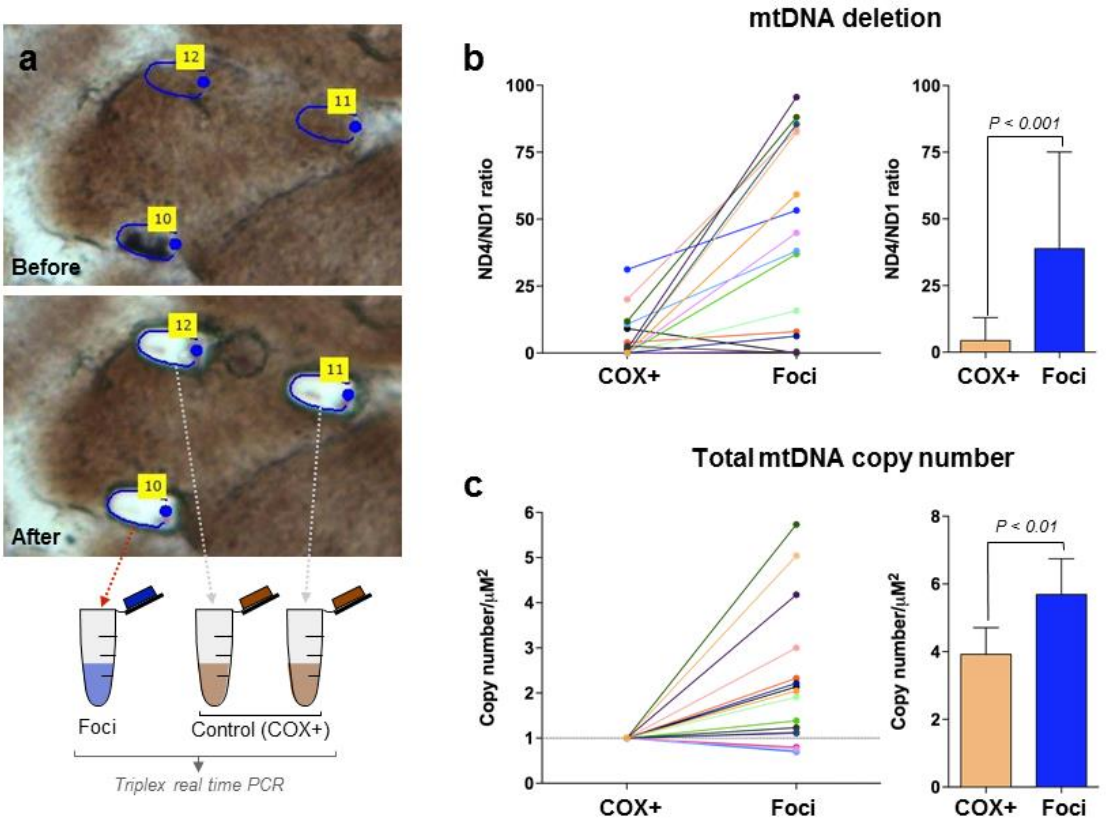

Figure 5.6 *Deletion level is higher in COX-negative foci than the COX-positive region of the same fibre. (a) Fibre before and after laser microdissection of COX- and two COX+ control regions. (b) MT-ND4/MT-ND1 as an indicator of deletion level in COX- foci and matched sub-cellular regions from single fibres. Matched sub-cellular regions are connected by a line and colour-coded with the same scheme. (c) Averages of data from (b), data are means ± SEM. Three patients, n=18, two-tailed paired T-tests. (d) MT-ND4/MT-ND4 in COX+ and COX- fibres. Each data point corresponds to a single fibre. Bars indicate mean values. Data points represent single fibres (n = 22, 3 patients, two-tailed T tests).*

5.4.6 Quantification of mtDNA copy number

Quantification of mtDNA copy number was completed using an optimised standard curve method (Rygiel *et al.*, 2015a) for quantification of absolute copy number of the real time PCR D-Loop amplicon, since *MT-ND1* and *MT-ND4* are both found to be deleted in some samples. As expected, mtDNA copy number was increased in the majority of foci, with some foci showing a greater than three-fold increase in mtDNA copy number when compared to COX-positive regions of the same fibre (**Figure 5.7a**). COX negative foci relative to COX positive regions shows a mean 1.8-fold (range 1.1 - 5.7, $P < 0.001$) higher mtDNA copy number (**Figure 5.7b**). In comparison, COX-negative fibres have a 1.4-fold (range 1.0 - 4.3, $P = 0.03$) higher mtDNA copy number than COX-positive fibres (**Figure 5.7c**). When taken in conjunction with the increased SDHA protein level (patient 24, ***Figure 5.5*e**), this implies increased mitochondrial biogenesis in both the focal regions of COX-deficiency and fully COX-deficient fibres.

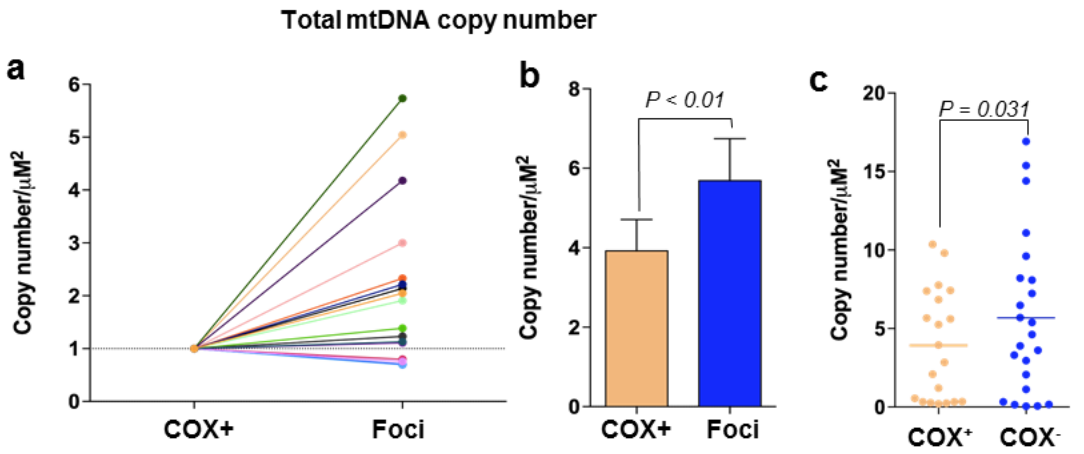

Figure 5.7 *Total mtDNA copy number is increased in foci. (a) Total mtDNA copy number in COX- foci and matched sub-cellular regions from single fibres. Matched sub-cellular regions are connected by a line and colour-coded with the same scheme. (b) Averages of fibres presented in (a), data are means ± SEM, 3 patients, n=18, two-tailed T-test. (c) Total mtDNA copy number in COX+ and COX- fibres. Each data point corresponds to a single fibre. Bars indicate mean values. Data points represent single fibres (n = 22, 3 patients, two-tailed T test).*

5.4.7 Assessing direction of spreading of respiratory chain deficiency

COX/SDH histochemistry and mitochondrial morphology as assessed by electron microscopy suggest that mtDNA deletions and respiratory chain deficiency are likely to spread quicker across the transverse plane of a myofibre than along the longitudinal. If this is the case we see segmental COX deficiency as in the mitochondrial network model rather than the shape created in a random spread model where deficiency spreads equally in both directions (**Figure 5.8a**). This is supported by the number of small segments if COX deficiency observed in the longitudinal myofibres (**Figure 5.8b**). In the fibres shown the aspect ratio (length y / width z) is 2 – 2.5, indicating that spread in the transverse plane is at least twice as high. Furthermore, electron microscopy of mitochondria in the transverse and longitudinal planes shows increased mitochondrial network connectivity in the transvers plane (**Figure 5.8c and d**). This is explored further and quantitatively assessed in **Chapter 7**.

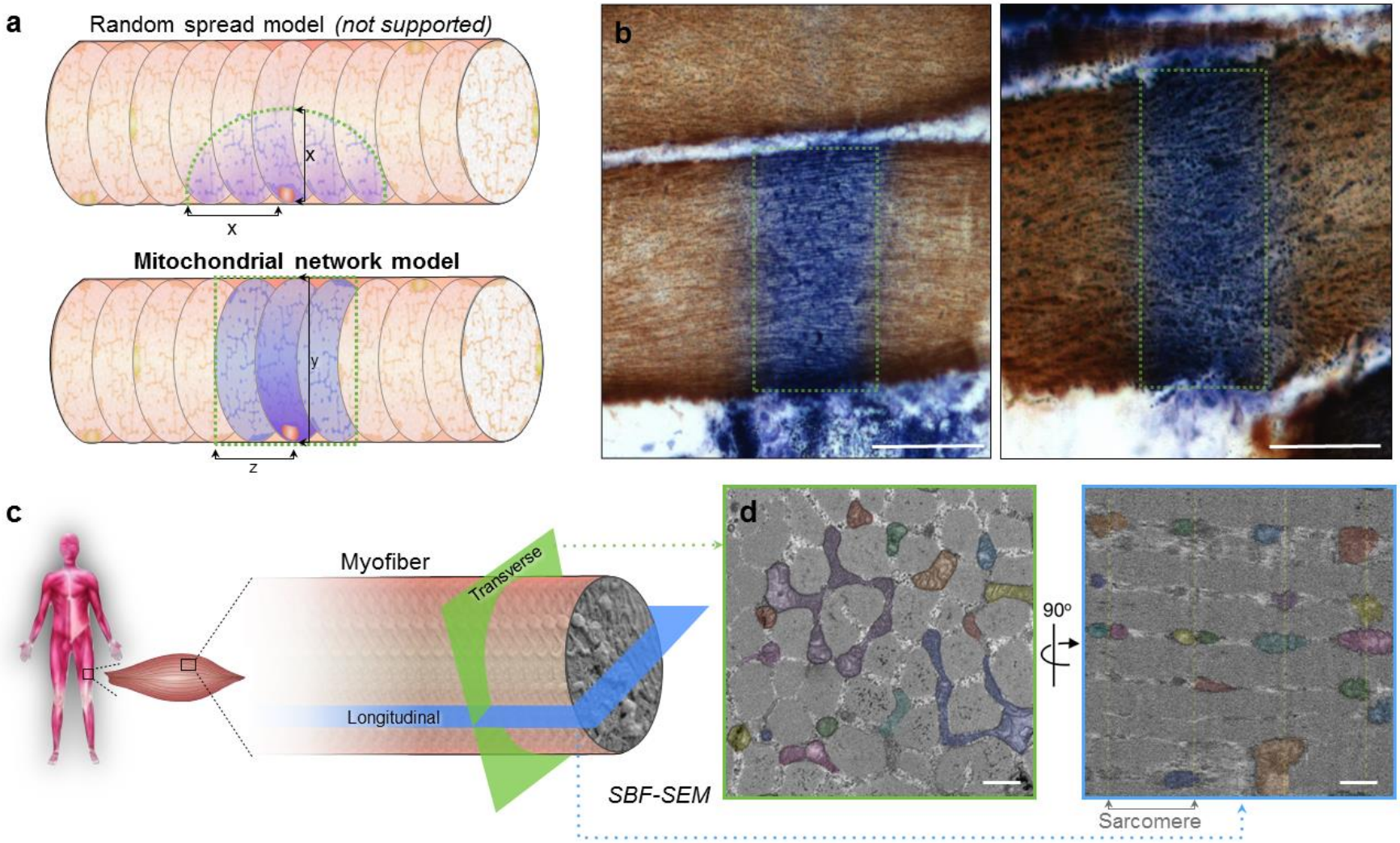
a
Random spread model (not supported)
x
x
Mitochondrial network model
y
z
b
c
Myofiber
Transverse
Longitudinal
SBF-SEM
d
90°
Sarcomere

***Figure* 5.8** *Skeletal muscle anisotropy in mitochondrial network connectivity. (a) Hypothetical models illustrating potential distributions of COX- niches at early stage of clonal expansion. In the random spread model (top), biochemical deficiency covers an equal distance (x) in both transverse and longitudinal orientations. In the mitochondrial network model (bottom), biochemical deficiency ca*n cover the width of the myo*fibre, a distance (y) that is greater than the distance covered in the longitudinal axis of the fibre (z). Dotted green boxes denote edges of biochemical deficiency. (b) Images of thin longitudinal regions of COX- segments support the mitochondrial network model. (c) Schematic demonstrating differences in mitochondrial network conne*ctivity when examining a myo*fibre in transverse or longitudinal orientation. (d) Results from serial block face scanning electron microscopy (SBFSEM) showing that in the transverse orientation (green), mitochondria form an interconnected network. In the longitudinal orientation (blue), mitochondria appear round and isolated, with few connections across sarcomeres. Each continuous mitochondrion is pseudocoloured, and Z-lines are denoted by dotted lines. Scale bars histochemistry (b), 50 µm; scale bars electron microscopy (d), 1 µm.*

5.5 Discussion:

Since the late 90s, several theories have been suggested to account for the clonal expansion of mtDNA deletions in post mitotic tissues. However, many of these do not fully explain the biological data and leave several questions unanswered. Some such questions include; i) where do mtDNA deletion originate in the cell? ii) What allows deleted mtDNA to accumulate such that it becomes present in higher levels than wild type mtDNA and is this driven by a selective advantage? iii) Why do we see segmental COX deficiency in longitudinal myofibres, and what dictates the directional spread of respiratory chain deficiency? The aim of this study is to attempt to answer some of these questions.

A combination of in-depth imaging and molecular investigations were performed to investigate human skeletal muscle biopsies across a number of disease conditions as well as ageing. By doing so the work aimed to identify and investigate a conserved principle simultaneously accounting for the origin, expansion, and directional spread of mtDNA deletions within myofibres. It was hypothesised that there is a proliferative perinuclear niche (**Figure 5.9**), where proximity of mtDNA deletions to the nucleus is a key factor which allows retrograde mito-nuclear signalling from respiratory chain-deficient mitochondria to initiate local mitochondrial biogenesis. Findings presented here suggest that SS perinuclear mitochondria acquire an mtDNA deletion and proliferate by driving mitochondrial biogenesis, and expand through the sarcomeric planes across the z-band via the path of least resistance and subsequently along the myofibre.

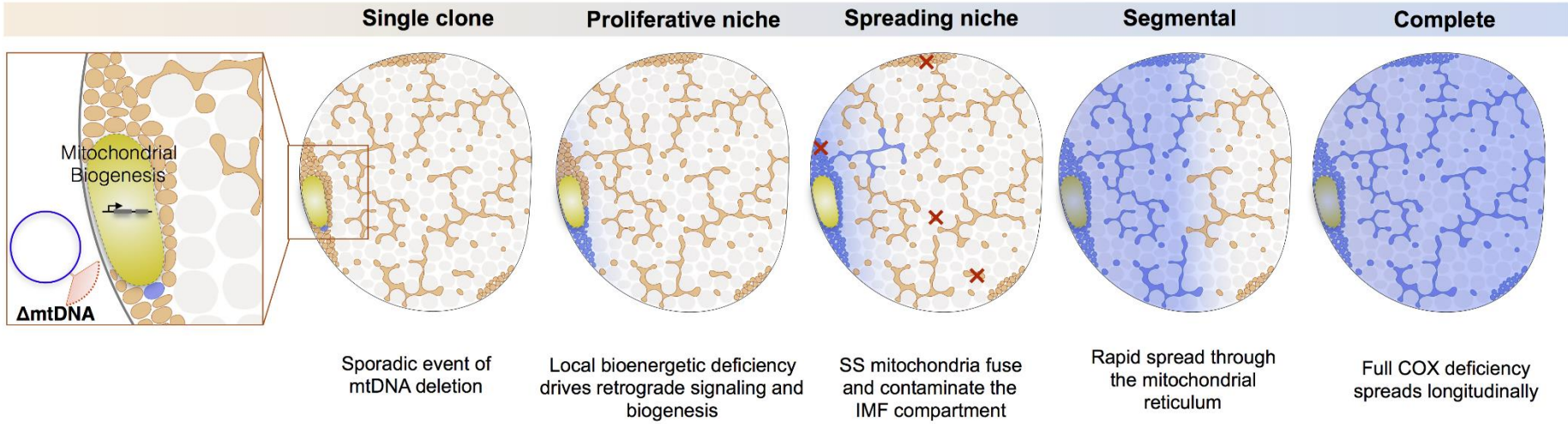

Figure 5.9 *Proliferative perinuclear niche model for clonal expansion of mitochondrial DNA deletions in skeletal muscle. Stages of clonal expansion from a single deleted mtDNA clone to a completely COX-deficient myofibre. Sporadic mtDNA deletion (ΔmtDNA) events that occur in close proximity to the nucleus expand by random genetic drift until biochemical deficiency develops. This engages "retrograde" signalling to the nucleus where it triggers compensatory mitochondrial biogenesis and mtDNA replication, driving proliferation of the perinuclear niche. Proliferating SS mitochondria with mtDNA deletions physically interact with IMF mitochondria via fusion and/or migration and spread through the path of least resistance (i.e., transversely) in a wave-like manner, creating myofibres with segmental COX deficiency. Constant mitochondrial turnover (red crosses) leads to the "replacement" of wild-type mtDNA by deleted mtDNA under the force of the proliferative niche. IMF mitochondria that acquire a spontaneous mtDNA deletion are likely degraded without having the capacity to drive biogenesis and replicate (red crosses), explaining why COX-deficient foci always arise from the SS compartment.*

Identifying the site of origin for mtDNA deletions could improve the understanding of clonal expansion. Myofibres contain two mitochondrial subpopulations, subsarcolemmal and intermyofibrillar, with distinct topological, morphological and functional differences (Ferreira *et al.*, 2010; Picard *et al.*, 2013). With this in mind several thousand myofibres were analysed and the smallest possible foci of COX deficiency identified. It was noted that the subsarcolemmal mitochondria are always implicated but never the IMF in isolation.

There are two possible explaination for the perinuclear localization of focal deficiency. Deletion events may occur sporadically with an equal probability of occurring in SS or IMF mitochondria. In this case the data here suggests that the mtDNA deletions in the IMF mitochondria either do not clonally expand or are eliminated through mitophagy. A factor in this failure to expand may be the distance from the nuclei (Davis and Clayton, 1996), situated in the subsarcolemmal area, which would allow biogenesis to be triggered through retrograde signaling due to respiratory chain deficiency. Diffusion of signaling molecules declines exponentially with distance, therefore distance from nuclei alone could determine the probability of a deleted mtDNA expanding. Since IMF mitochondria can be positioned tens of microns from a nuclei while SS mitochondria can be only hundreds of nanometers from a nuclear pore (**Figure 5.4**), the difference in probability of an mtDNA deletion expanding could be substantial. The proximity of SS mitochondria overcomes possible diffusion barriers between the mitochondria and nucleus, therefore giving the SS mitochondria a retrograde signaling advantage over their IMF counterparts.

Another explanation for the perinuclear location of focal deficiency, is that deletion evens occur more commonly in the perinuclear mitochondria. If the perinuclear mitochondria are the actively replicating mitochondria, then deletion events may occur more frequently here due to errors in replication. Similar to the above hypothesis mtDNA replication requires nuclear encoded proteins and given the fact that diffusion declines over distance this may also be true for nuclear derived mRNA or proteins. Even so the increase in mtDNA copy number and mitochondrial mass, suggests that mito-nuclear retrograde signaling and upregulation of mitochondrial biogenesis is still likely to play an important role.

The pathogenesis of mtDNA deletions is dependent on their accumulation to levels exceeding the mutational threshold. Some previous models of clonal expansion have

assumed that a change in mtDNA replication rate e.g. replicative advantage (Wallace, 1989) or survival of the slowest (de Grey, 1997) is required to give mitochondria with an mtDNA deletion the capability to expand and outnumber the wild type mitochondria. The debate over whether a replicate advantage is necessary or whether random genetic drift due to relaxed replication is sufficient to allow a deletion expand continues to date. Evidence both for (Diaz *et al.*, 2002; Fukui and Moraes, 2009; Samuels *et al.*, 2013; Kowald and Kirkwood, 2014) and against (Campbell *et al.*, 2014; Gitschlag *et al.*, 2016) a selective advantage has been reported. Whilst the proliferative perinuclear niche model presented here neither confirms nor disproves the need for a replicative advantage, it demonstrates that when a deleted mtDNA clone exceeds the threshold for biochemical deficiency, then a nuclear dependent proliferative mechanism is activated. This therefore gives the perinuclear niche a proliferative advantage and drives replication of the proximal mitochondria including those with deleted mtDNA. Notably, the data presented here suggests that the mtDNA size itself does not confer a replicative advantage of the deleted mtDNA (Campbell *et al.*, 2014; Gitschlag *et al.*, 2016), however the level of respiratory chain deficiency caused by the deletion could indeed influence the strength of the signals driving mitochondrial biogenesis. The magnitude of the proliferative drive may be dependent on the location and size of the deletion and thus the number of structural and tRNA genes which are affected. Mutations in tRNA genes are associated with a greater proliferative drive than mutations in structural genes as evidenced by RRF formation being more common in patients with tRNA point mutations versus patients with point mutations in structural genes (Montoya *et al.*, 2009). This is likely due to the fact that tRNA mutations impact on translation of multiple mtDNA encoded structural subunits and thus have a greater impact on respiratory chain dysfunction.

Increasing levels of mtDNA heteroplasmy activate nuclear transcriptional reprogramming, altering the transcription levels of thousands of genes (Picard *et al.*, 2014; Maeda *et al.*, 2016). Nuclear transcriptional reprogramming triggers an increase in mitochondrial mass and mtDNA copy number (Petruzzella *et al.*, 1994; Yu Wai Man *et al.*, 2010; Giordano *et al.*, 2014). In *C. elegans,* mtDNA deletions activate the unfolded protein response (UPR^{mt}) in order to promote mitochondrial biogenesis and mitochondrial dynamics (Gitschlag *et al.*, 2016; Lin *et al.*, 2016). This process

drives the mtDNA heteroplasmy up at a whole organism level. A UPR^{mt} has been identifed in mammals and is proposed to involve the AKT or JNK signaling pathways, however this is not well characterised and homologues of the key regulatory proteins identified in *C. elegans* have not been found (Pellegrino *et al.*, 2013). The proliferative perinuclear niche model presented here, suggests a conserved mechanism for clonal expansion across species, however the key effector pathways may vary from species to species and possibly from tissue to tissue.

Indeed there are a number of possible signaling pathways that could lead to the increased mtDNA heteroplasmy and mitochondrial mass. Firstly, a reduction in the ATP/ADP ratio or increased ROS due to respiratory chain dysfunction may upregulate mitochondrial biogenesis. Alternatively, mitochondrial biogenesis may upregulated through the mammalian UPR^{mt}, since evidence suggests that the AKT signaling pathway can transcriptionally upregulate *Nrf1* (Pellegrino *et al.*, 2013). This would be in agreement with findings by Lin *et al.* (2016) who find that the UPR^{mt} in *C. elegans* increases mitochondrial biogenesis and mitochondrial dynamics. An alternative to the proposed upregulation of mitochondrial biogenesis is a reduction in mitophagy, again this has been found by Gitschlag *et al.* (2016) to result from UPR^{mt} activation in *C. elegans.* Each of these possibilities needs to be considered and investigated further.

In addition to the proposed perinuclear niche hypothesis, it could be proposed that the perinuclear foci of COX-deficiency arises not from increased mitochondrial biogenesis, but from a deficiency in trafficking of dysfunctional mitochondria away from the nucleus or active trafficking of dysfunctional mitochondria back to the nucleus. While this should not be completely discounted, considering recently published findings in mice with photoactivatable mitochondria (Eisner *et al.*, 2014; Mishra *et al.*, 2015) and data reported in the present manuscript, neither of these hypotheses would accurately account for the observations.

First, although there is fusion between skeletal muscle mitochondria, there is very little movement or trafficking of mitochondria in mature myofibres (Eisner *et al.*, 2014; Mishra *et al.*, 2015). Mouse models with photoactivatable mitochondria find frequent fusion events between adjacent mitochondria, without apparent mitochondrial movement. This is in contrast to cultured cells and undifferentiated tissues. So trafficking is very unlikely to contribute to this process. There is also no reason to

suspect that mitochondria would be trafficked in the direction of the nucleus, since autophagosomes are observed by EM in the IMF space and autophagic removal of mitochondria takes place here (Masiero *et al.*, 2009).

Second, the correct model also needs to explain why mutant mitochondria originate as a very small area and accumulate around a single nucleus and not all the nuclei in a fibre. Mitochondrial biogenesis requires nuclear products and it is therefore unlikely that mitochondria would proliferate to a substantial degree away from nuclei. The proliferative perinuclear niche model does not stipulate that mtDNA deletions and mutations do not occur outside the perinuclear space. Rather, it stipulates that only those that do occur in the perinuclear niche eventually have the opportunity to recruit nuclear resources, replicate, and expand to pathogenic levels.

Finally, data presented here and the proliferative perinuclear niche model is entirely consistent with robust data published recently (Mishra *et al.*, 2015). The authors show how mitochondrial fluorescent proteins arising from a single nucleus propagate from the nucleus towards the middle of the cell. The pattern of propagation from this single myonuclear domain parallels findings presented here.

Following the formation of focal deficiency, an important process to consider in clonal expansion is the spread of COX-deficient mitochondria from one perinuclear niche to neighboring nuclear domains, thus allowing the propagation of the mitochondrial deficiency along the length of the myofibre. In isolated myofibres the average length of COX-deficient segments correlates with muscle homogenate mtDNA heteroplasmy (Matsuoka *et al.*, 1992), which may suggest that the longitudinal spread and thus involvement of more nuclei drives the rise in mtDNA deletion heteroplasmy over time. If the spread of COX deficiency were to occur at an equal speed the longitudinal and transverse orientations it would be expected that the frequency at which segmental COX deficiency is observed in cross section would be relatively high. However this is not the case, COX-negative foci are rarely seen in comparison to fully COX negative fibres and as such must transition from the former to the latter relatively rapidly. Furthermore, when longitudinal myofibres are examined segments of deficiency are often very small with the longitudinal length of the deficient segment being smaller than the width of the myofibre (**Figure 5.8**). This suggests that myofibres transition from focal COX deficiency to fully COX-deficient fibre in transverse before deficiency

then spreads along the longitudinal axis. This is explored more in more depth and quantitatively assessed in **Chapter 7**.

A possible hypothesis to explain this, is that mitochondria may be more networked or branched in the transverse plane than the longitudinal, thus providing less resistance to spread. Serial block face scanning electron microscopy demonstrated substantially more mitochondrial connections in the transverse plane across the Z-band (or I- band (Glancy *et al.*, 2015)), compared to those observed in the longitudinal (**Figure 5.8**), thus supporting this hypothesis.

However, a number of questions remain unanswered. Firstly, how the SS COX-negative mitochondria interact with the IMF mitochondria, allowing the spread of COX deficiency. Occasional connections between SS and IMF mitochondria have been reported (Picard *et al.*, 2013; Dahl *et al.*, 2015; Glancy *et al.*, 2015), indicating that both populations can physically interact, likely via fusion. Further to this low levels of mtDNA heteroplasmy can promote mitochondrial elongation (Picard *et al.*, 2014), likely to allow functional complementation (Nakada *et al.*, 2001; Chen *et al.*, 2010), a caveat of this may be that it contributes to the spread of mtDNA deletions into the IMF area.

Secondly, how it is that wild type mtDNA is lost and replaced by the deleted mtDNA? Mitochondria have been reported to have a half-life of days to weeks (Jaleel *et al.*, 2008; Poovathingal *et al.*, 2012). One of the signaling pathways promoting degradation of mitochondria is reactive oxygen species (ROS) (Chen *et al.*, 2009). Of interest, the IMF mitochondria have a 2-3 fold higher production of ROS than the SS mitochondria (Servais *et al.*, 2003; Adhihetty *et al.*, 2005). Furthermore the low oxygen tension in the IMF compartment may promote mitophagy in the IMF region, while mitochondrial biogenesis is occurring preferentially in the SS mitochondria (Pathi *et al.*, 2012). The combination of the proliferative perinuclear niche, selective degradation of IMF mitochondria and occasional interaction of SS and IMF mitochondria would result in a “wave-like” flow of deleted mtDNA from the SS mitochondria across the myofibre. Therefore, mitochondrial biogenesis, fission and fusion and mitophagy are likely to be factors in the overall process of clonal expansion.

Finally, the same focal deficiency is observed in acquired mtDNA mutations (e.g. mitochondrial DNA maintenance disorders with multiple deletions and ageing) as with

mtDNA mutations that are present since embryogenesis (e.g. single, large-scale mtDNA deletions.) Why is this, since the single mtDNA deletion must already have been present at low levels within an affected muscle fibre? One possibility is that the increase in mitochondrial DNA replication in the perinuclear area means that it is this region that accumulates a high level of the mutation first and thus this region that becomes COX-deficient first. However, this will warrant further investigation.

5.5.1 Limitations

The work presented here is a convincing hypothesis and tests a number of key assumptions for the hypothesis including the close proximity of focal COX-deficiency to nuclei and the higher level of mtDNA deletions in foci compared to the remainder of the fibre. However, repeats of these experiments and quantitative analysis of the proximity of foci to nuceli should be completed and more patients analysed. Furthermore, although close proximity to the nucleus and the increase in mtDNA copy number and SDH labelling in the foci is indicative of an upregulation of mitochondrial biogenesis the exact signaling pathway has not been identified.

One of the biggest advantages of this study is the use of human skeletal muscle, which provides insight into disease pathogenesis without the limitations of using a ‘disease model’, which may fall short of accurately representing the human disease state. However, the disadvantage of this is the inability to manipulate experimental conditions in order to gain mechanistic insight.

In addition, to this although the data provided is able to identify a conserved pattern across numerous diseases and ageing, only a small number of mtDNA deletion patients were analysed genetically (n=3). This could be increased to include more nuclear genes and more disease groups, however the reason that this was only completed in patients with mtDNA maintenance disorders causing mtDNA deletions was due to the high rate at which foci are observed in these patients.

Finally, this hypothesis is only relevant to skeletal muscle where mitochondrial movement is relatively restricted. Similar COX-deficient regions are unlikely to arise in the neurons where mitochondria are highly dynamic.

5.5.2 Further work

This work leaves a number of questions unanswered including the mito-nuclear signaling mechanism involved in the clonal expansion of mtDNA deletions. As such it would be interesting to look at expression levels of key mitochondrial biogenesis proteins such as PGC-1α, NRF1/2 and TFAM. Furthermore, is there a mitochondrial unfolded protein response in humans that plays a role in clonal expansion similar to

that observed in *C. elegans*? Investigation of this may yield insight into how conserved the mechanisms are between species. Given that findings indicate the mammalian UPR^{mt} may function through the JNK and AKT signaling pathways antibodies for phosphorylated and unphosphorylated forms of these proteins may be used to investigate this possibility. If there is a UPR^{mt}, the findings by Gitschlag *et al.* (2016) imply that the mechanism for accumulation may be a change in mitophagy rather than biogenesis. This possibility should be investigated also by looking at expression of proteins involved in mitophagy such as p62 and LC3.

Furthermore, the experiments to date have been restricted to mtDNA deletion clonal expansion and do not investigate whether the mechanism is conserved for mtDNA point mutations. As such, repeating the above investigation in a cohort of patients with mtDNA point mutations would be interesting to investigate this.

Finally, this mechanism does not explain is why mtDNA deletions accumulate in post-mitotic rather than mitotic tissues since it is specific to muscle fibres. It also does not yield insight into the mechanism of mtDNA deletion formation. As such, it would be interesting after elucidating the exact signaling mechanism by which clonal expansion of mtDNA deletions occurs in skeletal muscle to compare these pathways in other post-mitotic cells such as neurons and mitotic tissues such as the colon. Furthermore, it will be important to determine whether deletions arise during replication or repair.

5.5.3 Conclusions:

In conclusion, data presented here indicates that in human skeletal muscle mitochondrial respiratory chain deficiency starts as a proliferative perinuclear niche. Furthermore, the findings suggest mito-nuclear signaling triggering mitochondrial biogenesis is a key driver of clonal expansion in human disease and that anisotropy of the skeletal muscle mitochondrial network may dictate the spread of mtDNA deletions through the myofibres. High resolution subcellular imaging combined with methods allowing us to target selected nuclear domains (Mishra *et al.*, 2015), will be necessary to understand the signaling pathways implicated in the different stages of clonal expansion and how these relate to human disease pathology.

Chapter 6. Mitochondrial ultrastructure in human skeletal muscle of mitochondrial disease patients

6.1 Introduction

6.1.1 Electron microscopy

Electron microscopy as a technique was first developed by German physicist Ernest Ruska in 1931. In 1945, isolated mitochondria were first examined using electron microscopy (Claude and Fullam, 1945). The earliest papers that report ultrastructural changes in the mitochondria were published prior to the advent of genomics and the advances in molecular biology that have occurred over recent decades and as a consequence the functional and genetic context of many of the early observations is lacking. Furthermore, advances in genomics and molecular biology seem to have occurred in a period where the majority of electron microscopy reports were patient case studies or small cohorts, with few attempts to link structural observation with functional investigations.

Although a comparatively old technique, the frequency of reports using EM has not declined in recent years, quite the contrary. The mitochondrial genome was first sequenced in 1981 (Anderson *et al.*, 1981) and the first draft of the human nuclear genome was published by two groups almost simultaneously in 2001 (Lander *et al.*, 2001; Venter *et al.*, 2001). In the 15 years that followed (2001 -2015), 64 papers (mean 4.3 per year) were published that used EM to look at mitochondria in skeletal muscle of mitochondrial disease patients. In the previous 15 years (1986 - 2000) only 45 papers (mean 3 per year) were published doing the same (literature review in **Appendix 1**). As such it appears that newer technologies and molecular techniques have not reduced the applicability of EM. However very few studies link structural findings to functional studies and approximately 30% of reports since 2001 were reporting patients without a genetic diagnosis (literature review in **Appendix 1**). Therefore, so far many ultrastructural changes are regarded merely as non-specific pathological changes.

In recent years, advances in technology have seen an increase in the imaging options for electron microscopy. From improving resolution and imaging quality of scanning electron microscopes and transmission electron microscopes to EM tomography and serial block face techniques for three-dimensional reconstruction (discussed in detail in **Chapter 7**). As such there is now an opportunity to characterise mitochondrial ultrastructure in the context of recent advances in mitochondrial biology, particularly those in model organisms.

6.1.2 Regulating normal cristae structure

Normal mitochondrial ultrastructure is described in 1.2, here further detail on the regulation of cristae structure is provided. The cristae are regularly spaced invaginations along the inner mitochondria membrane the structure of which is organised by a number of proteins (Pfanner *et al.*, 2014). The mitochondrial contact site and cristae organizing system (MICOS) (Harner *et al.*, 2011), also termed the mitochondrial inner membrane organising system (MINOS) (von der Malsburg *et al.*, 2011; van der Laan *et al.*, 2012) or mitochondrial organising structure (MitOS) (Hoppins *et al.*, 2011) due to its simultaneous discovery by a number of groups, has been demonstrated to regulate normal cristae junction structure. The nomenclature used here is a uniform nomenclature proposed later by Pfanner *et al.* (2014). The MICOS complex consists of six proteins of which Mic60 (previously Mitofilin) and Mic10 (previously Mio10) are core components (van der Laan *et al.*, 2012). The remaining subunits are Mic19, Mic26, Mic12 and Mic28 (***Figure 6.1***). Numerous experiments interfering with expression of MICOS components in HeLa cells, yeast and *C. elegans* have demonstrated abnormal cristae morphology. Some examples include the knockdown of mitofiln in HeLa cells using RNAi (John *et al.*, 2005) and knockdown of the Mic19 homologue by RNAi in *C. elegans* (Head *et al.*, 2011), which have both been found to cause membrane stacking or concentrically organised cristae or stacked cristae membranes . However, in knock-out Mic60 yeast strains, generated by PCR based targeted homologous recombination, cristae junctions are not completely absent

(Hoppins *et al.*, 2011; von der Malsburg *et al.*, 2011), therefore Mic60 must not be essential for the formation of cristae junctions.

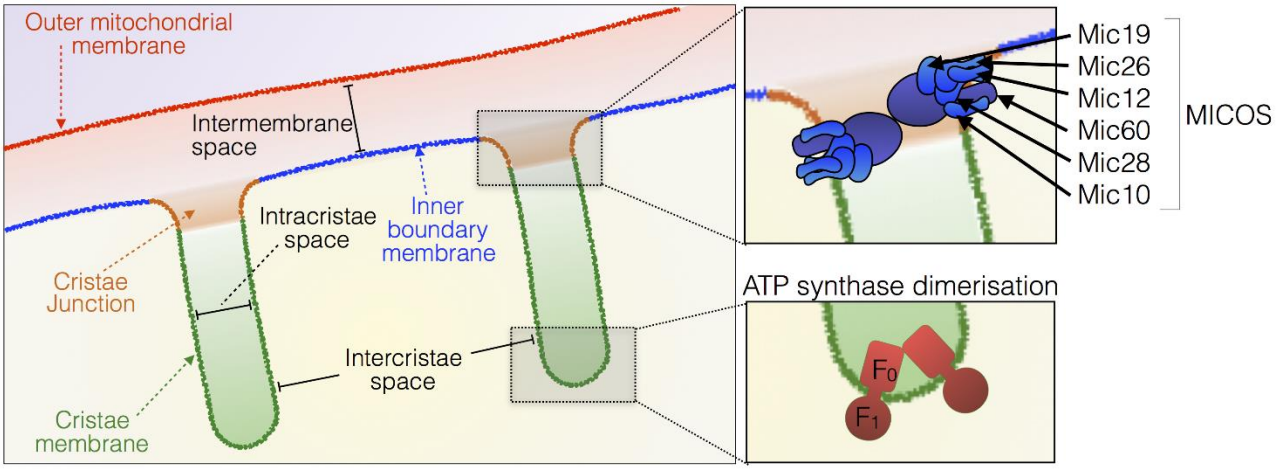

Figure 6.1 *Mitochondrial cristae structure regulation. The mitochondrial cristae organising system (MICOS) proteins regulate the size of cristae junctions and the bending of the inner mitochondrial membrane (IMM) between the inner boundary membrane and cristae membrane. Six proteins have been identified to be part of the MICOS complex so far. At the apex of the cristae ATP synthase dimerizes causing the IMM to bend. Figure based on Pfanner et al. (2014).*

Opa1 is also thought to be important in the regulation of normal cristae structure, since it remodels the cristae junction during apoptosis (Scorrano *et al.*, 2002; Frezza *et al.*, 2006), for more information see **1.3.3**. Yeast in which Mgm1 (the Opa1 homologue) is mutated show abnormal cristae structure (Meeusen *et al.*, 2006).

ATP synthase is located at the apex of the cristae membrane, where it dimerises at an angle of 70 ± 5° and causes the IMM to bend (***Figure 6.1***) (Dudkina *et al.*, 2005). ATP synthase subunits e and g are not necessary for ATP synthesis but for dimerisation and yeast lacking either subunit are found to have concentric cristae structures (Giraud *et al.*, 2002; Paumard *et al.*, 2002; Bornhovd *et al.*, 2006).

Electron tomogrophy in *Podospora anserine*, which is commonly used as an ageing model also demonstrates a reduction in ATP synthase dimerisation with ageing, which causes vesicularisation of the IMM (Daum *et al.*, 2013).

Finally, cardiolipin is also thought to play a role in IMM ultrastructure, since cardiolipin mutant hamster ovary cells with a drop of 30% in cardiolipin, had a swollen appearance with disorganised cristae and an electron dense matrix (Ohtsuka *et al.*, 1993). It has been demonstrated by NMR spectroscopy that cardiolipin interacts with ATP synthase (Eble *et al.*, 1990). It also has stabilising effects on respiratory chain supercomplexes (Bottinger *et al.*, 2012) and increases membrane fluidity and curvature of membranes (Phan and Shin, 2015). As such, it seems plausible that cardiolipin may interact with ATP synthase and aid in the curvature of the membrane at the apex of the cristae.

6.1.3 Literature review of mitochondrial ultrastructure in muscle of patients with mitochondrial disease

A systematic review of the literature for reports of electron microscopy in skeletal muscle of patients with clinically or genetically diagnosed mitochondrial disease resulted in 131 primary articles and 4 reviews. A summary of findings including; patient age, biopsy site, genetic and/or clinical diagnosis where available and a description of ultrastructural defect, can be found in **Appendix 1**.

Screening of these for specific mitochondrial ultrastructure revealed 69 reports of paracrystalline inclusions (including 2 reviews), a number of the reports also call these parking-lot mitochondria or parking-lot type inclusions (Mierau *et al.*, 2004; Thajeb *et al.*, 2006). Paracrystalline inclusions (See **6.4.2** and ***Figure 6.4*** for examples) have been found to label with antibodies for creatine kinase in rat cardiomyocytes cultured in creatine-deficient medium (Eppenberger-Eberhardt *et al.*, 1991). Creatine is the substrate for creatine kinase and when cells are cultured in medium containing creatine, paracrystalline inclusions are not observed. As such it is hypothesised that a deficiency in the creatine kinase shuttle (***Figure 6.2***),

which is responsible for the exchange of ATP in the mitochondrial matrix with ADP in the cytosol, leads to accumulation of creatine kinase as paracrystalline inclusions. Interestingly, these PCIs come in two structurally and topologically different types (Hammersen *et al.*, 1980; Stadhouders *et al.*, 1994), type-I are made of stacked sheets forming identical rectangular structures and found in the matrix and type-II PCIs are electron dense and found in the IMS. The precise reason for these structural and locational differences is unknown however reports suggest they may be mutually exclusive (Hammersen *et al.*, 1980).

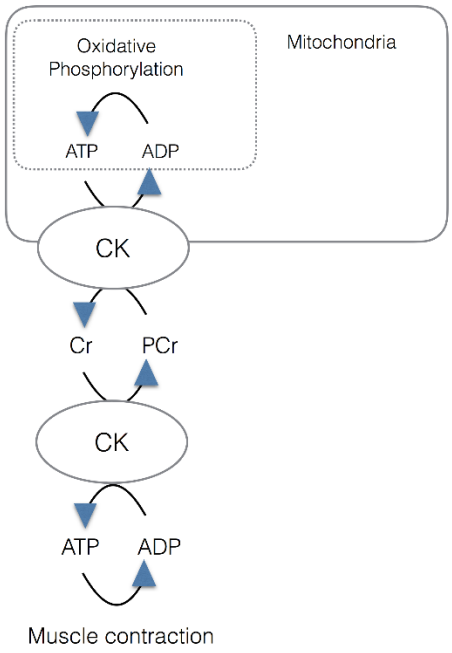

Figure 6.2 *Creatine phosphate shuttle. The creatine phosphate shuttle is responsible for the exchange of ATP in the mitochondrial matrix with ADP in the cytosol, thus removing the product of ATP synthase and providing more substrate. This exchange is mediated by creatine kinase via the sequential phosphorylation and dephosphorylation of creatine.*

Of the papers screened there were 35 reports of concentric cristae (including 1 review). There was however some degree of variability in the terminology used to describe these structures, which all appeared to be structurally identical. Terms used included; circular cristae, “onionoid”, concentric cristae, whorl mitochondria

and mitochondria with concentric lamellae. Similar structures have been reported in yeast where the mitochondrial cristae organising system (MICOS) proteins have been knocked down (see **1.2**).

In addition to this, the literature review highlighted some commonly used terms to describe mitochondrial appearance in mitochondrial myopathy which included; electron lucent (not very electron dense), giant and swollen. Furthermore, they also identified a number of inclusions other than PCIs described previously. The first is osmophilic bodies, which appear to be matrix located objects heavily stained with osmium. Granular inclusions according to (Munn, 1974), are not well characterised but have been suggested to be cation binding sites, areas with accumulation of calcium, strontium and barium and present at the sites for calcium binding and glycogen among other things (Munn, 1974). Filamentous inclusions or electron dense inclusions also appear to be poorly characterised and very variable in appearance but commonly described. Other than paracrystalline inclusions and concentric cristae, the remaining features reported and analysed below are the first report in human skeletal muscle (Vincent *et al.*, 2016b). This has been previously published and the paper is available in **Appendix 4.**

6.2 Aims of this study:

The aim of this study was to complete an in depth literature review for mitochondrial ultrastructure in human skeletal muscle and to document mitochondrial ultrastructural abnormalities found in mitochondrial patient skeletal muscle. Following this, the objective was to put these ultrastructural abnormalities into the context of recent literature in order to better understand the link between structure and function and the mechanism by which these structures form.

6.3 Methodology:

6.3.1 Patient cohort:

Patients were identified via the mitochondrial disease clinic in Newcastle over 12 consecutive weeks and consented for part of their muscle biopsy to be used for research. All work presented here was previously approved by the Newcastle and North Tyneside Local Research Ethics Committees (reference 2002/205) and is now approved under Newcastle and North Tyneside Local Research Ethics Committees (reference 16NE/0267). Patient details including genetic diagnosis plus relevant diagnostic and clinical information can be found in **Table 2.10**.

6.3.2 Transmission electron microscopy

Transmission microscopy was performed as described in **2.12.1.**

6.3.3 Serial block face scanning electron microscopy (SBFSEM)

SBFSEM was performed as described in **2.12.2.**

6.3.4 Image J analysis

Quantitative measurement of two-dimensional features e.g. nanotunnel diameter, intracristae and intercristae distance, intermembrane were performed in Image J (NIH, version 1.47v). For nanotunnel measurements, the narrowest and widest regions of each nanotunnel were averaged, yielding a mean diameter for each nanotunnel. Segments used for analysis were defined on the basis of lacking cristae and being of constant width.

6.3.5 IMOD reconstruction

3 view image stacks were converted to MRC files in Digital Micrograph (Gatan, v2.31.734.0) and 25 to 50 mitochondria reconstructed using IMOD (Boulder lab, v4.7.15) image analysis software. Mitochondria were manually traced using the 'sculpt' drawing tool, after which a mesh and cap were applied using 1.5 as the flat criteria. Following this surface area and volume inside the mesh were extracted.

6.3.6 Systematic review of the literature

Scopus, Embase and Medline were searched using the following search terms: "electron microscop* AND muscle AND human AND mitochondria*". Filtering these for "full text" and "human" yielded 1549 results from scopus, 1670 results from embase and 922 results from medline. Duplicates were removed, and search results screened on the basis of the following criteria: full text availability, English language, human, skeletal muscle, mitochondrial disease, any publication date up to the end of 2015. All included studies reported on patients with either a clinical or genetic diagnosis of mitochondrial disease; publications including cases where a diagnosis could not be reached have not been included. This resulted in 131 primary articles and four reviews. All articles were screened for the specific mitochondrial pathology reported, and for the diagnostic methodology used, which included restriction site mutation (RSM) assay, southern blotting, PCR, Sanger sequencing, restriction fragment length polymorphism (RFLP), solid phase mini sequencing, sequencing (general), next generation sequencing, or method not specified. **Appendix 5** is a table of results in chronological order including the biopsied muscle, age of subjects, clinical features, genetic diagnosis, and a summary of mitochondrial ultrastructural and morphological feature(s).

6.4 Results:

Initially a systematic review of the literature for electron microscopy in human skeletal muscle of patients with mitochondrial disease was performed (presented in the introduction for this chapter). Following this TEM and SBFSEM on skeletal muscle from seven genetically diagnosed mitochondrial disease patients was completed. This allowed demonstration and analyses of six mitochondrial ultrastructural abnormalities which, apart from paracrystalline inclusions (PCIs) and concentric cristae had not previously been reported in skeletal muscle of mitochondrial disease patients. A semi quantitative summary of these can be found in ***Table 6.1***.

6.4.1 Normal mitochondrial ultrastructure

Normal mitochondrial ultrastructure is extensively characterised in the literature to date. Further to this an aged muscle biopsy and a muscle biopsy of a 21 year old with hypertrophic cardiomyopathy and normal skeletal muscle were also examined (**Figure 6.3**). Normal ultrastructure was found in some muscle fibres of patient biopsies. Fibres with abnormal and normal mitochondrial ultrastructure were found in a mosaic pattern similar to that observed for COX positive and negative fibres in muscle sections treated for COX/SDH histochemistry.

Mitochondria are double membrane organelles with the IMM and OMM encasing the matrix. (**Figure 6.3**). The curved IMM bends inwards and can be subdivided into three sections; inner boundary membrane, the crista junction, and the cristae membrane (**Figure 6.3b**) (Pfanner *et al.*, 2014). In normal mitochondria, the matrix is a continuous space containing enzymes for biochemical reactions, as well as multiple copies of the mitochondrial genome (mtDNA). Although frequently depicted as bean-shaped, mitochondrial shape is dynamic and through continuous fission and fusion, switches between tubular and spherical morphology which also affect their size (Friedman and Nunnari, 2014).

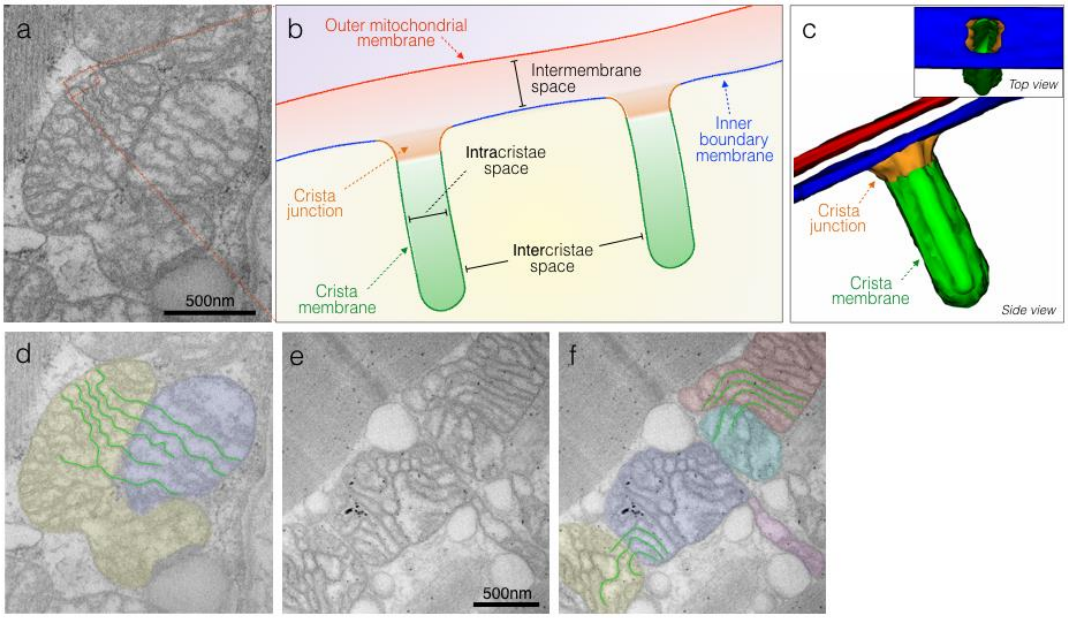

Figure 6.3 *Normal mitochondrial ultrastructure. (a) Transmission electron micrograph of normal mitochondria in human skeletal muscle. The mitochondria have typical tubular cristae and cristae junctions. (b) Schematic of cristae junctions, associated structures and parameters measured in this chapter. (c) Three dimensional schematic of a normal tubular cristae structure. The outer mitochondrial membrane (OMM, red), and three functionally distinct regions of the inner mitochondrial membrane (IMM): inner boundary membrane (blue), Cristae junction (orange) and crista membrane (green). (d) Electron micrograph from A with pseudocoloured adjacent mitochondria and lines to highlight cristae co-ordination as previously reported by Picard et al. (2015). (e) Unprocessed and (f) pseudcoloured transmission electron micrograph of normal Human skeletal muscle demonstrating normal mitochondrial shape and size. These mitochondria have electron dense curvilinear cristae, with some exhibiting trans-mitochondrial cristae co-ordination. Adapted from Vincent et al. (2016b).*

To date the literature describes what is considered normal mitochondrial morphology in skeletal muscle of humans and mice (Payne *et al.*, 1975; Larsen *et al.*, 2012; Picard *et al.*, 2013; Pfanner *et al.*, 2014). Comparable mitochondrial morphology is seen in a 78 year old healthy control and a 21 year old with hypertrophic cardiomyopathy but normal skeletal muscle mitochondrial histochemistry, validating the electron microscopy preparation used here.

Furthermore, normal mitochondrial morphology is found in some muscle fibers of mitochondrial disease patients examined. The normal morphology and ultrastructural defects presented here were present in a mosaic pattern of myofibres, comparable to that reported for mitochondrial respiratory chain deficiency by COX/SDH histochemistry.

Here, the aim was to document deviations from the normal mitochondrial ultrastructure described above, in genetically-defined cases of mitochondrial disease. This chapter looks at muscle biopsies from seven patients with a primary mtDNA mutation: single, large-scale mtDNA deletion (n = 3), m.8344A>G $tRNA^{Lys}$ (n = 3), or m.3243A>G $tRNA^{Leu(UUR)}$ (n = 1). Six mitochondrial ultrastructural abnormalities were identified as possible features linked to myopathy and are described below. A semi-quantitative summary of ultrastructural findings for all patients can be found in **Table 6.1**. Each ultrastructural finding is presented below and then discussed in the context of recent findings in mitochondrial biology.

The frequency at which each ultrastructural abnormality is observed varies between patients. This could be due to nuclear background, severity of mitochondrial dysfunction and cellular environment, along with other environmental factors such as diet and activity levels.

Patient	Type I PCI	Type II PCI	Linearization and geometrical features	Concentric cristae	Compartmentalisation	Nanotunnel	Hyperfusion and branching	Projections
P28	+++	-	-	-	-	-	++	-
P35	-	-	-	-	-	+	+	-
P36	-	-	-	-	+++	+	-	+++
P37	-	+	+++	++	-	-	-	-
P38	+	-	-	-	++	-	-	+
P39	-	-	-	+	-	-	++	+
P40	-	-	-	-	-	+++	+++	+++

Table 6.1 *Summary of mitochondrial ultrastructural abnormalities identified in patient skeletal muscle biopsies (n = 7). Patients coloured based on genetic diagnosis; blue: single, large scale mtDNA deletions; orange: m.8344A>G; green: m.3243A>G. PCI: Paracrystalline inclusion; + : Few; ++ : Frequent; +++ : Very frequent; - : none*

6.4.2 Paracrystalline inclusions

PCIs were observed in a patient with a single, large-scale mtDNA deletion (Patient 28) and chronic progressive external opthalmoplegia (CPEO) and in two patients with myopathy due to the m.8344A>G $tRNA^{Lys}$ point mutation (Patients 37 and 28). Paracrystalline inclusions (PCIs) are rigid rectangular crystals of approximately 250 nm x 50 nm. They comprise stacked sheets that either run obliquely (**Figure 6.4, a and d**) or parallel (**Figure 6.4, b and c**) to the length of the paracrystal. The rigidity is assumed based on their occasional distortion or damage of mitochondrial membranes (**Figure 6.4 c**). As with other ultrastructural abnormalities discussed below, considerable heterogeneity existed in the distribution of PCIs within single myofibres, with some mitochondria having normal ultrastructure, and adjacent mitochondria containing PCIs of various types and sizes. Although PCIs were observed in both SS and IMF mitochondria, they were typically more common in SS mitochondria (**Figure 6.4, e and f**).

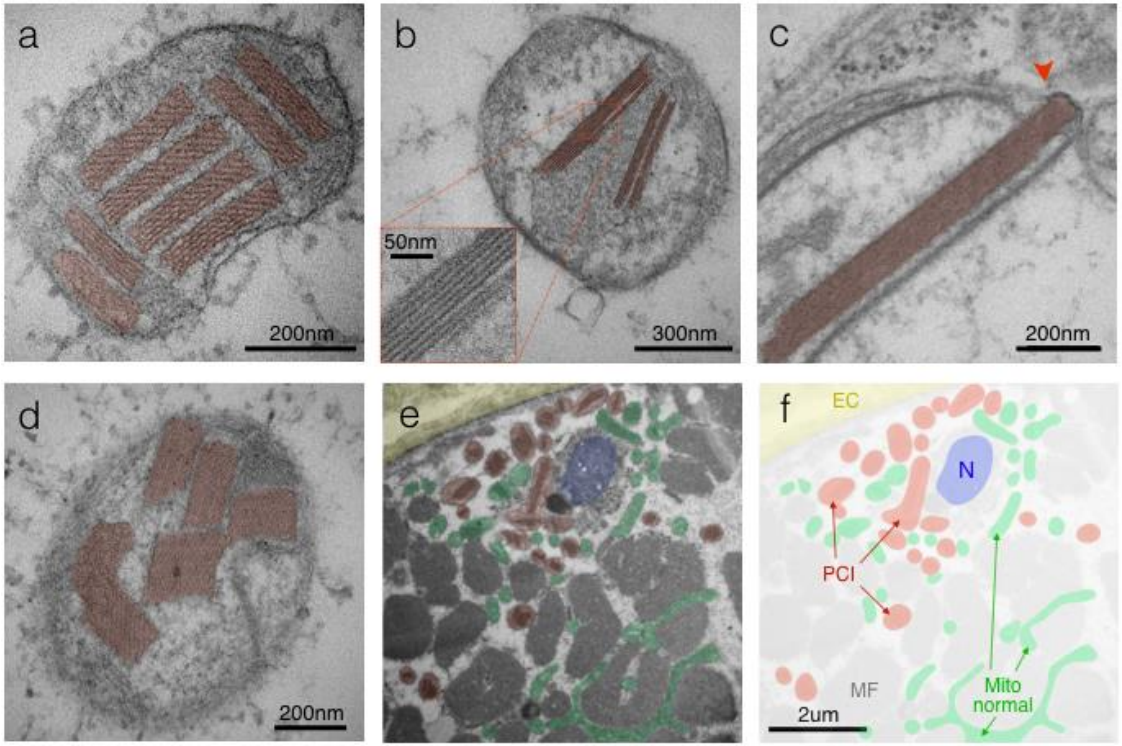

Figure 6.4 *Paracrystalline inclusions (PCIs). (a) Type I PCIs occupying the majority of a mitochondrion's volume in skeletal muscle from a patient with a single mtDNA deletion (patient 28) (b) Linear Type I PCIs in a mitochondrion from a case of m.8344A>G (patient 38). (c) Disruption of the IMM and OMM (arrow head) by a rigid type II PCI, and (d) other examples of type II PCIs from a case of m.8344A>G (patient 37). (e) Subsarcolemmal region of a myofibre showing extracellular space (EC, yellow) and sarcolemmal, Profile of nucleus (N, blue), myofibrils (MF), mitochondria with PCI (red) and normal mitochondria (green), with (f) Pseudocoloured mask (patient 28). Note the greater abundance of PCI-containing mitochondria in the perinuclear SS compartment relative to the intermyofibrillar compartment. This is consistent with the requirement for de novo protein synthesis for PCI formation. Adapted from Vincent et al. (2016b).*

PCIs fall into two classifications based on structure, size, and location within the mitochondria. Type-I PCIs consist of stacked sheets forming rectangular inclusions located in the intracristal space (**Figure 6.4, a and b**) and type-II PCIs are electron dense without layers and residing in the intracristal and intermembrane space (**Figure 6.4 d**). Both type I and II were observed here and consistent with previous observations (Hammersen *et al.*, 1980), were found to be mutually exclusive within individual patients, i.e. type-I PCIs were identified in patients 28 and 38, whereas type-II PCIs were observed in patient 37.

1.8.6 Cristae linearization and angular features

In contrast to the normal cristae invaginations of the IMM (**Figure 6.3**), linearisation of cristae IMM with angular (i.e., geometrical) features were observed in Patient 37 (**Figure 6.5, a-d**). These structures included rigid linear membranes at angles of 124.7 ± 7.4º (**Figure 6.5, a and b**) and are often observed in association with electron dense inclusions (**Figure 6.5, c and d**). Linear membrane segments show enhanced electron density, which may be due to the presence of large molecular weight proteins and/or substantial change in membrane lipid or protein composition. SBFSEM and three-dimensional reconstruction demonstrated that the linearised membranes actually formed sheets rather than isolated tubular structures as would be expected given normal cristae structure (**Figure 6.5, e and f**).

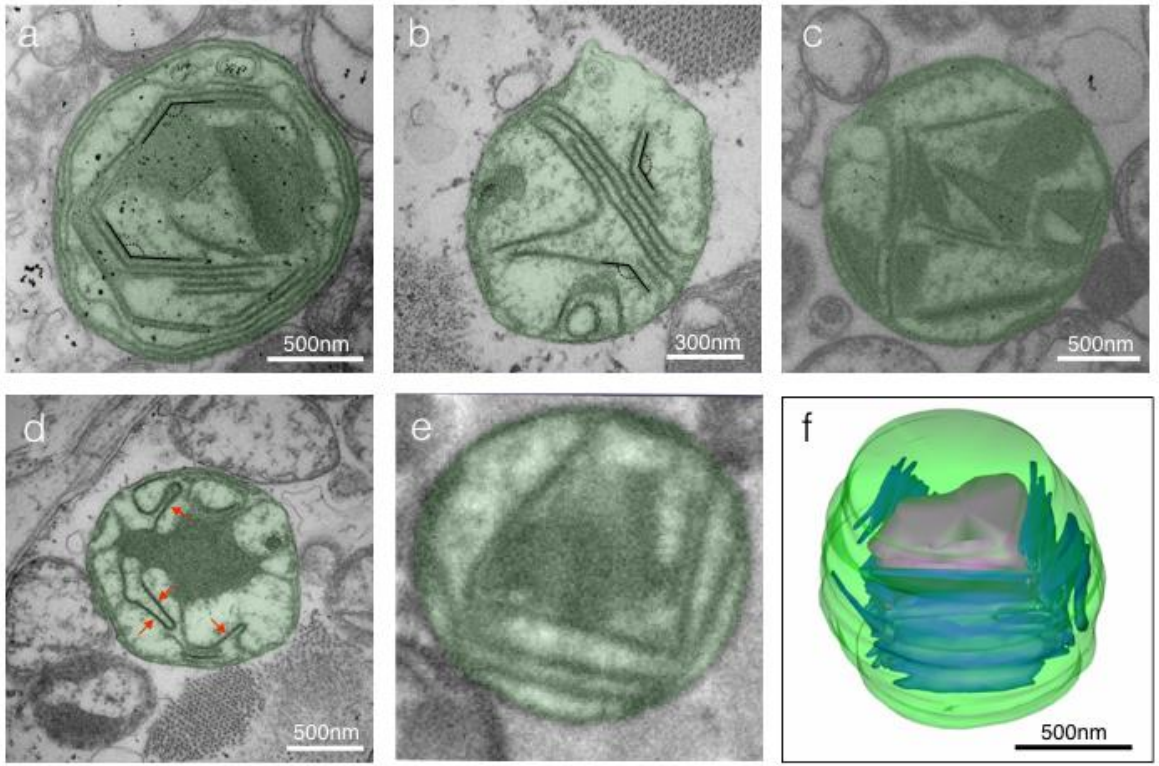

Figure 6.5 *Linearization and geometrical cristae features. (a, b) Enlarged mitochondria containing linearized cristae juxtaposed at nearly identical angles, and (c) linearized cristae forming various geometrical shapes, and (d) linearized IMM segments (arrows) joined by curved segments from a case of m.8344A>G (patient 37). (e) SBFSEM image with example of linearized cristae and geometrical shapes and (f) IMOD reconstruction of mitochondrion in (e) (patient 37). Adapted from Vincent et al. (2016b).*

6.4.3 Concentric "onion-like'' cristae

The IMM bends at regular intervals forming cristae and the connected cristae junction forms a pore. In contrast to the normal cristae invaginations TEM images from patients 37 and 39 who both have m.8344A>G $tRNA^{Lys}$ mutations have a large proportion of mitochondria with concentric "onion-like" cristae (**Figure 6.6, a and b**) which appear to be completely lacking cristae junctions. SBFSEM and three-dimensional reconstruction of one such onion-like mitochondria confirmed the tight layers of discontinuous membrane sheets (**Figure 6.6, c and d**).

The width of the IMS and intracristal space are known to be tightly regulated by specific proteins. Measurement of the IMS and intracristal space demonstrated that the IMS width was similar between mitochondria with concentric (7.1 ± 1.6 nm) and normal cristae structure (7.9 ± 1.2 nm, $P = 0.45$). However, the intracristae space was reduced by ~15% in mitochondria with concentric cristae (7.78 ± 1.2nm) when compared to normal cristae (9.20 ± 1.0nm, $P < 0.05$), possibly due to compaction of the cristae membranes in onion-like mitochondria. Furthermore the intercristal space (space between two adjacent cristae), was also significantly reduced in mitochondria with concentric cristae (22.2 ± 4.5nm) compared to normal mitochondria (60.2 ± 9.9nm, $P<0.001$). Together this suggests tightly packed membranes in dysfunctional mitochondria and implies a loss of regulation of the width of the intracristae space.

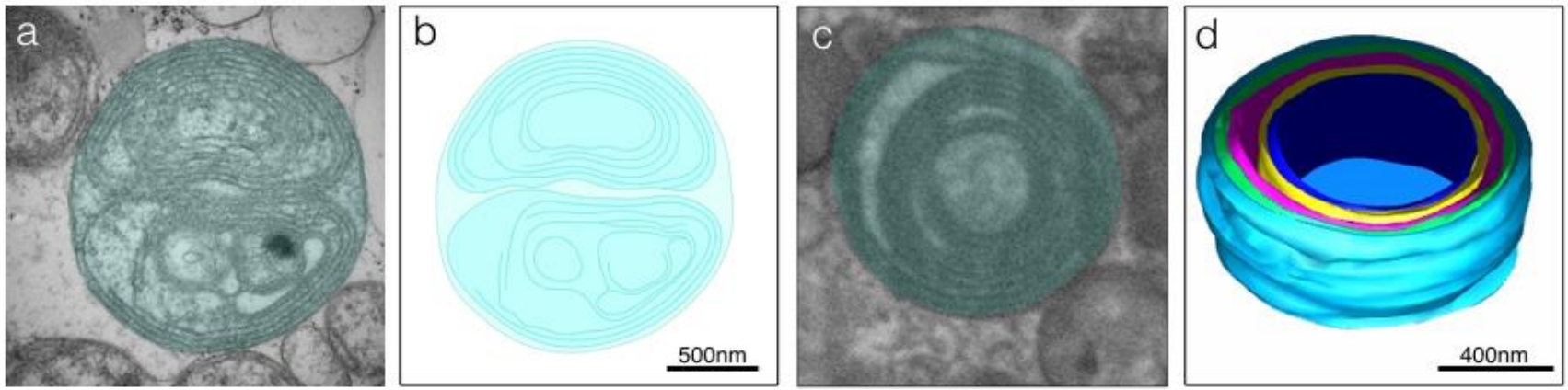

Figure 6.6 *Concentric "onion-shaped" cristae. (a) Multiple layers of double OMM and IMM membranes forming two major compartments in a case of m.8344A>G (patient 37), and (b) two-dimensional reconstruction of membrane structures. (c) Example pf concentric cristae compartments in patient 37, imaged with SBFSEM, with (d) corresponding three-dimensional reconstruction. Adapted from Vincent et al. (2016b).*

6.4.4 Compartmentalisation

Normal mitochondria have two compartments: a continuous mitochondrial matrix compartment, and the intermembranal space. In contrast, patient 36 with a single, large-scale mtDNA deletion and CPEO and patient 38 with an m.8344A>G $tRNA^{Lys}$ mutation and mild myopathy had abnormal matrix compartments surrounded by a single or double membrane and with a different electron density (**Figure 6.7, a and b**). This difference in electron density may indicate a difference in ionic content. Other examples showed dense amorphous material (**Figure 6.7c**) or were found in association with linearised electron dense membranes (**Figure 6.7d**). This extra compartmentalisation appeared in conjunction with complete absence of cristae junctions or normal cristae structures. SBFSEM and three-dimensional reconstruction of mitochondria with apparent compartmentalisation in cross-section showed the complete spatial insolation of individual compartments (**Figure 6.7, e and f**).

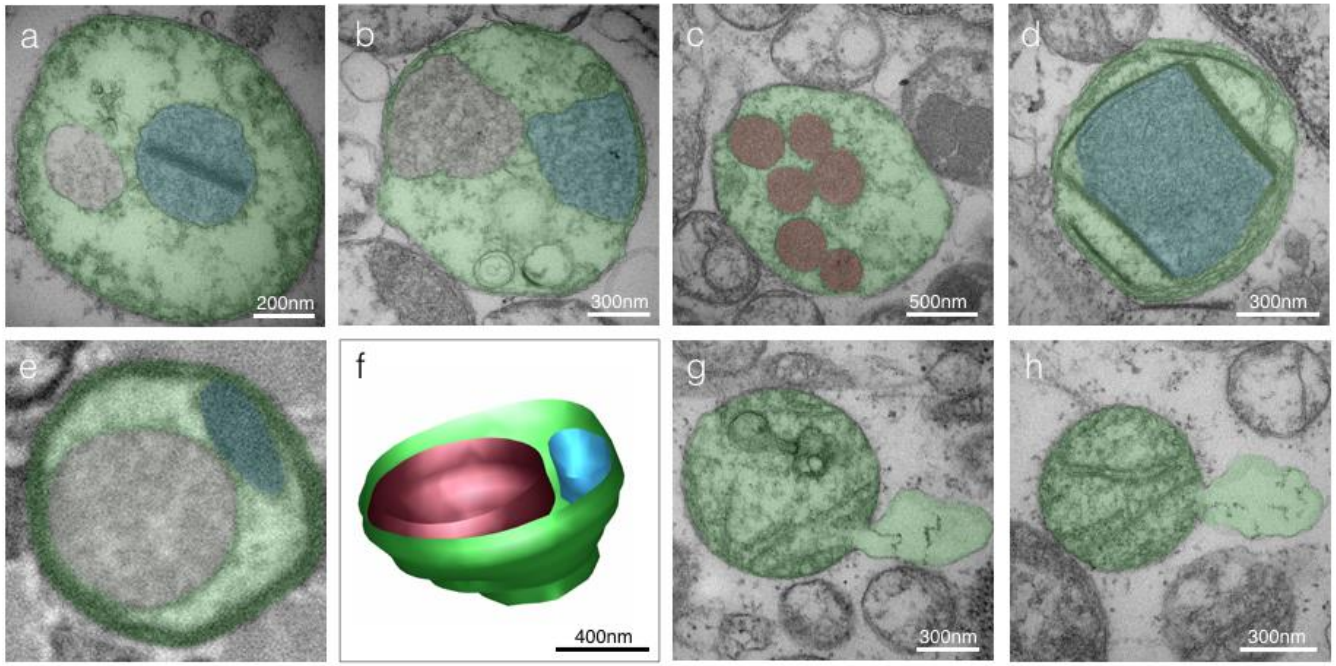

Figure 6.7 *Mitochondrial compartmentalisation. (a) Example of membrane-bound sub-mitochondrial compartments located centrally and (b) peripherally in contact with the inner boundary membrane, from cases of m.8344A>G mutation (patient 38) and single mtDNA deletion (patient 36), respectively. (c) Electron-dense round compartments, distributed in the mitochondrial matrix in a case of single mtDNA deletion (patient 36). (d) Compartment bund by linear electron dense membranes in a case of m.8344A>G (patient 37). (e) Cross sectional image of a mitochondrion with two distinct compartments of different electron densities and (f) corresponding three-dimensional reconstruction from SBFSEM. (g,h) Examples of OMM protrusion and distension consistent with the release of mitochondrial components in the cytoplasm in a case of m.8344A>G mutation (Patient 37). Pseudocoloured areas indicated the major compartment bound by the OMM (green), and sub-compartments (red and blue). Adapted from Vincent et al. (2016b).*

6.4.5 Nanotunnels

"Nanotunnels" have previously been reported in studies using confocal fluorescent microscopy in rat cardiomyocytes (Huang *et al.*, 2013) and also by TEM in cultured African grey monkey kidney cells (Bowes and Gupta, 2008). However, Vincent *et al.* (2016b) were the first to report mitochondrial nanotunnels in human skeletal muscle diseased or otherwise. Nanotunnels were found in three out of seven patients (P35, P36 and P40) (**Figure 6.8 a and b**). The average diameter of a nanotunnel was 62.3 ± 10.7 nm (**Figure 6.8 c**) and was similar in all three patients. The average nanotunnel length was 623 nm (range 206 nm to 2.3 µm). SBFSEM and three dimensional reconstruction of mitochondria connected by nanotunnels confirmed that they were thin tubular structures (**Figure 6.8 d**) and TEM images showed that nanotunnels lack cristae.

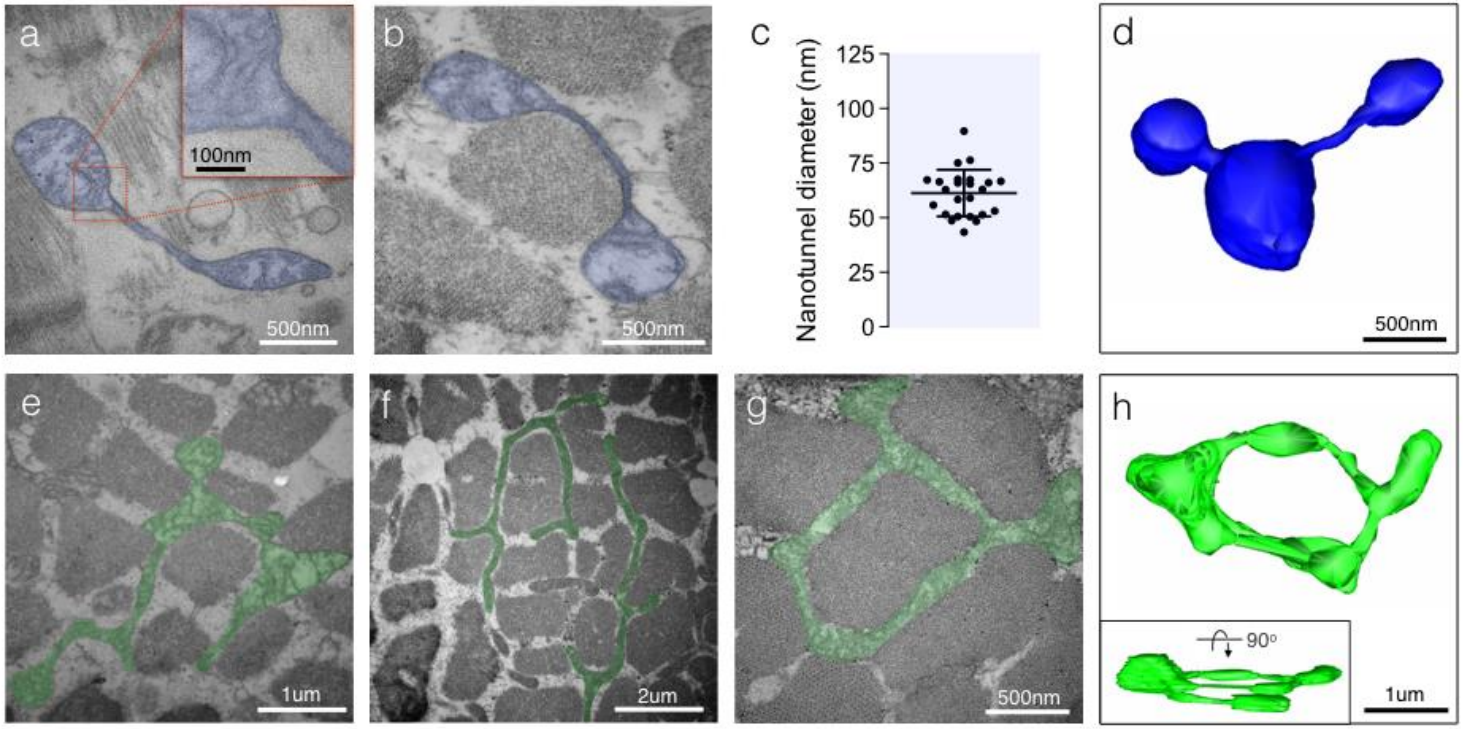

Figure 6.8 *Nanotunneling and hyperbranching. (a-b) Examples of mitochondrial nanotunnels composed of both OMM and IMM but devoid of cristae in a patient with m.3243 A>G mutation (patient 40). (c) Variation in nanotunnel diameter, with each point representing the average of the largest and smallest diameters measured for individual nanotunnels across all subjects (n=26). (d) 3D reconstruction of three mitochondria connected via nanotunnels from a case of m.3243A>G (patient 40). (e-f) Examples of highly branched mitochondria (hyperfusion) from cases of m.3243A>G (patient 40). (g) Donut-shaped mitochondrion denoting self-fusion from a single mtDNA deletion patient (patient 35). (h) Three-dimensional reconstruction of donut shaped mitochondrion from a case of m.8344A>G (patient 39). Adapted from Vincent et al. (2016b).*

6.4.6 Hyperbranching and donut mitochondria

A shift in mitochondrial dynamics towards greater mitochondrial fusion results in highly elongated and often branched mitochondria, this occurs in response to low levels of mitochondrial stress. For instance in the presence of m.3243A>G mutations up to 90% heteroplasmy mitochondria become increasingly elongated, however at mutational heteropmasy exceeding 90% the mitochondrial network fragments (Picard *et al.*, 2014). Also, in aged skeletal muscle of mice mitochondria are found to be elongated in atrophied muscle fibres (Leduc-Gaudet *et al.*, 2015). Highly branched mitochondria were observed in a case of m.3243A>G $tRNA^{Leu(UUR)}$ with 21% heteroplasmy (patient 40) (**Figure 6.8 e and f**). Donut-shaped mitochondria were also found in a patient with m.8344A>G $tRNA^{Lys}$ at 40% heteroplasmy (patient 39) (**Figure 6.8 g and h**). SBFSEM and three dimensional reconstruction supported the ring or toroid shape of the donut mitochondria (Figure 6.8h), which may be produced by either self-fusion or “splitting” of a mitochondrion.

6.5 Discussion

Mitochondrial ultrastructure is inexplicably linked to mitochondrial function (Mannella, 2006; Pernas and Scorrano, 2016). Initially electron microscopy studies identified ultrastructural abnormalities such as paracrystalline inclusions (**Appendix 5**), however a lot of early electron microscopy studies were completed before the understanding of molecular determinants of ultrastructure were known, which limits the potential interpretation. However with the genetic revolution and the improvements in identifying genetic determinants of disease, a large percentage of patients now receive a diagnosis (Taylor *et al.*, 2014). Therefore building on advances in genetic and molecular mitochondrial biology and imaging, the aim was to examine a small cohort of patients with genetically determined mitochondrial disease and assess the spectrum of ultrastructure present.

Normal mitochondrial morphology is well classified in the literature and we were able to document similar mitochondrial morphology in two individuals with normal skeletal muscle and also in normal myofibres of patients, confirming the biopsy and imaging methods preserve mitochondrial ultrastructure. We also confirmed previous findings that normal ultrastructure includes cristae-cristae co-ordination between neighbouring mitochondria (Picard *et al.*, 2015). It should also be noted that a mosaic distribution of mitochondrial ultrastructure was observed between individuals, between myofibres and within single myofibres which is consistent with what is seen with histology.

6.5.1 Paracrystalline inclusions

Although the patient sample size was small, PCI's were identified in three patients and type I and type II PCIs were found to be mutually exclusive which is in agreement with previous reports (Hammersen *et al.*, 1980). Of note two related patients with m.8344A>G $tRNA^{Lys}$ (mother and daughter, patients 37 and 38) had different types of PCIs, indicating that factors other than mtDNA mutation and nuclear background may be important determinates of disease phenotype. In order to determine specific conditions where PCIs form, a study in a larger disease

cohort would be necessary. However, it is worth noting that presence of PCIs correlated with severity of COX deficiency and lactic acidosis and also structurally with the presence of lineariSed IMM and concentric cristae.

PCIs also appear more common in the SS mitochondria than the IMF mitochondria. Since PCIs are composed of crystalised mitochondrial creatine kinase (CK) (Eppenberger-Eberhardt *et al.*, 1991), due to a compensatory upregulation of CK caused by a deficiency of the creatine phosphate shuttle activity. It seems likely that PCIs may result in patient tissue due to a reduction in ATP synthesis due to respiratory chain dysfunction, thus leading to an upregulation of CK synthesis and accumulation as PCIs. Since the upregulation required retrograde mitochondrial to nuclear signalling this may explain the preferential occurrence of PCIs in SS mitochondria.

6.5.2 Linearised IMM

Cristae with linearised membranes, altered electron density and rigid angular appearance were present in a single patient (Patient 37). These were commonly found in close proximity to mitochondria with PCIs and changes to both the membrane and matrix electron density. Changes to protein composition of the membrane or of the protein complex assembly could influence the shape of the IMM, in particular the ATP synthase, which determines the curvature of the membrane at the cristae junction (Strauss *et al.*, 2008). Variation in the cardiolipin content of the IMM could also lead to changes in rigidity of the IMM (Jiang *et al.*, 2000; Weber *et al.*, 2013; Phan and Shin, 2015). Interestingly these rigid lineariSed membranes regularly formed angles of ~120°. Previously hexagonal structures with membranes forming angles of 120° have been found in cardiolipid-containing phospholipid bilayer (Domènech *et al.*, 2007), which could indicate that these abnormal membrane structures maybe due to changes in the membrane lipid composition.

6.5.3 Concentric cristae

The presence of concentric cristae was noted in two related patients (P37 and P39), both harboring the m.8344A>G $tRNA^{Lys}$ mutation. This observation is similar to structures previously found in cultured human (HeLa) cells and yeast where the mitochondrial contact site and cristae organizing system (MICOS) components had been knocked down or knocked out resulting in concentric layering or stacking of the membrane (John *et al.*, 2005; Rabl *et al.*, 2009; van der Laan *et al.*, 2012; Pfanner *et al.*, 2014). Concentric cristae have also be found to form following abnormal ATP-synthase dimerization (Paumard *et al.*, 2002).

Measurements of the intra- and inter- cristae space demonstrate a significantly smaller size in mitochondria with concentric cristae compared to normal mitochondria. The width of both the intermembrane and intracristae spaces are tightly regulated by specific proteins and this regulation is believe to be of functional as well as structural importance (Mannella *et al.*, 2013; Varanita *et al.*, 2015). Cristae junctions were not noted in these mitochondria, however this does not mean they are not present in another plane. However, based on the studies in model systems mentioned above, defects of the nuclear-encoded MICOS components or other proteins regulating the cristae junction may cause cristae junction dysfunction and result in the concentric cristae observed. Such mutations are unlikely to be the cause of these ultrastructural changes in mitochondrial myopathy patients, particularly those described here with mtDNA mutations. However, mitochondrial dysfunction may lead to protein damage via an increase in ROS, which would have the same affect.

6.5.4 Compartmentalisation

Mitochondria showing increased compartmentalisation, were found in two patients (P28 and P38). This increased compartmentalisation could be a product of hemi-fusion i.e. OMM fusion in the absence of IMM fusion, therefore producing a single mitochondrion that has multiple matrix compartments (Zick *et al.*, 2009). In support

of this hypothesis suppression of Opa1 homologue eat-3 in *C. elegans* causes a similar phenotype (Kanazawa *et al.*, 2008).

Further to this a distension of the OMM was noted with what appeared to be release of mitochondrial matrix content. This was observed without other changes to mitochondrial ultrastructure and therefore could be distinguished from mitochondrial swelling induced by opening of the permeability transition pore. Recent reports show that mitochondrial proteins (e.g. Prohitibin and Hsp60) and mtDNA (in its oxidised form) are released into the cell cytoplasm or systemic circulation (Zhang *et al.*, 2010). This release of mitochondrial material acts as a damage associated mitochondrial protein (DAMP) and activates the inflammatory response pathways (Zhang *et al.*, 2010). Similarly, release of mitochondrially derived vesicles have also been found to be a quality control mechanism in the cardiac system (Cadete *et al.*, 2016).

6.5.5 Nanotunneling

Nanotunnels were first observed by transmission electron microscopy in African green kidney cells (Bowes and Gupta, 2008) and were subsequently named later upon visualisation using confocal microscopy in rat cardiomyocytes (Huang *et al.*, 2013). The first report of these structures in humans was in human skeletal muscle and relates to results presented here (Vincent *et al.*, 2016b). Here nanotunnels were found to be 62.3 ± 10.7 nm in diameter and 200 nm to 2.3 µm in length. In contrast others report diameters of 50 nm (Bowes and Gupta, 2008) and 90-120 nm (Huang *et al.*, 2013) respectively. Consistent with previous reports (Bakeeva *et al.*, 1978; Fujioka *et al.*, 2013) the nanotunnels observed here are double membrane structures lacking cristae. Consistent with their structure, live cell imaging demonstrates that nanotunnels are able to transport GFP targeted to both the mitochondrial matrix and also IMM (Huang *et al.*, 2013). However, based on the diameter of nanotunnels here it is unlikely that a nucleoid containing mtDNA which is reported to average around 110 nm in diameter (Kukat *et al.*, 2015), could be transported. Even so nanotunnels may be an effective method of

communication especially in skeletal muscle where mitochondrial movement is restricted (Huang *et al.*, 2013).

Live cell imaging has demonstrated that nanotunnels form in a KIF5B dependent manor, over a period of seconds (Wang *et al.*, 2015). An alternative suggestion is that nanotunnels are in fact the results of stalled fission (Zhang *et al.*, 2016), this may be supported by the similarity in diameter between the nanotunnels and restriction caused by dynamin Dnm1 during fission in yeast (Mears *et al.*, 2011).

An understanding of the function and conditions that initiate or prevent nanotunnel formation may offer new insights into the pathogenesis of mitochondrial myopathy. Nanotunnels are found here in three of seven patients, interestingly they were also found to be present in normal muscle without mitochondrial disease but not in the patients with the highest mutational heteroplasmy. However due to the small diameter of nanotunnels transmission electron microscopy is likely to provide an underestimate of the actual prevalence of nanotunnels, as such nanotunnels are analysed further, using SBFSEM in **Chapter 7**.

6.5.6 Hyperbranching and donut mitochondria

Increase in mitochondrial fusion or reduced fission results in mitochondrial elongation and hyperbranching. This switch in the balance between mitochondrial fission and fusion could be a response to mitochondrial stress (Shutt and McBride, 2013), such as the dose-dependent response to m.3243A>G heteroplasmy demonstrated in cybrid cells (Picard *et al.*, 2014). As such, hyperbranching witnessed here could therefore be indicators of stress due to respiratory chain dysfunction in patients with intermediate levels of mutational heteroplasmy (e.g. patient 40).

Also observed here were donut mitochondria, formed by self-fusion events or mitochondrial splitting. Respiratory chain inhibition and oxidative stress have also been shown to cause similar mitochondrial morphology *in vitro* (Ahmad *et al.*, 2013) and are found to be present in the synaptic boutons in the brains of aged

rhesus monkeys and to correlate inversely with memory (Hara *et al.*, 2014). As such the presence of Donut mitochondria may be an indicator of mitochondrial dysfunction and may be functionally relevant at the tissue or organism level.

6.5.7 Limitations

A number of limitations are important to remember when interpreting the data presented here. Firstly the aim of this investigation was to characterise the spectrum of mitochondrial ultrastructure in skeletal muscle. As such the methods for both sample collection and image capture reflect this. The samples were collected over sequential weeks in the mitochondrial clinic, yielding a small sample size with clinical and genetic heterogeneity. A large number of images were captured and fibres with clear signs of disease pathology were targeted preferentially. This means that although the methods yielded a large variety of different ultrastructural defects, the imaging strategy is not compatible with a quantitative assessment of the prevalence of these features, as such only a semi-quantitative assessment is provided. Furthermore, the small sample size and the fact that some observations are made in a single patient prevents us from making deductions on specificity of these defects to a particular mtDNA mutation.

6.5.8 Further work

Although some features described above can be well linked with recent mitochondrial biology, a number of functional experiments to better understand other structures described would be useful. For instance Amoscato *et al.* (2014), recently described the use of imaging mass spectrometry to analyse the cardiolipin content of mitochondrial membranes in the brain. Such an investigation in the patients where we see concentrically organised or linear and electron dense cristae may answer questions as to whether it is a change in cardiolipin density.

In addition, it was hypothesised that similar to PCI formation due to lack of Creatine a reduction in ATP production may have a similar impact. As such it would also be interesting to see whether respiratory chain inhibition induces formation of PCI's due to lack of ATP production.

It may also be interesting to look for possible nuclear modifiers via patient exome sequencing that may impact on the ultrastructural defects observed. However, it seems highly likely that many of the ultrastructural defects are in fact secondary to dysfunction caused by the primary disease causing mutation.

6.5.9 Conclusion

The results presented here broaden knowledge of the ultrastructural abnormalities witnessed in mitochondrial myopathy. A number of the features presented here are novel (e.g. linearised cristae membranes), or have not previously been witnessed in human tissue (e.g. nanotunnels and donut mitochondria). Furthermore some of the features identified have previously been observed in model organisms or induced *in vitro* (e.g. concentric cristae), allowing me to hypothesise their mechanistic, functional or pathological relevance. As such this study provides a foundation on which future investigations can be planned.

A larger-scale systematic assessment of mitochondrial ultrastructure using quantitative methods and a combination of TEM and serial block face scanning electron microscopy will be necessary to better understand the pathological relevance of these ultrastructural changes. Furthermore coupling this to molecular investigations such as whole exome studies may yield further insight into potential nuclear genetic modifiers to mitochondrial disease.

Chapter 7. Three-dimensional analysis of mitochondrial morphology in human skeletal muscle

7.1 Introduction:

7.1.1 Transmission electron microscopy and the limitations of two-dimensional electron microcopy

Transmission electron microscopy (TEM) and scanning electron microscopy (SEM) provide unrivalled resolution for visualising nanoscale structures and observing structural changes. However, as the scientific field has developed the demand for quantitative assessments over qualitative and observational studies is ever increasing. As such, TEM are commonly used to provide structural support to functional experimental findings. Alternatively, TEM sometimes allows the initial observation which guides the functional investigation but rarely forms the main component of an investigation.

However TEM has a number of useful outcomes; i) deriving valuable quantitative information on the shape and size of biological structures, contributing to hypothesis testing, ii) visualising biological structures yielding hints of mechanisms for pathophysiological processes and iii) discovery of novel structures that generate insight into complex functions. This is particularly so where the questions being asked are about the length or width of a particular object e.g. the size of the intermembrane space or length of nanotunnels, as presented in **Chapter 6**. Furthermore, TEM has been used to quantitatively assess morphological differences between subsarcolemmal (SS) and intermyofibrillar (IMF) mitochondria, finding SS mitochondria to be rounder and IMF mitochondria more branched (Picard *et al.*, 2013).

However, when the questions asked are about shape, area or perimeter, it has become increasingly apparent when the same tissue is observed in different orientations that measurements using two dimensional EM techniques, are often underestimates. A key example of this are observations of skeletal muscle mitochondria in transverse and longitudinal orientations. Here, findings suggest due to the complexity of the mitochondrial shape and branching (Leduc-Gaudet *et al.*,

2015), that assessing mitochondrial morphology in two dimensions grossly underestimates the mitochondrial network connectivity. As such investigations using serial semi-thin sections on TEM have looked to reconstruct mitochondrial networks (Bakeeva *et al.*, 1978; Kayar *et al.*, 1988) and advances in technology have been sought to allow faster less human intensive, high-throughput, high-resolution imaging technologies (Escovitz *et al.*, 1975; Denk and Horstmann, 2004).

7.1.2 Volume electron microscopy (EM) and the advent of three-dimensional EM

Traditionally three dimensional EM analysis has been performed by serial section transmission electron microscopy (ssTEM) (Bang and Bang, 1957). A rather painstaking and technically demanding technique ssTEM requires the investigator to; i) collect serial ultrathin sections for imaging by TEM without losing a section, ii) find the same area in each section and iii) orientate the images captured appropriately for reconstruction. Also commonly used is electron tomography which involves the imaging of a 200 nm to 1000 nm section by tilting the section up to ±70° within the path of the electron beam whilst imaging (McEwen and Marko, 2001). This method allows a 2 nm axial resolution but similar to ssTEM, the ability to acquire larger volume stacks and the field of view are limited.

Recent advances in technology have seen a surge of new methodologies for three dimensional nanoscale resolution imaging. These include array tomography, Automatic Tape-collecting Lathe Ultramicrotome (Hayworth *et al.*, 2006) or Automatic Tape-collecting Ultramicrotome (Schalek *et al.*, 2011) and finally serial block-face imaging techniques which include serial block-face SEM (SBFSEM) (Denk and Horstmann, 2004) and focused ion beam SEM (FIBSEM) (Escovitz *et al.*, 1975). Serial block face techniques allow large volume imaging without the need for manual serial sectioning and alignment and thus allow much larger volumes to be imaged.

An SBFSEM is essentially a microtome within an SEM, with a diamond knife cutting ultra-thin sections between imaging iterations. At present the maximum block-face of an SBFSEM sample is limited to approximately 800 μm^2 in size but with much larger volume imaging possible than with previous technologies. The disadvantage of SBFSEM is that minimum section thickness is 25 nm in optimal specimens (Peddie

and Collinson, 2014) and may be higher in non-optimal samples thus limiting the axial resolution. In comparison, FIBSEM uses a focused ion beam to mill away a layer of the block between imaging iterations, with the main advantage over SBFSEM being an increased maximum axial resolution to approximately 3 nm, however the process of ion beam milling is much slower than sectioning and as such SBFSEM is a fast way to acquire large data sets. SBFSEM is the method implemented here for large volume imaging at speed. In addition, the presence of an SBFSEM in the University's Electron Microscopy Research Services allowed for in house processing and imaging and thus Dr Kathryn White and Dr Tracey Davies technical expertise.

7.1.3 Three dimensional reconstructions of mitochondrial networks in mouse and human.

Three dimensional reconstruction of mitochondria in healthy human skeletal muscle from focused ion beam scanning electron microscopy (FIBSEM) has recently been completed by (Dahl *et al.*, 2015) , however no study has quantitatively assessed the mitochondrial network in three dimensions. The primary reason for this may be the lack of three-dimensional parameters to quantitatively assess the mitochondria compared to those already developed for two dimensional analysis (Koopman *et al.*, 2005; Picard *et al.*, 2013). As such we do not know what constitutes "normal" when we discuss mitochondrial network morphology in human skeletal muscles, how variable "normal" is or how IMF and SS mitochondria vary.

Although three dimensional quantitative analysis of human skeletal muscle mitochondria has not been completed mouse muscle mitochondria have been reconstructed and quantitatively assessed (Glancy *et al.*, 2015). However, given that mouse skeletal muscle fibre-types differ from those found in human skeletal muscle (Gorza, 1990; Smerdu *et al.*, 1994) intra–species differences in the mitochondrial morphology may be quite substantial. Furthermore research suggests that mitochondrial dynamics are a distinguishing feature between different fibre types in mice (Mishra *et al.*, 2015), which implies that mitochondrial morphology is also likely to differ between fibre types of humans.

7.2 Aims of this investigation

The first aim of this study was to develop a methodology for calculating mitochondrial complexity in three-dimensions and a validated approach to calculate the degree of branching. The purpose of this was to assess whether the mitochondrial network is anisotropic, that is it is more connected in one plane of the muscle fibre than the other. The second aim was to use this methodology to characterise the morphology (size, complexity and degree of branching) of mitochondria in skeletal muscle samples from patients with mitochondrial disease and healthy controls.

7.3 Methodology:

7.3.1 Patient cohort

Patients were identified via the mitochondrial disease clinic in Newcastle over 12 consecutive weeks and consented that part of their muscle biopsy be used for research. This study examines a group of six patients with genetically diagnosed mitochondrial disease; single large-scale mtDNA deletion (n = 2), m.8344A>G $tRNA^{Lys}$ (n = 3) and m.3243A>G $tRNA^{Leu(UUR)}$ (n = 1). Patient details including genetic diagnosis plus relevant diagnostic and clinical information can be found in Error! eference source not found.. All work presented here was previously approved by the Newcastle and North Tyneside Local Research Ethics Committees (reference 2002/205) and is now approved under Newcastle and North Tyneside Local Research Ethics Committees (reference 16NE/0267).

Control muscle biopsies (controls 5-12) were collected during routine anterior cruciate ligament (ACL) surgery with prior informed consent. Ethical approval for collection of ACL biopsies was given by Newcastle and North Tyneside Local Research Ethics Committees (reference 12/NE/0395, project number 42). Age and gender of controls can be found in **Table 2.6**.

7.3.2 Serial block face scanning electron microscopy

Preparation of samples was completed as described in **2.12.2**, by Drs Kathryn White and Tracey Davey. Fibres with a high mitochondrial content were selected from

cases with specific mitochondrial pathology and a series of serial images interspersed by 30 - 50 nm were captured at a magnification of 8,200x using the Gatan 3view system and digital micrograph software.

7.3.3 IMOD three dimensional reconstruction

Image stacks from Digital Micrograph (Gatan) were converted to MRC files and 25 to 50 mitochondria per myofibre were reconstructed using IMOD image analysis software. Mitochondria were manually traced using the 'sculpt' drawing tool, after which a mesh and cap were applied using 1.5 as the flat criteria. After which surface area and volume inside the mesh were extracted.

7.3.4 Mitochondrial volume density

Mitochondrial volume density was calculated for each intermyofibrillar fibre by reconstructing all mitochondria in two sarcomeres (A-band to A-band). Several myofibres had poor orientation and A- and Z-bands were not clear and so mitochondrial volume density could not be accurately assessed. An additional object was created to measure the muscle volume of two sarcomeres and the total mitochondrial volume divided by the total muscle volume and multiplied by 100 to give mitochondrial volume density as a percentage.

7.3.5 Quantification of mitochondrial complexity

Mitochondrial complexity index (MCI) was calculated using **Equation 7.1**, where SA is surface area and V is volume. This equation was developed as a three-dimensional equivalent to form factor (Koopman *et al.*, 2005). Testing similar to that used by Koopman *et al.* (2005) was completed to validate the formula.

Equation 7.1 *Mitochondrial complexity index (MCI)*

$$MCI = \left(\frac{SA^{3/2}}{4\pi V}\right)^{2}$$

7.3.6 Quantification of mitochondrial branching

Mitochondrial branching was quantified to assess mitochondrial anisotropy in skeletal muscle. In order to do this each mitochondrion was assessed in two planes; transverse (or cross-section) (x,y) and longitudinal (x,z) and a ratio was calculated for the two giving the mitochondrial branching index (**Equation 7.2**). Transverse branching index (TBI) (**Equation 7.3**), was assessed by quantifying the total number of myofibrils bridged. In instances where a mitochondrion wraps around one myofibril the side with the largest value was taken as shown in **Figure 7.1**. Longitudinal branching index (LBI) (**Equation 7.4**) was assessed by adding up the total score for "boundaries bridged", where a z-band or half sarcomere equates to a score of one and full sarcomere a score of two **Figure 7.1**.

Equation 7.2 *Mitochondrial branching index (MBI)*

$$MBI = \frac{TBI}{LBI}$$

Equation 7.3 *Transverse branching index (TBI)*

$$TBI = 1 + total\ myofibrils\ bridged$$

Equation 7.4 *Longitudinal branching index (LBI)*

$$LBI = 1 + total\ score\ for\ boundaries\ bridged$$

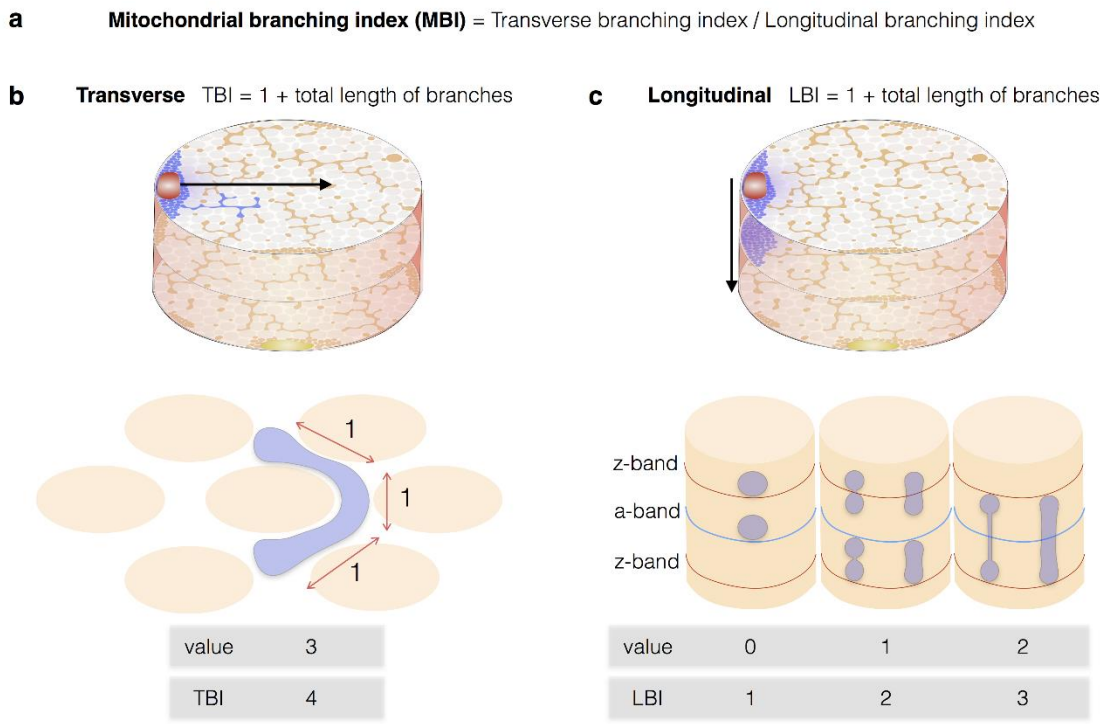

Figure 7.1. *Quantification of mitochondrial branching to assess anisotropy. (a) Mitochondrial branching index (MBI) = Transverse branching index (TBI) / Longitudinal branching index (LBI). In order to calculate MBI each mitochondrion is assessed first in the transverse orientation and then longitudinal orientation. As such any value greater than 1 indicates greater branching in the transverse orientation, 1 equates to equivalent branching in both directions and less than 1 more branching in the longitudinal orientation. (b) Branching in transverse is assessed as TBI = 1 + the total length of all branches. The total length of branches is the sum of each myofibril "bridged". In the event that a mitochondrion wraps around one myofibril as depicted the side with the greatest value is taken (i.e. this mitochondrion bridges three myofibrils.) (c) Branching in longitudinal orientation is assessed as LBI = 1 + total longitudinal boundaries bridged. Bridging of a z-band or half a sarcomere is valued as one, bridging of a full sarcomere is valued as 2.*

7.3.7 Statistical analysis of mitochondrial morphology data

A normality test was performed on all continuous data sets in Mini tab v17.1.0 and histograms plotted in Prism v7.0 (Graph Pad) to assess normality. All data sets were found not to be normally distributed as such a Cox-Box transformation was performed in Mini tab to try to normalise data and normality tests repeated. Volume was the only parameter that could be normalised, therefore all parameters were assessed non-parametrically using a combination of tests performed in Prism v7.0 (Graph Pad); Mann-Whitney test, Kruskal-Wallis test, one-way ANOVA and two-way ANOVA. Finally, linear regressions were plotted to assess the relationship of morphological parameters to each other and relevant clinical markers such as heteroplasmy, COX deficiency and NMDAS scores (Schaefer *et al.*, 2006). Statistical significance was set at 0.05.

Skewness and kurtosis were calculated in Prism v7.0. Skewness is a measure of symmetry of a distribution, with a symmetrical distribution having a skewness of 0, an asymmetrical distribution with a skew to the right (higher values) has a positive skewness and a skew to the left (lower values) has a negative skewness. Kurtosis is a measure of how well the distribution fits a Gaussian distribution. A Gaussian distribution will have a kurtosis of zero, a flatter distribution has a negative kurtosis and a more peaked distribution a positive kurtosis.

7.4 Results:

7.4.1 Testing Mitochondrial Complexity Index

Form factor is the parameter used to measure mitochondrial branching as assessed by two-dimension electron microscopy (Koopman *et al.*, 2005). In order to develop a three dimensional equivalent metric, which was named the mitochondrial complexity index (MCI), we first replaced perimeter and area in the form factor formula with surface area and volume, respectively (**Figure 7.2a**). However when tested this formula was variable dependent on volume, which form factor is not. As such, the power to which surface area is raised had to be modified to make a formula that is pure shape descriptor and therefore does not change when volume increases but shape remains equal.

In order to test this simulated three dimensional shapes made of 1 nm^3 cubes were constructed and used to test MCI (**Figure 7.2b**), volume (**Figure 7.2c**), surface area (**Figure 7.2d**) and MCI (**Figure 7.2e**) were calculated for each object. Objects 1, 19 and 20 are all the same shape and vary only in size, accordingly MCI is exactly the same for each of these. In comparison shapes 5, 10, 12 and 14 have none, one, two and three branches respectively and each have a slightly increased MCI. This therefore showed that MCI is a quantitative measure for three-dimensional mitochondrial branching that does not change dependent on size. Subsequently MCI was calculated for a range of reconstructed mitochondria to confirm that it appropriately increased as mitochondrial complexity increased. However, the overall increase in MCI did not reflect the apparent increase in mitochondrial complexity visually observed. As such a test in which MCI was squared and cubed was completed for a range of mitochondria to compare the values (**Figure 7.3**). The standard unmodified MCI did not appear to increase as dramatically as the shape changed and the cubed MCI formula showed too large an increase. Therefore the squared formula was selected as the most representative numerical assessment of mitochondrial complexity.

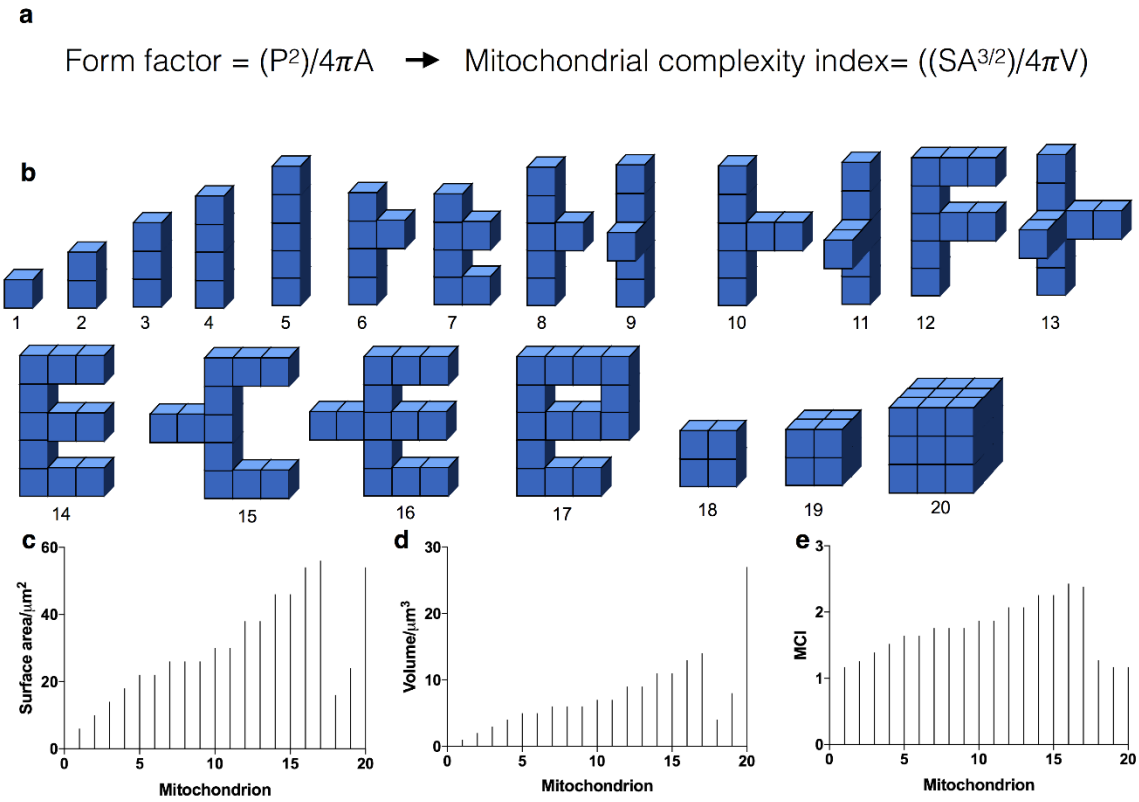

Figure 7.2. *Mitochondrial Complexity index (MCI) was tested as a shape descriptor. (a) Conversion of form factor formula to three dimensions, giving MCI formula. (b) Various 3D shapes were generated consisting of 1x1x1 blocks. These were then tested by plotting: (c) surface area, (d) volume and (e) MCI. Plotting MCI for shapes in (b) validated that it is a three-dimensional measure of mitochondrial branching which does not take change if volume is increased without a change in shape (e.g. 1, 19 and 20).*

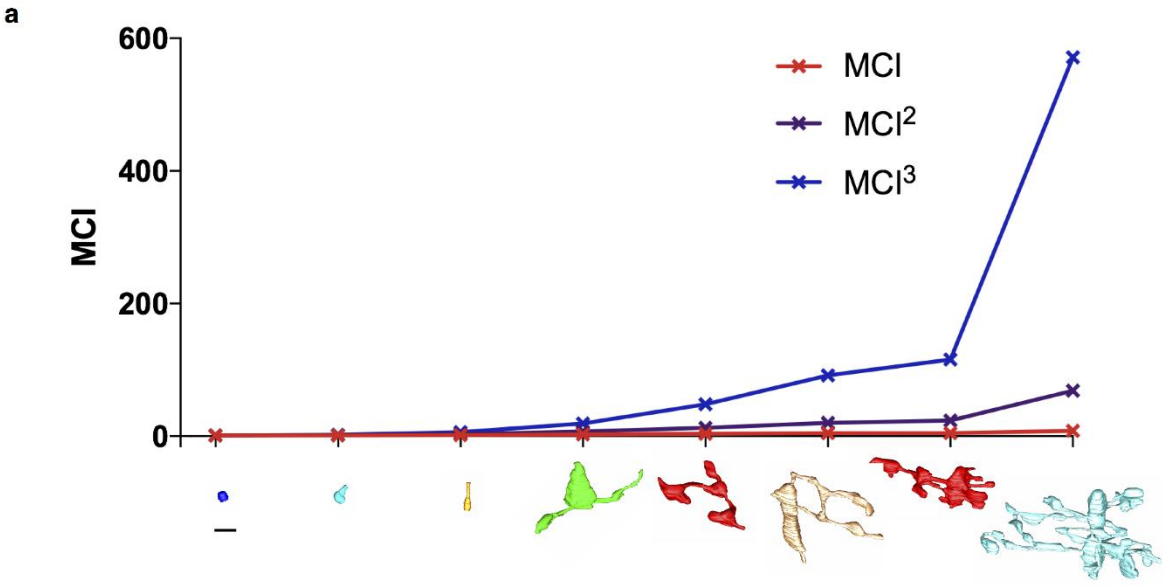

MCI	1.145	1.338	1.847	2.680	3.587	4.510	4.871	8.297
MCI^2	1.31	1.79	3.41	7.18	12.87	20.34	23.73	68.84
MCI^3	1.48	2.40	6.31	19.23	48.14	91.70	115.63	571.21

b

Mitochondrial complexity index= $((SA^{3/2})/4\pi V)^2$

Figure 7.3. *Modifying MCI formula to fit perceived increase in mitochondrial complexity. (A) However the change in MCI did not accurately reflect the increase in perceived complexity. Therefore, we transformed MCI by squaring and cubing the values and tested this on a sample of 8 mitochondria with varying complexities. This resulted in us selecting the formula MCI = $((SA^{3/2})/4\pi V)^2$. Scale bar 1000 nm. (B) Final MCI formula.*

7.4.2 Intermyofibrillar and subsarcolemmal mitochondria comparison

Similar to previous findings using TEM, comparison of SS and IMF mitochondria in images from SBF-SEM showed that IMF mitochondria are typically more branched than the smaller rounder SS mitochondria (**Figure 7.4 a-c**). Eight mitochondria representing the full range of volumes observed for IMF and SS mitochondria, presented in **Figure 7.4d** demonstrates a much wider range of volumes in the IMF mitochondria than the SS. Furthermore, other than the largest mitochondria presented for the SS group all the mitochondria are very simple in shape. The largest

SS mitochondria has a branch that reaches into the IMF area (red arrow), 6.1% of all SS mitochondria assessed (n = 573) had such protrusions into the IMF space. Such connections between SS and IMF mitochondria have previously been demonstrated in both mouse and human skeletal muscle (Picard *et al.*, 2013; Dahl *et al.*, 2015).

The difference between IMF and SS mitochondria is further exemplified in **Video 7.1** (on CD provided), where the nucleus and all SS (red) and IMF (blue) mitochondria have been reconstructed. During the video the IMF mitochondria are made transparent so that projections from the SS mitochondria into the IMF space can be visualised.

When IMF and SS mitochondrial populations were compared in the eight controls assessed, volume was typically higher in IMF mitochondria than in SS (**Figure 7.4e**). This difference was found to be significant in controls 5, 6, 11 and 12 (P = 0.0001) and control 10 (P = 0.0004). When MCI was compared SS mitochondria were found to be significantly less complex in all (P = 0.0001) but controls 8 and 10 (**Figure 7.4f**). Although the MCI mode was the same for IMF and SS mitochondria the IMF distribution was more skewed (**Figure 7.4g**) with higher skewness and kurtosis (skewness = 4.88, kurtosis = 37.09, n = 1201) than SS mitochondria (skewness = 4.02, kurtosis =27.14, n = 344). Skewness and Kurtosis are explained in section **7.3.7**.

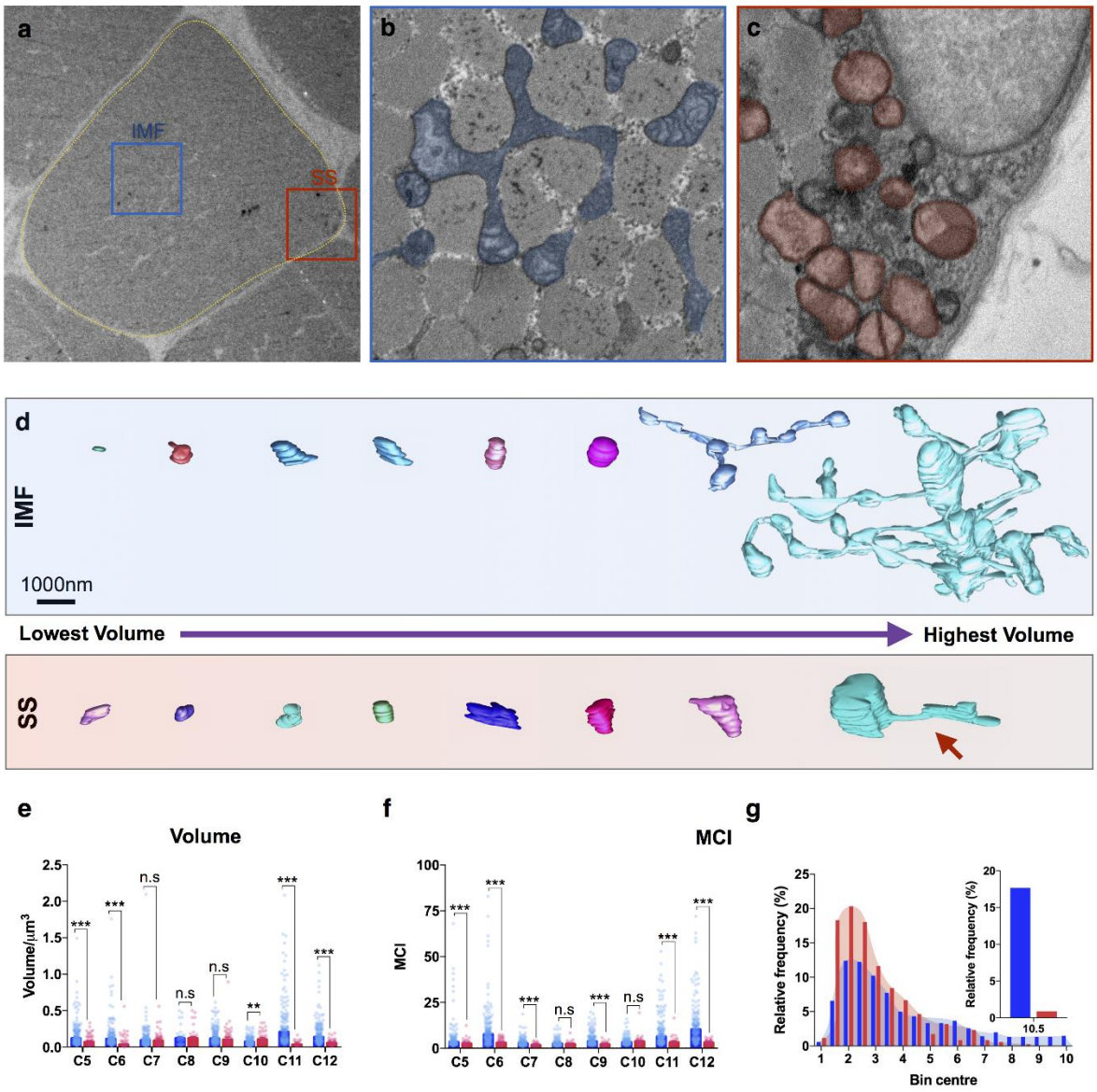
a
IMF
SS
b
c
d
IMF
1000nm
Lowest Volume
Highest Volume
SS
e
Volume
Volume/µm³
2.5
2.0
1.5
1.0
0.5
0.0
***
***
n.s
***
n.s
n.s
**
***
***
C5
C6
C7
C8
C9
C10
C11
C12
f
MCI
MCI
100
75
50
25
0
***
***
***
n.s
***
n.s
***
***
C5
C6
C7
C8
C9
C10
C11
C12
g
Relative frequency (%)
25
20
15
10
5
0
1
2
3
4
5
6
7
8
9
10
Bin centre
Relative frequency (%)
20
15
10
5
0
10.5

Figure 7.4 *Mitochondria are highly variable and exist in two morphologically different subpopulations; subsarcolemmal (SS - Red) and intermyofibillar (IMF- Blue) mitochondria. (a) Low magnification electron micrograph of a myofibre in transverse orientation, with higher magnification images of (b) IMF and (c) SS mitochondria. Note the difference in size and shape. (d) Illustration of the volume spectrum of IMF and SS mitochondria with the smallest volume mitochondria on the left and largest on the right. The SS mitochondrion with the highest volume actually has a protrusion into the IMF area (red arrow), 6.1% of all (n = 573) SS mitochondria have such a protrusion. (e) Bar graph of MCI median and 95% confidence intervals for IMF (blue) and SS (red) mitochondria in controls 5 to 12. MCI is typically higher in IMF mitochondria. MCI is statistically significant between SS and IMF mitochondria and between controls (two-way ANOVA, P < 0.0001). A Mann-Whitney test for each control found significance (***, P = 0.0001) for all but C9 (n.s, p = 0.5382) and C10 (P = 0.9781). (f) Bar graph of volume median and 95% confidence intervals for IMF (blue) and SS (red) mitochondria in controls 5 to 12. Volume is typically higher in IMF mitochondria. A Mann-Whitney test for each control found significance (***, P = 0.0001) for C5, C6, C11, C12 and (**, P = 0.0004) C10, but was not significant for C7 (n.s, P = 0.591), C8 (n.s, P = 0.324) and C9 (P = 0.289). (g) Frequency histogram of IMF and SS volumes in (f). In order to demonstrate differences the graph was truncated at 0.5 and then the region above this included in a smaller graph with higher bin values. It can be noted that SS mitochondria and IMF mitochondria have approximately the same mode however a larger percentage of SS mitochondria are in the smaller bins with non above bin centre 0.9, whereas as small percentages of IMF mitochondria can be seen right up to bin centre 2.*

Video 7.1 *The video can be found on the attached disk. This video shows one of the subsarcolemmal regions, fully reconstructed. This includes the nucleus (light blue), subsarcolemmal mitochondria (SS, red) and intermyofibrillar mitochondria (IMF, dark blue). The video pans through the full depth of the image stack in a transverse orientation, before rotating to a longitudinal orientation. The reconstruction then completes two full rotations in the y-axis one with all mitochondria present and one with just the SS mitochondria. Notice the projections from the SS mitochondria into the intermyofibrillar space.*

7.4.3 Complexity of intermyofibrillar mitochondria

The difference in size and morphology between IMF and SS mitochondria and the small spherical shape of the subsarcolemmal mitochondria was consistent with previous findings. What was more interesting was the number of very complex IMF mitochondria observed. Due to the lack of previous 3D analysis in human skeletal muscle the degree of connectivity assumed was largely based on TEM and SEM and thus underestimated the true complexity. The complexity of the IMF mitochondria in controls is illustrated in **Figure 7.5**. The images show reconstructions from control myofibres in both longitudinal and transverse orientations with annotations to demonstrate presence of the z-band. The mitochondria are highly complex in some fibres with a high degree of branching across the z-band. Branching can also be seen across the z-band and across the full sarcomere.

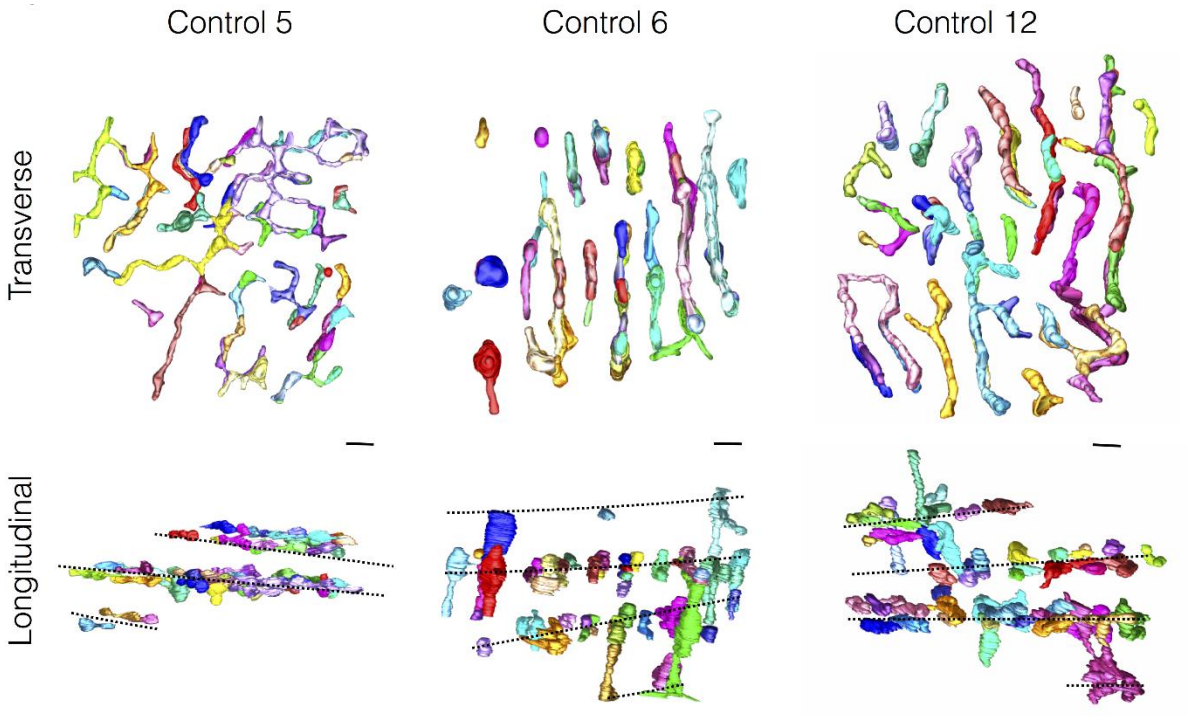

Figure 7.5 *Intermyofibrillar mitochondria exhibit complex morphology in controls. Figure shows a transverse and longitudinal view of resconstructed mitochondria in one fibre from controls 5, 6 and 12. Dashed lines in the longitudinal orientation represent location of the z-bands. Scale bar 1 µm.*

7.4.4 Variability of IMF MCI and volume within fibres, between fibres and between controls

Comparison of MCI and volume for three fibres for each control demonstrated surprisingly high variability both between controls and between the three IMF fibres of the same control. Median ± 95% CI of the volume and MCI values were plotted for each IMF fibres of the controls to compare variability both within and between cases (**Figure 7.6**). For some controls all fibres are very similar (e.g. control 9), whereas others show a greater degree of variation (e.g. control 11). In addition in some cases the variability of MCI and volume in a single fibre is very small and in others much larger. This is clearer in **Figure 7.7**, where MCI and volume for the individual mitochondria in each IMF fibre in each control have been plotted for comparison. Control 7 fibre 1 and control 12 fibre 1 have very similar values with little variability

within the fibre. In comparison, control 5 fibre 2 and control 6 fibre 2 both have a high range of MCI values and thus are very variable. It should also be noted that the mean MCI for the three fibres for controls 6 and 12 were quite variable. This further demonstrates that the variability both within a fibre and between fibres of the same control is very variable in itself.

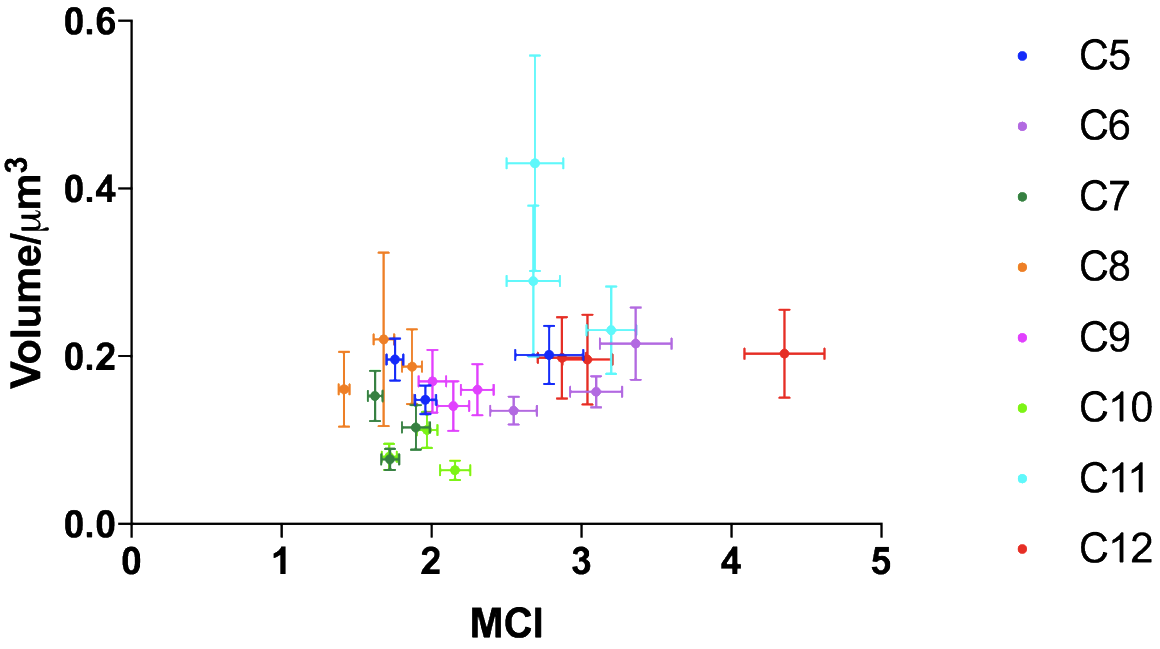

***Figure 7.6**. Mitochondrial complexity (MCI) and volume are variable in the IMF mitochondria in the majority of patients. Mean and SEM of Volume against mean and SEM of MCI for each IMF myofibre coloured by control. Between fibre variability is small in some controls but larger in others (e.g. Control 11). This should be considered when interpreting control and patient data.*

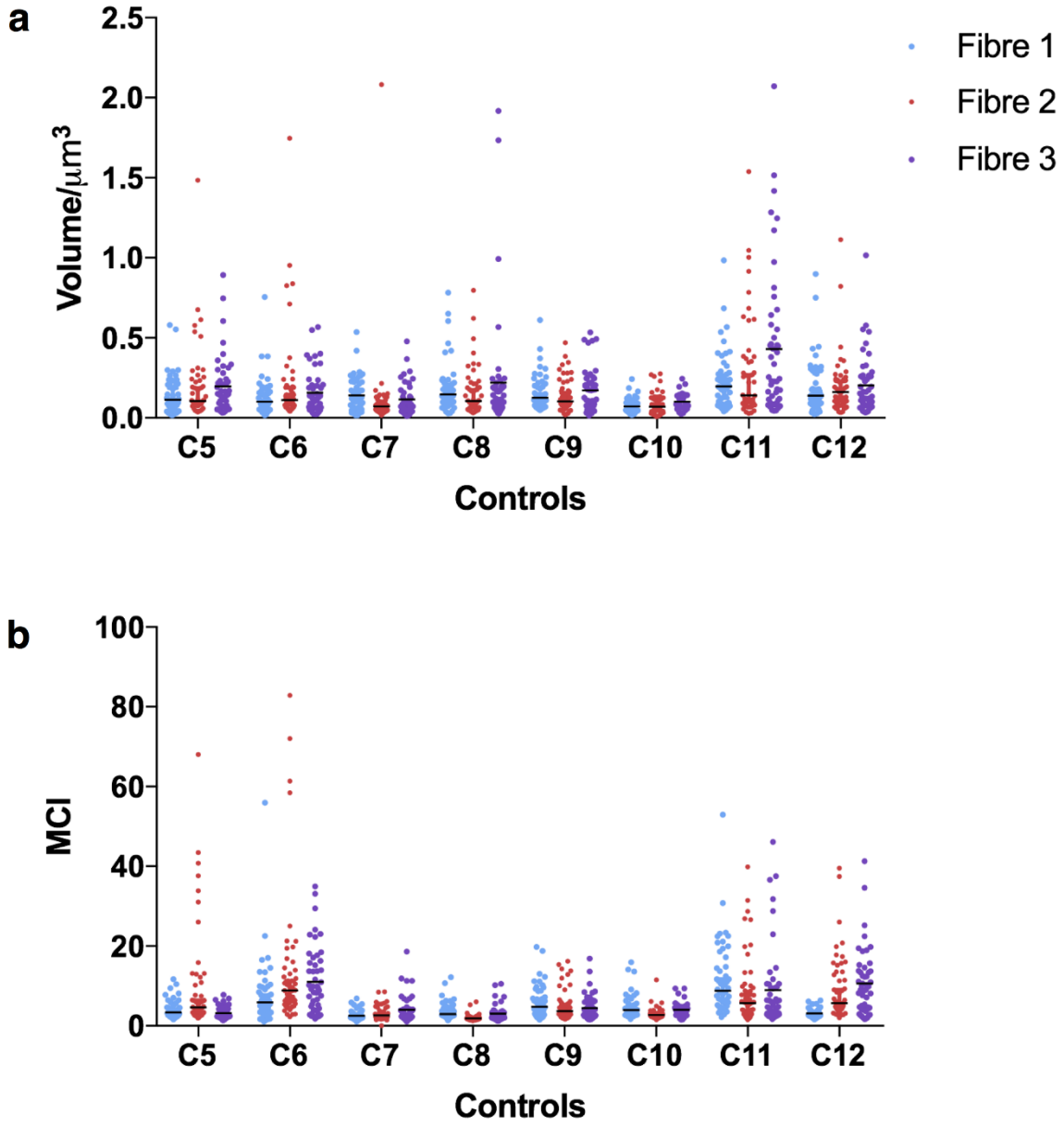

Figure 7.7 *Volume and MCI are variable within a single myofibre as well as between fibres. Comparison of (a) volume and (b) MCI for each mitochondrion in each the three IMF myofibres for the controls. Lines represent the mean for each fibre. Each data point represents one mitochondrion*

7.4.5 Is there a relationship between mitochondrial volume density and MCI?

It was hypothesised that MCI may increase in fibres where mitochondrial volume density was higher since the mitochondria would be in closer proximity and thus fusion events more likely. Mitochondrial volume density was assessed in each of the IMF myofibres as described in **7.3.4**. When mitochondrial volume density was plotted against mean MCI of the myofibre, for all controls there was no significant correlation (R^2 =0.09719, P = 0.1938) (**Figure 7.8**).The absence of relationship was even more evident when comparing single myofibres among individual subjects.

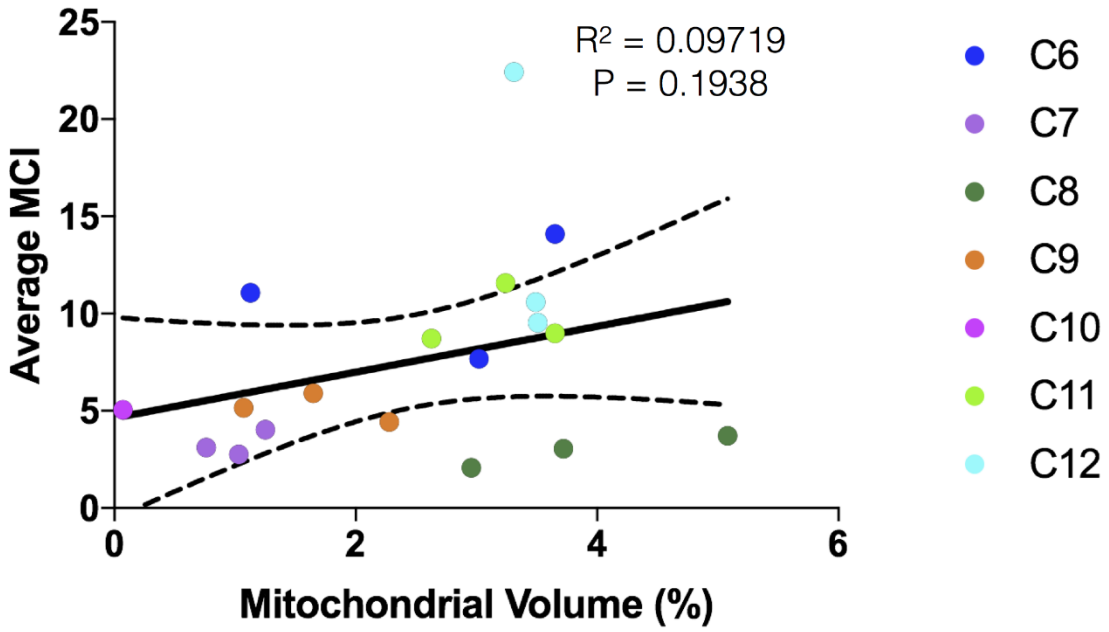

Figure 7.8 *Mitochondrial mass assessed over two sarcomeres from A-band to A-band. Mitochondrial volume as a percentage of muscle volume was plotted against average MCI for each myofibre. The solid line indicates linear regression, and the dotted lines the 95% confidence interval. No assessment was made for control 5 (C5) and two fibres from control 10 (C10) due to the orientation of the myofibres.*

7.4.6 How do patients with mtDNA mutations differ?

A cohort of six patients with mtDNA mutations including; single large-scale mtDNA deletion (n = 1) m.8344A>G $tRNA^{Lys}$ (n = 3) and m.3243A>$G^{Leu(URR)}$ (n = 1). This cohort is small, furthermore there are a number of confounding variables that must be considered and make the patients difficult to interpret. These variables include, mtDNA mutation, heteroplasmy, level of respiratory chain defect and age. This is made more difficult given the morphological variability observed in the controls (**Figure 7.9a**) and in patients also (**Figure 7.9b**).

Patients are colour coded based on the mtDNA mutation and ordered from left to right for patients 35 to 40. When compared to the combined control population using a Mann-Whitney test, patients 35, 37, 38 and 39 were significant. However, this is also the case if some of the controls are compared to the combined control population using a Mann-Whitney test, as such it is very difficult to make any firm conclusions from these data.

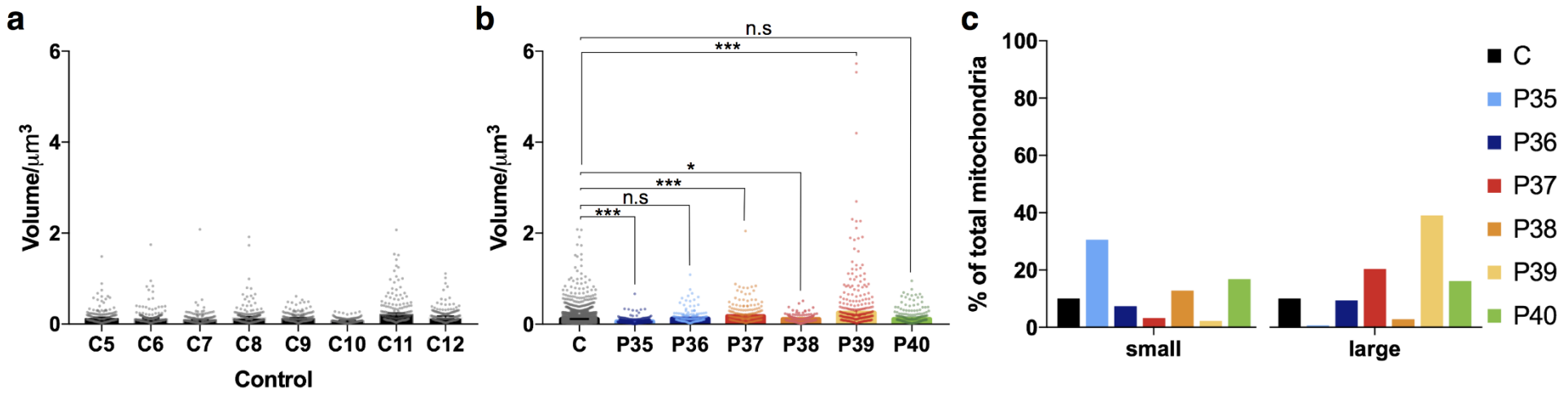

Figure 7.9 *Mitochondrial volume is variable between controls and patients analysed. Patients are organised by genetic mutation: controls; C, single, large-scale mitochondrial DNA deletion; P35 and P36, m.8344A>G $tRNA^{Lys}$: P37, P38 and P39, m.3243A>G $tRNA^{Leu(UUR)}$; P40. (a) Intermyofibrillar mitochondrial volume of controls 5 to 12 showing individual values, median and 95% confidence intervals. A Kruskal-Wallis test indicates that the controls are significantly different (P < 0.0001). (b) Intermyofibrillar mitochondrial volume of combined control and patients 25 to 40 showing individual values, median and 95% confidence intervals. A Mann-Whitney test was used to compare each patient to the control population (***; P < 0.0001, * = 0.0295; n.s.; not significant). (c) Intermyofibrillar mitochondrial volume of combined controls and patients 35 to 40. Data was plotted as a percentage of mitochondria that fall into the 10th (small) and 90th (large) percentile of the control population.*

It was expected that the most notable differences would be seen in the smallest and largest mitochondria. As such the tenth and ninetieth percentiles of the combined control population were used as a cut off to look at percentage of mitochondria that were either “small” (below the 10th percentile of controls) or “large” (above the 90th percentile of controls) respectively (**Figure 7.9c**). In doing so this made comparison of controls and patients easier. The first patient with a single mtDNA deletion (patient 35) has approximately three times the number of small mitochondria than were detected in the control population and very few large mitochondria. In comparison, the second patient with a single mtDNA deletion (patient 36) is very similar to the control population and has a slightly smaller deletion and a slightly lower heteroplasmy level (18%) than patient 35 (20%).

Within the patients analysed there are three related individuals with the m.8344A>G tRNA^{Lys} mutation (**Figure 7.10a**). The mother (patient 38) was 50 years old with 63% mutational heteroplasmy and mild myopathy. Her first daughter (patient 37) was 21 years old with 97% heteroplasmy, severe myopathy and exercise intolerance. In comparison her sister (patient 39) was 20 years old with 40% heteroplasmy and was asymptomatic. Patient 37 and her asymptomatic sister (patient 38), both had a much lower frequency of small mitochondria and the mother a marginally higher frequency of small mitochondria than was observed in the control population (**Figure 7.9c**). The opposite is observed for the large mitochondria and the asymptomatic sister had the highest frequency of large mitochondria with approximately four times that of the controls. Patient 37 had double the number of large mitochondria when compared to the controls whilst the mother had very few.

When the EM micrographs and reconstructed models were compared for each of these individuals it was very apparent that both patient 37 and 38 had relatively simple mitochondria that are small and round (**Figure 7.10b and c**). In comparison, patient 39, the asymptomatic sister, with a moderate level of heteroplasmy, had some very complex mitochondria with large degrees of branching and nanotunnels (**Figure 7.10d**). This patient also had small round mitochondria isolated from the mitochondrial network. Together, a substantial portion of very complex and very small mitochondria contributed to a greater spread of both MCI and volume (**Figure 7.10e and f**). Interestingly the volume of patient 38 is less positively skewed than patient 37 (skewness: patient 37 = 3.344 and patient 38 = 1.643), possibly suggesting that

some mitochondria in patient 37 are swollen, which is a common finding in mitochondrial myopathy. Finally, for the m.3243A>G $tRNA^{Leu(UUR)}$ patient (patient 40), both small mitochondria and large mitochondria are marginally more frequent than controls.

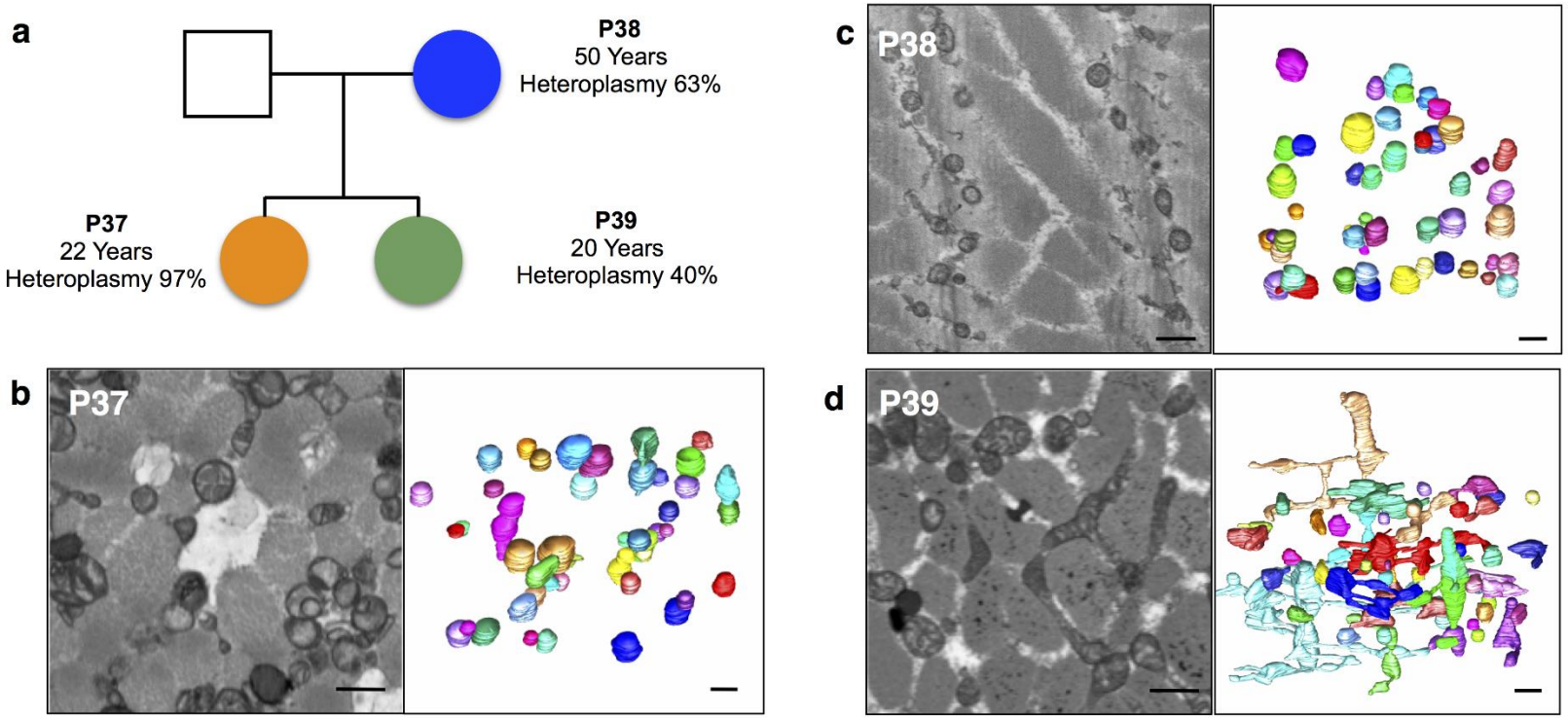

Figure 7.10 *A family variably affected with mitochondrial myopathy and m.8344A>G tRNA^{Lys} show a high degree of variability in mitochondrial morphology. (a) Family tree showing; patient 38 affected mother (blue) with 63% heteroplasmy, 22% COX deficiency and mild myopathy, patient 37 the proband (orange) with 97% heteroplasmy, 97% COX deficiency myofibres and severe myopathy and exercise intolerance and patient 39 unaffected sister (green) with 40% heteroplasmy and some intermediate COX-deficient fibres. (b-d) Single slice from serial block face scanning electron microscopy (SBFSEM) and reconstruction of 50 mitochondria in an IMF region of myofibre for patients 37 (b), 38 (c) and 39 (d). Note the small round morphology in the mother and proband (b and c) and the branched mitochondria in the unaffected sister (d). Scale bars; 1 µm.*

MCI was also highly variable in both controls (**Figure 7.11a**) and patients (**Figure 7.11b**). A Mann-Whitney test comparing patients to the combined control population found a significant difference in all patients. However, some but not all of the control cases also yielded this result when compared to the combined control population using a Mann-Whitney test. Similar to volume it was expected that the greatest changes would be observed at either end of the MCI spectrum. Therefore, the 10^{th} and 90^{th} percentiles of the MCI of the controls were used as cut offs to categorise patient mitochondria as simple (less than the 10^{th} percentile of the control population) or complex (greater than the 90^{th} percentile of the control population). This demonstrated that simple mitochondria, i.e. mitochondria that are more less branched and more round, are typically more frequent in patients than controls (**Figure 7.11c**).

In the patients with single, large-scale mtDNA deletions (patient 35 and 36), patient 36 was comparable to controls in frequency of simple and complex mitochondria, similar to results for volume (**Figure 7.11c**). Patient 35 also had a three times higher frequency of simple mitochondria than the control population, however the frequency of complex mitochondria was comparable to controls, a slight variation in the pattern observed with volume. This tends to indicate that the larger mitochondria in patient 35 are likely large and branched rather than simple and swollen.

In the three cases with the m.8344A>G $tRNA^{Lys}$ mutation, all patients had more simple mitochondria than the control population with patients 37 and 38; the proband and mother having the highest levels with approximately 70% and 80% of all mitochondria being classified as simple (**Figure 7.11c**). Of these three cases the symptomatic sister (patient 39) was the only patient to have complex mitochondria, with levels comparable to those of the control population. Finally, the m.3243A>G patient (patent 40) had an approximately six times higher frequency of simple mitochondria than the control population and very few simple mitochondria.

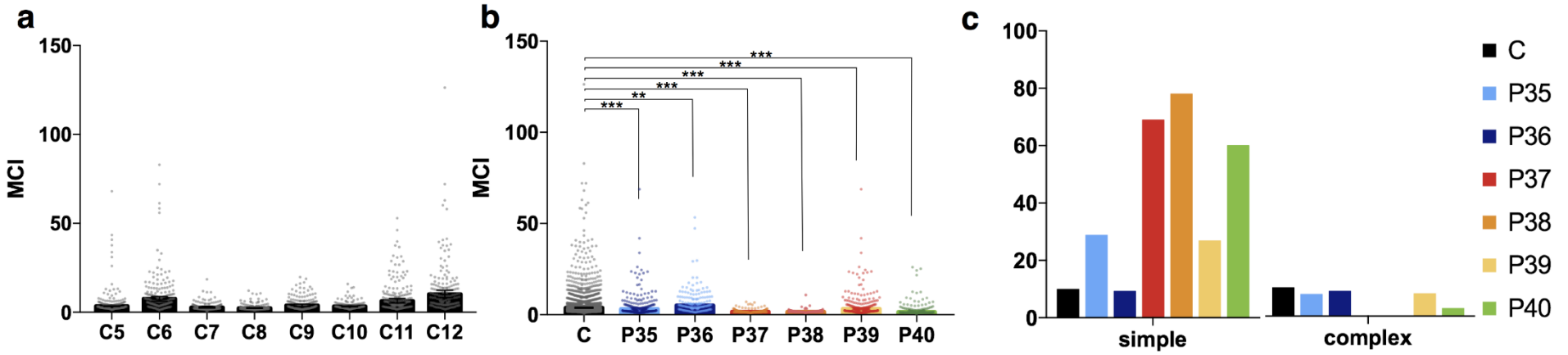

Figure 7.11 *Mitochondrial complexity index (MCI) is variable between controls and patients analysed. Patients are organised by genetic mutation: controls; C, single, large-scale mitochondrial DNA deletion; P35 and P36, m.8344A>G $tRNA^{Lys}$: P37, P38 and P39, m.3243A>G $tRNA^{Leu(UUR)}$; P40. (a) Intermyofibrillar mitochondrial MCI of controls one to eight showing individual values, median and 95% confidence intervals. A Kruskal-Wallis test indicates that the controls are significantly different ($p < 0.0001$). (b) Intermyofibrillar mitochondrial MCI of combined control and patients one to six showing individual values, median and 95% confidence intervals. A Mann-Whitney test was used to compare each patient to the control population, all were significant (***; $P < 0.0001$, **; $P = 0.0031$). (c) Intermyofibrillar mitochondrial MCI of combined controls and patients 35 to 40. Data as plotted as a percentage of mitochondria that fall into the 10th (simple) and 90th (complex) percentile of the control population*

7.4.7 Frequency of donut mitochondria and nanotunnels

For each of the mitochondria reconstructed the number of nanotunnels and donut mitochondria were counted. For each of these counts the total was normalized to the number of mitochondria assessed giving number of nanotunnels or donut mitochondria per 100 mitochondria assessed.

Donut mitochondria are those that have either fused back in on themselves or have split forming a ring shape. Once more these were found in both transverse and longitudinal orientations, and were in fact most commonly found in the longitudinal orientation. When the frequency was compared among all cases frequency of donut mitochondria had no clear trend in patients or controls (**Figure 7.12a-c**). However, it is difficult to draw robust conclusions on such a small sample size. The biological relevance and previous findings are discussed further in section **7.5.5**.

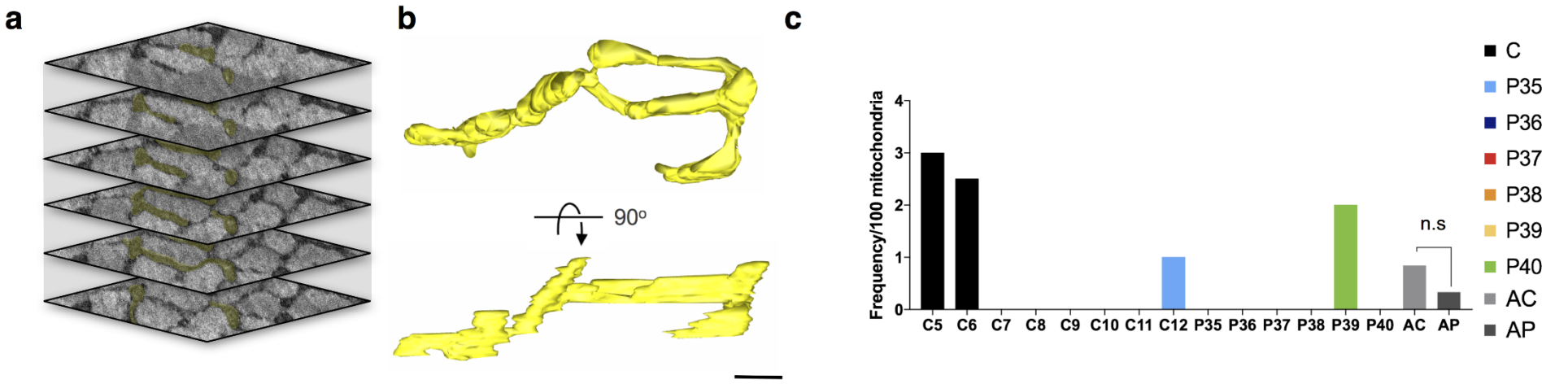

Figure 7.12 *Donut mitochondria were observed in patients and controls. (a) Stack of serial block face scanning electron microscopy images showing a donut mitochondrion and (b) three dimensional reconstruction of the donut mitochondrion in (a). (c) Frequency of donut mitochondria per 100 mitochondria in combined controls (black) and patients 35-40 (left to right). Patients are organised by genetic mutation: controls; C5 to C12, single, large-scale mitochondrial DNA deletion; P35 and P36, m.8344A>G $tRNA^{Lys}$: P37, P38 and P39, m.3243A>G $tRNA^{Leu(UUR)}$; P40. A Mann-Whitney test was used to compare all controls (AC) and all patients (AP), no significant (n.s) difference was detected. Of the mitochondria that had nanotunnels (n = 241) and those that were donut mitochondria (n = 17), five had both. Scale bars; 500 nm.*

Nanotunnels were thin projections connecting two close or distant mitochondria (**Figure 7.13 a and b**). Nanotunnels were present in both the transverse and longitudinal orientation increasing the likelihood that the frequency would be underestimated by two dimensional assessments. When the frequency of nanotunnels was compared for all subjects, number of nanotunnels were generally low in controls, with the exception of control 6 (**Figure 7.13c**). In comparison frequency of nanotunnels was high in patients with the greatest number found in patient 39. Interestingly, the patients with m.8344A>G $tRNA^{Lys}$ and m.3243A>G $tRNA^{Leu(UUR)}$ point mutations had higher levels of nanotunnels than those with large-scale single deletions (patients 35 and 36). Although with such a small number of patients with point mutations we do not have the statistical power to test this.

Because nanotunnels are newly discovered in human skeletal muscle, we attempted to derive some functional significance by analysing the correlation between the number of nanotunnels overserved and clinical parameters. Frequency of nanotunnels was plotted against key clinical and diagnostic parameters including percentage of COX deficiency (**Figure 7.14a**), heteroplasmy (**Figure 7.14b**) and NMDAS (**Figure 7.14c**), as well as MCI (**Figure 7.14d**). Regression lines demonstrated a lack of trend and significance.

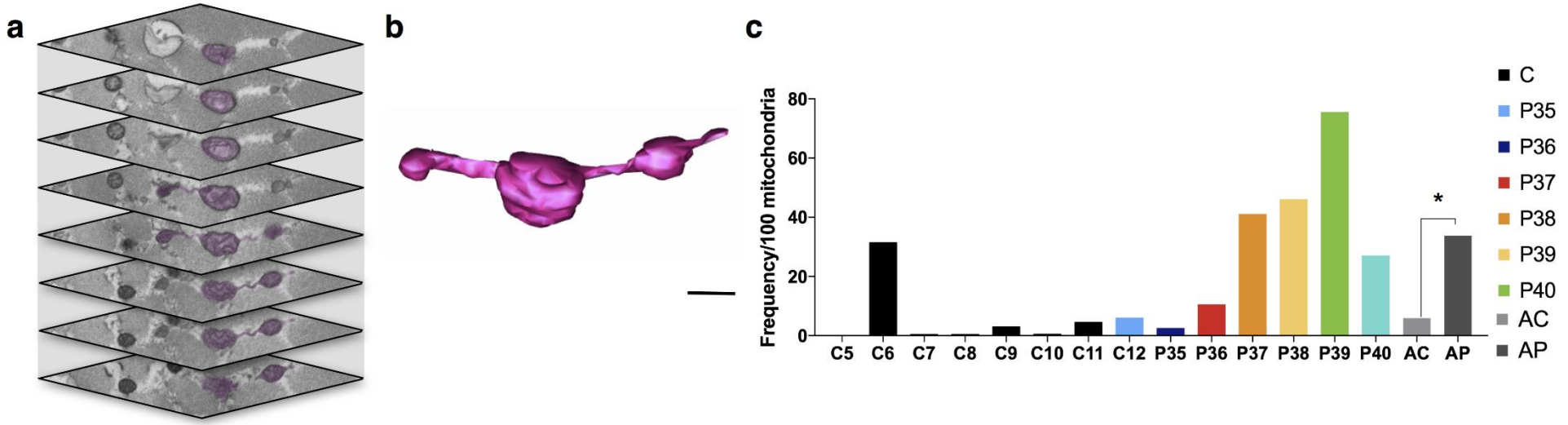

Figure 7.13 *Nanotunnels were observed in controls and patients but more frequenctly in patients. (a) Stack of serial block face scanning electron microscopy images showing a mitochondrion with a nanotunnel and (b) three dimensional reconstruction of the mitochondrion in (a). (c) Frequency of nanotunnels per 100 mitochondria in combined controls (black) and patients 35-40 (left to right). Patients are organised by genetic mutation: controls; C5 to C12, single, large-scale mitochondrial DNA deletion; P35 and P36, m.8344A>G* $tRNA^{Lys}$*: P37, P38 and P39, m.3243A>G* $tRNA^{Leu(UUR)}$*; P40. A Mann-Whitney test was used to compare all controls (AC) and all patients (AP) which are significantly different (p=0.01).*

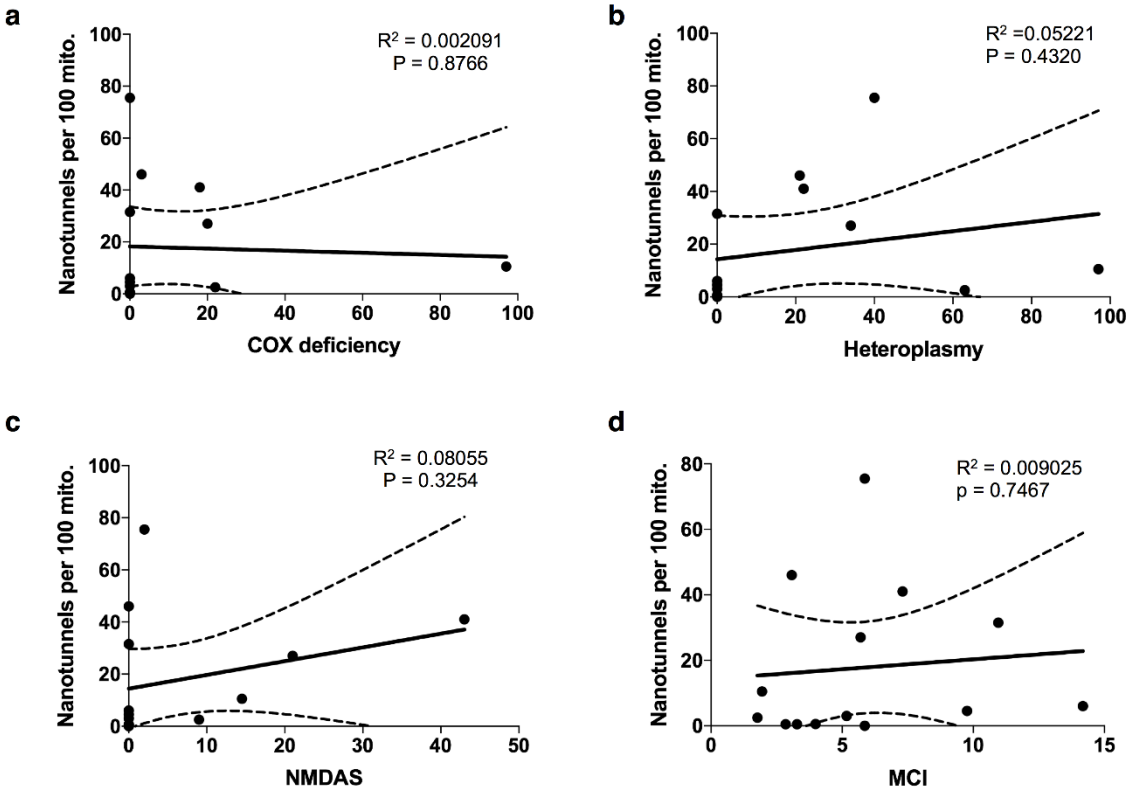

Figure 7.14 *Regressions plotted for frequency of nanotunnels per 100 mitochondria. Number of nanotunnels plotted against (a) percentage COX-deficient fibres (R^2 = 0.002091, P = 0.88), (b) heteroplasmy (R^2 = 0.052, p = 0.43), (c) NMDAS (R^2 = 0.08055, P = 0.33) and (d) MCI (R^2 = 0.0090, P = 0.7467)*

7.4.8 Looking for trends that improve the understanding of disease pathology

There were a number of confounding variables that needed to be considered when the patient data was interpreted, these included; mtDNA mutation, mutational heteroplasmy, degree of respiratory chain deficiency and age. As such it is helpful to look for correlations that may help yield a better understanding of the results. Plotting of MCI against heteroplasmy, percentage COX deficiency, age and also total NMDAS scores and NMDAS subscores for myopathy and exercise intolerance, yielded (***Table 7.1***) no strong or significant correlation (**Figure 7.15**).

Interestingly, the pattern for heteroplasmy appears to take an adverted U shape. This would fit with previous findings and a hypothesis that fusion at low levels of

mutational heteroplasmy allows complementation but at higher levels of heteroplasmy the network fragments.

Patient #	Assessment time relative to biopsy	NMDAS total	Exercise intolerance	Myopathy
35	6 months pre-biopsy	21	0	2
36	At biopsy	43	4	3
37	1 year pre-biopsy	14.5	4	3
38	At biopsy	9	0	2
39	At biopsy	2	0	0
40	N/A	N/A	N/A	N/A

Table 7.1 *Total NMDAS and NMDAS subscores for exercise intolerance and myopathy for all patients, apart from patient 40, for whom these were unavailable*

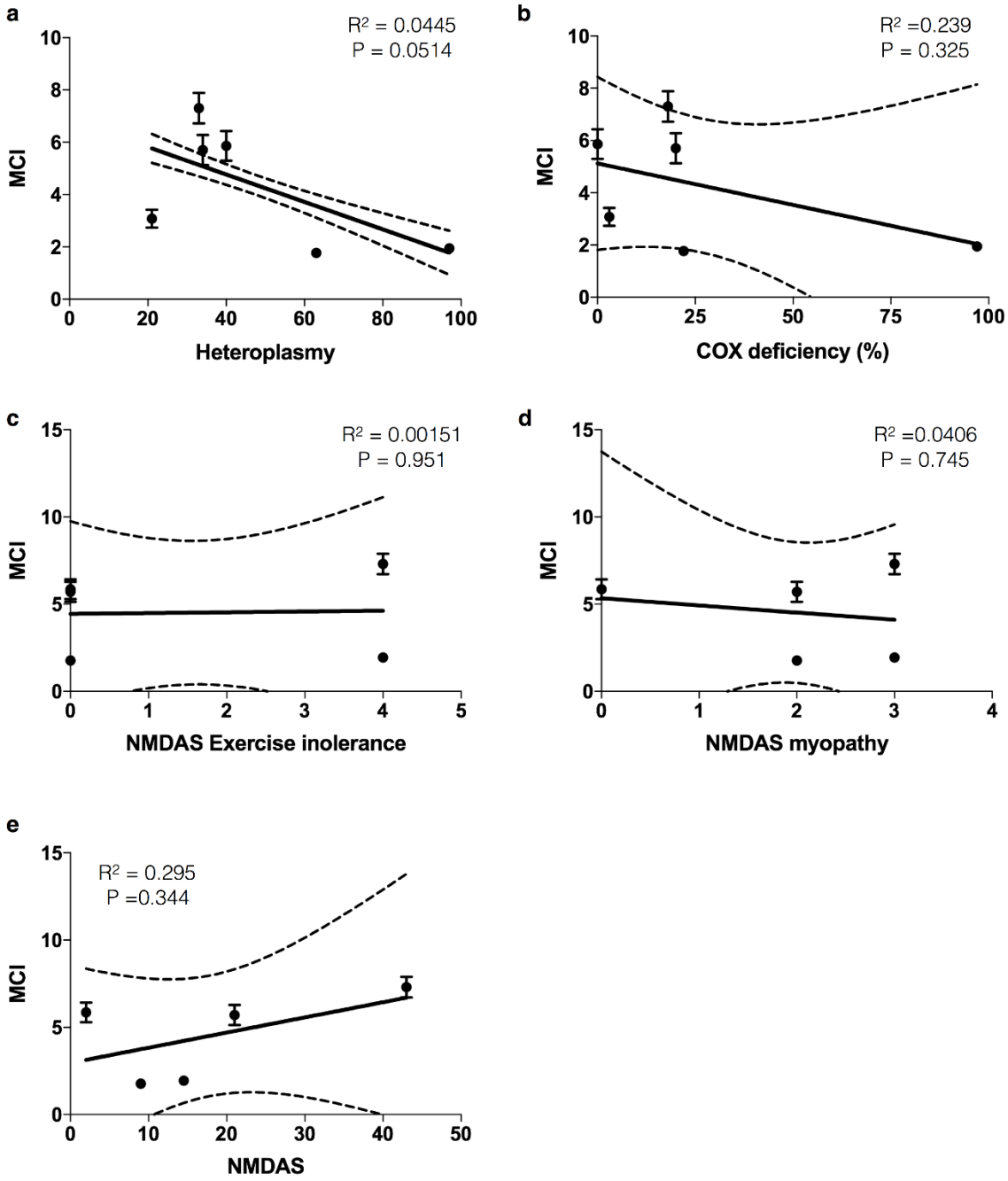

Figure 7.15 *Average mitochondrial complexity index for the muscle fibres of each patient was regressed against (a) heteroplasmy (R^2 = 0.0445, P = 0.0514) (b) percentage COX deficiency (R^2 = 0.239, P = 0.325), (c) NMDAS exercise intolerance subscore (R^2 = 0.00151, P = 0.951), (d) NMDAS myopathy subscore (R^2 = 0.0406, P = 0.745) and (e) NMDAS total (R^2 = 0.295, P = 0.344). Data for patient 40 was not plotted for c-e due to lack of NMDAS scores.*

As the largest, but still very small, patient group the m.8344A>G patients were examined further for possible correlations. When MCI was regressed against COX-deficiency (**Figure 7.16a**) and mutational heteroplasmy (**Figure 7.16b**) for the three m.8344A>G $tRNA^{Lys}$ patients, R squared values showed a strong relationship however neither heteroplasmy ($R^2 = 0.89$, P = 0.056) or percentage COX deficiency ($R^2 = 0.61$, P = 0.43) were significant. However, this should be interpreted with caution since these graphs include only a few data points and cannot really be used to draw conclusions, but were used to explore possible trends that may warrant investigation with a larger patient cohort.

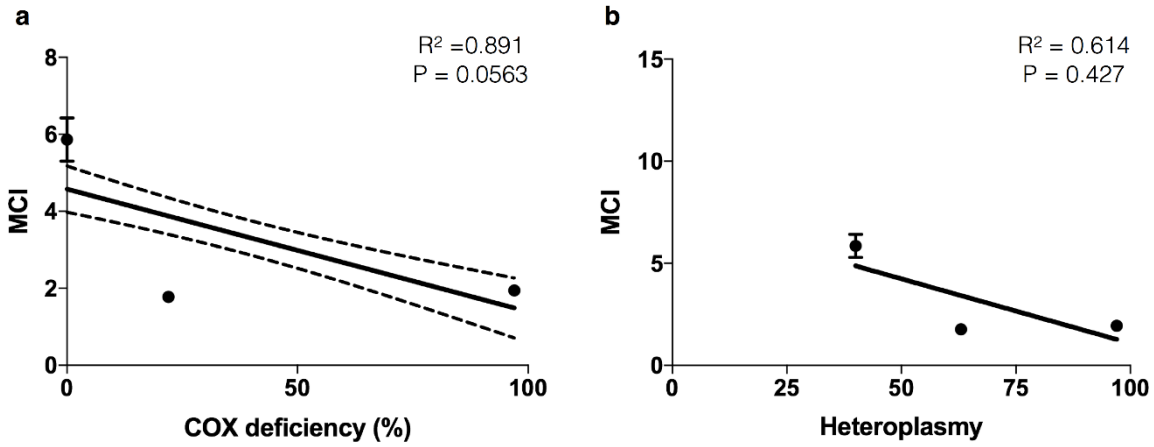

Figure 7.16 *Mean MCI regressed against (a) percentage COX deficiency ($R^2 = 0.89$, P = 0.056) and (b) heteroplasmy ($R^2 = 0.61$, P = 0.43). Error bars are SEM.*

7.4.9 Assessing mitochondrial anisotropy

COX deficiency in longitudinal skeletal myofibres is segmental and spreads slowly through the myofibre over time. The reason that short segments of COX deficiency are regularly observed and skeletal myofibres are rarely fully deficient is intriguing and has relevance for clinical pathology and disease progression. In order to test whether the mitochondrial network may be a limiting factor in the spread of respiratory chain deficiency, mitochondrial branching was assessed in the transverse and longitudinal planes and a ratio of the two calculated to quantitatively assess

mitochondrial anisotropy with a mitochondrial branching index (MBI). It was hypothesised that mitochondrial branching would be greater in the transverse orientation possibly accounting for faster spread in this orientation (**Figure 7.17a**). Mitochondria that are equally branched in both directions will have an MBI of one. Mitochondria that exhibited more branching longitudinally had an MBI of less than one (e.g. **Figure 7.17b**) and those that were more branched in the transverse orientation had an MBI of greater than one (e.g. **Figure 7.17c**). This demonstrated that 48.7% of all mitochondria analysed are equally branched in both directions (**Figure 7.17**), 40.9% were more branched in the transverse orientation and only 10.4% more branched longitudinally (**Figure 7.17d**). Taken together this suggests an approximately 4-fold greater degree of mitochondrial network connectivity across the plane of each z-band compared to the connections between mitochondria of different z-bands. This is noticeable upon visual assessment in some myofibres (e.g. **Video 7.2**, on CD provided).

Video 7.2 *The video can be found on the attached disk. This video shows a full reconstruction of an intermyofibrillar serial block face scanning electron microscopy image stack. Each mitochondrion is in a different colour. The video starts in a transverse orientation and rotates 360 degrees in the x-axis. Then rotates to a transverse orientation before rotating in the y-axis. Notice the variation in mitochondrial shape and size and the organisation of mitochondria in layers at the z-band. Also noticeable are nanotunnels connecting mitochondria at adjacent z-bands.*

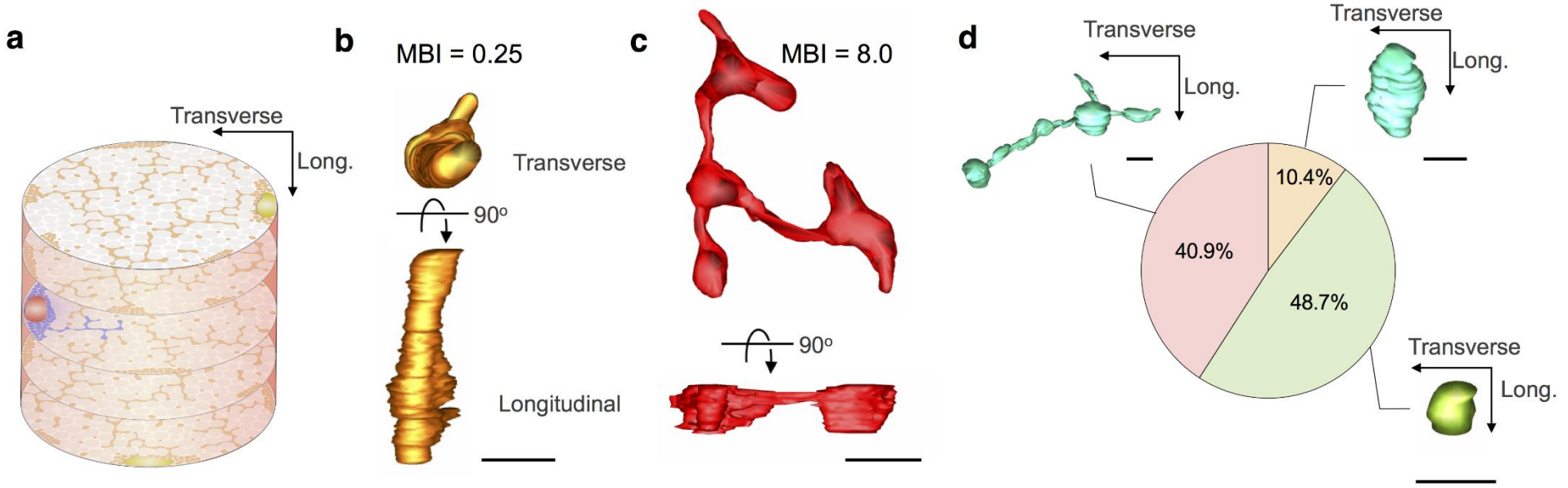

Figure 7.17 *Anisotropy of branching may impact the spread of mtDNA mutations through skeletal myofibres. (a) Schematic demonstrating increased likelihood of mutation expansion in direction with greatest mitochondrial "network connectivity" or branching. (b) A reconstructed mitochondrion that was longer or more branched in the longitudinal orientation of the myofibre and (c) a reconstructed mitochondrion that was more branched in transverse orientation. (d) Mitochondrial branching indicator (Transverse branching indicator/Longitudinal branching indicator) in combined controls and patients. A value of less than 1 (orange) indicated greater branching in the longitudinal orientation of the myofibre, equal to 1 (green) indicated equivalent branching in both planes and greater than 1 (red) indicated more branching in the transverse plane of the myofibre. Note that the percentage of mitochondria that were more branched in the transverse orientation (40.9%) was greater than those more branched longitudinally (10.4%). Scale bars; (b) and (c) 1 μm and (d) 500 nm.*

7.5 Discussion:

Mitochondrial morphology is intrinsically linked to mitochondrial function, with numerous studies finding correlations between mitochondrial morphology and mitochondrial function and tissue function (Trushina *et al.*, 2012; Hara *et al.*, 2014; Picard *et al.*, 2014; Leduc-Gaudet *et al.*, 2015). Mitochondria become more fused at intermediate levels of mutational heteroplasmy (50-80%) and the network fragments at high levels of heteroplasmy (90%) (Picard *et al.*, 2014). At the tissue level, frequency of donut mitochondria in synaptic boutons of aged rhesus monkeys inversely correlates with working memory (Hara *et al.*, 2014). SS mitochondria are swollen and less circular and IMF mitochondria were longer and more branched in atrophied skeletal muscle fibres in mice (Leduc-Gaudet *et al.*, 2015).

Prior to this investigation three-dimensional assessment of human skeletal muscle mitochondria using electron microscopy had been restricted to one study in controls, which also completed quantitative mitochondrial volume density using confocal microscopy (Dahl *et al.*, 2015). In addition, a study using FIBSEM to quantitatively assess mouse muscle mitochondrial morphology demonstrated a continuous mitochondrial reticulum (Glancy *et al.*, 2015).

7.5.1 Quantitative analysis of mitochondrial networks in three dimensions

Due to the lack of previous quantitative assessment in three-dimensions, it was necessary to develop morphological parameters. Form factor which had already been developed and validated as a two dimensional was modified to give a three dimensional branching indicator, which was subsequently validated. Testing of the Mitochondrial Complexity index (MCI), proved it to be the three dimensional equivalent of form factor and found it to be a valuable discriminating parameter when comparing both SS and IMF mitochondria.

7.5.2 Subsarcolemmal and intermyofibrillar mitochondrial are morphologically different

Subsarcolemmal mitochondria were found to be less complex and have a smaller volume than intermyofibrillar mitochondria. Upon visual analysis the majority of subsarcolemmal mitochondria are spherical, with a small proportion having projections that reach into the IMF space or are fused to an IMF mitochondrion. This observation is in agreement with previous reports both in mouse (Picard *et al.*, 2013) and humans (Dahl *et al.*, 2015).

7.5.3 Variability in mitochondrial morphology in control skeletal muscle

Assessing mitochondrial morphology in control myofibres demonstrated unexpected variability within fibres, between fibres of the same individual and between controls. Although it is apparent that mitochondrial morphology is likely to be variable both between muscles with different oxidative capacities and tissues with different energetic demands, the variability of mitochondrial volume and branching observed here within a single myofibre was surprising.

Since fibres were selected based on the mitochondrial mass within a fibre and fibre typing was not possible, it is possible that different fibre types were analysed. If so this may explain some of the variability observed, since fibre type has previously been demonstrated to alter mitochondrial morphology and dynamics (Dahl *et al.*, 2015; Mishra *et al.*, 2015). In particular Dahl *et al.* (2015), demonstrates that type I fibres have a higher mitochondrial volume and tubular mitochondria are generally thicker, whilst Mishra *et al.* (2015) demonstrates that fusion events are more frequent in oxidative muscle fibres.

Further to this when findings presented here in human skeletal muscle are compared to those of Glancy *et al.* (2015) in mouse skeletal muscle, there appear to be inherent differences between species. In mouse skeletal muscle the mitochondria form one reticular network with smaller isolated mitochondria being a rare occurrence and the overall mitochondrial volume density is greater. This may be a consequence of the variation of mitochondrial fibre types in humans and mice (Gorza, 1990; Smerdu *et al.*, 1994). Alternatively, it could be a methodological artefact since, they implement

automatic segmentation of mitochondria by thresholding based on the pixel grey scale. Particularly for the subsarcolemmal mitochondria in images presented it looks like mitochondria that are not joined may have been artificially joined.

However, Glancy *et al.* (2015) drop fixative on to the mouse muscle whilst the mouse is still alive. In comparison for human muscle biopsies there is typically up to an hour of ischemia following the biopsy prior to fixation. As such it should be considered that this could also be an artefact caused by the delay between biopsy and subsequent fixation of the tissue when we assess human samples. It is well known that mitochondria can change shape in seconds and that delay in fixation may result in a change in the structure observed on EM.

Given the lower mitochondrial volume density in human skeletal muscle, it seems unlikely that the difference in mitochondrial morphology observed here is due to fixation artefact, since delayed fixation will only cause a fragmentation of the network not a change in total mitochondrial volume. Furthermore, clear variability is noted throughout the cases assessed with some exhibiting marked mitochondrial complexity and others very simple mitochondrial morphology and yet all biopsies were processed the identically.

7.5.4 Mitochondrial morphology in mitochondrial myopathies

A further novelty of this work was the comparison of mitochondrial three dimensional morphology in a cohort of mitochondrial myopathy patients to the control population. Although this included only a small group of patients thus making it difficult to interpret and draw conclusions, this provides grounding for future studies. In addition to the confounding variables considered previously (mtDNA mutation, heteroplasmy, percentage COX deficiency and age), there are also a number of other variables to consider. Due to variation in clinical severity as well as age some patients are likely to be more active than others, indeed some of the patients analysed have a degree of exercise intolerance (**Table 7.1**). Since exercise is known to promote mitochondrial biogenesis based on substantial research connecting level of exercise to both mitochondrial morphology and mitochondrial mass.

This work has also allowed the identification of morphological indicators of mitochondrial dysfunction and mitochondrial stress, in particular mitochondrial network fusion and fragmentation, nanotunnels and donut mitochondria. Nanotunnels and donut mitochondria were previously unobserved in human skeletal muscle. In addition, the data presented here provides a clearer picture than that presented in **chapter 6**, since we get a better idea of the true frequency and 3D shape of these structures.

The mitochondrial network has been demonstrated to undergo stress induced mitochondrial fusion in response to low levels of mitochondrial stress or mutational heteroplasmy (Tondera *et al.*, 2009; Shutt and McBride, 2013; Picard *et al.*, 2014; Leduc-Gaudet *et al.*, 2015). However, when mutational heteroplasmy is increased or stress exceeds a functional threshold the mitochondrial network appears to fragment likely due to loss of membrane potential and proteolytic cleavage of Opa1 (Ehses *et al.*, 2009; Head *et al.*, 2009). This appears to be supported by what is observed here in the m.8344A>G $tRNA^{Lys}$ trio, where both mother and daughter with 60% and 97% heteroplasmy respectively have fragmented mitochondrial networks whereas the sister with lower (40%) mutational heteroplasmy in fact shows greater mitochondrial network connectivity than the combined control population but similar or less than some controls (controls 6, 11 and 12) when compared individually.

7.5.5 Donut mitochondria

Donut or toroid mitochondria have been found to be a morphological marker of cellular stress and are found in cells during hypoxia (Liu and Hajnoczky, 2011) as well as being inducible via respiratory chain inhibition (Ahmad *et al.*, 2013). They have been found to range in diameter from 0.5 – 2.4 μm with a nearly Gaussian distribution and to form by self-fusion due to increases in chemiosmotic pressure caused by opening of the permeability transition pore (PTP) and changes in the K^+ conductance of the IMM (Long *et al.*, 2015). This increase in pressure is relieved by mitochondrial swelling or donut formation (Long *et al.*, 2015). Furthermore, toroid mitochondria return more easily to their initial morphology than swollen mitochondria so as well as a stress response it is also a protective mechanism (Liu and Hajnoczky, 2011). Interestingly, frequency of donut mitochondria in presynaptic boutons of the

prefrontal cortex of aged rhesus monkey has also been found to correlate inversely with working memory (Hara *et al.*, 2014) demonstrating that they may be associated with tissue dysfunction.

Surprisingly, donut mitochondria were observed here in a small number of patients and controls and were not more prevalent in patients. In **Chapter 6**, donut mitochondria were observed in the transverse orientation, here using three-dimensional reconstruction we observed that these actually appear more commonly in the longitudinal orientation. Thus three-dimensional EM techniques provides us with a clearer picture of both frequency, size and morphology of these toroid mitochondria. Quantitative measurements similar to those made by (Long *et al.*, 2015), need to be made to assess whether these measurements are in agreement. However, based on the available data for the frequency of donut mitochondria in controls and patients they are perhaps not a useful morphological abnormality for diagnostic purposes.

7.5.6 Nanotunnels

The first visualisation of a nanotunnel-like structure was in 2008 (Bowes and Gupta, 2008) in African green monkey kidney cell, where transmission electron microscopy was used to demonstrate double membrane connections between mitochondria of roughly 50 nm in diameter. The term “nanotunnel” was introduced later by Huang *et al.* (2013). This study examined rat cardiomyocytes by live-cell confocal microscopy and found nanotunnel diameter to be 90-120 nm. In addition, measurements of nanotunnels in human skeletal muscle using TEM and reporting diameters of 62.3 ± 10.7 nm are presented in **Chapter 6** (Vincent *et al.*, 2016b). Additionally, Bowes and Gupta (2008) found the length of the projections to be variable, Huang *et al.* (2013) report nanotunnels to span up to seven sarcomeres and findings presented in **Chapter 6** (Vincent *et al.*, 2016b) show lengths between 200 nm and 2.3 µm. Three-dimensional analysis in this chapter finds nanotunnels more frequently than expected based on TEM analysis of the same patients in **Chapter 6**.

Most interestingly, comparison of controls and patients demonstrates that nanotunnel are noticeably more frequent in patients than controls. This seems to implicate

nanotunnels as a stress response, which both increases the understanding of their relevance and raises further questions.

Firstly, can nanotunnels transport mtDNA, thus allowing genetic complementation? Initial confocal live cell imaging demonstrated that nanotunnels can transport GFP localised to both the mitochondrial matrix and also the IMM. However, given that mammalian nucleoids are reported to have a uniform size of approximately 100 nm (Kukat *et al.*, 2011), it is unlikely that nanotunnels could transport nucleoids. This suggests that the functional importance of nanotunnels is not complementation of mitochondria with nucleoid packaged mtDNA, but possibly proteins and RNA.

In addition to this, are they only observed in skeletal and cardiac muscle where mitochondrial movement is restricted? It would make sense if nanotunnels were a morphological response to the fact that mitochondria are less motile in skeletal and cardiac muscle compared to other cells such as neurons where they are highly motile. If this were the case nanotunnels may function as an alternative communication method. In order to determine whether this is the case, studies similar to this one need to be performed in other tissues. In doing so it may be possible to find other morphological features with apparent tissue specificity.

Based on previous findings nanotunnels are both highly dynamic and occur between distant mitochondria (Huang *et al.*, 2013). As such the mechanism by which they form and whether there is a signalling involved to guide the projection of one mitochondrion to its target mitochondria should be investigated. Previous work has implicated a Kinesin family member 5B (Kif5b), a microtubule-dependent motor, dependent mechanism in their formation of nanotunnels between mitochondria that subsequently increase in diameter to form a fused network (Wang *et al.*, 2015). A similar structure has also been reported in Alzheimer's disease and is described as "mitochondria on a string", these structures have been suggested to form from failed fission. This is supported by Lee *et al.* (2016) who find nanotunnel like structures form in a number of cell lines when treated with dynamin-2 siRNA. These two mechanisms seems to be distinct and produce similar structures. Which of these is being observed here or whether there are other mechanisms at work has yet to be determined. A number of projections from one mitochondrion not yet connected to a second mitochondrion were observed, this seemed to indicate that this is not the result of failed fission.

As to whether a signalling mechanism exists this seems very plausible but would require further investigation. Nanotunnels often form connections between two distant mitochondria passing other mitochondria in the process (Huang *et al.*, 2013). As such, this could either be a random process and the nanotunnel fuses with the first mitochondrion it contacts or alternatively and perhaps more likely a signalling mechanism guides the nanotunnel projection to its intended target. This hypothesis is perhaps more appealing if we consider the that tube-like membranous communication mechanisms are known to occur in bacteria (Dubey and Ben-Yehuda, 2011), as are chemoattractant cell to cell signalling mechanisms (Brown and Berg, 1974). Furthermore chemoattractant signalling has been found to drive filipodia formation and tunnelling nanotube communication between cells (Gerdes *et al.*, 2013).

7.5.7 Mitochondrial anisotropy affects spread of mtDNA mutations and respiratory chain deficiency

In skeletal muscle COX-deficiency is found to be segmental when examined longitudinally (Matsuoka *et al.*, 1992; Elson *et al.*, 2002; Bua *et al.*, 2006) and to expand over time (Lopez *et al.*, 2000). The restricted spread of respiratory chain deficiency throughout the full length of the myofibre is of functional and clinical relevance to mitochondrial myopathy, skeletal muscle ageing and neuromuscular diseases for which respiratory deficiency is seen to varying degrees. Results presented here found that the mitochondrial network in human skeletal muscle is anisotropic with greater branching across the transverse myofibre than longitudinally. As such, this may explain the segmental histological pattern of COX-deficiency since mtDNA mutations and respiratory deficiency are likely to spread quicker along the path of least resistance (the transverse orientation) than longitudinally where there are fewer mitochondrial connections. When considered in the context of investigations into mechanisms of clonal expansion, (explored in detail in **Chapter 5**), this further suggests that the mechanism by which mtDNA mutations clonally expand may differ dependent of the tissue architecture and mitochondrial network morphology.

7.5.8 Limitations:

This study has a number of limitations that must be considered. Primarily the control and patient biopsies are taken from different muscles which may impact on the fibre type distribution and lead to differences in mitochondrial morphology. Furthermore, all patients are female, whilst only three of the eight controls are female and oestrogen levels have been known to affect mitochondrial morphology (Hara *et al.*, 2014). In addition when muscle biopsies are taken there is always a delay between the removal of the muscle biopsy from the leg muscle and its subsequent fixation which may induce artefacts when mitochondrial morphology is examined. Time of biopsy is also found to be an important variable when assessing mitochondrial morphology in liver (Jacobi *et al.*, 2015) and may also be important to consider in skeletal muscle. Finally activity levels of the controls and patients biopsied are likely to impact results since mitochondrial mass is known to increase with exercise (Holloszy, 1967).

Finally, when trying to correlate mitochondrial morphology with heteroplasmy, these results are potentially confounded by the fact that we are using heteroplasmy based on muscle homogenate mtDNA rather than single cell. Unfortunately using the present technique, the correlation with single cell heteroplasmy is not possible and therefore limits how we interpret the data.

7.5.9 Further work

Due to the large data set acquired here, it would be interesting to apply analysis methods used on large data sets like those acquired from metabolomics. As such the intention is to use the online web tool MetaboAnalyst v3.0 (Xia *et al.*, 2015), to generate a model and see if it is possible to identify key morphological discriminators to identify patients and controls.

Primarily an experiment comparing fixation protocols typically used in for electron microscopy in rodents with methods used here should be completed. This should elucidate whether the differences observed between mice and human muscle is a species related difference or an artifact induced by fixation delay.

Studies in mice could also be performed to assess the effect of exercise and metabolic state on the mitochondrial morphology. In addition, super resolution or expansion microscopy could be used to assess the mitochondrial morphology in the context of respiratory chain function and fibre type.

Another possibility is to try to correlate single cell heteroplasmy for known mtDNA mutations with mitochondrial morphology. This could be attempted using probes for mutant and wild type mtDNA in combination with expansion microscopy. This would hopefully allow us to assess the relative proportions of wild-type and mutant mtDNA as well as the morphology of the mitochondrial network with nanoscale resolution.

7.5.10 Conclusion:

This work developed methodology for three-dimensional quantification of mitochondrial branching and morphology. MCI was used in combination with volume, which provided the first quantitative assessment of mitochondrial morphology and network organisation in human skeletal muscle at EM resolution. Furthermore, it confirmed two dimensional findings that in muscle SS mitochondria are smaller and rounder than IMF mitochondria and reports that SS and IMF mitochondria interact (Picard *et al.*, 2013; Dahl *et al.*, 2015).

The data demonstrated unexpected variation both within fibres of the same control and among the control population, which lead to questions of whether fibre type, levels of activity and metabolic state may be confounding variables.

Interestingly, low levels of m.8344A>G $tRNA^{Lys}$ heteroplasmy presents with a hyperfused mitochondrial network, while high heteroplasmy results in fragmented mitochondria. This supports findings and suggestions by Picard *et al.* (2014) that mitochondria initially form a hyperfused and branched network at low levels of stress but fragment when stress exceeds a certain threshold.

Nanotunnels appear to be more frequent in patients but also appear to have a weak trend with age, which may suggest that these are a mitochondrial stress response. However, the presence of donut mitochondria, which are known to be a morphological indicator of mitochondrial stress, do not differ between patients and controls.

Finally, the data demonstrates anisotropy of the mitochondrial network which may have significance when we consider how mtDNA mutations and respiratory chain deficiency spread throughout the myofibre. Also data gathered here finds that the mitochondrial network is more connected along the numbers z-bands of skeletal myofibres than between z-bands. This may impact the spread of mitochondrial DNA mutations and respiratory chain deficiency and explain segmental respiratory chain deficiency inn skeletal myofibres of ageing and disease.

Chapter 8. Discussion

Skeletal muscle is one of the most energetically demanding tissues within the body, as such it is understandable that mitochondrial dysfunction in the skeletal muscle is linked to neuromuscular disease and ageing. Skeletal muscle respiratory chain deficiency arises in a mosaic pattern (Johnson *et al.*, 1983; Sciacco *et al.*, 1994), is segmental along the myofibre and is concomitant with mtDNA mutations (Wanagat *et al.*, 2001; Bua *et al.*, 2006; Herbst *et al.*, 2007). However, the mechanisms by which the mtDNA mutations accumulate and the factors governing this accumulation and spread of respiratory chain deficiency are not fully understood. As such, the work presented here aimed to improve the understanding of the mechanisms and pathological significance of mitochondrial dysfunction in skeletal muscle.

8.1 Major findings and future work

8.1.1 Levels of respiratory chain deficiency are higher in patients with Dysferlin mutations than age matched controls

Investigations into mitochondria in dysferlinopathy have previously reported COX-deficiency, paracrystalline inclusions and reduced complex I, II and IV activities (Gayathri *et al.*, 2011; Liu *et al.*, 2016). The findings presented in **Chapter 3** demonstrate a higher level of mitochondrial respiratory chain deficiency in muscle of patients with *DYSF* mutations than age matched controls. Although the underlying cause of the dysfunction is not fully elucidated, the potential relevance or role of Ca^{2+} homeostasis in disease pathogenesis, warrants further investigation. Fluorescence imaging of patient myoblasts to detect fluorescence intensity of Rhod2/AM (mitochondrial Ca^{2+} concentration) and Fluo3 (cytoplasmic Ca^{2+} concentration), as previously described (Csordás and Hajnóczky, 2003). Furthermore, since increases in Ca^{2+} concentration are known to disrupt the mitochondrial network and induce mitochondrial swelling (Chappell and Crofts, 1965), an electron microscopy investigation of the mitochondrial ultrastructure and morphology would also be valuable. SBFSEM, three-dimensional reconstruction of mitochondrial networks and quantitative morphological measures developed in **Chapter 7**, may be interesting to apply to the dysferlin patients. However, this would need to be approached in a new cohort of

patients since neither EM prepped muscle blocks nor myoblasts are available for the patients included here.

8.1.2 Mitochondrial mass is reduced in myofibrillar myopathy

Previously, research characterising mitochondrial dysfunction in myofibrillar myopathy has demonstrated respiratory chain deficiency, presence of mtDNA deletions and a change in the positioning of IMF mitochondria to the periphery of the cell (Reimann *et al.*, 2003; Schroder *et al.*, 2003; Claeys *et al.*, 2008; Dold *et al.*, 2012; Henderson *et al.*, 2013). However, no quantitative assessment of respiratory chain deficiency has been performed and so far no attempts have been made to link the mitochondrial changes observed, to the protein aggregates which accumulate as the hallmark of MFM.

As such, the most interesting finding from work presented in **Chapter 4** is that all mitochondrial proteins assayed (NDUFB8, MTCOI and VDAC1) are reduced in a large percentage of MFM skeletal myofibres. Attempts to correlate this with the presence of protein aggregates, however, showed no correlation. This suggests that the aggregation of proteins does not cause the reduction in mitochondrial mass, but does not provide answers as to the underlying cause of mitochondrial dysfunction.

Since the reduction of mitochondrial mass must result from a shift in the balance of mitochondrial biogenesis and mitophagy, quantifying key markers for both pathways may help to elucidate the pathological mechanisms. In addition, previous studies have indicated a shift in the ratio of IMF/SS mitochondria (Claeys *et al.*, 2008; Winter *et al.*, 2016). Therefore, application of the methodologies developed in **Chapter 7** to patients with myofibrillar myopathy may be useful to understand the effect that aggregates containing desmin, have on mitochondrial positioning and morphology. Unfortunately, samples processed for diagnostic EM were only available for a few patients and were mainly found to contain fatty tissue rather than muscle. Examining more biopsies in this manner and implementing the TEM, SBFSEM and reconstruction protocols, as described in this thesis, might provide further insight into the changes in mitochondrial volume density, positioning and morphology.

8.1.3 There is a much larger spectrum of ultrastructural changes in mitochondrial myopathy than previously reported

Previously, EM had been used only on small cohorts or in case studies and is at present commonly used to provide supportive data, rather than to generate the foundation of the results for an investigation (see review in **Appendix 5**). As such, a comprehensive, study of mitochondrial ultrastructure in skeletal muscle biopsies, from patients with mitochondrial myopathy was missing.

In doing this study, a wide range of ultrastructural changes were observed, some of which can already be linked to biological findings in model organisms (e.g. concentric cristae and MICOS (John *et al.*, 2005; Rabl *et al.*, 2009) and donut mitochondria (Long *et al.*, 2015). In addition, a number of other changes have not yet been fully investigated but have led to novel hypotheses and new avenues for investigation. One example is the presence of linearised cristae membranes. It is hypothesised that a change in membrane composition leads to linearised and electron dense cristae. This hypothesis requires an examination of membrane composition and, in particular, the percentage of cardiolipin present in the IMM of mitochondria with linearised and normal cristae. This could be achieved using imaging mass spectrometry as previously reported (Amoscato *et al.*, 2014).

In addition, for paracrystalline inclusions the biological make up has already been identified, and *in vitro* conditions for their development determined (Eppenberger-Eberhardt *et al.*, 1991). However, understanding how and why they develop in myopathic conditions requires further investigation.

8.1.4 Nanotunnels are more frequent in patient muscle biopsies than controls

A recently described and, as yet, not well characterised structure, the nanotunnel, was identified for the first time in human skeletal muscle in **Chapter 6** and **Chapter 7**. Previous investigations have provided information about the dimensions and lifetime of these structures in rodent models, and also about the movement of matrix and IMM located proteins (Bowes and Gupta, 2008; Huang *et al.*, 2013). Measurement of nanotunnel

diameters, made for the first time in human skeletal muscle (**Chapter 6**), allow predictions of the function and capacity of nanotunnels as a communicative mechanism. However, further work is required to investigate the mechanisms by which these nanotunnels form and the physiological conditions that promotes them. In particular, findings in **Chapter 7** demonstrate that they are much more common in patients compared to controls. By understanding the conditions under which they form, a better understanding of their functional capacity can be gleaned.

Nanotunnels are intriguing structures and their presence and potential relevance to mitochondrial pathology in skeletal muscle raises a number of questions that necessitate further investigation. First, are nanotunnels specific to skeletal muscle due to reduced mitochondrial motility? EM investigations in other tissues will be necessary to answer this. Second, is the membrane composition of nanotunnels similar to the two mitochondria it connects? This question might be investigated using imaging mass spectrometry (Amoscato *et al.*, 2014). Third, what controls their formation and are there multiple ways by which similar structures form? Work so far has partly elucidated two possible mechanisms, of which a microtubule dependent formation fits best with observations in mitochondrial myopathy. However, characterisation of this process and the machinery involved will be important future steps. Fourth, is there a signal that promotes their formation, or an “SOS” signal that guides them to the target mitochondria? This final question is perhaps the most intriguing and yet most difficult to investigate, possibly requiring some inspiration from the microbiology world, where similar mechanisms of cell-to-cell communication are observed.

8.1.5 Clonal expansion appears to start as a perinuclear niche

Previous investigations into the mechanism of clonal expansion have focused on a number of key questions. First, some studies have aimed to understand whether the process by which mtDNA deletions accumulate is random (Elson *et al.*, 2001), or if dysfunctional mitochondria are actively selected for (de Grey, 1997). Second, others have investigated the presence of a replicative advantage (Hayashi *et al.*, 1991; Moraes *et al.*, 1999; Diaz *et al.*, 2002; Campbell *et al.*, 2014; Gitschlag *et al.*, 2016), allowing smaller genomes to accumulate faster. Finally, a number of studies have aimed to investigate compensatory

mechanisms that may lead to the accumulation of mtDNA deletions (Kowald and Kirkwood, 2014; Gitschlag *et al.*, 2016; Lin *et al.*, 2016).

However, what these studies have not considered to date is whether the tissue-specific cytoarchitecture and the location of the initial deletion event is an important factor. Work presented here aimed to identify the first observable regions of respiratory chain deficiency and to consider the multinucleated myofibres, the lack of motility of mitochondria and the connectivity of the mitochondrial network as factors in the clonal expansion of mtDNA deletions in skeletal muscle.

Results in **Chapter 5** indicate that mtDNA deletions arise in the subsarcolemmal mitochondria causing an initial focus of respiratory chain deficiency. Investigation demonstrated close proximity of COX-deficient foci to myonuclei and found that both deletion level and mitochondrial mass appear to be increased in the perinuclear niche compared to the remainder of the fibre. This is suggestive of mito-nuclear signalling, facilitated by the close proximity to the nucleus, promoting mitochondrial biogenesis. However, evidence for the upregulation of mitochondrial biogenesis markers and an exact signalling pathway has not been elucidated. There are a number of possible signalling pathways that may be implicated and should be investigated.

As such proposed further work would include examining levels of mitochondrial biogenesis and mitophagy markers as well as intermediates in the AKT and JNK pathways which have been shown to be implicated in the mammalian UPR^{mt} (Pellegrino *et al.*, 2013). As proposed by the perinuclear niche hypothesis, the suspicion is that upregulation of mitochondrial biogenesis will be the main driving force behind the propagation of mtDNA deletions, however it will be interesting to investigate whether this occurs through the UPR^{mt} and the AKT pathway which upregulates *Nrf1* transcription (Pellegrino *et al.*, 2013). In addition, this mechanism is currently only investigated for mtDNA deletions and may also be applicable to mtDNA point mutations. Therefore, once the signalling pathways and mechanisms have been elucidated, examining these in a cohort of patients with mtDNA point mutations will be an important next step.

8.1.6 Mitochondrial network morphology is highly variable

Quantification of mitochondrial morphology has previously been underestimated by the use of two dimensional EM techniques and so far newer, three-dimensional EM, volume imaging techniques have only been quantitatively applied to skeletal muscle mitochondria in mice (Glancy *et al.*, 2015). This thesis includes the first quantitative assessment of three-dimensional mitochondrial morphology in human skeletal muscle and highlights striking variability within fibres, between fibres and between individuals in the control population. In addition, when compared to previous work in mice (Glancy *et al.*, 2015), it highlights a large difference in both mitochondrial network connectivity and mitochondrial volume density that should be considered when implementing mouse models for studies into human disease.

A cohort of mitochondrial myopathy patients were also investigated and compared to controls, with results from three related patients with the same mutation suggesting fragmentation of the mitochondrial network at higher levels of heteroplasmy followed by swelling of mitochondria with further increases in heteroplasmy. This is intriguing and fits with previous observations of mitochondrial dynamics in cybrids with variations in heteroplasmy (Picard *et al.*, 2014).

Further work, to understand whether an initial increase in fusion occurs at lower levels of heteroplasmy prior to fragmentation of the mitochondrial network should be completed. In addition, increasing the number of patients with each mutation and comparing between the mtDNA genetic defects may allow us to elucidate whether there is a heteroplasmy threshold for these changes in morphology and whether this differs between patients. Limitations in the present experimental design however, necessitate consideration of other techniques such as expansion microscopy, which allow functional assessment of the respiratory chain alongside mitochondrial morphology and may also allow us to probe for known mtDNA mutations. In addition to this, analysis as performed on metabolomics datasets may yield further insight into changes in mitochondrial morphology in healthy and diseased muscle.

8.1.7 The skeletal muscle mitochondrial network is anisotropic

Only one previous study visualises the mitochondrial network in human skeletal muscle at nanoscale resolution (Dahl *et al.*, 2015). In this study the analysis is restricted to characterising the interaction of SS and IMF mitochondria, and as such, no characterisation of mitochondrial branching orientation has been completed.

Therefore, the finding that the mitochondrial network is substantially more branched in the transverse plane than the longitudinal is both novel as well as interesting, even more so when we consider the potential pathological significance of this. Segmental respiratory chain deficiency has been a hallmark of mitochondrial myopathy and ageing alike, yet an explanation for why this deficiency does not propagate rapidly along the length of the fibre has been lacking.

However, this finding could be the missing link to explain this. In theory, in order for mtDNA mutations and dysfunctional respiratory chain proteins to spread there must be at least a transient connection of the mitochondria network. Therefore, the large degree of connectivity in the transverse plane may allow a relatively quick spread of mtDNA mutations and respiratory chain deficiency across the myofibre. In comparison, the smaller number of connections along the fibre may hinder spread in this direction, thus giving rise to segmental deficiency in the longitudinal orientation.

Contrary to this, imaging from mice with photoactivatable mitochondria demonstrates that fusion events are more frequent in the longitudinal orientation within the myofibre (Eisner *et al.*, 2014). This may, however, be an artefact of the imaging process or due to differences between the two species, possibly due to fibre type variations and differences in mitochondrial volume density. In order to assess this, similar live imaging would need to be completed for human skeletal muscle fibres. Since this is not possible, the closest representation may be the generation of a skeletal muscle organoid from human myoblasts (Shansky *et al.*, 1997). This would allow live cell study of human samples whilst replicating the cytoskeletal structure of developed myofibres, which it has been demonstrated in this thesis is an important factor to consider when designing experiments.

8.2 Final conclusion

This work provides a number of novel insights into mitochondrial involvement in neuromuscular disease pathology. Key findings include: the reduction of mitochondrial mass in myofibrillar myopathy, increased respiratory chain deficiency in some patients with dysferlinopathy, the spectrum of mitochondrial ultrastructural defects in mitochondrial myopathy, the anisotropic nature of the skeletal muscle mitochondria, the perinuclear origins of mtDNA deletions and their clonal expansion due to retrograde signalling and mitochondrial biogenesis. In addition to these findings, I believe that this work highlights the importance of considering tissue-specific and species-specific differences when investigating the mechanisms governing mitochondrial pathogenesis. On top of these differences, the changes that occur during myogenesis, both to cell structure and the mitochondria, also pose a number of challenges to the investigation of skeletal muscle mitochondrial pathology. Despite this, many questions are left to be answered and although each proposed experiment will have its limitations, in combination these will hopefully advance the understanding of the molecular mechanisms governing disease pathology and provide insight to develop informed and targeted treatments.

Chapter 9. Appendices

Appendix 1 Newcastle Adult Mitochondrial Disease scale (NMDAS) questionnaire. As used to assess mitochondrial disease severity and progression in the Newcastle Mitochondrial disease cohort.

THE NEWCASTLE

MITOCHONDRIAL DISEASE ADULT SCALE

(NMDAS)

Name: _____

Date of birth: _____

Age at assessment: _____

Date of assessment: _____

Checklist – please tick off when completed.

- ❑ **Height:** _____
- ❑ **FVC - 1st attempt** _____
- ❑ **FVC - 2nd attempt** _____
- ❑ **FVC - 3rd attempt** _____ **% Predicted** _____

	Raw Score	Scaled Score	Centile
❑ **SF-12v2 self completion questionnaire**	_____	_____	_____
❑ **WTAR reading test (1 minute)**	_____	_____	_____
❑ **Symbol Search (2 minutes)**	_____	_____	_____
❑ **Speed of comprehension test (2 minutes)**	_____	_____	_____

Disease score (sections I-III)_____

SF-12v2 Quality of Life score (section IV)_____

Section I- Current Function

Rate function over the preceding **4 week period, according to patient and/or caregiver** interview only. The clinician's subjective judgement of functional ability should **not** be taken into account.

1. **Vision** with usual glasses or contact lenses

0. Normal.
1. No functional impairment but aware of worsened acuities.
2. Mild - difficulty with small print or text on television.
3. Moderate - difficulty outside the home (eg bus numbers, road signs or shopping).
4. Severe - difficulty recognising faces.
5. Unable to navigate without help (eg carer, dog, cane).

2. **Hearing** with or without hearing aid

0. Normal.
1. No communication problems but aware of tinnitus **or** deterioration from prior 'normal' hearing.
2. Mild deafness (eg missing words in presence of background noise). **Fully** corrected with hearing aid.
3. Moderate deafness (eg regularly requiring repetition). **Not fully** corrected with hearing aid.
4. Severe deafness - poor hearing even with aid (see 3 above).
5. End stage - virtually no hearing despite aid. Relies heavily on non-verbal communication (eg lip reading) **or** has cochlear implant.

3. **Speech**

0. Normal.
1. Communication unaffected but patient or others aware of changes in speech patterns or quality.
2. Mild difficulties - usually understood and **rarely** asked to repeat things.
3. Moderate difficulties - poorly understood by strangers and **frequently** asked to repeat things.
4. Severe difficulties - poorly understood by family or friends.
5. Not understood by family or friends. Requires communication aid.

4. **Swallowing**

0. Normal.
1. Mild - sensation of solids 'sticking' (occasional).
2. Sensation of solids 'sticking' (most meals) **or** need to modify diet (eg avoidance of steak/salad).
3. Difficulty swallowing solids - affecting meal size or duration. Coughing, choking **or** nasal regurgitation infrequent (1 to 4 times per month) but more than peers.
4. Requires adapted diet - regular coughing, choking, **or** nasal regurgitation (more than once per week).
5. Requiring enteral feeding (eg PEG).

5. **Handwriting**

0. Normal.
1. Writing speed unaffected but aware of increasing untidiness.
2. Mild – Has to write slower to maintain tidiness/legibility.
3. Moderate – Handwriting takes at least twice as long **or** resorts to printing (must previously have used joined writing).
4. Severe – Handwriting mostly illegible. Printing very slow and untidy (eg 'THE BLACK CAT' takes in excess of 30 seconds).
5. Unable to write. No legible words.

6. **Cutting food and handling utensils** (irrespective of contributory factors – eg weakness, coordination, cognitive function etc. This is also true for questions 7-10)

0. Normal.
1. Slightly slow and/or clumsy but **minimal** effect on meal duration.
2. Slow and/or clumsy with extended meal duration, but no help required.
3. Difficulty cutting up food and inaccuracy of transfer pronounced. Can manage alone but avoids problem foods (eg peas) or carer typically offers minor assistance (eg cutting up steak).
4. Unable to cut up food. Can pass food to mouth with great effort or inaccuracy. Resultant intake minimal. Requires major assistance.
5. Needs to be fed.

7. **Dressing**

0. Normal.
1. Occasional difficulties (eg shoe laces, buttons etc) but no real impact on time or effort taken to dress.
2. Mild – Dressing takes longer and requires more effort than expected at the patient's age. No help required.
3. Moderate - Can dress unaided but takes at least twice as long and is a major effort. Carer typically helps with difficult tasks such as shoe laces or buttons.
4. Severe – Unable to dress without help but some tasks completed unaided.
5. Needs to be dressed.

8. **Hygiene**

0. Normal.
1. Occasional difficulties only but no real impact on time or effort required.
2. Mild – hygienic care takes longer but quality unaffected.
3. Moderate - bathes and showers alone with difficulty **or** needs bath chair / modifications. Dextrous tasks (eg brushing teeth, combing hair) performed poorly.
4. Severe - unable to bathe or shower without help. Major difficulty using toilet alone. Dextrous tasks require help.
5. Dependent upon carers to wash, bathe, and toilet.

9. **Exercise Tolerance**

0. Normal.
1. Unlimited on flat - symptomatic on inclines or stairs.
2. Able to walk < 1000m on the flat. Restricted on inclines or stairs - rest needed after 1 flight (12 steps).
3. Able to walk < 500m on the flat. Rest needed after 8 steps on stairs.
4. Able to walk < 100m on the flat. Rest needed after 4 steps on stairs.
5. Able to walk < 25m on the flat. Unable to do stairs alone.

10. **Gait stability**

0. Normal.
1. Normal gait - occasional difficulties on turns, uneven ground, or if required to balance on narrow base.
2. Gait reasonably steady. Aware of impaired balance. **Occasionally** off balance when walking.
3. Unsteady gait. **Always** off balance when walking. **Occasional** falls. Gait steady with support of stick or person.
4. Gait grossly unsteady without support. **High likelihood** of falls. Can only walk short distances (< 10m) without support.
5. Unable to walk without support. Falls on standing.

Section II – System Specific Involvement

Rate function according to patient and/or caregiver interview and consultation with the medical notes. Each inquiry should take into account the situation for the preceding **12 month period** only, unless otherwise stated in the question.

1. **Psychiatric**

0. None.
1. Mild & transient (eg reactive depression) - lasting **less** than 3 months.
2. Mild & persistent (lasting **more** than 3 months) **or** recurrent. Patient has consulted GP.
3. Moderate & warranting specialist treatment (e.g. from a psychiatrist) - eg. bipolar disorder or depression with vegetative symptoms (insomnia, anorexia, abulia etc).
4. Severe (eg self harm - psychosis etc).
5. Institutionalised or suicide attempt.

2. **Migraine Headaches** During **the last 3 months**, how many days have headaches prevented the patient from functioning normally at school, work, or in the home?

0. No past history.
1. Asymptomatic but past history of migraines.
2. One day per month.
3. Two days per month.
4. Three days per month.
5. Four days per month or more.

3. **Seizures**

0. No past history.
1. Asymptomatic but past history of epilepsy.
2. Myoclonic or simple partial seizures only.
3. Multiple absence, complex partial, or myoclonic seizures affecting function **or** single generalised seizure.
4. Multiple generalised seizures.
5. Status epilepticus.

4. **Stroke-like episodes** (exclude focal deficits felt to be of vascular aetiology)

0. None.
1. Transient focal sensory symptoms only (**less** than 24 hours).
2. Transient focal motor symptoms only (**less** than 24 hours).
3. Single stroke-like episode affecting one hemisphere (**more** than 24 hours).
4. Single stroke-like episode affecting both hemispheres (**more** than 24 hours).
5. Multiple stroke-like episodes (**more** than 24 hours each).

5. **Encephalopathic Episodes**

0. No past history.
1. Asymptomatic **but** past history of encephalopathy.
2. Mild - single episode of personality or behavioural change but retaining orientation in time/place/person.
3. Moderate - single episode of confusion or disorientation in time, place or person.

4. Severe – multiple moderate episodes (as above) **or** emergency hospital admission due to encephalopathy **without** associated seizures or stroke-like episodes.
5. Very severe - in association with seizures, strokes or gross lactic acidaemia.

6. **Gastro-intestinal symptoms**

0. None.
1. Mild constipation only **or** past history of bowel resection for dysmotility.
2. Occasional symptoms of 'irritable bowel' (pain, bloating or diarrhoea) with long spells of normality.
3. Frequent symptoms (as above) most weeks **or** severe constipation with bowels open less than once/week **or** need for daily medications.
4. Dysmotility requiring admission **or** persistent and/or recurrent anorexia/vomiting/weight loss.
5. Surgical procedures **or** resections for gastrointestinal dysmotility.

7. **Diabetes mellitus**

0. None.
1. Past history of gestational diabetes or transient glucose intolerance related to intercurrent illness.
2. Impaired glucose tolerance (in absence of intercurrent illness).
3. NIDDM (diet).
4. NIDDM (tablets).
5. DM requiring insulin (irrespective of treatment at onset).

8. **Respiratory muscle weakness**

0. FVC normal (≥ 85% predicted).
1. FVC < 85% predicted.
2. FVC < 75% predicted.
3. FVC < 65% predicted.
4. FVC < 55% predicted.
5. FVC < 45% predicted **or** ventilatory support for over 6 hours per 24 hr period (**not** for OSA alone).

9. **Cardiovascular system**

0. None.
1. Asymptomatic ECG change.
2. Asymptomatic LVH on echo **or** non-sustained brady/tachyarrhythmia on ECG.
3. Sustained or **symptomatic** arrhythmia, LVH **or** cardiomyopathy. Dilated chambers **or** reduced function on echo. Mobitz II AV block or greater.
4. Requires pacemaker, defibrillator, arrhythmia ablation, **or** LVEF < 35% on echocardiogram.
5. Symptoms of left ventricular failure **with** clinical and/or x-ray evidence of pulmonary oedema **or** LVEF < 30% on echocardiogram.

Section III – Current Clinical Assessment

Rate current status according to examination performed at **the time of** assessment

1. **Visual acuity** with usual glasses, contact lenses or pinhole.

0. CSD ≤ **12** (ie normal vision - 6/6, 6/6 or better).
1. CSD ≤ **18** (eg 6/9, 6/9).
2. CSD ≤ **36** (eg 6/12, 6/24).
3. CSD ≤ **60** (eg 6/24, 6/36).
4. CSD ≤ **96** (eg 6/60, 6/36).
5. CSD ≥ **120** (eg 6/60, 6/60 **or worse**).

2. **Ptosis**

0. None.
1. Mild ptosis - not obscuring **either** pupil.
2. Unilateral ptosis obscuring < 1/3 of pupil.
3. Bilateral ptosis obscuring < 1/3 **or** unilateral ptosis obscuring > 1/3 of pupil **or** prior unilateral surgery.
4. Bilateral ptosis obscuring > 1/3 of pupils **or** prior bilateral surgery.
5. Bilateral ptosis obscuring >2/3 of pupils **or** >1/3 of pupils **despite** prior bilateral surgery.

3. **Chronic Progressive External Ophthalmoplegia**

0. None.
1. Some restriction of eye movement (any direction). Abduction complete.
2. Abduction of worst eye incomplete.
3. Abduction of worst eye below 60% of normal.
4. Abduction of worst eye below 30% of normal.
5. Abduction of worst eye minimal (flicker).

4. **Dysphonia/Dysarthria**

0. None.
1. Minimal - noted on examination only.
2. Mild – clear impairment but easily understood.
3. Moderate – some words poorly understood and infrequent repetition needed.
4. Severe – many words poorly understood and frequent repetition needed.
5. Not understood. Requires communication aid.

5**. Myopathy**

0. Normal.
1. Minimal reduction in hip flexion and/or shoulder abduction **only** (eg MRC 4+/5).
2. Mild but clear proximal weakness in hip flexion and shoulder abduction (MRC 4/5). Minimal weakness in elbow flexion and knee extension (MRC 4+/5 - both examined with joint at 90 degrees).
3. Moderate proximal weakness including elbow flexion & knee extension (MRC 4/5 or 4 -/5) **or difficulty** rising from a 90 degree squat.
4. Waddling gait. **Unable** to rise from a 90 degree squat (=a chair) unaided.
5. Wheelchair dependent **primarily** due to proximal weakness.

6. **Cerebellar ataxia**

0. None.
1. Normal gait but hesitant heel-toe.
2. Gait reasonably steady. Unable to maintain heel-toe walking **or** mild UL dysmetria.
3. Ataxic gait (but walks unaided) **or** UL intention tremor & past-pointing. Unable to walk heel-toe - falls immediately.
4. Severe - gait grossly unsteady without support **or** UL ataxia sufficient to affect feeding.
5. Wheelchair dependent **primarily** due to ataxia **or** UL ataxia **prevents** feeding.

7**. Neuropathy**

0. None.
1. Subtle sensory symptoms **or** areflexia.
2. Sensory impairment only (eg glove & stocking sensory loss).
3. Motor impairment (distal weakness) **or** sensory ataxia.
4. Sensory ataxia **or** motor effects severely limit ambulation.
5. Wheelchair bound **primarily** due to sensory ataxia or neurogenic weakness.

8. **Pyramidal Involvement**

0. None.
1. Focal or generalised increase in tone or reflexes only.
2. Mild **focal** weakness, sensory loss or fine motor impairment (eg cortical hand).
3. Moderate hemiplegia allowing unaided ambulation **or** dense UL monoplegia.
4. Severe hemiplegia allowing ambulation with aids **or** moderate tetraplegia (ambulant).
5. Wheelchair dependant **primarily** due to hemiplegia or tetraplegia.

9. **Extrapyramidal**

0. Normal.
1. Mild and unilateral. Not disabling (H&Y stage 1).
2. Mild and bilateral. Minimal disability. Gait affected (H&Y stage 2).
3. Moderate. Significant slowing of body movements (H&Y stage 3)
4. Severe. Rigidity and bradykinesia. Unable to live alone. Can walk to limited extent (H&Y stage 4).
5. Cannot walk or stand unaided. Requires constant nursing care (H&Y stage 5).

10. **Cognitition**

Patients undergo testing using WTAR, Symbol Search and Speed of Comprehension Test.

0. Combined centiles **100 or more.**
1. Combined centiles **60 - 99**
2. Combined centiles **30 - 59**
3. Combined centiles **15 - 29**
4. Combined centiles **5 - 14**
5. Combined centiles **4 or below.**

WORD CARD

1. again
2. address
3. cough
4. preview
5. although
6. most
7. excitement
8. know
9. plumb
10. decorate
11. fierce
12. knead
13. aisle
14. vengeance
15. prestigious
16. wreathe
17. gnat
18. amphitheatre
19. lieu
20. grotesque
21. iridescent
22. ballet
23. equestrian
24. porpoise
25. aesthetic
26. conscientious
27. homily
28. malady
29. subtle
30. Fecund
31. Palatable
32. Menagerie
33. obfuscate
34. liaison
35. exigency
36. xenophobia
37. ogre
38. scurrilous
39. ethereal
40. paradigm
41. perspicuity
42. plethora
43. lugubrious
44. treatise
45. dilettante
46. vertiginous
47. ubiquitous
48. hyperbole
49. insouciant
50. hegemony

	Item	Pronunciation	Score (0,1)		Item	Pronunciation	Score (0,1)
1	again	ah-GEHN ah-Gain or uh-GEHN or uh-GAIN		26	Conscientious	con-shee-EN-shss	
2	address	ah-DRESS or uh-DRESS		27	homily	HOM-ih-lay or HOM-ih-lee	
3	cough	kawf or kof		28	malady	MAL-uh-day or MAL-uh-dee	
4	preview	PREE-vyue		29	subtle	SUH-tl	
5	although	awl-THO		30	fecund	FE-cund or FEE-cund	
6	most	Mohst		31	palatable	PAL-ah-tuh-bul or PAL-uh-tuh-bul	
7	excitement	eck-SITE-munt or ik-SITE-munt		32	menagerie	meh-NA-juh-ree	
8	know	noh or no		33	obfuscate	OB-fuh-skate	
9	plump	Plum		34	liaison	lee-AY-zon or lee-AY-zn	
10	decorate	DEK-oh-rate or DEK-uh-rate		35	exigency	eks-IH-jen-say or eks-IH-jen-see	
11	fierce	fee-us or feerss		36	xenophobia	zen-oh-FO-bee-uh	
12	knead	need		37	ogre	OH-gur	
13	aisle	iyle		38	scurrilous	SKUR-ih-lus or SKUR-uh-lus	
14	vengeance	VEN-jnss		39	ethereal	ih-THEE-ree-ul or ih-THEER-ee-ul	
15	prestigious	pre-STIJ-us or pre-STEEJ-us		40	paradigm	PAH-rah-dime	
16	wreathe	reeTH		41	perspicuity	per-spuh-KYEW-uh-tee	
17	gnat	nat		42	plethora	PLETH-oh-rah or PLETH-eh-rah	
18	amphitheatre	AM-fih-thee-uh-ter		43	Lugubrious	loo-GOOB-ree-uss or loo-GOO-bree-uss	
19	lieu	loo or l(y)oo		44	treatise	TREE-tiz or TREET-iz	
20	grotesque	gro-TESK		45	dilettante	DILL-ih-tan-tay or DILL-uh-tahnt	
21	iridescent	ihr-ih-DESS-unt or ihr-uh-DESS-unt		46	vertiginous	ver-TIDJ-in-iss	
22	ballet	BA-lay or ba-LAY or bal-ay		47	ubiquitous	you-BIC-wuh-tiss or you-BIC-wuh-tus	
23	equestrian	eh-KWESS-tree-un or ih-KWESS-tree-un		48	hyperbole	hy-PER-bul-lay or hy-PUR-bul-lay	
24	propoise	PAW-pss or POR-opyz (scots)		49	insouciant	in-SOO-see-yunt	
25	aesthetic	ess-THET-ik or ees-THET-ik		50	hegemony	heh-GEM-o-nee or heh-JEM-o-nee or HEH-geh-mon-ee	
						WTAR Raw Score	
						WTAR Standard Score	

WTAR Word List – UK pronunciation guide

Say, I will show you some words that I will ask you to pronounce. Place the WTAR Word Card in front of the examinee. As you point to the card, say, **Beginning with the first word on the list, pronounce each word aloud. Start with this word** (point to item 1), **and go down this column, one after the other, without skipping any. When you finish this column, go to the next column** (point to the second column). **Pronounce each word even if you are unsure. Do you understand?** When you are sure that the examinee understands the task, say, **Ready? Begin.**

Response Booklet — 2 minutes to complete

Symbol Search	Ricerca di Simboli	Symbol Sek	Hledání symbolů
Symbòles	Símbolos	Symboler	Hl'andanie symbolov
Symboltest	Pesquisa de simbolos	Merkintinnistus	
Symbolletnign	Figuren Vergelijken		

Sample Items

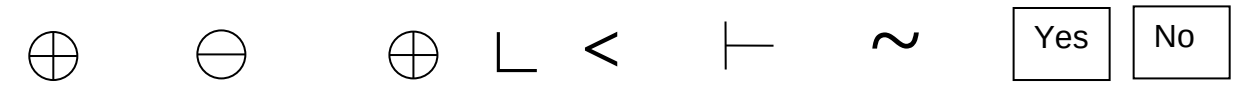

The Speed of Comprehension Test VersionA

Many of the things we do rely on ‘common sense’, a knowledge of the world and an ability to make use of such knowledge. This test looks at the speed and accuracy with which people can use such information. It consists of a series of sentences, about half of which are true and half false. The true sentences are all obviously true, e.g. ;dogs have four legs’, or ‘birds have wings’. The false sentences are made up by combining two true sentences. ‘dogs have wings’, or ‘birds have four legs’. While the true sentences may not be all quite as obvious at this, there are no trick questions. If you do find a question that you really cannot answer, mark it with a ‘?’.

Work as quickly as you can without making errors, and put a tick against sentences which are true and a cross against those which are false. Are there any questions?

Then try the following at your own speed, but do not turn over until you are given the signal to begin the main test.

Practice

P1 Rats have teeth
P2 Nuns are made in factories
P3 Ants are living creatures
P4 Tractors grow in gardens
P5 Pythons move around searching for food
P6 Desks wear clothes

1 Admirals are people
2 Footstools are small
3 Beef steaks can be bought in shops
4 Dragonflies have wings
5 Grapes are people
6 Grass snakes move around searching for food
7 Prime Ministers have feathers
8 Bishops wear clothes
9 Bedroom slippers are made in factories
10 Beavers have strong teeth
11 Forks are manufactured goods
12 Architects can be bought in shops
13 Prime Ministers hold a political office
14 Vans grow in gardens
15 Pliers are found in tool chests
16 Tomato soup is a liquid
17 Admirals have fins
18 Wives often have husbands
19 Beef steaks are footwear
20 Grapes come from plants
21 Wives are made in factories
22 Beer lives in trees
23 Penguins are living creatures
24 Dragonflies are manufactured goods
25 Haddocks are fish
26 Beer is an alcoholic drink
27 Bishops are islands
28 Architects undergo a long training
29 Tomato soup moves around searching for food
30 Vans are vehicles
31 Haddocks have wheels
32 Footstools wear clothes
33 Pencils undergo a long training
34 Fish and chips move around searching for food
35 Climbing boots are made in factories
36 Gin is sold by butchers
37 Potatoes can be eaten
38 Can – openers are said to have loud voices
39 Fish and chips are fried
40 Mothers are parents
41 Crows are in charge of ships
42 U.S Presidents have feathers
43 Grass snakes come from pigs
44 Corporals are people
45 U.S Presidents hold a political office
46 Popes wear clothes
47 Drills are found in tool chests

48 Trucks grow in gardens
49 Popes are footwear
50 Corporals come from calves
51 Pliers are made in factories
52 Forks have feet
53 Carrots come from cattle
54 Wives can be bough in shops
55 Roses grow in gardens
56 Beavers are manufactured goods
57 Radishes can be bough in shops
58 Wool comes from sheep
59 Books are vegetables
60 Tomato soup is people
61 Haddocks are a liquid
62 Biscuits can be eaten
63 Snails are make from apples
64 Radishes are furniture
65 Books can be bought in shop
66 Grass snakes have shops
67 Penguins are birds
68 Vans wear clothes
69 Pliers have a profession
70 Wool have handles
71 Grass snakes are living creatures
72 Spoons are used for eating soup
73 Mothers are part if the family
74 Crows are a liquid
75 Pineapples are used for storage
76 Drills have a profession
77 Sharks are good swimmers
78 Trucks wear clothes
79 Biscuits come in long strands
80 Hammers are found in tool chests
81 Oranges are furniture
82 Pencils are made in factories
83 Squirrels are manufactures goods
84 Carrots ca be eaten
85 Cobras serve on city councils
86 U.S Presidents are made in factories
87 Can-openers have feet
88 Bees move around searching for food
89 Potatoes are cooked
90 Gin is alcoholic
91 Gin moves around searching for food
92 Can-openers are kitchen utensils
93 Popes are people
94 Roses deliver sermons
95 Beef steaks crawl on their bellies

96 Oranges can be eaten
97 Climbing boots live in monasteries
98 Ladles are kitchen utensils
99 Pineapples are fruit
100 Trucks carry loads

Your Health and Well-Being

This Survey asks for you views about your health. This information will help keep track of how you feel and how well you are able to do you usual activities. ***Thank you for completing this survey.***

For each of the following questions, please tick the one box that best describes your answer.

1. In general, would you say your health is:

Excellent	Very good	Good	Fair	Poor
▼	▼	▼	▼	▼
☐	☐	☐	☐	☐

2. The Following questions are about activities you might do during a typical day. Does <u>your health now limit you</u> in these activates? If so, how much?

	Yes, limited a lot ▼	Yes, limited a little ▼	No, not limited at all ▼
A	**<u>Moderate activities</u>, such as moving a table, pushing A vacuum cleaner, bowling or playing golf……**	☐……	☐……..☐
B	**Climbing <u>several</u> flights of stairs……**	☐……	☐……..☐

3. During the <u>past 4 weeks,</u> how much of the time have you had any of the following problems with your work or other regular daily activities <u>as a result of your physical health.</u>

	All of the time	Most of the time	Some of the time	A little of the time	None of the time
	▼	▼	▼	▼	▼
A	**Accomplished less than you would like……**	☐	☐	☐	☐	☐
b	**Were limited in the kind of work or other activities..**	☐	☐	☐	☐	☐

4. During the part 4 weeks, how much of the time have you had any of the following problems with your work or other regular daily activities as a result of any emotional problems (such as feeling depressed or anxious)?

	All of the time	Most of the time	Some of the time	A little of the time	None of the time
	▼	▼	▼	▼	▼
A	**Accomplished less than you would like……**	☐	☐	☐	☐	☐
b	**Did work or other activities less carefully than usual ……**	☐	☐	☐	☐	☐

5. During the past 4 weeks, how much did pain interfere with your normal work (including both work outside the home and housework)?

Not at all	A little bit	Moderately	Quite a bit	Extremely
▼	▼	▼	▼	▼
☐	☐	☐	☐	☐

6. These questions are about how you feel and how things have been with you <u>during the past 4 weeks</u>. For each question, please give the one answer that comes closest to the way you have been feeling. How much of the time during the <u>past 4 weeks</u>…

	All of the time ▼	Most of the time ▼	Some of the time ▼	A little of the time ▼	None of the time ▼
A Have you felt calm & Peaceful?	☐	☐	☐	☐	☐
B Did you have a lot of Energy?	☐	☐	☐	☐	☐
C Have you felt Downhearted & low……..	☐	☐	☐	☐	☐

7. During the past 4 weeks, how much of the time has your physical health or emotional problems interfered with your social activities (like visiting with friend's relatives, etc.)?

Not at all ▼	A little bit ▼	Moderately ▼	Quite a bit ▼	Extremely ▼
☐	☐	☐	☐	☐

Thank you for completing these questions!

Appendix 2 “Dysferlin mutations and Mitochondrial Dysfunction”. Vincent et al. (2016). Manuscript published in Neuromuscular disorders.

Available online at www.sciencedirect.com

ScienceDirect

Neuromuscular Disorders 26 (2016) 782–788

www.elsevier.com/locate/nmd

Dysferlin mutations and mitochondrial dysfunction

Amy E. Vincent [a], Hannah S. Rosa [a], Charlotte L. Alston [a], John P. Grady [a], Karolina A. Rygiel [a], Mariana C. Rocha [a], Rita Barresi [b], Robert W. Taylor [a], Doug M. Turnbull [a,*]

[a] *Wellcome Trust Centre for Mitochondrial Research, Institute of Neuroscience, Newcastle University, Newcastle upon Tyne, NE2 4HH, UK*

[b] *Rare Diseases Advisory Group Service for Rare Neuromuscular Diseases, Muscle Immunoanalysis Unit, Newcastle-upon-Tyne Hospitals NHS Foundation Trust, Newcastle upon Tyne NE2 4AZ, UK*

Received 9 May 2016; received in revised form 3 August 2016; accepted 15 August 2016

Abstract

Dysferlinopathies are caused by mutations in the *DYSF* gene and patients may present with proximal or distal myopathy. Dysferlin is responsible for membrane resealing, and mutations may result in a defect in membrane repair following mechanical or chemical stress, causing an influx of Ca^{2+}. Since mitochondria are involved in Ca^{2+} buffering, we hypothesised that mitochondrial defects may be present in skeletal muscle biopsies from patients with mutations in this gene. The aim was to characterise mitochondrial defects in muscle from patients with dysferlinopathies. Here, we analysed skeletal muscle biopsies for eight patients by quadruple immunofluorescent assay to assess oxidative phosphorylation protein abundance. Long-range PCR in single muscle fibres was used to look for presence of clonally expanded large-scale mitochondrial DNA rearrangements in patients' skeletal muscle (n = 3). Immunofluorescence demonstrated that the percentage of complex I- and complex IV-deficient fibres was higher in patients with *DYSF* mutations than in age-matched controls. No clonally expanded mtDNA deletions were detected using long-range PCR in any of the analysed muscle fibres. We conclude that complex I and complex IV deficiency is higher in patients than age matched controls but patients do not have rearrangements of the mtDNA. We hypothesise that respiratory chain deficiency may be the results of an increased cytosolic Ca^{2+} concentration (due to a membrane resealing defect) causing mitochondrial aberrations.

Keywords: Dysferlin; Mitochondria; LGMD2B; Immunofluorescence; Histochemistry; Cytochrome *c* oxidase deficiency

1. Introduction

Dysferlin mutations cause a number of different phenotypes including limb girdle muscle dystrophy type 2B (LGMD2B), Miyoshi distal myopathy (MM) [1,2] and distal myopathy with Anterior Tibialis onset (DMAT) [3]. Links between mutation type, location and phenotype are not straight forward [4,5]. These conditions demonstrate a multitude of dystrophic features including necrotic fibres, fibre splitting, variation in fibre size, and sometimes inflammatory infiltrates [6]. Dysferlin is responsible for plasma membrane repair, vesicle fusion and membrane trafficking. The ferlin protein group to which dysferlin belongs all have Ca^{2+} sensitive C2 domains [7]; dysferlin itself has seven C2 domains with variable affinities for Ca^{2+} [8]. It has previously been demonstrated that an influx of Ca^{2+} through the site of membrane injury triggers dysferlin-mediated membrane repair [9]. Patients with mutations in the dysferlin gene often have impaired membrane resealing following mechanical or chemical stress, causing an influx of Ca^{2+}. This is particularly relevant in muscle where mechanical stress due to muscle contraction is quite common and Ca^{2+} regulation is highly important.

To date, two reports have been published documenting mitochondrial abnormalities in patients with dysferlin mutations. The first report demonstrated accumulation of subsarcolemmal mitochondria in some patients' muscle fibres including one patient with ragged red fibres and paracrystalline mitochondrial inclusions [10]. More recently up to 10% of muscle fibres were reported to be cytochrome *c* oxidase (COX or complex IV) deficient, and some of these fibres have increased mtDNA copy number [11]. In the same study, a reduced complex IV and complex III levels were observed in some patients, while others showed a significant downregulation of complex I and complex IV activities and only a mild reduction of complex III.

Here, we employ a recently developed immunofluorescent technique [12] to measure levels of complex I and complex IV

* Corresponding author. Wellcome Trust Centre for Mitochondrial Research, Institute of Neuroscience, Newcastle University, Newcastle upon Tyne NE2 4HH, UK. Fax: 0044-1912228553.

E-mail address: doug.turnbull@ncl.ac.uk (D.M. Turnbull).

http://dx.doi.org/10.1016/j.nmd.2016.08.008

normalised to porin as a mitochondrial mass marker. This technique, unlike COX/SDH histochemistry allows us to accurately and objectively quantify the extent of mitochondrial respiratory chain deficiency. We also hypothesise that increased mitochondrial fission due to increased cytosolic Ca^{2+} may reduce mtDNA stability. Therefore, we also employ long-range PCR to look for the presence of large-scale mtDNA rearrangements. Accurate and objective quantification of complex I and complex IV levels and mtDNA deletion analysis provide a novel addition to previous investigations in patients with dysferlin mutations.

2. Patients and methods

2.1. Patient cohort

Muscle biopsies were taken for diagnostic purposes from patients (n = 8), with a suspected neuromuscular condition; all patients consented to the use of the sample for research. Diagnostic immunohistochemistry and western blotting showed an absence of dysferlin. Sequencing of the *DYSF* gene identified pathogenic mutations (Table 1), confirming a diagnosis of dysferlinopathy. Eight patients included in the study (numbered 1–8 based on age); six were diagnosed with Limb Girdle Muscular Dystrophy type 2B (LGMD2B) and two with Miyoshi myopathy (MM). Patients were numbered 1 to 8 based on age at biopsy. A muscle biopsy from a previously-reported patient with an mtDNA maintenance disorder and multiple deletions due to recessive *RRM2B* variants [13] was used as a positive control, as well as 3 healthy control biopsies from subjects aged 18, 35 and 52 years at the time of biopsy.

2.2. Histochemistry

Cryosections (10 μm) were obtained from transversely-orientated muscle blocks and subjected to COX/SDH (cytochrome c oxidase/succinate dehydrogenase) histochemistry. Three serial sections were used to detect: COX activity, SDH activity and combined COX/SDH activity, as described previously [14]. Numbers of COX-deficient fibres were counted in a defined area for each section using the meander scan function in Stereo Investigator and a Stereology microscope (Olympus BX51). Serial sections were stained with haematoxylin and eosin (H&E) to examine muscle morphology. Slides were assessed independently by two investigators.

2.3. Quadruple immunofluorescence

A recently developed immunofluorescent assay was used to assess levels of complex I and complex IV relative to mitochondrial mass [12]. Images were stitched using ZEN (blue edition) before analysis in IMARIS (v.8) software, and statistical analysis was completed as described previously [12].

2.4. Laser microdissection and cell lysis

Three serial cryosections were cut. The first and last tissue sections underwent sequential COX/SDH histochemistry and were used to assess the degree of COX deficiency. The second tissue section underwent SDH histochemistry only and was used for mtDNA analysis. Single muscle fibres were laser microdissected from the second tissue section using a PALM system (Zeiss). Fibres from the second tissue section were captured into 15 μl single cell lysis buffer (0.5% SDS, 10 mM EDTA, 5% proteinase K).

2.5. Long-range PCR

Two rounds of PCR were employed to screen isolated muscle fibres for large-scale mtDNA rearrangements using PrimeSTAR GXL (TaKaRa, Clonetech). The reaction was prepared as follows: 1 μl cell lysate, 1× PrimeSTAR GXL reaction buffer, 0.2 μM dNTPs, 0.2 μM forward and reverse primers and 0.625 unit polymerase, in a total volume of 50 μl. The first round of PCR amplified a 16,179 bp region using primers 2180F (nucleotides m.2180–2209) and 1789R (nucleotides m.1760–1789) and the second round reaction amplified a 16,029 bp region using primers 2330F (nucleotides m.2330–2359) and 1789R (nucleotides m.1760–1789) (NC_012920.1). Cycling conditions were: 35 cycles of 10 seconds at 98 °C and 11 minutes at 68 °C. PCR products were separated through a 0.7% agarose gel with a 1 Kb ladder used to size amplicons.

Table 1
Dysferlinopathy patient information.

Patient number	Gender	Age at onset (if known)	Age at biopsy	Mutation	CK	Phenotype
DYSF 1	F	10 (distal)	15.7	c.855+1delG; c.3031G>C, p.(Gly1011Arg)	3012	MM
DYSF 2	F	26	20.5	c.2434dup p.(His812Profs*53); c.1745G>T p.(Arg582Leu)	7586	LGMD2B
DYSF 3	F	26	21.9	Hom. c.2163-1G>T	13,000	LGMD2B
DYSF 4	M	Birth	24.7	Hom. c.1480+18T>C; c.4999G>A, p.(Glu1667Lys)	400–700	LGMD2B
DYSF 5	M	9	28.9	exon 5–10 deletion; c.757C>T, p.(Arg253Trp)	5000	LGMD2B
DYSF 6	M	Late teens (distal)	30.4	Hom. c.3059dupC, p.(Glu1021Glyfs*10)	20,000	MM
DYSF 7	F	N/K	47.1	c. 5509G>A, p.(Asp1837Asn); c.6124C>T, p.(Arg2042Cys)	5110	LGMD2B
DYSF 8	M	13	52.5	c.3512_3513delCT, p.(Ser1171Phefs*3); c.5908C>T, p.(Pro19070Ser)	6000	LGMD2B

Notes: Patients are organised in age order and all mutation nomenclature uses the primary transcript (NM_003494.3). All biopsies were taken from the quadriceps via needle biopsy.
N/K; Not known; M: Male; F: Female; Hom.: homozygous; LGMD2B: Limb girdle muscular dystrophy type 2B; MM: Miyoshi Myopathy.

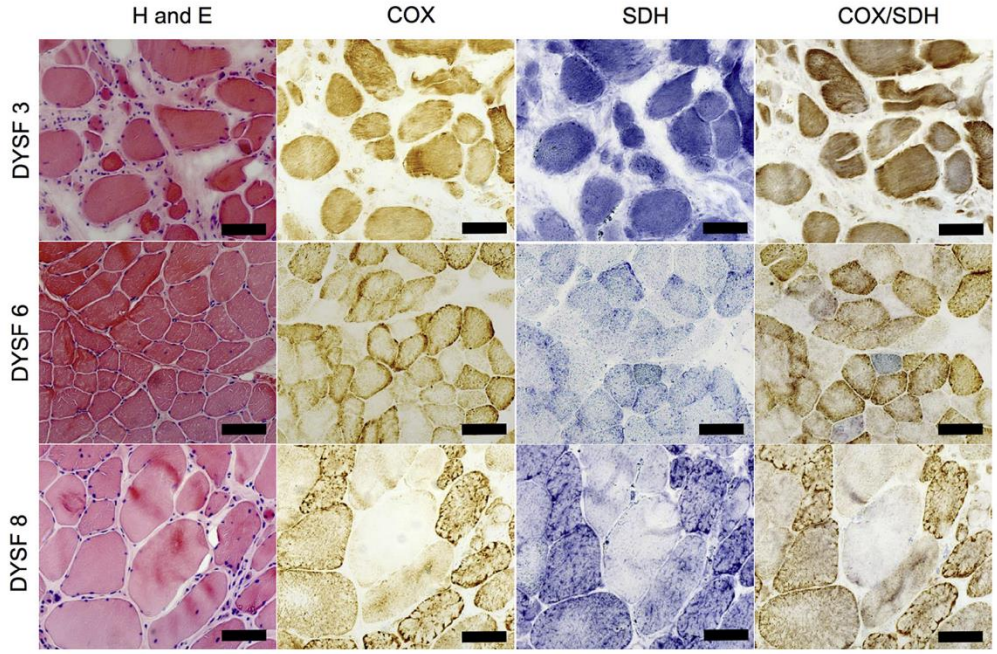

Fig. 1. Histochemical analysis of serial muscle section.
Notes: Serial muscle sections from patients 3, 6 and 8, for H&E, COX, SDH and sequential COX/SDH histochemistry. H&E demonstrates large variation in fibre size, with occasional internal nuclei and inflammation. Only DYSF 6 shows a clear cut COX negative fibre but all three biopsies show evidence of intermediate fibres.

3. Results

3.1. COX/SDH histochemistry and haematoxylin and eosin

H&E staining demonstrated a large variability in fibre size. There were also many necrotic fibres, internal nuclei and in some cases inflammatory infiltrates mostly associated with (but not limited to) necrotic fibres (Fig. 1, left column). COX/SDH histochemistry demonstrated a small number (typically less than 1%) of COX deficient fibres (Fig. 1, right column). However, many biopsies had a large number of fibres that appeared to have intermediate levels of COX deficiency, which was difficult to assess visually (Fig. 1, DYSF 3). Stereoinvestigator and a stereology microscope were used to count the number of COX positive, intermediate positive, intermediate negative and negative fibres in a defined region (Table 2). Due to very few truly COX-deficient fibres and many more COX-intermediate muscle fibres, deficiency level was likely to be under- or overestimated. Furthermore, counts between 2 investigators varied due to a large number of fibres intermediate for COX activity, which demonstrated the necessity of applying the objective quantitative immunofluorescence to more accurately assess COX levels.

3.2. Immunofluorescent analysis of respiratory chain complexes

Quadruple immunofluorescence allowed objective quantification of complex I and complex IV protein abundance. Results are summarised in Table 3. Immunofluorescent images for DYSF 4, 6 and 8 (Fig. 2) demonstrate complex I- and complex IV-deficient fibres. In 18 and 34 year old control biopsies, complex I deficiency is absent, but present in

Table 2
COX deficiency for dysferlin patients (n = 8) as assessed by sequential COX/SDH histochemistry.

Investigator	Patient	Total fibres	% COX positive	% Intermediate positive	% Intermediate negative	% COX negative
1	DYSF 1	1491	98.2%	1.8%	0.0%	0.0%
	DYSF 2	577	75.4%	18.4%	6.1%	0.1%
	DYSF 3	963	65.5%	21.9%	11.9%	0.6%
	DYSF 4	1774	97.7%	5.0%	0.1%	0.0%
	DYSF 5	397	86.9%	12.8%	0.3%	0.0%
	DYSF 6	563	80.8%	17.9%	0.9%	0.4%
	DYSF 7	132	69.7%	30.3%	0.0%	0.0%
	DYSF 8	453	92.5%	4.9%	2.0%	0.7%
2	DYSF 1	1357	83.6%	16.3%	0.07%	0.0%
	DYSF 2	382	71.7%	26.9%	1.5%	0.0%
	DYSF 3	328	65.9%	30.4%	3.7%	0.0%
	DYSF 4	1131	97.1%	2.6%	0.2%	0.1%
	DYSF 5	395	77.7%	22.0%	0.3%	0.0%
	DYSF 6	726	70.4%	27.1%	1.9%	0.6%
	DYSF 7	135	58.5%	31.1%	10.4%	0.0%
	DYSF 8	463	78.2%	20.3%	1.2%	0.4%

Notes: Fibres were classified as COX positive, COX intermediate positive, COX intermediate negative or negative in order to make it comparable with immunofluorescent assessment.

Table 3
Immunofluorescent analysis of respiratory chain protein expression.

Patient	Age/ years	Complex I negative/%	Complex I deficient/%	Complex IV negative/%	Complex IV deficient/%
DYSF 1	15.7	2.03	12.26	*0.58*	6.62
18 years (-ve C)	18	0	0	*0*	0
DYSF 2	20.5	0	0.00	*0*	0.05
DYSF 3	21.9	26.1	29.42	*0*	11.05
DYSF 4	24.7	0.09	0.85	*1.13*	4.7
DYSF 5	28.9	0.15	0.48	*0.12*	0.33
DYSF 6	30.4	1.78	7.43	*1.24*	3.05
34 years (-ve C)	34	*0.18*	0.6	*0.18*	0.3
DYSF 7	47.1	0	0.00	*0*	5.05
52 years (-ve C)	52	*0*	0	*0*	0
DYSF 8	52.5	1.96	10.79	*0.44*	1.31

Notes: Summary of percentage of fibres classified as complex-I and complex-IV negative or deficient (negative and intermediate categories). Controls and patients are organised in age for easy comparison.

approximately 0.5% fibres in the 52 year old control. In contrast, complex I deficiency ranged from 0% in two patients to 29.4% in patient 3. These levels were much higher than we expected in age matched healthy individuals but lower than those found in the patient with recessive *RRM2B* variants (36.2%).

The 18 and 34 year old control biopsies demonstrated no complex IV deficient fibres and the 52 year old had approximately 0.5%. In contrast to this, 0.1–11.1% of patients' muscle fibres had evidence of complex IV deficiency. A higher proportion of muscle fibres are complex IV deficient than in the age-matched controls and previous reports of age-related complex IV deficiency [15]. However, in comparison to the patient with *RRM2B* variants whose biopsy harboured 23.2% complex IV deficient fibres, the degree of deficiency in the dysferlin patient is low.

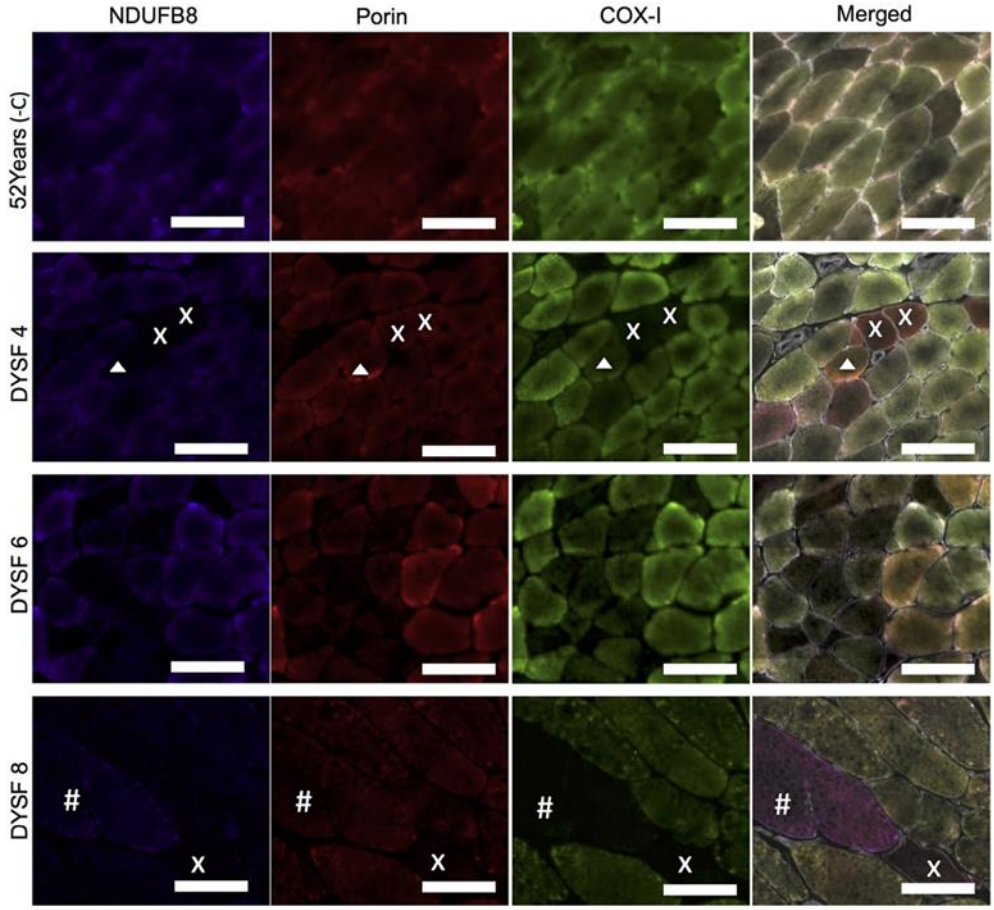

Fig. 2. Quadruple immunofluorescent analysis of mitochondrial respiratory chain deficiency.
Notes: Representative images of NDUFB8 (complex I) (purple), porin (red) and COX-I (complex IV) (red). Immunofluorescent staining in a 52 year old negative control and dysferlin patients 4, 6 and 8. Fibres deficient for complex I and complex IV (x in DYSF4 and DYSF8), complex IV only (# in DYSF8) and complex I only (arrow head in DYSF8) can be seen. Scale bar 100 μm.

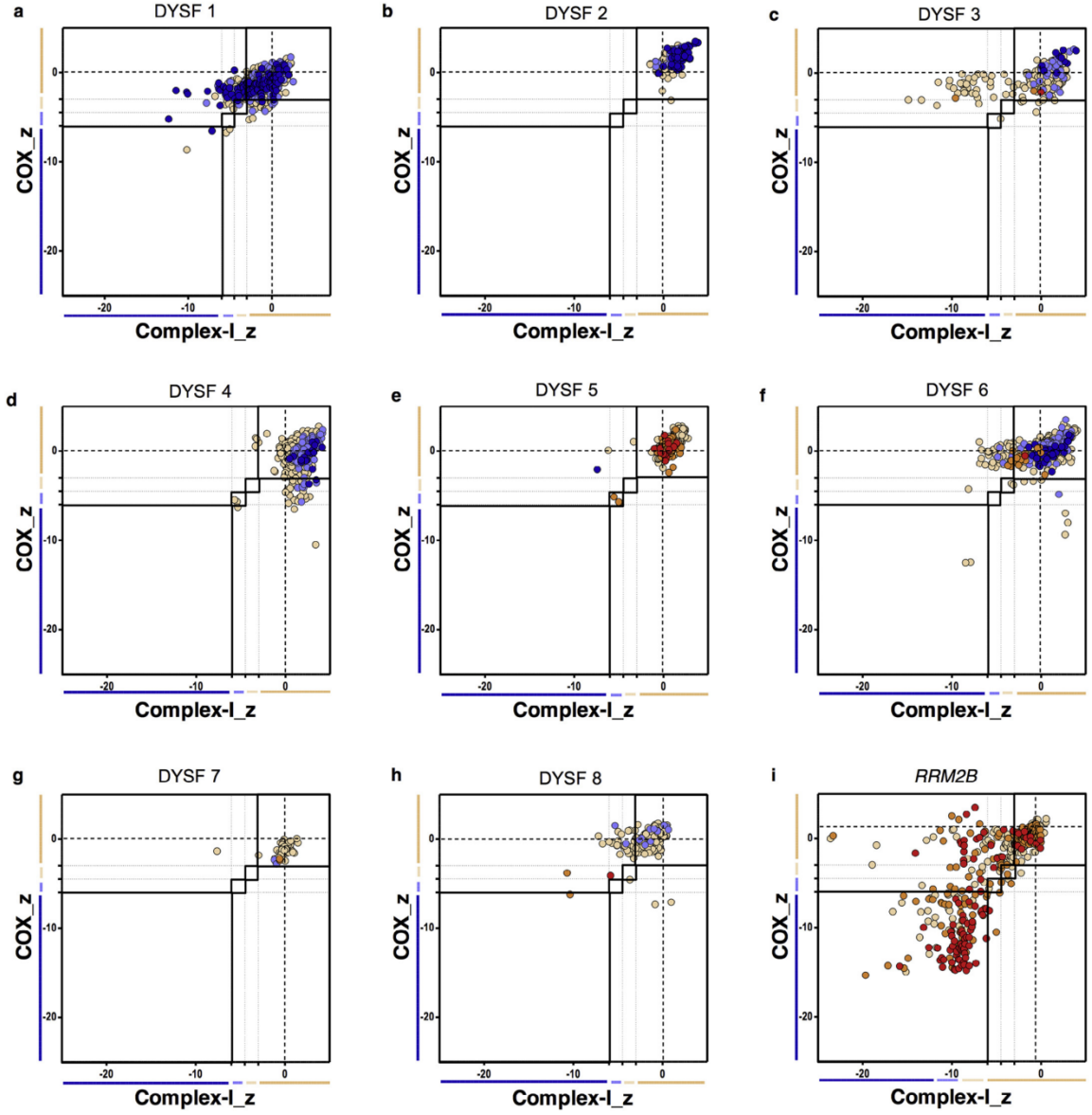

Fig. 3. Mitochondrial respiratory chain expression profiles displaying complex I, complex IV and porin levels in patients with *DYSF* mutations and an *RRM2B* mutation as a mitochondrial disease control. (a) DYSF 1, (b) DYSF 2, (c) DYSF 3, (d) DYSF 4, (e) DYSF 5, (f) DYSF 6, (g) DYSF 7, (h) DYSF 8 and (i) RRM2B patient positive control.

Notes: Each point gives the complex I and complex IV z-scores for a single fibre and is colour coded to indicate the porin category of the fibre (very low, dark blue; low, light blue; normal, beige; high, orange; or very high red). Bars next to the X and Y-axes indicate category of complex I or complex IV levels (dark blue, negative; light blue, intermediate negative; light beige, intermediate positive and beige, normal).

The respiratory expression profiles in Fig. 3 demonstrate three clear patterns of mitochondrial respiratory chain protein levels. Dysferlin patients 1, 3 and 6 (Fig. 3a, c and f respectively) had large number of fibres which were complex I-deficient. Dysferlin patient 4 (Fig. 3d) had a larger number of complex IV-deficient fibres than complex I-deficient fibres. Patients, 2, 5, 7 and 8 (Fig. 3b, e, g and h respectively) demonstrated very little deficiency affecting either respiratory chain complex. All dysferlinopathy patients had lower levels of respiratory chain deficiency than the *RRM2B* patient (Fig. 3i)

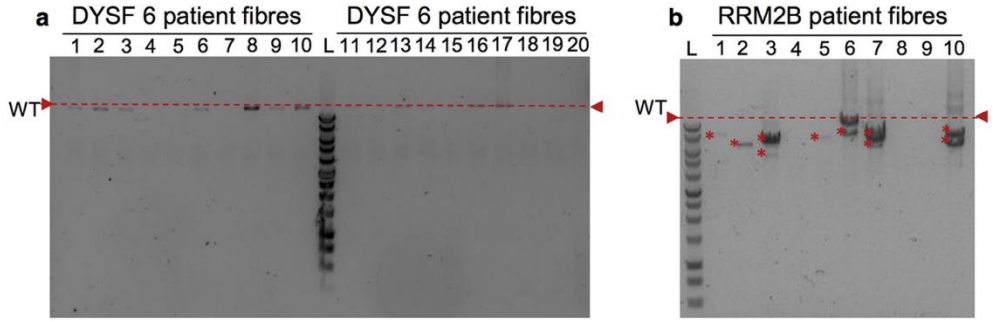

Fig. 4. Long-range PCR analysis of mtDNA. Long-range analysis of dysferlin patient 6 (DYSF6) (representative).
Notes: Red dashed line on all gels indicates wild type mitochondrial DNA size. 1Kb ladder (Promega) run on every agarose gel to size bands and a non-deleted, wild type DNA sample and a no template were included as controls. (a) Long-range PCR results for 20 single fibre lysates from DYSF 6 showed no deletions to be present, while (b) the *RRM2B* positive control long-range PCR results show multiple large-scale mtDNA deletions detected (*).

but at 43 years of age, this disease control is older than the majority of dysferlin patients (many of whom are below the age of 35 years).

3.3. Mitochondrial DNA genetic analysis

Patients 4, 6 and 8 were selected for genetic analysis, as these demonstrated the most COX-deficient fibres in sections subjected to COX/SDH histochemistry. Long-range PCR indicated a lack of deletions in all fibres for which a product was successfully amplified for each patient (Fig. 4a), while the patient harbouring compound *RRM2B* variants demonstrated multiple mtDNA deletions (Fig. 4b). In each of the dysferlin patients and an RRM2B patient, a small number of fibres failed to amplify.

4. Discussion

This study has demonstrated that the levels of complex IV (COX) and complex I deficiency are higher in some dysferlinopathy patients than in age-matched controls. The majority of deficient fibres were categorised as intermediate positive or intermediate negative rather than completely negative. Furthermore, the percentage of complex I-deficient fibres was higher than the percentage of complex IV deficient fibres in many of these patients.

Long-range PCR analysis of mtDNA from three patients, with high percentage of complex I and complex IV deficient fibres, demonstrated only full-length mtDNA amplicons. Despite an absence of large-scale mtDNA deletions, it is possible that the respiratory chain dysfunction may be due to deletions or duplications smaller than the resolution of the technique, or indeed mtDNA point mutations. As there is a greater percentage of complex I and complex IV deficiency in patients compared to controls, we hypothesise that mutations in the dysferlin protein which cause a defect in membrane resealing and alter the ability of dysferlin to maintain Ca^{2+} homeostasis may also have an impact on the mitochondria. If so, mitochondrial respiratory chain dysfunction could be secondary to the increased cytosolic calcium concentration which may affect mitochondrial topology.

Dysferlin, which has ferlin Ca^{2+} domains with variable affinities for Ca^{2+} helps to regulate cytosolic Ca^{2+} [10]. In the absence of functional dysferlin, cytosolic Ca^{2+} levels become abnormally high. Regulation of cytosolic Ca^{2+} levels is also a role of the mitochondria; as such, a shift in Ca^{2+} will affect their function. Ca^{2+} influx into the cytoplasm increases in mitochondrial fission and leads to fragmentation of the mitochondrial network [16]. Mitochondrial fusion is necessary for mtDNA stability and tolerance of mtDNA mutations, as it allows equilibration of the mtDNA maintenance machinery throughout the network and dilutes mutated mitochondrial DNA reducing the impact on mitochondrial function [17]. As such, mutations in the dysferlin gene that increase Ca^{2+} influx and impair muscle Ca^{2+} homeostatic ability of the muscle cause an increase in cytosolic Ca^{2+} concentration, fragmentation of the mitochondrial network and therefore allow mitochondrial dysfunction to accumulate and impact on tissue functionality.

Here, we demonstrate that complex I and complex IV deficiency is higher in patients with dysferlin mutations than in age-matched controls. We hypothesise that this may be due to interruption of calcium homeostasis because of the mutation in dysferlin and defect in membrane resealing. Further testing will be required to confirm this but may offer a potential therapeutic target.

Acknowledgements

AEV is funded by an MRC studentship (MR/K501074/1) as part of the MRC Centre for Neuromuscular Disease (MR/K000608/1). This work was supported by The Wellcome Trust Centre for Mitochondrial Research (096919Z/11/Z), the Medical Research Council (UK) Centre for Translational Muscle Disease Research (G0601943), the UK NIHR Biomedical Research Centre in Age and Age Related Diseases award to the Newcastle upon Tyne Hospitals NHS Foundation Trust, The Lily Foundation and the UK NHS Highly

Specialised Commissioners, which funds the "Rare Mitochondrial Disorders of Adults and Children" Diagnostic Service in Newcastle upon Tyne. CLA is the recipient of a National Institute for Health Research (NIHR) doctoral fellowship (NIHR-HCS-D12-03-04). The views expressed are those of the author(s) and not necessarily those of the NHS, the NIHR or the Department of Health.

References

[1] Liu J, Aoki M, Illa I, et al. Dysferlin, a novel skeletal muscle gene, is mutated in Miyoshi myopathy and limb girdle muscular dystrophy. Nat Genet 1998;20:31–6.
[2] Bashir R, Britton S, Strachan T, et al. A gene related to Caenorhabditis elegans spermatogenesis factor fer-1 is mutated in limb-girdle muscular dystrophy type 2B. Nat Genet 1998;20:37–42.
[3] Bansal D, Campbell KP. Dysferlin and the plasma membrane repair in muscular dystrophy. Trends Cell Biol 2004;14:206–13.
[4] Illarioshkin SN, Ivanova-Smolenskaya IA, Greenberg CR, et al. Identical dysferlin mutation in limb-girdle muscular dystrophy type 2B and distal myopathy. Neurology 2000;55:1931–3.
[5] Weiler T, Bashir R, Anderson LV, et al. Identical mutation in patients with limb girdle muscular dystrophy type 2B or Miyoshi myopathy suggests a role for modifier gene(s). Hum Mol Genet 1999;8:871–7.
[6] Gallardo E, Rojas-Garcia R, de Luna N, Pou A, Brown RH Jr, Illa I. Inflammation in dysferlin myopathy: immunohistochemical characterization of 13 patients. Neurology 2001;57:2136–8.
[7] Lek A, Lek M, North KN, Cooper ST. Phylogenetic analysis of ferlin genes reveals ancient eukaryotic origins. BMC Evol Biol 2010;10:231.
[8] Abdullah N, Padmanarayana M, Marty NJ, Johnson CP. Quantitation of the calcium and membrane binding properties of the C2 domains of dysferlin. Biophys J 2014;106:382–9.
[9] Bansal D, Miyake K, Vogel SS, et al. Defective membrane repair in dysferlin-deficient muscular dystrophy. Nature 2003;423:168–72.
[10] Gayathri N, Alefia R, Nalini A, et al. Dysferlinopathy: spectrum of pathological changes in skeletal muscle tissue. Indian J Pathol Microbiol 2011;54:350–4.
[11] Liu F, Lou J, Zhao D, et al. Dysferlinopathy: mitochondrial abnormalities in human skeletal muscle. Int J Neurosci 2015;doi:10.3109/00207454.2015.1034801.
[12] Rocha MC, Grady JP, Grunewald A, et al. A novel immunofluorescent assay to investigate oxidative phosphorylation deficiency in mitochondrial myopathy: understanding mechanisms and improving diagnosis. Sci Rep 2015;5:15037.
[13] Pitceathly RD, Smith C, Fratter C, et al. Adults with RRM2B-related mitochondrial disease have distinct clinical and molecular characteristics. Brain 2012;135:3392–403.
[14] Taylor RW, Barron MJ, Borthwick GM, et al. Mitochondrial DNA mutations in human colonic crypt stem cells. J Clin Invest 2003;112:1351–60.
[15] Bua E, Johnson J, Herbst A, et al. Mitochondrial DNA-deletion mutations accumulate intracellularly to detrimental levels in aged human skeletal muscle fibers. Am J Hum Genet 2006;79:469–80.
[16] Han XJ, Lu YF, Li SA, et al. CaM kinase I alpha-induced phosphorylation of Drp1 regulates mitochondrial morphology. J Cell Biol 2008;182:573–85.
[17] Chen H, Vermulst M, Wang YE, et al. Mitochondrial fusion is required for mtDNA stability in skeletal muscle and tolerance of mtDNA mutations. Cell 2010;141:280–9.

Appendix 3 “Mitochondrial dysfunction in myofibrillar myopathy”. Vincent et al. (2016). Manuscript published in Neuromuscular disorders.

Available online at www.sciencedirect.com

ScienceDirect

Neuromuscular Disorders 26 (2016) 691–701

www.elsevier.com/locate/nmd

Mitochondrial dysfunction in myofibrillar myopathy

Amy E. Vincent [a], John P. Grady [a], Mariana C. Rocha [a], Charlotte L. Alston [a], Karolina A. Rygiel [a], Rita Barresi [b], Robert W. Taylor [a], Doug M. Turnbull [a,*]

[a] *Wellcome Trust Centre for Mitochondrial Research, Institute of Neuroscience, Newcastle University, Newcastle upon Tyne, NE2 4HH, UK*

[b] *Rare Diseases Advisory Group Service for Neuromuscular Diseases, Muscle Immunoanalysis Unit, Newcastle upon Tyne Hospitals NHS Foundation Trust, Newcastle upon Tyne, NE2 4AZ, UK*

Received 6 April 2016; received in revised form 5 August 2016; accepted 9 August 2016

Abstract

Myofibrillar myopathies (MFM) are characterised by focal myofibrillar destruction and accumulation of myofibrillar elements as protein aggregates. They are caused by mutations in the *DES*, *MYOT*, *CRYAB*, *FLNC*, *BAG3*, *DNAJB6* and *ZASP* genes as well as other as yet unidentified genes. Previous studies have reported changes in mitochondrial morphology and cellular positioning, as well as clonally-expanded, large-scale mitochondrial DNA (mtDNA) deletions and focal respiratory chain deficiency in muscle of MFM patients. Here we examine skeletal muscle from patients with desmin (n = 6), ZASP (n = 1) and myotilin (n = 2) mutations and MFM protein aggregates, to understand how mitochondrial dysfunction may contribute to the underlying mechanisms causing disease pathology. We have used a validated quantitative immunofluorescent assay to study respiratory chain protein levels, together with oxidative enzyme histochemistry and single cell mitochondrial DNA analysis, to examine mitochondrial changes. Results demonstrate a small number of clonally-expanded mitochondrial DNA deletions, which we conclude are due to both ageing and disease pathology. Further to this we report higher levels of respiratory chain complex I and IV deficiency compared to age matched controls, although overall levels of respiratory deficient muscle fibres in patient biopsies are low. More strikingly, a significantly higher percentage of myofibrillar myopathy patient muscle fibres have a low mitochondrial mass compared to controls. We concluded this is mechanistically unrelated to desmin and myotilin protein aggregates; however, correlation between mitochondrial mass and muscle fibre area is found. We suggest this may be due to reduced mitochondrial biogenesis in combination with muscle fibre hypertrophy.

Keywords: Myofibrillar myopathy; Mitochondria; Mitochondrial DNA deletion; Immunofluorescence; Histochemistry; Cytochrome *c* oxidase deficiency

1. Introduction

Myofibrillar myopathies (MFMs) are a group of myopathies characterised by aggregation of the Z-disk proteins and focal myofibrillar destruction. MFMs or Z-disk diseases are clinically and genetically heterogeneous. Mutations causing MFM can be found in genes encoding a range of Z-disk proteins including; desmin (*DES*) [1], αB-crystallin (*CRYAB*) [2], myotilin (*MYOT*) [3], filamin C (*FLNC*) [4], ZASP (*LDB3/ZASP*) [5] and Bcl2-associated athanogene 3 (*BAG3*) [6]. Novel MFM causing genes are continuously being identified and at present only 50% of suspected MFM cases have a genetic diagnosis.

They are typically present in the third or fourth decade of life or later, though rare cases of adolescent onset have also been reported. Most commonly they present as distal myopathies initially, progressing to involve proximal limb muscles. However, myofibrillar myopathies can vary in clinical presentation and can lead to cardiomyopathy associated with skeletal muscle myopathy or isolated cardiomyopathy. Key clinical patterns in presentation can be noted for some of the causative genes; however, once more, these are not clear cut and there are exceptions.

Mitochondrial dysfunction is a common finding in many proteinopathies including protein aggregate myopathies (PAMs) [7–15], and some neurodegenerative conditions [16]. Cytochrome *c* oxidase (COX) deficiency has been found to be associated with clonally-expanded mtDNA rearrangements in sarcopenia, patients with single or multiple mitochondrial DNA (mtDNA) deletions and inclusion body myositis. However, mtDNA point mutations [17] and depletion of mtDNA copy number [18] may also lead to focal respiratory chain deficiency.

Previous reports have noted that both mitochondrial morphology and positioning are altered in muscle of MFM

* Corresponding author. Wellcome Trust Centre for Mitochondrial Research, Institute of Neuroscience, The Medical School, Newcastle University, Newcastle upon Tyne, NE2 4HH, UK. Fax: 0044-1912228553.

E-mail address: doug.turnbull@ncl.ac.uk (D.M. Turnbull).

http://dx.doi.org/10.1016/j.nmd.2016.08.004

patients [19], as well as the presence of clonally-expanded large-scale mtDNA deletions [20,21] and focal respiratory chain deficiency [22,23]. However, there have only been a few previous publications to date and only small numbers of patients reported in these studies. As such it is unclear what role, if any, clonally expanded mtDNA deletion and mitochondrial respiratory chain deficiency may play in the pathogenesis of myofibrillar myopathy.

In this paper we investigate a cohort of nine genetically determined MFM patients for evidence of mitochondrial dysfunction. From this cohort, we further selected a group of six patients based on the frequency of COX-deficient fibres identified by sequential COX/SDH histochemistry to study for presence of clonally-expanded large-scale mtDNA deletions. We also subjected all patient muscle biopsies to a recently developed immunofluorescence assay [24] to assess NDUFB8 (complex-I) and COX-I (complex-IV) protein levels normalised to mitochondrial mass (Porin).

2. Materials and methods

2.1. Patient cohort

Muscle biopsies were taken for diagnostic purposes from patients with a suspected neuromuscular condition (see Table 1). Informed consent was obtained from all patients in the study. Ethical approval was granted by the Newcastle and North Tyneside local research and ethics committee (LREC2002/205). Inclusion criteria were the presence of protein aggregates on sections stained with anti-desmin and anti-myotilin antibodies and confirmed molecular diagnosis for MFM genes. We studied nine MFM patients with mutations in *DES* (n = 6), *MYOT* (n = 2) and *ZASP* (n = 1). A patient with compound heterozygous *RRM2B* variants, leading to a disturbance of mtDNA maintenance and multiple mtDNA deletions [25], was used as a positive control, as well as two healthy control muscle biopsies from individuals aged 52 and 63 years.

2.2. Histochemistry

Muscle was cryosectioned (10 μm) from transversely-orientated muscle blocks and subjected to histochemical reactions for the individual activities of COX, SDH and the sequential assay of COX/SDH activity [26]. COX-deficient fibres were counted using a stereomicroscope, by outlining the full muscle biopsy section and using the meander scan function in Stereo Investigator. Fibres were categorised by eye with blue fibres being categorised as COX negative, blue-grey fibres as intermediate negative and grey-brown fibres as intermediate positive. Intermediate categories were included to make comparison with immunofluorescent quantification easier. The minimum number of fibres counted was 127, which was for patient DES3 who had the smallest muscle biopsy section. Serial sections were stained with Haematoxylin and Eosin (H&E) to examine muscle morphology.

2.3. Quadruple immunofluorescence

A quadruple immunofluorescent method using antibodies recognising laminin (membrane marker), NDUFB8 (complex I marker), COX-I (complex IV marker), and porin as a mitochondrial mass marker, was employed to assess the degree of respiratory chain deficiency [24]. Briefly, one 10 μm cryosection from each patient and age matched controls was labelled with all four antibodies and a serial 10 μm section with just laminin to be used as a negative (no primary antibody) control. Sections were incubated with secondary antibodies coupled with Alexa Fluor 405, 488, 546 and 647 (Life Technologies). Using a Zeiss AxioImager and AxioCam MRm with AxioVision software tiled images scanning of the full section were acquired and stitched using ZEN (blue edition). Analysis using IMARIS version 7.6 involved creating a surface over the laminin staining, which was masked, allowing a second surface covering each fibre to be created and average fluorescent intensity for each muscle fibre to be collected.

Using values from the negative (no primary antibody) control for each case, non-specific background was subtracted and NDUFB8 and COX-1 intensity was normalised to porin intensity as the mitochondrial mass marker. Control case values then created a "normal population" for which the patient fibres could then be assigned a z-score describing their deviation from the normal population. Statistical analysis is described in more detail by Rocha et al. [24]. Total fibres analysed was dependent on section size and ranged from n = 111 to n = 1883 in patients and controls.

Table 1
Myofibrillar myopathy patient information (n = 9). Patients are organised by gene then age order and all mutation nomenclature uses the primary transcripts for *DES* (NM_001927) and *MYOT* (NM_006790) and for *ZASP* transcript variant 2 (NM_001080114.1).

Patient	Gender	Mutated gene	Mutation	CK	Biopsy site	Age at biopsy	Age at onset (if known)
DES 1	M	*DES*	Het. c.1069G > C, p.(Ala357Pro)	480	Quadriceps	31.2	29
DES 2	M	*DES*	Het. c.1069G > C, p.(Ala357Pro)	NK	NK	32.1	NK
DES 3	M	*DES*	Hom. c.46C > T, p.(Arg16Cys)	450	Quadriceps	33.8	20s
DES 4	F	*DES*	Het. c.735 + 20C > T (MAF = 0.01); c.638C > T, p.(Ala213Val)	NK	Quadriceps	51.3	Early childhood
DES 5	F	*DES*	Het. c.638 C > T, p.(Ala213Val)	74	Quadriceps	53	40s
DES 6	F	*DES*	Het. c.1346A > C , p.(Lys449Thr)	287	NK	64.3	46
MYOT 1	M	*MYOT*	Het. c.179C > G, p.(Ser60Cys)	446	Quadriceps	60.5	55
MYOT 2	M	*MYOT*	c.179C > G, p.(Ser60Cys)	400–500	Tibialis anterior	65.7	NK
ZASP 1	F	*ZASP*	Het. c.494C > T, p.(Ala165Val); Het. c.728C > T, p.(Pro243Leu)	300	Quadriceps	69.6	60s

DES: desmin; MYOT: myotilin; Hom.: homozygous; Het.: heterozygous; MAF: maternal allele frequency; CK: creatine kinase; NK: not known.

2.4. Measurement of porin across the muscle fibre

A total pool of normal (n = 10), low (n = 10) and very low porin (n = 10) fibres were selected to assess porin level across the muscle fibre. The profile tab in ZEN (blue edition) was used to draw a segmenting line across the full muscle fibre and generate a graph of fluorescent intensity in each channel across the fibre.

2.5. Mitochondrial mass

To assess mitochondrial mass, labelling of a second marker, succinate dehydrogenase subunit A (SDHA), was compared to porin. Cryosectioned muscle was subject to an immunofluorescence protocol, following a similar protocol as in Section 2.3, but without anti-COXI and replacing anti-NDUFB8 with anti-SDHA. Total fibres analysed across all patients was n = 5565, with fibres per patient ranging from n = 114 to n = 1283 in individual patients and controls.

2.6. Analysis of MFM protein aggregates and mitochondrial mass

Muscle sections were co-labelled with antibodies recognising laminin, desmin, myotilin and porin. Following image capture, processing and analysis as in Section 2.3, myofibres containing very low (n = 436), low (n = 338) and normal porin (n = 150) content (across all patients) were analysed in turn and categorised as either being positive or negative for the presence of desmin and myotilin aggregates. Following this, fibres with or without aggregates were plotted against z-score for porin protein level as an indicator of mitochondrial mass.

2.7. Laser microdissection and cell lysis

Six patients were selected for mtDNA analysis based on the presence of COX deficient fibres. For each patient four serial muscle sections were cryosectioned. The first and last tissue sections underwent sequential COX/SDH histochemistry and were used to assess deficiency of the second and third sections, which underwent SDH histochemistry only. Sequential single muscle fibres were laser micro-dissected from the second and third tissue section using a PALM system (Zeiss). Fibres from the second tissue section were captured into 15 µl SDS/EDTA/Proteinase K single cell lysis buffer (0.5% SDS, 10 mM EDTA, 5% proteinase K) and incubated for 2 hours at 37 °C to lyse. Fibres from the third were captured into 15 µl Tris/Tween/Proteinase K single cell lysis buffer (0.5M Tris-HCl, 0.5% Tween 20, 1% Proteinase K, pH 8.5) and incubated for 2 hours at 55 °C, followed by 10 minutes at 95 °C to lyse. For each patient 20 single fibres were analysed for both long range PCR and real time PCR.

2.8. Long range PCR

Two rounds of PCR were employed to screen isolated muscle fibres for large-scale mtDNA rearrangements: 1 µl cell lysate, 1× PrimeSTAR GXL reaction buffer, 0.2 µM dNTPs, 0.2 µM forward and reverse primers and 0.625 unit polymerase, in a total volume of 50 µl. The first round of PCR amplified a 16179 bp region using primers 2180F (nucleotides m.2180–2209) and 1789R (nucleotides m.1760–1789) and the second round reaction amplified a 16029 bp region using primers 2330F (nucleotides m.2330–2359) and 1789R (nucleotides m.1760–1789) (NC_012920.1). Cycling conditions were: 35 cycles of 10 seconds at 98 °C and 11 minutes at 68 °C. PCR products were separated through a 0.7 % agarose gel with a 1 Kb ladder used to size amplicons.

2.9. Triplex real time PCR

A triplex real time PCR assay was used to quantify mtDNA deletion level as described previously [27]. This method quantifies relative levels of *MT-ND4* and *MT-ND1* and D-Loop, using TaqMan chemistry. Primers and TaqMan MGB probes used to detect *MT-ND1*, *MT-ND4* and D-Loop have been previously reported [27]. PCR amplification was completed in a 25 µl reaction in triplicate for each sample, with each plate containing a serial dilution of p7D1 plasmid for standard curve generation, as reported previously [27].

2.9.1. Analysis and statistics

Percentage classification of fibres for NDUFB8, COX-I and porin were compared between the patient group and control group using a Wilcoxon Signed-Rank Test. Spearman's rank correlation (src) was used to assess the relationship between fibre area and complex I, complex IV and porin protein levels.

3. Results

3.1. Histology and histochemistry

H&E demonstrated a variety of pathological features consistent with a diagnosis of myofibrillar myopathy including: variation in fibre size, rimmed vacuoles, internal nuclei, nuclear bags, basophilic and eosinophilic inclusions, fibre splitting, and necrotic and regenerating fibres. Sequential COX/SDH histochemistry showed a low number of COX-deficient fibres (typically not more than 5%) (Table 2). Furthermore, fibres that were pale for COX activity were also pale for SDH activity, indicating low mitochondrial content (Fig. 1, denoted by asterisk). Many fibres also showed a core-like depletion of mitochondria in the centre and accumulation in the subsarcolemmal region (Fig. 1, DES patient 2).

Table 2
COX deficiency counts for myofibrillar myopathy patients based on sequential COX/SDH histochemistry.

Patient	Total fibres	COX-positive	Intermediate-positive	Intermediate-negative	COX negative
DES 1	494	94.3	4.45	1.01	0.202
DES 2	611	87.7	10.3	1.80	0.164
DES 3	127	81.9	18.1	0.0	0.0
DES 4	863	95.6	4.06	0.348	0.0
DES 5	1086	93.6	5.06	0.829	0.552
DES 6	248	45.16	39.1	12.9	2.82
MYOT 1	848	96.6	2.48	0.943	0.0
MYOT 2	697	91.1	5.67	3.73	0.0
ZASP 1	835	99.4	0.479	0.120	0.0

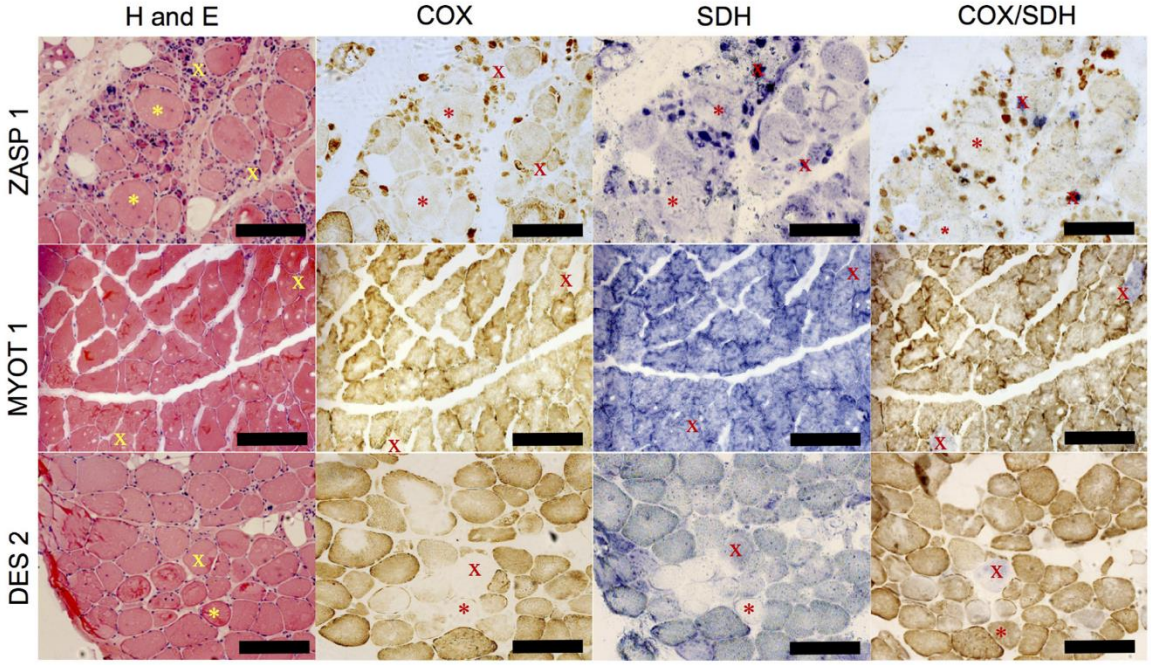

Fig. 1. Histochemistry for serial muscle sections. Sections from ZASP 1, MYOT 1 and DES 2 were subject to H&E staining, COX histochemistry, SDH histochemistry and sequential COX/SDH histochemistry. H&E staining demonstrates morphological changes compatible with diagnosis. Many fibres appear COX-deficient but also demonstrate low SDH reactivity, indicative of a reduction in mitochondrial mass. X, COX-deficient fibre, and asterisk (*), mitochondrial depletion fibres. Scale bar 200 μm.

3.2. Clonally-expanded mtDNA deletions

Long range PCR and real time PCR were used to investigate the presence of clonally-expanded mtDNA deletions in 20 COX-deficient single cell lysates from MFM patients with *DES* (n = 4), *MYOT* (n = 1) and *ZASP* (n = 1) mutations and a positive control (patient with multiple mtDNA deletions caused by genetically inherited pathogenic *RRM2B* variants). For every fibre analysed both long range and real time PCR were performed. Long range PCR analysis of 20 fibres from the patient with *RRM2B* variants demonstrated products of varying size indicative of different sized mtDNA deletions (Fig. 2a). In comparison to the *RRM2B* patient, of the 120 fibres analysed from six MFM patients, an mtDNA deletion was detected in only five fibres (DES4: n = 1, DES5: n = 1 and ZASP1: n = 3). The remaining fibres either had a full-length wild type (WT) product or failed to amplify a product (n = 31) (Fig. 2b and c). Failure to amplify a product is common in long range PCR from single cell lysates. This also occurred in two fibres from the *RRM2B* patient. The percentage of fibres that did not amplify is lower in the *RRM2B* case, likely due to the presence of ragged-red fibres indicative of high mitochondrial mass in the *RRM2B* patient and core-like fibres suggesting low mitochondrial mass in the MFM patients.

Real time PCR analysis showed that the majority of individual COX-deficient myofibres obtained from the *RRM2B* patient muscle contained different levels of mtDNA deletion (Fig. 2d), which was in agreement with long range PCR results (Fig. 2a). Real time PCR also confirmed that only a few MFM muscle fibres contained clonally-expanded mtDNA deletion. Of 120 fibres deletions were found by real time PCR in 12 fibres (DES 4: n = 1, DES5: n = 2, DES7: n = 1 and ZASP1: n = 8), as presented in Fig. 2c and d.

Out of the 120 fibres on which both long range PCR and real time PCR were completed, a deletion was found by both methods in five fibres and a further seven were shown to have a deletion by real time PCR alone. In these seven fibres unfortunately no long range product was amplified. Inclusion of the D-loop allowed confirmation that MFM patient fibres did not contain any deletions affecting *MT-ND1* (data not shown). This was in agreement with long range PCR.

3.3. Immunofluorescent analysis of respiratory chain deficiency

Based on the low number of fibres in which COX-deficiency was found by histochemistry and an mtDNA deletion detected, we explored the nature of the respiratory chain protein abundance in more detail. We employed a quantitative immunofluorescence assay to assess porin, NDUFB8 (complex I) and COX-I (complex IV) protein levels.

Immunofluorescent analysis was used to compare the myofibrillar myopathy patients and a patient with compound

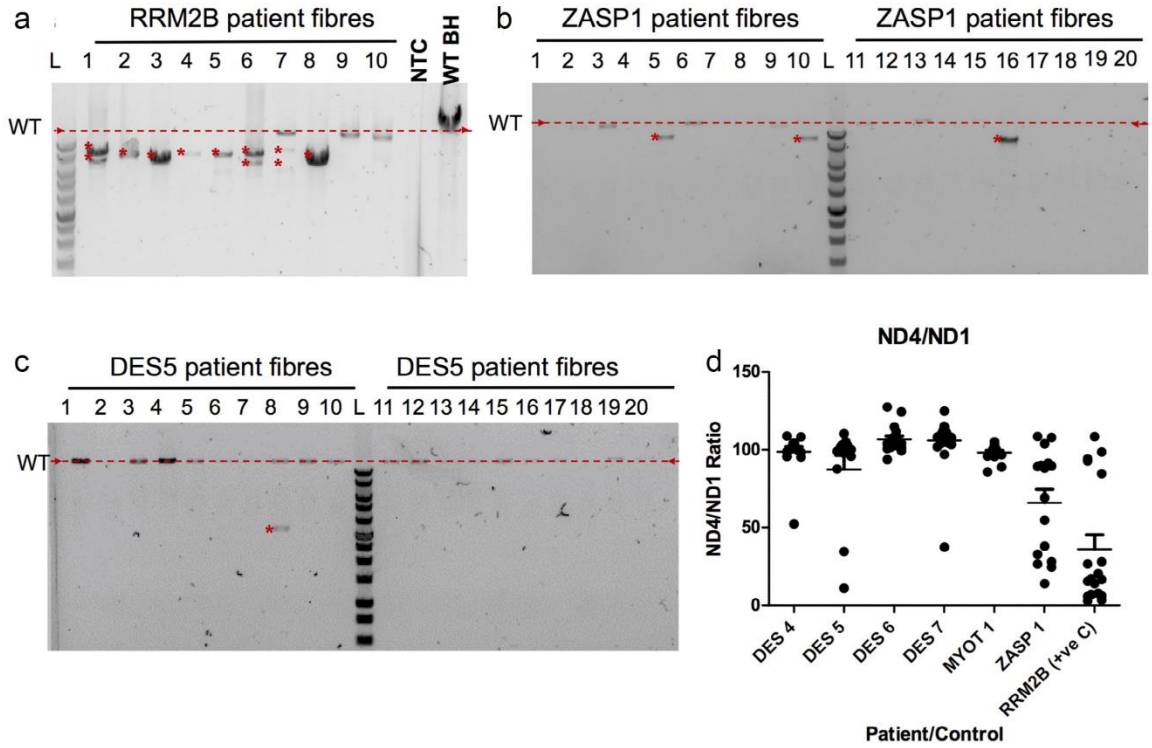

Fig. 2. Long range and real time PCR analysis of mtDNA deletions in each patient (n = 20). In long range PCR gels (a–c) red arrows and dashed line indicates size of wild type mtDNA product, red asterisk (*) indicates deletion products. (a) Long range PCR results for 10 single fibre lysates relative to a wild type (WT) blood homogenate, no template control (NTC) and 1 Kb ladder (Promega), multiple and single deletions present due to variants in RRM2B. (b) Long range PCR results for 20 single fibre lysates from ZASP1 demonstrating 3 fibres with a single deletion. (c) Long range PCR results for 20 single fibre lysates from DES 5 demonstrating 1 fibre with an mtDNA deletion. (d) Real time PCR results for DES4, DES5, DES6, DES7, MYOT1 and ZASP1 showing ratios of ND4 to ND1. Lines represent mean and standard error of the mean (SEM).

heterozygous *RRM2B* variants to age matched controls. Immunofluorescent images showed a number of fibres with combined and isolated complex I and complex IV-deficiency, plus fibres with reduced mitochondrial mass (Fig. 3). Respiratory chain protein level profiles for each MFM patient and the RRM2B patient can be found in Fig. 4. A summary of results can be found in Table 3.

Controls aged 52 years and 60 years showed no complex I or complex IV deficiency. In comparison, desmin patients showed some levels of complex I and complex IV deficiency, reaching 6.5% and 4.2% deficient fibres for complex I and complex IV respectively. However, respiratory chain deficiency was low in the majority of desmin patients. Although MYOT1 also had low levels of deficiency, MYOT2 exhibited higher levels of deficiency with percentage deficiencies of 45.5% for complex I and 24.7% for complex IV. Finally, the ZASP patient had 11.5% complex I deficient fibres and 9% complex IV deficient fibres.

By comparing these patients with the *RRM2B* patient (32.6% complex I and 23% complex IV deficiency), it is apparent that MYOT2 and ZASP1 exhibit levels of deficiency closer to that of a mitochondrial disease patient.

3.4. Reduction in mitochondrial mass

MFM patients showed very low porin fibres between 11% and 51.4%. Low and very low porin fibres are presented by light blue and dark blue circles in the respiratory chain profiles in Fig. 4. There was a significant difference in percentage of normal ($p = 0.03$), low ($p = 0.03$) and very low ($p = 0.04$) porin fibres between patients and controls (tested using a Wilcoxon Signed-Rank Test.) Total fibres were analysed and range of fibres per patient can be found in Section 2.4.

During the image analysis process (using IMARIS), the surfaces created above the fibres did not cover the full area within the laminin membrane staining due to limitations in threshold values used to generate the surfaces for analysis. Previous reports and our findings suggest core-like depletion of mitochondria in the intermyofibrillar regions and aggregation in the subsarcolemmal regions. If this is the case, it is possible that the image analysis process missed the majority of the mitochondria located in the subsarcolemma, explaining the high number of low porin fibres.

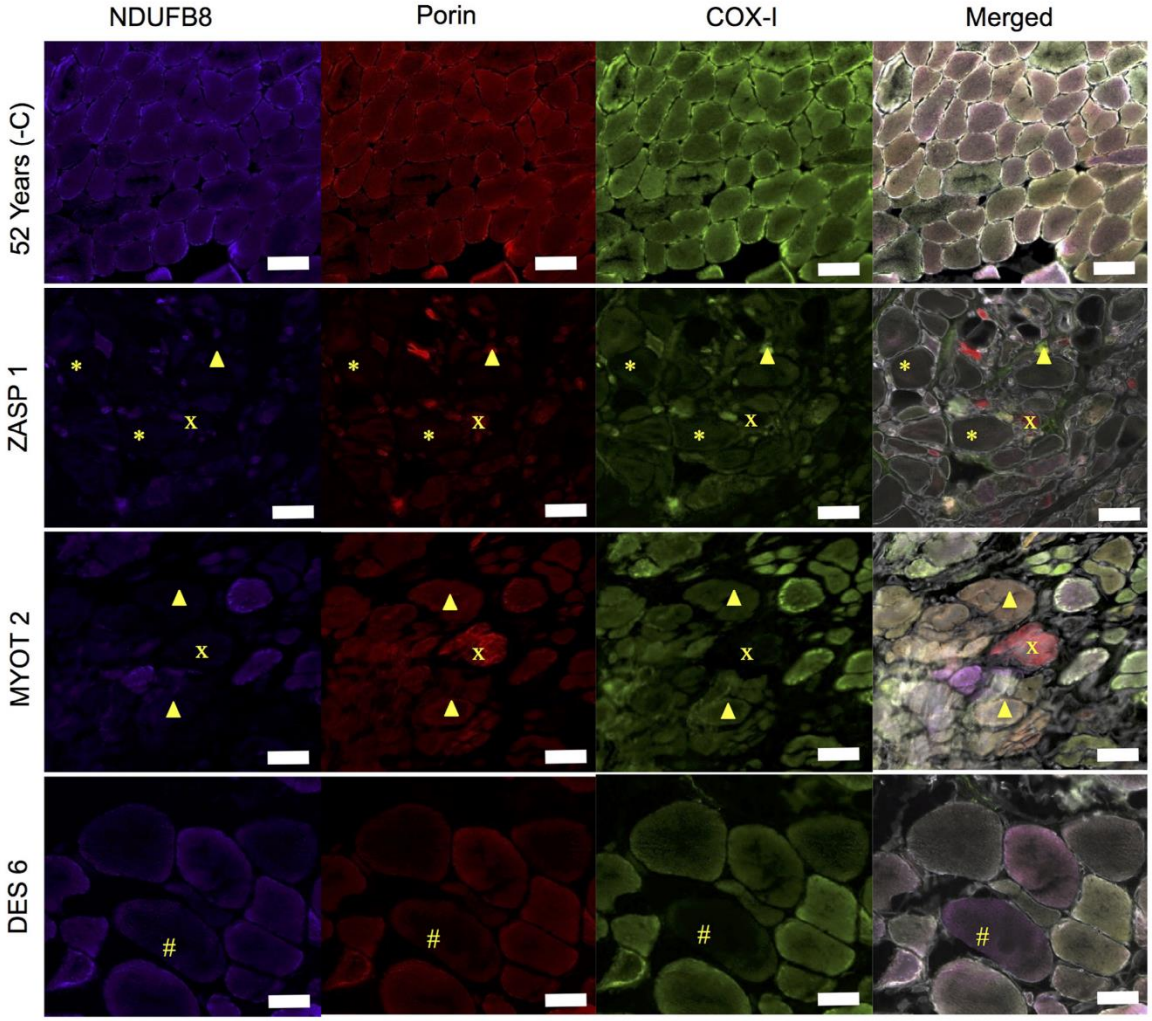

Fig. 3. Immunofluorescent analysis of respiratory chain function. Representative immunofluorescence for NDUFB8 (complex I), porin and COX-I (complex IV) in ZASP 1, MYOT 2 and DES 6. Complex I and complex IV deficient fibres, complex IV deficient fibres and complex I deficient fibres can be seen. Most strikingly fibres with low porin, complex I and complex IV can be seen in a number of patients, most pronounced in ZASP1(*). Asterisk (*), low porin complex I and complex IV; Cross, complex I and IV deficient fibres; Arrow head, complex I deficient fibres; and hash, complex IV deficient fibres. Scale bar 100 μm.

In order to test whether we are underestimating the level of porin due to our analysis methods, we analysed the fluorescent signal intensity across a pool of normal, low and very low porin fibres (Supplementary Fig. S1). This demonstrated a reduction in porin fluorescent intensity across the full diameter of the muscle fibre in both low and very low porin fibres when compared to normal fibres.

To further verify mitochondrial mass reduction, porin was compared to SDHA, a nuclearly encoded subunit of complex II. Porin and SDHA immunohistochemistry was carried out using sections from patients and controls. When SDHA is linearly regressed against porin, the r^2 values suggest a strong positive relationship in the cases with the largest range of porin and SDHA levels. For those cases with a smaller range the relationship was still apparent but the r^2 value was smaller due to the spread of the data points. This indicates that mitochondrial mass is reduced in a higher percentage of myofibrillar myopathy patient fibres compared to controls (2.6% and 6.4%).

3.5. Relation of respiratory chain deficiencies, mitochondrial mass and fibre size

To determine whether levels of porin, complex I and complex IV could be related to fibre atrophy we compared

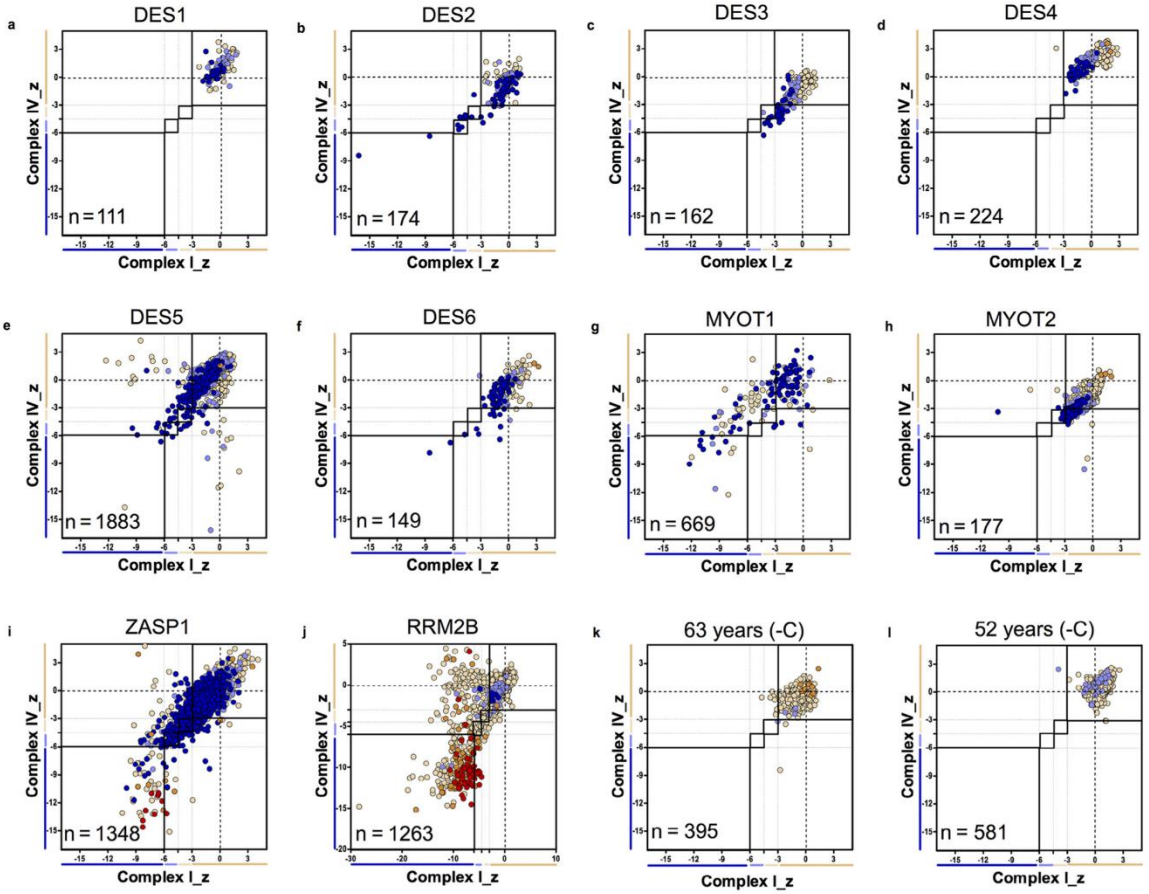

Fig. 4. Mitochondrial respiratory chain protein expression profiles. Immunofluorescence results for MFM patients and *RRM2B* patient positive control. Graphs demonstrate distribution of z-scores for complex I and complex IV with each point colour coded for porin category. Number (n) of fibres analysed on each plot. (a) DES1, (b) DES2, (c) DES3, (d) DES4, (e) DES5, (f) DES6, (g) MYOT1, (h) MYOT2, (i) ZASP1, (j) RRM2B, (k) 63 years (negative control) and (l) 52 years (negative control). Each point gives the COX and complex-I z-scores for a single fibre and is colour coded to indicate the porin category of the fibre (very low, dark blue; low, light blue; normal, beige; high, orange; or very high, red). Bars next to the X and Y-axes indicate category complex I or complex IV levels (dark blue, negative; light blue, intermediate negative; light beige, intermediate positive and beige, normal). In addition solid and dashed lines running vertically and horizontally also mark the boundaries between each category of complex I and complex IV.

fluorescent intensity for each channel with fibre area. Correlation was examined using Spearman's rank correlation (src) coefficient (summarised in Table 4.). Plotting of muscle fibre area against complex I level (Supplementary Fig. S2) demonstrated a positive correlations in DES5 (src = 0.4389, $p < 0.0001$), and DES3 (src = 0.4389, $p = < 0.0001$), a negative correlation in DES6 (src = −0.4817, $p < 0.0001$). For muscle fibre area and complex IV levels (Supplementary Fig. S3) only very weak to no correlation was found. We also found a negative correlation between muscle fibre area and porin level (Supplementary Fig. S4) in ZASP1 (src = −0.4487, $p < 0.0001$) and DES6 (src = −0.4583, $p < 0.0001$). Spearman's rank correlations were also significant for DES2, DES5, DES6, MYOT1 and MYOT2; however, the correlation between porin and muscle fibre area was weak in these patients (Table 4). Porin level plotted against muscle fibre area, for patient ZASP1, in particular, shows that large muscle fibres all have a low porin level whilst smaller muscle fibres have a range of high to low porin. Low Spearman's rank correlations in some patients appear to be due to the smaller range of fibre area.

3.6. *Association of low porin with protein aggregates*

As protein aggregates are the hallmark of myofibrillar myopathy we hypothesised they may be mechanistically linked to the low porin levels. Analysis of sections co-labelled with antibodies for myotilin, desmin, porin and laminin demonstrated a similar percentage of low and very low porin fibres relative to controls as previously shown. Very low, low and normal

Table 3
Immunofluorescent analysis of respiratory chain protein expression. Summary of percentage of fibres classified as complex I and complex IV negative or deficient (negative and intermediate categories). Controls and patients are organised in age order for easy comparison.

Patient	Age/ years	Complex I negative (%)	Complex I deficient (%)	Complex IV negative (%)	Complex IV deficient (%)	Total fibres analysed
DES 1	31.2	0.00	0.00	0.00	0.00	111
DES 2	32.1	0.12	6.48	0.12	3.62	174
DES 3	33.8	0.00	0.00	0.58	4.18	162
DES 4	51.3	0.00	0.00	0.00	0.00	224
52 Years (-ve C)	52.0	0.00	0.00	0.00	0.00	581
DES 5	53.0	0.79	1.41	0.8	1.63	1883
60 Years (-ve C)	60.0	0.00	0.73	0.07	0.07	395
MYOT 1	60.5	0.18	0.18	0.12	0.44	669
DES 6	64.3	1.91	2.50	3.52	4.99	149
MYOT 2	65.7	38.5	45.51	13.57	24.73	177
ZASP 1	69.6	6.43	11.47	5.34	8.96	1348

porin fibres were analysed for the presence of myotilin and desmin aggregates. This analysis demonstrated no significant relationship between presence of protein aggregates and porin level (Fig. 5b). Furthermore, in fibres with aggregates in ZASP1 (the patient with the highest percentage of low porin fibres), we found that only 22.9% had very low porin levels.

4. Discussion

Mitochondrial DNA deletions [20,21] and respiratory chain deficiency [20,22,23] have been shown to accumulate in the skeletal muscle of patients with myofibrillar myopathy. Furthermore changes in mitochondrial positioning have also been found [19]. As such, we aimed to examine a cohort of myofibrillar myopathy patients for the presence of mitochondrial dysfunction, and attempt to understand what correlation, if any, this has with disease pathology.

Here we demonstrate clonally-expanded mtDNA deletions in a small number of fibres from MFM patients by both long range PCR and real time PCR. A further seven fibres were found to have deletions by real time PCR but failed to amplify a product by long range PCR, a common problem for single cell long range PCR especially if mitochondrial content is low as in MFM patient muscle fibres. We conclude that the low levels of mtDNA deletions detected are likely due, at least in part, to the age on top of the disease process. Sporadic deletions are known to form and accumulate in mtDNA of aged muscle [28] and here we find the highest number of deletions in the oldest patient (ZASP1). However, due to the fact that there is only one patient with a ZASP mutation it is difficult to conclude to what extent this is due to age or the genotype.

Table 4
Summary of Spearman's rank correlation (src) analysis of muscle fibre are area against levels of porin, complex I and complex IV.

Patient	Porin		Complex I		Complex IV	
	src	p value	src	p value	src	p value
DES 1	−0.0564	0.5546	0.1389	0.144	0.09819	0.303
DES 2	−0.2492	0.0009	0.1161	0.1261	−0.1738	0.0214
DES 3	0.3776	<0.0001	0.4389	<0.0001	0.2808	0.0003
DES 4	0.06009	0.3707	0.1249	0.0619	0.05067	0.4504
DES 5	−0.1733	<0.0001	0.26	<0.0001	0.2933	<0.0001
DES 6	−0.4583	<0.0001	−0.4817	<0.0001	−0.3073	0.0001
MYOT 1	−0.2093	<0.0001	−0.09169	0.0187	−0.2006	<0.0001
MYOT 2	0.1302	0.1064	0.2428	0.0023	0.0483	0.5506
ZASP 1	−0.4487	<0.0001	−0.1716	<0.0001	−0.1634	<0.0001

In fibres where an mtDNA deletion was not detected, it is possible that mtDNA point mutations or mtDNA depletion may be the cause of COX deficiency. In particular, it should be noted that based on both COX/SDH histochemistry and immunofluorescent analysis, COX-deficient fibres are present at lower levels comparable to those with reduced mitochondrial mass. Both quantification of mtDNA copy number and deep sequencing of the mitochondrial genome would be necessary to fully assess this.

Immunofluorescent analysis demonstrated percentage complex I and complex IV deficiency higher than would be expected in age matched controls for four out of six desmin patients, one of two MYOT patients and a ZASP patient.

Most strikingly porin is reduced in all patients, in a significantly high percentage of fibres relative to controls, indicating a reduction in mitochondrial mass. This reduction in mitochondrial mass may simply be due to the depletion of mitochondria in the intermyofibrillar space and aggregation in the subsarcolemmal space previously described in myofibrillar myopathy patients [19,22,23]. Analysis of porin fluorescent intensity across a number of normal, low and very low porin fibres demonstrated this is not the case and porin intensity is reduced across the whole fibre. Furthermore, there is no correlation between the presence of desmin and myotilin protein aggregates and the reduction in porin. Throughout the analysis, however, it became apparent that in some fibres where large aggregates are present (Fig. 5c), there is a lack of porin and therefore reduction of mitochondrial mass. In these fibres mitochondria are accumulated in the subsarcolemmal regions or other myofibrillar regions of the fibres, which agrees with previous studies using electron microscopy.

It has been demonstrated that aggregate prone desmin mutations cause a change in Ca^{2+} homeostatic ability, due to lack of appropriate positioning of the mitochondria close to the sarcoplasmic reticulum [29]. Therefore, it may be that aggregate prone mutations in MFM related genes, including

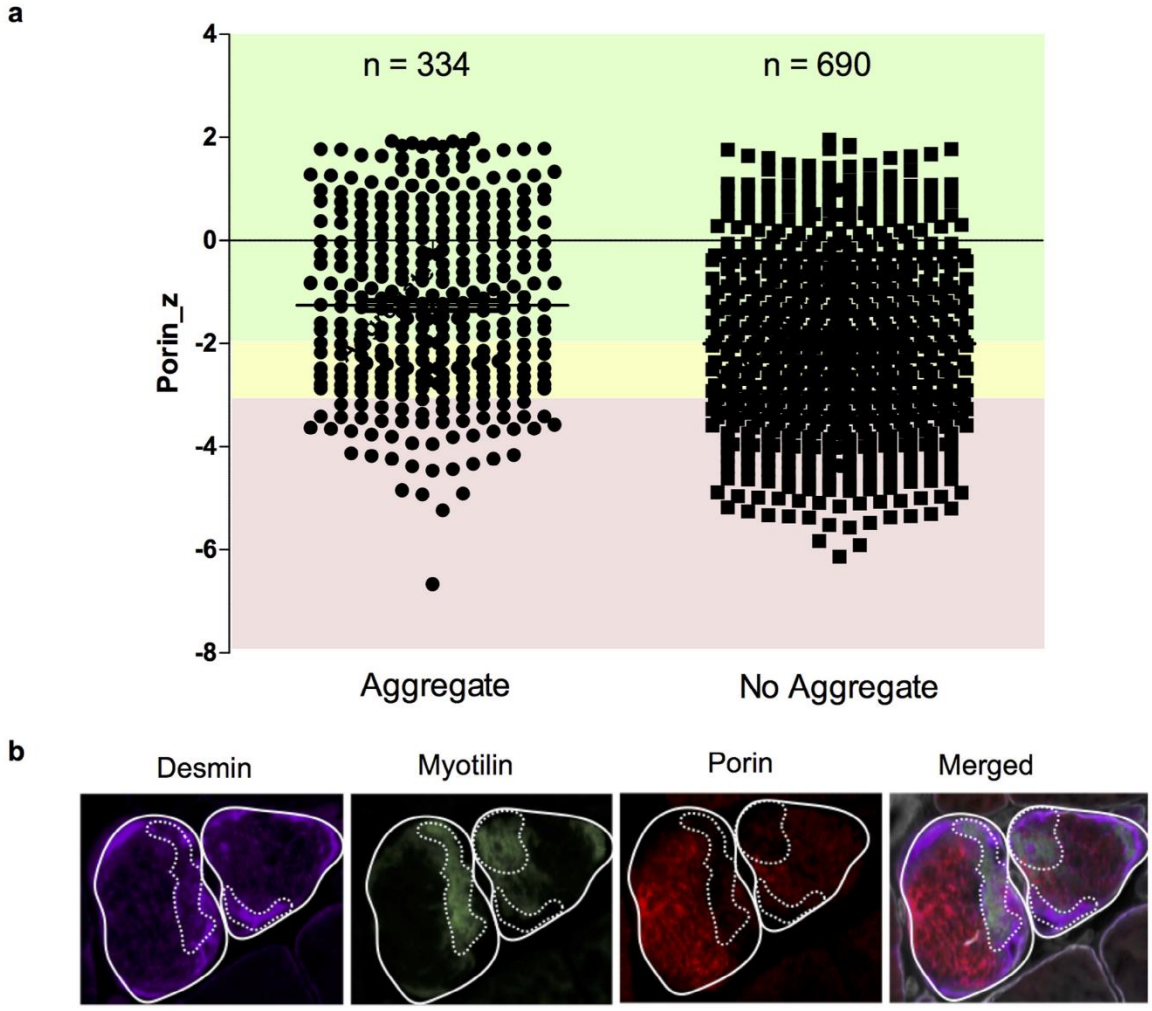

Fig. 5. Immunofluorescent analysis of mitochondrial mass and MFM aggregates. ZASP 1 as a representative example of analysis of desmin and myotilin protein aggregation and porin levels. (a) ZASP 1 fibres classified as very low (pink), low (yellow) or normal (green) porin fibres analysed for presence of aggregates. No clear relationship detected. Very low porin fibres accounted for 22.9% of all fibres with aggregates. (b) Immunofluorescent images from ZASP 1 showing individual channel images (desmin, myotilin, porin) and merged. The staining demonstrates a lack of porin in regions with large aggregates (regions within dashed lines).

MYOT and *ZASP* also cause this same effect and therefore lead to increased cytoplasmic Ca^{2+}. An increase in cytoplasmic Ca^{2+} concentration in neurons has been found to increased fission and therefore fragment the mitochondrial network [30]. Mitochondrial fusion and interaction of the mitochondrial network are necessary for mitochondrial DNA stability and ability to cope with mtDNA mutation [31]. So, this could explain both the formation and accumulation of mtDNA deletions in some MFM patients and also respiratory chain deficiency. However, whether this could be a relevant mechanism in the reduction of mitochondrial mass or whether a shift in mitochondrial biogenesis and mitophagy might be responsible is unclear.

Comparison of complex I and complex IV levels with muscle fibre cross sectional area yielded mixed relationships, making it hard to determine whether complex I and complex IV levels may be linked to muscle fibre atrophy or hypertrophy. On the other hand, comparison of muscle fibre area with porin levels demonstrated a negative relationship in the majority of patients. The relationship demonstrates that hypertrophic muscle fibres with a greater area typically have a lower level of porin than atrophic fibres with a smaller area, which have more variable levels of porin. This might suggest that mitochondrial mass is not involved in the process of muscle atrophy but may indicate either a lack of mitochondrial biogenesis or increased mitophagy during muscle fibre hypertrophy. Alternatively it

could indicate that fibre atrophy is more common in oxidative muscle fibres whilst fibre hypertrophy is more common in glycolytic muscle fibres. It seems most likely that a lack of mitochondrial biogenesis be responsible for the low levels of porin in the hypertrophic muscle fibres; however, further testing would be needed to confirm this.

The low occurrence of mtDNA deletions, lack of relationship between complex I and IV deficiency and muscle fibre cross sectional area and between pathological protein aggregates and mitochondrial dysfunction, found here, are very different to our previous findings in sporadic IBM. In sporadic IBM, approximately 50% of COX-deficient fibres were shown to have one or more large-scale mtDNA rearrangements [32]. Furthermore, inflammatory infiltrates correlated with the extent of the mitochondrial respiratory chain deficiency and muscle fibre atrophy [13]. Therefore, in comparison to IBM where we can conclude mitochondrial dysfunction is pathologically important, and to mitochondrial myopathies where a clear mechanistic link exists between mutations in mtDNA maintenance genes, mtDNA deletions and mitochondrial respiratory chain deficiency, further work needs to be undertaken to determine whether mitochondrial dysfunction is pathologically relevant in MFM. Nevertheless, the decrease in mitochondrial mass and weak relationship between mitochondrial mass and muscle fibre cross sectional area certainly infers that mitochondrial dysfunction may be both mechanistically- and pathologically-relevant.

In conclusion, we have demonstrated clonally-expanded mtDNA deletions in a small number of single cells, similar to previous findings in muscle homogenate DNA from similar patients [20,21], although do note the increased frequency of these mutations in the oldest patient with a ZASP mutation. Given this and previous work we conclude that mtDNA deletions likely arise due to the combined effect of sarcopenia and disease pathogenesis. We also present evidence that myofibrillar myopathies can manifest depletion of mitochondria and respiratory chain deficiency of varying degrees among patients. Previous reports also report a core-like reduction of mitochondria, something we confirm. Such a depletion of mitochondria may be a contributing factor to overall disease pathogenesis and could be related to muscle fibre hypertrophy.

Acknowledgements

AEV is funded by an MRC studentship (MR/K501074/1) as part of the MRC Centre for Neuromuscular disease (MR/K000608/1). This work was supported by The Wellcome Trust Centre for Mitochondrial Research (096919Z/11/Z), the Medical Research Council (UK) Centre for Translational Muscle Disease Research (G0601943), the UK NIHR Biomedical Research Centre in Age and Age Related Diseases award to the Newcastle upon Tyne Hospitals NHS Foundation Trust, The Lily Foundation and the UK NHS Highly Specialised Commissioners, which funds the "Rare Mitochondrial Disorders of Adults and Children" and the "Rare Diseases Advisory Group Service for Neuromuscular Diseases" Diagnostic Services in Newcastle upon Tyne. CLA is the recipient of a National Institute for Health Research (NIHR) doctoral fellowship (NIHRHCS-D12-03-04).

Appendix: Supplementary material

Supplementary data to this article can be found online at doi:10.1016/j.nmd.2016.08.004.

References

[1] Goldfarb LG, Park KY, Cervenakova L, et al. Missense mutations in desmin associated with familial cardiac and skeletal myopathy. Nat Genet 1998;19:402–3.
[2] Vicart P, Caron A, Guicheney P, et al. A missense mutation in the alphaB-crystallin chaperone gene causes a desmin-related myopathy. Nat Genet 1998;20:92–5.
[3] Selcen D, Engel AG. Mutations in myotilin cause myofibrillar myopathy. Neurology 2004;62:1363–71.
[4] Vorgerd M, van der Ven PF, Bruchertseifer V, et al. A mutation in the dimerization domain of filamin c causes a novel type of autosomal dominant myofibrillar myopathy. Am J Hum Genet 2005;77:297–304.
[5] Selcen D, Engel AG. Mutations in ZASP define a novel form of muscular dystrophy in humans. Ann Neurol 2005;57:269–76.
[6] Selcen D, Muntoni F, Burton BK, et al. Mutation in BAG3 causes severe dominant childhood muscular dystrophy. Ann Neurol 2009;65:83–9.
[7] Oldfors A, Larsson NG, Lindberg C, Holme E. Mitochondrial DNA deletions in inclusion body myositis. Brain 1993;116(Pt 2):325–36.
[8] Oldfors A, Moslemi AR, Fyhr IM, Holme E, Larsson NG, Lindberg C. Mitochondrial DNA deletions in muscle fibers in inclusion body myositis. J Neuropathol Exp Neurol 1995;54:581–7.
[9] Santorelli FM, Sciacco M, Tanji K, et al. Multiple mitochondrial DNA deletions in sporadic inclusion body myositis: a study of 56 patients. Ann Neurol 1996;39:789–95.
[10] Moslemi AR, Lindberg C, Oldfors A. Analysis of multiple mitochondrial DNA deletions in inclusion body myositis. Hum Mutat 1997;10:381–6.
[11] Askanas V, Engel WK. Inclusion-body myositis: a myodegenerative conformational disorder associated with Abeta, protein misfolding, and proteasome inhibition. Neurology 2006;66:S39–48.
[12] Oldfors A, Moslemi AR, Jonasson L, Ohlsson M, Kollberg G, Lindberg C. Mitochondrial abnormalities in inclusion-body myositis. Neurology 2006;66:S49–55.
[13] Rygiel KA, Miller J, Grady JP, Rocha MC, Taylor RW, Turnbull DM. Mitochondrial and inflammatory changes in sporadic inclusion body myositis. Neuropathol Appl Neurobiol 2015;41:288–303.
[14] Chariot P, Ruet E, Authier FJ, Labes D, Poron F, Gherardi R. Cytochrome c oxidase deficiencies in the muscle of patients with inflammatory myopathies. Acta Neuropathol 1996;91:530–6.
[15] Askanas V, Engel WK, Nogalska A. Pathogenic considerations in sporadic inclusion-body myositis, a degenerative muscle disease associated with aging and abnormalities of myoproteostasis. J Neuropathol Exp Neurol 2012;71:680–93.
[16] Bender A, Krishnan KJ, Morris CM, et al. High levels of mitochondrial DNA deletions in substantia nigra neurons in aging and Parkinson disease. Nat Genet 2006;38:515–17.
[17] Greaves LC, Yu-Wai-Man P, Blakely EL, et al. Mitochondrial DNA defects and selective extraocular muscle involvement in CPEO. Invest Ophthalmol Vis Sci 2010;51:3340–6.
[18] Grunewald A, Rygiel KA, Hepplewhite PD, Morris CM, Picard M, Turnbull DM. Mitochondrial DNA depletion in respiratory chain-deficient Parkinson disease neurons. Ann Neurol 2016;79:366–78.
[19] Claeys KG, Fardeau M, Schroder R, et al. Electron microscopy in myofibrillar myopathies reveals clues to the mutated gene. Neuromuscul Disord 2008;18:656–66.
[20] Dold T, Reimann J, Zsurka G, Kunz WS, Kornblum C. On mitochondrial function and genome integrity in myofibrillar myopathies. Neuromuscul Disord 2012;22:822.

[21] Joshi PR, Hauburger A, Kley R, et al. Mitochondrial abnormalities in myofibrillar myopathies. Clin Neuropathol 2014;33:134–42.
[22] Henderson M, De Waele L, Hudson J, et al. Recessive desmin-null muscular dystrophy with central nuclei and mitochondrial abnormalities. Acta Neuropathol 2013;125:917–19.
[23] Schroder R, Goudeau B, Simon MC, et al. On noxious desmin: functional effects of a novel heterozygous desmin insertion mutation on the extrasarcomeric desmin cytoskeleton and mitochondria. Hum Mol Genet 2003;12:657–69.
[24] Rocha MC, Grady JP, Grunewald A, et al. A novel immunofluorescent assay to investigate oxidative phosphorylation deficiency in mitochondrial myopathy: understanding mechanisms and improving diagnosis. Sci Rep 2015;5:15037.
[25] Pitceathly RD, Smith C, Fratter C, et al. Adults with RRM2B-related mitochondrial disease have distinct clinical and molecular characteristics. Brain 2012;135:3392–403.
[26] Taylor RW, Barron MJ, Borthwick GM, et al. Mitochondrial DNA mutations in human colonic crypt stem cells. J Clin Invest 2003;112:1351–60.
[27] Rygiel KA, Grady JP, Taylor RW, Tuppen HAL, Turnbull DM. Triplex real-time PCR – an improved method to detect a wide spectrum of mitochondrial DNA deletions in single cells. Sci Rep 2015; 5:9906.
[28] McKenzie D, Bua E, McKiernan S, Cao Z, Aiken JM. Mitochondrial DNA deletion mutations: a causal role in sarcopenia. Eur J Biochem 2002;269:2010–15.
[29] Smolina N, Bruton J, Sjoberg G, Kostareva A, Sejersen T. Aggregate-prone desmin mutations impair mitochondrial calcium uptake in primary myotubes. Cell Calcium 2014;56:269–75.
[30] Han XJ, Lu YF, Li SA, et al. CaM kinase I alpha-induced phosphorylation of Drp1 regulates mitochondrial morphology. J Cell Biol 2008;182: 573–85.
[31] Chen H, Vermulst M, Wang YE, et al. Mitochondrial fusion is required for mtDNA stability in skeletal muscle and tolerance of mtDNA mutations. Cell 2010;141:280–9.
[32] Rygiel KA, Tuppen HA, Grady JP, et al. Complex mitochondrial DNA rearrangements in individual cells from patients with sporadic inclusion body myositis. Nucleic Acids Res 2016;44:5313–29.

Appendix 4 “The spectrum of Mitochondrial Ultrastructral Defects in Mitochondrial Myopathy”. Vincent et al. (2016). Manuscript published in Neuromuscular disorders.

www.nature.com/scientificreports

SCIENTIFIC REPORTS

OPEN

The Spectrum of Mitochondrial Ultrastructural Defects in Mitochondrial Myopathy

Received: 07 April 2016
Accepted: 07 July 2016
Published: 10 August 2016

Amy E. Vincent[1], Yi Shiau Ng[1], Kathryn White[2], Tracey Davey[2], Carmen Mannella[3], Gavin Falkous[1], Catherine Feeney[1], Andrew M. Schaefer[1], Robert McFarland[1], Grainne S. Gorman[1], Robert W. Taylor[1], Doug M. Turnbull[1] & Martin Picard[4,5]

Mitochondrial functions are intrinsically linked to their morphology and membrane ultrastructure. Characterizing abnormal mitochondrial structural features may thus provide insight into the underlying pathogenesis of inherited and acquired mitochondrial diseases. Following a systematic literature review on ultrastructural defects in mitochondrial myopathy, we investigated skeletal muscle biopsies from seven subjects with genetically defined mtDNA mutations. Mitochondrial ultrastructure and morphology were characterized using two complimentary approaches: transmission electron microscopy (TEM) and serial block face scanning EM (SBF-SEM) with 3D reconstruction. Six ultrastructural abnormalities were identified including i) paracrystalline inclusions, ii) linearization of cristae and abnormal angular features, iii) concentric layering of cristae membranes, iv) matrix compartmentalization, v) nanotunelling, and vi) donut-shaped mitochondria. In light of recent molecular advances in mitochondrial biology, these findings reveal novel aspects of mitochondrial ultrastructure and morphology in human tissues with implications for understanding the mechanisms linking mitochondrial dysfunction to disease.

Skeletal muscle fibers contain large numbers of mitochondria classically known for their role in ATP synthesis through oxidative phosphorylation (OXPHOS), which fuels the energy-demanding process of muscle contraction[1,2]. However, research in recent decades has revealed that beyond energy production mitochondria also perform a number of additional functions. They contribute to Ca^{2+} homeostasis[3,4] and redox signalling[5,6], release pro-apoptotic factors regulating cell death[7], synthesize essential macromolecules including heme molecules[8], regulate nuclear gene expression[9,10], and can release immunogenic pro-inflammatory molecules into the cytoplasm and systemic circulation[11]. Beyond expanding our fundamental understanding of mitochondrial biology[12], these advances have challenged the commonly reported view of mitochondria as a cellular powerhouse and thus revealed new cellular mechanisms whereby mitochondrial dysfunction causes clinical disease[13–16].

Of particular interest to neuromuscular disorders is the link between mitochondrial ultrastructure and function[17–19]. Abnormal mitochondrial ultrastructure, particularly the highly conserved inner mitochondrial membrane (IMM) cristae where a number of OXPHOS enzymes reside, is linked to altered mitochondrial function and signalling that may contribute to pathophysiology (e.g., ref. 20). Furthermore, the molecular machinery that regulates mitochondrial morphology and ultrastructural transitions has in part been defined and experimental manipulation of various components in model systems has reinforced causal links between mitochondrial structures and functions[21]. Thus, the determinants of mitochondrial ultrastructure and its functional bearings have implications for understanding the pathophysiology in human mitochondrial disease[22]. However, mitochondrial ultrastructural defects in mitochondrial myopathy have not been thoroughly examined in light of recent molecular advances in mitochondrial biology.

The first description of mitochondrial structures in human skeletal muscle using electron microscopy appeared in the 1960s[23–25]. Abnormal skeletal muscle mitochondrial morphology and ultrastructure has since

[1]Wellcome Trust Centre for Mitochondrial Research, Institute of Neurosciences, Newcastle University, Newcastle upon Tyne, UK. [2]EM Research Services, Newcastle University, Newcastle upon Tyne, UK. [3]Wadsworth Center, New York State Department of Health, Albany, NY, USA. [4]Department of Psychiatry, Division of Behavioral Medicine, Columbia University Medical Center, New York, NY, USA. [5]Department of Neurology and Columbia Translational Neuroscience Initiative, H. Houston Merritt Center, Columbia University Medical Center, New York, NY, USA. Correspondence and requests for materials should be addressed to M.P. (email: mp3484@columbia.edu)

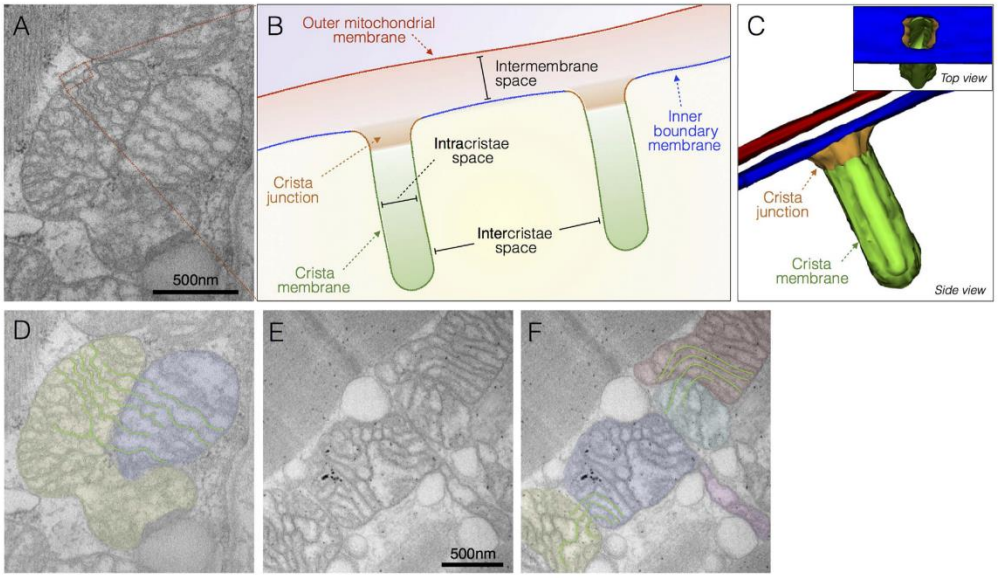

Figure 1. Normal mitochondrial ultrastructure. (**A**) Transmission electron micrograph of normal mitochondria in human skeletal muscle showing typical tubular cristae, and crista junctions. (**B**) Schematic representation of crista junctions, associated structures, and parameters measured in this study. (**C**) Three-dimensional schematic of normal tubular cristae structure. The outer mitochondrial membrane (OMM, red), and three functionally distinct regions of the inner mitochondrial membrane (IMM): inner boundary membrane (blue), crista junction (orange), and crista membrane (green). (**D**) Same image as in A with pseudocolored adjacent but distinct mitochondria and outlined crisate membranes undergoing trans-mitochondrial cristae coordination (see ref. 34 and text for discussion). (**E**) Unprocessed and (**F**) pseudocolored transmission electron micrographs of normal human skeletal muscle illustrating mitochondria with normal shapes and sizes, with electron-dense curvilinear cristae, with some exhibiting trans-mitochondrial cristae coordination.

been reported in the context of aging and several neuromuscular disorders, but most previous studies involved only a limited spectrum of defects and/or poorly-defined genetic disorders (e.g., refs 26, 27 see Table S1). Previous investigations of mitochondrial ultrastructure in clinical samples were also limited to standard (single-plane) transmission electron microscopy (TEM), precluding analysis of complex three-dimensional mitochondrial structures of potential functional significance.

Here, we first conducted a systematic review of the literature to document mitochondrial ultrastructural abnormalities in skeletal muscle of individuals with mitochondrial disease published to date. We then combined two electron microscopy methods: TEM and serial block face scanning electron microscopy (SBF-SEM) to examine muscle biopsies from individuals with molecularly defined mitochondrial DNA (mtDNA) mutations. This in depth re-examination of skeletal muscle mitochondrial ultrastructure in light of recent advances in mitochondrial biology reveals abnormal features not previously reported in human tissues, thus expanding the spectrum of mitochondrial EM pathology in mitochondrial disease.

Results

Systematic review of the literature. We first performed a systematic review of the literature that identified 135 publications reporting EM findings in skeletal muscle biopsies of individuals with mitochondrial disease. These are summarized in Table S1, including information about the muscle biopsied, subject ages, clinical phenotype, and genetic diagnosis where available. Among the most commonly reported features were enlarged mitochondrial size with swelling, paracrystalline inclusions (PCIs), and electron-dense precipitates in the mitochondrial matrix. This systematic review indicated that most articles were case studies, published prior to technological progress enabling genetic diagnosis, or prior to recent discoveries of the molecular aspects of mitochondrial ultrastructure, thus limiting the interpretation of these observations.

Normal mitochondrial ultrastructure. Parameters for normal mitochondrial ultrastructure are established (e.g., refs 28–30) and were confirmed in biopsies from two individuals with normal skeletal muscle mitochondrial histochemistry. Mitochondria are double membrane organelles with the inner (IMM) and outer mitochondrial membranes (OMM) surrounding the mitochondrial matrix and intermembrane space, respectively (Fig. 1). The convoluted IMM bends inwards[31,32] and can be divided into three regions; inner

Patient #	Sex	Age at biopsy	Genetic diagnosis	Heteroplasmy (if applicable)	% deficiency	% RRF	CK (IU/L)	Lactate (mmol/L)	Clinical phenotype	Diagnostic notes
1	F	47	Large-scale single mtDNA deletion	N/A	20	10	226	2.4	CPEO, proximal myopathy	—
2	F	62	Large-scale single mtDNA deletion	34	20	15	122–197	2.1–3.1	CPEO, proximal myopathy	—
3	F	70	Large-scale single mtDNA deletion	22	18	9	318–1238	1.4–2	CPEO, proximal myopathy	Asymmetric myopathy
4	F	22	*m.8344A>G*	97	97	10	145–291	7.4	Axial, proximal myopathy, lactic acidosis	—
5	F	50	*m.8344A>G*	63	22	7	43	1.6	Mild myopathy	Mother of patient 4
6	F	20	*m.8344A>G*	40	COX intermediate	0	267	1.2	Asymptomatic	Sister of patient 4
7	F	69	*m.3243A>G*	21	3	2	180–375	1.3	Diabetes mellitus, deafness, gut dysmotility	—

Table 1. Case information for patients with mitochondrial disease. N/A: non-available; % COX: proportion of myofibers with cytochrome c oxidase deficiency; RRF: ragged red fibers; CK: creatine kinase; CPEO: chronic progressive external opthalmoplegia; HCM: hypertrophic cardiomyopathy; OA: optic atrophy; MERRF: myoclonic epilepsy with ragged red fibers. Deletions position and sizes for patient 1: N/A; patient 2: *m.8482-13460,* 4978 bp; patient 3: *m.8576-12968*, 4392 bp. Normal clinical range for CK: 25–200 IU/L; lactate: <2.2 mmol/L. All biopsies from the *tibialis anterior* muscle.

Patient #	Type I PCI	Type II PCI	Linearization and geometrical features	Concentric cristae	Compartmentalisation	Nanotunneling	Hyperbranching/ hyperfusion	Projections
1	+++	–	–	–	–	–	++	–
2	–	–	–	–	–	+	+	–
3	–	–	–	–	+++	+	–	+++
4	–	+	+++	++	–	–	–	–
5	+	–	–	–	++	–	–	+
6	–	–	–	+	–	–	++	+
7	–	–	–	–	–	+++	+++	+++

Table 2. Summary of mitochondrial ultrastructural abnormalities identified in patient skeletal muscle biopsies. PCI: Paracrystalline inclusion; +: Few; ++: Frequent; +++: Very frequent; –: none.

boundary membrane, the crista junction, and the cristae membrane (Fig. 1B,C)[33]. In some cases where mitochondria are tethered by an inter-mitochondrial junction (IMJ), trans-mitochondrial cristae coordination between distinct organelles can be observed[34] (Fig. 1A,D). Also in normal mitochondria, the matrix is a single continuous space that contains enzymes involved in biochemical transformations and biosynthetic reactions, as well as several copies of the mitochondrial genome. Although frequently depicted as ovoid or bean-shaped, mitochondria oscillate between tubular and spherical morphology determined by highly dynamic fusion and fission processes, which also determine their sizes[21].

Here, we aimed to document deviations from normal mitochondrial ultrastructure in molecularly-defined cases of mitochondrial disease. We examined muscle biopsies from seven patients who harboured a primary mtDNA mutation: single large-scale mtDNA deletion (n = 3), *m.8344A>G tRNA*^{Lys} (n = 3), or *m.3243A>G tRNA*$^{Leu(UUR)}$ (n = 1). Six mitochondrial ultrastructural abnormalities were identified as candidate features linked to known myopathic mechanisms. Demographic, genetic, biochemical, and clinical information for each subject is provided in Table 1. A summary of ultrastructural findings for all subjects is provided in Table 2. Each observed feature is first presented below, and their potential biological and clinical significance subsequently discussed in light of recent advanced in mitochondrial biology.

Paracrystalline inclusions (PCIs). PCIs were observed in a patient harbouring a single, large-scale mtDNA deletion (patient 1) and chronic progressive external opthalmoplegia (CPEO) and in two patients manifesting with myopathy with the *m.8344A>G* mutation (patients 4 and 5). PCIs present as rigid rectangular crystals of approximately 250 nm in length and 50 nm in width. They consist of stacked sheets that either run obliquely (Fig. 2A,D) or parallel (Fig. 2B,C) relative to the length of the paracrystal. Their rigidity is evidenced by their occasional deformation or rupture of membranes (Fig. 2C). As for the other defects discussed below, substantial heterogeneity existed in PCI distribution even within single cells, with some mitochondria exhibiting normal ultrastructure, and other containing PCIs of various types and sizes. Although PCIs were observed in both subsarcolemmal (SS, beneath the plasma membrane and near nuclei) and intermyofibrillar (IMF, between myofibrils) compartments, PCIs were generally more prevalent in SS mitochondria (Fig. 2E,F).

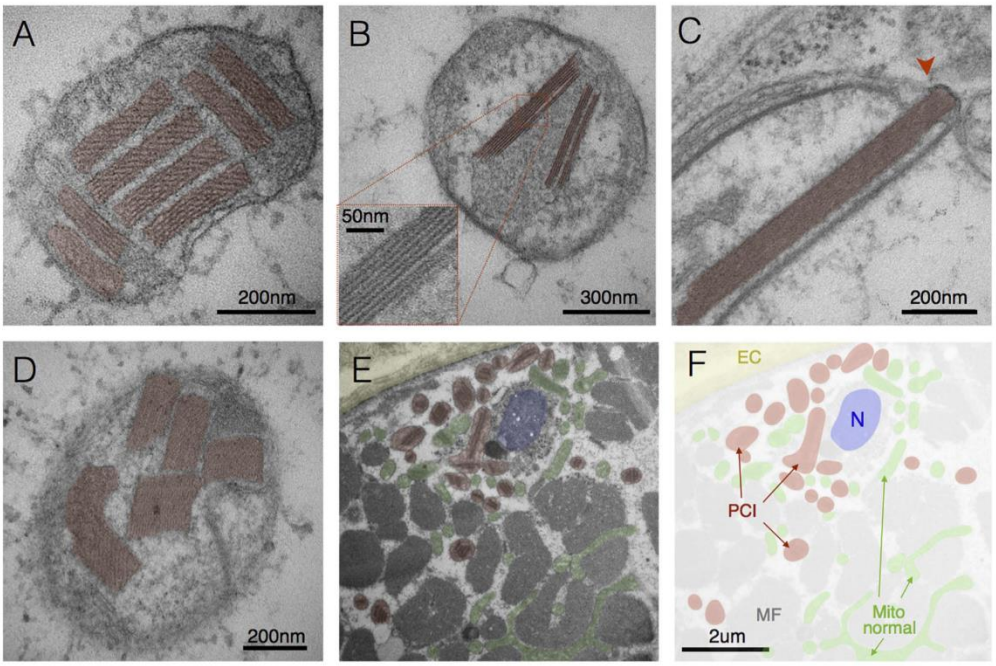

Figure 2. Paracrystalline inclusions (PCIs). (**A**) Type I PCIs occupying most of a mitochondrion's volume in skeletal muscle with a single mtDNA deletion (patient 1). (**B**) Linear Type I PCI in mitochondrion from a case of m.8344A>G (patient 5). (**C**) Disruption of IMM and OMM (arrowhead) by a rigid type II PCI, and (**D**) other examples of type II PCIs from a case of *m.8344A>G* (patient 4). (**E**) Subsarcolemmal region of a muscle fiber showing the extracellular space (EC, yellow) and sarcolemma, profile of a nucleus (N, blue), myofibrils (MF), mitochondria with PCI (red) and normal mitochondria (green), with (**F**) pseudocolored mask (patient 1). Note the greater abundance of PCI-containing mitochondria in the perinuclear SS compartment compared to the intermyofibrillar compartment, consistent with the distinctive requirement for *de novo* protein synthesis for PCI formation.

PCIs are classified in two major types characterized by defined structural pattern, size, and location within the mitochondria[35]. Both type-I PCIs comprised of stacked sheets with discernible structure forming rectangular inclusions in the intracristae space (Fig. 2A,B) and type-II PCIs with electron dense substructure and residing in the intracristae and intermembrane space (Fig. 2D) were observed here. Consistent with previous observations[35], we found type-I and type-II PCIs to be mutually exclusive within individual patients; type-I PCIs were identified in patients 1 and 5, whereas type-II PCIs were observed in patient 4.

Cristae linearization and angular features. In contrast to the normal invaginations of the IMM (Fig. 1), we observed linearization of cristae membranes and abnormal angular (i.e., geometrical) features in patient 4 (Fig. 3). These structures included rigid linear cristae juxtaposed at angles of $124.7 \pm 7.4°$ (Fig. 3A,B), often in association with electron dense inclusions (Fig. 3C,D). Linear cristae segments show enhanced electron density, suggesting the presence of large molecular weight proteins and/or substantial change in membrane lipid composition. Three-dimensional reconstruction from SBF-SEM data demonstrated the organization of linearized electron-dense cristae as continuous sheets encompassing cargo, rather than isolated tubular structures (Fig. 3E,F).

Concentric cristae or "onion-like" mitochondria. In normal mitochondria the inner boundary membrane periodically invaginates into tubular or fenestrated laminar cristae, with the resulting crista junctions forming pores between the intermembrane and intracristae spaces (Fig. 1). Contrary to this pattern, in TEM from patients 4 and 6 with the *m.8344A>G* mutation we observed several mitochondria devoid of normal cristae and crista junctions (CJs), but with abnormal "onion-like" concentric membranes free of fenestration (Fig. 4), also previously referred to as "tubular parallel cristae" or "concentric laminated bodies" (see Table S1). Three-dimensional reconstructions confirmed the tight layering of discontinuous concentric membranes sheets (Fig. 4C,D).

The intermembrane space separating the OMM-IMM was similar between mitochondria with concentric (7.1 ± 1.6 nm) and normal cristae (7.9 ± 1.2 nm, $P = 0.45$). However, the width of the intracristae spaces (Fig. 1B) was reduced by approximately 15% in mitochondria with concentric cristae (7.78 ± 1.0 nm) compared to normal mitochondria (9.20 ± 1.0 nm, $P < 0.05$), indicating a tightening of cristae membranes in

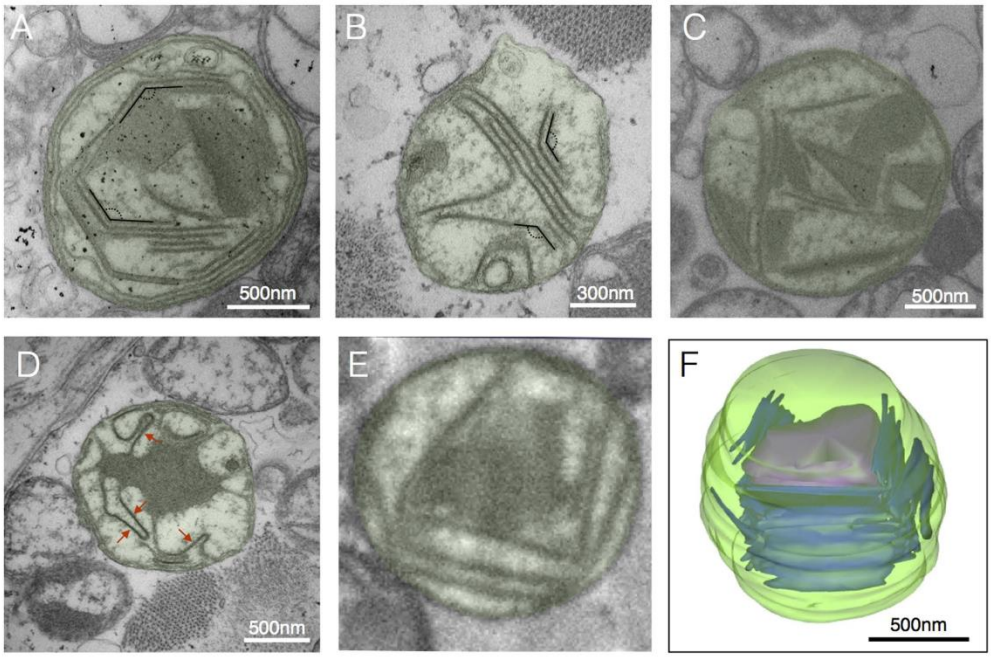

Figure 3. Linearization and geometrical cristae features. (**A,B**) Enlarged mitochondria containing linearized cristae juxtaposed at nearly identical angles, and (**C**) linearized cristae forming various geometrical shapes, and (**D**) linearized IMM segments (arrows) joined by curved segments from a case of *m.8344A>G* (patient 4). **(E)** SBF-SEM image with example of linearized cristae and geometrical shapes and **(F)** three-dimensional reconstruction of mitochondrion in E (patient 4).

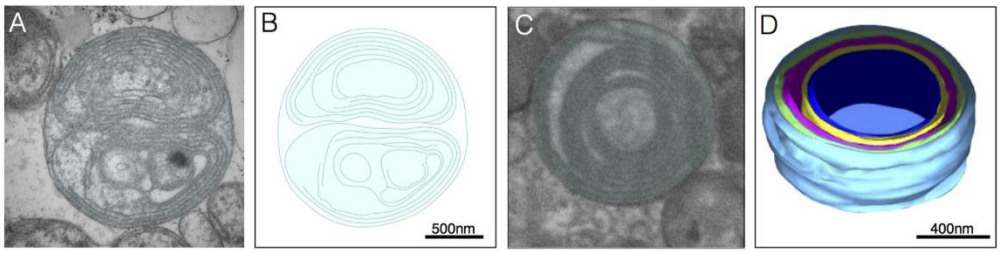

Figure 4. Concentric "onion-shaped" cristae. (**A**) Multiple overlaid layers of double OMM/IMM membranes forming two major compartments in a case of the *m.8344A>G* (patient 4), and (**B**) two-dimensional reconstruction of membrane structures. (**C**) Example of concentric cristae compartments (patient 4) imaged with SBF-SEM, with (**D**) corresponding three-dimensional reconstruction.

onion-like mitochondria. Furthermore, as expected the distance between two adjacent cristae (Fig. 1B, intercristae space) was substantially smaller in mitochondria with concentric cristae (22.5 ± 4.5 nm) than in normal mitochondria (60.2 ± 9.9 nm, $P < 0.001$), indicating denser packaging of membranes in dysfunctional mitochondria.

Compartmentalisation. Normal mitochondria consist of 2 compartments: a single mitochondrial matrix compartment, and a contiguous intermembrane/intracristae space. We observed an increased number of compartments per mitochondrion particularly in patient 3 with a single, large-scale mtDNA deletion and CPEO, and patient 5 with a *m.8344A>G* mutation and mild myopathy. Abnormal compartments were bound by a single or double membrane with distinct molecular or ionic composition evidenced by differences in electron density between each compartment (Fig. 5A,B), dense amorphous material (Fig. 5C), occasionally bounded by electron-dense linearized membranes (Fig. 5D). Notably, compartmentalization appears to involve the complete

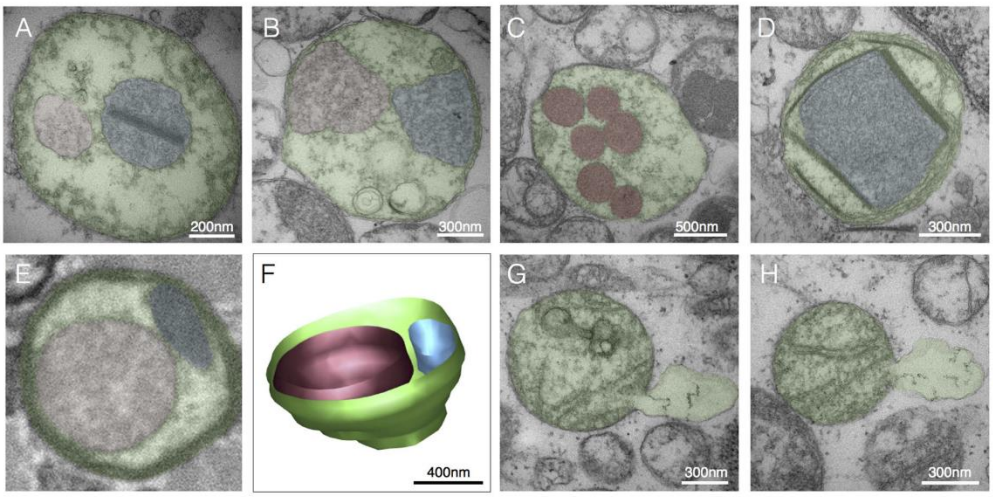

Figure 5. Compartmentalization. (**A**) Example of membrane-bound sub-mitochondrial compartments located centrally and (**B**) peripherally in contact with the inner boundary membrane, from cases of *m.8344A>G* mutation (patient 5) and single mtDNA deletion (patient 3), respectively. (**C**) Electron-dense round compartments distributed in the mitochondrial matrix in a case of single mtDNA deletion (patient 3). (**D**) Compartment bound by linearized electron-dense membranes in a case of *m.8344A>G* (patient 4). (**E**) Cross-sectional image of a mitochondrion with two distinct compartments of different electron density, and (**F**) three-dimensional reconstruction from SBF-SEM. (**G,H**) Examples of OMM protrusion and distension consistent with the release of mitochondrial components in the cytoplasm in a case of *m.8344A>G* mutation (patient 4). Pseudocolored areas indicate the major compartment bound by the OMM (green), and sub-compartments (red and blue).

absence of crista junction and normal cristae structures. Three-dimensional reconstruction of mitochondria exhibiting apparent compartmentalization in cross-section confirmed the complete spatial isolation of individual compartments without connection to the outer boundary membrane (Fig. 5E,F). Localized distension of the OMM with apparent release of mitochondrial matrix content into the cytoplasm was also observed (Fig. 4G,H).

Nanotunneling. We observed mitochondrial nanotunnels (Fig. 6A,B) in three of the seven patients (patients 2, 3 and 7). The average diameter of nanotunnels was 62.3 ± 10.7 nm (Fig. 6C) and was similar between patients. Three-dimensional reconstructions further demonstrated that nanotunnels consist of thin tubular projections extending from one or more mitochondria. The nanotunnel length averaged 623 nm, ranging from 206 nm to 2.3 μm (Fig. 6D).

Hyperbranching and donut mitochondria. Extensively branched mitochondria were particularly abundant in a case of *m.3243A>G* with 21% heteroplasmy (patient 7) (Fig. 6E,F). Interestingly, donut-shaped mitochondria arising from self-fusion of a mitochondrion were also observed in cases single mtDNA deletion at 34% heteroplasmy (patient 2) and *m.8344A>G* at 40% heteroplasmy (patient 6) (Fig. 6G,H). Three-dimensional reconstruction confirmed the unique toroid nature of donut mitochondria (Fig. 6H).

Discussion

Mitochondrial biology is replete with examples where mitochondrial ultrastructure is mechanistically linked to functions[17,18], and vice versa. In an attempt to understand the pathogenesis of mitochondrial disease, early electron microscopy investigations identified common ultrastructural abnormalities such as swelling and PCIs. However, most observations were mainly made prior to the identification of molecular determinants of mitochondrial structure and function (Table S1), thus limiting the spectrum of conceivable observations and the interpretation of their mechanistic significance. Improved diagnosis enable the identification of pathogenic mutations in an unprecedentedly large proportion of patients[36]. Here, building from recent advances in mitochondrial biology imaging technology, and genetic diagnosis, we examined the spectrum of mitochondrial ultrastructural features in a clinically characterized group of patients with genetically defined mitochondrial disease.

The literature to date characterizes what constitutes normal mitochondrial morphology in human and mouse skeletal muscle, including the organization of the IMM into cristae (Fig. 1). Using our electron microscopy approaches, we documented comparable normal mitochondrial morphology in two individuals with normal skeletal muscle mitochondrial function[34], confirming that our biopsy and imaging methods preserved normal mitochondrial ultrastructure. Normal ultrastructure notably included the physical coordination of cristae between pairs of distinct mitochondria linked by an inter-mitochondrial junction (Fig. 1A,D), a phenomenon which has been shown to be resistant to genetic disruption of respiratory chain function in mice, independent of mitofusins,

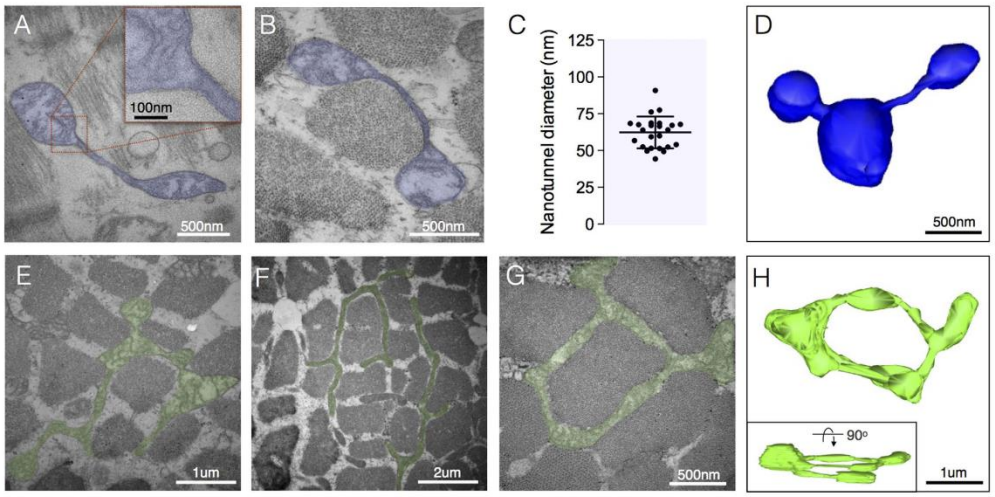

Figure 6. Nanotunelling and hyperbranching. (**A,B**) Examples of mitochondrial nanotunnels composed of both OMM and IMM, but devoid of cristae in a case of *m.3243A>G* (patient 7). (**C**) Variation in nanotunnel diameter, with each datapoint representing the average of the smallest and largest diameters measured for individual nanotunnels across all subjects (n = 26). (**D**) Three-dimensional reconstruction of three mitochondria connected via nanotunnels from a case of *m.3242A>G* (patient 7). (**E,F**) Examples of highly branched mitochondria (hyperfusion) from cases of *m.3243A>G* (patient 7) (**G**) Donut-shaped mitochondrion denoting self-fusion from a case of single mtDNA deletion (patient 2). (**H**) Three-dimensional reconstruction of a donut-shaped mitochondrion from a case of *m.8344A>G* (patient 6).

evolutionary conserved from mollusk to mammals, and inducible to some extent by the physical rapprochement of energized mitochondria *in vitro*[34]. In general, from a methodological perspective, it must be noted that consistent with the mosaic distribution of affected and non-affected cells in mitochondrial myopathy, substantial heterogeneity and mosaicism in mitochondrial ultrastructure exists between individuals, between muscle fibers, and even within single cells (Fig. S1).

Overall, the electron microscopic survey described here expands the spectrum of mitochondrial ultrastructural abnormalities known to exist in human. Some previously reported features are non-specific pathological hallmarks of mitochondrial myopathy such as PCIs, enlarged mitochondria, concentric "onion-like" cristae. Other features not previously reported include linearization and angular arrangement of cristae, localized membrane distension, nanotunnels, and donut-shaped mitochondria. These features are discussed below in context of recent findings in mitochondrial biology, with an emphasis on their potential significance to mitochondrial function and pathology.

Paracrystalline inclusions. Although sample size was small, type-I (n = 2) and type-II (n = 1) PCIs were found to be mutually exclusive similar to previous reports[35]. The cause of this mutual exclusivity is, to date, unknown. Notably, two related patients with the *m.8344A>G* mutation (mother and daughter, patients 4 and 5) manifested different PCIs, indicating that factors other than the mtDNA mutation and nuclear background likely interact to determine disease phenotype. PCI analysis in larger cohorts of patients would be required to understand the specific conditions leading to different types of PCIs. However, it is worth noting that in our study occurrence of type II PCIs correlated clinically with most severe cytochrome c oxidase deficiency and lactic acidosis, and structurally with highest occurrence of concentric and linearized inner membranes.

We further note that PCIs appear more commonly in subsarcolemmal mitochondria. PCIs are composed of crystallized mitochondrial creatine kinase (CK)[37], likely as a result of a compensatory upregulation of CK due to a deficiency of creatine phosphate shuttle activity. Reduced shuttle activity likely results from reduced ATP synthesis secondary to OXPHOS defects, leading to CK protein accumulation and PCI formation. Thus, contrary to most known pathognomonic processes triggered by loss-of-function mutations (i.e., absence of a protein or functional mutation), PCI formation involves the accumulation of a functional protein. Protein accumulation requires *de novo* synthesis, which depends upon upregulation of the CK gene in the nuclear compartment, and local translation of the gene product. This molecular requirement for PCI could explain the preferential abundance in the SS mitochondria that are inherently closer to myonuclei than IMF mitochondria.

Linearized cristae membranes. Linearized cristae membranes with altered electron density and a rigid angular appearance were observed in a single patient (patient 4). These were commonly found in association with PCIs and changes to both membrane and matrix electron density. Altered protein composition or supramolecular

assembly of protein complexes, particularly of the ATP synthase, which is heavily involved in determining IMM folding[32,38], influence membrane curvature. Changes in the fluidity or rigidity of the IMM could also be caused by altered cardiolipin content in the IMM[39–41]. Interestingly, we noted linearized cristae membranes juxtaposed at an angle of approximately 120°. Domènech *et al.* also reported hexagonal structures with membranes exhibiting 120° angles in cardiolipin-containing phospholipid bilayer[42], suggesting that cristae linearization and abnormal angular features in mitochondrial myopathy could result from altered membrane lipid composition. The sole case with prominent linearized inner membranes in our study (patient 4) was concurrent with the only example of type II PCIs.

Concentric cristae. Concentric cristae were limited to two related patients (patients 4 and 6) with the *m.8344A>G* mutation. Nevertheless, the existence of onion-like IMM organisation in human tissue extends previous observations in cultured human (HeLa) cells and yeast where down-regulation or knock down of mitochondrial contact site and cristae organising system (MICOS) components causes membrane stacking and/or onion-like concentric layering[33,43–45]. Abnormal dimerization of the ATP-synthase in yeast also promotes concentric cristae formation[46].

Measurement of the intra- and inter- cristae space in normal mitochondria and those with concentric cristae demonstrated a significant reduction in size in concentric cristae indicating tighter packing of cristae membranes. The widths of intermembrane and intracristae spaces (Fig. 1) are regulated by specific proteins and are believed to be of functional relevance[19,47]. We did not observe cristae junctions in mitochondria with concentric cristae. Based on studies in model systems, potential causes of crista junction dysfunction and the resulting layering pattern include defects of nuclear-encoded MICOS components, or other crista junction or IMS proteins interacting with both OMM and IMM.

Compartmentalization. An increase in the number of compartments observed within mitochondria was noted in two patients (patients 3 and 5). Sub-mitochondrial compartmentalization could be the product of partial or hemi-fusion subsequent to OMM fusion in the absence of IMM fusion, thus resulting in a single enlarged mitochondrion with multiple matrix spaces from the original smaller precursor mitochondria[48]. Consistent with this hypothesis, suppression of the IMM pro-fusion Opa1 homologue eat-3 in *Caenorhabditis elegans* causes a similar compartmentalisation phenotype[49].

We observed localized distension of the OMM with apparent release of mitochondrial matrix content into the cytoplasm (Fig. 4G,H). This occurred without gross alteration of mitochondrial ultrastructure, distinguishing this process from permeability transition-induced swelling. Interestingly, recent evidence indicates that mitochondrial proteins (e.g. prohibitin, Hsp60) and mtDNA (in oxidized form) are released into the cytoplasm and systemic circulation[11]. Such ectopic mitochondrial material acts as damage associated mitochondrial proteins (DAMPs) or "alarmins", triggering activation of inflammatory responses both intracellularly and systemically[11]. The factors determining mitochondrial compartmentalization and local release of mitochondrial material, and their relevance to myopathy, remain to be established.

Nanotunneling. To our knowledge, this is the first report of nanotunnels in human skeletal muscle. The existence of "nanotunnels" was initially demonstrated in rat cardiomyocytes[50]. Consistent with earlier reports where similar structures were observed[51,52], mitochondrial nanotunnels are stretches of both IMM and OMM devoid of cristae (Fig. 5A, inset), measure 50–200 nm in diameter[50], able to transport large soluble proteins such as GFP between non-adjacent mitochondria[50]. Such communication system may be particularly relevant for physically constrained mitochondria in striated muscle, which cannot easily move and undergo fusion[50].

In vitro, nanotunnels appear to grow between mitochondria in a kinesin KIF5B-dependent mechanism within seconds[53]. However, upon fusion with a distant mitochondrion newly established nanotunnels may increase in diameter, accommodate respiratory complexes via diffusion through the IMM, and thus contribute to the expansion of mitochondrial tubules and of the mitochondrial network[53]. Alternatively, nanotunnels could result from failed or stalled fission, a possibility supported by the fact that nanotunnels have a diameter at the lower limit of the constrictions (60–150 nm) induced by the dynamin Dnm1 during mitochondrial fission in yeast[54]. Failed fission could contribute to accelerate the spread of molecular defects across the mitochondrial network[55].

Understanding the physiological and pathological conditions that promote or inhibit mitochondrial nanotunelling could offer new insights into the pathogenesis of mitochondriopathies, mutation load threshold, and progression of mitochondrial myopathy. It is worth noting that in this study nanotunnels were observed in specimens from three of seven patients, exclusively in those lacking PCIs. Nanotunnels were also observed in normal muscle without mitochondrial disease (n = 2), but not in those with the highest heteroplasmy levels and the most severe mitochondrial dysfunction. Therefore, nanotunnels may be indicative of normal or moderately impaired mitochondrial respiratory chain function.

Hyperbranching and donut mitochondria. Excessive mitochondrial fusion or absence of fission leads to mitochondrial elongation and hyperbranching, possibly representing a compensatory acute response to mitochondrial stress[56]. Dose-response increase in the *m.3243A>G* mutation load *in vitro* also leads to progressive mitochondrial elongation[9], and has been observed in aged mouse sarcopenic muscle[57]. Thus, hyperbranching and donut mitochondria may reflect cellular stress[58] in mitochondrial myopathy patients with intermediate states of dysfunction, such as patient 7 (Fig. 6E,F).

Further to this we observe donut mitochondria in a further two patients (patients 2 and 6). The donut shape results from self-fusion or "splitting" of mitochondria and are induced experimentally by respiratory chain inhibition and oxidative stress *in vitro*[59], and have been reported in brain presynaptic boutons of aged cognitively

impaired non-human primates[60]. The presence of these features in human skeletal muscle may be reflective of the degree or nature of mitochondrial dysfunction, although more work is required to establish their physiological significance.

Some limitations of the present study should be noted. The aim of this investigation was to characterize the spectrum of mitochondrial ultrastructural features in human skeletal muscle. Accordingly, our approach consisted in capturing a large number of images depicting specific mitochondrial ultrastructural abnormalities, targeting myofibers with clear signs of pathology. While this sampling approach enabled the identification of multiple examples for known and novel ultrastructural defects, it is not compatible with a systematic unbiased quantification of the prevalence or frequency of the ultrastructural defects. Furthermore, muscle biopsies were collected from a convenience sample of consecutive individuals attending the diagnostic clinic, yielding a relatively small group of patients with different genetic defects. While this precludes conclusions regarding disease specificity, it has allowed to document and characterize a larger spectrum of ultrastructural abnormalities, and conclude that some structural defects are in fact not unique to specific mutations.

Conclusion

Collectively, these results advance our understanding of mitochondrial dysfunction in several ways. First, in seeking to understand the relative contributions of sub-cellular compartmentalization in disease pathogenesis and progression, the recognition that certain features (i.e. PCIs) require the accumulation rather than the depletion of proteins may offer new insights into both the kinetics and nature of the underlying bioenergetics defects. Second, some of the reported features were previously observed *in vitro* or in model organisms following genetic disruption of specific mitochondrial proteins. For example, alteration of MICOS components disrupt CJs in various model systems (e.g., ref. 61), and could contribute to some observed features such as compartmentalization that completely lack CJs, and concentric cristae formation where CJs are rare. This opens the door to investigating the pathophysiological signficance of MICOS components in primary mtDNA diseases. Third, the origin of transcriptional dysregulation and pro-inflammatory gene activation in certain musculoskeletal disorders remains unclear. Given that mitochondria can transcriptionally regulate a large number of nuclear genes[9,10] and trigger intracellular inflammatory processes[11], localized membrane distension (Fig. 5G,H) or PCI-induced membrane rupture (Fig. 2C) could contribute to the cytoplasmic release of mitochondrial material that trigger these "non-energetic" pathogenic features. Finally, nanotunnel formation, donut-shaped mitochondria, and hyperbranching could represent evolutionary conserved compensatory responses to "mild" mitochondrial stress[56,62].

Systematic assessment of mitochondrial morphology using quantitative EM methodologies sensitive mitochondrial size, shape, and branching complexity (e.g., refs 29,57), and particularly three-dimensional reconstruction methods such as serial block face (SBF-SEM) and focused-ion beam (FIB-SEM), will be required to ascertain the role of structural remodelling in certain mitochondrial and other musculoskeletal diseases. In addition, the functional significance of these changes will also need to be established through targeted molecular studies coupled to clinical investigations of mitochondrial ultrastructure. Expanding the spectrum of mitochondrial ultrastructure in human tissues should help us identify different mechanisms by which mitochondrial dysfunction contributes to disease.

Material and Methods

Literature review. Scopus, Embase and Medline were searched using the following search terms: "electron microscop* AND muscle AND human AND mitochondria*". Filtering these for "full text" and "human" yielded 1549 results from Scopus, 1670 results from Embase and 922 results from Medline. Duplicates were removed, and search results screened on the basis of the following criteria: full text availability, English language, human, skeletal muscle, mitochondrial disease, any publication date up to the end of 2015. All included studies reported on patients with either a clinical or genetic diagnosis of mitochondrial disease; publications including cases where a diagnosis could not be reached have not been included. This resulted in 131 primary articles and four reviews (total n = 135). All articles were screened for the specific mitochondrial pathology reported, and for the diagnostic methodology used, which included restriction site mutation (RSM) assay, southern blotting, PCR, Sanger sequencing, restriction fragment length polymorphism (RFLP), solid phase mini sequencing, sequencing (general), next generation sequencing, or method not specified. Table S1 reports in chronological order the biopsied muscle, age of subjects, clinical features, genetic diagnosis, and a summary of mitochondrial ultrastructural and morphological feature(s).

Patient cohort. This study was approved by the Newcastle and North Tyneside Local Research Ethics Committees (reference 2002/205) and prior informed consent was obtained from each participant. All experiments were carried out in accordance with the approved guidelines. Samples were collected in our diagnostic service over a period of approximately ten weeks where 11 consecutive cases underwent a muscle biopsy, seven of which were diagnosed with a primary mtDNA defect and reported upon here. For cases of single, large scale mtDNA deletions, sequencing was performed in two of the three cases to determine the breakpoint and size. Muscle biopsies were performed using the conchotome method under local anaesthesia (2% lidocaine) from tibialis anterior muscle of all diagnosed patients. Biopsy specimens were subsequently dissected and processed for electron microscopy. Demographic information and clinical data for each patient is summarized in Table 1.

Transmission electron microscopy (TEM). Muscle fiber bundles were teased from a fresh biopsy and fixed overnight in 2% glutaradehyde in 0.1 M Sorenson's buffer (pH 7.4) at 4 °C as described previously[29]. Briefly, fibers were post fixed in 1% osmium tetroxide for 1 hour. Samples are dehydrated in a graded series of acetone (25%, 50%, 75%, 100%) before being embedded in epoxy resin (TAAB medium grade) and polymerised at 60 °C. Sections are cut on a Leica EM UC7 ultramicrotome, firstly semi-thin sections (0.5 um) are stained with toluidine blue for LM to identify the area of interest/confirm orientation of tissue. Ultrathin sections (70 nm) were then

transferred to copper grids, and stained with uranyl acetate and lead citrate, and examined on a Phillips CM 100 Compustage (FEI) transmission electron microscope and digital micrographs were captured with an AMT CCD camera (Deben). On average seven individual fibers were thoroughly examined for each patient, for a total of 750 analysed images. Mitochondrial respiratory chain deficiency exists as a mosaic in skeletal muscle and cannot be conclusively ascertained for individual muscle fibers in ultrathin sections. We therefore focused our survey on myofibers with the highest mitochondrial content and/or showing signs of pathology at low magnification, such as vacuolization, mitochondrial hyperproliferation, or myofibrillar disarray. Regions of interest were scanned at 5,800x, images were captured at magnifications between 7,900x and 96,000x. Muscle fibers were examined in longitudinal and transverse orientations using methodology reported previously[29].

Serial block face scanning electron microscopy (SBF-SEM). Tissue was fixed in 2% glutaraldehyde in 0.1 M cacodylate buffer (pH 7.4), and processed with heavy metal impregnation as described previously[63]. Briefly, tissue was immersed in 3% potassium ferrocyanide and 2% osmium tetroxide, followed by 0.1% thiocarbohydrazide, then 2% osmium tetroxide and finally left overnight in 1% uranyl acetate (with water washes between each step). The next day the samples were immersed in 0.6% lead aspartate solution and then dehydrated in graded acetone and embedded in epoxy tab 812 hard resin. After polymerisation blocks were trimmed and sectioned for standard TEM to identify areas of interest for SBF-SEM imaging. Fibers with high mitochondrial content were selected from cases with specific mitochondrial pathology and a series of serial images interspersed by 30–50 nm were captured at a magnification of 8,000–12,000x on a Zeiss Sigma scanning electron microscope with Gatan 3view system and digital micrograph software.

Analysis and statistics. Image stacks were exported, processed, and used for reconstruction of abnormal features with IMOD 3dmod (IMOD 4.7, Boulder Laboratory for 3-D Electron Microscopy of Cells). Abnormal ultrastructure features detected in patients 4, 6 and 7 were reconstructed in 3dmod. Ultrastructural features were manually traced in consecutive image series and meshed. Surface transparency and smoothness were adjusted to facilitate visualization of features of interest in final reconstructed models. Each ultrastructural component was analysed separately to accurately quantify 3-dimensional features. Mitochondrial were pseudocolored (Keynote 6.6.1) to facilitate visualization of distinct organelles and structrures of interest.

Quantitative measurement of two-dimensional features (nanotunnel diameter and length, intracristae and intercristae distance, and intermembrane space) were performed in Image J (NIH, version 1.47v). For nanotunnel width measurements, the narrowest and widest regions of each nanotunnel were averaged, yielding a mean diameter for each nanotunnel ($n = 26$). Segments used for analysis were defined on the basis of lacking cristae and being of constant width. Data are reported as means $\pm$ S.D. Two-tailed T-test assuming unequal variance was used to evaluate differences in cristae measurements between normal and abnormal mitochondria, with the level of significance set at 0.05.

References

1. Chance, B. & Williams, G. R. The respiratory chain and oxidative phosphorylation. *Advances in enzymology and related subjects of biochemistry* **17,** 65–134 (1956).
2. Mitchell, P. Chemiosmotic coupling in oxidative and photosynthetic phosphorylation. *Biological reviews of the Cambridge Philosophical Society* **41,** 445–502 (1966).
3. Eisner, V., Lenaers, G. & Hajnóczky, G. Mitochondrial fusion is frequent in skeletal muscle and supports excitation–contraction coupling. *The Journal of cell biology* **205,** 179–195 (2014).
4. De Stefani, D., Raffaello, A., Teardo, E., Szabo, I. & Rizzuto, R. A forty-kilodalton protein of the inner membrane is the mitochondrial calcium uniporter. *Nature* **476,** 336–340 (2011).
5. Finkel, T. Signal transduction by reactive oxygen species. *The Journal of cell biology* **194,** 7–15 (2011).
6. Sena, L. A. & Chandel, N. S. Physiological roles of mitochondrial reactive oxygen species. *Molecular cell* **48,** 158–167 (2012).
7. Frezza, C. *et al.* OPA1 controls apoptotic cristae remodeling independently from mitochondrial fusion. *Cell* **126,** 177–189 (2006).
8. Lill, R. *et al.* The role of mitochondria in cellular iron-sulfur protein biogenesis and iron metabolism. *Biochimica et Biophysica Acta-Molecular Cell Research* **1823,** 1491–1508 (2012).
9. Picard, M. *et al.* Progressive increase in mtDNA 3243A >G heteroplasmy causes abrupt transcriptional reprogramming. *Proceedings of the National Academy of Sciences of the United States of America* **111,** E4033–E4042 (2014).
10. Chae, S. *et al.* A systems approach for decoding mitochondrial retrograde signaling pathways. *Science signaling* **6,** rs4 (2013).
11. Zhang, Q. *et al.* Circulating mitochondrial DAMPs cause inflammatory responses to injury. *Nature* **464,** 104–107 (2010).
12. Nunnari, J. & Suomalainen, A. Mitochondria: in sickness and in health. *Cell* **148,** 1145–1159 (2012).
13. Logan, C. V. *et al.* Loss-of-function mutations in MICU1 cause a brain and muscle disorder linked to primary alterations in mitochondrial calcium signaling. *Nature genetics* **46,** 188–193 (2014).
14. Shaw, G. C. *et al.* Mitoferrin is essential for erythroid iron assimilation. *Nature* **440,** 96–100 (2006).
15. Tesson, C. *et al.* Alteration of Fatty-Acid-Metabolizing Enzymes Affects Mitochondrial Form and Function in Hereditary Spastic Paraplegia. *American journal of human genetics* **91,** 1051–1064 (2012).
16. Meimaridou, E. *et al.* Mutations in NNT encoding nicotinamide nucleotide transhydrogenase cause familial glucocorticoid deficiency. *Nature genetics* **44,** 740–742 (2012).
17. Mannella, C. A. The relevance of mitochondrial membrane topology to mitochondrial function. *Biochimica et Biophysica Acta (BBA)-Molecular Basis of Disease* **1762,** 140–147 (2006).
18. Pernas, L. & Scorrano, L. Mito-Morphosis: Mitochondrial Fusion, Fission, and Cristae Remodeling as Key Mediators of Cellular Function. *Annual Review of Physiology* **78,** null (2016).
19. Mannella, C. A., Lederer, W. J. & Jafri, M. S. The connection between inner membrane topology and mitochondrial function. *Journal of molecular and cellular cardiology* **62,** 51–57 (2013).
20. Cogliati, S. *et al.* Mitochondrial Cristae Shape Determines Respiratory Chain Supercomplexes Assembly and Respiratory Efficiency. *Cell* **155,** 160–171 (2013).
21. Friedman, J. R. & Nunnari, J. Mitochondrial form and function. *Nature* **505,** 335–343 (2014).
22. Cogliati, S., Enriquez, J. A. & Scorrano, L. Mitochondrial Cristae: Where Beauty Meets Functionality. *Trends in Biochemical Sciences* (2016).

23. van Wijngaarden, G. K., Bethlem, J., Meijer, A. E., Hulsmann, W. C. & Feltkamp, C. A. Skeletal muscle disease with abnormal mitochondria. *Brain: a journal of neurology* **90,** 577–592 (1967).
24. Price, H. M., Gordon, G. R., Munsat, T. L. & Pearson, C. M. Myopathy with atypical mitochondria in type I skeletal muscle fibers. A histochemical and ultrastructural study. *Journal of neuropathology and experimental neurology* **26,** 475–497 (1967).
25. Hulsmann, W. C., Bethlem, J., Meijer, A. E., Fleury, P. & Schellens, J. P. Myopathy with abnormal structure and function of muscle mitochondria. *Journal of neurology, neurosurgery, and psychiatry* **30,** 519–525 (1967).
26. Mitsumoto, H., Aprille, J. R., Wray, S. H., Nemni, R. & Bradley, W. G. Chronic progressive external ophthalmoplegia (CPEO): Clinical, morphologic, and biochemical studies. *Neurology* **33,** 452 (1983).
27. Melberg, A., Lundberg, P. O., Henriksson, K. G., Olsson, Y. & Stalberg, E. Muscle-nerve involvement in autosomal dominant progressive external ophthalmoplegia with hypogonadism. *Muscle & nerve* **19,** 751–757 (1996).
28. Larsen, S. *et al.* Biomarkers of mitochondrial content in skeletal muscle of healthy young human subjects. *The Journal of physiology* **590,** 3349–3360 (2012).
29. Picard, M., White, K. & Turnbull, D. M. Mitochondrial morphology, topology, and membrane interactions in skeletal muscle: a quantitative three-dimensional electron microscopy study. *Journal of applied physiology (Bethesda, Md.: 1985)* **114,** 161–171 (2013).
30. Payne, C. M., Stern, L. Z., Curless, R. G. & Hannapel, L. K. Ultrastructural fiber typing in normal and diseased human muscle. *Journal of the neurological sciences* **25,** 99–108 (1975).
31. Dudkina, N. V., Heinemeyer, J., Keegstra, W., Boekema, E. J. & Braun, H.-P. Structure of dimeric ATP synthase from mitochondria: An angular association of monomers induces the strong curvature of the inner membrane. *FEBS Letters* **579,** 5769–5772 (2005).
32. Strauss, M., Hofhaus, G., Schroder, R. R. & Kuhlbrandt, W. Dimer ribbons of ATP synthase shape the inner mitochondrial membrane. *Embo j* **27,** 1154–1160 (2008).
33. Pfanner, N. *et al.* Uniform nomenclature for the mitochondrial contact site and cristae organizing system. *The Journal of cell biology* **204,** 1083–1086 (2014).
34. Picard, M. *et al.* Trans-mitochondrial coordination of cristae at regulated membrane junctions. *Nat Commun* **6,** 6259 (2015).
35. Hammersen, F., Gidlöf, A., Larsson, J. & Lewis, D. The occurrence of paracrystalline mitochondrial inclusions in normal human skeletal muscle. *Acta neuropathologica* **49,** 35–41 (1980).
36. Taylor, R. W. *et al.* Use of whole-exome sequencing to determine the genetic basis of multiple mitochondrial respiratory chain complex deficiencies. *JAMA* **312,** 68–77 (2014).
37. Eppenberger-Eberhardt, M. *et al.* Adult rat cardiomyocytes cultured in creatine-deficient medium display large mitochondria with paracrystalline inclusions, enriched for creatine kinase. *The Journal of cell biology* **113,** 289–302 (1991).
38. Daum, B., Walter, A., Horst, A., Osiewacz, H. D. & Kühlbrandt, W. Age-dependent dissociation of ATP synthase dimers and loss of inner-membrane cristae in mitochondria. *Proceedings of the National Academy of Sciences* **110,** 15301–15306 (2013).
39. Phan, Minh D. & Shin, K. Effects of Cardiolipin on Membrane Morphology: A Langmuir Monolayer Study. *Biophysical Journal* **108,** 1977–1986 (2015).
40. Weber, T. A. *et al.* APOOL is a cardiolipin-binding constituent of the Mitofilin/MINOS protein complex determining cristae morphology in mammalian mitochondria. *PloS one* **8,** e63683 (2013).
41. Jiang, F. *et al.* Absence of cardiolipin in the crd1 null mutant results in decreased mitochondrial membrane potential and reduced mitochondrial function. *Journal of Biological Chemistry* **275,** 22387–22394 (2000).
42. Domènech, Ò., Morros, A., Cabañas, M. E., Teresa Montero, M. & Hernández-Borrell, J. Supported planar bilayers from hexagonal phases. *Biochimica et Biophysica Acta (BBA)-Biomembranes* **1768,** 100–106 (2007).
43. John, G. B. *et al.* The Mitochondrial Inner Membrane Protein Mitofilin Controls Cristae Morphology. *Molecular biology of the cell* **16,** 1543–1554 (2005).
44. Rabl, R. *et al.* Formation of cristae and crista junctions in mitochondria depends on antagonism between Fcj1 and Su e/g. *The Journal of cell biology* **185,** 1047–1063 (2009).
45. van der Laan, M., Bohnert, M., Wiedemann, N. & Pfanner, N. Role of MINOS in mitochondrial membrane architecture and biogenesis. *Trends in cell biology* **22,** 185–192 (2012).
46. Paumard, P. *et al.* The ATP synthase is involved in generating mitochondrial cristae morphology. *The EMBO Journal* **21,** 221–230 (2002).
47. Varanita, T. *et al.* The Opa1-Dependent Mitochondrial Cristae Remodeling Pathway Controls Atrophic, Apoptotic, and Ischemic Tissue Damage. *Cell Metabolism* **21,** 834–844 (2015).
48. Zick, M., Rabl, R. & Reichert, A. S. Cristae formation—linking ultrastructure and function of mitochondria. *Biochimica et Biophysica Acta (BBA)-Molecular Cell Research* **1793,** 5–19 (2009).
49. Kanazawa, T. *et al.* The *C. elegans* Opa1 Homologue EAT-3 Is Essential for Resistance to Free Radicals. *PLoS Genet* **4,** e1000022 (2008).
50. Huang, X. *et al.* Kissing and nanotunneling mediate intermitochondrial communication in the heart. *Proceedings of the National Academy of Sciences of the United States of America* **110,** 2846–2851 (2013).
51. Amchenkova, A. A., Bakeeva, L. E., Chentsov, Y. S., Skulachev, V. P. & Zorov, D. B. Coupling membranes as energy-transmitting cables. I. Filamentous mitochondria in fibroblasts and mitochondrial clusters in cardiomyocytes. *The Journal of cell biology* **107,** 481–495 (1988).
52. Fujioka, H., Tandler, B., Haldar, S. M., Jain, M. K. & Hoppel, C. L. String mitochondria in mouse soleus muscle. *Microscopy research and technique* **76,** 237–241 (2013).
53. Wang, C. *et al.* Dynamic tubulation of mitochondria drives mitochondrial network formation. *Cell research* **25,** 1108–1120 (2015).
54. Mears, J. A. *et al.* Conformational changes in Dnm1 support a contractile mechanism for mitochondrial fission. *Nature structural & molecular biology* **18,** 20–26 (2011).
55. Bhandari, P., Song, M., Chen, Y., Burelle, Y. & Dorn, G. W. 2nd. Mitochondrial contagion induced by Parkin deficiency in Drosophila hearts and its containment by suppressing mitofusin. *Circ Res* **114,** 257–265 (2014).
56. Shutt, T. E. & McBride, H. M. Staying cool in difficult times: mitochondrial dynamics, quality control and the stress response. *Biochimica et biophysica acta* **1833,** 417–424 (2013).
57. Leduc-Gaudet, J. P. *et al.* Mitochondrial morphology is altered in atrophied skeletal muscle of aged mice. *Oncotarget* **6,** 17923–17937 (2015).
58. Liu, X. & Hajnoczky, G. Altered fusion dynamics underlie unique morphological changes in mitochondria during hypoxia-reoxygenation stress. *Cell Death Differ* **18,** 1561–1572 (2011).
59. Ahmad, T. *et al.* Computational classification of mitochondrial shapes reflects stress and redox state. *Cell death & disease* **4,** e461 (2013).
60. Hara, Y. *et al.* Presynaptic mitochondrial morphology in monkey prefrontal cortex correlates with working memory and is improved with estrogen treatment. *Proceedings of the National Academy of Sciences* **111,** 486–491 (2014).
61. Barbot, M. *et al.* Mic10 Oligomerizes to Bend Mitochondrial Inner Membranes at Cristae Junctions. *Cell Metabolism* **21,** 756–763 (2015).
62. Picard, M. & Burelle, Y. Mitochondria: starving to reach quorum?: Insight into the physiological purpose of mitochondrial fusion. *Bioessays* **34,** 272–274 (2012).
63. Deerinck, T., Bushong, E., Thor, A. & M. E. NCMIR methods for 3D EM: A new protocol for preparation of biological specimens for serial block face scanning electron microscopy. *Micrscopy* 6–8 (2010).

Acknowledgements

This work was supported by grants from the Biotechnology and Biological Sciences Research Council BB/M012093/1, Engineering and Physical Sciences Research Council, Economic and Social Research Council and Medical Research Council G0700718, The Wellcome Trust Centre for Mitochondrial Research G906919, The MRC Centre for Translational Research in Neuromuscular Disease Mitochondrial Disease Patient Cohort G0800674, the UK NIHR Biomedical Research Centre in Age and Age Related Diseases award to the Newcastle upon Tyne Hospitals NHS Foundation Trust, The Lily Foundation and the UK NHS Specialist Commissioners "Rare Mitochondrial Disorders of Adults and Children" Service. AEV is funded by an MRC studentship (MR/K501074/1) as part of the MRC Centre for Neuromuscular disease (MR/K000608/1).

Author Contributions

Experimental conception and design: M.P., D.M.T. and A.E.V. Facilitation of tissue acquisition and clinical information: Y.S.N., D.M.T., R.W.T., G.F., C.F., A.M.S. and R.M.F. Acquisition of data: A.E.V., K.W., T.D. and M.P. Analysis and interpretation of data: A.E.V. and M.P. Drafting of manuscript: A.E.V., M.P. and D.M.T. Critical revision of manuscript: C.M., Y.S.N., R.W.T., G.S.G. and R.M.F.

Additional Information

Supplementary information accompanies this paper at http://www.nature.com/srep

Competing financial interests: The authors declare no competing financial interests.

How to cite this article: Vincent, A. E. *et al.* The Spectrum of Mitochondrial Ultrastructural Defects in Mitochondrial Myopathy. *Sci. Rep.* **6**, 30610; doi: 10.1038/srep30610 (2016).

Appendix 5: Results from a systematic review of literature of electron microscopy studies (n = 135) in skeletal muscle of patients with confirmed mitochondrial myopathy.

*Age at biopsy for EM study

AV: Atrioventricular

CPEO: Chronic progressive external opthalmoplegia

IMF: Intermyofibrillar

KSS: Kearns-sayer syndrome

MELAS: Mitochondrial encephalomyopathy, lactic acidosis and stoke-like episodes

mtDNA: Mitochondrial DNA

MERRF: Myoclonic epilepsy and ragged red fibres

N.S.: Not specified

PCI: Paracrystalline inclusion

PEO: progressive external opthalmoplegia

RRF: Ragged-red fibers

SS: Subsarcolemmal
1: common large-scale deletion, 4977bp in length between two 13-bp direct repeats at positions m.13447-13459 and m.8470-8482.

Genetic diagnostic methodology: aRestriction site mutation assay; bSouthern blot, cPCR, dSanger sequencing, eRFLP, fSolid phase mini sequencing, gSequencing, hNext generation sequencing, iNot specified.

Author (Year)	Muscle	Age*	Clinical	Genetics	Ultrastructural abnormality
van Wijngaarden et al. (1967)	Deltoid and gastrocnemius	15 years	[Pediatric] Myopathy without muscle atrophy, deltoid muscle weakened, paresis of pelvic muscles (n=1).	N.S.	Matrix swelling and electron lucent mitochondria; clumped and filamentous, small osmiophilic dense bodies present in mitochondrial matrix; larger electron-dense round granules or irregularly shaped inclusions of moderately electron dense granular material.
(Afifi et al., 1972)	N.S.	19 years	Hypermetabolic “mitochondrial” disease. Substantial muscle weakness (n=1).	N.S.	Osmiophilic inclusions of variable size and density within mitochondria; dense inclusions replacing most of the cristae, with cristae reduced to a thin circular rim at the periphery of affected mitochondria.
(Hudgson et al., 1972)	Peroneus longus and biceps	35 years (proband) and 12 years (niece).	Familial “mitochondrial” myopathy. Facial and ocular, pectoralis major and bicep weakness, considerable lower limb weakness (n=2).	Dominant inheritance; high penetrance; maternal transmission. Mutation N.S.	Giant mitochondria measuring up to 3 µm containing concentric cristae and small electron-dense inclusions; mitochondria with “parking-lot” type inclusions between inner and outer mitochondrial membranes; mitochondrial with six layers with periodicity between both their transverse and axial cristae of approximately 75 A.
(Adachi et al., 1973)	Ocular muscles	37 years	CPEO, cerebella ataxia and	N.S.	Enlarged mitochondria with parallel or concentric cristae.

			cardiomyopathy (n=1).		
	Deltoid	37 years (same individual as above)	CPEO, cerebella ataxia and cardiomyopathy (n=1).	N.S.	Unusually large mitochondria ranging from 5-8 µm in greatest diameter with cristae usually located at the periphery of the organelle and rectangular inclusions; cross sections of the PCI structures disclosed well-organized arrays of tubules oriented in parallel rows with a diameter of 70-80 A, with a lumen of 30-40 A, and interspace between the tubules of 20-30 A, arranged in a helical pattern; abnormal mitochondria almost completely replaced by dense rectangular inclusions and occasionally showed complete transition to crystalline structures obscuring the original mitochondrial morphology.
(Shibasaki et al., 1973)	Deltoid	60 years	Late onset myopathy; marked atrophy of shoulder girdle and proximal upper limb, pelvic and proximal lower limb muscles; mild atrophy of distal lower limb muscles (n=1).	N.S.	Elongated, giant mitochondria up to 5 µm in greatest diameter, particularly in the SS region; PCIs including lattice pattern, four-fold array, or amorphous form.

(Crosby and Chou, 1974)	Left bicep	10 years	[Pediatric] Leigh disease (n=1).	N.S.	Enlarged mitochondria (in cross section); whirled cristae membranes; electron dense spheroid bodies; electron-lucent mitochondrial matrix spaces; complex, convoluted membrane systems; PCI within cristae membrane.
(Black et al., 1975)	Anterior tibialis or Quadriceps	30 years	Mitochondrial disorder, RRFs, and ptosis (n=1).	N.S.	Enlarged mitochondria with “wavy” cristae and central electron dense granular material; round dense osmiophilic inclusions; occasional lipid inclusions and concentric cristae.
(Karpati et al., 1975)	Quadriceps	11 years	[Pediatric] KSS biopsied before and after Carnitine supplementation (n=1).	N.S.	PCI; concentric cristae; swollen mitochondria.
(McLeod et al., 1975)	Quadriceps (vastus lateralis)	27 years	Mitochondrial myopathy (n=1).	N.S.	PCI with parallel bands of amorphous material surrounded by a membrane; mitochondria with “empty” electron-lucent spaces; amorphous material between the mitochondrial membranes; mitochondria containing “empty space” surrounded by double membranes.
(Bastiaensen et al., 1979)	Ocular and skeletal	>30 years [review]	PEO plus.	N.S.	[Review] Aggregates of swollen mitochondria with parallel or concentric cristae.
(Linden and Ansink, 1979)	Gastrocnemius	11 years	[Pediatric] KSS. Ptosis, mental and physical	N.S.	PCI; large mitochondria.

			retardation, dysarthria (n=1).		
(Fitzsimons and Tyer, 1980)	Left deltoid	10 and 17 years	Mitochondrial myopathy. Myopathy, scoliosis, respiratory failure. (n=2)	N.S.	Rectangular inclusions, PCI, amorphous material and concentric cristae in mitochondria.
(Fukuhara et al., 1980)	Quadriceps femoris	21 years	MERRF. Myoclonic jerk, seizures, hypotonia, ataxia (n=1).	N.S.	Electron-lucent homogenous matrix space; enlarged mitochondria; markedly proliferated IMM; PCIs.
(Land et al., 1981)	Left deltoid	14 years	[Pediatric] Mitochondrial myopathy, opthalmoplegia (n=1).	N.S.	Mitochondria with “finger-print” like patterns (i.e., densely packed parallel cristae); concentric cristae.
(Shah et al., 1982)	Quadriceps	N.S.	KSS, polymyositis, neurogenic atrophy, mitochondrial myopathy.	N.S.	PCIs (30-45 nm long and 22-23 nm wide); round or oval swollen mitochondria; presence of various inclusions; densely packed or tubular cristae formation; concentric cristae or “lamellar bodies”; parallel destruction of cristae and presence of amorphous material.
(Holliday et al., 1983)	N.S.	18 and 26 years	Mitochondrial myopathy,	N.S.	Rectangular or curvilinear PCIs composed of four parallel lamina within a boundary membrane.

			encephalopathy (n=2).		
(Mitsumoto et al., 1983)	Deltoid	11 to 49 years (m=34.5)	CPEO with RRF (n=8).	N.S.	Mitochondria with absent cristae; irregular vacuoles; PCIs; concentric cristae; dark inclusion; whirl formation.
(Müller-Höcker et al., 1983)	N.S.	N.S.	PEO (n=8).	N.S.	Enlarged mitochondria with high cristae content; concentric cristae and PCIs.
(Prick et al., 1983)	N.S.	2 and 5 years	[Pediatric] Alper's disease (n=2).	N.S.	Aggregates of enlarged mitochondria with PCIs in SS region.
(Sarnat et al., 1983)	Quadriceps femoris, deltoid, extensor digitorum longus of the forearm (post mortem)	3 weeks and 4 months	[Pediatric] Mitochondrial myopathy, cerebro-hepato renal (Zellweger) syndrome (n=2).	N.S.	Electron dense granules in mitochondrial matrix; myelin figures, degeneration and other degenerative changes (e.g. membrane rupture) to mitochondria.
(Sengers et al., 1983)	Quadriceps	4 years	[Pediatric] Mitochondrial myopathy, carnitine deficiency (n=1).	N.S.	Large mitochondria with densely packed or whirled cristae; granular or fibrillary electron dense material in intercristal space.
(Hayes et al., 1984)	Intercostal muscle	20 years	Mitochondrial myopathy, bilateral ptosis, muscle bulk normal, mild	N.S.	SS mitochondria with concentric cristae and inclusions; central droplets of neutral or osmiophilic lipid or areas of central necrosis.

			diffuse weakness (n=1).		
(Kennaway et al., 1984)	N.S.	17 years	Mitochondrial myopathy, lactic acidosis (n=1).	N.S.	Abnormally large mitochondria some with PCIs.
(Bresolin et al., 1985)	Quadriceps	2, 3, 6 and 7 months	[Pediatric] Mitochondrial myopathy, hypertonia and severe limb weakness, tendon and pharyngeal weakness absent (n=1).	N.S.	Large mitochondria with irregular or concentric tubular cristae.
(Müller-Höcker et al., 1985)	N.S.	12 years	[Pediatric] Mitochondrial myopathy, excercise induced muscle weakness and pain, tachycardia and dyspnoea (n=1).	N.S.	Swollen mitochondria with PCIs.
(Niebrój-Doblosz et al., 1985)	Biceps brachii and quadriceps	7 years	[Pediatric] KSS. Biceps and quadriceps	N.S.	Giant mitochondria; PCIs; concentric cristae.

			weakness, mental retardation, progressive limb weakness (n=1).		
(Fischer et al., 2006)	Quadriceps	17 years	Mitochondrial enchephalomyopathy, seizures, myoclonic contractures, retarded motor and speech development (n=1).	N.S.	Small mitochondria with swollen matrix; concentric cristae or “concentric laminated bodies”.
(Lehmann et al., 1986)	Deltoid	44 years	Myopathy with rimmed vacuoles, mild shoulder girdle weakness, exercise intolerance (n=1).	N.S.	PCIs of Type I and II.
(Stadhouders and Sengers, 1987)	N.S.	N.S.	Mitochondrial myopathy (KSS, MELAS, MERRF)	N.S.	[Review] PCIs and concentric cristae; suggests model of PCI formation; classify 2 types of PCI (Type I, Type II); suggests different types of PCI for different fibre types.
(van Ekeren et al., 1987)	N.S.	6 days	Hereditary mitochondrial hypertrophic	N.S.	Mitochondria with vesicular inclusions; matrix crystals.

			cardiomyopathy (n=1).		
(Colombo et al., 1988)	Left quadriceps	27 years	Mitochondrial occuloskeletal myopathy (n=1).	N.S.	PCIs; globular dense bodies; cristae running concentrically.
(Dias-Tosta, 1988)	N.S.	N.S.	CPEO. Sporadic muscle weakness (n=10), familial isolated myopathy (n=9), myopathy with retinopathy, cerebellar ataxia, or peripheral neuropathy (n=15).	N.S.	PCIs; concentric cristae; “parking lot” and “intramural type” inclusions.
(Federico et al., 1988)	Quadriceps	N.S.	LHON (n=3).	N.S.	Enlarged mitochondria with PCIs.
(Mizusawa et al., 1988)	Rectus femoris or tibialis	46 and 48 years	Familial mitochondrial myopathy, pptic atrophy, muscle wasting, weakness (n=2).	N.S.	Aggregates of mitochondria with PCIs; electron dense globular bodies; concentric cristae.

(Kim et al., 1989)	Left deltoid	53 years	CPEO. Mild proximal limb weakness (n=1)	N.S.	PCIs; irregularly orientated cristae.
(Paulus et al., 1989)	Left quadriceps	33 years	Mitochondrial encephalomyopathy with perivacuolar inclusions, bilateral hearing loss, seizures, cerebral atrophy, moderate muscle atrophy (n=1).	N.S.	Small osmiophilic rod-like inclusions; piles within round or oval vacuoles (perivacuolar inclusions).
(Rivner et al., 1989)	N.S	25 years	KSS. Cerebellar and cortical atrophy, mild ataxia and generalised weakness of proximal and distal muscles (n=1).	N.S.	Deformed internal architecture; PCI arrays; concentric cristae or “cristae arranged circumferentially”.
(Suzuki et al., 1989)	Quadriceps	35 years	Mitochondrial encephalomyopathy, general muscle atrophy, psychiatric	N.S.	Enlarged mitochondria with PCIs.

			disturbance (n=1).		
(Arruda et al., 1990)	Quadriceps	32 and 34 years	Mitochondrial myopathy with myoclonic epilepsy. Myoclonic jerks and seizures (n=2).	N.S.	Enlarged mitochondria.
(Haginoya et al., 1990)	Quadriceps (vastus femoris)	8-43 years (m=25)	MERRF and MELAS. Mixed, myoclonic seizure, ataxia, stroke-like episodes, ptosis (n=3).	N.S.	Aggregated mitochondria in areas of segmental COX deficiency.
(Korenke et al., 1990)	N.S.	2 weeks - 9 years (m=2 years)	[Pediatric] Mitochondrial myopathy. Mixture; respiratory insufficiency, hypotonia, motor retardation and feeding problems (n=8).	N.S.	Abnormally small and large mitochondria; PCIs; polymorphy; altered cristae.

(Schapira et al., 1990)	Quadriceps (vastus lateralis)	14 years	Mitochondrial myopathy. Weakness of limbs and trunk, high CK.	Defect in protein transport? Molecular cause N.S.	Disordered “labyrinth” cristae with electron dense and granular inclusions.
(Sumegi et al., 1990)	N.S.	45 days	[Pediatric] COX deficiency.	N.S.	Swollen mitochondria, and often “tennis-racket” like mitochondria (swollen at one end); mitochondria with honeycomb cristae.
(Takeda et al., 1990)	Extraocular muscles	14 to 30 years (m=20)	MELAS and MERRF. Mixed symptoms (n=3).	N.S.	Mitochondria of irregular shape with tubule-vesicular cristae; morphological changes more prominent in MELAS than MERRF. No PCI.
(Kim et al., 1991)	N.S.	16 and 22 years	Mitochondrial myopathy. Severe respiratory dysfunction, mild myopathy.	N.S.	Sickle shaped mitochondria containing curvilinear PCI, regular PCIs.
(McKelvie et al., 1991)	Quadriceps (vastus lateralis)	48 years (n=1)	KSS. Opthalmoplegia, limb weakness, ataxia (n=1).	3.5Kb single mtDNA deletioni	PCIs in subsarcolemmal aggregates of mitochondria.
(Letellier et al., 1992)	Deltoid	1 week to 4 months (m=2 months)	[Pediatric] Mitochondrial myopathy. Mixture of symptoms (n=6).	N.S.	Enlarged and swollen mitochondria.

(Linda et al., 1992)	N.S.	N.S.	Mitochondrial myopathy. MELAS (n=3), Marinesco-Sjogren syndrome (n=7) and KSS (n=2).	mtDNA mutations N.S.	PCIs; pleoconial mitochondria; enlarged “megamitochondria”; thickening, unfolding, and parallelization of cristae; concentric cristae or “concentric lamellar cristae”; augmented matrix space; amorphous inclusion bodies.
(Modi et al., 1992)	Biceps brachii	20 years	Mitochondrial myopathy. Proximal myopathy, cardiomyopathy, bilateral deafness and ptosis.	N.S.	Laminated PCIs.
(Telerman-Toppet et al., 1992)	N.S.	8 weeks	[Pediatric] COX deficiency and mtDNA depletion (n=1).	N.S.	PCIs; abnormal spatial arrangement of mitochondrial cristae.
(Angelini et al., 1993)	Biceps and quadriceps	19 and 25 years	Hypertrophic cardiomyopathy with mitochondrial myopathy. Weakness in upper limb girdle muscles and Gower’s signs and waddling	Dystrophin and mtDNA deletions ruled out. Cause N.S.i	Enlarged mitochondria with irregular cristae.

			gait, no cerebellar abnormalities (n=2).		
(Coquet et al., 1993)	N.S.	15 and 17 years	MERRF. Myoclonic jerks, epileptic seizures, ataxia, deafness, lower limb weakness (n=2).	m.8344A>Ga tRNALys	PCIs; concentric cristae.
(Reichmann et al., 1993)	Biceps brachii	53 years	KSS. Mild generalized muscle weakness and exercise intolerance, diabetes, slowly progressive ataxia (n=1).	Multiple deletionsb (causative mutation N.S.)	PCIs; concentric cristae.
(Ionasescu et al., 1994)	Quadriceps (vastus lateralis)	9 years	[Pediatric] MERRF. Progressive proximal weakness (n=1).	m.15990A>Ga tRNAPro	PCIs.

(Norby et al., 1994)	Quadriceps (vastus medialis)	15 years	[Pediatric] KSS. Epileptic seizures, ataxia, myopathy (n=1).	11Kb single mtDNA deletionb	Enlarged mitochondria with PCIs.
(Stadhouders et al., 1994)	N.S.	N.S.	CPEO, KKS, MELAS	N.S.	PCIs (Types I and II).
(Gilbert and Emms, 1996)	N.S.	21 months	Pearson's syndrome. Pancreatic atrophy, enlarged kidneys, metabolic acidosis, high blood lactate and hypomagnesemi a (n=1).	N.S.	Aggregated SS and IMF mitochondria; concentric cristae, enlarged mitochondria with disrupted membranes; central follicular (granular) matrix.
(Melberg et al., 1996)	Quadriceps (vastus lateralis) or bicularis oculi	16 to 63 years (m=52 years)	Dominant PEO. Ocular myopathy, hypogonadism (n=14).	Dominant genetic cause N.S.	Densely packed cristae; size variation; longitudinally or circular cristae; crystalloid-like alterations.
(Toscano et al., 1996)	N.S.	73 to 75 years (m=74 years)	Late-onset mitochondrial neuropathy. Muscle weakness and cramps, ataxia,	No mtDNA mutations foundb,c. Genetic cause N.S.	PCIs, enlarged or bizarrely shaped mitochondria.

			exercise intolerance (n=3).		
(van Domburg et al., 1996)	Soleus, quadriceps, ocular rectus superior	25 to 36 years (m=30 years)	CPEO plus. Ocular myopathy, encephalomyopathy, sensory neuropathy, ataxia, polyneuropathy (n=6).	No evidence of maternal inheritance, common point mutations and deletions ruled outi. Genetic cause N.S.	PCIs, mitochondria with deranged cristae; concentric cristae.
(Wada et al., 1996)	Quadriceps femoris	11 weeks	[Pediatric] Mitochondrial myopathy. Muscular hyoptonia, profound acidosis, difficulty suckling, no muscle weakness (n=1).	N.S.	Enlarged mitochondria with sparse cristae; concentric cristae.
(Heiman-Patterson et al., 1997)	N.S.	4 to 63 years (m=28 years)	Family with mitochondrial myopathy. Exercise intolerance, proximal lower limb weakness in	mtDNA deletions and common point mutations ruled out, a number of non-pathogenic point mutations	Uneven and electron dense cristae; globular inclusions.

			first decade of life (n=11).	foundd. Genetic cause N.S.	
(Kim and Chi, 1997)	Deltoid	22 and 23 years	KSS. Neck and proximal limb weakness, severe ptosis, AV block.	Single mtDNA deletion1,c	PCIs, enlarged mitochondria with distorted cristae.
(Smith et al., 1997)	Quadriceps	N.S.	Mother of MELAS patient, with insulin dependent diabetes (n=1).	m.3243A>Ga tRNALeu	Pleomorphic mitochondria; concentric cristae; electron-dense bodies.
(Takahashi et al., 1998)	Quadriceps femoris	9 months	[Pediatric] Leigh disease. Generalized hypotonia at birth, apnea attacks, irregular breathing, poor head control (n=1).	m.8993T>Ga MT-ATP6	Variably sized mitochondria; aberrant cristae.
(Castro-Gago et al., 1999)	Deltoid	Fetus	Hydranencephalic-hydrocephalic syndrome in association with mitochondrial	Common mtDNA point mutations and deletions ruled	Enlarged SS mitochondria; abnormal cristae (honey-comb-like).

			encephalomyopathy.	outi. Genetic cause N.S.	
(Kyriacou et al., 1999)	N.S.	6 days to 10 years (m=2 years)	[Pediatric] Mitochondrial enchephalomyopathy. Hypotonia and psychomotor retardation (n=5), multisystemic (n=2), Pearson syndrome (n=1), Leigh disease (n=1). (Adult) Myalgia and proximal limb weakness (n=8), PEO (n=3).	N.S.	Pleomorphic mitochondria; simplified cristae; vesicular cristae.
(Melegh et al., 1999)	N.S.	5 months	Mitochondrial enchephalomyopathy. Myoclonic jerk, uncoordinated eye movement (n=1).	Multiple mtDNA deletionsb. Nuclear mutation N.S.	Enlarged mitochondria with no or few cristae.
(Carta et al., 2000)	Quadriceps (rectus medialis)	48 years	CPEO (n=1)	Single common mtDNA deletion1,b	PCIs; “onion-like” concentric cristae, “ghost-like” mitochondria (devoid of cristae).

(Makino et al., 2000)	N.S.	N.S.	Leigh syndrome. Hypotonia, necrotic lesions in basal ganglia and brainstem (n=1).	m.8993T>Ga MT-ATP6	Enlarged mitochondria.
(Wang et al., 2000)	N.S.	9 years	No prominent muscle weakness or hypotonia, but wobbling gait early on. Proximal limb myopathy 1 month prior to biopsy (n=1).	N.S.	Loss of matrix and cristae.
(De Kremer et al., 2001)	N.S	N.S.	[Pediatric] Barth-syndrome like disorder, marked muscle weakness.	m.3243A>Gd tRNALeu	Round swollen mitochondria; fine fibrillary matrix; poorly define cristae.
(Higashikata et al., 2001)	Biceps brachii	80 years	MELAS. Cardiomyopathy.	m.3243A>Ga tRNALeu	Aggregates of enlarged mitochondria with PCIs.
(Rollins et al., 2001)	N.S.	1 to 70 years (m=12.5 years)	Mitochondrial cytopathy (n=113)	Mutation of “maternal inheritance” N.S.	PCI; enlarged mitochondria.

(Vogel, 2001)	N.S.	N.S.	Mitochondrial myopathy	N.S.	[Review] Swollen, elongated, devoid of cristae, PCIs.
(Fagiolari et al., 2002)	N.S.	27 to 73 years (m=55 years)	CPEO (n=7), PEO and ptosis (n=7), myopathy (n=1).	Multiple mtDNA deletionsb due to ANT1 mutation – p.114A>P and p.98L>Pi	Mitochondrial proliferation and PCIs.
(Fillano et al., 2002)	N.S.	2 to 12 years (m=7 years)	HEADD syndrome (hypotonia, epilepsy, autism, and developmental delay) (n=3)	Multiple mtDNA deletionsc (nuclear cause N.S.) or 7.4Kb single mtDNA deletionc	Stacked cristae; electron dense deposits.
(Kim et al., 2002)	Biceps brachii	18 Years	MERRF. Myoclonic epilepsy, myopathy, ataxia, dysarthria (n=1).	m.8344A>Ge tRNALys	PCI; concentric cristae.
(Marín-García et al., 2002)	N.S.	15 years	PEO (n=1)	Multiple mtDNA deletionsb	Vacuolated cristae; variation in size and morphology.
(Nevo et al., 2002)	Quadriceps	11 to 26 months	[Pediatric] Mitochondrial myopathy. Motor	TK2 mutation causing	Pleomorphic mitochondria; enlarged mitochondria; concentric cristae or “concentric lamellae”.

		(m=16 months)	deterioration, dyspneic, muscle weakness, bilateral ptosis.	mtDNA depletioni	
(Kyriakides et al., 2003)	N.S.	6 days to 18 months (m=6 months, n=19), 19 to 75 years (m=42 years, n=14)	Mitochondrial encephalomyopathies: myopathic, multisystemic or CPEO. Pediatric (n=19) and adult (n=14).	N.S.	Mitochondrial dysmorphology more common in children than adults and vice versa.
(Uusimaa et al., 2003)	N.S.	10 months	Alpers-Huttenlocher-like disease (n=1)	m.7706G>Ad MT-COII	Enlarged mitochondria; variable shape and size.
(Mierau et al., 2004)	Quadriceps	8 years	[Pediatric] Lactic acidosis, proximal weakness, cognitive delay.	N.S.	PCIs; enlarged or abnormally small; concentric cristae; parking lot type inclusions; spherical electron dense inclusions.
(Patterson, 2004)	N.S.	16 years	KSS.	5Kb mtDNA deletionf	PCIs.

(Carta et al., 2005)	Quadriceps (rectus medialis)	42 to 75 years (m=63 years)	CPEO and LHON (n=3)	Single common mtDNA deletion1,i	“Ghost” mitochondrial profiles (lack of cristae) with partial to complete matrix emptying rearrangement of the cristae with an “onion ring-like” appearance
(Coulbault et al., 2005)	N.S.	10 months	[Pediatric] Psychomotor retardation, failure to thrive, hypotonia, hepatocellular dysfunction, thrombocytopenia. Multiple organ failure (lethal) (n=1).	m.5693T>Ce, tRNAASN	PCIs; stacked cristae.
(Dinopoulos et al., 2005)	Quadriceps	1 to 15 months (n=9 months)	[Pediatric] Hypotonia, myoclonic epilepsy, cardiomyopathy, psychomotor regression, failure to thrive, lactic acidosis (mixed) (n=4).	NDUFS2 c.237T>C, NDUFS8 c.236C>T and c.302G>A, NDUFVI c.175C>X and c.1268C>T mutations (CI)i	Concentric cristae or “concentric laminated bodies”; osmiophilic mitochondria.

(Enns et al., 2005)	Quadriceps (vastus lateralis) and deltoid	6 weeks to 5 years (m=1.5 years)	Electron transport chain abnormalities, RRFs. (n=7)	N.S.	Enlarged mitochondria; swelling with electron-lucent matrix space; proliferation of mitochondria; elongated and branched.
(Güçer et al., 2005)	N.S.	4 months and 9 years	[Pediatric] Seizures, ptosis, failure to thrive, high serum lactate and pyruvate, RRF (n=2).	Single common mtDNA deletion1,b	Increased matrix density and cristae; SS mitochondrial accumulation.
(Karppa et al., 2005)	Quadriceps (vastus lateralis) or tibialis anterior	16 to 70 years (m=45 years)	MELAS	m.3243A>Gi tRNALeu	PCIs (Types I and II); variation in size and ultrastructure.
(Kyriacou et al., 2005)	N.S.	6 days to 18 years (median= 4 years, n=31) and 19 to 75 years (median= 46 years, n=17)	Mitochondrial encephalomyopa thy (n=48).	N.S.	Elongated and enlarged mitochondria more common in children than adults; subsarcolemmal aggregation of mitochondrial (RRF) more common in adults.
(Pulkes et al., 2005)	N.S.	16 and 23 years	MERRF. Proximal upper	m.7472_insCi tRNASer	Type 2 fibres larger and dense matrix components and contain either or both type 1 or 2 crystalline intra-

			and lower limb weakness, ataxia, seizures and myoclonus (n=2).		membranous inclusions. Type 1 myofiber mitochondria, have many large and abnormal forms, show a more orderly arrangement of their cristae, a lesser quantity of less dense matrix, and only type 1 intra-membranous crystalline inclusions.
(Stenqvist et al., 2005)	Quadriceps (vastus lateralis)	10 years	[Pediatric] MELAS. Mild central and cortical brain atrophy, encephalopathy, no mention of myopathy (n=1).	m.3271T>Cf tRNALeu	Dense granular inclusions, parallel cristae arrays, open matrix spaces.
(Zeharia et al., 2005)	N.S.	19 years	Mitochondrial myopathy (n=1).	Autosomal recessive PUS1d	PCIs.
(Cardaioli et al., 2006)	Quadriceps	31 years	Deafness, mental retardation, brain atrophy (n=1).	m.7472insCe tRNAser (UCN) and m.7472A>Ce tRNAser (UCN)	Swollen mitochondria with reduced cristae and PCIs.
(Deschauer et al., 2006)	N.S.	66 years	Exercise intolerance, walking difficulty, muscle cramps,	m.622G>Ad tRNAPhe	Enlarged mitochondria with PCIs.

			hearing impairment, mild myopathy and peripheral neuropathy (n=1).		
(Miles et al., 2006)	N.S.	2 weeks to 21 years (median=2.7 years)	KSS (n=4), Leigh syndrome (n=2), lethal infantile COX deficiency (n=2), MERRF (n=1), encephalopathy with (n=72) and without myopathy (n=46).	N.S.	PCIs; abnormal patterns of cristae; concentric cristae or “circular cristae” and fingerprint cristae; abnormal matrix density.
(Saneto and Bouldin, 2006)	N.S.	11 years	[Pediatric] Muscle weakness, hypercarbia, lactic acidosis, absent deep tendon reflexes, respiratory difficulty (n=1).	m.3243A>G tRNALeu	Enlarged rounded mitochondria; distorted cristae; electron dense inclusions.
(Thajeb et al., 2006)	N.S.	65 years	Oculopharangyl somatic myopathy,	Single mtDNA deletionc,d and homoplasmic	“Parking lot” type PCIs.

			bilateral ptosis and difficulty swallowing (n=1).	m.5814T>Cd tRNACys	
(Wabbels et al., 2007)	M. levator palpebrae, and/or the M. orbicularis oculi	4 to 81 years (m=40 years)	Adult/child Ptosis/CPEO (n=21).	N.S.	PCIs; concentric and wavy cristae; pleomorphy; intermitochondrial granules.
(Perry and Sladky, 2008)	Quadriceps	3 days	[Pediatric] Sengers syndrome. Bilateral ptosis, hypotonia, trace reflexes, skeletal muscle myopathy and cardiomyopathy (n=1).	N.S.	Diffuse dysmorphic mitochondria.
(Pronicki et al., 2008)	Quadriceps (vastus lateralis)	9 months to 12 years (m=3.5 years)	[Pediatric)] Leigh Syndrome. Motor regression, bulbar symptoms, difficulty walking, hypotonia, failure to thrive, floppiness, disturbed eye	SURF1i mutation	Enlarged or elongated mitochondria; dark matrix with densely packed, concentric lamellae cristae; mitochondrial matrix displaced by amorphous granular material; small electron-dense osmiophilic granules.

			movement (n=21).		
(Yerdelen et al., 2008)	Biceps brachii	38 years	KSS. Delayed motor and mental development, arrhythmia (n=1).	N.S.	PCIs; swollen mitochondria with few electron dense cristae; osmiophilic and electron-dense structures.
(Abu-Amero et al., 2009)	N.S.	34 years	MELAS (n=1)	No mtDNA mutations or POLG mutations. Genetic cause N.S.	Mitochondria with parallel cristae and PCIs, osmiophilic inclusions and mitochondrial vacuoles.
(DeBrosse et al., 2009)	Deltoid	67 years	CPEO. Ptosis, mild upper limb weakness, mild memory difficulty and imbalance (n=1).	N.S.	PCIs; dystrophic mitochondria.
(Yau et al., 2009)	Quadriceps	14 years	[Pediatric] KSS, short stature, mental deficiency, lower limb weakness, mild ataxic gait (n=1).	Single 7.2Kb mtDNA deletionc	PCIs; irregular structure and cristae; central core-like fibres (IMF mitochondrial depletion).

(Ali et al., 2010)	Triceps brachii	62 years	CPEO. Diplopia, no muscle weakness (n=1).	Single mtDNA deletion1,b,c,d	PCIs (Type I); swollen rounded mitochondria.
(Ascaso et al., 2010)	N.S.	48 years	KSS. Bilateral ptosis, proximal muscle weakness and RRFs (n=1).	Single mtDNA deletion1b,c,d	Large atypical mitochondria; round electron dense bodies.
(Cardenas and Amato, 2010)	N.S.	14 years	[Pediatric] Alpers disease. Neuropathalogical degeneration of cerebral grey matter (n=1).	POLG mutations (compound heterozygous) c.911T>G (p. L304R), c.1174C>G (p.L392V) and a duplication (pR1081dup)f	Reduced mitochondrial content, absence of cristae, vacuolization.
(Chi et al., 2010)	Quadriceps	1 month to 15 years (median=15 months, n=69)	[Pediatric] Leigh disease (n=6).	m.8993T>G (n=3) MT-ATP6, m.8993T>C MT-ATP6 (n=1), m.10191T>C MT-ND3 (n=1) and	Tubular cristae; swollen mitochondrial accumulation; variable shapes; concentric “whirl” cristae; inclusion bodies.

				m.8344A>G (n=1)c,d,e	
			[Pediatric] MELAS (n=4).	m.3243A>G tRNALeu (n=4)c,d,e	
			[Pediatric] Pearson syndrome (n=1)	6 Kb mtDNA deletion (n=1)c,d,e	
			Mixed mitochondrial disease (n=58)	Genetic cause N.S.	
(Han et al., 2010)	Rectus femoris	4 to 48 years (m=N.S)	Spinocerebellar ataxia type 7. Unsteady gait, visual problems, cerebellum and brain stem atrophy (n=34).	SCA7 mutationc CAG repeat	Mitochondrial with tubular or absent cristae.
(Herrero-Marti et al., 2010)	N.S.	50 years	MELAS MERRF overlap (n=1)	m.5521G>Ag tRNATrp	PCIs.
(Lang et al., 2010)	Ocular medial rectus	47 and 67 years	CPEO, ptosis, exercise intolerance and	Multiple mtDNA deletionsi	Enlarged mitochondria; hypertrophic concentric lamellar cristae.

			mild myopathy (n=2).	(nuclear mutation not defined)	
(Baskin et al., 2011)	N.S.	9 years	Mitochondrial myopathy. Myopathic findings by electromyography, deafness, ocular and neurological findings (n=1).	NPHS3g mutation	Abnormal mitochondrial shape and cristae patterns.
(Cenacchi et al., 2011)	Quadriceps, Tricep, deltoid	19 to 79 years (m=56 years)	Mitochondrial myopathy (=14).	N.S.	Accumulation of SS mitochondria; rounded, elongated, or cup-shaped mitochondria; abnormally large or “mega-mitochondria”; concentric cristae; lipid-dense; PCIs in matrix.
(Conway et al., 2011)	gastrocnemius	29 years	MELAS. Seizures, hearing loss (n=1).	m.3243A>GitRNALeu	Abnormally arranged cristae and aberrant electron density.
(Schaaf et al., 2011)	N.S.	3 and 8 years	Optic nerve atrophy, hypotonic, ataxia (n=2).	OPA1 mutation c.2708_2711delTTAG (p.V903GfsX3) and c.1146A>G (p.I382M)d	Mitochondrial with dense osmiophilic bodies.

(Blakely et al., 2012)	Quadriceps	21 years	Neuropathy and leukoencephalopathy, walking difficulties, distal numbness, muscle wasting of hands and distal lower limbs (n=1).	MPV17 mutationd causing 12.5Kb mtDNA deletionc	Enlarged, “parking lot” type inclusions.
(Bostan et al., 2012)	Deltoid	52 years	Ptosis, ataxia, neuropathy, gastroparesis, myopathy (n=1).	POLG mutationi	PCIs.
(Gotz et al., 2012)	N.S.	5 days	[Pediatric] Fatal neonatal lactic acidosis (n=1).	m.7453G>Ad tRNASer	Enlarged and swollen mitochondria, concentric cristae.
(Kendall, 2012)	Multiple	N.S.	Multiple mitochondrial disorders.	N.S.	[Review] Previous reports suggest electron microscopy is not a good diagnostic tool. However other sources report the frequency of 30-44% of aberrant mitochondrial morphology in pediatric mitochondrial disease and conclude its usefulness.
(Pfeffer et al., 2012)	Levator palpebrae	34 to 72 years (m=52 years)	CPEO (n=8)	POLG1 (n=1), single mtDNA deletion (n=4), multiple mtDNA	Large mitochondrial aggregates, pleomorphism, various inclusions.

				deletion (n=1, NS (n=2)b,c,e	
(Roefs et al., 2012)	Orbicularis	46 to 64 years (m=58 years)	Progressive bilateral ptosis and generalised muscle weakness (n=3).	Single mtDNA deletionb,c	Enlarged mitochondria; densley packed parallel cristae; electron dense inclusions.
(Baric et al., 2013)	Deltoid	17 years	Elevated CK, mild myopathy in brachial muscles.	m.5522G>Ac,g tRNATrp	Swollen globular looking mitochondria, occasional branching and angular OMM.
(Lopez et al., 2013)	Tibialis anterior	22 years	[Pediatric] Fatal infantile mitochondrial DNA depletion (n=1).	TK2 mutationc,g	Elongated mitochondria with PCIs.
(Lu and Huang, 2013)	Biceps brachii	1 to 13 years (m=8 years)	MELAS (n=6)	m.3243A>Gi tRNALeu	Globualar looking mitochondrial shape elongated with swollen regions and PCIs.
(Nolte et al., 2013)	N.S.	16 and 17 years	Seizures, myoclonic jerk, PEO (n=2).	POLG1 c.2243G>C (p.W748S) and c.1879C>T (p.R627W)g	Elongated mitochondria with “globoid” inclusions (amorphous lipid-like); SS mitochondrial accumulation or “aggregates”.

(Polimeno et al., 2013)	N.S.	N.S.	Mitochondrial myopathy (other symptoms N.S.).	N.S.	PCIs; mitochondria assuming bizarre and/or giant forms.
(Siriwardena et al., 2013)	N.S.	15 months	Sengers syndrome (n=1)	AGK mutationg	Pentagonal mitochondrial crystals with a dense outer layer.
(Yuan et al., 2013)	N.S.	51 and 54 years	RRF, rimmed vacuoles, muscle weakness in facial, cervical and proximal muscles, wasting of shoulder girdle (n=2).	m.8344A>Gd tRNALys	PCIs; Mitochondrial proliferation, concentric cristae.
(Zhao et al., 2013)	Biceps brachii	66 years	CPEO, RRF and diffuse muscle weakness (n=1)g.	Large 4Kb mtDNA mutation	PCIs.
(Chen et al., 2014)	N.S.	44 years	CPEO, ptosis, diplopia, bulbar paresis, inflammatory myopathy, neck muscle weakness (n=1).	Single mtDNA deletion1,h	PCIs preferentially in SS mitochondria.

(Hopmann et al., 2014)	N.S.	72 years	Mitochondrial myopathy, muscle atrophy and proximal weakness of arms trunk and legs (n=1).	Multiple mtDNA deletionsb,c	“Parking lot” inclusions; swollen aggregated mitochondria; loss of cristae.
(Chatfield et al., 2015)	N.S.	2 months	Mild enchephalomyopathy, diffusion of the perirolandic white matter (n=1).	HSD10 mutationg c.740A>G (p.N247S)	Loss of cristae; swollen vacuolated mitochondria.
(Nozuma et al., 2015)	N.S.	32 and 76 years	Mitochondrial myopathy, limb weakness and general fatigue, high CK, myalgia (n=2).	16 non-pathogenic mtDNA alterations[i]: Pathogenic N.S.	Accumulation of mitochondria, vacuolated mitochondria.

Chapter 10. References

Abdullah, N., Padmanarayana, M., Marty, N.J. and Johnson, C.P. (2014) 'Quantitation of the calcium and membrane binding properties of the C2 domains of dysferlin', *Biophys J*, 106(2), pp. 382-9.

Abu-Amero, K., Al-Dhalaan, H., Bohlega, S., Hellani, A. and Taylor, R. (2009) 'A patient with typical clinical features of mitochondrial encephalopathy, lactic acidosis and stroke-like episodes (MELAS) but without an obvious genetic cause: A case report', *Journal of Medical Case Reports*, 3 (no pagination)(77).

Adachi, M., Torii, J., Volk, B.W., Briet, P., Wolintz, A. and Schneck, L. (1973) 'Electron microscopic and enzyme histochemical studies of cerebellum, ocular and skeletal muscles in chronic progressive ophthalmoplegia with cerebellar ataxia', *Acta Neuropathologica*, 23(4), pp. 300-312.

Adhihetty, P.J., Ljubicic, V., Menzies, K.J. and Hood, D.A. (2005) 'Differential susceptibility of subsarcolemmal and intermyofibrillar mitochondria to apoptotic stimuli', *American Journal of Physiology - Cell Physiology*, 289(4), pp. C994-C1001.

Afifi, A.K., Ibrahim, M.Z.M., Bergman, R.A., Haydar, N.A., Mire, J., Bahuth, N. and Kaylani, F. (1972) 'Morphologic features of hypermetabolic mitochondrial disease. A light microscopic, histochemical and electron microscopic study', *Journal of the Neurological Sciences*, 15(3), pp. 271-290.

Ahmad, T., Aggarwal, K., Pattnaik, B., Mukherjee, S., Sethi, T., Tiwari, B.K., Kumar, M., Micheal, A., Mabalirajan, U., Ghosh, B., Sinha Roy, S. and Agrawal, A. (2013) 'Computational classification of mitochondrial shapes reflects stress and redox state', *Cell Death Dis*, 4, p. e461.

Al-Dosary, M., Whittaker, R.G., Haughton, J., McFarland, R., Goodship, J., Turnbull, D.M. and Taylor, R.W. (2009) 'Neuromuscular disease presentation with three genetic defects involving two genomes', *Neuromuscular Disorders*, 19(12), pp. 841-844.

Alexander, C., Votruba, M., Pesch, U.E.A., Thiselton, D.L., Mayer, S., Moore, A., Rodriguez, M., Kellner, U., Leo-Kottler, B., Auburger, G., Bhattacharya, S.S. and Wissinger, B. (2000) 'OPA1, encoding a dynamin-related GTPase, is mutated in autosomal dominant optic atrophy linked to chromosome 3q28', *Nat Genet*, 26(2), pp. 211-215.

Ali, N., Woodward, C.E., Sweeney, M., Phadke, R., Holton, J.L., Acheson, J., Plant, G.T. and Bremner, F.D. (2010) 'Pupillary dysfunction in an atypical case of mitochondrial myopathy with tubular aggregates', *J Neuroophthalmol*, 30(2), pp. 153-6.

Altmann, J., Buchner, B., Nadaj-Pakleza, A., Schafer, J., Jackson, S., Lehmann, D., Deschauer, M., Kopajtich, R., Lautenschlager, R., Kuhn, K.A., Karle, K., Schols, L., Schulz, J.B., Weis, J., Prokisch, H., Kornblum, C., Claeys, K.G. and Klopstock, T. (2016) 'Expanded phenotypic spectrum of the m.8344A>G "MERRF" mutation: data from the German mitoNET registry', *J Neurol*, 263(5), pp. 961-72.

Amati-Bonneau, P., Valentino, M.L., Reynier, P., Gallardo, M.E., Bornstein, B., Boissiere, A., Campos, Y., Rivera, H., de la Aleja, J.G., Carroccia, R., Iommarini, L., Labauge, P., Figarella-Branger, D., Marcorelles, P., Furby, A., Beauvais, K., Letournel, F., Liguori, R., La

Morgia, C., Montagna, P., Liguori, M., Zanna, C., Rugolo, M., Cossarizza, A., Wissinger, B., Verny, C., Schwarzenbacher, R., Martin, M.A., Arenas, J., Ayuso, C., Garesse, R., Lenaers, G., Bonneau, D. and Carelli, V. (2008) 'OPA1 mutations induce mitochondrial DNA instability and optic atrophy 'plus' phenotypes', *Brain*, 131(Pt 2), pp. 338-51.

Amoscato, A.A., Sparvero, L.J., He, R.R., Watkins, S., Bayir, H. and Kagan, V.E. (2014) 'Imaging Mass Spectrometry of Diversified Cardiolipin Molecular Species in the Brain', *Analytical Chemistry*, 86(13), pp. 6587-6595.

Anderson, S., Bankier, A.T., Barrell, B.G., de Bruijn, M.H., Coulson, A.R., Drouin, J., Eperon, I.C., Nierlich, D.P., Roe, B.A., Sanger, F., Schreier, P.H., Smith, A.J., Staden, R. and Young, I.G. (1981) 'Sequence and organization of the human mitochondrial genome', *Nature*, 290(5806), pp. 457-65.

Andrews, R.M., Kubacka, I., Chinnery, P.F., Lightowlers, R.N., Turnbull, D.M. and Howell, N. (1999) 'Reanalysis and revision of the Cambridge reference sequence for human mitochondrial DNA', *Nat Genet*, 23(2), p. 147.

Angelini, C., Melacini, P., Valente, M.L., Reichmann, H., Carrozzo, R., Fanin, M., Vergani, L., Boffa, G.M., Martinuzzi, A. and Fasoli, G. (1993) 'Hypertrophic cardiomyopathy with mitochondrial myopathy - A new phenotype of complex II defect', *Japanese Heart Journal*, 34(1), pp. 63-77.

Arruda, W.O., Torres, L.F., Lombes, A., DiMauro, S., Cardoso, B.A., Teive, H.A., De Paola, D. and Seixas, R.R. (1990) 'Mitochondrial myopathy and myoclonic epilepsy', *Arquivos de neuro-psiquiatria*, 48(1), pp. 32-43.

Ascaso, F.J., Lopez-Gallardo, E., Del Prado, E., Ruiz-Pesini, E. and Montoya, J. (2010) 'Macular lesion resembling adult-onset vitelliform macular dystrophy in Kearns-Sayre syndrome with multiple mtDNA deletions', *Clinical and Experimental Ophthalmology*, 38(8), pp. 812-816.

Bacman, S.R., Williams, S.L. and Moraes, C.T. (2009) 'Intra- and inter-molecular recombination of mitochondrial DNA after in vivo induction of multiple double-strand breaks', *Nucleic Acids Research*, 37(13), pp. 4218-4226.

Baines, H.L., Stewart, J.B., Stamp, C., Zupanic, A., Kirkwood, T.B., Larsson, N.G., Turnbull, D.M. and Greaves, L.C. (2014) 'Similar patterns of clonally expanded somatic mtDNA mutations in the colon of heterozygous mtDNA mutator mice and ageing humans', *Mech Ageing Dev*, 139, pp. 22-30.

Bakeeva, L.E., Chentsov Yu, S. and Skulachev, V.P. (1978) 'Mitochondrial framework (reticulum mitochondriale) in rat diaphragm muscle', *Biochim Biophys Acta*, 501(3), pp. 349-69.

Bang, B.G. and Bang, F.B. (1957) 'Graphic reconstruction of the third dimension from serial electron microphotographs', *Journal of Ultrastructure Research*, 1(2), pp. 138-146.

Bansal, D. and Campbell, K.P. (2004) 'Dysferlin and the plasma membrane repair in muscular dystrophy', *Trends in Cell Biology*, 14(4), pp. 206-213.

Bansal, D., Miyake, K., Vogel, S.S., Groh, S., Chen, C.C., Williamson, R., McNeil, P.L. and Campbell, K.P. (2003) 'Defective membrane repair in dysferlin-deficient muscular dystrophy', *Nature*, 423(6936), pp. 168-72.

Baric, I., Fumic, K., Petkovic Ramadza, D., Sperl, W., Zimmermann, F.A., Muacevic-Katanec, D., Mitrovic, Z., Pazanin, L., Cvitanovic Sojat, L., Kekez, T., Reiner, Z. and Mayr, J.A. (2013) 'Mitochondrial myopathy associated with a novel 5522G>A mutation in the mitochondrial tRNA(Trp) gene', *Eur J Hum Genet*, 21(8), pp. 871-5.

Barrell, B.G., Anderson, S., Bankier, A.T., de Bruijn, M.H., Chen, E., Coulson, A.R., Drouin, J., Eperon, I.C., Nierlich, D.P., Roe, B.A., Sanger, F., Schreier, P.H., Smith, A.J., Staden, R. and Young, I.G. (1980) 'Different pattern of codon recognition by mammalian mitochondrial tRNAs', *Proceedings of the National Academy of Sciences*, 77(6), pp. 3164-3166.

Bartz, R.R., Suliman, H.B. and Piantadosi, C.A. (2015) 'Redox mechanisms of cardiomyocyte mitochondrial protection', *Frontiers in Physiology*, 6, p. 291.

Bashir, R., Britton, S., Strachan, T., Keers, S., Vafiadaki, E., Lako, M., Richard, I., Marchand, S., Bourg, N., Argov, Z., Sadeh, M., Mahjneh, I., Marconi, G., Passos-Bueno, M.R., Moreira Ede, S., Zatz, M., Beckmann, J.S. and Bushby, K. (1998) 'A gene related to Caenorhabditis elegans spermatogenesis factor fer-1 is mutated in limb-girdle muscular dystrophy type 2B', *Nat Genet*, 20(1), pp. 37-42.

Bashir, R., Strachan, T., Keers, S., Stephenson, A., Mahjneh, I., Marconi, G., Nashef, L. and Bushby, K.M. (1994) 'A gene for autosomal recessive limb-girdle muscular dystrophy maps to chromosome 2p', *Hum Mol Genet*, 3(3), pp. 455-7.

Baskin, E., Selda Bayrakci, U., Alehan, F., Ozdemir, H., Oner, A., Horvath, R., Vega-Warner, V., Hildebrandt, F. and Ozaltin, F. (2011) 'Respiratory-chain deficiency presenting as diffuse mesangial sclerosis with NPHS3 mutation', *Pediatr Nephrol*, 26(7), pp. 1157-61.

Bastiaensen, L.A.K., Jaspar, H.H.J. and Stadhouders, A.M. (1979) 'Ophthalmoplegia-plus', *Documenta Ophthalmologica*, 46(2), pp. 365-380.

Baughman, J.M., Perocchi, F., Girgis, H.S., Plovanich, M., Belcher-Timme, C.A., Sancak, Y., Bao, X.R., Strittmatter, L., Goldberger, O., Bogorad, R.L., Koteliansky, V. and Mootha, V.K. (2011) 'Integrative genomics identifies MCU as an essential component of the mitochondrial calcium uniporter', *Nature*, 476(7360), pp. 341-345.

Bender, A., Krishnan, K.J., Morris, C.M., Taylor, G.A., Reeve, A.K., Perry, R.H., Jaros, E., Hersheson, J.S., Betts, J., Klopstock, T., Taylor, R.W. and Turnbull, D.M. (2006) 'High levels of mitochondrial DNA deletions in substantia nigra neurons in aging and Parkinson disease', *Nat Genet*, 38(5), pp. 515-7.

Beraud, N., Pelloux, S., Usson, Y., Kuznetsov, A.V., Ronot, X., Tourneur, Y. and Saks, V. (2009) 'Mitochondrial dynamics in heart cells: very low amplitude high frequency fluctuations in adult cardiomyocytes and flow motion in non beating Hl-1 cells', *J Bioenerg Biomembr*, 41(2), pp. 195-214.

Bereiter-Hahn, J. (1978) 'Intracellular motility of mitochondria: role of the inner compartment in migration and shape changes of mitochondria in XTH-cells', *J Cell Sci*, 30, pp. 99-115.

Bereiter-Hahn, J. and Voth, M. (1994) 'Dynamics of mitochondria in living cells: shape changes, dislocations, fusion, and fission of mitochondria', *Microsc Res Tech*, 27(3), pp. 198-219.

Berg, J., Tymoczko, J. and Stryer, L. (2012a) *Biochemsitry 7th edition. Glycolysis and gluconeogenesis.* New York: W.H. Freeman and Comapny.

Berg, J., Tymoczko, J. and Stryer, L. (2012b) *Biochemsitry 7th edition. Oxidative phosphorylation.* New York: W.H. Freeman and Comapny.

Berg, J., Tymoczko, J. and Stryer, L. (2012c) *Biochemsitry 7th edition. The citric acid cycle.* New York: W.H. Freeman and Comapny.

Black, J.T., Judge, D., Demers, L. and Gordon, S. (1975) 'Ragged-red fibers: A biochemical and morphological study', *Journal of the Neurological Sciences*, 26(4), pp. 479-488.

Blakely, E.L., Butterworth, A., Hadden, R.D., Bodi, I., He, L., McFarland, R. and Taylor, R.W. (2012) 'MPV17 mutation causes neuropathy and leukoencephalopathy with multiple mtDNA deletions in muscle', *Neuromuscul Disord*, 22(7), pp. 587-91.

Bleazard, W., McCaffery, J.M., King, E.J., Bale, S., Mozdy, A., Tieu, Q., Nunnari, J. and Shaw, J.M. (1999) 'The dynamin-related GTPase Dnm1 regulates mitochondrial fission in yeast', *Nature Cell Biology*, 1(5), pp. 298-304.

Bogenhagen, D. and Clayton, D.A. (1977) 'Mouse L cell mitochondrial DNA molecules are selected randomly for replication throughout the cell cycle', *Cell*, 11(4), pp. 719-27.

Boldogh, I.R. and Pon, L.A. (2007) 'Mitochondria on the move', *Trends in Cell Biology*, 17(10), pp. 502-510.

Bonawitz, N.D., Clayton, D.A. and Shadel, G.S. (2006) 'Initiation and beyond: multiple functions of the human mitochondrial transcription machinery', *Mol Cell*, 24(6), pp. 813-25.

Bornhovd, C., Vogel, F., Neupert, W. and Reichert, A.S. (2006) 'Mitochondrial membrane potential is dependent on the oligomeric state of F1F0-ATP synthase supracomplexes', *J Biol Chem*, 281(20), pp. 13990-8.

Bostan, A., Glibert, G., Dachy, B. and Dan, B. (2012) 'Novel mutation in spacer region of POLG associated with ataxia neuropathy spectrum and gastroparesis', *Autonomic Neuroscience: Basic and Clinical*, 170(1-2), pp. 70-72.

Bottinger, L., Horvath, S.E., Kleinschroth, T., Hunte, C., Daum, G., Pfanner, N. and Becker, T. (2012) 'Phosphatidylethanolamine and cardiolipin differentially affect the stability of mitochondrial respiratory chain supercomplexes', *J Mol Biol*, 423(5), pp. 677-86.

Bowes, T. and Gupta, R.S. (2008) 'Novel mitochondrial extensions provide evidence for a link between microtubule-directed movement and mitochondrial fission', *Biochem Biophys Res Commun*, 376(1), pp. 40-5.

Boyman, L., Williams, G.S., Khananshvili, D., Sekler, I. and Lederer, W.J. (2013) 'NCLX: the mitochondrial sodium calcium exchanger', *J Mol Cell Cardiol*, 59, pp. 205-13.

Brandt, U. (2006) 'Energy converting NADH:quinone oxidoreductase (complex I)', *Annu Rev Biochem*, 75, pp. 69-92.

Braun, T. and Gautel, M. (2011) 'Transcriptional mechanisms regulating skeletal muscle differentiation, growth and homeostasis', *Nat Rev Mol Cell Biol*, 12(6), pp. 349-61.

Bresolin, N., Zeviani, M., Bonilla, E., Miller, R.H., Leech, R.W., Shanske, S., Nakagawa, M. and DiMauro, S. (1985) 'Fatal infantile cytochrome c oxidase deficiency: decrease of immunologically detectable enzyme in muscle', *Neurology*, 35(6), pp. 802-12.

Brierley, E.J., Johnson, M.A., Lightowlers, R.N., James, O.F. and Turnbull, D.M. (1998) 'Role of mitochondrial DNA mutations in human aging: implications for the central nervous system and muscle', *Ann Neurol*, 43(2), pp. 217-23.

Brini, M. and Carafoli, E. (2009) 'Calcium Pumps in Health and Disease', *Physiological Reviews*, 89(4), pp. 1341-1378.

Brown, D.A. and Berg, H.C. (1974) 'Temporal stimulation of chemotaxis in Escherichia coli', *Proc Natl Acad Sci U S A*, 71(4), pp. 1388-92.

Brown, D.T., Samuels, D.C., Michael, E.M., Turnbull, D.M. and Chinnery, P.F. (2001) 'Random genetic drift determines the level of mutant mtDNA in human primary oocytes', *Am J Hum Genet*, 68(2), pp. 533-6.

Brown, T.A., Tkachuk, A.N., Shtengel, G., Kopek, B.G., Bogenhagen, D.F., Hess, H.F. and Clayton, D.A. (2011) 'Superresolution Fluorescence Imaging of Mitochondrial Nucleoids Reveals Their Spatial Range, Limits, and Membrane Interaction', *Molecular and Cellular Biology*, 31(24), pp. 4994-5010.

Brown, W.M., George, M. and Wilson, A.C. (1979) 'Rapid evolution of animal mitochondrial DNA', *Proceedings of the National Academy of Sciences*, 76(4), pp. 1967-1971.

Bua, E., Johnson, J., Herbst, A., Delong, B., McKenzie, D., Salamat, S. and Aiken, J.M. (2006) 'Mitochondrial DNA-deletion mutations accumulate intracellularly to detrimental levels in aged human skeletal muscle fibers', *Am J Hum Genet*, 79(3), pp. 469-80.

Bukau, B., Weissman, J. and Horwich, A. (2006) 'Molecular chaperones and protein quality control', *Cell*, 125(3), pp. 443-51.

Burke, R.E., Levine, D.N. and Zajac, F.E., 3rd (1971) 'Mammalian motor units: physiological-histochemical correlation in three types in cat gastrocnemius', *Science*, 174(4010), pp. 709-12.

Cadete, V.J., Deschenes, S., Cuillerier, A., Brisebois, F., Sugiura, A., Vincent, A., Turnbull, D., Picard, M., McBride, H.M. and Burelle, Y. (2016) 'Formation of mitochondrial-derived vesicles is an active and physiologically relevant mitochondrial quality control process in the cardiac system', *J Physiol*, 594(18), pp. 5343-62.

Campbell, G., Krishnan, K.J., Deschauer, M., Taylor, R.W. and Turnbull, D.M. (2014) 'Dissecting the mechanisms underlying the accumulation of mitochondrial DNA deletions in human skeletal muscle', *Hum Mol Genet*, 23(17), pp. 4612-20.

Candé, C., Cohen, I., Daugas, E., Ravagnan, L., Larochette, N., Zamzami, N. and Kroemer, G. (2002) 'Apoptosis-inducing factor (AIF): a novel caspase-independent death effector released from mitochondria', *Biochimie*, 84(2–3), pp. 215-222.

Canto, C., Gerhart-Hines, Z., Feige, J.N., Lagouge, M., Noriega, L., Milne, J.C., Elliott, P.J., Puigserver, P. and Auwerx, J. (2009) 'AMPK regulates energy expenditure by modulating NAD+ metabolism and SIRT1 activity', *Nature*, 458(7241), pp. 1056-60.

Cardaioli, E., Pozzo, P.D., Cerase, A., Sicurelli, F., Malandrini, A., Stefano, N.D., Stromillo, M.L., Battisti, C., Dotti, M.T. and Federico, A. (2006) 'Rapidly progressive neurodegeneration in a case with the 7472insC mutation and the A7472C polymorphism in the mtDNA tRNAser(UCN) gene', *Neuromuscular Disorders*, 16(1), pp. 26-31.

Cardenas, J.F. and Amato, R.S. (2010) 'Compound heterozygous polymerase gamma gene mutation in a patient with alpers disease', *Seminars in Pediatric Neurology*, 17(1), pp. 62-64.

Carta, A., Carelli, V., D'Adda, T., Ross-Cisneros, F.N. and Sadun, A.A. (2005) 'Human extraocular muscles in mitochondrial diseases: comparing chronic progressive external ophthalmoplegia with Leber's hereditary optic neuropathy', *Br J Ophthalmol*, 89(7), pp. 825-7.

Carta, A., D'Adda, T., Carrara, F. and Zeviani, M. (2000) 'Ultrastructural analysis of extraocular muscle in chronic progressive external ophthalmoplegia', *Arch Ophthalmol*, 118(10), pp. 1441-5.

Castro-Gago, M., Alonso, A., Pintos-Martínez, E., Beiras-Iglesias, A., Campos, Y., Arenas, J., Novo-Rodríguez, M.I. and Eirís-Puñal, J. (1999) 'Congenital hydranencephalic-hydrocephalic syndrome associated with mitochondrial dysfunction', *Journal of Child Neurology*, 14(2), pp. 131-135.

Cavalier-Smith, T. (1987) 'The Origin of Eukaryote and Archaebacterial Cells', *Annals of the New York Academy of Sciences*, 503(1), pp. 17-54.

Cenacchi, G., Valentina, P., Marina, F., Elena, P. and Corrado, A. (2011) 'Comparison of muscle ultrastructure in myasthenia gravis with anti-MuSK and anti-AChR antibodies', *Journal of Neurology*, 258(5), pp. 746-752.

Chan, D.C. (2006) 'Mitochondrial fusion and fission in mammals', *Annu Rev Cell Dev Biol*, 22, pp. 79-99.

Chance, B., Estabrook, R.W. and Lee, C.-p. (1963) 'Electron Transport in the Oxysome', *Science*, 140(3565), pp. 379-380.

Chandel, N.S., Maltepe, E., Goldwasser, E., Mathieu, C.E., Simon, M.C. and Schumacker, P.T. (1998) 'Mitochondrial reactive oxygen species trigger hypoxia-induced transcription', *Proceedings of the National Academy of Sciences of the United States of America*, 95(20), pp. 11715-11720.

Chang, C.R. and Blackstone, C. (2010) 'Dynamic regulation of mitochondrial fission through modification of the dynamin-related protein Drp1', *Ann N Y Acad Sci*, 1201, pp. 34-9.

Chang, D.D. and Clayton, D.A. (1984) 'Precise identification of individual promoters for transcription of each strand of human mitochondrial DNA', *Cell*, 36(3), pp. 635-43.

Chappell, J.B. and Crofts, A.R. (1965) 'Calcium ion accumulation and volume changes of isolated liver mitochondria. Calcium ion-induced swelling.', *Biochem J*, 95, pp. 378-86.

Charge, S.B. and Rudnicki, M.A. (2004) 'Cellular and molecular regulation of muscle regeneration', *Physiol Rev*, 84(1), pp. 209-38.

Chatfield, K.C., Coughlin, C.R., Friederich, M.W., Gallagher, R.C., Hesselberth, J.R., Lovell, M.A., Ofman, R., Swanson, M.A., Thomas, J.A., Wanders, R.J.A., Wartchow, E.P. and Van Hove, J.L.K. (2015) 'Mitochondrial energy failure in HSD10 disease is due to defective mtDNA transcript processing', *Mitochondrion*, 21, pp. 1-10.

Chen, H., Chomyn, A. and Chan, D.C. (2005) 'Disruption of fusion results in mitochondrial heterogeneity and dysfunction', *J Biol Chem*, 280(28), pp. 26185-92.

Chen, H., Detmer, S.A., Ewald, A.J., Griffin, E.E., Fraser, S.E. and Chan, D.C. (2003) 'Mitofusins Mfn1 and Mfn2 coordinately regulate mitochondrial fusion and are essential for embryonic development', *The Journal of Cell Biology*, 160(2), pp. 189-200.

Chen, H., McCaffery, J.M. and Chan, D.C. (2007) 'Mitochondrial fusion protects against neurodegeneration in the cerebellum', *Cell*, 130(3), pp. 548-62.

Chen, H., Vermulst, M., Wang, Y.E., Chomyn, A., Prolla, T.A., McCaffery, J.M. and Chan, D.C. (2010) 'Mitochondrial fusion is required for mtDNA stability in skeletal muscle and tolerance of mtDNA mutations', *Cell*, 141(2), pp. 280-289.

Chen, T., Pu, C., Shi, Q., Wang, Q., Cong, L., Liu, J., Luo, H., Fei, L., Tang, W. and Yu, S. (2014) 'Chronic progressive external ophthalmoplegia with inflammatory myopathy', *Int J Clin Exp Pathol*, 7(12), pp. 8887-92.

Chen, Y., Azad, M.B. and Gibson, S.B. (2009) 'Superoxide is the major reactive oxygen species regulating autophagy', *Cell Death Differ*, 16(7), pp. 1040-52.

Chi, C.S., Lee, H.F., Tsai, C.R., Lee, H.J. and Chen, L.H. (2010) 'Clinical manifestations in children with mitochondrial diseases', *Pediatr Neurol*, 43(3), pp. 183-9.

Cipolat, S., de Brito, O.M., Dal Zilio, B. and Scorrano, L. (2004) 'OPA1 requires mitofusin 1 to promote mitochondrial fusion', *Proceedings of the National Academy of Sciences of the United States of America*, 101(45), pp. 15927-15932.

Claeys, K.G., Fardeau, M., Schroder, R., Suominen, T., Tolksdorf, K., Behin, A., Dubourg, O., Eymard, B., Maisonobe, T., Stojkovic, T., Faulkner, G., Richard, P., Vicart, P., Udd, B., Voit, T. and Stoltenburg, G. (2008) 'Electron microscopy in myofibrillar myopathies reveals clues to the mutated gene', *Neuromuscular Disorders*, 18(8), pp. 656-666.

Claude, A. and Fullam, E.F. (1945) 'An Electron Microscope Study of Isolated Mitochondria: Method and Preliminary Results', *J Exp Med*, 81(1), pp. 51-62.

Clay Montier, L.L., Deng, J.J. and Bai, Y. (2009) 'Number matters: control of mammalian mitochondrial DNA copy number', *Journal of Genetics and Genomics*, 36(3), pp. 125-131.

Clayton, D.A. (1982) 'Replication of animal mitochondrial DNA', *Cell*, 28(4), pp. 693-705.

Clayton, D.A., Doda, J.N. and Friedberg, E.C. (1974) 'The absence of a pyrimidine dimer repair mechanism in mammalian mitochondria', *Proc Natl Acad Sci U S A*, 71(7), pp. 2777-81.

Cogliati, S., Enriquez, J.A. and Scorrano, L. (2016) 'Mitochondrial Cristae: Where Beauty Meets Functionality', *Trends in Biochemical Sciences*, 41(3), pp. 261-273.

Coller, H.A., Khrapko, K., Bodyak, N.D., Nekhaeva, E., Herrero-Jimenez, P. and Thilly, W.G. (2001) 'High frequency of homoplasmic mitochondrial DNA mutations in human tumors can be explained without selection', *Nat Genet*, 28(2), pp. 147-50.

Colombo, A., Merelli, E., Sola, P., Panzetti, P., Quaglino Jr, D. and Fornieri, C. (1988) 'Mitochondrial oculoskeletal myopathy: case report', *The Italian Journal of Neurological Sciences*, 9(4), pp. 385-389.

Conway, L.J., Robertson, T.E., McGill, J.J. and Hanson, J.P. (2011) 'MELAS syndrome in an Indigenous Australian woman', *Medical Journal of Australia*, 195(10), pp. 581-582.

Coquet, M., Degoul, F., Vital, A., Malgat, M., Mazat, J.P., Louvet-Giendaj, C., Fontan, D., Tison, F., Diry, M. and Marsac, C. (1993) 'Merrf family with 8344 mutation in tRNA (lys). Evidence of a mitochondrial vasculopathy in muscle biopsies', *Neuromuscul Disord*, 3(5-6), pp. 593-7.

Cory, S. and Adams, J.M. (2002) 'The Bcl2 family: regulators of the cellular life-or-death switch', *Nat Rev Cancer*, 2(9), pp. 647-56.

Coulbault, L., Herlicoviez, D., Chapon, F., Read, M.H., Penniello, M.J., Reynier, P., Fayet, G., Lombès, A., Jauzac, P. and Allouche, S. (2005) 'A novel mutation in the mitochondrial tRNAAsn gene associated with a lethal disease', *Biochemical and Biophysical Research Communications*, 329(3), pp. 1152-1154.

Cree, L.M., Samuels, D.C., de Sousa Lopes, S.C., Rajasimha, H.K., Wonnapinij, P., Mann, J.R., Dahl, H.-H.M. and Chinnery, P.F. (2008) 'A reduction of mitochondrial DNA molecules during embryogenesis explains the rapid segregation of genotypes', *Nat Genet*, 40(2), pp. 249-254.

Crick, F.H.C. (1966) 'Codon—anticodon pairing: The wobble hypothesis', *Journal of Molecular Biology*, 19(2), pp. 548-555.

Crosby, T.W. and Chou, S.M. (1974) '"Ragged-red" fibers in Leigh's disease', *Neurology*, 24(1), pp. 49-54.

Csordás, G. and Hajnóczky, G. (2003) 'Plasticity of Mitochondrial Calcium Signaling', *Journal of Biological Chemistry*, 278(43), pp. 42273-42282.

Cui, H., Kong, Y. and Zhang, H. (2012) 'Oxidative Stress, Mitochondrial Dysfunction, and Aging', *Journal of Signal Transduction*, 2012, p. 13.

Daems, W.T. and Wisse, E. (1966) 'Shape and attachment of the cristae mitochondriales in mouse hepatic cell mitochondria', *J Ultrastruct Res*, 16(1), pp. 123-40.

Dahl, R., Larsen, S., Dohlmann, T.L., Qvortrup, K., Helge, J.W., Dela, F. and Prats, C. (2015) 'Three-dimensional reconstruction of the human skeletal muscle mitochondrial network as a tool to assess mitochondrial content and structural organization', *Acta Physiol (Oxf)*, 213(1), pp. 145-55.

Damas, J., Carneiro, J., Amorim, A. and Pereira, F. (2014a) 'MitoBreak: the mitochondrial DNA breakpoints database', *Nucleic Acids Research*, 42(D1), pp. D1261-D1268.

Damas, J., Samuels, D.C., Carneiro, J., Amorim, A. and Pereira, F. (2014b) 'Mitochondrial DNA Rearrangements in Health and Disease—A Comprehensive Study', *Human Mutation*, 35(1), pp. 1-14.

Daum, B., Walter, A., Horst, A., Osiewacz, H.D. and Kühlbrandt, W. (2013) 'Age-dependent dissociation of ATP synthase dimers and loss of inner-membrane cristae in mitochondria', *Proceedings of the National Academy of Sciences*, 110(38), pp. 15301-15306.

Davis, A.F. and Clayton, D.A. (1996) 'In situ localization of mitochondrial DNA replication in intact mammalian cells', *J Cell Biol*, 135(4), pp. 883-93.

Davis, K.A. and Hatefi, Y. (1971) 'Succinate dehydrogenase. I. Purification, molecular properties, and substructure', *Biochemistry*, 10(13), pp. 2509-16.

de Brito, O.M. and Scorrano, L. (2008) 'Mitofusin 2 tethers endoplasmic reticulum to mitochondria', *Nature*, 456(7222), pp. 605-610.

de Grey, A.D. (1997) 'A proposed refinement of the mitochondrial free radical theory of aging', *Bioessays*, 19(2), pp. 161-6.

De Kremer, R.D., Paschini-Capra, A., Bacman, S., Argarana, C., Civallero, G., Kelley, R.I., Guelbert, N., Latini, A., Noher de Halac, I., Giner-Ayala, A., Johnston, J., Proujansky, R., Gonzalez, I., Depetris-Boldini, C., Oller-Ramirez, A., Angaroni, C., Theaux, R.A., Hliba, E. and Juaneda, E. (2001) 'Barth's syndrome-like disorder: a new phenotype with a maternally inherited A3243G substitution of mitochondrial DNA (MELAS mutation)', *Am J Med Genet*, 99(2), pp. 83-93.

De Stefani, D., Raffaello, A., Teardo, E., Szabo, I. and Rizzuto, R. (2011) 'A forty-kilodalton protein of the inner membrane is the mitochondrial calcium uniporter', *Nature*, 476(7360), pp. 336-340.

DeBrosse, S., Ubogu, E.E., Yaniglos, S., Hassan, M.O. and Leigh, R.J. (2009) 'Dynamic properties of eye movements in mitochondrial chronic progressive external ophthalmoplegia', *Eye (Lond)*, 23(2), pp. 382-8.

Deerinck T, Bushong E, Thor A and M, E. (2010) 'NCMIR methods for 3D EM: A new protocol for preparation of biological specimens for serial block face scanning electron microscopy', *Micrscopy*, pp. 6-8.

Delettre, C., Griffoin, J.-M., Kaplan, J., Dollfus, H., Lorenz, B., Faivre, L., Lenaers, G., Belenguer, P. and Hamel, C.P. (2001) 'Mutation spectrum and splicing variants in the OPA1 gene', *Human Genetics*, 109(6), pp. 584-591.

Denk, W. and Horstmann, H. (2004) 'Serial Block-Face Scanning Electron Microscopy to Reconstruct Three-Dimensional Tissue Nanostructure', *PLoS Biology*, 2(11), p. e329.

Deschauer, M., Swalwell, H., Strauss, M., Zierz, S. and Taylor, R.W. (2006) 'Novel mitochondrial transfer RNA(Phe) gene mutation associated with late-onset neuromuscular disease', *Arch Neurol*, 63(6), pp. 902-5.

Di Lisa, F., Menabo, R., Canton, M., Barile, M. and Bernardi, P. (2001) 'Opening of the mitochondrial permeability transition pore causes depletion of mitochondrial and cytosolic NAD+ and is a causative event in the death of myocytes in postischemic reperfusion of the heart', *J Biol Chem*, 276(4), pp. 2571-5.

Dias-Tosta, E. (1988) 'Chronic progressive external ophthalmoplegia. II. A qualitative and quantitative electronmicroscopy study of skeletal muscles', *Arquivos de Neuro-Psiquiatria*, 46(2), pp. 143-155.

Diaz, F., Bayona-Bafaluy, M.P., Rana, M., Mora, M., Hao, H. and Moraes, C.T. (2002) 'Human mitochondrial DNA with large deletions repopulates organelles faster than full-length genomes under relaxed copy number control', *Nucleic Acids Res*, 30(21), pp. 4626-33.

Dinopoulos, A., Smeitink, J. and ter Laak, H. (2005) 'Unusual features of mitochondrial degeneration in skeletal muscle of patients with nuclear complex I mutation', *Acta Neuropathol*, 110(2), pp. 199-202.

Dold, T., Reimann, J., Zsurka, G., Kunz, W.S. and Kornblum, C. (2012) 'On mitochondrial function and genome integrity in myofibrillar myopathies', *Neuromuscular Disorders*, 22(9-10), pp. 822-822.

Domènech, Ò., Morros, A., Cabañas, M.E., Teresa Montero, M. and Hernández-Borrell, J. (2007) 'Supported planar bilayers from hexagonal phases', *Biochimica et Biophysica Acta (BBA) - Biomembranes*, 1768(1), pp. 100-106.

Dong, D.W., Pereira, F., Barrett, S.P., Kolesar, J.E., Cao, K., Damas, J., Yatsunyk, L.A., Johnson, F.B. and Kaufman, B.A. (2014) 'Association of G-quadruplex forming sequences with human mtDNA deletion breakpoints', *BMC Genomics*, 15, p. 677.

Droge, W. (2002) 'Free radicals in the physiological control of cell function', *Physiol Rev*, 82(1), pp. 47-95.

Dubey, G.P. and Ben-Yehuda, S. (2011) 'Intercellular nanotubes mediate bacterial communication', *Cell*, 144(4), pp. 590-600.

Dubowitz, V. (2007) *Muscle biopsy : a practical approach*. 3rd ed. edn. Edinburgh: Edinburgh : Elsevier Saunders.

Dudkina, N.V., Heinemeyer, J., Keegstra, W., Boekema, E.J. and Braun, H.P. (2005) 'Structure of dimeric ATP synthase from mitochondria: an angular association of monomers induces the strong curvature of the inner membrane', *FEBS Lett*, 579(25), pp. 5769-72.

Duvezin-Caubet, S., Jagasia, R., Wagener, J., Hofmann, S., Trifunovic, A., Hansson, A., Chomyn, A., Bauer, M.F., Attardi, G., Larsson, N.G., Neupert, W. and Reichert, A.S. (2006) 'Proteolytic processing of OPA1 links mitochondrial dysfunction to alterations in mitochondrial morphology', *J Biol Chem*, 281(49), pp. 37972-9.

Eble, K.S., Coleman, W.B., Hantgan, R.R. and Cunningham, C.C. (1990) 'Tightly associated cardiolipin in the bovine heart mitochondrial ATP synthase as analyzed by 31P nuclear magnetic resonance spectroscopy', *J Biol Chem*, 265(32), pp. 19434-40.

Efremov, R.G., Baradaran, R. and Sazanov, L.A. (2010) 'The architecture of respiratory complex I', *Nature*, 465(7297), pp. 441-5.

Efremov, R.G. and Sazanov, L.A. (2011) 'Structure of the membrane domain of respiratory complex I', *Nature*, 476(7361), pp. 414-20.

Ehses, S., Raschke, I., Mancuso, G., Bernacchia, A., Geimer, S., Tondera, D., Martinou, J.C., Westermann, B., Rugarli, E.I. and Langer, T. (2009) 'Regulation of OPA1 processing and mitochondrial fusion by m-AAA protease isoenzymes and OMA1', *Journal of Cell Biology*, 187(7), pp. 1023-1036.

Eisner, V., Lenaers, G. and Hajnóczky, G. (2014) 'Mitochondrial fusion is frequent in skeletal muscle and supports excitation–contraction coupling', *The Journal of Cell Biology*, 205(2), pp. 179-195.

Elson, J.L., Samuels, D.C., Johnson, M.A., Turnbull, D.M. and Chinnery, P.F. (2002) 'The length of cytochrome c oxidase-negative segments in muscle fibres in patients with mtDNA myopathy', *Neuromuscul Disord*, 12(9), pp. 858-64.

Elson, J.L., Samuels, D.C., Turnbull, D.M. and Chinnery, P.F. (2001) 'Random intracellular drift explains the clonal expansion of mitochondrial DNA mutations with age', *Am J Hum Genet*, 68(3), pp. 802-6.

Enns, G.M., Hoppel, C.L., DeArmond, S.J., Schelley, S., Bass, N., Weisiger, K., Horoupian, D. and Packman, S. (2005) 'Relationship of primary mitochondrial respiratory chain dysfunction to fiber type abnormalities in skeletal muscle', *Clin Genet*, 68(4), pp. 337-48.

Eppenberger-Eberhardt, M., Riesinger, I., Messerli, M., Schwarb, P., Muller, M., Eppenberger, H.M. and Wallimann, T. (1991) 'Adult rat cardiomyocytes cultured in creatine-deficient medium display large mitochondria with paracrystalline inclusions, enriched for creatine kinase', *J Cell Biol*, 113(2), pp. 289-302.

Escovitz, W.H., Fox, T.R. and Levi-Setti, R. (1975) 'Scanning transmission ion microscope with a field ion source', *Proceedings of the National Academy of Sciences of the United States of America*, 72(5), pp. 1826-1828.

Esser, C., Ahmadinejad, N., Wiegand, C., Rotte, C., Sebastiani, F., Gelius-Dietrich, G., Henze, K., Kretschmann, E., Richly, E., Leister, D., Bryant, D., Steel, M.A., Lockhart, P.J., Penny, D. and Martin, W. (2004) 'A genome phylogeny for mitochondria among alpha-proteobacteria and a predominantly eubacterial ancestry of yeast nuclear genes', *Mol Biol Evol*, 21(9), pp. 1643-60.

Estaquier, J., Vallette, F., Vayssiere, J.L. and Mignotte, B. (2012) 'The mitochondrial pathways of apoptosis', *Adv Exp Med Biol*, 942, pp. 157-83.

Fagiolari, G., Sciacco, M., Chiveri, L., Lamperti, C., Comi, G.P., Scarlato, G., Moggio, M. and Prelle, A. (2002) 'Lack of apoptosis in patients with progressive external ophthalmoplegia and mutated adenine nucleotide translocator-1 gene', *Muscle and Nerve*, 26(2), pp. 265-269.

Falkenberg, M., Gaspari, M., Rantanen, A., Trifunovic, A., Larsson, N.G. and Gustafsson, C.M. (2002) 'Mitochondrial transcription factors B1 and B2 activate transcription of human mtDNA', *Nat Genet*, 31(3), pp. 289-94.

Fanin, M. and Angelini, C. (2002) 'Muscle pathology in dysferlin deficiency', *Neuropathol Appl Neurobiol*, 28(6), pp. 461-70.

Fannjiang, Y., Cheng, W.C., Lee, S.J., Qi, B., Pevsner, J., McCaffery, J.M., Hill, R.B., Basanez, G. and Hardwick, J.M. (2004) 'Mitochondrial fission proteins regulate programmed cell death in yeast', *Genes Dev*, 18(22), pp. 2785-97.

Faulkner, G., Pallavicini, A., Formentin, E., Comelli, A., Ievolella, C., Trevisan, S., Bortoletto, G., Scannapieco, P., Salamon, M., Mouly, V., Valle, G. and Lanfranchi, G. (1999) 'ZASP: a new Z-band alternatively spliced PDZ-motif protein', *J Cell Biol*, 146(2), pp. 465-75.

Faxen, K., Gilderson, G., Adelroth, P. and Brzezinski, P. (2005) 'A mechanistic principle for proton pumping by cytochrome c oxidase', *Nature*, 437(7056), pp. 286-9.

Federico, A., Manneschi, L., Meloni, M., Alessandrini, C., Bardelli, A.M., Dotti, M.T. and Sabatelli, P. (1988) 'Histochemical, ultrastructural and biochemical study of muscle mitochondria in Leber's hereditary optic atrophy', *Journal of Inherited Metabolic Disease*, 11(2 Supplement), pp. 193-197.

Ferreira, R., Vitorino, R., Alves, R.M., Appell, H.J., Powers, S.K., Duarte, J.A. and Amado, F. (2010) 'Subsarcolemmal and intermyofibrillar mitochondria proteome differences disclose functional specializations in skeletal muscle', *Proteomics*, 10(17), pp. 3142-54.

Ferrer, I. and Olive, M. (2008) 'Molecular pathology of myofibrillar myopathies', *Expert Rev Mol Med*, 10, p. e25.

Fillano, J.J., Goldenthal, M.J., Rhodes, C.H. and Marin-Garcia, J. (2002) 'Mitochondrial dysfunction in patients with hypotonia, epilepsy, autism, and developmental delay: HEADD syndrome', *J Child Neurol*, 17(6), pp. 435-9.

Fischer, D., Herasse, M., Bitoun, M., Barragan-Campos, H.M., Chiras, J., Laforet, P., Fardeau, M., Eymard, B., Guicheney, P. and Romero, N.B. (2006) 'Characterization of the muscle involvement in dynamin 2-related centronuclear myopathy', *Brain*, 129(Pt 6), pp. 1463-9.

Fitzsimons, R.B. and Tyer, H.D.D. (1980) 'A study of a myopathy presenting as idiopathic scoliosis. Multicore disease or mitochondrial myopathy?', *Journal of the Neurological Sciences*, 46(1), pp. 33-48.

Fleischer, S., Klouwen, H. and Brierley, G. (1961) 'Studies of the electron transfer system. 38. Lipid composition of purified enzyme preparations derived from beef heart mitochondria', *J Biol Chem*, 236, pp. 2936-41.

Frank, S., Gaume, B., Bergmann-Leitner, E.S., Leitner, W.W., Robert, E.G., Catez, F., Smith, C.L. and Youle, R.J. (2001) 'The role of dynamin-related protein 1, a mediator of mitochondrial fission, in apoptosis', *Dev Cell*, 1(4), pp. 515-25.

Frey, T.G. and Mannella, C.A. (2000) 'The internal structure of mitochondria', *Trends Biochem Sci*, 25(7), pp. 319-24.

Frezza, C., Cipolat, S., Martins de Brito, O., Micaroni, M., Beznoussenko, G.V., Rudka, T., Bartoli, D., Polishuck, R.S., Danial, N.N., De Strooper, B. and Scorrano, L. (2006) 'OPA1 controls apoptotic cristae remodeling independently from mitochondrial fusion', *Cell*, 126(1), pp. 177-89.

Friedman, J.R. and Nunnari, J. (2014) 'Mitochondrial form and function', *Nature*, 505(7483), pp. 335-43.

Fujioka, H., Tandler, B., Haldar, S.M., Jain, M.K. and Hoppel, C.L. (2013) 'String mitochondria in mouse soleus muscle', *Microscopy Research and Technique*, 76(3), pp. 237-241.

Fukuhara, N., Tokiguchi, S., Shirakawa, K. and Tsubaki, T. (1980) 'Myoclonus epilepsy associated with ragged-red fibres (mitochondrial abnormalities): disease entity or a syndrome? Light-and electron-microscopic studies of two cases and review of literature', *J Neurol Sci*, 47(1), pp. 117-33.

Fukui, H. and Moraes, C.T. (2009) 'Mechanisms of formation and accumulation of mitochondrial DNA deletions in aging neurons', *Hum Mol Genet*, 18(6), pp. 1028-36.

Gall, J.M., Wang, Z., Liesa, M., Molina, A., Havasi, A., Schwartz, J.H., Shirihai, O., Borkan, S.C. and Bonegio, R.G.B. (2012) 'Role of Mitofusin 2 in the Renal Stress Response', *PLOS ONE*, 7(1), p. e31074.

Garrido, N., Griparic, L., Jokitalo, E., Wartiovaara, J., van der Bliek, A.M. and Spelbrink, J.N. (2003) 'Composition and Dynamics of Human Mitochondrial Nucleoids', *Molecular Biology of the Cell*, 14(4), pp. 1583-1596.

Gayathri, N., Alefia, R., Nalini, A., Yasha, T., Anita, M., Santosh, V. and Shankar, S. (2011) 'Dysferlinopathy: Spectrum of pathological changes in skeletal muscle tissue', *Indian Journal of Pathology and Microbiology*, 54(2), pp. 350-354.

Gehlert, S., Bloch, W. and Suhr, F. (2015) 'Ca2+-dependent regulations and signaling in skeletal muscle: from electro-mechanical coupling to adaptation', *Int J Mol Sci*, 16(1), pp. 1066-95.

Gerdes, H.-H., Rustom, A. and Wang, X. (2013) 'Tunneling nanotubes, an emerging intercellular communication route in development', *Mechanisms of Development*, 130(6–8), pp. 381-387.

Gilbert, R.D. and Emms, M. (1996) 'Pearson's syndrome presenting with Fanconi syndrome', *Ultrastructural Pathology*, 20(5), pp. 473-475.

Giles, R.E., Blanc, H., Cann, H.M. and Wallace, D.C. (1980) 'Maternal inheritance of human mitochondrial DNA', *Proc Natl Acad Sci U S A*, 77(11), pp. 6715-9.

Giordano, C., Iommarini, L., Giordano, L., Maresca, A., Pisano, A., Valentino, M.L., Caporali, L., Liguori, R., Deceglie, S., Roberti, M., Fanelli, F., Fracasso, F., Ross-Cisneros, F.N., D'Adamo, P., Hudson, G., Pyle, A., Yu-Wai-Man, P., Chinnery, P.F., Zeviani, M., Salomao, S.R., Berezovsky, A., Belfort, R., Jr., Ventura, D.F., Moraes, M., Moraes Filho, M., Barboni, P., Sadun, F., De Negri, A., Sadun, A.A., Tancredi, A., Mancini, M., d'Amati, G., Loguercio Polosa, P., Cantatore, P. and Carelli, V. (2014) 'Efficient mitochondrial biogenesis drives incomplete penetrance in Leber's hereditary optic neuropathy', *Brain*, 137(Pt 2), pp. 335-53.

Giraud, M.F., Paumard, P., Soubannier, V., Vaillier, J., Arselin, G., Salin, B., Schaeffer, J., Brethes, D., di Rago, J.P. and Velours, J. (2002) 'Is there a relationship between the supramolecular organization of the mitochondrial ATP synthase and the formation of cristae?', *Biochim Biophys Acta*, 1555(1-3), pp. 174-80.

Gitschlag, B.L., Kirby, C.S., Samuels, D.C., Gangula, R.D., Mallal, S.A. and Patel, M.R. (2016) 'Homeostatic responses regulate selfish mitochondrial genome dynamics in C. elegans', *Cell Metab*, (In press).

Glancy, B., Hartnell, L.M., Malide, D., Yu, Z.-X., Combs, C.A., Connelly, P.S., Subramaniam, S. and Balaban, R.S. (2015) 'Mitochondrial reticulum for cellular energy distribution in muscle', *Nature*, 523(7562), pp. 617-620.

Glater, E.E., Megeath, L.J., Stowers, R.S. and Schwarz, T.L. (2006) 'Axonal transport of mitochondria requires milton to recruit kinesin heavy chain and is light chain independent', *J Cell Biol*, 173(4), pp. 545-57.

Goldfarb, L.G., Park, K.Y., Cervenakova, L., Gorokhova, S., Lee, H.S., Vasconcelos, O., Nagle, J.W., Semino-Mora, C., Sivakumar, K. and Dalakas, M.C. (1998) 'Missense mutations in desmin associated with familial cardiac and skeletal myopathy', *Nat Genet*, 19(4), pp. 402-3.

Gorman, G.S., Schaefer, A.M., Ng, Y., Gomez, N., Blakely, E.L., Alston, C.L., Feeney, C., Horvath, R., Yu-Wai-Man, P., Chinnery, P.F., Taylor, R.W., Turnbull, D.M. and McFarland, R. (2015) 'Prevalence of nuclear and mitochondrial DNA mutations related to adult mitochondrial disease', *Ann Neurol*, 77(5), pp. 753-9.

Gorza, L. (1990) 'Identification of a novel type 2 fiber population in mammalian skeletal muscle by combined use of histochemical myosin ATPase and anti-myosin monoclonal antibodies', *J Histochem Cytochem*, 38(2), pp. 257-65.

Gotz, A., Isohanni, P., Liljestrom, B., Rummukainen, J., Nikolajev, K., Herrgard, E., Marjavaara, S. and Suomalainen, A. (2012) 'Fatal neonatal lactic acidosis caused by a novel de novo mitochondrial G7453A tRNA-Serine ((UCN)) mutation', *Pediatr Res*, 72(1), pp. 90-4.

Greaves, L.C., Nooteboom, M., Elson, J.L., Tuppen, H.A., Taylor, G.A., Commane, D.M., Arasaradnam, R.P., Khrapko, K., Taylor, R.W., Kirkwood, T.B., Mathers, J.C. and Turnbull, D.M. (2014) 'Clonal expansion of early to mid-life mitochondrial DNA point mutations drives mitochondrial dysfunction during human ageing', *PLoS Genet*, 10(9), p. e1004620.

Grünewald, A., Lax, N.Z., Rocha, M.C., Reeve, A.K., Hepplewhite, P.D., A. Rygiel, K., Taylor, R.W. and Turnbull, D.M. (2014) 'Quantitative quadruple-label immunofluorescence of mitochondrial and cytoplasmic proteins in single neurons from human midbrain tissue', *Journal of Neuroscience Methods*, 232(100), pp. 143-149.

Gu, J., Wu, M., Guo, R., Yan, K., Lei, J., Gao, N. and Yang, M. (2016) 'The architecture of the mammalian respirasome', *Nature*, 537(7622), pp. 639-643.

Güçer, Ş., Talim, B., Aşan, E., Korkusuz, P., Özen, S., Ünal, Ş., Kalkanoğlu, S.H., Kale, G. and Çağlar, M. (2005) 'Focal segmental glomerulosclerosis associated with mitochondrial cytopathy: Report of two cases with special emphasis on podocytes', *Pediatric and Developmental Pathology*, 8(6), pp. 710-717.

Guerrero-Castillo, S., Baertling, F., Kownatzki, D., Wessels, H.J., Arnold, S., Brandt, U. and Nijtmans, L. (2016) 'The Assembly Pathway of Mitochondrial Respiratory Chain Complex I', *Cell Metab*.

Guja, K.E. and Garcia-Diaz, M. (2012) 'Hitting the Brakes: Termination of Mitochondrial Transcription', *Biochimica et biophysica acta*, 1819(9-10), pp. 939-947.

Hackenbrock, C.R., Chazotte, B. and Gupte, S.S. (1986) 'The random collision model and a critical assessment of diffusion and collision in mitochondrial electron transport', *J Bioenerg Biomembr*, 18(5), pp. 331-68.

Hagerhall, C. (1997) 'Succinate: quinone oxidoreductases. Variations on a conserved theme', *Biochim Biophys Acta*, 1320(2), pp. 107-41.

Haginoya, K., Miyabayashi, S., Iinuma, K. and Tada, K. (1990) 'Mosaicism of mitochondria in mitochondrial myopathy: an electronmicroscopic analysis of cytochrome c oxidase', *Acta Neuropathologica*, 80(6), pp. 642-648.

Halestrap, A.P., Quinlan, P.T., Whipps, D.E. and Armston, A.E. (1986) 'Regulation of the mitochondrial matrix volume in vivo and in vitro. The role of calcium', *Biochemical Journal*, 236(3), pp. 779-787.

Hammersen, F., Gidlöf, A., Larsson, J. and Lewis, D. (1980) 'The occurrence of paracrystalline mitochondrial inclusions in normal human skeletal muscle', *Acta Neuropathologica*, 49(1), pp. 35-41.

Han, X.J., Lu, Y.F., Li, S.A., Kaitsuka, T., Sato, Y., Tomizawa, K., Nairn, A.C., Takei, K., Matsui, H. and Matsushita, M. (2008) 'CaM kinase I alpha-induced phosphorylation of Drp1 regulates mitochondrial morphology', *J Cell Biol*, 182(3), pp. 573-85.

Han, Y., Deng, B., Liu, M., Jiang, J., Wu, S. and Guan, Y. (2010) 'Clinical and genetic study of a Chinese family with spinocerebellar ataxia type 7', *Neurol India*, 58(4), pp. 622-6.

Handschin, C., Chin, S., Li, P., Liu, F., Maratos-Flier, E., Lebrasseur, N.K., Yan, Z. and Spiegelman, B.M. (2007) 'Skeletal muscle fiber-type switching, exercise intolerance, and myopathy in PGC-1alpha muscle-specific knock-out animals', *J Biol Chem*, 282(41), pp. 30014-21.

Hara, Y., Yuk, F., Puri, R., Janssen, W.G.M., Rapp, P.R. and Morrison, J.H. (2014) 'Presynaptic mitochondrial morphology in monkey prefrontal cortex correlates with working memory and is improved with estrogen treatment', *Proceedings of the National Academy of Sciences*, 111(1), pp. 486-491.

Harner, M., Korner, C., Walther, D., Mokranjac, D., Kaesmacher, J., Welsch, U., Griffith, J., Mann, M., Reggiori, F. and Neupert, W. (2011) 'The mitochondrial contact site complex, a determinant of mitochondrial architecture', *Embo j*, 30(21), pp. 4356-70.

Hatefi, Y. (1976) 'The Enzymes and the Enzyme Complexes of the Mitochondrial Oxidative Phosphorylation System', in Martonosi, A.N. (ed.) *The Enzymes of Biological Membranes: Volume 4: Electron Transport Systems and Receptors*. Boston, MA: Springer US, pp. 3-41.

Hatefi, Y. (1985) 'The mitochondrial electron transport and oxidative phosphorylation system', *Annu Rev Biochem*, 54, pp. 1015-69.

Hatefi, Y., Jurtshuk, P. and Haavik, A.G. (1961) 'Studies on the electron transport system. XXXI. DPNH-cytochrome c reductase II', *Biochim Biophys Acta*, 52, pp. 119-29.

Hayashi, J.I., Ohta, S., Kikuchi, A., Takemitsu, M., Goto, Y.I. and Nonaka, I. (1991) 'Introduction of disease-related mitochondrial DNA deletions into HeLa cells lacking mitochondrial DNA results in mitochondrial dysfunction', *Proceedings of the National Academy of Sciences of the United States of America*, 88(23), pp. 10614-10618.

Hayes, D.J., Lecky, B.R.F., Landon, D.N., Morgan-Hughes, J.A. and Clark, J.B. (1984) 'A new mitochondrial myopathy. Biochemical studies revealing a deficiency in the cytochrome b-c1 complex (complex III) of the respiratory chain', *Brain*, 107(4), pp. 1165-1177.

Hayworth, K.J., Kasthuri, N., Schalek, R. and Lichtman, J.W. (2006) 'Automating the Collection of Ultrathin Serial Sections for Large Volume TEM Reconstructions', *Microscopy and Microanalysis*, 12(S02), pp. 86-87.

Head, B., Griparic, L., Amiri, M., Gandre-Babbe, S. and van der Bliek, A.M. (2009) 'Inducible proteolytic inactivation of OPA1 mediated by the OMA1 protease in mammalian cells', *The Journal of Cell Biology*, 187(7), pp. 959-966.

Head, B.P., Zulaika, M., Ryazantsev, S. and van der Bliek, A.M. (2011) 'A novel mitochondrial outer membrane protein, MOMA-1, that affects cristae morphology in Caenorhabditis elegans', *Mol Biol Cell*, 22(6), pp. 831-41.

Heiman-Patterson, T.D., Argov, Z., Chavin, J.M., Kalman, B., Alder, H., DiMauro, S., Bank, W. and Tahmoush, A.J. (1997) 'Biochemical and genetic studies in a family with mitochondrial myopathy', *Muscle Nerve*, 20(10), pp. 1219-24.

Henderson, M., De Waele, L., Hudson, J., Eagle, M., Sewry, C., Marsh, J., Charlton, R., He, L.P., Blakely, E.L., Horrocks, I., Stewart, W., Taylor, R.W., Longman, C., Bushby, K. and Barresi, R. (2013) 'Recessive desmin-null muscular dystrophy with central nuclei and mitochondrial abnormalities', *Acta Neuropathologica*, 125(6), pp. 917-919.

Herbst, A., Pak, J.W., McKenzie, D., Bua, E., Bassiouni, M. and Aiken, J.M. (2007) 'Accumulation of Mitochondrial DNA Deletion Mutations in Aged Muscle Fibers: Evidence for a Causal Role in Muscle Fiber Loss', *The journals of gerontology. Series A, Biological sciences and medical sciences*, 62(3), pp. 235-245.

Herrero-Marti, N.M.D., Ayuso, T., Tunon, M.T., Martin, M.A., Ruiz-Pesini, E. and Montoya, J. (2010) 'A MELAS/MERRF phenotype associated with the mitochondrial DNA 5521G>A mutation', *Journal of Neurology, Neurosurgery and Psychiatry*, 81(4), pp. 471-472.

Herrmann, J.M. and Neupert, W. (2000) 'Protein transport into mitochondria', *Current Opinion in Microbiology*, 3(2), pp. 210-214.

Higashikata, T., Koyama, J., Shimada, H., Yazaki, M., Owa, M. and Ikeda, S. (2001) 'An 80-year-old mitochondrial disease patient with A3243G tRNA(Leu(UUR)) gene presenting cardiac dysfunction as the main symptom', *Intern Med*, 40(5), pp. 405-8.

Hollenbeck, P.J. and Saxton, W.M. (2005) 'The axonal transport of mitochondria', *Journal of Cell Science*, 118(23), pp. 5411-5419.

Holliday, P.L., Climie, A.R., Gilroy, J. and Mahmud, M.Z. (1983) 'Mitolchondrial myopathy and encephalopathy: Three cases—a deficiency of NADH-CoQ dehydrogenase?', *Neurology*, 33(12), pp. 1619-1622.

Holloszy, J.O. (1967) 'Biochemical adaptations in muscle. Effects of exercise on mitochondrial oxygen uptake and respiratory enzyme activity in skeletal muscle', *J Biol Chem*, 242(9), pp. 2278-82.

Holt, I.J., Harding, A.E., Cooper, J.M., Schapira, A.H., Toscano, A., Clark, J.B. and Morgan-Hughes, J.A. (1989) 'Mitochondrial myopathies: clinical and biochemical features of 30 patients with major deletions of muscle mitochondrial DNA', *Ann Neurol*, 26(6), pp. 699-708.

Holt, I.J., Lorimer, H.E. and Jacobs, H.T. (2000) 'Coupled Leading- and Lagging-Strand Synthesis of Mammalian Mitochondrial DNA', *Cell*, 100(5), pp. 515-524.

Hood, D.A. (2001) 'Invited Review: Contractile activity-induced mitochondrial biogenesis in skeletal muscle', *Journal of Applied Physiology*, 90(3), pp. 1137-1157.

Hopmann, D., Kivi, A., Stenzel, W., Ehret, R. and Mueller, J. (2014) 'Late onset myopathy and hyperkinetic movement disorder', *Clinical Neurophysiology*, 125, p. S209.

Hoppins, S., Collins, S.R., Cassidy-Stone, A., Hummel, E., Devay, R.M., Lackner, L.L., Westermann, B., Schuldiner, M., Weissman, J.S. and Nunnari, J. (2011) 'A mitochondrial-focused genetic interaction map reveals a scaffold-like complex required for inner membrane organization in mitochondria', *J Cell Biol*, 195(2), pp. 323-40.

Howell, N., Chinnery, P.F., Ghosh, S.S., Fahy, E. and Turnbull, D.M. (2000) 'Transmission of the human mitochondrial genome', *Hum Reprod*, 15 Suppl 2, pp. 235-45.

Huang, X., Sun, L., Ji, S., Zhao, T., Zhang, W., Xu, J., Zhang, J., Wang, Y., Wang, X., Franzini-Armstrong, C., Zheng, M. and Cheng, H. (2013) 'Kissing and nanotunneling mediate intermitochondrial communication in the heart', *Proc Natl Acad Sci U S A*, 110(8), pp. 2846-51.

Hudgson, P., Bradley, W.G. and Jenkison, M. (1972) 'Familial "mitochondrial" myopathy. A myopathy associated with disordered oxidative metabolism in muscle fibres Part 1. Clinical,

electrophysiological and pathological findings', *Journal of the Neurological Sciences*, 16(3), pp. 343-370.

Hurd, D.D. and Saxton, W.M. (1996) 'Kinesin mutations cause motor neuron disease phenotypes by disrupting fast axonal transport in Drosophila', *Genetics*, 144(3), pp. 1075-85.

Ionasescu, V.V., Hart, M., DiMauro, S. and Moraes, C.T. (1994) 'Clinical and morphologic features of a myopathy associated with a point mutation in the mitochondrial tRNA(Pro) gene', *Neurology*, 44(5), pp. 975-7.

Iqbal, S. and Hood, D.A. (2014) 'Cytoskeletal regulation of mitochondrial movements in myoblasts', *Cytoskeleton (Hoboken)*, 71(10), pp. 564-72.

Itoh, K., Weis, S., Mehraein, P. and Muller-Hocker, J. (1996) 'Cytochrome c oxidase defects of the human substantia nigra in normal aging', *Neurobiol Aging*, 17(6), pp. 843-8.

Iwata, S., Lee, J.W., Okada, K., Lee, J.K., Iwata, M., Rasmussen, B., Link, T.A., Ramaswamy, S. and Jap, B.K. (1998) 'Complete structure of the 11-subunit bovine mitochondrial cytochrome bc1 complex', *Science*, 281(5373), pp. 64-71.

Jacobi, D., Liu, S., Burkewitz, K., Kory, N., Knudsen, N.H., Alexander, R.K., Unluturk, U., Li, X., Kong, X., Hyde, A.L., Gangl, M.R., Mair, W.B. and Lee, C.H. (2015) 'Hepatic Bmal1 Regulates Rhythmic Mitochondrial Dynamics and Promotes Metabolic Fitness', *Cell Metab*, 22(4), pp. 709-20.

Jaleel, A., Short, K.R., Asmann, Y.W., Klaus, K.A., Morse, D.M., Ford, G.C. and Nair, K.S. (2008) 'In vivo measurement of synthesis rate of individual skeletal muscle mitochondrial proteins', *Am J Physiol Endocrinol Metab*, 295(5), pp. E1255-68.

James, D.I., Parone, P.A., Mattenberger, Y. and Martinou, J.C. (2003) 'hFis1, a novel component of the mammalian mitochondrial fission machinery', *J Biol Chem*, 278(38), pp. 36373-9.

Jeppesen, M.G., Navratil, T., Spremulli, L.L. and Nyborg, J. (2005) 'Crystal structure of the bovine mitochondrial elongation factor Tu.Ts complex', *J Biol Chem*, 280(6), pp. 5071-81.

Jeppesen, T.D., Schwartz, M., Frederiksen, A.L., Wibrand, F., Olsen, D.B. and Vissing, J. (2006) 'Muscle phenotype and mutation load in 51 persons with the 3243A>G mitochondrial DNA mutation', *Arch Neurol*, 63(12), pp. 1701-6.

Jiang, F., Ryan, M.T., Schlame, M., Zhao, M., Gu, Z., Klingenberg, M., Pfanner, N. and Greenberg, M.L. (2000) 'Absence of cardiolipin in the crd1 null mutant results in decreased mitochondrial membrane potential and reduced mitochondrial function', *Journal of Biological Chemistry*, 275(29), pp. 22387-22394.

John, G.B., Shang, Y., Li, L., Renken, C., Mannella, C.A., Selker, J.M., Rangell, L., Bennett, M.J. and Zha, J. (2005) 'The mitochondrial inner membrane protein mitofilin controls cristae morphology', *Mol Biol Cell*, 16(3), pp. 1543-54.

Johnson, M.A., Turnbull, D.M., Dick, D.J. and Sherratt, H.S.A. (1983) 'A partial deficiency of cytochrome c oxidase in chronic progressive external ophthalmoplegia', *Journal of the Neurological Sciences*, 60(1), pp. 31-53.

Jonckheere, A.I., Smeitink, J.A.M. and Rodenburg, R.J.T. (2012) 'Mitochondrial ATP synthase: architecture, function and pathology', *Journal of Inherited Metabolic Disease*, 35(2), pp. 211-225.

Joshi, P.R., Hauburger, A., Kley, R., Claeys, K.G., Schneider, I., Kress, W., Stoltenburg, G., Weis, J., Vorgerd, M., Deschauer, M. and Hanisch, F. (2014) 'Mitochondrial abnormalities in myofibrillar myopathies', *Clin Neuropathol*, 33(2), pp. 134-42.

Kanazawa, T., Zappaterra, M.D., Hasegawa, A., Wright, A.P., Newman-Smith, E.D., Buttle, K.F., McDonald, K., Mannella, C.A. and van der Bliek, A.M. (2008) 'The <italic>C. elegans</italic> Opa1 Homologue EAT-3 Is Essential for Resistance to Free Radicals', *PLoS Genet*, 4(2), p. e1000022.

Kanki, T. and Klionsky, D.J. (2008) 'Mitophagy in yeast occurs through a selective mechanism', *J Biol Chem*, 283(47), pp. 32386-93.

Karpati, G., Carpenter, S., Engel, A.G., Watters, G., Allen, J., Rothman, S., Klassen, G. and Mamer, O.A. (1975) 'The syndrome of systemic carnitine deficiency. Clinical, morphologic, biochemical, and pathophysiologic features', *Neurology*, 25(1), pp. 16-24.

Karppa, M., Herva, R., Moslemi, A.R., Oldfors, A., Kakko, S. and Majamaa, K. (2005) 'Spectrum of myopathic findings in 50 patients with the 3243A>G mutation in mitochondrial DNA', *Brain*, 128(Pt 8), pp. 1861-9.

Kassar-Duchossoy, L., Gayraud-Morel, B., Gomes, D., Rocancourt, D., Buckingham, M., Shinin, V. and Tajbakhsh, S. (2004) 'Mrf4 determines skeletal muscle identity in Myf5:Myod double-mutant mice', *Nature*, 431(7007), pp. 466-471.

Katunin, V.I., Savelsbergh, A., Rodnina, M.V. and Wintermeyer, W. (2002) 'Coupling of GTP Hydrolysis by Elongation Factor G to Translocation and Factor Recycling on the Ribosome', *Biochemistry*, 41(42), pp. 12806-12812.

Kayar, S.R., Hoppeler, H., Mermod, L. and Weibel, E.R. (1988) 'Mitochondrial size and shape in equine skeletal muscle: a three-dimensional reconstruction study', *Anat Rec*, 222(4), pp. 333-9.

Kazak, L., Reyes, A. and Holt, I.J. (2012) 'Minimizing the damage: repair pathways keep mitochondrial DNA intact', *Nat Rev Mol Cell Biol*, 13(10), pp. 659-671.

Kelly, R.D.W., Mahmud, A., McKenzie, M., Trounce, I.A. and St John, J.C. (2012) 'Mitochondrial DNA copy number is regulated in a tissue specific manner by DNA methylation of the nuclear-encoded DNA polymerase gamma A', *Nucleic Acids Research*, 40(20), pp. 10124-10138.

Kendall, F.D. (2012) 'Mitochondrial disorders: Overview of diagnostic tools and new diagnostic trends', *Journal of Pediatric Biochemistry*, 2(4), pp. 193-203.

Kennaway, N.G., Buist, N.R.M., Darley–usmar, V.M., Papadimitriou, A., Dimauro, S., Kelley, R.I., Capaldi, R.A., Blank, N.K. and D'Agostino, A. (1984) 'Lactic acidosis and mitochondrial myopathy associated with deficiency of several components of complex III of the respiratory chain', *Pediatric Research*, 18(10), pp. 991-999.

Kerr, J.F., Wyllie, A.H. and Currie, A.R. (1972) 'Apoptosis: a basic biological phenomenon with wide-ranging implications in tissue kinetics', *Br J Cancer*, 26(4), pp. 239-57.

Kim, D.S., Jung, D.S., Park, K.H., Kim, I.J., Kim, C.M., Lee, W.H. and Rho, S.K. (2002) 'Histochemical and molecular genetic study of MELAS and MERRF in Korean patients', *J Korean Med Sci*, 17(1), pp. 103-12.

Kim, G.W., Kim, S.M., Sunwoo, I.N. and Chi, J.G. (1991) 'Two cases of mitochondrial myopathy with predominant respiratory dysfunction', *Yonsei Med J*, 32(2), pp. 184-9.

Kim, I., Rodriguez-Enriquez, S. and Lemasters, J.J. (2007) 'Selective degradation of mitochondria by mitophagy', *Arch Biochem Biophys*, 462(2), pp. 245-53.

Kim, J.S., Kim, C.J., Chi, J.G. and Myung, H.J. (1989) 'Chronic progressive external ophthalmoplegia (CPEO) with 'ragged red fibers'. A case report', *Journal of Korean Medical Science*, 4(2), pp. 91-96.

Kim, S.H. and Chi, J.G. (1997) 'Characterization of a mitochondrial DNA deletion in patients with mitochondrial myopathy', *Mol Cells*, 7(6), pp. 726-9.

Kim, T.Y., Wang, D., Kim, A.K., Lau, E., Lin, A.J., Liem, D.A., Zhang, J., Zong, N.C., Lam, M.P. and Ping, P. (2012) 'Metabolic labeling reveals proteome dynamics of mouse mitochondria', *Mol Cell Proteomics*, 11(12), pp. 1586-94.

Kitada, T., Asakawa, S., Hattori, N., Matsumine, H., Yamamura, Y., Minoshima, S., Yokochi, M., Mizuno, Y. and Shimizu, N. (1998) 'Mutations in the parkin gene cause autosomal recessive juvenile parkinsonism', *Nature*, 392(6676), pp. 605-8.

Kley, R.A. (2014) 'O07 Using proteomic profiling to decipher the pathogenesis of myofibrillar myopathies', *Neuromuscular Disorders*, 24(S1), p. S2.

Koopman, W.J.H., Visch, H.-J., Verkaart, S., van den Heuvel, L.W.P.J., Smeitink, J.A.M. and Willems, P.H.G.M. (2005) 'Mitochondrial network complexity and pathological decrease in complex I activity are tightly correlated in isolated human complex I deficiency', *American Journal of Physiology - Cell Physiology*, 289(4), p. C881.

Korenke, G.C., Bentlage, H.A.C.M., Ruitenbeek, W., Sengers, R.C.A., Sperl, W., Trijbels, J.M.F., Gabreels, F.J.M., Wijburg, F.A., Wiedermann, V., Hanefeld, F., Wendel, U., Reckmann, M., Griebel, V. and Wölk, H. (1990) 'Isolated and combined deficiencies of NADH dehydrogenase (complex I) in muscle tissue of children with mitochondrial myopathies', *European Journal of Pediatrics*, 150(2), pp. 104-108.

Kowald, A. and Kirkwood, T.B. (2014) 'Transcription could be the key to the selection advantage of mitochondrial deletion mutants in aging', *Proc Natl Acad Sci U S A*, 111(8), pp. 2972-7.

Kraytsberg, Y., Kudryavtseva, E., McKee, A.C., Geula, C., Kowall, N.W. and Khrapko, K. (2006) 'Mitochondrial DNA deletions are abundant and cause functional impairment in aged human substantia nigra neurons', *Nat Genet*, 38(5), pp. 518-20.

Krebs, H.A. and Johnson, W.A. (1937) 'Metabolism of ketonic acids in animal tissues', *Biochem J*, 31(4), pp. 645-60.

Krishnan, K.J., Reeve, A.K., Samuels, D.C., Chinnery, P.F., Blackwood, J.K., Taylor, R.W., Wanrooij, S., Spelbrink, J.N., Lightowlers, R.N. and Turnbull, D.M. (2008) 'What causes mitochondrial DNA deletions in human cells?', *Nat Genet*, 40(3), pp. 275-9.

Kroemer, G., Petit, P., Zamzami, N., Vayssiere, J.L. and Mignotte, B. (1995) 'The biochemistry of programmed cell death', *Faseb j*, 9(13), pp. 1277-87.

Kukat, C., Davies, K.M., Wurm, C.A., Spahr, H., Bonekamp, N.A., Kuhl, I., Joos, F., Polosa, P.L., Park, C.B., Posse, V., Falkenberg, M., Jakobs, S., Kuhlbrandt, W. and Larsson, N.G. (2015) 'Cross-strand binding of TFAM to a single mtDNA molecule forms the mitochondrial nucleoid', *Proc Natl Acad Sci U S A*, 112(36), pp. 11288-93.

Kukat, C., Wurm, C.A., Spahr, H., Falkenberg, M., Larsson, N.G. and Jakobs, S. (2011) 'Super-resolution microscopy reveals that mammalian mitochondrial nucleoids have a uniform size and frequently contain a single copy of mtDNA', *Proc Natl Acad Sci U S A*, 108(33), pp. 13534-9.

Kunkel, T.A. and Loeb, L.A. (1981) 'Fidelity of mammalian DNA polymerases', *Science*, 213(4509), pp. 765-767.

Kuwana, T., Mackey, M.R., Perkins, G., Ellisman, M.H., Latterich, M., Schneiter, R., Green, D.R. and Newmeyer, D.D. (2002) 'Bid, Bax, and lipids cooperate to form supramolecular openings in the outer mitochondrial membrane', *Cell*, 111(3), pp. 331-42.

Kuznetsov, A.V., Hermann, M., Saks, V., Hengster, P. and Margreiter, R. (2009) 'The cell-type specificity of mitochondrial dynamics', *Int J Biochem Cell Biol*, 41(10), pp. 1928-39.

Kyriacou, K., Hadjisavvas, A., Zenios, A., Papacharalambous, R. and Kyriakides, T. (2005) 'Morphological methods in the diagnosis of mitochondrial encephalomyopathies: the role of electron microscopy', *Ultrastruct Pathol*, 29(3-4), pp. 169-74.

Kyriacou, K., Mikellidou, C., Hadjianastasiou, A., Middleton, L., Panousopoulos, A. and Kyriakides, T. (1999) 'Ultrastructural diagnosis of mitochondrial encephalomyopathies revisited', *Ultrastructural Pathology*, 23(3), pp. 163-170.

Kyriakides, T., Drousiotou, A., Panasopoulou, A., Hadjisavvas, A., Zenios, A., Hadjigeorgiou, G.M. and Kyriacou, K. (2003) 'A comparative morphological study in 33 cases of respiratory chain encephalomyopathies', *Acta Myologica*, 22(SEPT.), pp. 48-51.

Land, J.M., Hockaday, J.M., Hughes, J.T. and Ross, B.D. (1981) 'Childhood mitochondrial myopathy with ophthalmoplegia', *Journal of the Neurological Sciences*, 51(3), pp. 371-382.

Lander, E.S., Linton, L.M., Birren, B., Nusbaum, C., Zody, M.C., Baldwin, J., Devon, K., Dewar, K., Doyle, M., FitzHugh, W., Funke, R., Gage, D., Harris, K., Heaford, A., Howland, J., Kann, L., Lehoczky, J., LeVine, R., McEwan, P., McKernan, K., Meldrim, J., Mesirov, J.P., Miranda, C., Morris, W., Naylor, J., Raymond, C., Rosetti, M., Santos, R., Sheridan, A., Sougnez, C., Stange-Thomann, Y., Stojanovic, N., Subramanian, A., Wyman, D., Rogers, J., Sulston, J., Ainscough, R., Beck, S., Bentley, D., Burton, J., Clee, C., Carter, N., Coulson, A., Deadman, R., Deloukas, P., Dunham, A., Dunham, I., Durbin, R., French, L., Grafham, D., Gregory, S., Hubbard, T., Humphray, S., Hunt, A., Jones, M., Lloyd, C., McMurray, A., Matthews, L., Mercer, S., Milne, S., Mullikin, J.C., Mungall, A., Plumb, R., Ross, M., Shownkeen, R., Sims, S., Waterston, R.H., Wilson, R.K., Hillier, L.W., McPherson, J.D., Marra, M.A., Mardis, E.R., Fulton, L.A., Chinwalla, A.T., Pepin, K.H., Gish, W.R., Chissoe, S.L., Wendl, M.C., Delehaunty, K.D., Miner, T.L., Delehaunty, A., Kramer, J.B., Cook, L.L., Fulton, R.S., Johnson, D.L., Minx, P.J., Clifton, S.W., Hawkins, T., Branscomb, E., Predki, P., Richardson, P., Wenning, S., Slezak, T., Doggett, N., Cheng, J.F., Olsen, A., Lucas, S., Elkin, C., Uberbacher, E., Frazier, M., et al. (2001) 'Initial sequencing and analysis of the human genome', *Nature*, 409(6822), pp. 860-921.

Lang, T., Laver, N., Strominger, M.B., Witking, A., Pfannl, R. and Alroy, J. (2010) 'Morphological findings of extraocular myopathy with chronic progressive external ophthalmoplegia', *Ultrastruct Pathol*, 34(2), pp. 78-81.

Larsen, S., Nielsen, J., Hansen, C.N., Nielsen, L.B., Wibrand, F., Stride, N., Schroder, H.D., Boushel, R., Helge, J.W., Dela, F. and Hey-Mogensen, M. (2012) 'Biomarkers of mitochondrial content in skeletal muscle of healthy young human subjects', *The Journal of Physiology*, 590(Pt 14), pp. 3349-3360.

Leduc-Gaudet, J.P., Picard, M., St-Jean Pelletier, F., Sgarioto, N., Auger, M.J., Vallee, J., Robitaille, R., St-Pierre, D.H. and Gouspillou, G. (2015) 'Mitochondrial morphology is altered in atrophied skeletal muscle of aged mice', *Oncotarget*, 6(20), pp. 17923-37.

Lee, C.M., Lopez, M.E., Weindruch, R. and Aiken, J.M. (1998) 'Association of age-related mitochondrial abnormalities with skeletal muscle fiber atrophy', *Free Radic Biol Med*, 25(8), pp. 964-72.

Lee, J.E., Westrate, L.M., Wu, H., Page, C. and Voeltz, G.K. (2016) 'Multiple dynamin family members collaborate to drive mitochondrial division', *Nature*, advance online publication.

Lee, Y.-j., Jeong, S.-Y., Karbowski, M., Smith, C.L. and Youle, R.J. (2004) 'Roles of the Mammalian Mitochondrial Fission and Fusion Mediators Fis1, Drp1, and Opa1 in Apoptosis', *Molecular Biology of the Cell*, 15(11), pp. 5001-5011.

Legesse-Miller, A., Massol, R.H. and Kirchhausen, T. (2003) 'Constriction and Dnm1p Recruitment Are Distinct Processes in Mitochondrial Fission', *Molecular Biology of the Cell*, 14(5), pp. 1953-1963.

Lehmann, J., Ziegan, J., Oertel, G., Lößner, J. and Kühn, H.J. (1986) 'Myopathy with mitochondrial abnormalities and rimmed vacuoles', *Acta Neuropathologica*, 70(1), pp. 86-90.

Leiber, R.L. (2010) *Skeletal muscle structure, function and plastictity*. Philidelphia, USA: Lippincott Williams & Wilkins.

Lek, A., Lek, M., North, K.N. and Cooper, S.T. (2010) 'Phylogenetic analysis of ferlin genes reveals ancient eukaryotic origins', *BMC Evol Biol*, 10, p. 231.

Letellier, T., Malgat, M., Coquet, M., Moretto, B., Parrot-Roulaud, F. and Mazat, J.P. (1992) 'Mitochondrial myopathy studies on permeabilized muscle fibers', *Pediatr Res*, 32(1), pp. 17-22.

Letts, J.A., Fiedorczuk, K. and Sazanov, L.A. (2016) 'The architecture of respiratory supercomplexes', *Nature*, 537(7622), pp. 644-648.

Levine, T.D. and Pestronk, A. (1998) 'Inflammatory myopathy with cytochrome oxidase negative muscle fibers: methotrexate treatment', *Muscle Nerve*, 21(12), pp. 1724-8.

Lin, Y.F., Schulz, A.M., Pellegrino, M.W., Lu, Y., Shaham, S. and Haynes, C.M. (2016) 'Maintenance and propagation of a deleterious mitochondrial genome by the mitochondrial unfolded protein response', *Nature*, 533(7603), pp. 416-9.

Linda, S., Lund, I., Torbergsen, T., Aasly, J., Mellgren, S.I., Borud, O. and Monstad, P. (1992) 'Mitochondrial diseases and myopathies: A series of muscle biopsy specimens with ultrastructural changes in the mitochondria', *Ultrastructural Pathology*, 16(3), pp. 263-275.

Linden, G.J.v.d. and Ansink, B.J.J. (1979) 'A case of the Kearns - Shy syndrome', *Clinical Neurology and Neurosurgery*, 81(1), pp. 45-52.

Litonin, D., Sologub, M., Shi, Y., Savkina, M., Anikin, M., Falkenberg, M., Gustafsson, C.M. and Temiakov, D. (2010) 'Human mitochondrial transcription revisited: only TFAM and TFB2M are required for transcription of the mitochondrial genes in vitro', *J Biol Chem*, 285(24), pp. 18129-33.

Liu, F., Lou, J., Zhao, D., Li, W., Zhao, Y., Sun, X. and Yan, C. (2016) 'Dysferlinopathy: mitochondrial abnormalities in human skeletal muscle', *International Journal of Neuroscience*, 126(6), pp. 499-509.

Liu, J., Aoki, M., Illa, I., Wu, C., Fardeau, M., Angelini, C., Serrano, C., Urtizberea, J.A., Hentati, F., Hamida, M.B., Bohlega, S., Culper, E.J., Amato, A.A., Bossie, K., Oeltjen, J., Bejaoui, K., McKenna-Yasek, D., Hosler, B.A., Schurr, E., Arahata, K., de Jong, P.J. and Brown, R.H., Jr. (1998) 'Dysferlin, a novel skeletal muscle gene, is mutated in Miyoshi myopathy and limb girdle muscular dystrophy', *Nat Genet*, 20(1), pp. 31-6.

Liu, P., Qian, L., Sung, J.-S., de Souza-Pinto, N.C., Zheng, L., Bogenhagen, D.F., Bohr, V.A., Wilson, D.M., Shen, B. and Demple, B. (2008) 'Removal of Oxidative DNA Damage via FEN1-Dependent Long-Patch Base Excision Repair in Human Cell Mitochondria', *Molecular and Cellular Biology*, 28(16), pp. 4975-4987.

Liu, X. and Hajnoczky, G. (2011) 'Altered fusion dynamics underlie unique morphological changes in mitochondria during hypoxia-reoxygenation stress', *Cell Death Differ*, 18(10), pp. 1561-72.

Long, Q., Zhao, D., Fan, W., Yang, L., Zhou, Y., Qi, J., Wang, X. and Liu, X. (2015) 'Modeling of Mitochondrial Donut Formation', *Biophys J*, 109(5), pp. 892-9.

Longley, M.J., Prasad, R., Srivastava, D.K., Wilson, S.H. and Copeland, W.C. (1998) 'Identification of 5'-deoxyribose phosphate lyase activity in human DNA polymerase gamma and its role in mitochondrial base excision repair in vitro', *Proc Natl Acad Sci U S A*, 95(21), pp. 12244-8.

Lopez-Fabuel, I., Le Douce, J., Logan, A., James, A.M., Bonvento, G., Murphy, M.P., Almeida, A. and Bolaños, J.P. (2016) 'Complex I assembly into supercomplexes determines differential mitochondrial ROS production in neurons and astrocytes', *Proceedings of the National Academy of Sciences*, 113(46), pp. 13063-13068.

Lopez-Gallardo, E., Lopez-Perez, M.J., Montoya, J. and Ruiz-Pesini, E. (2009) 'CPEO and KSS differ in the percentage and location of the mtDNA deletion', *Mitochondrion*, 9(5), pp. 314-7.

Lopez, C.P., Rios, P.G., Infante, E.R., Carbonell, P., Hirano, M. and DiMauro, S. (2013) 'TK2 mutation presenting as indolent myopathy', *Neurology. Conference: 65th American Academy of Neurology Annual Meeting San Diego, CA United States. Conference Start*, 80(1 MeetingAbstracts).

Lopez, M.E., Van Zeeland, N.L., Dahl, D.B., Weindruch, R. and Aiken, J.M. (2000) 'Cellular phenotypes of age-associated skeletal muscle mitochondrial abnormalities in rhesus monkeys', *Mutat Res*, 452(1), pp. 123-38.

Loson, O.C., Song, Z., Chen, H. and Chan, D.C. (2013) 'Fis1, Mff, MiD49, and MiD51 mediate Drp1 recruitment in mitochondrial fission', *Mol Biol Cell*, 24(5), pp. 659-67.

Lu, J. and Huang, Y. (2013) 'Childhood mitochondrial encephalomyopathies: clinical course, diagnosis, neuroimaging findings, mtDNA mutations and outcome in six children', *Ital J Pediatr*, 39, p. 60.

Ma, J. and Spremulli, L.L. (1996) 'Expression, purification, and mechanistic studies of bovine mitochondrial translational initiation factor 2', *J Biol Chem*, 271(10), pp. 5805-11.

Maeda, K., Kawai, H., Sanada, M., Terashima, T., Ogawa, N., Idehara, R., Makiishi, T., Yasuda, H., Sato, S.I., Hoshi, K.I., Yahikozawa, H., Nishi, K., Itoh, Y., Ogasawara, K., Tomita, K., Indo, H.P. and Majima, H.J. (2016) 'Clinical Phenotype and Segregation of Mitochondrial 3243A>G Mutation in 2 Pairs of Monozygotic Twins', *JAMA Neurol*.

Mai, N., Chrzanowska-Lightowlers, Z.M.A. and Lightowlers, R.N. (2016) 'The process of mammalian mitochondrial protein synthesis', *Cell and Tissue Research*, pp. 1-16.

Makino, M., Horai, S., Goto, Y.I. and Nonaka, I. (2000) 'Mitochondrial DNA mutations in Leigh syndrome and their phylogenetic implications', *Journal of Human Genetics*, 45(2), pp. 69-75.

Mancuso, M., Orsucci, D., Angelini, C., Bertini, E., Carelli, V., Comi, G.P., Donati, A., Minetti, C., Moggio, M., Mongini, T., Servidei, S., Tonin, P., Toscano, A., Uziel, G., Bruno, C., Ienco, E.C., Filosto, M., Lamperti, C., Catteruccia, M., Moroni, I., Musumeci, O., Pegoraro, E., Ronchi, D., Santorelli, F.M., Sauchelli, D., Scarpelli, M., Sciacco, M., Valentino, M.L., Vercelli, L., Zeviani, M. and Siciliano, G. (2014) 'The m.3243A>G mitochondrial DNA mutation and related phenotypes. A matter of gender?', *Journal of Neurology*, 261(3), pp. 504-510.

Mancuso, M., Orsucci, D., Angelini, C., Bertini, E., Carelli, V., Comi, G.P., Donati, M.A., Federico, A., Minetti, C., Moggio, M., Mongini, T., Santorelli, F.M., Servidei, S., Tonin, P., Toscano, A., Bruno, C., Bello, L., Caldarazzo Ienco, E., Cardaioli, E., Catteruccia, M., Da Pozzo, P., Filosto, M., Lamperti, C., Moroni, I., Musumeci, O., Pegoraro, E., Ronchi, D., Sauchelli, D., Scarpelli, M., Sciacco, M., Valentino, M.L., Vercelli, L., Zeviani, M. and Siciliano, G. (2015) 'Redefining phenotypes associated with mitochondrial DNA single deletion', *J Neurol*, 262(5), pp. 1301-9.

Mancuso, M., Orsucci, D., Angelini, C., Bertini, E., Carelli, V., Comi, G.P., Minetti, C., Moggio, M., Mongini, T., Servidei, S., Tonin, P., Toscano, A., Uziel, G., Bruno, C., Caldarazzo Ienco, E., Filosto, M., Lamperti, C., Martinelli, D., Moroni, I., Musumeci, O., Pegoraro, E., Ronchi, D., Santorelli, F.M., Sauchelli, D., Scarpelli, M., Sciacco, M., Spinazzi, M., Valentino, M.L., Vercelli, L., Zeviani, M. and Siciliano, G. (2013) 'Phenotypic heterogeneity of the 8344A>G mtDNA "MERRF" mutation', *Neurology*, 80(22), pp. 2049-54.

Mannella, C.A. (2006) 'The relevance of mitochondrial membrane topology to mitochondrial function', *Biochimica et Biophysica Acta (BBA) - Molecular Basis of Disease*, 1762(2), pp. 140-147.

Mannella, C.A., Lederer, W.J. and Jafri, M.S. (2013) 'The connection between inner membrane topology and mitochondrial function', *J Mol Cell Cardiol*, 62, pp. 51-7.

Mannella, C.A., Marko, M. and Buttle, K. (1997) 'Reconsidering mitochondrial structure: new views of an old organelle', *Trends Biochem Sci*, 22(2), pp. 37-8.

Marín-García, J., Goldenthal, M.J., Flores-Sarnat, L. and Sarnat, H.B. (2002) 'Severe mitochondrial cytopathy with complete A-V block, PEO, and mtDNA deletions', *Pediatric Neurology*, 27(3), pp. 213-216.

Martin, M., Cho, J., Cesare, A.J., Griffith, J.D. and Attardi, G. (2005) 'Termination factor-mediated DNA loop between termination and initiation sites drives mitochondrial rRNA synthesis', *Cell*, 123(7), pp. 1227-1240.

Martin, M.A., Iyadurai, S.J., Gassman, A., Gindhart Jr, J.G., Hays, T.S. and Saxton, W.M. (1999) 'Cytoplasmic dynein, the dynactin complex, and kinesin are interdependent and essential for fast axonal transport', *Molecular Biology of the Cell*, 10(11), pp. 3717-3728.

Martin Schmeing, T., Huang, K.S., Strobel, S.A. and Steitz, T.A. (2005) 'An induced-fit mechanism to promote peptide bond formation and exclude hydrolysis of peptidyl-tRNA', *Nature*, 438(7067), pp. 520-524.

Martin, W. and Muller, M. (1998) 'The hydrogen hypothesis for the first eukaryote', *Nature*, 392(6671), pp. 37-41.

Martinus, R.D., Garth, G.P., Webster, T.L., Cartwright, P., Naylor, D.J., Hoj, P.B. and Hoogenraad, N.J. (1996) 'Selective induction of mitochondrial chaperones in response to loss of the mitochondrial genome', *Eur J Biochem*, 240(1), pp. 98-103.

Marzo, I., Brenner, C., Zamzami, N., Jurgensmeier, J.M., Susin, S.A., Vieira, H.L., Prevost, M.C., Xie, Z., Matsuyama, S., Reed, J.C. and Kroemer, G. (1998) 'Bax and adenine nucleotide translocator cooperate in the mitochondrial control of apoptosis', *Science*, 281(5385), pp. 2027-31.

Masiero, E., Agatea, L., Mammucari, C., Blaauw, B., Loro, E., Komatsu, M., Metzger, D., Reggiani, C., Schiaffino, S. and Sandri, M. (2009) 'Autophagy is required to maintain muscle mass', *Cell Metab*, 10(6), pp. 507-15.

Matsuoka, T., Goto, Y., Hasegawa, H. and Nonaka, I. (1992) 'Segmental cytochrome c-oxidase deficiency in CPEO: teased muscle fiber analysis', *Muscle Nerve*, 15(2), pp. 209-13.

McEwen, B.F. and Marko, M. (2001) 'The emergence of electron tomography as an important tool for investigating cellular ultrastructure', *J Histochem Cytochem*, 49(5), pp. 553-64.

McKelvie, P.A., Morley, J.B., Byrne, E. and Marzuki, S. (1991) 'Mitochondrial encephalomyopathies: A correlation between neuropathological findings and defects in mitochondrial DNA', *Journal of the Neurological Sciences*, 102(1), pp. 51-60.

McKenzie, D., Bua, E., McKiernan, S., Cao, Z. and Aiken, J.M. (2002) 'Mitochondrial DNA deletion mutations: a causal role in sarcopenia', *Eur J Biochem*, 269(8), pp. 2010-5.

McLelland, G.L., Soubannier, V., Chen, C.X., McBride, H.M. and Fon, E.A. (2014) 'Parkin and PINK1 function in a vesicular trafficking pathway regulating mitochondrial quality control', *Embo j*, 33(4), pp. 282-95.

McLeod, J.G., Baker, D.C., Shorey, C.D. and Kerr, C.B. (1975) 'Mitochondrial myopathy with multisystem abnormalities and normal ocular movements', *Journal of the Neurological Sciences*, 24(1), pp. 39-52.

Mears, J.A., Lackner, L.L., Fang, S., Ingerman, E., Nunnari, J. and Hinshaw, J.E. (2011) 'Conformational changes in Dnm1 support a contractile mechanism for mitochondrial fission', *Nat Struct Mol Biol*, 18(1), pp. 20-6.

Meeusen, S., DeVay, R., Block, J., Cassidy-Stone, A., Wayson, S., McCaffery, J.M. and Nunnari, J. (2006) 'Mitochondrial inner-membrane fusion and crista maintenance requires the dynamin-related GTPase Mgm1', *Cell*, 127(2), pp. 383-95.

Meissner, C., Bruse, P. and Oehmichen, M. (2006) 'Tissue-specific deletion patterns of the mitochondrial genome with advancing age', *Exp Gerontol*, 41(5), pp. 518-24.

Meissner, C., Lorenz, H., Weihofen, A., Selkoe, D.J. and Lemberg, M.K. (2011) 'The mitochondrial intramembrane protease PARL cleaves human Pink1 to regulate Pink1 trafficking', *Journal of Neurochemistry*, 117(5), pp. 856-867.

Melberg, A., Lundberg, P.O., Henriksson, K.G., Olsson, Y. and Stålberg, E. (1996) 'Muscle-nerve involvement in autosomal dominant progressive external ophthalmoplegia with hypogonadism', *Muscle and Nerve*, 19(6), pp. 751-757.

Melegh, B., Seress, L., Bedekovics, T., Kispál, G., Sümegi, B., Trombitás, K. and Méhes, K. (1999) 'Muscle carnitine acetyltransferase and carnitine deficiency in a case of mitochondrial encephalomyopathy', *Journal of Inherited Metabolic Disease*, 22(7), pp. 827-838.

Mierau, G.W., Tyson, R.W. and Freehauf, C.L. (2004) 'Role of electron microscopy in the diagnosis of mitochondrial cytopathies', *Pediatr Dev Pathol*, 7(6), pp. 637-40.

Miles, L., Wong, B.L., Dinopoulos, A., Morehart, P.J., Hofmann, I.A. and Bove, K.E. (2006) 'Investigation of children for mitochondriopathy confirms need for strict patient selection, improved morphological criteria, and better laboratory methods', *Hum Pathol*, 37(2), pp. 173-84.

Miller, F.J., Rosenfeldt, F.L., Zhang, C., Linnane, A.W. and Nagley, P. (2003) 'Precise determination of mitochondrial DNA copy number in human skeletal and cardiac muscle by a PCR-based assay: lack of change of copy number with age', *Nucleic Acids Research*, 31(11), pp. e61-e61.

Milner, D.J., Mavroidis, M., Weisleder, N. and Capetanaki, Y. (2000) 'Desmin Cytoskeleton Linked to Muscle Mitochondrial Distribution and Respiratory Function', *The Journal of Cell Biology*, 150(6), pp. 1283-1298.

Minamikawa, T., Williams, D.A., Bowser, D.N. and Nagley, P. (1999) 'Mitochondrial permeability transition and swelling can occur reversibly without inducing cell death in intact human cells', *Exp Cell Res*, 246(1), pp. 26-37.

Miralles Fusté, J., Shi, Y., Wanrooij, S., Zhu, X., Jemt, E., Persson, Ö., Sabouri, N., Gustafsson, C.M. and Falkenberg, M. (2014) 'In Vivo Occupancy of Mitochondrial Single-Stranded DNA Binding Protein Supports the Strand Displacement Mode of DNA Replication', *PLoS Genetics*, 10(12), p. e1004832.

Mishra, P., Varuzhanyan, G., Pham, A.H. and Chan, D.C. (2015) 'Mitochondrial Dynamics is a Distinguishing Feature of Skeletal Muscle Fiber Types and Regulates Organellar Compartmentalization', *Cell Metab*, 22(6), pp. 1033-44.

Mitchell, P. (1961) 'Coupling of phosphorylation to electron and hydrogen transfer by a chemi-osmotic type of mechanism', *Nature*, 191, pp. 144-8.

Mitchell, P. (1976) 'Possible molecular mechanisms of the protonmotive function of cytochrome systems', *J Theor Biol*, 62(2), pp. 327-67.

Mitsumoto, H., Aprille, J.R., Wray, S.H., Nemni, R. and Bradley, W.G. (1983) 'Chronic progressive external ophthalmoplegia (CEPO): Clinical, morphologic, and biochemical studies', *Neurology*, 33(4), pp. 452-461.

Mizusawa, H., Watanabe, M., Kanazawa, I., Nakanishi, T., Kobayashi, M., Tanaka, M., Suzuki, H., Nishikimi, M. and Ozawa, T. (1988) 'Familial mitochondrial myopathy associated with peripheral neuropathy: Partial deficiencies of complex I and complex IV', *Journal of the Neurological Sciences*, 86(2-3), pp. 171-184.

Modi, G., Heckman, J.M. and Saffer, D. (1992) 'Vitelliform macular degeneration associated with mitochondrial myopathy', *Br J Ophthalmol*, 76(1), pp. 58-60.

Montoya, J., Gaines, G.L. and Attardi, G. (1983) 'The pattern of transcription of the human mitochondrial rRNA genes reveals two overlapping transcription units', *Cell*, 34(1), pp. 151-9.

Montoya, J., López-Gallardo, E., Díez-Sánchez, C., López-Pérez, M.J. and Ruiz-Pesini, E. (2009) '20 years of human mtDNA pathologic point mutations: Carefully reading the pathogenicity criteria', *Biochimica et Biophysica Acta (BBA) - Bioenergetics*, 1787(5), pp. 476-483.

Moraes, C.T., DiMauro, S., Zeviani, M., Lombes, A., Shanske, S., Miranda, A.F., Nakase, H., Bonilla, E., Werneck, L.C., Servidei, S. and et al. (1989) 'Mitochondrial DNA deletions in progressive external ophthalmoplegia and Kearns-Sayre syndrome', *N Engl J Med*, 320(20), pp. 1293-9.

Moraes, C.T., Kenyon, L. and Hao, H. (1999) 'Mechanisms of human mitochondrial DNA maintenance: the determining role of primary sequence and length over function', *Mol Biol Cell*, 10(10), pp. 3345-56.

Moreira, D. and Lopez-Garcia, P. (1998) 'Symbiosis between methanogenic archaea and delta-proteobacteria as the origin of eukaryotes: the syntrophic hypothesis', *J Mol Evol*, 47(5), pp. 517-30.

Morgan-Hughes, J.A., Sweeney, M.G., Cooper, J.M., Hammans, S.R., Brockington, M., Schapira, A.H.V., Harding, A.E. and Clark, J.B. (1995) 'Mitochondrial DNA (mtDNA) diseases: correlation of genotype to phenotype', *Biochimica et Biophysica Acta (BBA) - Molecular Basis of Disease*, 1271(1), pp. 135-140.

Morozov, Y.I., Agaronyan, K., Cheung, A.C.M., Anikin, M., Cramer, P. and Temiakov, D. (2014) 'A novel intermediate in transcription initiation by human mitochondrial RNA polymerase', *Nucleic Acids Research*, 42(6), pp. 3884-3893.

Morozov, Y.I., Parshin, A.V., Agaronyan, K., Cheung, Alan C.M., Anikin, M., Cramer, P. and Temiakov, D. (2015) 'A model for transcription initiation in human mitochondria', *Nucleic Acids Research*, 43(7), pp. 3726-3735.

Moslemi, A.R., Tulinius, M., Holme, E. and Oldfors, A. (1997) 'Threshold expression of the tRNA^{lys} A8344G mutation in single muscle fibres', *Neuromuscular Disorders*, 7(6), p. 450.

Mozdy, A.D., McCaffery, J.M. and Shaw, J.M. (2000) 'Dnm1p Gtpase-Mediated Mitochondrial Fission Is a Multi-Step Process Requiring the Novel Integral Membrane Component Fis1p', *The Journal of Cell Biology*, 151(2), pp. 367-380.

Müller-Höcker, J., Paetzke, I., Pongratz, D. and Hübner, G. (1985) 'Mitochondrial myopathy with diffuse activation and focal deficiency of mitochondrial ATPase and carnitine deficiency', *Virchows Archiv B Cell Pathology Including Molecular Pathology*, 48(1), pp. 185-196.

Müller-Höcker, J., Pongratz, D. and Hübner, G. (1983) 'Focal deficiency of cytochrome-c-oxidase in skeletal muscle of patients with progressive external ophthalmoplegia - Cytochemical-fine-structural study', *Virchows Archiv A Pathological Anatomy and Histopathology*, 402(1), pp. 61-71.

Muller-Hocker, J., Seibel, P., Schneiderbanger, K. and Kadenbach, B. (1993) 'Different in situ hybridization patterns of mitochondrial DNA in cytochrome c oxidase-deficient extraocular muscle fibres in the elderly', *Virchows Arch A Pathol Anat Histopathol*, 422(1), pp. 7-15.

Munn, E.A. (1974) *The structure of mitochondria*. Academic Press.

Nakada, K., Inoue, K., Ono, T., Isobe, K., Ogura, A., Goto, Y.I., Nonaka, I. and Hayashi, J.I. (2001) 'Inter-mitochondrial complementation: Mitochondria-specific system preventing mice from expression of disease phenotypes by mutant mtDNA', *Nat Med*, 7(8), pp. 934-40.

Narendra, D., Tanaka, A., Suen, D.F. and Youle, R.J. (2008) 'Parkin is recruited selectively to impaired mitochondria and promotes their autophagy', *J Cell Biol*, 183(5), pp. 795-803.

Narendra, D.P., Kane, L.A., Hauser, D.N., Fearnley, I.M. and Youle, R.J. (2010) 'p62/SQSTM1 is required for Parkin-induced mitochondrial clustering but not mitophagy; VDAC1 is dispensable for both', *Autophagy*, 6(8), pp. 1090-1106.

Nesbitt, V. and McFarland, R. (2011) 'Phenotypic spectrum of m.3243A>G mitochondrial DNA mutation in children', *Archives of Disease in Childhood*, 96(Suppl 1), p. A28.

Neuspiel, M., Schauss, A.C., Braschi, E., Zunino, R., Rippstein, P., Rachubinski, R.A., Andrade-Navarro, M.A. and McBride, H.M. (2008) 'Cargo-selected transport from the mitochondria to peroxisomes is mediated by vesicular carriers', *Curr Biol*, 18(2), pp. 102-8.

Nevo, Y., Soffer, D., Kutai, M., Zelnik, N., Saada, A., Jossiphov, J., Messer, G., Shaag, A., Shahar, E., Harel, S. and Elpeleg, O. (2002) 'Clinical characteristics and muscle pathology in myopathic mitochondrial DNA depletion', *J Child Neurol*, 17(7), pp. 499-504.

Nicastro, D., Frangakis, A.S., Typke, D. and Baumeister, W. (2000) 'Cryo-electron tomography of neurospora mitochondria', *J Struct Biol*, 129(1), pp. 48-56.

Nichol, D., Christian, M., Steel, J.H., White, R. and Parker, M.G. (2006) 'RIP140 expression is stimulated by estrogen-related receptor alpha during adipogenesis', *J Biol Chem*, 281(43), pp. 32140-7.

Nicholls, T.J. and Minczuk, M. (2014) 'In D-loop: 40 years of mitochondrial 7S DNA', *Experimental Gerontology*, 56, pp. 175-181.

Niebrój-Doblosz, I., Ryniewicz, B., Fidziańska, A. and Badurska, B. (1985) 'Lipid storage myopathy in Kearns-Sayre syndrome', *Neurology*, 35(11), pp. 1582-1586.

Noji, H., Yasuda, R., Yoshida, M. and Kinosita, K. (1997) 'Direct observation of the rotation of F1-ATPase', *Nature*, 386(6622), pp. 299-302.

Nolte, K.W., Trepels-Kottek, S., Honnef, D., Weis, J., Bien, C.G., van Baalen, A., Ritter, K., Czermin, B., Rudnik-Schoneborn, S., Wagner, N. and Hausler, M. (2013) 'Early muscle and brain ultrastructural changes in polymerase gamma 1-related encephalomyopathy', *Neuropathology*, 33(1), pp. 59-67.

Norby, S., Lestienne, P., Nelson, I., Nielsen, I.M., Schmalbruch, H., Sjo, O. and Warburg, M. (1994) 'Juvenile Kearns-Sayre syndrome initially misdiagnosed as a psychosomatic disorder', *J Med Genet*, 31(1), pp. 45-50.

Nozuma, S., Okamoto, Y., Higuchi, I., Yuan, J., Hashiguchi, A., Sakiyama, Y., Yoshimura, A., Higuchi, Y. and Takashima, H. (2015) 'Clinical and electron microscopic findings in two patients with mitochondrial myopathy associated with episodic hyper-creatine kinase-emia', *Internal Medicine*, 54(24), pp. 3209-3214.

Ohtsuka, T., Nishijima, M., Suzuki, K. and Akamatsu, Y. (1993) 'Mitochondrial dysfunction of a cultured Chinese hamster ovary cell mutant deficient in cardiolipin', *J Biol Chem*, 268(30), pp. 22914-9.

Ojala, D., Montoya, J. and Attardi, G. (1981) 'tRNA punctuation model of RNA processing in human mitochondria', *Nature*, 290(5806), pp. 470-4.

Oldfors, A., Larsson, N.G., Lindberg, C. and Holme, E. (1993) 'Mitochondrial DNA deletions in inclusion body myositis', *Brain*, 116 (Pt 2), pp. 325-36.

Oldfors, A., Moslemi, A.R., Fyhr, I.M., Holme, E., Larsson, N.G. and Lindberg, C. (1995) 'Mitochondrial DNA deletions in muscle fibers in inclusion body myositis', *J Neuropathol Exp Neurol*, 54(4), pp. 581-7.

Oldfors, A., Moslemi, A.R., Jonasson, L., Ohlsson, M., Kollberg, G. and Lindberg, C. (2006) 'Mitochondrial abnormalities in inclusion-body myositis', *Neurology*, 66(2 Suppl 1), pp. S49-55.

Olivé, M., Odgerel, Z., Martínez, A., Poza, J.J., Bragado, F.G., Zabalza, R.J., Jericó, I., Gonzalez-Mera, L., Shatunov, A., Lee, H.S., Armstrong, J., Maraví, E., Arroyo, M.R., Pascual-Calvet, J., Navarro, C., Paradas, C., Huerta, M., Marquez, F., Gutierrez-Rivas, E., Pou, A., Ferrer, I. and Goldfarb, L.G. (2011) 'Clinical and myopathological evaluation of early- and late-onset subtypes of myofibrillar myopathy', *Neuromuscular disorders : NMD*, 21(8), pp. 533-542.

Pagliuso, A., Tham, T.N., Stevens, J.K., Lagache, T., Persson, R., Salles, A., Olivo-Marin, J.C., Oddos, S., Spang, A., Cossart, P. and Stavru, F. (2016) 'A role for septin 2 in Drp1-mediated mitochondrial fission', *EMBO reports*, 17(6), pp. 858-873.

Palade, G.E. (1953) 'An electron microscope study of the mitochondrial structure', *J Histochem Cytochem*, 1(4), pp. 188-211.

Palau, F., Estela, A., Pla-Martin, D. and Sanchez-Piris, M. (2009) 'The role of mitochondrial network dynamics in the pathogenesis of Charcot-Marie-Tooth disease', *Adv Exp Med Biol*, 652, pp. 129-37.

Palty, R., Silverman, W.F., Hershfinkel, M., Caporale, T., Sensi, S.L., Parnis, J., Nolte, C., Fishman, D., Shoshan-Barmatz, V., Herrmann, S., Khananshvili, D. and Sekler, I. (2010) 'NCLX is an essential component of mitochondrial Na+/Ca2+ exchange', *Proc Natl Acad Sci U S A*, 107(1), pp. 436-41.

Papa, L. and Germain, D. (2011) 'Estrogen receptor mediates a distinct mitochondrial unfolded protein response', *J Cell Sci*, 124(Pt 9), pp. 1396-402.

Papanicolaou, K.N., Khairallah, R.J., Ngoh, G.A., Chikando, A., Luptak, I., O'Shea, K.M., Riley, D.D., Lugus, J.J., Colucci, W.S., Lederer, W.J., Stanley, W.C. and Walsh, K. (2011) 'Mitofusin-2 maintains mitochondrial structure and contributes to stress-induced permeability transition in cardiac myocytes', *Mol Cell Biol*, 31(6), pp. 1309-28.

Paradas, C., Gonzalez-Quereda, L., De Luna, N., Gallardo, E., Garcia-Consuegra, I., Gomez, H., Cabello, A., Illa, I. and Gallano, P. (2009) 'A new phenotype of dysferlinopathy with congenital onset', *Neuromuscul Disord*, 19(1), pp. 21-5.

Pathi, B., Kinsey, S.T., Howdeshell, M.E., Priester, C., McNeill, R.S. and Locke, B.R. (2012) 'The formation and functional consequences of heterogeneous mitochondrial distributions in skeletal muscle', *J Exp Biol*, 215(Pt 11), pp. 1871-83.

Patterson, K. (2004) 'Mitochondrial muscle pathology', *Pediatr Dev Pathol*, 7(6), pp. 629-32.

Paulus, W., Stevens, A. and Roggendorf, W. (1989) 'Mitochondrial encephalomyopathy with pilovacuolar inclusion or phenocopy with mitochondrial artefact?', *Journal of Neurology*, 236(6), pp. 361-363.

Paumard, P., Vaillier, J., Coulary, B., Schaeffer, J., Soubannier, V., Mueller, D.M., Brethes, D., di Rago, J.P. and Velours, J. (2002) 'The ATP synthase is involved in generating mitochondrial cristae morphology', *Embo j*, 21(3), pp. 221-30.

Payne, C.M., Stern, L.Z., Curless, R.G. and Hannapel, L.K. (1975) 'Ultrastructural fiber typing in normal and diseased human muscle', *Journal of the Neurological Sciences*, 25(1), pp. 99-108.

Peddie, C.J. and Collinson, L.M. (2014) 'Exploring the third dimension: volume electron microscopy comes of age', *Micron*, 61, pp. 9-19.

Pellegrino, M.W., Nargund, A.M. and Haynes, C.M. (2013) 'Signaling the mitochondrial unfolded protein response', *Biochim Biophys Acta*, 1833(2), pp. 410-6.

Perkins, G., Renken, C., Martone, M.E., Young, S.J., Ellisman, M. and Frey, T. (1997) 'Electron tomography of neuronal mitochondria: three-dimensional structure and organization of cristae and membrane contacts', *J Struct Biol*, 119(3), pp. 260-72.

Pernas, L. and Scorrano, L. (2016) 'Mito-Morphosis: Mitochondrial Fusion, Fission, and Cristae Remodeling as Key Mediators of Cellular Function', *Annual Review of Physiology*, 78(1), p. null.

Perry, M.S. and Sladky, J.T. (2008) 'Neuroradiologic findings in Sengers syndrome', *Pediatr Neurol*, 39(2), pp. 113-5.

Peter, J.B., Barnard, R.J., Edgerton, V.R., Gillespie, C.A. and Stempel, K.E. (1972) 'Metabolic profiles of three fiber types of skeletal muscle in guinea pigs and rabbits', *Biochemistry*, 11(14), pp. 2627-2633.

Petruzzella, V., Moraes, C.T., Sano, M.C., Bonilla, E., DiMauro, S. and Schon, E.A. (1994) 'Extremely high levels of mutant mtDNAs co-localize with cytochrome c oxidase-negative ragged-red fibers in patients harboring a point mutation at nt 3243', *Hum Mol Genet*, 3(3), pp. 449-54.

Pfanner, N., van der Laan, M., Amati, P., Capaldi, R.A., Caudy, A.A., Chacinska, A., Darshi, M., Deckers, M., Hoppins, S., Icho, T., Jakobs, S., Ji, J., Kozjak-Pavlovic, V., Meisinger, C., Odgren, P.R., Park, S.K., Rehling, P., Reichert, A.S., Sheikh, M.S., Taylor, S.S., Tsuchida, N., van der Bliek, A.M., van der Klei, I.J., Weissman, J.S., Westermann, B., Zha, J., Neupert, W. and Nunnari, J. (2014) 'Uniform nomenclature for the mitochondrial contact site and cristae organizing system', *J Cell Biol*, 204(7), pp. 1083-6.

Pfeffer, G., Waters, P.J., Maguire, J., Vallance, H.D., Wong, V.A. and Mezei, M.M. (2012) 'Levator palpebrae biopsy and diagnosis of progressive external ophthalmoplegia', *Can J Neurol Sci*, 39(4), pp. 520-4.

Pham, A.H., McCaffery, J.M. and Chan, D.C. (2012) 'Mouse lines with photo-activatable mitochondria (PhAM) to study mitochondrial dynamics', *Genesis (New York, N.Y. : 2000)*, 50(11), pp. 833-843.

Phan, Minh D. and Shin, K. (2015) 'Effects of Cardiolipin on Membrane Morphology: A Langmuir Monolayer Study', *Biophysical Journal*, 108(8), pp. 1977-1986.

Picard, M., Jung, B., Liang, F., Azuelos, I., Hussain, S., Goldberg, P., Godin, R., Danialou, G., Chaturvedi, R., Rygiel, K., Matecki, S., Jaber, S., Des Rosiers, C., Karpati, G., Ferri, L., Burelle, Y., Turnbull, D.M., Taivassalo, T. and Petrof, B.J. (2012) 'Mitochondrial dysfunction and lipid accumulation in the human diaphragm during mechanical ventilation', *Am J Respir Crit Care Med*, 186(11), pp. 1140-9.

Picard, M., McManus, M.J., Csordas, G., Varnai, P., Dorn, G.W., 2nd, Williams, D., Hajnoczky, G. and Wallace, D.C. (2015) 'Trans-mitochondrial coordination of cristae at regulated membrane junctions', *Nat Commun*, 6, p. 6259.

Picard, M., White, K. and Turnbull, D.M. (2013) 'Mitochondrial morphology, topology, and membrane interactions in skeletal muscle: a quantitative three-dimensional electron microscopy study', *J Appl Physiol (1985)*, 114(2), pp. 161-71.

Picard, M., Zhang, J., Hancock, S., Derbeneva, O., Golhar, R., Golik, P., O'Hearn, S., Levy, S., Potluri, P., Lvova, M., Davila, A., Lin, C.S., Perin, J.C., Rappaport, E.F., Hakonarson, H., Trounce, I.A., Procaccio, V. and Wallace, D.C. (2014) 'Progressive increase in mtDNA 3243A>G heteroplasmy causes abrupt transcriptional reprogramming', *Proc Natl Acad Sci U S A*, 111(38), pp. E4033-42.

Pierce, G.B., Parchment, R.E. and Lewellyn, A.L. (1991) 'Hydrogen peroxide as a mediator of programmed cell death in the blastocyst', *Differentiation*, 46(3), pp. 181-186.

Piñol-Ripoll, G., Shatunov, A., Cabello, A., Larrodé, P., de la Puerta, I., Pelegrín, J., Ramos, F.J., Olivé, M. and Goldfarb, L.G. (2009) 'Severe infantile-onset cardiomyopathy associated with a homozygous deletion in desmin', *Neuromuscular disorders : NMD*, 19(6), pp. 418-422.

Pitceathly, R.D., Rahman, S. and Hanna, M.G. (2012a) 'Single deletions in mitochondrial DNA--molecular mechanisms and disease phenotypes in clinical practice', *Neuromuscul Disord*, 22(7), pp. 577-86.

Pitceathly, R.D., Smith, C., Fratter, C., Alston, C.L., He, L., Craig, K., Blakely, E.L., Evans, J.C., Taylor, J., Shabbir, Z., Deschauer, M., Pohl, U., Roberts, M.E., Jackson, M.C., Halfpenny, C.A., Turnpenny, P.D., Lunt, P.W., Hanna, M.G., Schaefer, A.M., McFarland, R., Horvath, R., Chinnery, P.F., Turnbull, D.M., Poulton, J., Taylor, R.W. and Gorman, G.S. (2012b) 'Adults with RRM2B-related mitochondrial disease have distinct clinical and molecular characteristics', *Brain*, 135(Pt 11), pp. 3392-403.

Pohjoismaki, J.L., Wanrooij, S., Hyvarinen, A.K., Goffart, S., Holt, I.J., Spelbrink, J.N. and Jacobs, H.T. (2006) 'Alterations to the expression level of mitochondrial transcription factor A, TFAM, modify the mode of mitochondrial DNA replication in cultured human cells', *Nucleic Acids Res*, 34(20), pp. 5815-28.

Polimeno, L., Rossi, R., Mastrodonato, M., Montagnani, M., Piscitelli, D., Pesetti, B., De Benedictis, L., Girardi, B., Resta, L., Napoli, A. and Francavilla, A. (2013) 'Augmenter of liver regeneration, a protective factor against ROS-induced oxidative damage in muscle tissue of mitochondrial myopathy affected patients', *Int J Biochem Cell Biol*, 45(11), pp. 2410-9.

Ponnalagu, D. and Singh, H. (2016) 'Anion Channels of Mitochondria', *Handb Exp Pharmacol*.

Poovathingal, S.K., Gruber, J., Lakshmanan, L., Halliwell, B. and Gunawan, R. (2012) 'Is mitochondrial DNA turnover slower than commonly assumed?', *Biogerontology*, 13(5), pp. 557-564.

Porteous, W.K., James, A.M., Sheard, P.W., Porteous, C.M., Packer, M.A., Hyslop, S.J., Melton, J.V., Pang, C.-Y., Wei, Y.-H. and Murphy, M.P. (1998) 'Bioenergetic consequences of accumulating the common 4977-bp mitochondrial DNA deletion', *European Journal of Biochemistry*, 257(1), pp. 192-201.

Prick, M.J.J., M. Gabreëls, F.J., Trijbels, J.M.F., Janssen, A.J.M., le Coultre, R., van Dam, K., J. Jaspar, H.H., J. Ebels, E. and de Coul, A.A.W.O. (1983) 'Progressive poliodystrophy (alpers') disease) with a defect in cytochromeaa3 in muscle: a report of two unrelated patients', *Clinical Neurology and Neurosurgery*, 85(1), pp. 57-70.

Pronicki, M., Matyja, E., Piekutowska-Abramczuk, D., Szymanska-Debinska, T., Karkucinska-Wieckowska, A., Karczmarewicz, E., Grajkowska, W., Kmiec, T., Popowska, E. and Sykut-Cegielska, J. (2008) 'Light and electron microscopy characteristics of the muscle of patients with SURF1 gene mutations associated with Leigh disease', *J Clin Pathol*, 61(4), pp. 460-6.

Pulkes, T., Liolitsa, D., Eunson, L.H., Rose, M., Nelson, I.P., Rahman, S., Poulton, J., Marchington, D.R., Landon, D.N., Debono, A.G., Morgan-Hughes, J.A. and Hanna, M.G. (2005) 'New phenotypic diversity associated with the mitochondrial tRNA(SerUCN) gene mutation', *Neuromuscul Disord*, 15(5), pp. 364-71.

Rabl, R., Soubannier, V., Scholz, R., Vogel, F., Mendl, N., Vasiljev-Neumeyer, A., Korner, C., Jagasia, R., Keil, T., Baumeister, W., Cyrklaff, M., Neupert, W. and Reichert, A.S. (2009) 'Formation of cristae and crista junctions in mitochondria depends on antagonism between Fcj1 and Su e/g', *J Cell Biol*, 185(6), pp. 1047-63.

Reeve, A.K., Krishnan, K.J., Elson, J.L., Morris, C.M., Bender, A., Lightowlers, R.N. and Turnbull, D.M. (2008) 'Nature of mitochondrial DNA deletions in substantia nigra neurons', *Am J Hum Genet*, 82(1), pp. 228-35.

Rehling, P., Brandner, K. and Pfanner, N. (2004) 'Mitochondrial import and the twin-pore translocase', *Nat Rev Mol Cell Biol*, 5(7), pp. 519-530.

Reichmann, H., Gold, R., Meurers, B., Naumann, M., Seibel, P., Walter, U. and Klopstock, T. (1993) 'Progression of myopathology in Kearns-Sayre syndrome: a morphological follow-up study', *Acta Neuropathologica*, 85(6), pp. 679-681.

Reimann, J., Kunz, W.S., Vielhaber, S., Kappes-Horn, K. and Schroder, R. (2003) 'Mitochondrial dysfunction in myofibrillar myopathy', *Neuropathol Appl Neurobiol*, 29(1), pp. 45-51.

Reipert, S., Steinbock, F., Fischer, I., Bittner, R.E., Zeold, A. and Wiche, G. (1999) 'Association of mitochondria with plectin and desmin intermediate filaments in striated muscle', *Exp Cell Res*, 252(2), pp. 479-91.

Reiser, P.J., Moss, R.L., Giulian, G.G. and Greaser, M.L. (1985) 'Shortening velocity and myosin heavy chains of developing rabbit muscle fibers', *J Biol Chem*, 260(27), pp. 14403-5.

Riva, A., Tandler, B., Loffredo, F., Vazquez, E. and Hoppel, C. (2005) 'Structural differences in two biochemically defined populations of cardiac mitochondria', *American Journal of Physiology - Heart and Circulatory Physiology*, 289(2), pp. H868-H872.

Rivner, M.H., Shamsnia, M., Swift, T.R., Trefz, J., Roesel, R.A., Carter, A.L., Yanamura, W. and Hommes, F.A. (1989) 'Kearns-Sayre syndrome and complex II deficiency', *Neurology*, 39(5), pp. 693-6.

Robberson, D.L., Kasamatsu, H. and Vinograd, J. (1972) 'Replication of Mitochondrial DNA. Circular Replicative Intermediates in Mouse L Cells', *Proceedings of the National Academy of Sciences of the United States of America*, 69(3), pp. 737-741.

Rocha, M.C., Grady, J.P., Grunewald, A., Vincent, A., Dobson, P.F., Taylor, R.W., Turnbull, D.M. and Rygiel, K.A. (2015) 'A novel immunofluorescent assay to investigate oxidative phosphorylation deficiency in mitochondrial myopathy: understanding mechanisms and improving diagnosis', *Sci Rep*, 5, p. 15037.

Roefs, A.M., Waters, P.J., Moore, G.R.W. and Dolman, P.J. (2012) 'Orbicularis oculi muscle biopsies for mitochondrial DNA analysis in suspected mitochondrial myopathy', *British Journal of Ophthalmology*, 96(10), pp. 1296-1299.

Rollins, S., Prayson, R.A., McMahon, J.T. and Cohen, B.H. (2001) 'Diagnostic yield of muscle biopsy in patients with clinical evidence of mitochondrial cytopathy', *American Journal of Clinical Pathology*, 116(3), pp. 326-330.

Rorbach, J., Richter, R., Wessels, H.J., Wydro, M., Pekalski, M., Farhoud, M., Kuhl, I., Gaisne, M., Bonnefoy, N., Smeitink, J.A., Lightowlers, R.N. and Chrzanowska-Lightowlers, Z.M. (2008) 'The human mitochondrial ribosome recycling factor is essential for cell viability', *Nucleic Acids Res*, 36(18), pp. 5787-99.

Rossignol, R., Faustin, B., Rocher, C., Malgat, M., Mazat, J.P. and Letellier, T. (2003) 'Mitochondrial threshold effects', *Biochem J*, 370(Pt 3), pp. 751-62.

Rouzier, C., Bannwarth, S., Chaussenot, A., Chevrollier, A., Verschueren, A., Bonello-Palot, N., Fragaki, K., Cano, A., Pouget, J., Pellissier, J.F., Procaccio, V., Chabrol, B. and Paquis-

Flucklinger, V. (2012) 'The MFN2 gene is responsible for mitochondrial DNA instability and optic atrophy 'plus' phenotype', *Brain*, 135(Pt 1), pp. 23-34.

Rygiel, K.A., Grady, J.P., Taylor, R.W., Tuppen, H.A. and Turnbull, D.M. (2015a) 'Triplex real-time PCR--an improved method to detect a wide spectrum of mitochondrial DNA deletions in single cells', *Sci Rep*, 5, p. 9906.

Rygiel, K.A., Miller, J., Grady, J.P., Rocha, M.C., Taylor, R.W. and Turnbull, D.M. (2015b) 'Mitochondrial and inflammatory changes in sporadic inclusion body myositis', *Neuropathol Appl Neurobiol*, 41(3), pp. 288-303.

Rygiel, K.A., Tuppen, H.A., Grady, J.P., Vincent, A., Blakely, E.L., Reeve, A.K., Taylor, R.W., Picard, M., Miller, J. and Turnbull, D.M. (2016) 'Complex mitochondrial DNA rearrangements in individual cells from patients with sporadic inclusion body myositis', *Nucleic Acids Research*, 44(11), pp. 5313-5329.

Sacconi, S., Salviati, L., Nishigaki, Y., Walker, W.F., Hernandez-Rosa, E., Trevisson, E., Delplace, S., Desnuelle, C., Shanske, S., Hirano, M., Schon, E.A., Bonilla, E., De Vivo, D.C., DiMauro, S. and Davidson, M.M. (2008) 'A functionally dominant mitochondrial DNA mutation', *Hum Mol Genet*, 17(12), pp. 1814-20.

Sagan, L. (1967) 'On the origin of mitosing cells', *Journal of Theoretical Biology*, 14(3), pp. 225-IN6.

Salmikangas, P., van der Ven, P.F., Lalowski, M., Taivainen, A., Zhao, F., Suila, H., Schroder, R., Lappalainen, P., Furst, D.O. and Carpen, O. (2003) 'Myotilin, the limb-girdle muscular dystrophy 1A (LGMD1A) protein, cross-links actin filaments and controls sarcomere assembly', *Hum Mol Genet*, 12(2), pp. 189-203.

Samuels, D.C., Li, C., Li, B., Song, Z., Torstenson, E., Boyd Clay, H., Rokas, A., Thornton-Wells, T.A., Moore, J.H., Hughes, T.M., Hoffman, R.D., Haines, J.L., Murdock, D.G., Mortlock, D.P. and Williams, S.M. (2013) 'Recurrent tissue-specific mtDNA mutations are common in humans', *PLoS Genet*, 9(11), p. e1003929.

Saneto, R.P. and Bouldin, A. (2006) 'A boy with muscle weakness, hypercarbia, and the mitochondrial DNA A3243G mutation', *Journal of Child Neurology*, 21(1), pp. 77-79.

Santos, R.X., Correia, S.C., Wang, X., Perry, G., Smith, M.A., Moreira, P.I. and Zhu, X. (2010) 'A synergistic dysfunction of mitochondrial fission/fusion dynamics and mitophagy in Alzheimer's disease', *J Alzheimers Dis*, 20 Suppl 2, pp. S401-12.

Sarnat, H.B., Machin, G., Darwish, H.Z. and Rubin, S.Z. (1983) 'Mitochondrial myopathy of cerebro-hepato-renal (Zellweger) syndrome', *Canadian Journal of Neurological Sciences*, 10(3), pp. 170-177.

Sazanov, L.A. (2007) 'Respiratory complex I: mechanistic and structural insights provided by the crystal structure of the hydrophilic domain', *Biochemistry*, 46(9), pp. 2275-88.

Scarpulla, R.C. (2011) 'Metabolic control of mitochondrial biogenesis through the PGC-1 family regulatory network', *Biochim Biophys Acta*, 1813(7), pp. 1269-78.

Schaaf, C.P., Blazo, M., Lewis, R.A., Tonini, R.E., Takei, H., Wang, J., Wong, L.J. and Scaglia, F. (2011) 'Early-onset severe neuromuscular phenotype associated with compound heterozygosity for OPA1 mutations', *Mol Genet Metab*, 103(4), pp. 383-7.

Schaefer, A.M., McFarland, R., Blakely, E.L., He, L., Whittaker, R.G., Taylor, R.W., Chinnery, P.F. and Turnbull, D.M. (2008) 'Prevalence of mitochondrial DNA disease in adults', *Ann Neurol*, 63(1), pp. 35-9.

Schaefer, A.M., Phoenix, C., Elson, J.L., McFarland, R., Chinnery, P.F. and Turnbull, D.M. (2006) 'Mitochondrial disease in adults: a scale to monitor progression and treatment', *Neurology*, 66(12), pp. 1932-4.

Schagger, H. and Pfeiffer, K. (2000) 'Supercomplexes in the respiratory chains of yeast and mammalian mitochondria', *Embo j*, 19(8), pp. 1777-83.

Schägger, H. and Pfeiffer, K. (2001) 'The Ratio of Oxidative Phosphorylation Complexes I–V in Bovine Heart Mitochondria and the Composition of Respiratory Chain Supercomplexes', *Journal of Biological Chemistry*, 276(41), pp. 37861-37867.

Schalek, R., Kasthuri, N., Hayworth, K., Berger, D., Tapia, J., Morgan, J., Turaga, S., Fagerholm, E., Seung, H. and Lichtman, J. (2011) 'Development of High-Throughput, High-Resolution 3D Reconstruction of Large-Volume Biological Tissue Using Automated Tape Collection Ultramicrotomy and Scanning Electron Microscopy', *Microscopy and Microanalysis*, 17(S2), pp. 966-967.

Schapira, A.H.V., Cooper, J.M., Morgan-Hughes, J.A., Landon, D.N. and Clark, J.B. (1990) 'Mitochondrial myopathy with a defect of mitochondrial-protein transport', *New England Journal of Medicine*, 323(1), pp. 37-42.

Scherz-Shouval, R., Shvets, E., Fass, E., Shorer, H., Gil, L. and Elazar, Z. (2007) 'Reactive oxygen species are essential for autophagy and specifically regulate the activity of Atg4', *EMBO Journal*, 26(7), pp. 1749-1760.

Schiaffino, S., Murgia, M., Serrano, A.L., Calabria, E. and Pallafacchina, G. (1999) 'How is muscle phenotype controlled by nerve activity?', *Ital J Neurol Sci*, 20(6), pp. 409-12.

Schreiber, S.N., Emter, R., Hock, M.B., Knutti, D., Cardenas, J., Podvinec, M., Oakeley, E.J. and Kralli, A. (2004) 'The estrogen-related receptor alpha (ERRalpha) functions in PPARgamma coactivator 1alpha (PGC-1alpha)-induced mitochondrial biogenesis', *Proc Natl Acad Sci U S A*, 101(17), pp. 6472-7.

Schroder, R., Goudeau, B., Simon, M.C., Fischer, D., Eggermann, T., Clemen, C.S., Li, Z., Reimann, J., Xue, Z., Rudnik-Schoneborn, S., Zerres, K., van der Ven, P.F., Furst, D.O., Kunz, W.S. and Vicart, P. (2003) 'On noxious desmin: functional effects of a novel heterozygous desmin insertion mutation on the extrasarcomeric desmin cytoskeleton and mitochondria', *Hum Mol Genet*, 12(6), pp. 657-69.

Schroder, R., Kunz, W.S., Rouan, F., Pfendner, E., Tolksdorf, K., Kappes-Horn, K., Altenschmidt-Mehring, M., Knoblich, R., van der Ven, P.F., Reimann, J., Furst, D.O., Blumcke, I., Vielhaber, S., Zillikens, D., Eming, S., Klockgether, T., Uitto, J., Wiche, G. and Rolfs, A. (2002) 'Disorganization of the desmin cytoskeleton and mitochondrial dysfunction in plectin-related epidermolysis bullosa simplex with muscular dystrophy', *J Neuropathol Exp Neurol*, 61(6), pp. 520-30.

Schultz, R.A., Swoap, S.J., McDaniel, L.D., Zhang, B., Koon, E.C., Garry, D.J., Li, K. and Williams, R.S. (1998) 'Differential expression of mitochondrial DNA replication factors in mammalian tissues', *J Biol Chem*, 273(6), pp. 3447-51.

Sciacco, M., Bonilla, E., Schon, E.A., DiMauro, S. and Moraes, C.T. (1994) 'Distribution of wild-type and common deletion forms of mtDNA in normal and respiration-deficient muscle fibers from patients with mitochondrial myopathy', *Hum Mol Genet*, 3(1), pp. 13-9.

Scorrano, L., Ashiya, M., Buttle, K., Weiler, S., Oakes, S.A., Mannella, C.A. and Korsmeyer, S.J. (2002) 'A distinct pathway remodels mitochondrial cristae and mobilizes cytochrome c during apoptosis', *Dev Cell*, 2(1), pp. 55-67.

Sebastian, D., Hernandez-Alvarez, M.I., Segales, J., Sorianello, E., Munoz, J.P., Sala, D., Waget, A., Liesa, M., Paz, J.C., Gopalacharyulu, P., Oresic, M., Pich, S., Burcelin, R., Palacin, M. and Zorzano, A. (2012) 'Mitofusin 2 (Mfn2) links mitochondrial and endoplasmic reticulum function with insulin signaling and is essential for normal glucose homeostasis', *Proc Natl Acad Sci U S A*, 109(14), pp. 5523-8.

Selcen, D. and Engel, A.G. (2004) 'Mutations in myotilin cause myofibrillar myopathy', *Neurology*, 62(8), pp. 1363-1371.

Selcen, D. and Engel, A.G. (2005) 'Mutations in ZASP define a novel form of muscular dystrophy in humans', *Ann Neurol*, 57(2), pp. 269-76.

Selcen, D., Muntoni, F., Burton, B.K., Pegoraro, E., Sewry, C., Bite, A.V. and Engel, A.G. (2009) 'Mutation in BAG3 causes severe dominant childhood muscular dystrophy', *Ann Neurol*, 65(1), pp. 83-9.

Sengers, R.C.A., Fischer, J.C., Trijbels, J.M.F., Ruitenbeek, W., Stadhouders, A.M., ter Laak, H.J. and Jaspar, H.H.J. (1983) 'A mitochondrial myopathy with a defective respiratory chain and carnitine deficiency', *European Journal of Pediatrics*, 140(4), pp. 332-337.

Servais, S., Couturier, K., Koubi, H., Rouanet, J.L., Desplanches, D., Sornay-Mayet, M.H., Sempore, B., Lavoie, J.M. and Favier, R. (2003) 'Effect of voluntary exercise on H2O2 release by subsarcolemmal and intermyofibrillar mitochondria', *Free Radic Biol Med*, 35(1), pp. 24-32.

Shadel, G.S. and Clayton, D.A. (1997) 'Mitochondrial DNA maintenance in vertebrates', *Annu Rev Biochem*, 66, pp. 409-35.

Shah, A.J., Sahgal, V., Muschler, G., Subramani, V. and Singh, H. (1982) 'Morphogenesis of the mitochondrial alterations in muscle diseases', *J Neurol Sci*, 55(1), pp. 25-37.

Shansky, J., Del Tatto, M., Chromiak, J. and Vandenburgh, H. (1997) 'A simplified method for tissue engineering skeletal muscle organoids in vitro', *In Vitro Cell Dev Biol Anim*, 33(9), pp. 659-61.

Sharma, N., Medikayala, S., Defour, A., Rayavarapu, S., Brown, K.J., Hathout, Y. and Jaiswal, J.K. (2012) 'Use of Quantitative Membrane Proteomics Identifies a Novel Role of Mitochondria in Healing Injured Muscles', *The Journal of Biological Chemistry*, 287(36), pp. 30455-30467.

Shibasaki, H., Santa, T. and Kuroiwa, Y. (1973) 'Late onset mitochondrial myopathy', *Journal of the Neurological Sciences*, 18(3), pp. 301-310.

Shimizu, S., Narita, M. and Tsujimoto, Y. (1999) 'Bcl-2 family proteins regulate the release of apoptogenic cytochrome c by the mitochondrial channel VDAC', *Nature*, 399(6735), pp. 483-7.

Shmookler Reis, R.J. and Goldstein, S. (1983) 'Mitochondrial DNA in mortal and immortal human cells. Genome number, integrity, and methylation', *J Biol Chem*, 258(15), pp. 9078-85.

Shoffner, J.M., Lott, M.T., Voljavec, A.S., Soueidan, S.A., Costigan, D.A. and Wallace, D.C. (1989) 'Spontaneous Kearns-Sayre/chronic external ophthalmoplegia plus syndrome associated with a mitochondrial DNA deletion: a slip-replication model and metabolic therapy', *Proc Natl Acad Sci U S A*, 86(20), pp. 7952-6.

Shoubridge, E.A. and Wai, T. (2007) 'Mitochondrial DNA and the mammalian oocyte', *Curr Top Dev Biol*, 77, pp. 87-111.

Shutt, T.E. and McBride, H.M. (2013) 'Staying cool in difficult times: mitochondrial dynamics, quality control and the stress response', *Biochim Biophys Acta*, 1833(2), pp. 417-24.

Sicheritz-Ponten, T., Kurland, C.G. and Andersson, S.G. (1998) 'A phylogenetic analysis of the cytochrome b and cytochrome c oxidase I genes supports an origin of mitochondria from within the Rickettsiaceae', *Biochim Biophys Acta*, 1365(3), pp. 545-51.

Siriwardena, K., Mackay, N., Levandovskiy, V., Blaser, S., Raiman, J., Kantor, P.F., Ackerley, C., Robinson, B.H., Schulze, A. and Cameron, J.M. (2013) 'Mitochondrial citrate synthase crystals: novel finding in Sengers syndrome caused by acylglycerol kinase (AGK) mutations', *Mol Genet Metab*, 108(1), pp. 40-50.

Slomovic, S., Laufer, D., Geiger, D. and Schuster, G. (2005) 'Polyadenylation and Degradation of Human Mitochondrial RNA: the Prokaryotic Past Leaves Its Mark', *Molecular and Cellular Biology*, 25(15), pp. 6427-6435.

Smerdu, V., Karsch-Mizrachi, I., Campione, M., Leinwand, L. and Schiaffino, S. (1994) 'Type IIx myosin heavy chain transcripts are expressed in type IIb fibers of human skeletal muscle', *Am J Physiol*, 267(6 Pt 1), pp. C1723-8.

Smirnova, E., Griparic, L., Shurland, D.L. and van der Bliek, A.M. (2001) 'Dynamin-related protein Drp1 is required for mitochondrial division in mammalian cells', *Mol Biol Cell*, 12(8), pp. 2245-56.

Smith, M.L., Hua, X.Y., Marsden, D.L., Liu, D., Kennaway, N.G., Ngo, K.Y. and Haas, R.H. (1997) 'Diabetes and mitochondrial encephalomyopathy with lactic acidosis and stroke-like episodes (MELAS): radiolabeled polymerase chain reaction is necessary for accurate detection of low percentages of mutation', *J Clin Endocrinol Metab*, 82(9), pp. 2826-31.

Smits, P., Smeitink, J. and van den Heuvel, L. (2010) 'Mitochondrial translation and beyond: processes implicated in combined oxidative phosphorylation deficiencies', *J Biomed Biotechnol*, 2010, p. 737385.

Smolina, N., Bruton, J., Sjoberg, G., Kostareva, A. and Sejersen, T. (2014) 'Aggregate-prone desmin mutations impair mitochondrial calcium uptake in primary myotubes', *Cell Calcium*, 56(4), pp. 269-75.

Soleimanpour-Lichaei, H.R., Kuhl, I., Gaisne, M., Passos, J.F., Wydro, M., Rorbach, J., Temperley, R., Bonnefoy, N., Tate, W., Lightowlers, R. and Chrzanowska-Lightowlers, Z. (2007) 'mtRF1a is a human mitochondrial translation release factor decoding the major termination codons UAA and UAG', *Mol Cell*, 27(5), pp. 745-57.

Soubannier, V., McLelland, G.-L., Zunino, R., Braschi, E., Rippstein, P., Fon, Edward A. and McBride, Heidi M. (2012a) 'A Vesicular Transport Pathway Shuttles Cargo from Mitochondria to Lysosomes', *Current Biology*, 22(2), pp. 135-141.

Soubannier, V., Rippstein, P., Kaufman, B.A., Shoubridge, E.A. and McBride, H.M. (2012b) 'Reconstitution of Mitochondria Derived Vesicle Formation Demonstrates Selective Enrichment of Oxidized Cargo', *PLOS ONE*, 7(12), p. e52830.

Spelbrink, J.N., Li, F.Y., Tiranti, V., Nikali, K., Yuan, Q.P., Tariq, M., Wanrooij, S., Garrido, N., Comi, G., Morandi, L., Santoro, L., Toscano, A., Fabrizi, G.M., Somer, H., Croxen, R., Beeson, D., Poulton, J., Suomalainen, A., Jacobs, H.T., Zeviani, M. and Larsson, C. (2001) 'Human mitochondrial DNA deletions associated with mutations in the gene encoding Twinkle, a phage T7 gene 4-like protein localized in mitochondria', *Nat Genet*, 28(3), pp. 223-31.

Spendiff, S., Reza, M., Murphy, J.L., Gorman, G., Blakely, E.L., Taylor, R.W., Horvath, R., Campbell, G., Newman, J., Lochmüller, H. and Turnbull, D.M. (2013) 'Mitochondrial DNA deletions in muscle satellite cells: implications for therapies', *Human Molecular Genetics*, 22(23), pp. 4739-4747.

Srinivasula, S.M., Hegde, R., Saleh, A., Datta, P., Shiozaki, E., Chai, J., Lee, R.A., Robbins, P.D., Fernandes-Alnemri, T., Shi, Y. and Alnemri, E.S. (2001) 'A conserved XIAP-interaction motif in caspase-9 and Smac/DIABLO regulates caspase activity and apoptosis', *Nature*, 410(6824), pp. 112-6.

Stadhouders, A.M., Jap, P.H.K., Winkler, H.P., Eppenberger, H.M. and Wallimann, T. (1994) 'Mitochondrial creatine kinase: A major constituent of pathological inclusions seen in mitochondrial myopathies', *Proceedings of the National Academy of Sciences of the United States of America*, 91(11), pp. 5089-5093.

Stadhouders, A.M. and Sengers, R.C.A. (1987) 'Morphological observations in skeletal muscle from patients with a mitochondrial myopathy', *Journal of Inherited Metabolic Disease*, 10(1 Supplement), pp. 62-80.

Stenqvist, L., Paetau, A., Valanne, L., Suomalainen, A. and Pihko, H. (2005) 'A juvenile case of MELAS with T3271C mitochondrial DNA mutation', *Pediatr Res*, 58(2), pp. 258-62.

Stowers, R.S., Megeath, L.J., Gorska-Andrzejak, J., Meinertzhagen, I.A. and Schwarz, T.L. (2002) 'Axonal transport of mitochondria to synapses depends on milton, a novel Drosophila protein', *Neuron*, 36(6), pp. 1063-77.

Strauss, M., Hofhaus, G., Schroder, R.R. and Kuhlbrandt, W. (2008) 'Dimer ribbons of ATP synthase shape the inner mitochondrial membrane', *Embo j*, 27(7), pp. 1154-60.

Sumegi, B., Melegh, B., Adamovich, K. and Trombitas, K. (1990) 'Cytochrome oxidase deficiency affecting the structure of the myofibre and the shape of mitochondrial cristae membrane', *Clinica Chimica Acta*, 192(1), pp. 9-18.

Sun, F., Huo, X., Zhai, Y., Wang, A., Xu, J., Su, D., Bartlam, M. and Rao, Z. (2005) 'Crystal structure of mitochondrial respiratory membrane protein complex II', *Cell*, 121(7), pp. 1043-57.

Suzuki, T., Koizumi, J., Shiraishi, H., Ofuku, K., Sasaki, M., Hori, T. and Oskoshi, N. (1989) 'Psychiatric disturbance in mitochondrial encephalomyopathy', *J Neurol Neurosurg Psychiatry*, 52(7), pp. 920-2.

Takahashi, S., Makita, Y., Oki, J., Miyamoto, A., Yanagawa, J., Naito, E., Goto, Y. and Okuno, A. (1998) 'De novo mtDNA nt 8993 (T-->G) mutation resulting in Leigh syndrome', *Am J Hum Genet*, 62(3), pp. 717-9.

Takeda, S., Ohama, E. and Ikuta, F. (1990) 'Involvement of extraocular muscle in mitochondrial encephalomyopathy', *Acta Neuropathologica*, 80(2), pp. 118-122.

Takeuchi, N., Kawakami, M., Omori, A., Ueda, T., Spremulli, L.L. and Watanabe, K. (1998) 'Mammalian mitochondrial methionyl-tRNA transformylase from bovine liver. Purification, characterization, and gene structure', *J Biol Chem*, 273(24), pp. 15085-90.

Tang, Y., Schon, E.A., Wilichowski, E., Vazquez-Memije, M.E., Davidson, E. and King, M.P. (2000) 'Rearrangements of human mitochondrial DNA (mtDNA): new insights into the regulation of mtDNA copy number and gene expression', *Mol Biol Cell*, 11(4), pp. 1471-85.

Tatsuta, T. and Langer, T. (2009) 'AAA proteases in mitochondria: diverse functions of membrane-bound proteolytic machines', *Research in Microbiology*, 160(9), pp. 711-717.

Taylor, R.W., Pyle, A., Griffin, H., Blakely, E.L., Duff, J., He, L., Smertenko, T., Alston, C.L., Neeve, V.C., Best, A., Yarham, J.W., Kirschner, J., Schara, U., Talim, B., Topaloglu, H., Baric, I., Holinski-Feder, E., Abicht, A., Czermin, B., Kleinle, S., Morris, A.A., Vassallo, G., Gorman, G.S., Ramesh, V., Turnbull, D.M., Santibanez-Koref, M., McFarland, R., Horvath, R. and Chinnery, P.F. (2014) 'Use of whole-exome sequencing to determine the genetic basis of multiple mitochondrial respiratory chain complex deficiencies', *JAMA*, 312(1), pp. 68-77.

Taylor, R.W. and Turnbull, D.M. (2005) 'Mitochondrial DNA Mutations in Human Disease', *Nature reviews. Genetics*, 6(5), pp. 389-402.

Telerman-Toppet, N., Biarent, D., Bouton, J.M., de Meirleir, L., Elmer, C., Noel, S., Vamos, E. and DiMauro, S. (1992) 'Fatal cytochrome c oxidase-deficient myopathy of infancy associated with mtDNA depletion. Differential involvement of skeletal muscle and cultured fibroblasts', *Journal of Inherited Metabolic Disease*, 15(3), pp. 323-326.

Temperley, R., Richter, R., Dennerlein, S., Lightowlers, R.N. and Chrzanowska-Lightowlers, Z.M. (2010) 'Hungry Codons Promote Frameshifting in Human Mitochondrial Ribosomes', *Science*, 327(5963), pp. 301-301.

Thajeb, P., Ma, Y.S., Tzen, C.Y., Chuang, C.K., Wu, T.Y., Chen, S.C. and Wei, Y.H. (2006) 'Oculopharyngeal somatic myopathy in a patient with a novel large-scale 3,399 bp deletion and a homoplasmic T5814C transition of the mitochondrial DNA', *Clin Neurol Neurosurg*, 108(4), pp. 407-10.

Tomecki, R., Dmochowska, A., Gewartowski, K., Dziembowski, A. and Stepien, P.P. (2004) 'Identification of a novel human nuclear-encoded mitochondrial poly(A) polymerase', *Nucleic Acids Research*, 32(20), pp. 6001-6014.

Tondera, D., Grandemange, S., Jourdain, A., Karbowski, M., Mattenberger, Y., Herzig, S., Da Cruz, S., Clerc, P., Raschke, I., Merkwirth, C., Ehses, S., Krause, F., Chan, D.C., Alexander, C., Bauer, C., Youle, R., Langer, T. and Martinou, J.C. (2009) 'SLP-2 is required for stress-induced mitochondrial hyperfusion', *The EMBO Journal*, 28(11), pp. 1589-1600.

Tong, W.-H. and Rouault, T. (2000) 'Distinct iron–sulfur cluster assembly complexes exist in the cytosol and mitochondria of human cells', *The EMBO Journal*, 19(21), pp. 5692-5700.

Tong, W.H., Jameson, G.N., Huynh, B.H. and Rouault, T.A. (2003) 'Subcellular compartmentalization of human Nfu, an iron-sulfur cluster scaffold protein, and its ability to assemble a [4Fe-4S] cluster', *Proc Natl Acad Sci U S A*, 100(17), pp. 9762-7.

Toscano, A., Santoro, M., Vita, G., Girlanda, P., Sinicropi, S., Fazio, M.C., Mazzeo, A., Rodolico, C., Aguennouz, M., Bartolone, S., Bet, L., Comi, G.P. and Messina, C. (1996) 'Late-onset mitochondrial neuromyopathy: An age-related phenomenon?', *Archives of Gerontology and Geriatrics*, 22(SUPPL.1), pp. 577-583.

Trushina, E., Nemutlu, E., Zhang, S., Christensen, T., Camp, J., Mesa, J., Siddiqui, A., Tamura, Y., Sesaki, H., Wengenack, T.M., Dzeja, P.P. and Poduslo, J.F. (2012) 'Defects in mitochondrial dynamics and metabolomic signatures of evolving energetic stress in mouse models of familial Alzheimer's disease', *PLoS One*, 7(2), p. e32737.

Tsuboi, M., Morita, H., Nozaki, Y., Akama, K., Ueda, T., Ito, K., Nierhaus, K.H. and Takeuchi, N. (2009) 'EF-G2mt is an exclusive recycling factor in mammalian mitochondrial protein synthesis', *Mol Cell*, 35(4), pp. 502-10.

Tsukihara, T., Aoyama, H., Yamashita, E., Tomizaki, T., Yamaguchi, H., Shinzawa-Itoh, K., Nakashima, R., Yaono, R. and Yoshikawa, S. (1996) 'The whole structure of the 13-subunit oxidized cytochrome c oxidase at 2.8 A', *Science*, 272(5265), pp. 1136-44.

Tuppen, H.A.L., Blakely, E.L., Turnbull, D.M. and Taylor, R.W. (2010) 'Mitochondrial DNA mutations and human disease', *Biochimica et Biophysica Acta (BBA) - Bioenergetics*, 1797(2), pp. 113-128.

Turrens, J.F. (2003) 'Mitochondrial formation of reactive oxygen species', *The Journal of Physiology*, 552(2), pp. 335-344.

Twig, G., Elorza, A., Molina, A.J., Mohamed, H., Wikstrom, J.D., Walzer, G., Stiles, L., Haigh, S.E., Katz, S., Las, G., Alroy, J., Wu, M., Py, B.F., Yuan, J., Deeney, J.T., Corkey, B.E. and Shirihai, O.S. (2008) 'Fission and selective fusion govern mitochondrial segregation and elimination by autophagy', *Embo j*, 27(2), pp. 433-46.

Tyynismaa, H., Ylikallio, E., Patel, M., Molnar, M.J., Haller, R.G. and Suomalainen, A. (2009) 'A heterozygous truncating mutation in RRM2B causes autosomal-dominant progressive external ophthalmoplegia with multiple mtDNA deletions', *Am J Hum Genet*, 85(2), pp. 290-5.

Urata, M., Wada, Y., Kim, S.H., Chumpia, W., Kayamori, Y., Hamasaki, N. and Kang, D. (2004) 'High-sensitivity detection of the A3243G mutation of mitochondrial DNA by a combination of allele-specific PCR and peptide nucleic acid-directed PCR clamping', *Clin Chem*, 50(11), pp. 2045-51.

Uusimaa, J., Finnila, S., Vainionpaa, L., Karppa, M., Herva, R., Rantala, H., Hassinen, I.E. and Majamaa, K. (2003) 'A mutation in mitochondrial DNA-encoded cytochrome c oxidase II gene in a child with Alpers-Huttenlocher-like disease', *Pediatrics*, 111(3), pp. e262-8.

Valente, E.M., Abou-Sleiman, P.M., Caputo, V., Muqit, M.M., Harvey, K., Gispert, S., Ali, Z., Del Turco, D., Bentivoglio, A.R., Healy, D.G., Albanese, A., Nussbaum, R., Gonzalez-Maldonado, R., Deller, T., Salvi, S., Cortelli, P., Gilks, W.P., Latchman, D.S., Harvey, R.J., Dallapiccola, B., Auburger, G. and Wood, N.W. (2004) 'Hereditary early-onset Parkinson's disease caused by mutations in PINK1', *Science*, 304(5674), pp. 1158-60.

van der Laan, M., Bohnert, M., Wiedemann, N. and Pfanner, N. (2012) 'Role of MINOS in mitochondrial membrane architecture and biogenesis', *Trends Cell Biol*, 22(4), pp. 185-92.

van Domburg, P.H., Gabreels-Festen, A.A., Gabreels, F.J., de Coo, R., Ruitenbeek, W., Wesseling, P. and ter Laak, H. (1996) 'Mitochondrial cytopathy presenting as hereditary sensory neuropathy with progressive external ophthalmoplegia, ataxia and fatal myoclonic epileptic status', *Brain*, 119 (Pt 3), pp. 997-1010.

van Ekeren, G.J., Stadhouders, A.M., Egberink, G.J.M., Sengers, R.C.A., Daniëls, O. and Kubat, K. (1987) 'Hereditary mitochondrial hypertrophic cardiomyopathy with mitochondrial myopathy of skeletal muscle, congenital cataract and lactic acidosis', *Virchows Archiv A Pathological Anatomy and Histopathology*, 412(1), pp. 47-52.

Van Goethem, G., Dermaut, B., Lofgren, A., Martin, J.J. and Van Broeckhoven, C. (2001) 'Mutation of POLG is associated with progressive external ophthalmoplegia characterized by mtDNA deletions', *Nat Genet*, 28(3), pp. 211-2.

Van Laar, V.S. and Berman, S.B. (2009) 'Mitochondrial dynamics in Parkinson's disease', *Exp Neurol*, 218(2), pp. 247-56.

van Wijngaarden, G.K., Bethlem, J., Meijer, A.E., Hulsmann, W.C. and Feltkamp, C.A. (1967) 'Skeletal muscle disease with abnormal mitochondria', *Brain*, 90(3), pp. 577-92.

Varanita, T., Soriano, Maria E., Romanello, V., Zaglia, T., Quintana-Cabrera, R., Semenzato, M., Menabò, R., Costa, V., Civiletto, G., Pesce, P., Viscomi, C., Zeviani, M., Di Lisa, F., Mongillo, M., Sandri, M. and Scorrano, L. (2015) 'The Opa1-Dependent Mitochondrial Cristae Remodeling Pathway Controls Atrophic, Apoptotic, and Ischemic Tissue Damage', *Cell Metabolism*, 21(6), pp. 834-844.

Vendelin, M., Beraud, N., Guerrero, K., Andrienko, T., Kuznetsov, A.V., Olivares, J., Kay, L. and Saks, V.A. (2005) 'Mitochondrial regular arrangement in muscle cells: a "crystal-like" pattern', *Am J Physiol Cell Physiol*, 288(3), pp. C757-67.

Venter, J.C., Adams, M.D., Myers, E.W., Li, P.W., Mural, R.J., Sutton, G.G., Smith, H.O., Yandell, M., Evans, C.A., Holt, R.A., Gocayne, J.D., Amanatides, P., Ballew, R.M., Huson, D.H., Wortman, J.R., Zhang, Q., Kodira, C.D., Zheng, X.H., Chen, L., Skupski, M., Subramanian, G., Thomas, P.D., Zhang, J., Gabor Miklos, G.L., Nelson, C., Broder, S., Clark, A.G., Nadeau, J., McKusick, V.A., Zinder, N., Levine, A.J., Roberts, R.J., Simon, M., Slayman, C., Hunkapiller, M., Bolanos, R., Delcher, A., Dew, I., Fasulo, D., Flanigan, M., Florea, L., Halpern, A., Hannenhalli, S., Kravitz, S., Levy, S., Mobarry, C., Reinert, K., Remington, K., Abu-Threideh, J., Beasley, E., Biddick, K., Bonazzi, V., Brandon, R., Cargill, M., Chandramouliswaran, I., Charlab, R., Chaturvedi, K., Deng, Z., Di Francesco, V., Dunn, P., Eilbeck, K., Evangelista, C., Gabrielian, A.E., Gan, W., Ge, W., Gong, F., Gu, Z., Guan, P., Heiman, T.J., Higgins, M.E., Ji, R.R., Ke, Z., Ketchum, K.A., Lai, Z., Lei, Y., Li, Z., Li, J., Liang, Y., Lin, X., Lu, F., Merkulov, G.V., Milshina, N., Moore, H.M., Naik, A.K., Narayan, V.A., Neelam, B., Nusskern, D., Rusch, D.B., Salzberg, S., Shao, W., Shue, B., Sun, J., Wang, Z., Wang, A., Wang, X., Wang, J., Wei, M., Wides, R., Xiao, C., Yan, C., et al. (2001) 'The sequence of the human genome', *Science*, 291(5507), pp. 1304-51.

Vicart, P., Caron, A., Guicheney, P., Li, Z., Prevost, M.C., Faure, A., Chateau, D., Chapon, F., Tome, F., Dupret, J.M., Paulin, D. and Fardeau, M. (1998) 'A missense mutation in the alphaB-crystallin chaperone gene causes a desmin-related myopathy', *Nat Genet*, 20(1), pp. 92-5.

Vila, M.C., Rayavarapu, S., Hogarth, M.W., Van der Meulen, J.H., Horn, A., Defour, A., Takeda, S.i., Brown, K.J., Hathout, Y., Nagaraju, K. and Jaiswal, J.K. (2016) 'Mitochondria mediate cell membrane repair and contribute to Duchenne muscular dystrophy', *Cell Death Differ*.

Vincent, A.E., Grady, J.P., Rocha, M.C., Alston, C.L., Rygiel, K.A., Barresi, R., Taylor, R.W. and Turnbull, D.M. (2016a) 'Mitochondrial dysfunction in myofibrillar myopathy', *Neuromuscular Disorders*, 26(10), pp. 691-701.

Vincent, A.E., Ng, Y.S., White, K., Davey, T., Mannella, C., Falkous, G., Feeney, C., Schaefer, A.M., McFarland, R., Gorman, G.S., Taylor, R.W., Turnbull, D.M. and Picard, M. (2016b) 'The Spectrum of Mitochondrial Ultrastructural Defects in Mitochondrial Myopathy', *Sci Rep*, 6, p. 30610.

Vincent, A.E., Rosa, H.S., Alston, C.L., Grady, J.P., Rygiel, K.A., Rocha, M.C., Barresi, R., Taylor, R.W. and Turnbull, D.M. (2016c) 'Dysferlin mutations and mitochondrial dysfunction', *Neuromuscul Disord*.

Virbasius, J.V. and Scarpulla, R.C. (1994) 'Activation of the human mitochondrial transcription factor A gene by nuclear respiratory factors: a potential regulatory link between nuclear and mitochondrial gene expression in organelle biogenesis', *Proceedings of the National Academy of Sciences of the United States of America*, 91(4), pp. 1309-1313.

Vogel, H. (2001) 'Mitochondrial myopathies and the role of the pathologist in the molecular era', *J Neuropathol Exp Neurol*, 60(3), pp. 217-27.

von der Malsburg, K., Muller, J.M., Bohnert, M., Oeljeklaus, S., Kwiatkowska, P., Becker, T., Loniewska-Lwowska, A., Wiese, S., Rao, S., Milenkovic, D., Hutu, D.P., Zerbes, R.M., Schulze-Specking, A., Meyer, H.E., Martinou, J.C., Rospert, S., Rehling, P., Meisinger, C., Veenhuis, M., Warscheid, B., van der Klei, I.J., Pfanner, N., Chacinska, A. and van der Laan, M. (2011) 'Dual role of mitofilin in mitochondrial membrane organization and protein biogenesis', *Dev Cell*, 21(4), pp. 694-707.

Vorgerd, M., van der Ven, P.F., Bruchertseifer, V., Lowe, T., Kley, R.A., Schroder, R., Lochmuller, H., Himmel, M., Koehler, K., Furst, D.O. and Huebner, A. (2005) 'A mutation in the dimerization domain of filamin c causes a novel type of autosomal dominant myofibrillar myopathy', *Am J Hum Genet*, 77(2), pp. 297-304.

Wabbels, B., Schroeder, J.A., Voll, B., Siegmund, H. and Lorenz, B. (2007) 'Electron microscopic findings in levator muscle biopsies of patients with isolated congenital or acquired ptosis', *Graefes Arch Clin Exp Ophthalmol*, 245(10), pp. 1533-41.

Wada, H., Woo, M., Nishio, H., Nagaki, S., Yanagawa, H., Imamura, A., Yokoyama, S., Ohbayashi, C., Matsuo, M., Itoh, H. and Nakamura, H. (1996) 'Vascular involvement in benign infantile mitochondrial myopathy caused by reversible cytochrome c oxidase deficiency', *Brain Dev*, 18(4), pp. 263-8.

Walberg, M.W. and Clayton, D.A. (1981) 'Sequence and properties of the human KB cell and mouse L cell D-loop regions of mitochondrial DNA', *Nucleic Acids Res*, 9(20), pp. 5411-21.

Wallace, D.C. (1989) 'Mitochondrial DNA mutations and neuromuscular disease', *Trends Genet*, 5(1), pp. 9-13.

Wanagat, J., Cao, Z., Pathare, P. and Aiken, J.M. (2001) 'Mitochondrial DNA deletion mutations colocalize with segmental electron transport system abnormalities, muscle fiber atrophy, fiber splitting, and oxidative damage in sarcopenia', *Faseb j*, 15(2), pp. 322-32.

Wang, C., Du, W., Su, Q.P., Zhu, M., Feng, P., Li, Y., Zhou, Y., Mi, N., Zhu, Y., Jiang, D., Zhang, S., Zhang, Z., Sun, Y. and Yu, L. (2015) 'Dynamic tubulation of mitochondria drives mitochondrial network formation', *Cell Res*, 25(10), pp. 1108-20.

Wang, C. and Youle, R.J. (2009) 'The role of mitochondria in apoptosis*', *Annu Rev Genet*, 43, pp. 95-118.

Wang, L.C., Lee, W.T., Tsai, W.Y., Tsau, Y.K. and Shen, Y.Z. (2000) 'Mitochondrial cytopathy combined with Fanconi's syndrome', *Pediatr Neurol*, 22(5), pp. 403-6.

Wang, X. and Schwarz, T.L. (2009) 'The Mechanism of Ca2+-Dependent Regulation of Kinesin-Mediated Mitochondrial Motility', *Cell*, 136(1), pp. 163-174.

Wang, Y. and Bogenhagen, D.F. (2006) 'Human mitochondrial DNA nucleoids are linked to protein folding machinery and metabolic enzymes at the mitochondrial inner membrane', *J Biol Chem*, 281(35), pp. 25791-802.

Wanrooij, S. and Falkenberg, M. (2010) 'The human mitochondrial replication fork in health and disease', *Biochim Biophys Acta*, 1797(8), pp. 1378-88.

Watt, I.N., Montgomery, M.G., Runswick, M.J., Leslie, A.G.W. and Walker, J.E. (2010) 'Bioenergetic cost of making an adenosine triphosphate molecule in animal mitochondria', *Proceedings of the National Academy of Sciences*, 107(39), pp. 16823-16827.

Weber, K., Wilson, J.N., Taylor, L., Brierley, E., Johnson, M.A., Turnbull, D.M. and Bindoff, L.A. (1997) 'A new mtDNA mutation showing accumulation with time and restriction to skeletal muscle', *American Journal of Human Genetics*, 60(2), pp. 373-380.

Weber, T.A., Koob, S., Heide, H., Wittig, I., Head, B., van der Bliek, A., Brandt, U., Mittelbronn, M. and Reichert, A.S. (2013) 'APOOL is a cardiolipin-binding constituent of the Mitofilin/MINOS protein complex determining cristae morphology in mammalian mitochondria', *PLoS One*, 8(5), p. e63683.

West, A.P., Brodsky, I.E., Rahner, C., Woo, D.K., Erdjument-Bromage, H., Tempst, P., Walsh, M.C., Choi, Y., Shadel, G.S. and Ghosh, S. (2011) 'TLR signalling augments macrophage bactericidal activity through mitochondrial ROS', *Nature*, 472(7344), pp. 476-480.

Westrate, L.M., Drocco, J.A., Martin, K.R., Hlavacek, W.S. and MacKeigan, J.P. (2014) 'Mitochondrial Morphological Features Are Associated with Fission and Fusion Events', *PLoS ONE*, 9(4), p. e95265.

Wilkens, V., Kohl, W. and Busch, K. (2013) 'Restricted diffusion of OXPHOS complexes in dynamic mitochondria delays their exchange between cristae and engenders a transitory mosaic distribution', *Journal of Cell Science*, 126(1), p. 103.

Williams, S.L., Mash, D.C., Zuchner, S. and Moraes, C.T. (2013) 'Somatic mtDNA mutation spectra in the aging human putamen', *PLoS Genet*, 9(12), p. e1003990.

Winter, L., Wittig, I., Peeva, V., Eggers, B., Heidler, J., Chevessier, F., Kley, R.A., Barkovits, K., Strecker, V., Berwanger, C., Herrmann, H., Marcus, K., Kornblum, C., Kunz, W.S., Schroder, R. and Clemen, C.S. (2016) 'Mutant desmin substantially perturbs mitochondrial

morphology, function and maintenance in skeletal muscle tissue', *Acta Neuropathol*, 132(3), pp. 453-73.

Wu, S.-B., Ma, Y.-S., Wu, Y.-T., Chen, Y.-C. and Wei, Y.-H. (2010) 'Mitochondrial DNA Mutation-Elicited Oxidative Stress, Oxidative Damage, and Altered Gene Expression in Cultured Cells of Patients with MERRF Syndrome', *Molecular Neurobiology*, 41(2), pp. 256-266.

Xia, D., Yu, C.A., Kim, H., Xia, J.Z., Kachurin, A.M., Zhang, L., Yu, L. and Deisenhofer, J. (1997) 'Crystal structure of the cytochrome bc1 complex from bovine heart mitochondria', *Science*, 277(5322), pp. 60-6.

Xia, J., Sinelnikov, I.V., Han, B. and Wishart, D.S. (2015) 'MetaboAnalyst 3.0—making metabolomics more meaningful', *Nucleic Acids Research*.

Yamashita, S., Nishino, I., Nonaka, I. and Goto, Y. (2008) 'Genotype and phenotype analyses in 136 patients with single large-scale mitochondrial DNA deletions', *J Hum Genet*, 53(7), pp. 598-606.

Yau, E.K.C., Chan, K.Y., Au, K.M., Chow, T.C. and Chan, Y.W. (2009) 'A novel mitochondrial DNA deletion in a Chinese girl with Kearns-Sayre syndrome', *Hong Kong Medical Journal*, 15(5), pp. 374-377.

Yerdelen, D., Koc, F. and Koc, Z. (2008) 'Delayed diagnosis of Kearns-Sayre syndrome in a 38-year-old male patient: a case report', *Int J Neurosci*, 118(2), pp. 267-75.

Yin, X., Wang, Q., Chen, T., Niu, J., Ban, R., Liu, J., Mao, Y. and Pu, C. (2015) 'CD4(+) cells, macrophages, MHC-I and C5b-9 involve the pathogenesis of dysferlinopathy', *International Journal of Clinical and Experimental Pathology*, 8(3), pp. 3069-3075.

Yoon, T. and Cowan, J.A. (2003) 'Iron-sulfur cluster biosynthesis. Characterization of frataxin as an iron donor for assembly of [2Fe-2S] clusters in ISU-type proteins', *J Am Chem Soc*, 125(20), pp. 6078-84.

Youle, R.J. and van der Bliek, A.M. (2012) 'Mitochondrial Fission, Fusion, and Stress', *Science (New York, N.Y.)*, 337(6098), pp. 1062-1065.

Young, M.J. and Copeland, W.C. (2016) 'Human mitochondrial DNA replication machinery and disease', *Current Opinion in Genetics & Development*, 38, pp. 52-62.

Yu Wai Man, P., Sitarz, K.S., Samuels, D.C., Griffiths, P.G., Reeve, A.K., Bindoff, L.A., Horvath, R. and Chinnery, P.F. (2010) 'OPA1 mutations cause cytochrome c oxidase deficiency due to loss of wild-type mtDNA molecules', *Hum Mol Genet*, 19(15), pp. 3043-52.

Yuan, J.H., Sakiyama, Y., Higuchi, I., Inamori, Y., Higuchi, Y., Hashiguchi, A., Higashi, K., Yoshimura, A. and Takashima, H. (2013) 'Mitochondrial myopathy with autophagic vacuoles in patients with the m.8344A>G mutation', *J Clin Pathol*, 66(8), pp. 659-64.

Yusuf, F. and Brand-Saberi, B. (2012) 'Myogenesis and muscle regeneration', *Histochemistry and Cell Biology*, 138(2), pp. 187-199.

Zeharia, A., Fischel-Ghodsian, N., Casas, K., Bykhovskaya, Y., Tamari, H., Lev, D., Mimouni, M. and Lerman-Sagie, T. (2005) 'Mitochondrial myopathy, sideroblastic anemia, and lactic acidosis: An automosal recessive syndrome in persian jews caused by a mutation in the PUS1 gene', *Journal of Child Neurology*, 20(5), pp. 449-452.

Zeviani, M., Moraes, C.T., DiMauro, S., Nakase, H., Bonilla, E., Schon, E.A. and Rowland, L.P. (1988) 'Deletions of mitochondrial DNA in Kearns-Sayre syndrome', *Neurology*, 38(9), pp. 1339-46.

Zhang, L., Trushin, S., Christensen, T.A., Bachmeier, B.V., Gateno, B., Schroeder, A., Yao, J., Itoh, K., Sesaki, H., Poon, W.W., Gylys, K.H., Patterson, E.R., Parisi, J.E., Diaz Brinton, R., Salisbury, J.L. and Trushina, E. (2016) 'Altered brain energetics induces mitochondrial fission arrest in Alzheimer's Disease', *Sci Rep*, 6, p. 18725.

Zhang, Q., Raoof, M., Chen, Y., Sumi, Y., Sursal, T., Junger, W., Brohi, K., Itagaki, K. and Hauser, C.J. (2010) 'Circulating mitochondrial DAMPs cause inflammatory responses to injury', *Nature*, 464(7285), pp. 104-7.

Zhao, D., Wang, Z., Hong, D., Zhang, W. and Yuan, Y. (2013) 'Chronic progressive external ophthalmoplegia coexistent with motor neuron disease in a patient with a novel large-scale mitochondrial DNA deletion', *Clinical Neurology and Neurosurgery*, 115(8), pp. 1490-1492.

Zhao, Q., Wang, J., Levichkin, I.V., Stasinopoulos, S., Ryan, M.T. and Hoogenraad, N.J. (2002) 'A mitochondrial specific stress response in mammalian cells', *Embo j*, 21(17), pp. 4411-9.

Zheng, L., Zhou, M., Guo, Z., Lu, H., Qian, L., Dai, H., Qiu, J., Yakubovskaya, E., Bogenhagen, D.F., Demple, B. and Shen, B. (2008) 'Human DNA2 is a mitochondrial nuclease/helicase for efficient processing of DNA replication and repair intermediates', *Mol Cell*, 32(3), pp. 325-36.

Zhu, J., Vinothkumar, K.R. and Hirst, J. (2016) 'Structure of mammalian respiratory complex I', *Nature*, 536(7616), pp. 354-358.

Zick, M., Rabl, R. and Reichert, A.S. (2009) 'Cristae formation—linking ultrastructure and function of mitochondria', *Biochimica et Biophysica Acta (BBA) - Molecular Cell Research*, 1793(1), pp. 5-19.

Zollo, O., Tiranti, V. and Sondheimer, N. (2012) 'Transcriptional requirements of the distal heavy-strand promoter of mtDNA', *Proceedings of the National Academy of Sciences of the United States of America*, 109(17), pp. 6508-6512.

Zong, W.X., Lindsten, T., Ross, A.J., MacGregor, G.R. and Thompson, C.B. (2001) 'BH3-only proteins that bind pro-survival Bcl-2 family members fail to induce apoptosis in the absence of Bax and Bak', *Genes Dev*, 15(12), pp. 1481-6.